INTER

International Network on Timber Engineering Research

INTER - International Network on Timber Engineering Research

2014 the International Network on Timber Engineering Research (INTER) was founded.

Scope
Presentation, discussion and documentation of research results in timber engineering and development of application rules for timber design codes or standards related to timber engineering.
Approach
Annual meetings in different countries/places hosted by meeting participants
Presentation and discussion of papers
Peer review of the abstracts before the meeting and of the papers during the meeting
Decision of the acceptance of the abstracts before the meeting by a well-defined review process
Decision of the acceptance of the papers for the proceedings during the meeting
Publication of the papers and the discussion in proceedings
Rules
All decisions including the appointment of the chairperson or the location of annual meetings are made by the participants attending a meeting.
Membership
Persons contributing to or being interested in research related to timber engineering.

INTER PROCEEDINGS MEETING FORTY-EIGHT 2015

MEETING FORTY-EIGHT

ŠIBENIK, CROATIA

AUGUST 2015

INTER

International Network on Timber Engineering Research

Proceedings

Meeting 48

24 - 27 August 2015

Šibenik, Croatia

Edited by Rainer Görlacher

Timber Scientific Publishing
KIT Holzbau und Baukonstruktionen
Karlsruhe, Germany
2015

Publisher:
Timber Scientific Publishing
KIT Holzbau und Baukonstruktionen
Reinhard-Baumeister-Platz 1
76131 Karlsruhe
Germany
2015

ISSN 2199-9740

Table of Contents

1 List of participants

AUSTRIA	
T Bogensperger	holz.bau forschungs gmbh
M Retuznik	proHolz Austria, Vienna
G Schickhofer	Technical University of Graz
CANADA	
M Kovacs	McMaster University, Hamilton
F Lam	University of British Columbia, Vancouver
M Popovski	FPInnovations, Vancouver
A Salenikovich	Université Laval, Québec
I Smith	University of New Brunswick
T Tannert	University of British Columbia, Vancouver
CHINA	
Minjuan He	Tongji University
Zheng Li	Tongji University
CROATIA	
M Jelec	University of Osijek
V Rajcic	University of Zagreb
M Stepinac	University of Zagreb
J Barbalic	University of Zagreb
ESTONIA	
A Just	Tallinn University of Technology
M Tiso	Tallinn University of Technology
FINLAND	
A Kevarinmäki	VTT, Expert Services Ltd.
T Toratti	Wood Working Industries Federation, Helsinki
FRANCE	
L Franzoni	Université Paris-Est
R Pommier	University of Bordeaux

GERMANY

H J Blaß	Karlsruhe Institute of Technology (KIT)
P Dietsch	Technical University of Munich
M Flaig	Karlsruhe Institute of Technology (KIT)
M Frese	Karlsruhe Institute of Technology (KIT)
R Görlacher	Karlsruhe Institute of Technology (KIT)
M Gräfe	Technical University of Munich
J Hummel	University Kassel
M Kleinhenz	Technical University of Munich
K Kudla	University of Stuttgart
U Kuhlmann	University of Stuttgart
S Loebus	Technical University of Munich
W Seim	University Kassel
S Winter	Technical University of Munich

ITALY

C Bedon	University of Trieste
A Ceccotti	University of Venice
M Follesa	University of Sassari
L Marchi	University of Padova
C Nuti	RomaTre
L Pozza	University of Padova
A Polastri	CNR-IVALSA

JAPAN

M Yasumura	Shizuoka University

NEW ZEALAND

D Moroder	University of Canterbury
F Sarti	University of Canterbury
F Scheibmair	University of Auckland
P Zarnani	University of Auckland

NORWAY

P AAnensen	Norwegian Institute of Wood Technology (NTI)
A S Nygård	Norwegian University of Life Sciences
G Glaso	Norwegian Institute of Wood Technology (NTI)
K A Malo	NTNU Trondheim
H Stamatopoulos	NTNU Trondheim

SLOWENIA

A Blatnik	Plata d.o.o
B Dujic	Contemporary building design, Celje

SWEDEN

H Danielsson	Lund University
P J Gustafsson	Lund University
J Schmid	SP Wood Technology
E Serrano	Lund University

SWITZERLAND

T Ehrhart	ETH Zürich
G Fink	Swiss Federal Laboratories for Material Science (EMPA)
S Franke	Bern University of Applied Sciences
R Jockwer	Swiss Federal Laboratories for Material Science (EMPA)
P Kobel	ETH Zürich
J Ogrizovic	ETH Zürich

UNITED KINGDOM

R Harris	University of Bath
K Ranasinghe	TRADA, High Wycombe
Wen-Shao Chang	University of Bath
Cong Zhang	University of Bath

USA

T Skaggs	American Plywood Association, Tacoma
B Yeh	American Plywood Association, Tacoma

2 Minutes of the Meeting

by F Lam, Canada

CHAIRMAN'S INTRODUCTION

Prof. Hans Blass welcomed the delegates to the International Network on Timber Engineering Research (INTER). More than 70 participants registered for the meeting. This shows the continued interest in and the tradition of our meeting in light of changing the name of our group to INTER in Bath last year. The chairman thanks our host V Rajčić for the arrangement of the venue and looks forward to interesting presentations and discussions during our meeting. INTER will continue our tradition of yearly meetings to discuss research results with the aim of transferring the information into practical application.

There are 24 papers accepted for this meeting. Papers brought directly to the meeting would not be accepted for presentation, discussions, or publication. The same rule applies to papers where none of the authors are present and papers which are not defended by one of the authors. In the second case, we have made a one-time exception as the flights of authors for Paper 48-2-2 were unexpectedly cancelled and R Jockwer will present the work.

The presentations are limited to 20 minutes each, allowing time for meaningful discussions after each presentation. The Chair asked the presenters to conclude their respective presentations with a general proposal or statements concerning impact of the research results on existing or future potential applications and development in codes and standards.

There are 7 topics covered in this meeting: Timber columns (2), Stresses for solid timber (1), Timber joints and fasteners (5), Laminated members (5), Structural stability (4), Fire (1), Fracture Mechanics (2), and Structural design codes (4). Numbers in parentheses are the number of papers presented in each topic.

The participants have the possibility of presenting notes towards the end of the technical session. R Görlacher has brought a list of intended note presentations. Participants intending to present notes that are not on the list should notify R Görlacher accordingly.

An address list of the participants will be circulated for verification of accuracy.

The Vice Dean of International Cooperation from the University of Zagreb, Faculty of Civil Engineering gave a welcome address to our group. V Rajčić introduced the host University of Zagreb and the current state of using wood in buildings in Croatia. V Rajčić also welcomed the delegates.

GENERAL TOPICS

S Winter gave a presentation on the status report of CEN/TC 250/SC5. New items in Eurocode 5 include: CLT & reinforcements and Timber concrete composites. I Smith commented that Canadian code also faces similar challenges. E Serrano received clarifications about project team formation, timing and next phase.

TIMBER COLUMNS

48 - 2 - 1 Proposal of a Eurocode-based Method for the Buckling Design of Timber Log-walls – **C Bedon, M Fragiacomo, C Amadio**

Presented by C Bedon

H Blass asked about the G value of 500 MPa in Slide 10 and suggested that shear in buckling would be rolling shear in these walls. C Bedon responded that the chosen value was based on calibration with test results. Preliminary study showed that using a lower G value did not agree with data. Also they did not notice a lot of shear deformation as the rotation was almost a rigid body motion.

G Schickhofer commented that it would be better to consider a minimum requirement rather than such a complicated approach for a simple block wall house.

F Lam asked why the cases with design properties were higher than the cases with mean properties. C Bedon agreed and responded that the process also involved a normalization process.

A Ceccotti asked if the authors checked how far the designs are away from capacities in terms of safety. C Bedon answered that cases where stiffness of walls with large openings can be important and cases where top restraints were not available can also be important.

U Kuhlmann commented that compressive strength versus critical loading is confusing.

48 - 2 - 2 Design of Timber Members Subjected to Axial Compression or Combined Axial Compression and Bending Based on 2nd Order Theory – **A Frangi, M Theiler, R Steiger**

Presented by R Jockwer

S Winter asked why machine grading was not used to select the laminates. R Jockwer responded that no machine grading was available at the time of the project and visual grading is more common.

R Harris commented that the text of the paper seemed to suggest used of E_{mean} for single member design but the slides clarified that E_{mean} is used for system approach.

P Dietsch commented that there did not seem to be a difference between Eurocode 5 and the approach proposed by the paper where γ_m is already used.

I Smith asked how often the failures occurred at mid height. R Jockwer responded that the columns quite often failed at mid height. I Smith commented that failure locations in timber can be more random.

STRESSES FOR SOLID TIMBER

48 - 6 - 1 Rolling Shear Properties of some European Timber Species with Focus on Cross Laminated Timber (CLT): Test Configuration and Parameter Study – **T Ehrhart, R Brandner, G Schickhofer, A Frangi**

Presented by T Ehrhart

S Franke commented that the test did not consider different laminate thicknesses but only focused on the increase of board width. He stated that Beech CLT showed influence of laminate thickness rather than the laminate thickness to width ratio. T Ehrhart asked whether the ratio was kept constant in the Beech CLT tests so that thickness effect could be isolated. S Franke said no. G Schickhofer added that in future standardized procedures for LCT, 20 30 and 40 mm thickness will be available; therefore, in this study 30 mm thickness was used.

H Blass asked about the low G value. G Schickhofer responded that higher G values up to 100 MPa can be used.

P Zarnani commented that the rolling shear test results using the two plate configuration are not pure shear as tension can play a role.

M Flaig commented that the work was well done and agreed with higher values of ~100 MPa for G values. The rolling shear strength of spruce of 1.4 MPa cannot be confirmed with bending test results. G Schickhofer discussed 3 layer CLT has lower strength values possibly due to rolling shear volume effect. Also rolling shear strength should be between 1.2 and 1.5 MPa.

F Lam commented that in CLT bending tests for rolling shear strength, a high speed camera was used to capture the actual failure mode confirming existing tension perpendicular to grain stresses causing cracks that preceded rolling shear like failure. The interaction is complicated and requires more attention. He also commented that the current study for basic rolling strength is valid.

TIMBER JOINTS AND FASTENERS

48 - 7 - 1 A Universal Approach for Withdrawal Properties of Self-Tapping Screws in Solid Timber and Laminated Timber Products – **A Ringhofer, R Brandner, G Schickhofer**

Presented by G Schickhofer

H Blass commented and discussed about the usefulness of K_{ser} (screw's withdrawal stiffness) as K_{ser} is very much dependent on test configuration. G Schickhofer agreed as the test configuration dependency of stiffness is different from that of strength. R Jockwer commented that there are discussions in EC5 about test configuration. G Schickhofer agreed that the availability of a standardized test configuration would be good.

S Winter commented that he did not doubt the accuracy of the equations but they should be further simplified for practising engineers. G Schickhofer disagreed as there are so many products but the equation has three main variables for consideration.

H Stamatopoulos commented that withdrawal stiffness had more factors affecting the values.

P Zarnani asked about different screw manufacturers. G Schickhofer answered that different screws should have little effect in terms of the values. T Tannert commented that some believe in Canada that the design method for self-tapping wood screws should be extended to all types of screws. He asked whether the model fits to other data or other types of screws. G Schickhofer answered that this would be a good idea.

A Salenikovich agreed that diameter mattered and not the product type and that the difference between self-tapping and non self-tapping screws is small. H Blass stated that this would depend on density of the wood as some species would need predrilling.

K Malo supported that withdrawal stiffness would be important for vibration cases.

M Flaig commented that using a probabilistic approach about gap influence would be valuable. F Lam commented that angle application of screws would lessen the influence of gaps. G Schickhofer agreed.

48 - 7 - 2 Characteristic Withdrawal Capacity and Stiffness of Threaded Rods – **H Stamatopoulos, K A Malo**

Presented by H Stamatopoulos

H Blass commented about the stiffness dependence on the embedment and asked why FEM predictions were higher than experimental values except for the 90 degrees case. H Stamatopoulos answered that the rod slipped with the interface more at 0 degrees than with 90 degrees. Therefore, with less relative slip at 90 degrees, there was better agreement.

S Franke asked how was the load slip evaluated in relation to the strength. H Stamatopoulos answered that small embedment length was used only. FEM calculation for strength would be more difficult as crack formation could be issues that needed to be considered; therefore, only used for stiffness prediction. S Franke stated that he has a student working on strength prediction.

P Zarnani and H Stamatopoulos discussed local shear failure mode such as block shear failure issues.

W Seim asked about the definition of fracture energy and from where these values were obtained. H Stamatopoulos clarified that he did not use fracture energy and just used a bilinear constitutive law. E Serrano commented that you needed f_w and two slopes for the bilinear constitutive law; therefore, you have defined the fracture energy. H Stamatopoulos agreed.

I Smith and H Stamatopoulos discussed progressive collapse and the use of a long rod to get steel yielding rather than withdrawal.

R Jockwer asked about pull-pull rather than push-pull test configuration. H Stamatopoulos responded that there was work done and support conditions played an important role in withdrawal stiffness.

48 - 7 - 3 Load-carrying Capacity of Dowelled Connections – H J Blass, F Colling

Presented by H Blass

K Malo asked whether the approach is valid for stainless steel. H Blass responded yes. S Franke and H Blass discussed about the fitting process for screws are more difficult.

A Salenikovich asked for comments for multiple fasteners in a row. H Blass responded that EC5 equations were used.

S Franke commented that the attempt was to justify changes to EC5. H Blass responded that the old allowable values were not based on tests of steel strength, therefore over-strength situations were not correctly considered. Here the old code is still non-conservative by ~ 10% but not 25% as previously thought.

V Rajčić and H Blass discussed the lack of conservatism of the old code when different failure cases were considered.

R Jockwer commented the yield strength of the dowels were very important. H Blass responded that high strength steel dowel compared to mild steel would still be more beneficial although it would be dependent on cost and economics.

I Smith commented that this is a manifestation of system effect.

U Kuhlmann commented about target failure mode in relationship to the type steel used.

48 - 7 - 4 Evaluation of the Reliability of Design Approaches for Connections Perpendicular to the Grain – R Jockwer, R Steiger, A Frangi

Presented by R Jockwer

F Lam commented that 3 P Weibull distribution would provide a better fit for the distribution tails. R Jockwer agreed.

I Smith suggested use of reinforcement rather than depending on design approaches that rely on stable crack growth.

H Blass asked about reinforcement between the dowels. R Jockwer responded that they thought about this but did not use it because of the arrangement of steel plates and dowels were rather close. H Blass and R Jockwer further discussed the diameter of the dowel in relationship to the size of the potential reinforcement screws.

P Zarnani and R Jockwer discussed issues related to recording the crack opening.

P Gustafsson asked if this is only valid for symmetric test set up. R Jockwer answered that they had considered one sided loading and it seemed to be okay. However the experimental base for unsymmetrical loading is quite weak.

48 - 7 - 5 Simplified Fatigue Design of Typical Timber-Concrete Composite Road Bridges – K Kudla, U Kuhlmann

Presented by K Kudla

I Smith commented that we do not really know what the damage accumulation rule should be. Creep rupture rather than cyclic load effect would be more important with the concept of killer load. He asked about the experimental verification of the work. K Kudla answered that experimental verification was not done. Miner’s rule should be on the safe side.

W Seim received clarification that the S-N line results are conservative. U Kuhlmann commented that this is a typical approach.

P Zarnani asked about the geometry of the concrete slab compared to the beam. K Kudla answered that it would not make sense to change the geometry as they had aimed for optimal conditions.

K Malo asked if temperature rise was experienced during testing. U Kuhlmann responded yes, but that it should not be a big issue.

LAMINATED MEMBERS

48 - 12 - 1 Concentrated Load Introduction in CLT Elements Perpendicular to Plane – **T Bogensperger, R A Jöbstl**

Presented by T Bogensperger

F Lam received confirmation that the equation involved $f_{r,90mean}$ and the characteristic strength was incorrect and should be modified. F Lam asked about the softening procedure used in FEM analysis. T Bogensperger provided some explanation and agreed to add information in text of paper.

H Blass received clarification for the justification of punching factor k of 1.75 as possible localized effect where rolling shear failure was assumed not to be brittle. F Lam asked about the deflection in compression perpendicular to grain. T Bogensperger stated that the deflection was small because reinforcement screws were used. These screws did not add to the shear strength.

48 - 12 - 2 Shear Properties of Cross Laminated Timber (CLT) under in-plane Load: Test Configuration and Experimental Study – **R Brandner, P Dietsch, J Dröscher, M Schulte-Wrede, H Kreuzinger, M Sieder, G Schickhofer, S Winter**

Presented by P Dietsch

F Lam received clarification that the effect of compressive stresses on rolling shear strength was taken into considered using adjustment factors.

H Blass and P Dietsch discussed the roller bearing details and member under pure shear such as the case of shear wall. They also discussed the case of CLT as bending members on edge where standard bending test would be available but difficult to achieve shear failure of the members. Here torsional shear and rolling shear would coexist. A Ceccotti stated that in a 3x3 m wall in shear connection design would be more critical.

I Smith asked how the specimen size was selected. P Dietsch responded that they were chosen to avoid localized stresses therefore a ratio of 1:3 for width to height was chosen. G Schickhofer added that the tests are good for wall and diaphragm cases but beam solutions would need more work.

P Zarnani asked whether mechanistic modelling approach would be used. P Dietsch answered that the model is already mechanics based.

48 - 12 - 3 Advanced Modelling for Design Helping of Heterogeneous CLT Panels in Bending – **L Franzoni, A Lebée, F Lyon, G Foret**

Presented by L Franzoni

H Blass asked if the effect of board width was considered. L Franzoni said not yet and 3.5 is the ratio between boards. H Blass asked why were tension and compression properties established using small clear tests. L Franzoni answered that they tried to be consistent with modelling approach using clear properties and agreed that the material in reality has defects.

K Malo asked why there were sharp changes shown in the curves in slide 9 where with in-plane shear failure one would expected smooth rather than sharp changes. L Franzoni said that this could be caused by numerical issues

G Fink received clarification that the model was based on small clear properties.

K Malo and L Franzoni further discussed sharp changes were due to change in failure mode because the model could not determine mixed failure mode and therefore sharp changes were seen.

G Schickhofer asked whether the end goal should be aimed towards design code. L Franzoni said that this was not their goal at this moment.

48 - 12 - 4 Performance of Canadian Glulam Columns with New Laminae E Requirements –**F Lam, J K Oh, B J Yeh, J J Lee**

Presented by F Lam

T Bogensperger received clarification of the definition of column length being the total length of the column minus the length of the supporting shoes.

H Blass asked about the orientation of the column in relation to the buckling direction. Since the columns buckled in the direction parallel to the glue-line of the laminae, would the bending strength of the column be different if the columns buckled in the other direction. F Lam responded the “bending” strength is governed by the compression strength of the laminae when maximum load was reached. The final failure of tension occurred at a lower load level; therefore, orientation should not matter.

I Smith asked whether pin-pin conditions were tried. F Lam said that it was considered but not adopted given that the literature reported friction issues from pin-ended cases. H Blass commented that in reality pin-ended conditions do not exist so the code would be conservative if one assumed pin-ended case. F Lam agreed especially at high load levels.

A Salenikovich received clarification that the laminae were sampled from a mixed pool with MOE ranged of 11 to 13.1 GPa.

48 - 12 - 5 Design of CLT Beams with Large Finger Joints at Different Angles –**M Flaig**

Presented by M Flaig

G Schickhofer asked about the 0.3 reduction factor as a constant and suggested it would be better to have this as a function.

S Winter asked why there was a nominal reduction of 14% but found a 30% reduction for the profile. M Flaig responded that these specimens were from industry and they did not have control over the production accuracy. Here, optimized production of CLT as beams was not yet available.

W Seim received clarification that E_{local} as shear free MOE. He asked for examples of where these members could replace glulam. M Flaig responded that CLT beam has higher strengths in the perpendicular to grain direction therefore, these members could be suitable for cases where higher stress in perpendicular to grain directions as well as cases where cracks might be important.

L Franzoni asked given a straight beam why were those dimensions given. M Flaig said that bending strength of straight beams would depend on the specimen size; so standardized test span to depth ratio of 18 to 25 are typically used. In the current tests finger joint governed so the specimen length did not matter.

G Fink commented that based a sample size of 5 to get a characteristic strength might be too low. M Flaig agreed but stated that it would be too expensive to test many beams and that they relied on prior knowledge about CLT as beam element and used this information as guidance. G Fink commented they could consider different models to estimate characteristic properties.

T Bogensperger was surprised by the large stiffness degradation and asked if the strength depended on the glue. M Flaig stated that they did not know whether different glue would affect the strength but did not expect so. He also did not expect the large stiffness degradation at first but the test results clearly showed this.

T Bogensperger also asked about gluing large finger joint on site. M Flaig stated that it could be done but would not be recommended.

STRUCTURAL STABILITY

48 - 15 - 1 Performance-Based Seismic Design of Light-frame Structures - Proposed Values for Equivalent Damping –**J Hummel, W Seim**

Presented by J Hummel

M Popovski received confirmation that light frame and not CLT was shown in slide 7; also 2.8 mm diameter nails 65 mm in length and 75 mm spacing were used in the test. M Popovski commented that μ=1.64 from the data seemed too low.

D Moroder and J Hummel discussed the use of elastic spectrum and equal displacement approach. J Hummel also clarified issues related to rocking in the steel plate and the provision of ball bearing guides.

M Yasumura commented that in Japan a similar approach is available via the BSL using equivalent single mass. Here, long wall would depend on the joint at the end of the panel. Also in multi-story cases, different rotations of wall exist in each story. He asked how one would handle these cases. J Hummel answered that long walls were not considered yet. This could be considered in a model. Also multi-story cases need hold down to confine rotation such that shear would govern. M Yasumura commented that one would need a load displacement relationship and one should model the structure not just the wall. J Hummel agreed.

A Ceccotti stated that the CLT hysteresis loops would depend on different boundary conditions and the vertical load and paper reference on the topic is available.

B Dujič asked if this method would be applicable to timber structures. J Hummel responded that it has the potential to, but they would still need to work on inelastic spectrum for timber structures.

S Winter commented on editorial issues where details about the test specimens should be added. He also questioned the test with gypsum fibre boards and what would be the difference. J Hummel has the gypsum results where higher but similar load characteristics were observed. Also fatigue failures of staples and nails were observed.

WS Chang and J Hummel discussed about the flag shape hysteresis loops for CLT and the real building would behaviour differently because of centring effect. Also shear walls have relatively high equivalent viscous damping and the issue of building information from a wall to the whole structure.

F Lam received clarification the PGA used was 1g and it was chosen to drive the walls into the inelastic range. He commented that the spectrum of time histories looked strange.

I Smith discussed about missing wood based material with other material.

B Dujič commented about viscous damping issues.

D Moroder and J Hummel discussed the spectrum, time history shifting and scaling procedures.

48 - 15 - 2 Simplified Wall Bracing Method Using Wood Structural Panel Continuous Sheathing –T Skaggs, B J Yeh, E Keith

Presented by T Skaggs

I Smith received confirmation that there are plan limitations for diaphragm and wall to match each other.

G Schickhofer asked if it would be possible to introduce CLT with this approach. T Skaggs responded yes and that it could be possible although the market demand in N America for CLT in residential construction is low.

A Salenikovich asked if calculation tools would be available. T Skaggs said yes but the calculations are so simple that the tools would not really be needed.

W Seim and T Skaggs discussed how to deal with symmetrical and asymmetrical cases where location of the bracing elements would have to be within certain distance of the centre of the building plan.

F Lam and T Skaggs discussed consideration of CLT for tornado resistance structures although tornado forces are not considered in N American codes. Here, CLT for safe room tornado has been considered.

48 - 15 - 3 Structural Characterization of Multi-storey CLT Buildings Braced with Cores and Additional Shear Walls –**A Polastri, L Pozza, C Loss, I Smith**

Presented by A Polastri

D Moroder commented that the proposed interactive effort for design included FEM model for tall building but no practicing engineers are doing this. A Polastri agreed but stated that the FEM model is important and needed for tall buildings. D Moroder asked about higher mode effect. A Polastri said that only regular buildings were considered so there was no higher mode effect. D Moroder commented that higher mode was observed even in three story buildings but perhaps not in those made of CLT.

M Follesa asked about the bonding connection to the foundation. A Polastri responded that they did not consider the difference of the behaviour of hold down between wood elements and between wood wall and concrete foundation elements.

P Zarnani asked about the coupling issues between CLT panels at the corner of a building. A Polastri agreed that this would be important; here, crossed screws would be used to connect the corner panels to achieve high stiffness.

S Winter commented about the use of FEM for tall buildings. This type of study would not only be needed for earthquake, but wind issues would also need consideration. Also non-standardized hold downs should be considered. X Rad connectors have to be considered beyond strength including issues with fire, sound, airtightness etc.

A Polastri responded that they are looking at different covers to address these issues. In traditional steel plate solutions with the steel exposed, poor fire resistance would also be expected.

A Salenikovich received clarification about comparison between balloon and platform construction.

I Smith commented in Canada, a related study was done with taller buildings and wind forces tended to govern the design above 8 stories.

48 - 15 - 4 Dissipative Connections for Squat or Scarcely Jointed CLT Buildings - Experimental Tests and Numerical Validation –R Scotta, L Pozza, D Trutalli, L Marchi, A Ceccotti

Presented by R Scotta

F Sarti asked whether the differential movement between the wall and the connector was considered. R Scotta said the connector was assumed to be well connected to the wall and the differential movement was not considered. F Sarti discussed about vertical load that could help the self-centring in rocking systems. R Scotta responded that in squat systems, shear deformation is more important and has to be considered first.

T Tannert asked about the fancy shape of the connector. R Scotta said that this was made for production efficiency and consideration to use less material.

H Blass asked whether a steel angle type connector would be needed for the wall to floor connection. R Scotta said yes especially in wall to concrete foundation some steel plates would be needed to help transfer the high forces.

F Sarti asked about buckling and low cycle fatigue issues. R Scotta responded that when designing the connector, limiting the maximum strain would be needed to take low cycle fatigue into consideration. Buckling was observed and modelled, but did not influence the strength much.

B Dujič and R Scotta discussed that friction needed to be considered.

Z Li commented that the buckling would change the force distribution and one might need to avoid this failure mode. He received confirmation that mild steel with 275 MPa yield strength was used.

W Seim commented that this component test was a steel to steel connection but in buildings this would be steel to wood connection. R Scotta agreed and will use model to take this aspect into consideration.

U Kuhlmann stated that when using mild steel one must consider the over strength in the steel.

I Smith commented about practicality and tolerance, and whether the potential users have any opinions. R Scotta stated that the study mainly focused on the structural performance issues first.

FIRE

48 - 16 - 1 Analysis of Fire Resistance Tests on Timber Members in Compression with Respect to the Reduced Cross-Section Method –J Schmid, M Klippel, A Liew, A Just, A Frangi

Presented by J Schmid

H Blass commented that if these values could be trusted would you use the mean value or 5th percentile values. J Schmid responded that he would use the mean values and that there would be many other areas where safety could be added.

K Ranasinghe commented that in the UK they have huge difficulties in accepting the concept that 7 mm is too high. He asked if J Schmid would be insisting to increase 7 mm in the next EC5 revision. J Schmid responded that they are aiming to build a model to reduce the variability in the data to establish a better value. He stated that the starting value should be ~14 mm and then one can reduce it later as variability in the data base is reduced.

S Winter agreed that more investigation would be needed and that the old data base has limitations. He stated that the problem of zero strength layer concept as the actual reduction curve is questionable. Comparison with FEM is very difficult as exact properties with increase in temperature are not available. The use of 7 mm has worked well for more than 20 years and worked well all over the world. S Winter commented that he has never heard of a collapse before expected time of fire resistance in a real fire. We need to oppose making changes to the current rules now. J Schmid related to the example of weakness of steel connection in fire design and that the old standard was built on one unreliable database. The main problem is missing information on influence of temperature on timber properties if we want to replace fire testing with models.

BJ Yeh commented on the use of 7 mm for CLT and increase of char rate to account for falling off of the char layer. J Schmid responded that CLT is more complicated with many producers and issues with loading directions.

FRACTURE MECHANICS

48 - 19 - 1 A Beam Theory Fracture Mechanics Approach for Strength Analysis of Beams with a Hole –H Danielsson, P J Gustafsson

Presented by H Danielsson

H Blass commented that the stress distribution shown in slide 8 close to the hole is very different from reality. He questioned why the results are so good. H Danielsson agreed but stated that the beam theory is exact for normal stresses but might be different for shear stresses. PJ Gustafsson added that the solution should be exact in terms of energy release rate. As the crack propagated, the normal forces due to the moment should be exact but shear would not be true.

BJ Yeh asked how close the hole can be to the support and if there were two holes, how close can they be. H Danielsson responded the distances should be such that the support would not influence the hole. This would also apply to the multiple holes cases.

K Malo asked if there would be a limitation to the hole size. H Danielsson said that there would be no limit and the analysis would also work for notched beams.

I Smith commented that good results need accurate analysis, real structure, and accurate material properties; when results do not agree, maybe some of these are not working.

P Dietsch and H Danielsson discussed the cases of round and square holes and limitations to the model.

R Jockwer received clarifications that at this moment there is no recommendation for the size of the hole without reinforcement.

48 - 19 - 2 A Strongest Link Model Applied to Fracture Propagating Along Grain –P J Gustafsson, R Jockwer, E Serrano, R Steiger

Presented by R Jockwer

F Lam and R Jockwer discussed the factor K_{knot} as being established based on judgement with LN(2,0.8). F Lam commented that the fitting at the tail of the distribution was not very good. R Jockwer responded that there could be other factors such as influence of slope of grain involved.

I Smith commented about the load control testing situation versus displacement control and received information that this case related to crack arrest. He commented that how a dynamically developing crack growth could be handled with Weibull approach where Weibull did not consider stability issues. P Gustafsson responded that quasi static for dynamic loading was considered here and one could integrate the energy release rate as the crack propagates.

P Dietsch questioned if one applied the information from 48-7-4 in this situation what would happen. R Jockwer responded that one would expect little difference if the height adjustment model was applied as it might fit better than the volume adjustment model. With strongest link approach better fit could result.

T Tannert questioned the situation where the predefined failure plane in the FEM was the weak plane but failure could occur in the strong plane and how strongest link approach could consider the case with failure in the strong plane.   R Jockwer responded that one could lower the fracture energy of a predefined strong crack plane so that the crack could develop along the strong plane.

STRUCTURAL DESIGN CODES

48 - 102 - 1 A proposal for a new Background Document of Chapter 8 of Eurocode 8 – M Follesa, M Fragiacomo, D Vassallo, M Piazza, R Tomasi, S Rossi, D Casagrande

Presented by M Follesa

G Schickhofer stated that many structural types were considered here and that some should be considered only in the national annex such as log houses. M Follesa said that log houses would be interesting for Italy.

T Toratti commented that the two floor diaphragm cases where the floor went through the whole building would result in acoustic issues

F Lam commented that the ductility factor for screws connected light wood frame walls is too high. M Follesa agreed.

D Moroder discussed the information in slide 28 where β to reduce over-strength also has a β reduction; it seemed double reduction.

A Ceccotti commented that slide 7 stated that the current provisions are not always met. He asked whether the provisions are on the safe side. M Follesa said no and commented that for example some Xlam connectors have lower ductility ratio.

G Schickhofer and M Follesa discussed the definition of ductility as some of these are not consistent.

S Winter stated that the production of background documents is good; he asked about time schedule and finalization. M Follesa said that the proposal would be finalized by 2016. S Winter commented that the document should be circulated as soon as possible even as a draft.

48 - 102 - 2 Aspects of Code Based Design of Timber Structures –J Köhler, G Fink

Presented by G Fink

K Ranasinghe commented that simplicity would be needed by practicing engineers and asked the group whether we know who the target audience are for the standards. G Fink responded that the user of the standards is our aim; however, they needed to look deep into the problem to get the basic understanding to come up with provisions. H Blass commented that one would have to find the tools to translate these findings to the engineering world and practicing engineers would have deadlines and budget constraints and would use simple tools.

I Smith commented that sizing members would have easy ways but structural system considerations would be more challenging.

F Lam commented that the most needed area for reliability based design consideration would be connection design.

S Franke agreed that one needed a deeper understanding to transfer the information into simple equations; however, PhD students could be involved in the useful step of documentation of the steps from the deep understanding to the simple equation. G Fink responded that PhD students needed to be more focused and work on a topic in depth rather than looking into too many areas.

G Schickhofer agreed that COV should be considered but how to do this in a standard would be the question. G Fink agreed that it would not make sense to have different γ_m values to consider COV. F Lam added that in Canada, a reliability normalization procedure is available to consider different COVs in a reliability based approach.

U Kuhlmann suggested only one γ_m and provide calibration factor for γ_m and document clearly where these factors come from.

P Dietsch and G Fink discussed the aim of Eurocode 5 and the target audience. The fact that practicing engineers not familiar with wood might complain that the code would be too complicated.

48 - 102 - 3 The Reality of Seismic Engineering in a Modern Timber World –**T Smith, D Moroder, F Sarti, S Pampanin, A H Buchanan**

Presented by D Moroder

M Popovski commented that N America is moving away from ductility factor as yield point of connections is difficult to define. The focus would be on system and the use of nonlinear deformation level would be the new approaches. D Moroder agreed but it would be difficult to translate such information to code provisions.

P Dietsch commented that in some cases the steel braces that were designed for wood are different from what is used on site. He questioned about timber thicknesses when we design for ductility. D Moroder agreed and stated that it would be more a problem for the quality of steel in connection and perhaps some testing should be performed for important and special buildings.

A Ceccotti asked how to define ductility in NZ. D Moroder said that the 1994 RILEM committee has some information. In NZ, actually no information is available in this area in standards. They would define ultimate capacity and yield capacity as the base.

W Seim asked how to deal with low cycle fatigue in NZ code for connection design. D Moroder said that in N American light frame system this is primarily based on prescriptive code. In NZ special elements are usually tested to give guidance and would take into consideration low cyclic fatigue.

H Stamatopoulos and D Moroder discussed performance based design principles and how this would be taken into consideration in NZ.

M Follesa stated that in Eurocode we have serviceability limit state and ultimate limit state. Capacity based design deals with ultimate limit state but we need to consider both limit states.

I Smith stated in the last 5 years we have experienced extreme wind and snow load and commented that it is very tricky to handle the load side and he commented about proper design of structural system would be needed. D Moroder agreed and commented that this would be an education issue including builders, engineers to get global understanding. Educating insurance agencies would also be needed.

F Lam and D Moroder discussed issues related to performance of the connections in service where perhaps drying cracks could negatively impact their performance and change their failure mode. Reinforcement can be considered but not currently available in NZ standards.

48 - 102 - 4 An Execution Standard Initiative for Timber Construction –T Toratti

Presented by T Toratti

U Kuhlmann commented and explained in steel there is an independent executive standard EN1090 which depends on executive class. The executive class and consequence classes are critical. U Kuhlmann recommended similar approach to be considered for timber.

S Winter commented that we need to learn from other material and people doing execution on site always fear too much regulation even though this is needed. He stated that national specification document not national standard would be interesting for industry. S Winter and T Toratti discussed responsibility of different parties in a building project as this is a grey area.

R Jockwer and T Toratti discussed issues related to tolerances in relationship to workability and practicality. Design equations have to consider these tolerances including length of members etc.

M Follesa stated in Italy foundation tolerances might not be compatible with timber tolerance. There are discussions that tolerance is an issue for all materials. In steel, basic tolerances are available with the consideration of additional tolerance. If basic tolerance is not followed, redesign might be needed to check if this is ok.

NOTES

Three notes were presented.

ANY OTHER BUSINESS

University of Zagreb Civil Engineering provided an overview of their timber engineering research program.

Chairman restated the importance to relate the findings to codes or standards and suggested that the abstract review process need to take this into consideration.

E Serrano suggested that the authors should be provided with feedback from the review process. Chairman agreed that overall scores and acceptance level would be made available to the authors. Options to provide more detailed comment would be available to the reviewers but not mandatory for the reviewers.

Chairman will continue to chair the meeting for two more years and suggest to the group to find a successor and options for transition should be considered. Secretariat could still stay with KIT if the new chair would agree.

Discussion relating to the review process and mini-session for WCTE Vienna took place.

VENUE AND PROGRAMME FOR NEXT MEETING

G Schickhofer invited the group to INTER 2016 in Graz Austria August 16 to 19, 2016. The WCTE 2016 in Vienna will follow from August 22 to 25, 2016.

Tentative venues for INTER are Shizuoka, Japan 2017, Seattle, USA 2018, Tallinn, Estonia 2019, Munich, Germany 2020 and Biel, Switzerland 2021.

CLOSE

Chairman thanked the host university and the organizing group for organizing INTER 2015. Chairman thanked F Lam for the minutes and R Görlacher for his work.

3 INTER Papers, Šibenik, Croatia 2015

48 - 2 - 1	Proposal of a Eurocode-based Method for the Buckling Design of Timber Log-walls - C Bedon, M Fragiacomo, C Amadio
48 - 2 - 2	Design of Timber Members Subjected to Axial Compression or Combined Axial Compression and Bending Based on 2nd Order Theory - A Frangi, M Theiler, R Steiger
48 - 6 - 1	Rolling Shear Properties of some European Timber Species with Focus on Cross Laminated Timber (CLT): Test Configuration and Parameter Study - T Ehrhart, R Brandner, G Schickhofer, A Frangi
48 - 7 - 1	A Universal Approach for Withdrawal Properties of Self-Tapping Screws in Solid Timber and Laminated Timber Products - A Ringhofer, R Brandner, G Schickhofer
48 - 7 - 2	Characteristic Withdrawal Capacity and Stiffness of Threaded Rods - H Stamatopoulos, K A Malo
48 - 7 - 3	Load-carrying Capacity of Dowelled Connections - H J Blass, F Colling
48 - 7 - 4	Evaluation of the Reliability of Design Approaches for Connections Perpendicular to the Grain - R Jockwer, R Steiger, A Frangi
48 - 7 - 5	Simplified Fatigue Design of Typical Timber-Concrete Composite Road Bridges - K Kudla, U Kuhlmann
48 - 12 - 1	Concentrated Load Introduction in CLT Elements Perpendicular to Plane - T Bogensperger, R A Jöbstl
48 - 12 - 2	Shear Properties of Cross Laminated Timber (CLT) under in-plane Load: Test Configuration and Experimental Study - R Brandner, P Dietsch, J Dröscher, M Schulte-Wrede, H Kreuzinger, M Sieder, G Schickhofer, S Winter
48 - 12 - 3	Advanced Modelling for Design Helping of Heterogeneous CLT Panels in Bending - L Franzoni, A Lebée, F Lyon, G Foret
48 - 12 - 4	Performance of Canadian Glulam Columns with New Laminae E Requirements - F Lam, Jung Kwon Oh, BJ Yeh, Jun-Jae Lee
48 - 12 - 5	Design of CLT Beams with Large Finger Joints at Different Angles - M Flaig
48 - 15 - 1	Performance-Based Seismic Design of Light-frame Structures – Proposed Values for Equivalent Damping - J Hummel, W Seim
48 - 15 - 2	Simplified Wall Bracing Method Using Wood Structural Panel Continuous Sheathing - T Skaggs, B J Yeh, E Keith
48 - 15 - 3	Structural Characterization of Multi-storey CLT Buildings Braced with Cores and Additional Shear Walls. - A Polastri, L Pozza, C Loss, I Smith

48 - 15 - 4 Dissipative Connections for Squat or Scarcely Jointed CLT Buildings - Experimental Tests and Numerical Validation - R Scotta, L Pozza, D Trutalli, L Marchi, A Ceccotti

48 - 16 - 1 Analysis of Fire Resistance Tests on Timber Members in Compression with Respect to the Reduced Cross-Section Method - J Schmid, M Klippel, A Liew, A Just, A Frangi

48 - 19 - 1 A Beam Theory Fracture Mechanics Approach for Strength Analysis of Beams with a Hole - H Danielsson, P J Gustafsson

48 - 19 - 2 A Strongest Link Model Applied to Fracture Propagating Along Grain - P-J Gustafsson, R Jockwer, E Serrano, R Steiger

48 - 102 - 1 A proposal for a new Background Document of Chapter 8 of Eurocode 8 - M Follesa, M Fragiacomo, D Vassallo, M Piazza, R Tomasi, S Rossi, D Casagrande

48 - 102 - 2 Aspects of Code Based Design of Timber Structures - J Köhler, G Fink

48 - 102 - 3 The Reality of Seismic Engineering in a Modern Timber World - T Smith, D Moroder, F Sarti, S Pampanin, A H Buchanan

48 - 102 - 4 An Execution Standard Initiative for Timber Construction - T Toratti

Proposal of a Eurocode-based method for the buckling design of timber log-walls

Chiara Bedon, Dept. of Engineering and Architecture, University of Trieste, Italy

Massimo Fragiacomo, Dept. of Architecture, Design and Urban Planning, University of Sassari, Alghero (SS), Italy

Claudio Amadio, Dept. of Engineering and Architecture, University of Trieste, Italy

Keywords: timber log-walls, buckling, design method, buckling curves

1 Introduction

Blockhaus structural systems are commonly obtained by assembling multiple timber logs, which are stacked horizontally on the top of one another. Although based on simple resisting mechanisms, the structural behaviour of *Blockhaus* systems is rather complex to predict, and few design recommendations are available in current standards for timber structures. In this context, the paper focuses on the assessment of the typical buckling behaviour of vertically compressed timber log-walls. The effects of various mechanical and geometrical variables such as possible load eccentricities and/or initial curvatures, openings (e.g. doors or windows), fully flexible or in-plane rigid inter-storey floors are investigated by means of detailed finite-element (FE) numerical models validated on buckling test results available in literature (Heimeshoff and Kneidl 1992; Bedon et al. 2015). By taking into account a wide set of geometrical configurations of practical interest, the effects of the main input parameters on the observed compressive buckling responses are first highlighted. In order to provide buckling design recommendations of practical use, normalized design curves derived from standards (e.g. the buckling design approach provided in the Eurocode 5 for timber members in compression) are calibrated and validated for log-wall assemblies.

2 *Blockhaus* structural systems

In current practice (e.g. www.rubnerhaus.com), the traditional *Blockhaus* log-wall with height H and length L is obtained by stacking horizontally a series of spruce logs with strength class C24, according to (EN 338: 2009). These logs typically have cross-sectional dimensions of height h by width b, with the h/b ratio generally in the range 1.6 to 2.4 but, in some cases, also down to ≈0.8, and are characterized by small protrusions and tongues providing interlocking with the upper and lower logs (Fig.1a). Several log-wall profiles are available on the market (see for example Figs.1b-1c). Independently of the cross-sectional properties of logs, however, the design concept and structural assembly of log-wall structural systems is strictly related to interlocking of multiple timber elements.

In *Blockhaus* buildings, the structural interaction between the main perpendicular walls composing the full structural assembly is in fact provided by appropriate corner joints (Figs.1d-1e). Each log-wall is connected to the RC foundation slab by means of steel angular brackets. The permanent gravity loads are thus transferred onto each main wall by the inter-storey floors. Depending on their assembly, these inter-storey floors can realize an in-plane rigid diaphragm (e.g. by using OSB panels, timber joists and blocking, with the OSB sheathing properly nailed along the entire perimeter, or glulam panels arranged on their edges with proper connection between adjacent panels), hence resulting in a further lateral restraint able to avoid possible out-of plane deflections of the wall top logs (Fig.2).

(a) (b) (c) (d) (e)

Fig. 1 Examples of timber log cross-sections: (a) www.rubnerhaus.com; (b): www.lincolnlogs.com; (c): www.polarlifehaus.com. Typical corner joints: (d) 'Standard' and (e) 'Tirolerschloss' (www.rubnerhaus.com)

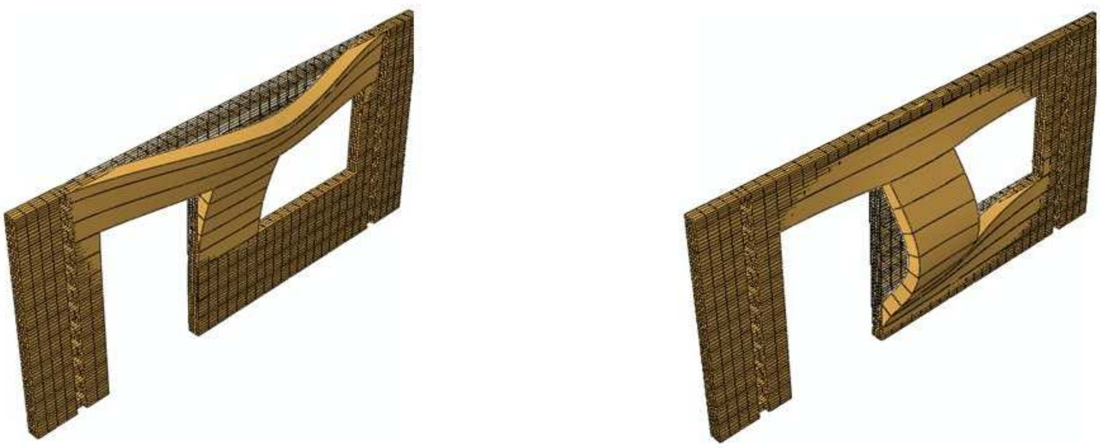

(a) Fully flexible inter-storey floor (FF) (b) In-plane rigid inter-storey floor (RF)

Fig. 2. Qualitative fundamental buckling shape for log-walls under in-plane compressive loads (Bedon and Fragiacomo 2015)

As also highlighted in (Bedon and Fragiacomo 2015), since metal connectors are generally minimized, the typical *Blockhaus* wall can sustain the vertical loads as far as a minimum level of contact among the logs is ensured. At the same time, the low modulus of elasticity (MOE) of timber in the direction perpendicular to the grain makes the usually slender (high H/b ratio) *Blockhaus* walls susceptible to flexural buckling.

3 Existing design buckling methods for timber structural members

3.1 Log-wall assemblies

The current Eurocode 5 for timber structures does not provide formulations and recommendations for the prediction of the critical load of log-walls under in-plane compressive loads. In order to provide practical design recommendations, an analytical and FE investigation was proposed in (Bedon and Fragiacomo 2015), where a preliminary assessment and calibration of closed-form formulations derived from classical buckling theories was presented. Validation of FE models was then carried out against full-scale buckling experiments discussed in (Bedon et al. 2015). Based on the performed parametric studies, it was shown that the critical buckling load of a given log-wall with top rigid lateral restraint (RF) can be calculated as (see also Fig. 3):

$$N_{cr,0}^{(E)} = k_\sigma \frac{\pi^2}{12}\frac{b^3}{L}\frac{E_\perp}{\left(1-\nu^2\right)} = k_\sigma \frac{\pi^2}{12}\frac{b^3}{L}\frac{E_\perp}{\left(1-\left(\frac{E_\perp}{2G}-1\right)^2\right)} \tag{1}$$

with k_σ= 6.97 for log-walls without openings and k_σ= 1.277 for log-walls with a single door/window opening (with $L= L_{ef}$ the reference length in Eq.(1), in accordance with Fig.3a). In Eq.(1), $E_\perp$ and G denote respectively the MOE in the direction perpendicular to the grain and the average shear modulus of C24 spruce. If double door/window openings are present, the theoretical critical buckling load is given by:

$$N_{cr,0}^{(E)} = \frac{\pi^2\left(EI_{ef}\right)}{\overline{H}^2}, \tag{2}$$

where (see Fig.3):

$$\overline{H} = 0.7H_d \tag{3}$$

and

$$EI_{ef} = E_\perp \frac{b^3 L_i}{12} + 2E_{steel}I_{steel} \tag{4}$$

represents the equivalent bending stiffness of the 'composite' portion of wall with metal stiffeners (see Fig.3b).

As shown in (Bedon and Fragiacomo 2015) by means of extended comparative investigations, Eqs.(1) and (2) can predict with close accuracy the Euler's critical load of timber log-walls of various geometrical properties, leading – especially for single or double door/window openings – to conservative estimations of the expected theoretical resistance for the same log-walls. A further imperfection factor was also proposed, so that the actual load-carrying capacity of a given log-wall affected by possible initial geometrical curvatures and eccentricities could be estimated based on the expected value of the theoretical compressive buckling resistance $N_{cr,0}^{(E)}$ as:

$$N_{cr} = \chi_{imp} N_{cr,0}^{(E)} \tag{5}$$

where

$$\chi_{imp} = \left(1 - \frac{e_{tot}}{b}\right) \tag{6}$$

and $e_{tot} \equiv (u_{0,max} + e_{load})$, with $u_{0,max} \geq H/400$ the minimum initial curvature amplitude.

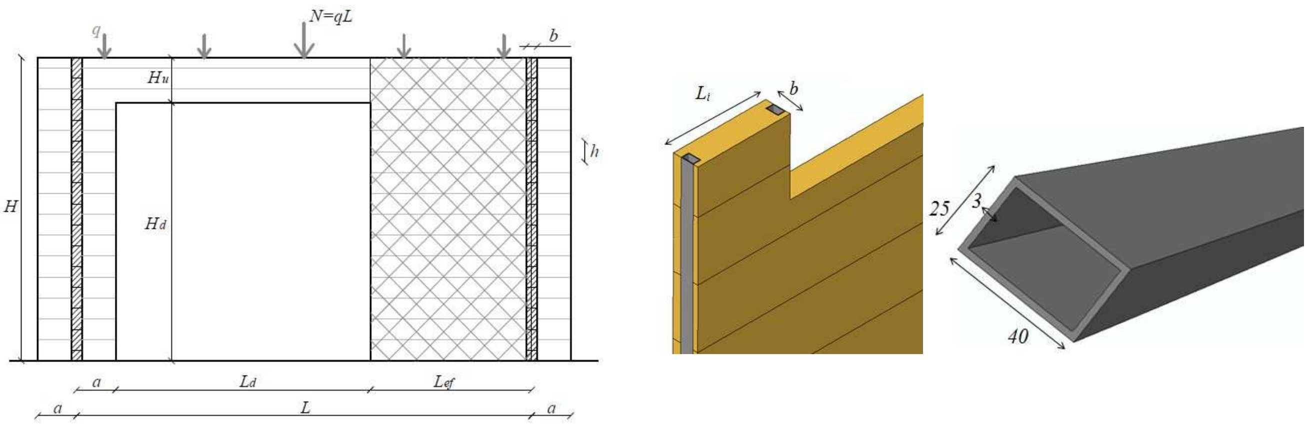

Fig. 3. (a) Example of log-wall configuration and (b) detail of the steel hollow stiffeners introduced along the vertical edges of door and window openings (www.rubnerhaus.com)

3.2 Timber members in compression

In accordance with the Eurocode 5 (point 6.3. *"Stability of members"*), a more general, standardized buckling design method for log-walls under in-plane compression could take the form of non-dimensional curves, properly calibrated so that the effects of a multitude of mechanical and geometrical parameters (e.g. material mechanical properties, initial curvatures, load and boundary eccentricities, inter-storey floor typology, etc.) could be conservatively taken into account. Based on the Eurocode 5, for example, the flexural buckling verification of a timber column is usually performed by taking into account its minimum relative slenderness ratio:

$$\lambda_{rel} = \frac{\lambda}{\pi}\sqrt{\frac{f_{c,0,k}}{E_{0.05}}}\ , \tag{5}$$

where

$$\lambda = \frac{L_0}{\rho_{\min}} = L_0\sqrt{\frac{A}{I_{\min}}}\text{, with } A \text{ the cross-sectional area,} \tag{6}$$

$f_{c,0,k}$ is the characteristic compressive strength parallel to the grain, and

$E_{0.05}$ represents the fifth percentile value of the MOE parallel to the grain.

The stability check of the member in pure compression requires that the design compressive stress $\sigma_{c,0,d}$ along the member would satisfy the condition:

$$\sigma_{c,0,d} \leq k_c \cdot f_{c,0,d}\ , \tag{7}$$

with $f_{c,0,d}$ the design compressive strength in the direction parallel to the gain and k_c a buckling reduction factor given by:

$$k_c = \frac{1}{k + \sqrt{k^2 - \lambda_{rel}}}\ , \tag{8}$$

with

- λ_{rel} defined by Eq.(5)
- k a coefficient taking into account the effects of initial imperfections, given by:
  $$k = 0.5 \cdot \left(1 + \beta_c\left(\lambda_{rel} - \beta_0\right) + \lambda_{rel}^2\right), \tag{9}$$
- β_c an imperfection factor equal to 0.2 or 0.1 for solid timber or glued laminated timber and LVL, respectively, while
- the coefficient β_0= 0.3 in Eq.(9) represents the minimum relative slenderness ratio λ_{rel} necessary to induce column buckling phenomena.

In accordance with Equation (7), in this work a standardized design method consisting of non-dimensional buckling curves is proposed for timber log-walls under in-plane compression. The novelty of the current proposal is given by the application of the existing normalized buckling design procedure to the studied structural system, as well as by the accurate calibration and validation of the method. As a result, the actual buckling resistance of a generic timber log-wall can be calculated – for each specific configuration – as a k_c fraction of the corresponding Euler's critical resistance.

4 Extended Finite-Element investigations

4.1 General numerical approach

The typical Finite-Element (FE) model used in this investigation consisted of 8-node, linear brick, solid elements with reduced integration (C3D8R), available in the ABAQUS element library. In each numerical simulation, a single log-wall laterally restrained by two portions of orthogonal log-walls working as outriggers was analysed (Fig.4). Each timber log was described with a regular *b*×*h* cross section. While the characteristic small protrusions and tongues along the top and bottom surfaces of logs (Figs. 1(a), 1(b)) were reasonably neglected, the nominal geometry of logs near their end restraints, as well as near the doors or windows openings, was correctly reproduced (Fig.4). In accordance with (Bedon and Fragiacomo 2015), moreover, the presence of the lateral outriggers or fully rigid inter-storey floors was taken into account in the form of equivalent nodal restraints for the main log nodes (Fig.4) .

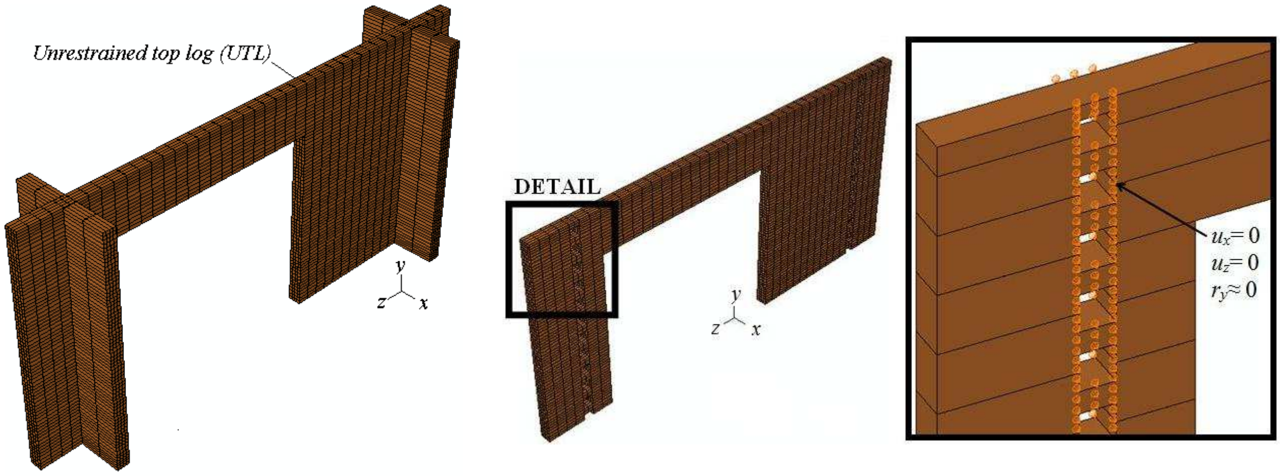

(a) FE-model with outriggers

(b) FE-model with equivalent boundaries along the vertical edges

Fig .4. Example of the typical FE-numerical model of a timber log-wall with single door opening (ABAQUS/Standard)

The mechanical interaction between the logs composing the main tested walls was reproduced by means of suitable surface contact algorithms. Possible tangential sliding was allowed between the logs (*tangential behaviour*), with μ= 0.5 being the static friction coefficient (Bedon and Fragiacomo 2015). The detachment of logs in the direction perpendicular to the contact surfaces was also taken into account (*normal behaviour*), so that the influence of partial uplift and overturning of logs on the overall bending deformations of the examined log-walls could be investigated. Due to the presence of geometrical global curvatures and/or load eccentricities, this modelling feature was a key parameter for the development of extended parametric studies for the derivation of practical design rules, as also discussed in Section 4.

Concerning the mechanical characterization of timber, C24 spruce was first described in the form of an equivalent elasto-plastic, isotropic material having density ρ= 420kg/m^3, nominal average MOE *E*= 370MPa, average shear modulus *G*= 500MPa and Poisson's ratio calculated in accordance with Eq.(1). The main effect of this simplified modelling assumption – in conjunction with the equivalent nodal restraints introduced along the lateral edges of each log-wall – resulted in a computationally efficient FE model able to properly describe the full structural response of the examined log-walls, with out-of-plane stiffness and load bearing capacity predictions in close agreement with both full-scale and small-scale buckling test results (Bedon and Fragiacomo 2015). The occurrence of possible compressive damage and local failure mechanisms in the timber logs (e.g. localized crushing mechanisms along protrusions and grooves of main logs) was also taken into account by limiting the compression stresses to the average compressive strength $f_{c,90,m}$= 3.57MPa of timber in the direction perpendicular to the grain.

Throughout the full parametric investigations, linear bifurcation analyses (LBA) were first carried out on each FE model, so that the fundamental buckling shape could be separately collected for each log-wall configuration. The same FE models were then analyzed under linearly increasing in-plane compressive loads N, by means of incremental nonlinear (INL) static simulations able to describe the full structural response of the examined log walls up to collapse. FE investigations were carried out to log-walls with both in-plane rigid (RF configuration) and fully flexible (FF) inter-storey floors. In both the cases, additional boundary restraints along the top log of each wall were properly implemented or removed, respectively (e.g. Fig.4a).

4.2. Parametric study

Throughout the parametric FE-investigations, log-walls characterized by specific geometrical properties were assembled as described in Section 4.1, by varying the:

a) Total length L, with H= 2.9m the reference nominal height for a single-storey building. In the parametric investigations, a total length ranging from 3m to 6m with incremental steps of 0.5m for each log wall configuration was considered;
b) Nominal width b of each timber log, with h= 16cm and 19cm respectively. Based on the cross-sections of timber log walls currently available on the market (*www.rubnerhaus.com*, *www.perr-blockhaus.de*, *www.rusticasa.pt*, *www.lincolnlogs.com*; *www.polarlifehaus.com*; *www.loghomescotland.co.uk*, etc.), the total width of each log was varied from 8cm to 24cm, with an incremental step of 2cm, for each one of the examined log wall configurations;
c) Number and position of openings (single or double door and window openings);
d) Metal stiffeners for the openings (see Fig.3b): for a given log-wall with door/window openings, INL simulations were carried out both with and without metal stiffeners along their vertical edges;
e) Restraint on the top log of the wall: either an in-plane fully rigid (RF) or flexible (FF) inter-storey floor was considered;

f) Initial geometrical curvature ($u_{0,max}$ =H/400 or H/300) and/or load eccentricity e_{load} (with $b/6 \leq e_{load} \leq b/3$).

A total number of 890 combinations of the variables (a) to (f) were analyzed through the INL parametric study.

5 Discussion of FE results

The main results of this extended numerical investigation were properly analyzed and compared, so that practical information related to the structural effects of the main input parameters could be separately identified.

5.1. Initial curvature

Log-walls of several geometrical properties were first analysed considering an initial global curvature with different maximum amplitude $u_{0,max}$, defined as the scaled LBA fundamental configuration. As shown in (Bedon and Fragiacomo 2015), initial geometrical imperfections typically result – depending on their maximum amplitude – in moderate decrease of the initial elastic stiffness for the examined log-walls. This leads to a premature overturning and detachment of few top logs only, with a progressive decrease of the global log-wall compressive resistance with respect to its corresponding Euler's critical load (e.g. Eqs.(1) and (2)).

In this work, additional INL calculations were carried out, and the ultimate compressive load $(N_{max})_{INL}$ attained by each log-wall was separately collected. The so obtained FE parametric results are displayed in dimensionless format in Figs.5 and 6, for log-walls with RF or FF restraints, respectively (with $u_{0,max}$= H/400 and H/300). In these figures, the numerically predicted buckling coefficient:

$$\left(k_c\right)^* = k_c = \frac{\left(N_{\max}\right)_{INL}}{N_{res}} = \frac{\left(N_{\max}\right)_{INL}}{f_{c,90,m} \cdot bL} \tag{10}$$

is plotted versus the log-wall normalized slenderness ratio:

$$\left(\lambda_{crit,c}\right)^* = \lambda_{crit,c} = \sqrt{\frac{f_{c,90,m} \cdot bL}{N_{cr,0}^{(E)}}} = \frac{\lambda}{\pi}\sqrt{\frac{f_{c,90,m}}{E_\perp}} \tag{11}$$

In Eqs.(10) and (11), $f_{c,90,m}$ denotes the mean compressive resistance of C24 spruce in the direction perpendicular to the grain, while $N_{cr,0}^{(E)}$ is calculated – depending on the presence of none/single/double openings – in accordance with Eqs.(1) and (2).

FE data are compared in each plot with additional analytical approximating curves, calculated in accordance with Eq.(8) and obtained by means of an appropriate numerical calibration of the β_c coefficient in Eq.(9), with β_0= 0.3. In Fig.5a, FE data are also separately collected for log-walls without openings or single/double openings, respectively.

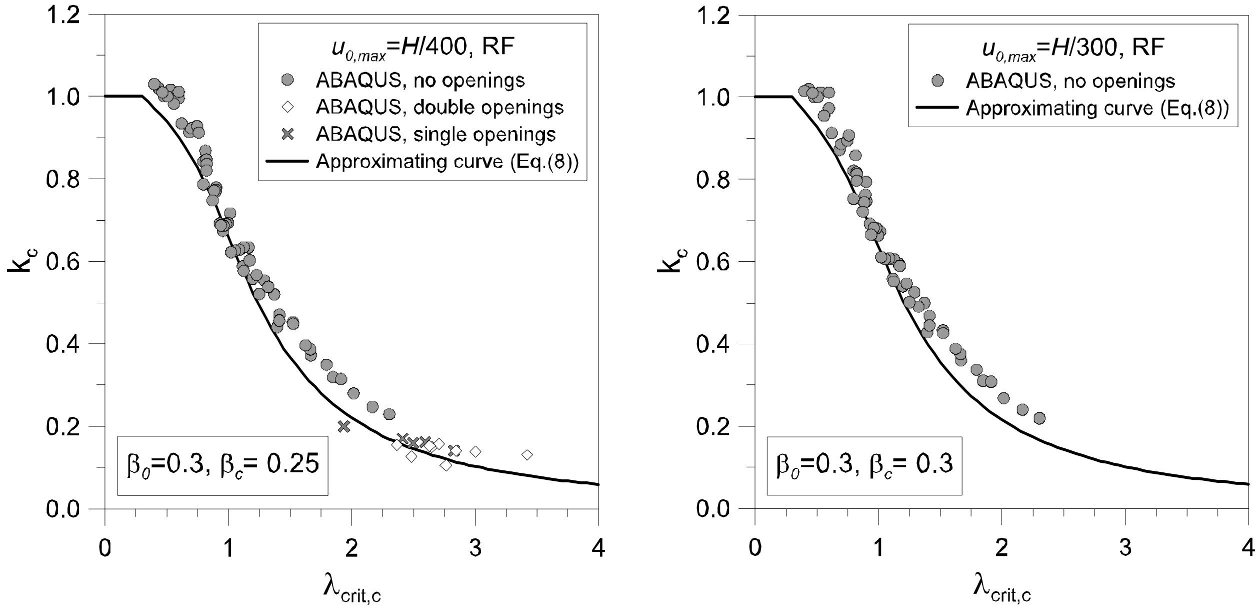

(a) *(b)*

Fig 5. Effect of initial curvature $u_{0,max}$ on the buckling response of timber log-walls under in-plane compression (ABAQUS/Standard). Hypothesis of in-plane rigid inter-storey floor (RF)

As shown, the presence of door and window openings typically results in a marked increase of the normalized slenderness ratio (Eq.(11)) and decrease of the overall buckling resistance (Eq.(10)), compared to log-walls without openings. However, a sufficiently regular behaviour was found for all the investigated geometrical configurations, hence suggesting the assumption of the proposed approximating curves for log-walls of general geometrical properties.

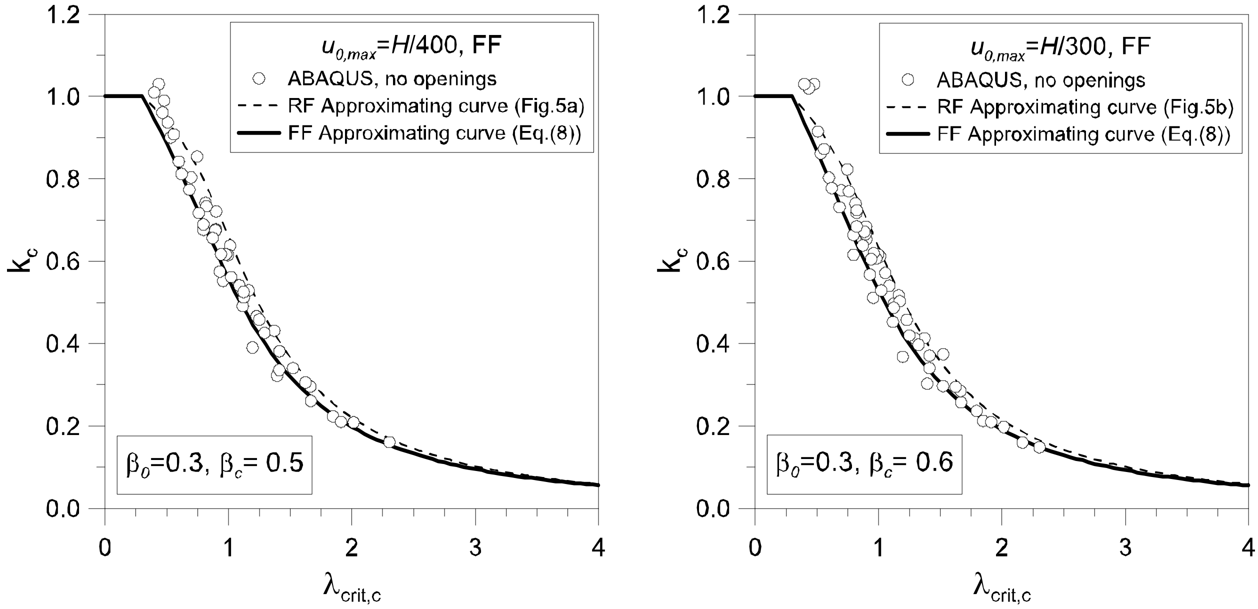

(a) *(b)*

Fig. 6. Effect of initial curvature $u_{0,max}$ on the buckling response of timber log-walls under in-plane compression (ABAQUS/Standard). Hypothesis of fully flexible inter-storey floor (FF)

5.2. Load eccentricity

All the tested log-walls also showed a high sensitivity to possible load eccentricities e_{load} (with $b/6 \leq e_{load} \leq b/3$, in the current parametric study), due to the intrinsic design concept of timber log-wall structural systems. Due to the implicit null tensile resistance of the examined structural system, the application of compressive loads N with a small eccentricity e_{load}, typically resulted in fact in the premature, partial overturning of the top logs (Fig.7), with progressive detachment of the resisting surfaces in contact ad hence an abrupt decrease of the overall compressive load-carrying capacity. Comparative examples are proposed in Fig.7 for a selected geometrical configuration (b=12cm; H= 2.9m; L= 4m, RF configuration), by changing the amplitude of the assigned load eccentricity e_{load}.

Additional comparative FE parametric results are also collected in dimensionless format (e.g. see Eqs.(10) and (11)) in Fig.8. In general, the FE collected data highlighted that for all the examined geometrical configurations, an almost exponential relationship can be found between the log-wall slenderness ratio and the corresponding buckling reduction coefficient k_c, for a given load eccentricity, given by:

$$k_c = A_1 \cdot \left(A_2^{\lambda_{crit,c}}\right) \qquad (12)$$

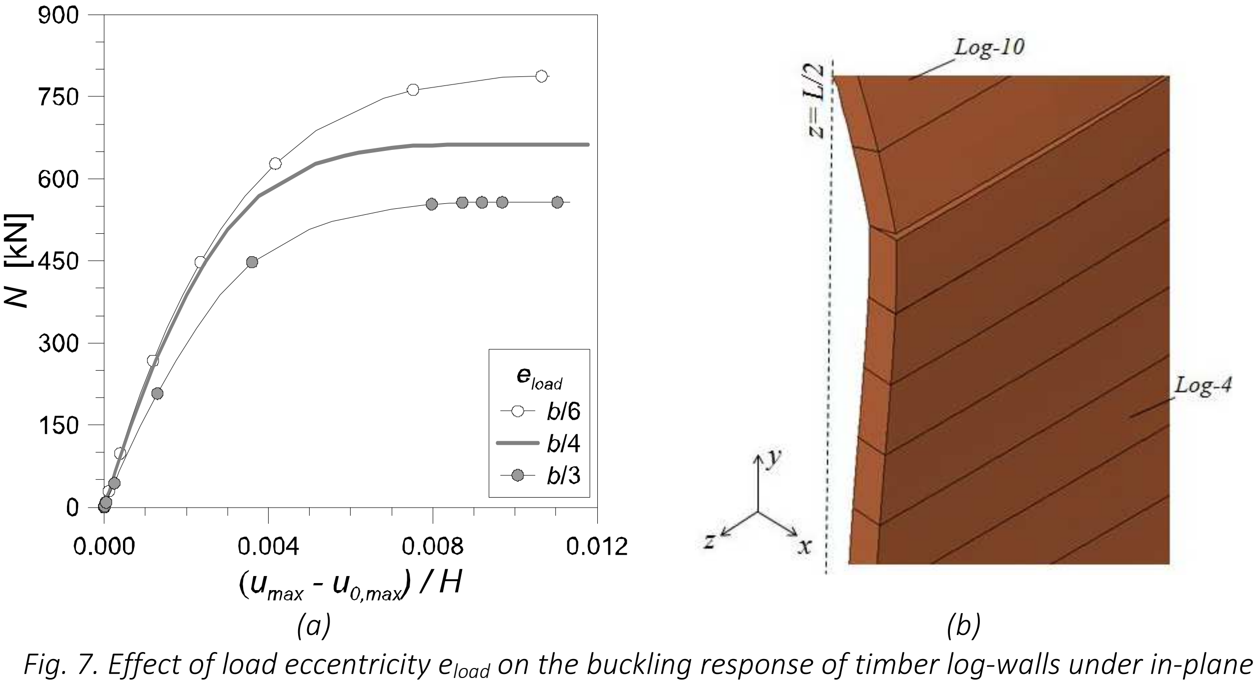

Fig. 7. Effect of load eccentricity e_{load} on the buckling response of timber log-walls under in-plane compression (ABAQUS/Standard). Hypothesis of in-plane rigid inter-storey floor (RF). (a) Compressive load vs. non-dimensional out-of-plane deformations; (b) detail of the qualitative deformed shape (ABAQUS/Standard)

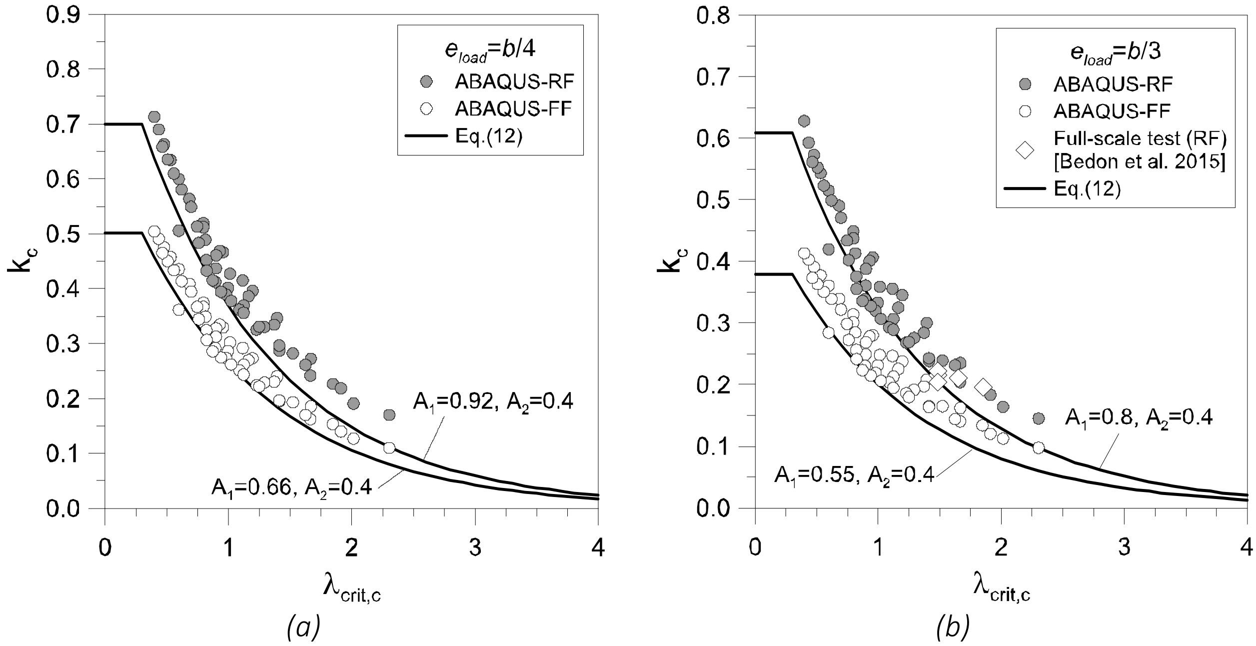

Fig. 8. Effect of load eccentricity e_{load} on the compressive buckling resistance of timber log-walls. Hypothesis of in-plane rigid (RF) or fully flexible (FF) inter-storey floor. FE numerical data (ABAQUS/Standard) and corresponding approximating curves (Eq.(12))

In Eq.(12), the constants A_1 and A_2 depend on the sensitivity of each log-wall configuration and top restraint condition (e.g. RF or FF restraint) on the assigned load eccentricity e_{load}, and can approximately be estimated as suggested in Fig.8 (with $0.3 \leq \lambda_{crit,c} \leq 4$). The parametric study highlighted that for A_2 an almost stable value of 0.4 can be used, independently of the assigned eccentricity amplitude.

In the same Fig.8, it can be seen that the absence of the top lateral restraints (e.g. FF configuration) markedly affects the actual compressive resistance of the log-walls, and in the current study typically resulted in overestimations up to ≈30% of the actual compressive resistance of the same log-walls with in-plane rigid inter-storey floors (e.g. RF restraint). Largest sensitivity and scatter of the collected FE data was found especially for large eccentricities (Fig.8b). However, a fairly regular structural behaviour was generally observed for all the examined configurations, hence suggesting the application of a standardized buckling design procedure for in-plane compressed log-walls. In the same Fig.8b, the experimental data obtained from full-scale (RF) buckling experiments discussed in (Bedon et al. 2015) are also shown, as a further assessment of the calibrated approximating curves.

5.3. Combined initial curvature and load eccentricity

The application of combined initial geometrical curvature $u_{0,max}$ and load eccentricity e_{load} was also investigated, being this case of relevance for the development of general design recommendations.

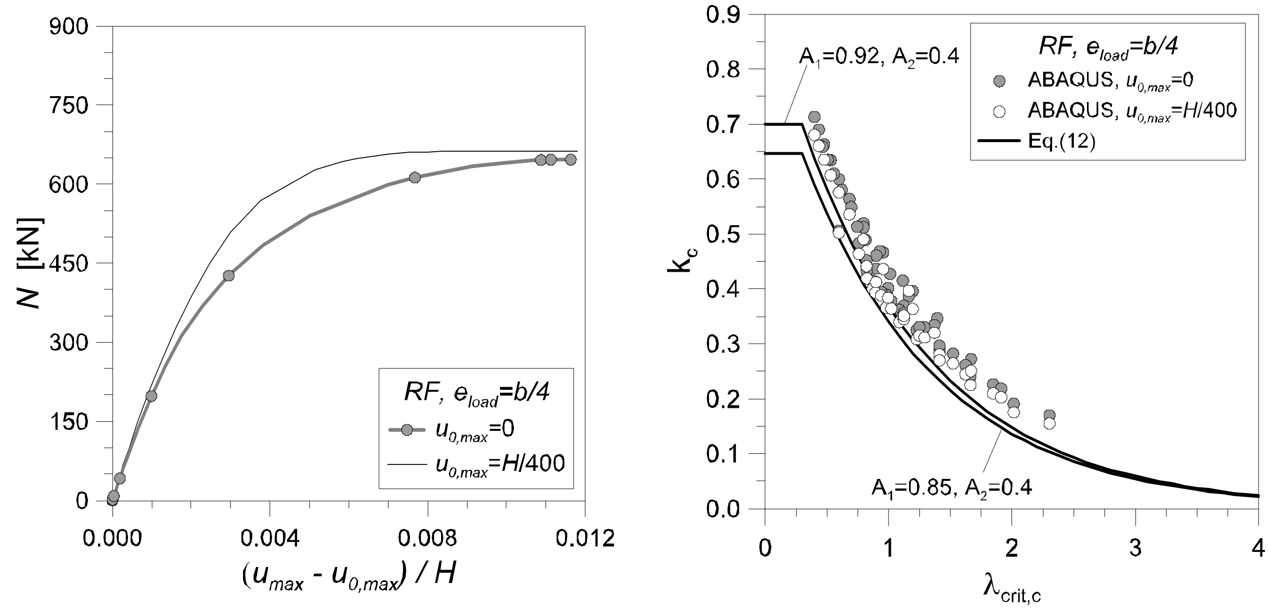

(a) *(b)*

Fig. 9. Effect of combined initial curvature and load eccentricity e_{load} on the compressive buckling resistance of timber log-walls. Hypothesis of in-plane rigid inter-storey floor (RF). (a) Compressive load vs. non-dimensional out-of-plane deformations; (b) FE numerical data (ABAQUS/Standard) and corresponding fitting curves (Eq.(12))

This last series of parametric analyses typically resulted – compared to Sections 5.1 and 5.2 – in a further amplification of the destabilizing effects deriving from curvatures or eccentricities only, hence leading to a further decrease of the log-wall initial stiffness (see for example Fig.9a), a premature detachment of the top logs and consequently a reduction of the actual load-carrying capacity for the studied log-walls. For all the examined geometrical configurations, the application of an initial global curvature of maximum amplitude $u_{0,max}=H/400$ and a simultaneous load eccentricity e_{load} generally led to an average ≈5% decrease of the buckling resistances calculated, for the same set of log-wall configurations, in presence of a load eccentricity e_{load} only. This phenomenon is displayed in Fig.9b, for example, for log-walls with fully rigid top lateral restraint (RF), in dimensionless format of INL parametric results (Eqs.(10) and (11)) and corresponding analytical fitting curves (Eq.(12)).

6 Proposal of a standardized buckling design method for timber log-walls

In order to implement a standardized buckling design method of practical use, further INL parametric investigations were finally carried out on the same log-wall configurations described in Section 4.2 (e.g. 890 combinations of (a) to (f) variables), by replacing in all the FE models the mean mechanical properties of C24 spruce with the corresponding design values:

$$E_{\perp,d} = \frac{E_\perp}{\gamma_M}\,, \quad G_d = \frac{G}{\gamma_M} \quad \text{and} \quad f_{c,90,d} = \frac{k_{\mathrm{mod}} f_{c,90,k}}{\gamma_M} \qquad (13a)\ (13b)\ (13c)$$

with γ_M= 1.3 the partial safety factor of wood, $f_{c,90,k}$= 2.5MPa the characteristic value of compressive strength perpendicular to the grain (EN 338:2009) and k_{mod}= 0.7 the partial modification factor for moisture and load duration influence (service class 1 and 2, and imposed load of long-term duration). A practical example is proposed in Fig.10, where the INL results obtained for a same log-wall (L=4.5m, H= 2.95m, b= 8cm, with $u_{0,max}$= H/400) by taking into account the mean ('ABAQUS, mean properties') or design ('ABAQUS, design properties', e.g. Eqs.(13a)-(13c)) mechanical properties of timber are shown. In both cases, the INL data are normalized by means of Eqs.(10) and (11), with the corresponding mean or design elastic properties for timber. For the same reason, the critical load $N_{cr,0}^{(E)}$ in Eq.(11) is calculated by means of Eq.(1), with 'mean' or 'design' elastic moduli respectively. As shown by Fig.10a, where 'A', 'B' and 'C' denote three different log-wall geometries, the main effect deriving from the use of the design elastic moduli and compressive strength for timber is a shift of the predicted INL data discussed in Section 5 towards lowest slenderness ratios $\lambda_{crit,c}$ and higher buckling reduction coefficients k_c. The first effect is strictly related to the used normalization approach, e.g. Eq.(11) and Eqs.(13a)-(13c). The apparent higher resistance of log-walls with design mechanical properties (e.g. the increase of k_c) – compared to the same log-walls with mean mechanical properties – also depends on the normalization of the collected FE data (Eq.(10)), e.g. on the decrease of the ultimate design compressive resistance $((N_{max})_{INL})_d$and the corresponding design compressive resistance $(N_{res})_d$. Due to the appropriate calibration of the β_0 and β_c imperfection factors for the approximating curve (Eq.(8)), however, being these values representative of the effects deriving from a possible initial curvature $u_{0,max}$, the same values 0.3 and 0.25 proposed in Section 5.1 can be used also for design purposes (see Fig.10b). Similarly, in the case of load eccentricity e_{load} or combined curvature / eccentricity, the constants A_1 and A_2 collected in Section 5.2 and 5.3 for the approximating curve (Eq.(12)) are proposed for the buckling design of the examined log-walls.

In conclusion, in accordance with the existing Eurocode 5 approach for timber members in compression (e.g. Eq.(7)) and on the discussed parametric results, the buckling design verification of log-walls subjected to in-plane compressive design stresses per unit length of wall σ_{sd} can take the form of:

$$\sigma_{sd} \leq \sigma_{b,Rd} = k_c \cdot \left(\sigma_{cr,0}^{(E)}\right)_d , \qquad (14)$$

with k_c the buckling reduction factor, $\sigma_{b,Rd}$ the design buckling strength and $\left(\sigma_{cr,0}^{(E)}\right)_d = \left(N_{cr,0}^{(E)}\right)_d \big/ L = f\left(E_{\perp,d}, G_d\right)$ the Euler's critical stress calculated as given in Table 1, depending on the log-wall geometry (e.g. imperfection, inter-storey floor typology, number of openings). In presence of double openings, specifically, the possible presence of metal stiffeners along the vertical edges of doors and windows (e.g.

Fig.3) can be taken into account by means of Eq.(4). When steel stiffeners are not used, the introduction at least of solid hardwood elements along the openings edges is recommended, in order to ensure a minimum structural continuity and interaction between the interrupted logs, as well as a certain stiffness against out-of-plane deformations. In the same Table, the calibrated imperfection factors for the approximating curves are also provided. For intermediate values of initial imperfection $u_{0,max}$ and load eccentricity e_{load}, a linear interpolation between the imperfection factors of Table 1 can be used to estimate the corresponding load-carrying capacity of a given in-plane loaded log-wall, hence suggesting the general applicability of the proposed method.

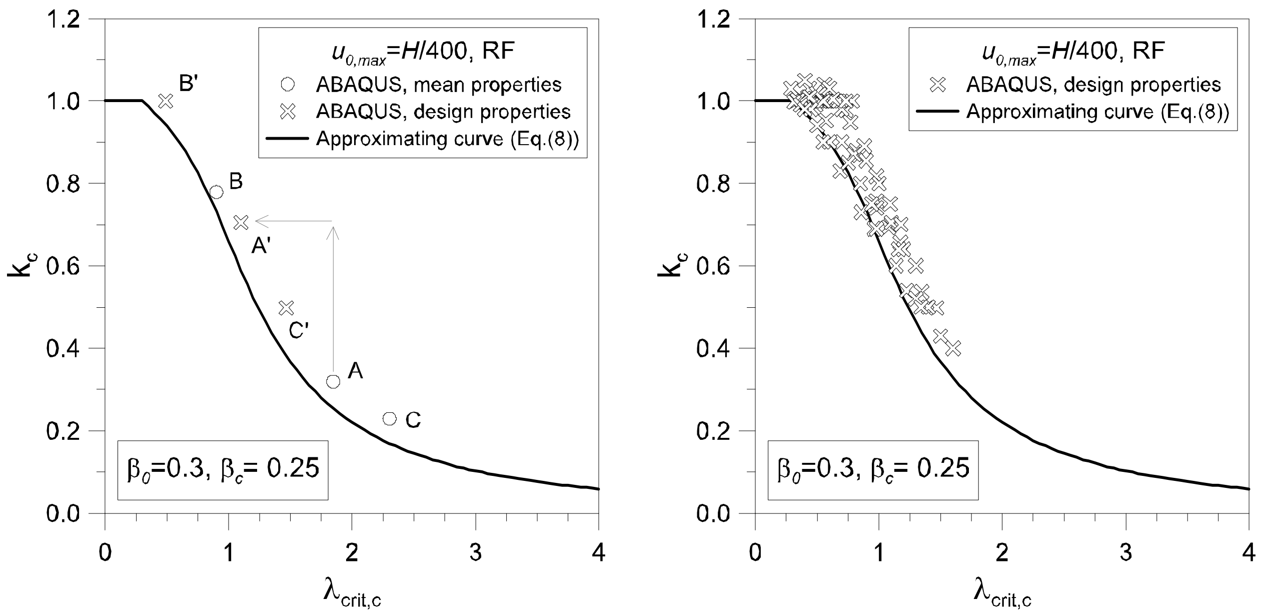

(a) *(b)*

Fig. 10. Validation of the buckling design approach for log-walls with initial geometrical curvature. (a) Qualitative effect of design mechanical properties; (b) parametric FE study with design properties

Table 1. Reference approximating curves of k_c, imperfection factors and design critical loads for timber log-walls under in-plane compression subjected to initial curvature and/or load eccentricity

		No openings / Single opening / Double openings		$(N_{cr,0}^{(E)})_d$		
Imperfection / Eccentricity	Approximating curve	Fully rigid floor (RF)	Fully flexible floor (FF)	No openings	Single opening	Double openings
$u_{0,max}$= H/400	Eq.(8), with β_0= 0.3	β_c= 0.25	β_c= 0.3	Eq.(1)	Eq.(1) with L= L_{ef}	Eq.(2)
$u_{0,max}$= H/300		β_c= 0.5	β_c= 0.6			
e_{load}= b/4	Eq.(12), with A_2= 0.4	A_1= 0.92	A_1= 0.66			
e_{load}= b/3		A_1= 0.80	A_1= 0.55			
$u_{0,max}$= H/400 + e_{load}= b/4		A_1= 0.85	A_1= 0.6			

6. Conclusions

Based on extended FE parametric investigations validated towards past analytical and experimental data, in the paper the buckling response of timber log-walls under in-plane compression has been investigated. Careful consideration has been given both to the influence of geometrical aspects (e.g. log-wall dimensions, timber log cross-section, presence and position of door / window openings) and to further influencing parameters, like initial curvatures and / or load eccentricities of variable amplitude. Approximating curves have been properly calibrated, in order to provide normalized design curves for all the examined log-walls. Finally, a standardized buckling design method is proposed. This method is conceptually similar to that used for the design of timber columns, and could be easily implemented in the ongoing revision of the Eurocode 5 – Part 1-1.

7. References

Bedon, C, Fragiacomo, M (2015): Numerical and analytical assessment of the buckling behaviour of Blockhaus log-walls under in-plane compression. Engineering Structures, 82: 134-150.

Bedon, C, Rinaldin, G, Izzi, M, Fragiacomo, M, Amadio, C (2015): Assessment of the structural stability of Blockhaus timber log-walls under in-plane compression via full-scale experiments. Construction and Building Materials, 78: 474-490.

EN 338:2009: Structural timber-strength classes.

Eurocode 5 (2004): Design of timber structures - Part 1-1: General and rules for buildings. CEN. (EN 1995-1-1).

Heimeshoff, B, Kneidl, R (1992): Zur Abtragung vertikaler Lasten in Blockwänden – Experimentelle Untersuchungen. Holz als Roh – und Werkstoff, 50: 173-180. Springer-Verlag.

Heimeshoff, B, Kneidl, R (1992): Bemessungsverfahren zur Abtragung vertikaler Lasten in Blockwänded. Holz als Roh – und Werkstoff, 50: 441-448. Springer-Verlag.

LogHomeScotland (United Kingdom), *www.loghomescotland.co.uk*

PERR Blockhäuser (Germany), *www.perr-blockhaus.de*

Polar Life Haus® (Finland), *www.polarlifehaus.com*

Rubner Haus AG Spa (Italy), *www.rubnerhaus.com*

Rusticasa Construções Lda (Portugal), *www.rusticasa.pt*

Simulia (2012). ABAQUS v.6.12 Computer Software, Dassault Systems, Providence, RI, USA.

The Original Lincoln Logs© (NY, USA), *www.lincolnlogs.com*

Discussion

The paper was presented by C Bedon

H Blass asked about the G value of 500 MPa in Slide 10 and suggested that shear in buckling would be rolling shear in these walls. C Bedon responded that the chosen value was based on calibration with test results. Preliminary study showed that using a lower G value did not agree with data. Also they did not notice a lot of shear deformation as the rotation was almost a rigid body motion.

G Schickhofer commented that it would be better to consider a minimum requirement rather than such a complicated approach for a simple block wall house.

F Lam asked why the cases with design properties were higher than the cases with mean properties. C Bedon agreed and responded that the process also involved a normalization process.

A Ceccotti asked if the authors checked how far the designs are away from capacities in terms of safety. C Bedon answered that cases where stiffness of walls with large openings can be important and cases where top restraints were not available can also be important.

U Kuhlmann commented that compressive strength versus critical loading is confusing.

Design of timber members subjected to axial compression or combined axial compression and bending based on 2nd order theory

Andrea Frangi, ETH Zurich, Institute of Structural Engineering IBK, Zurich, Switzerland

René Steiger, Empa, Materials Science and Technology, Structural Engineering Research Laboratory, Dübendorf, Switzerland

Matthias Theiler, dsp Ingenieure & Planer AG, Greifensee, Switzerland

Keywords: Timber structures, columns, compression parallel to the grain, stability, global buckling, P-delta effect, 2nd order structural analysis

1 Introduction

Axial compression or combined axial compression and bending are encountered in many types of timber members such as columns, frame structures or compression members of truss girders. The behaviour of these structural members is primarily characterised by the non-linear increase of the deformation due to the increasing eccentricity of the axial load (P-delta effect). In addition to this geometric non-linear behaviour, the non-linear material behaviour of timber members subjected to compression parallel to the grain has to be accounted for. The influence of the P-delta effect on the load-bearing capacity of timber members subjected to axial compression was investigated first by Tetmajer (1896). Tetmajer's studies set up the basis for the design of timber members subjected to axial compression for a long time. Tests performed by Larsen and Pedersen (1975) confirmed the results obtained by Tetmajer. The experimental investigation showed the great influence of varying material properties on the load-bearing capacity. In order to account for these variations and hence, to estimate the resistance of glued laminated timber members subjected to compression more accurately, Blaß (1987 and 1991) performed Monte Carlo simulations. The buckling curves given in different design codes (SIA 265:2012, EN 1995-1-1:2004 and DIN 1052:2008) were derived from these investigations.

For timber members subjected to combined axial compression and bending, Buchanan (1984 and 1985) developed a numerical model capable of investigating the influence of the non-linear material behaviour on the moment – axial force interaction. In addition Buchanan investigated the influence of the size of the member. Current design codes such as Eurocode 5 (EN 1995-1-1:2004), the Swiss national code for the design of timber structures (SIA 265:2012) or the withdrawn German code (DIN 1052:2008) provide two different approaches for the design of centrically and eccentrically loaded timber columns:

– a simplified calculation model based on the Effective Length Method (ELM),

– 2nd order analysis of the structure.

In ELM, the buckling problem of a structural system is reduced to that of an equivalent simply supported (pinned) column. The 2nd order analysis of the structure is a method which takes into account the non-linearity by studying the equilibrium of the deformed structural system. In general, non-linearity caused by the increasing eccentricity of the external load as well as non-linearity caused by the non-linear material behaviour of timber subjected to compression should be considered. However, the 2nd order analysis is often understood as a theory based on linear elastic material behaviour and the effects caused by the non-linearity of the material are neglected. Even the design codes (SIA 265:2012, EN 1995-1-1:2004 and DIN 1052:2008) only provide rules for this 2nd order linear elastic analysis of the structure. In this paper, a clear distinction between the 2nd order linear elastic analysis and the generalised 2nd order analysis is made.

The two approaches (ELM and 2nd order linear elastic analysis of the structure) given in the codes are not consistent and can lead to different results. This situation led to controversial discussions in the scientific community (Kessel et al. 2005 and 2006; Möller 2007; Köhler et al. 2008). The discussion in particular showed that there are inconsistencies concerning the consideration of the effect of moisture content (MC) and duration of load (DOL) as well as inconsistencies concerning the implementation of the 2nd order linear elastic analysis in the design codes. While recent research on the load-bearing behaviour of timber members subjected to axial compression or combined axial compression and bending was mainly focused on MC and DOL (Kessel et al. 2005 and 2006; Möller 2007, Becker and Rautenstrauch 2001, Hartnack et al. 2002) this paper deals with the influence of the non-linear material behaviour and with the implementation of 2nd order linear elastic analysis in the design codes such that there are only minor differences between 2nd order linear elastic analysis and the Effective Length Method. The results presented here are only valid for short-term response under load at constant interior climate. In fact, MC and DOL and in particular the creep behaviour and the climate take a major impact on the load-bearing behaviour of timber columns and should also be considered for the design of timber members subjected to compression or combined compression and bending (Hartnack 2004, Hartnack and Rautenstrauch 2005, Becker 2002).

2 Design of timber members in compression parallel to the grain

In general, the Effective Length Method is used for simple design situations (e.g. verification of stability of single members) while the 2nd order linear elastic analysis of the structure provides some advantages for more complex design situations (e.g. impact of stiffness of members and connections on the force distribution in truss and frame structures, design of bracing).

2.1 Effective Length Method (ELM)

The simplified calculation model is based on the Effective Length Method (ELM). The buckling problem of a structural system is reduced to that of an equivalent simply supported (pinned) column (Blass, 1995). For the design, the internal forces and moments are calculated based on a simple 1st order analysis and the non-linear P-delta effect is taken into account by means of a buckling factor k_c. This factor describes the ratio between the axial stress at buckling failure of a member subjected to axial compression and its compressive strength parallel to the grain. k_c depends on the effective length of the structural system which can be expressed by the slenderness ratio λ.

The buckling factor k_c as given in different design codes (EN 1995-1-1:2004, SIA 265:2012 and DIN 1052:2008) is based on extensive investigations performed by Blaß (1987). In order to determine the characteristic value (i.e. 5th percentile) of the load-bearing capacity of timber columns Blass performed Monte Carlo simulations. The numerical model and the parameter study considered the P-delta effect, the variability of the strength and the stiffness properties within the timber members, the geometric imperfection of the timber members and the non-linear material behaviour of timber when subjected to compression parallel to the grain and bending.

For the ultimate limit state analysis, the design codes (EN 1995-1-1:2004, SIA 265:2012 and DIN 1052:2008) recommend using a linear interaction model for combined axial compression and bending. In this interaction model, the buckling factor k_c is used to reduce the compressive strength parallel to the grain of the timber member in order to account for buckling.

2.2 2nd order linear elastic analysis

As an alternative to the calculation model based on the ELM, timber members subjected to axial compression or combined axial compression and bending can be designed by performing a 2nd order linear elastic analysis. The 2nd order linear elastic analysis is a method which takes into account the geometric non-linearity by studying the equilibrium of the deformed structural member. An initial deformation is introduced into the calculation in order to account for the geometric imperfection of the member as e.g. deviation from a perfectly straight shape.

For a simply supported, axially loaded column the 2nd order linear elastic analysis can easily be performed, assuming sinusoidal distributed initial deformations. The initial deformation in combination with the axial load leads to an initial bending moment M_I. The P-delta effect causes a magnified moment M_{II}. M_{II} can be calculated by multiplying the initial bending moment M_I with a magnification factor μ (Bazant and Cedolin 1991):

$$M_{II} = \mu \cdot M_I \tag{1}$$

$$\mu = \frac{1}{1-\frac{N}{N_{Euler}}} \text{ and } N_{Euler} = \frac{\pi^2 \cdot EI}{\ell_{cr}^2} \tag{2}$$

With

M_{II}: magnified bending moment (2nd order linear elastic theory, deformed structure)
M_I: initial bending moment (1st order theory, undeformed structure)
μ: magnification factor
N: normal force acting on the column
N_{Euler}: Euler buckling load
E: modulus of elasticity (MOE)
I: 2nd moment of inertia
ℓ_{cr}: effective length

Timber members subjected to combined axial compression and bending tend to develop non-linear deformations of the compression zone before failure occurs. This non-linearity leads to a curved shape of the moment – axial force interaction diagram depending on the ratio between the tensile strength $f_{t,m,0}$ and the compressive strength $f_{c,m,0}$ parallel to the grain (Buchanan 1985, Steiger and Fontana 2005). For the ultimate limit state analysis of timber columns the design codes (SIA 265:2012, EN 1995-1-1:2004 and DIN 1052:2008) consider this non-linear interaction behaviour by squaring the compression part in the interaction model (Eq. (3)). However, the non-linear material behaviour also influences the deformations of the structural system, and as a consequence, also the magnified moment M_{II} is influenced by the non-linear material behaviour. However, these effects are neglected when performing a 2nd order linear elastic analysis.

$$\left(\frac{\sigma_{c,0,d}}{f_{c,0,d}}\right)^2 + \frac{\sigma_{m,II,d}}{f_{m,d}} \leq 1.0 \tag{3}$$

With

$\sigma_{c,0,d}$: design value of the acting compressive stress parallel to the grain
$f_{c,0,d}$: design compressive strength parallel to the grain
$\sigma_{m,II,d}$: design value of the acting bending stress from a 2nd order structural analysis
$f_{m,d}$: design bending strength

3 Strain-based model

In order to predict the global buckling behaviour of timber columns, a numerical strain-based model has been implemented. Strain-based models are widely used in the design of structural members made from other construction materials than timber. E.g. for reinforced concrete columns, a strain-based model is suggested in CEB/FIP Manual (1978). Due to the failure mechanism in timber being influenced by the distinct nonlinear stress-strain relationship and leading to a more complex calculation procedure, up to now, only a few applications of these models to timber structures are reported in literature (Buchanan 1984, Hörsting 2008).

Figure 1 shows the calculation procedure of the strain-based model. On the left hand side, the calculation of the internal force N_i and bending moment M_i is illustrated. The calculation starts with selecting values for the strain ε_0 at the mass centre of the cross-section and for the curvature χ_y. These two parameters define the strain distribution within the whole cross-section, when assuming that plane sections remain plane. Based on the strain distribution, the stress distribution is calculated using the relationship given by the stress-strain curve. Any shape of stress-strain curve can be applied in the calculation. Finally, the internal force N_i and moment M_i are estimated by integrating the stresses over the whole cross-section. The right hand side of Figure 1 shows the calculation of the external force N_e and bending moment M_e. The external bending moment M_e depends on the external force N_e as well as on the deformation of the column due to the initial imperfections and the P-delta effect. Since the curvature is equal to the 2nd derivation of the deflection curve, the maximal deflection e_{II} of the column due to the P-delta effect can be calculated as a function of the curvature χ_y. Both the internal moment M_i and the external moment M_e depend on the curvature χ_y. Hence, equilibrium between internal and external forces and moments can be obtained iteratively.

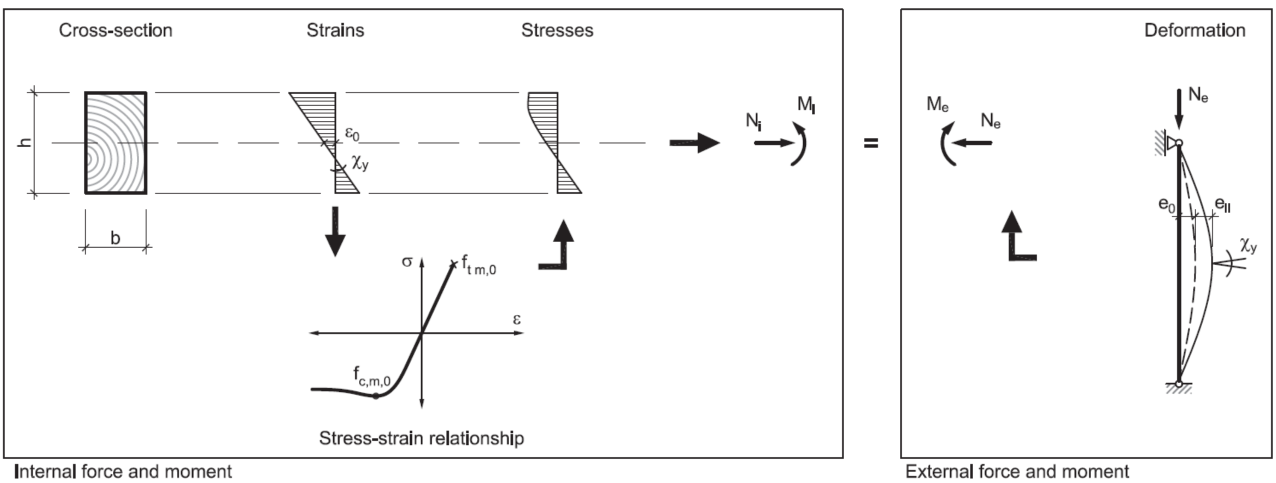

Figure 1. Calculation procedure in the strain-based model (Theiler et al. 2013)

The strain-based model has been used for studying the influence of various parameters. E.g. it can be shown that the plastic behaviour of timber when subjected to compression parallel to the grain considerably influences the buckling behaviour of columns (Theiler et al. 2013). Therefore, the application of an adequate material model (stress-strain relation) is essential when modelling the behaviour of timber members subjected to compression. In the present study, the model proposed by Glos (1978) has been used, since it appears to be more suitable than other material models because it is based on extensive experimental investigations on solid timber boards. In addition, Glos (1981) developed the model for timber members subjected to compression and bending while other models are mainly focused on timber members subjected to pure bending. Glos's model accounts for the reduction of stiffness before reaching the ultimate compression strength as well as for the subsequent softening. Figure 2 qualitatively shows the stress-strain relationship proposed by Glos. The description of the full curve in a mathematical form asks for six parameters (Figure 2 right).

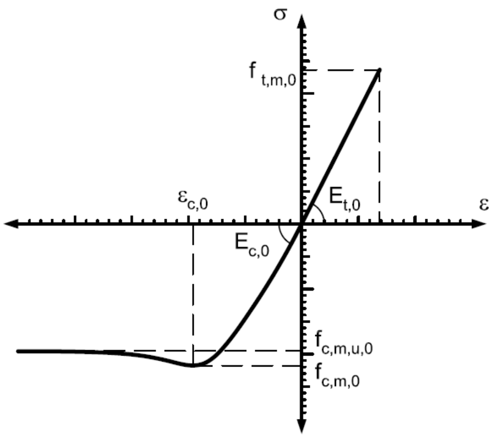

$E_{t,0}$ =	MOE in tension
$E_{c,0}$ =	MOE in compression
$f_{t,m,0}$ =	tension strength at extreme fibres position
$f_{c,m,0}$ =	compression strength of the plastic zone
$\varepsilon_{c,0}$ =	strain at ultimate compression strength
$f_{c,m,u,0}$ =	residual strength after reaching the compression strength

Figure 2. Qualitative representation of the stress-strain relationship in the material model proposed by Glos (1978).

4 Experiments

An experimental campaign on glued laminated timber members subjected to eccentric compression has been performed at ETH Zurich (Theiler and Frangi 2015). The aim of the experimental investigations was to create a data base, which could be used to validate theoretical calculation models and to assess the accurateness of the design approaches given in codes for the design of timber structures. The specimens were produced using lamellas made of Norway spruce (*picea abies*) grown in Switzerland. A total of 336 lamellas were available. In the first step, non-destructive tests on the lamellas were performed. These tests aimed at collecting data in order to characterise the raw material. In the second step, the lamellas were strength graded. The aim of the grading process was to select two classes of lamellas for the production of the test specimens. The lamellas were selected so that they were suitable to produce glued laminated timber of strength classes GL24h and GL32h.

Within the grading process, visual grading criteria as well as machine grading criteria (dynamic MOE) were used. Specimens for five tests series were produced, three series of glued laminated timber GL24h and two series of glued laminated timber GL32h (Table 1). Each of the test series consisted of ten specimens. The length of the timber members was varied between the different test series: *L* = 1’400 mm, *L* = 2’300 mm and *L* = 3’200 mm. The cross-section was 140 mm x 160 mm.

Table 1. Overview of test series on glued laminated timber members subjected to eccentric compression performed at ETH Zurich (Theiler and Frangi 2015)

Test series	Number of tests	Strength class	Cross-section [mm]	Length *L* (Slenderness λ)	Mean value of axial stress at failure (COV)
1	10	GL24h	140 x 160	1'400 mm (30.3)	25.6 N/mm^2 (0.07)
2	10	GL24h	140 x 160	3'200 mm (69.3)	15.3 N/mm^2 (0.11)
3	10	GL24h	140 x 160	2'300 mm (49.8)	20.3 N/mm^2 (0.12)
4	10	GL32h	140 x 160	1'400 mm (30.3)	31.1 N/mm^2 (0.09)
5	10	GL32h	140 x 160	3'200 mm (69.3)	18.1 N/mm^2 (0.10)

During the glulam production, the setup of the test specimens was recorded. Hence, the position and the orientation of every lamella within each test specimen were documented. Finally, the glued laminated timber members were subjected to buckling tests. The test specimens were loaded with an eccentric (15 mm) compression force up to failure. During the tests, the applied loads as well as horizontal and vertical deformations were recorded. For a subsample of 20 test specimens, additional local deformation measurements were performed using an optical measurement system.

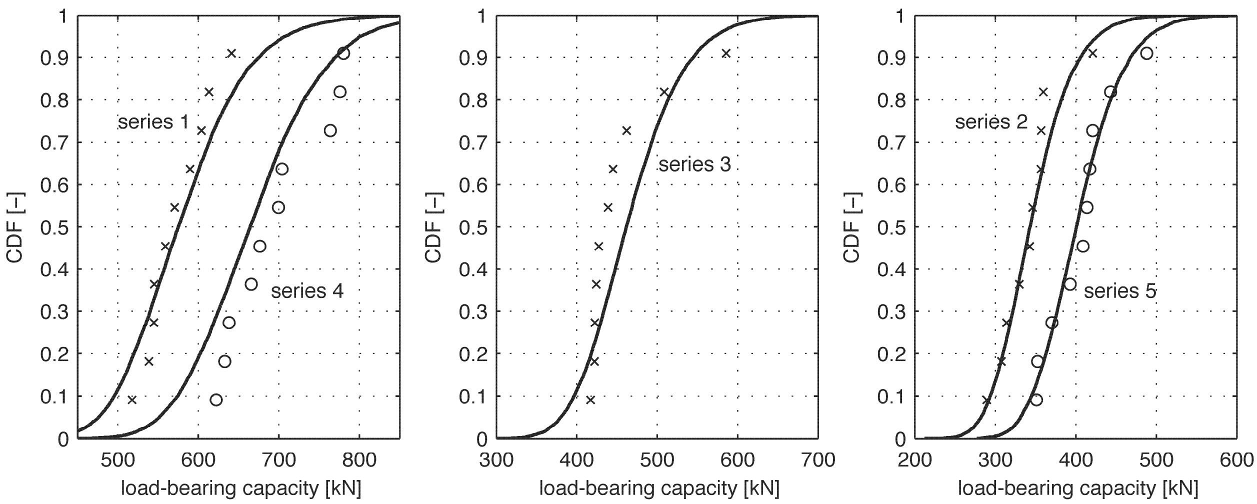

Figure 3. Measured load-bearing capacity for all tests performed in comparison with the assumed lognormal distribution estimated from the test results (Theiler 2014).

The graphs in Figure 3 show the results of all tests performed in comparison with the assumed lognormal distribution estimated from the tests. A good agreement between test results and estimated lognormal distribution can be seen. The coefficient of variation (COV) was in the range of 10% for all test series (Table 1). All details of the tests are presented in a test report (Theiler and Frangi 2015). The results of the tests have been used for the validation of the strain-based model.

5 Numerical simulations

In order to account for the variation in material properties, Monte Carlo simulations were performed. Columns of different slenderness and different strength grades were modelled with the strain-based model by assigning them randomly selected material properties. Six different parameters are needed to describe the full stress-strain relationship (Figure 2). The distributions of the properties in terms of probability density function PDF as well as the correlation between the different properties have to be taken into account. The study was performed for two different grades of solid timber (C24 and C30) and glued laminated timber (GL24h and GL32h). Characteristic values given in EN 338:2009 and EN 14080:2013 were considered. However, the characteristic values are not sufficient for the stochastic modelling. Further information on the variability of the mechanical properties is required that for example can be found in the JCSS Probabilistic Model Code (2007). In addition, Glos (1978) investigated variability and correlation of the model parameters. Using these investigations and the characteristic values as a basis, for each material property a mean value, a standard deviation and a probabilistic density function was estimated (Table 2).

Table 2. Mean value, standard deviation and probability distribution function PDF used for the numerical simulations (see figure 2 for the definition of the material properties) (Theiler 2014)

Material property			C24	C30	GL24h	GL32h
		Mean value	11’000	12’000	11’500	14’200
$E_{t,0}$, $E_{c,0}$	[N/mm^2]	Standard deviation	2’200	2’400	1’500	1’850
		PDF	Lognormal		Lognormal	
		Mean value	38.8	48.6	34.0	45.5
$f_{t,m,0}$	[N/mm^2]	Standard deviation	9.7	12.2	5.1	6.8
		PDF	Lognormal		Lognormal	
		Mean value	29.9	32.6	30.4	40.2
$f_{c,m,0}$	[N/mm^2]	Standard deviation	5.3	5.6	3.9	5.2
		PDF	Lognormal		Lognormal	
		Mean value	$3.40*10^{-3}$	$3.40*10^{-3}$	$3.27*10^{-3}$	$3.51*10^{-3}$
$\varepsilon_{c,0}$	[-]	Standard deviation	$6.80*10^{-4}$	$6.80*10^{-4}$	$4.25*10^{-4}$	$4.57*10^{-4}$
		PDF	Lognormal		Lognormal	
		Mean value	25.4	27.7	25.6	33.9
$f_{c,m,u,0}$	[N/mm^2]	Standard deviation	3.8	4.2	2.6	3.4
		PDF	Lognormal		Lognormal	

Starting from the stochastically modelled material properties, 2nd order simulations were carried out with the strain-based model. For each timber grade and slenderness ratio 10'000 simulations were performed allowing an accurate estimation of the mean value and the 5% fractile value of the load-carrying capacity. Altogether, about two million simulations were performed in this research project.

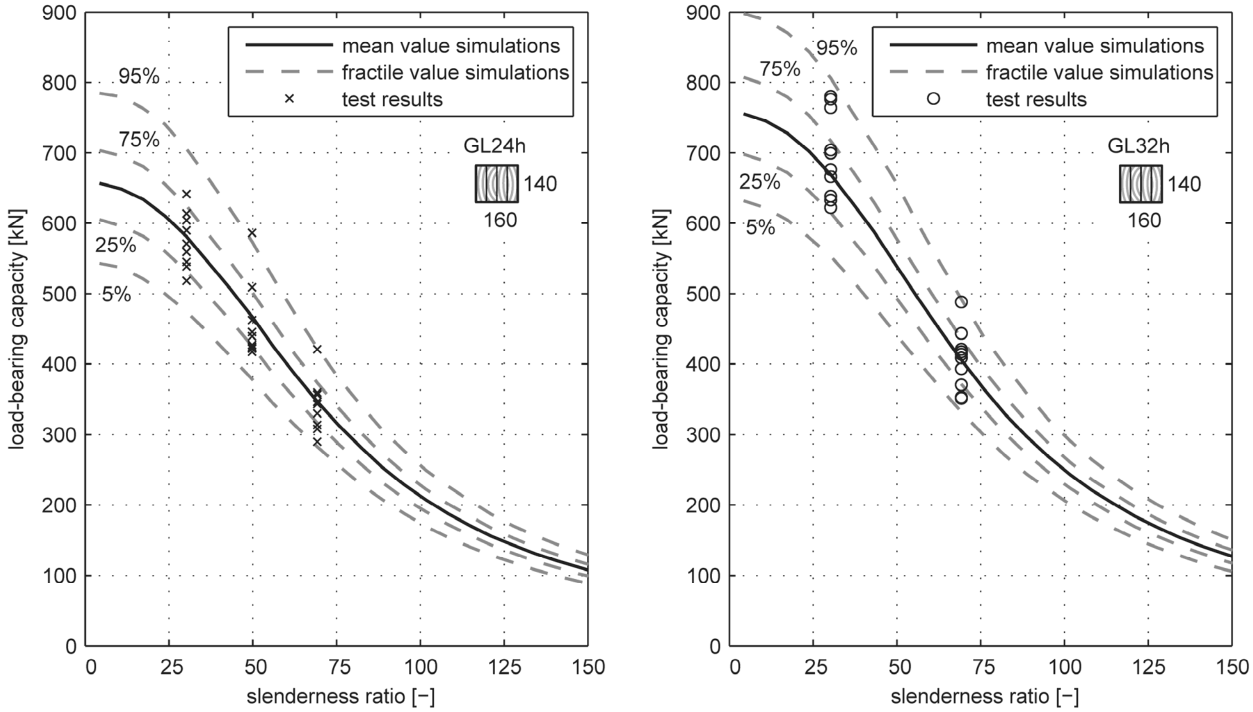

Figure 4. Comparison between experimental data and numerical simulations for glued laminated timber of strength classes GL24 and GL32h (Theiler 2014).

Figure 4 shows the results of the numerical simulations performed for the analysis of the test results for glued laminated timber of strength classes GL24h and GL32h. It can be seen that the variation in the numerical prediction is larger for stocky columns than for slender ones. This can be explained by the variation of the input parameters. The load-bearing capacity of stocky columns is governed by the compression strength parallel to the grain while the load-bearing capacity of slender columns is governed by the modulus of elasticity MOE. Therefore, the variation in the numerical prediction is a direct consequence of the variation of these parameters. For columns of intermediate slenderness various material properties as well as the initial deflection influence the load-bearing capacity.

6 Assessment and improvement of the Eurocode 5 design approach

The Monte Carlo simulations performed allow checking the accurateness of the design approaches given in Eurocode 5. In Figure 5 the results of the numerical simulations using as input parameters the values given in Table 2 are compared to analytical calculations by means of ELM and 2nd order linear elastic analysis for glued laminated timber GL24h and GL32h. Results of the numerical simulations for solid timber C24 and C30 can be found in Theiler (2014).

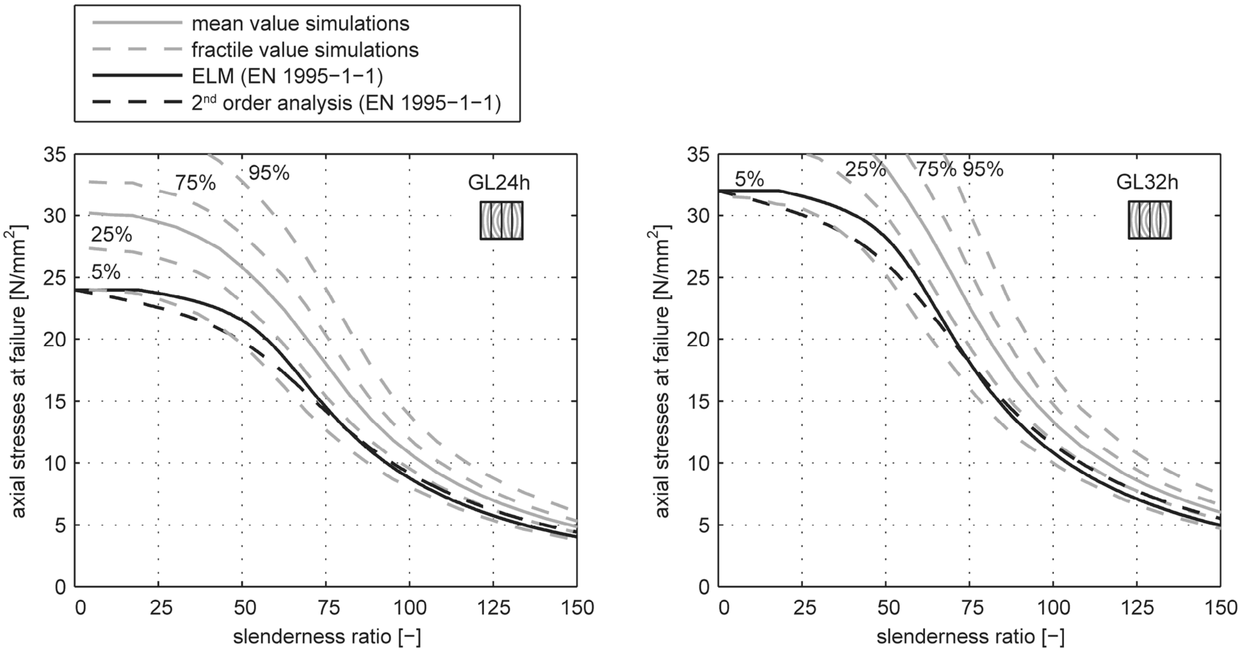

Figure 5. Comparison between ELM, 2nd order linear elastic analysis and numerical simulations for glued laminated timber GL 24h and GL 32h. Design equations taken from Eurocode 5.

It can be seen that the 2nd order linear elastic analysis may lead to an overestimation of the load-bearing capacity especially for columns of intermediate and high slenderness ($\lambda > 50$). For slender columns ($\lambda > 100$), the characteristic values obtained from 2nd order linear elastic analysis are in the range of the 25th percentile rather than in the range of the 5th percentile. This indicates that the design rules for the 2nd order linear elastic analysis given in Eurocode 5 do not ensure an accurate design of timber members subjected to compression and therefore should be modified. However, this conclusion is only valid for simply supported columns.

In Eurocode 5 and other design codes the 2nd order linear elastic analysis is based on the assumption of linear elastic material behaviour, which means that the reduction in stiffness caused by the non-linear material behaviour is neglected and the load-bearing capacity is overestimated. In order to reach a better agreement a correction factor has to be introduced in the design equation. Possibilities to modify the design approach are to enlarge the initial deformations or to reduce the design stiffness.

In particular, the reduction of the design stiffness seems to be a practicable solution, since it describes the physical phenomena accurately. In 1889 Engesser introduced the design concept of reduction in stiffness for steel columns and suggested to use a tangent modulus instead of the MOE. Engesser’s theory was first questioned by other scientists but Shanley showed in 1947, that Engesser’s method was a valuable possibility to account for non-linear deformations in the compression zone.

Based on the results of the research project (Theiler 2014) a very good agreement between 2nd order linear elastic analysis and numerical simulations is obtained when using a buckling modulus defined as follows:

$$T_{k,d} = \frac{E_{0,05}}{\gamma_M} \qquad \text{for} \quad \sigma_{c,0,d} / f_{c,0d} \leq 0.5 \qquad (5)$$

$$T_{k,d} = \frac{E_{0,05}}{\gamma_M} \cdot \left[1 - \left(2 \cdot \frac{\sigma_{c,0,d}}{f_{c,0,d}} - 1 \right)^{\beta_T} \right] \qquad \text{for} \quad \sigma_{c,0,d} / f_{c,0d} > 0.5 \qquad (6)$$

With $\beta_T = 3.0$ for solid timber and $\beta_T = 4.0$ for glued laminated timber.

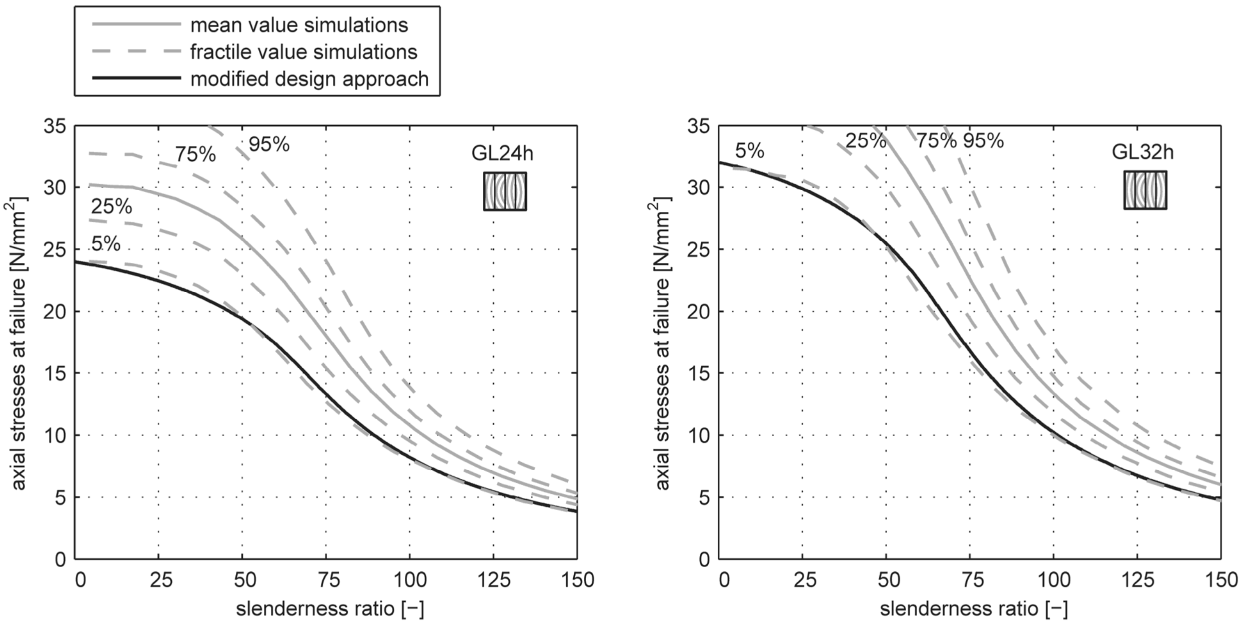

Figure 6. Comparison between 2nd order linear elastic analysis based on a buckling moduslus $T_{k,d}$ and numerical simulations for glued laminated timber of strength classes GL24h and GL32h.

A similar approach was already proposed by Roš and Brunner (1931) and used in the previous standard SIA 164:1981 (Dubas 1981). The investigations have shown that the strength-dependent reduction of the stiffness (Eq. (5) and (6)) leads to a very good agreement between the 2nd order linear elastic analysis and the numerical simulations (Figure 6). On the other hand, the strength-dependent reduction of the stiffness for high load levels leads to more laborious design procedure. The buckling modulus has to be determined by means of iteration and can be different for different design situation. Additional calculations have shown that for practical design the estimation of the buckling modulus $T_{k,d}$ according to Equation 5 is a reasonable solution even for high load levels ($\sigma_{c,0,d} / f_{c,0d} > 0.5$) making the design easier for the engineers as no iteration is needed.

This study concentrates on the behaviour of simply supported timber columns. For structural systems such as frame structures the behaviour is different due to the distribution of the axial load in the single members. Since the axial load influences the reduction of the stiffness due to the plastic deformations, the buckling behaviour depends on the distribution of the axial load and, as a consequence, the results obtained with the ELM or the adjusted 2nd order linear elastic analysis (Eq. (5) and (6)) would be too safe as shown in a reliability assessment performed in a previous analysis (Köhler et al. 2008).

7 Conclusions

When designing timber members subjected to simultaneously acting axial compression and bending moment, the increase of the bending moment due to the eccentricity of the axial force and due to the non-linear material behaviour of timber subjected to compressive stress has to be taken into account. The current design codes provide two different approaches for the design of respective members (simplified analysis based on the Effective Length Method and 2nd order linear elastic analysis of the structure). However, the two design approaches are not consistent and can lead to different results. Based on the investigations performed, the following conclusions can be drawn:

- The load-bearing capacity of stocky columns ($\lambda < 20$) is governed by the compression strength parallel to the grain. For slender columns ($\lambda > 100$) the modulus of elasticity (MOE) is the dominant material property. For columns of intermediate slenderness ratio ($50 < \lambda < 100$), the compression strength parallel to the grain, the MOE and the non-linear material behaviour impact the load-bearing capacity.
- When performing a 2nd order linear elastic analysis, the non-linear material behaviour of timber cannot be taken into account. Consequently, an adjustment of the results obtained with this method is required. This can be done by reducing the design stiffness of the structural member. The use of a buckling modulus for columns appears to be an appropriate solution.
- When designing *single columns or beam-columns* using a 2nd order linear elastic analysis, the calculation of the design value of the buckling modulus $T_{k,d}$ should be based on *5th percentile values of the modulus of elasticity $E_{0,05}$*. The investigations have shown that the strength-dependent reduction of the stiffness (Eq. (5) and (6)) leads to a very good agreement between the 2nd order linear elastic analysis and the numerical simulations. However, the estimation of the buckling modulus $T_{k,d}$ according to Equation 5 is a reasonable solution even for high load levels ($\sigma_{c,0,d}/f_{c,0d} > 0.5$) making the design easier for the engineers as no iteration is needed.
- When designing *structural systems* using a 2nd order linear elastic analysis, the calculation of the design value of the buckling modulus $T_{k,d}$ should be based on *mean values of the modulus of elasticity $E_{0,mean}$*, as the use of 5th percentile values would lead to too safe results.

8 References

Bazant Z.P., Cedolin L. (1991). Stability of structures: elastic, inelastic, fracture, and damage theories. Oxford University Press, New York.

Becker P., Rautenstrauch K. (2001). Time-dependent material behavior applied to timber columns under combined loading. Part II: Creep-buckling. Holz als Roh- und Werkstoff 59(6):491–5.

Becker P. (2002). Modellierung des zeit- und feuchteabhängigen Materialverhaltens zur Untersuchung des Langzeittragverhaltens von Druckstäben aus Holz. Dissertation. Bauhaus-Universität Weimar, Weimar.

Blaß H.J. (1987). Tragfähigkeit von Druckstäben aus Brettschichtholz unter Berücksichtigung streuender Einflussgrössen. Dissertation, Universität Fridericiana Karlsruhe, Karlsruhe.

Blaß H.J. (1991). Design of columns. In: Proceedings of the 1991 international timber engineering conference, vol. 1. London: TRADA. p. 1.75–1.81.

Blaß H.J. (1995). Buckling length. In: Timber engineering, STEP 1. Almere, Netherlands: Centrum Hout.

Buchanan AH. (1984). Strength model and design methods for bending and axial load interaction in timber members. Dissertation, University of British Columbia, Vancouver.

Buchanan AH., Johns KC., Madsen B. (1985). Column design methods for timber engineering. Can J Civil Eng 12(4):731–44.

CEB/FIP (1978). Manual of buckling and instability. Comité Euro-International du Béton and Fédération Internationale de la Précontrainte; The Construction Press Ltd; Lancaster.

DIN 1052 (2008). Entwurf, Berechnung und Bemessung von Holzbauwerken – Allgemeine Bemessungsregeln und Bemessungsregeln für den Hochbau. Deutsches Institut für Normung e.V., Berlin.

Dubas P. (1981). Stabilitätsprobleme. In: Einführung in die Norm SIA 164 (1981) – Holzbau, Lehrstuhl für Baustatik und Stahlbau, ETH Zurich, Zurich. 119–154.

EN 338 (2009). Bauholz für tragende Zwecke - Festigkeitsklassen. Europäisches Komitee für Normung, Brüssel.

EN 1995-1-1 (2004) + AC:2006 + A1:2008 + A2:2014. Eurocode 5: Bemessung und Konstruktion von Holzbauten – Teil 1-1: Allgemeines – Allgemeine Regeln und Regeln für den Hochbau. Europäisches Komitee für Normung, Brüssel.

EN 14080 (2013). Holzbauwerke - Brettschichtholz und Balkenschichtholz - Anforderungen. Europäisches Komitee für Normung, Brüssel.

Engesser F. (1889). Über die Knickfestigkeit gerader Stäbe. Zeitschrift des Architekten- und Ingenieur-Vereins zu Hannover, 35. 455–462.

Glos P. (1978). Zur Bestimmung des Festigkeitsverhaltens von Brettschichtholz bei Druckbeanspruchung aus Werkstoff- und Einwirkungskenngrössen, Dissertation, TU München. Munich.

Glos P. (1981). Zur Modellierung des Festigkeitsverhaltens von Bauholz bei Druck-, Zug- und Biegebeanspruchung. Sonderforschungsbereich 96 & Laboratorium für den konstruktiven Ingenieurbau – TU München, Munich.

Hartnack R., Schober K-U., Rautenstrauch K. (2002). Computer simulations on the reliability of timber columns regarding hygrothermal effects. In: Proceedings of CIB-W18 meeting 35: Paper No. 35-2-1. Kyoto, Japan.

Hartnack R. (2004). Langzeitverhalten von druckbeanspruchten Bauteilen aus Holz. Dissertation. Bauhaus-Universität Weimar, Weimar.

Hartnack R., Rautenstrauch K. (2005). Long-term load bearing of wooden columns influenced by climate – view on code. In: Proceedings of CIB-W18 meeting 38: Paper No. 38-2-1. Karlsruhe, Germany.

Hörsting O.P. (2008). Zum Tragverhalten druck- und biegebeanspruchter Holzbauteile. Dissertation; TU Braunschweig; Braunschweig.

Joint Committee on Structural Safety (2007). Probabilistic Model Code; JCSS Joint Committee on Structural Safety; www.jcss.byg.dtu.dk.

Kessel MH., Schönhoff T., Hörsting P. (2005). Zum Nachweis von druckbeanspruchten Bauteilen nach DIN 1052:2004–08, Teil 1. Bauen mit Holz 107(12):88–96.

Kessel MH., Schönhoff T., Hörsting P. (2006). Zum Nachweis von druckbeanspruchten Bauteilen nach DIN 1052:2004–08, Teil 2. Bauen mit Holz 108(1):41–4.

Köhler J., Frangi A., Steiger R. (2008). On the role of stiffness properties for ultimate limit state design of slender columns. In: Proceedings of CIB-W18 Meeting 41, Paper No. 41-1-1, St. Andrews.

Larsen HJ., Pedersen SS. (1975). Tests with centrally loaded timber columns. In: Proceedings of CIB-W18 meeting 4: Paper No. 4-2-1. Paris.

Möller G. (2007). Zur Traglastermittlung von Druckstäben im Holzbau. Bautechnik 84(5):329–34.

Roš M., Brunner J. (1931). Die Knickfestigkeit der Bauhölzer. In: Kongress des internationalen Verbandes für Materialprüfung, Zurich.

Shanley F. (1947). Inelastic column theory. Journal of the Aeronautical Sciences, 14(5). 261–268.

SIA 164 (1981). Holzbau. Schweizerischer Ingenieur- und Architektenverein, Zurich.

SIA 265 (2012). Holzbau. Schweizerischer Ingenieur- und Architektenverein, Zurich.

Steiger R., Fontana M. (2005). Bending moment and axial force interacting on solid timber beams. Materials and Structures, 38 (279). 507–513.

Tetmajer L. (1896). Die Gesetze der Knickungs- und der zusammengesetzten Druckfestigkeit der technisch wichtigsten Baustoffe. Materialprüfungs-Anstalt am Schweiz. Polytechnikum Zurich. Zurich.

Theiler M., Frangi A., Steiger R. (2013). Strain-based calculation model for centrically and eccentrically loaded timber columns. Engineering Structures, 56. 1103–1116.

Theiler M. (2014). Stabilität von axial auf Druck beanspruchten Bauteilen aus Vollholz und Brettschichtholz. Dissertation No. 22062, ETH Zurich, Zurich.

Theiler M., Frangi A. (2015). Knickversuche mit Brettschichtholzstützen unter exzentrischer Normalkraftbeanspruchung. IBK-Bericht No. 361, Institute of Structural Engineering IBK, ETH Zurich, Zurich.

Discussion

The paper was presented by R Jockwer

S Winter asked why machine grading was not used to select the laminates. R Jockwer responded that no machine grading was available at the time of the project and visual grading is more common.

R Harris commented that the text of the paper seemed to suggest used of E_{mean} for single member design but the slides clarified that E_{mean} is used for system approach.

P Dietsch commented that there did not seem to be a difference between Eurocode 5 and the approach proposed by the paper where γ_m is already used.

I Smith asked how often the failures occurred at mid height. R Jockwer responded that the columns quite often failed at mid height. I Smith commented that failure locations in timber can be more random.

Rolling Shear Properties of some European Timber Species with Focus on Cross Laminated Timber (CLT): Test Configuration and Parameter Study

Thomas Ehrhart*); ETH Zurich, Institute of Structural Engineering, www.ibk.ethz.ch, Stefano-Franscini-Platz 5, 8093 Zurich, Switzerland

Reinhard Brandner; Graz University of Technology, Institute of Timber Engineering and Wood Technology, www.lignum.at, Inffeldgasse 24, 8010 Graz, Austria

Gerhard Schickhofer; Graz University of Technology, Institute of Timber Engineering and Wood Technology, www.lignum.at, Inffeldgasse 24, 8010 Graz, Austria

Andrea Frangi; ETH Zurich, Institute of Structural Engineering, www.ibk.ethz.ch, Stefano-Franscini-Platz 5, 8093 Zurich, Switzerland

*) phone +41 44 633-3178, fax -1093, e-mail ehrhart@ibk.baug.ethz.ch

Keywords: rolling shear strength & modulus, European timber species, cross laminated timber, CLT, test configuration, parameter study

1 Introduction

Cross laminated timber (CLT) has gained popularity and relevance in the construction industry during the past decade. Its versatile applicability, economic competitiveness as well as an increasing social consciousness for sustainable constructions have been main reasons for this positive development. Its laminar composition enables CLT to withstand in- and out-of-plane loads. Due to its structure featuring orthogonally oriented adjacent layers, in CLT loaded out-of-plane, shear and more specific rolling shear has to be considered in ultimate (ULS) as well as serviceability limit state (SLS) design. This is because rolling shear constitutes a potential failure mechanism and contributes a noticeable amount to the overall deflection. Comprehensive knowledge on rolling shear modulus (G_R) and strength (f_R) is therefore of utmost importance for an adequate design of CLT structures. Previous investigations on rolling shear properties and their influential parameters have primarily been performed numerically and using Norway spruce (*Picea abies*).

The main goal of our contribution, based on investigations detailed in *Ehrhart* (2014), was to identify the most important parameters for rolling shear characteristics and to quantify their influence. Furthermore, information about the rolling shear performance of several timber species was analysed to investigate their potential for use in CLT-products. In view of upcoming new timber species increasingly pushed into the market, investigations on rolling shear comprised also some hardwood and other softwood species with a potential to be used for (cross) laminated timber products.

1.1 Available test configurations

Robust and replicable test configurations are essential to assess mechanical properties of timber. For most timber properties, such configurations are already implemented in international standards. Regarding rolling shear, standardised configurations and methods are not available yet. Studies reflect a variety of diverse testing methods to determine rolling shear modulus and / or strength by using quite different approaches (*Figure 1.1*).

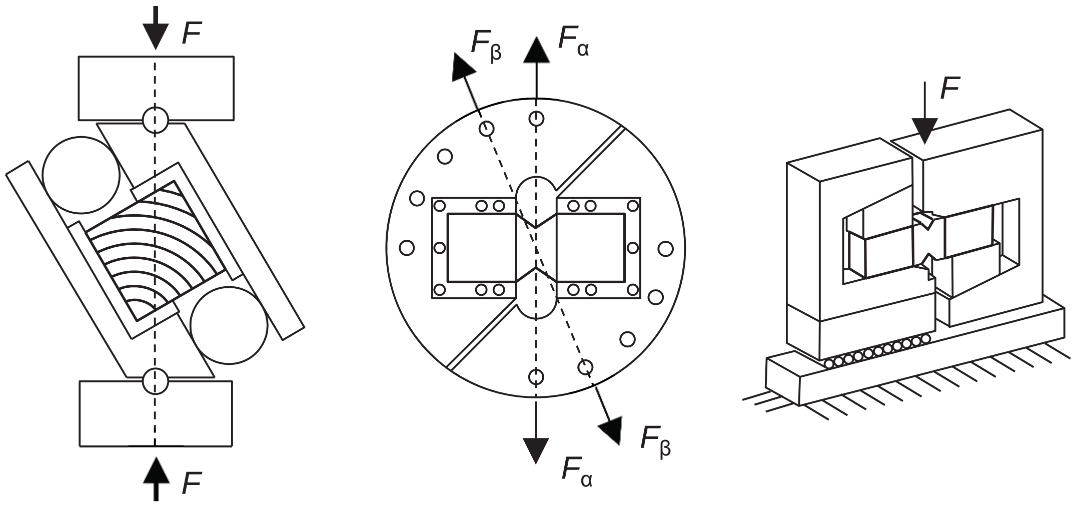

Figure 1.1 Some test configurations for determining rolling shear properties proposed by Hassel et al. (2009), Xavier et al. (2009) and Dumail et al. (2000) (left to right)

Neuhaus (1981) determined G_R using torsion bars, *Dumail et al.* (2000) investigated the applicability of the Iosipescu method for spruce wood, *Blass & Görlacher* (2001) used a tension-shear configuration proposed by *Gahl* (not published). *Görlacher* (2002) calculated G_R by means of eigenfrequency, *Hassel et al.* (2009) presented the single-cube apparatus (SCA) for determination of (rolling-) shear, *Xavier et al.* (2009) proposed the Arcan shear test for the measurement of shear properties of clear wood. *Mestek* (2011) used and optimised a sandwich configuration – similar to the one given in EN 408 (2010) for testing shear parallel to the grain – to determine rolling shear properties of Norway spruce. *Bendsten* (1976) had already used this method to investigate twelve structural softwood species about 40 years ago.

Beside these configurations, which focus on testing clear wood and board segments, there are additional configurations in discussion emphasizing the determination of rolling shear properties of the product CLT. *Mestek* (2011) adapted the sandwich configuration to allow also testing of CLT-elements. The draft version of prEN 16351 (2011) provides bending configurations with reduced spans from which rolling shear stiffness and strength can be derived. *Gehri* (2011) suggested a bending test of a five-layer CLT-plate with only the outermost layers oriented parallel to the supporting direction. This to enlarge the potential area for shear field measurements in the area exposed to rolling shear (*Figure 1.2*).

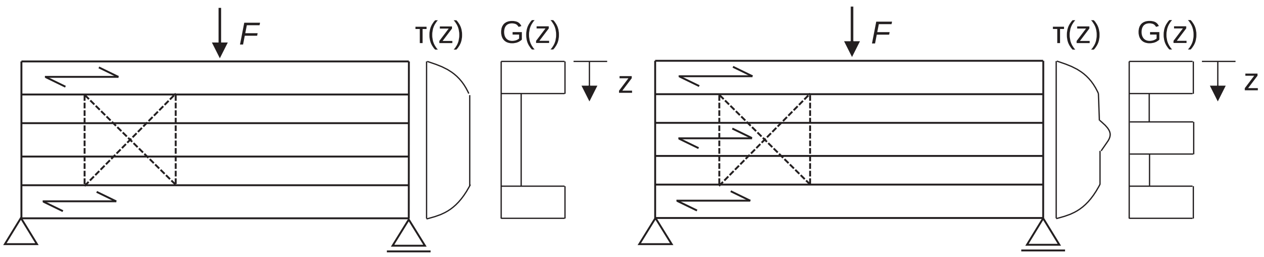

Figure 1.2 Left: setup suggested by Gehri (2011); Right: standard CLT structure

1.2 Potential influencing parameters on rolling shear properties

Beside others, the timber species itself is one major "parameter" for mechanical properties. Regarding strength and stiffness at all grain angles, most European hardwood timber species show higher characteristics than softwoods, *Kollmann* (1936). *Bendtsen* (1976) reported also significant differences between the rolling shear characteristics found by analysing nine structural softwoods.

Numerous studies have proven significant correlation between density and most mechanical properties of timber, at least for clear wood. *Görlacher* (2002) carried out bending vibration tests using board segments of Norway spruce and found positive (but low) correlation between density and rolling shear modulus.

Past investigations outline sawing pattern as one major parameter for the rolling shear modulus G_R. This was concluded in *Aicher & Dill-Langer* (2001), *Jakobs* (2005) and *Feichter* (2013) by numerical studies and in *Görlacher* (2002) based on eigenfrequency measurements.

Theoretical analysis on the load bearing behaviour of CLT in shear by *Kreuzinger & Scholz* (2001) showed that rolling shear strength depends on the ratio of undisturbed board's width – which can be either the actual width or the distance between stress reliefs – and its thickness. To consider this geometric effect, a reduction of strength by means of the factor k_{Red} is proposed. Experimental tests by *Mestek* (2011) confirmed the dependency and the results agreed well with values predicted using k_{Red}.

2 Material and methods

2.1 Material

2.1.1 Timber species

Because of its major importance to the construction industry and data availability from previous experimental and numerical studies on rolling shear, Norway spruce (*Picea abies* (L.) Karst.) was chosen as the reference timber species. This comprises also all parameter variations, which are described hereafter. For comparison a second coniferous wood, pine (*Pinus sylvestris* L.), was investigated.

Regarding the microstructure of wood, a general distinction between coniferous- and deciduous wood is given (*Figure 2.1*). Due to the concentrated clustering of vessels in the earlywood of ringporous hardwood species with subsequent potential to influence at least the failure mechanism, species featuring these characteristics have to be distinguished from diffuse porous species. Birch (*Betula pendula* Roth), beech (*Fagus sylvatica* L.) and poplar (*Populus spp.*) were investigated as representatives of the group of diffuse-porous deciduous timber species. Ash (*Fraxinus excelsior* L.) was the only ringporous timber species in this study.

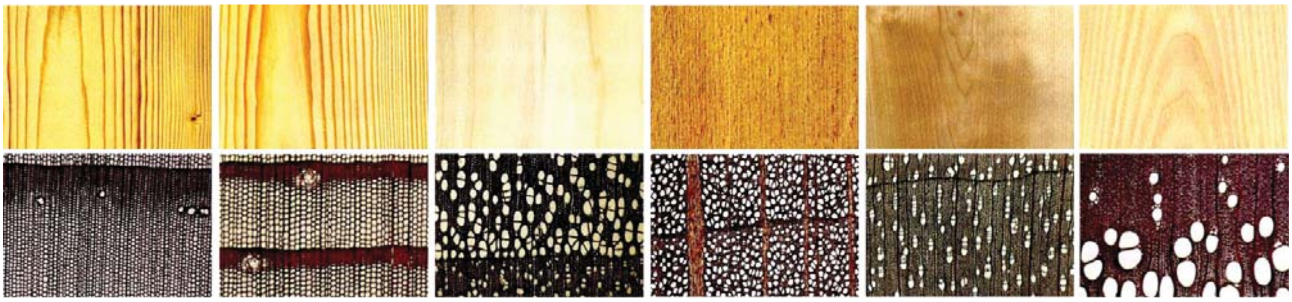

Figure 2.1 Tangential cuts (above) and microscopic cross cut (below) of spruce, pine, poplar, beech, birch and ash (from left to right) (from Grosser & Teez 1985)

2.1.2 Adjustment factors for physical properties in regard to moisture content

According to EN 408, all specimens were conditioned at 20 °C and 65 % relative humidity. Density, rolling shear modulus and strength were related to the reference moisture content of u_{ref} = 12 % by considering 0.5 % (EN 384), 2 % (*Neuhaus* 1981) and 3 % (*Brandner et al.* 2012*; Ringhofer et al.* 2014), respectively, per percent moisture difference. Density of all specimens was determined to investigate the influence on rolling shear properties for different timber species, sawing patterns and boards' geometries.

2.1.3 Geometry of the boards

The cross sectional geometry of CLT-products has not been standardised yet. Dimensions of boards and plates vary depending on the manufacturer, although – at least in Europe – board or layer thicknesses of 20, 30 and 40 mm are more and more common. Furthermore, specific production-techniques requiring stress reliefs influence the final setup. To cover common geometries, boards with a constant thickness (t_l) of

30 mm and a varying width w_l of 120 (reference), 60 and 180 mm were investigated (*Figure 2.2*). Thus, the tested ratios w_l / t_l were two, four and six. To separate the parameter "board geometry" from other parameters, like density, annual ring width, sawing pattern, reaction wood and other timber characteristics, specimens for both w_l / t_l ratios were cut subsequently from the boards. Consequently, in both series comparable densities were achieved (*Table 2*).

2.1.4 Sawing pattern

Depending on the former location in the log, the radial distance between specimen's cross section centre and the pith (*r*), different grain patterns are generated. We investigated radial distances *r* of 30 (± 10) (rift and half-rift grain), 60 and 100 mm (flat grain) by a realized but negligible eccentricity *e* of ± 5 mm (*Figure 2.2*).

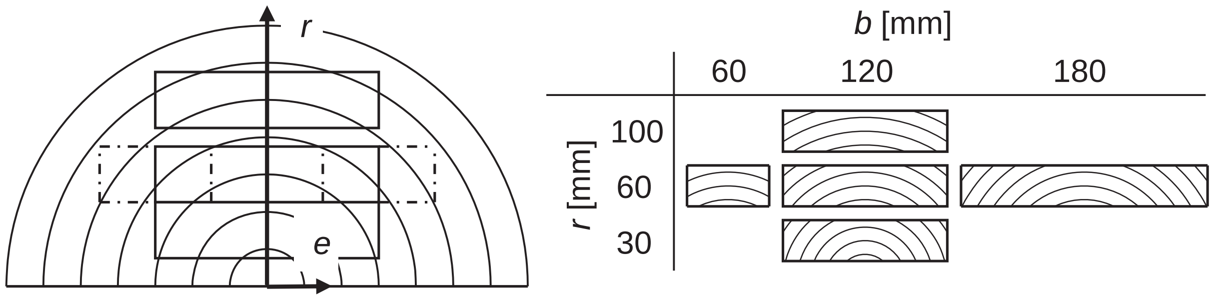

Figure 2.2 Investigated sawing patterns and board geometries

2.1.5 Test plan

The test plan is outlined in *Table 1*. For getting significant statistics on a reference basis, the so-called "reference sample" comprised 40 specimens of Norway spruce, with a radial distance *r* of 60 mm and a width w_l of 120 mm. All other samples comprised 20 specimens each and a setting where only one parameter was changed while the others remained according to the reference sample. In each sample, only one segment per board was used to assure representative results and to maintain full variability.

Table 1 Test plan

	group	*no.*	*species*	*r*	w_l / t_l
variation of	[-]	[-]	[-]	[mm]	[-]
reference	1	40	spruce	60	4
species	2.1	20	**birch**	60	4
	2.2	20	**ash**	60	4
	2.3	20	**poplar**	60	4
	2.4	20	**beech**	60	4
	2.5	20	**pine**	60	4
r	3.1	20	spruce	**30**	4
	3.2	20	spruce	**100**	4
w_l / t_l	4.1	20	spruce	60	**2**
	4.2	20	spruce	60	**6**

2.2 Methods

2.2.1 Test configuration

Purity of shear stress, variability of specimen dimensions and necessary effort were taken into account as most important decision parameters in choosing the method used in this work (*Figure 2.3*). It is based on the shear configuration given in EN 408 (2010) and considers the modifications suggested by *Mestek* (2011). Beech wood loading plates were used for softwood timber species and poplar. All other hardwood timber species were tested using steel plates. Additionally conducted numerical finite element (FE) analysis confirmed the suitability of the configuration and a uniform distribution of shear stresses in the main field of interest. Stresses perpendicular to the shear plane were relatively low, but exceeded transverse tensile- respectively compression strength locally in areas very close to the edges (*Figure 2.3*, middle and right).

Rolling shear strength was calculated according to EN 408 (2010) using Eq. (1). By means of displacement transducers, the relative displacement of the loading plates (x) was measured and G_R could be calculated using Eq. (2).

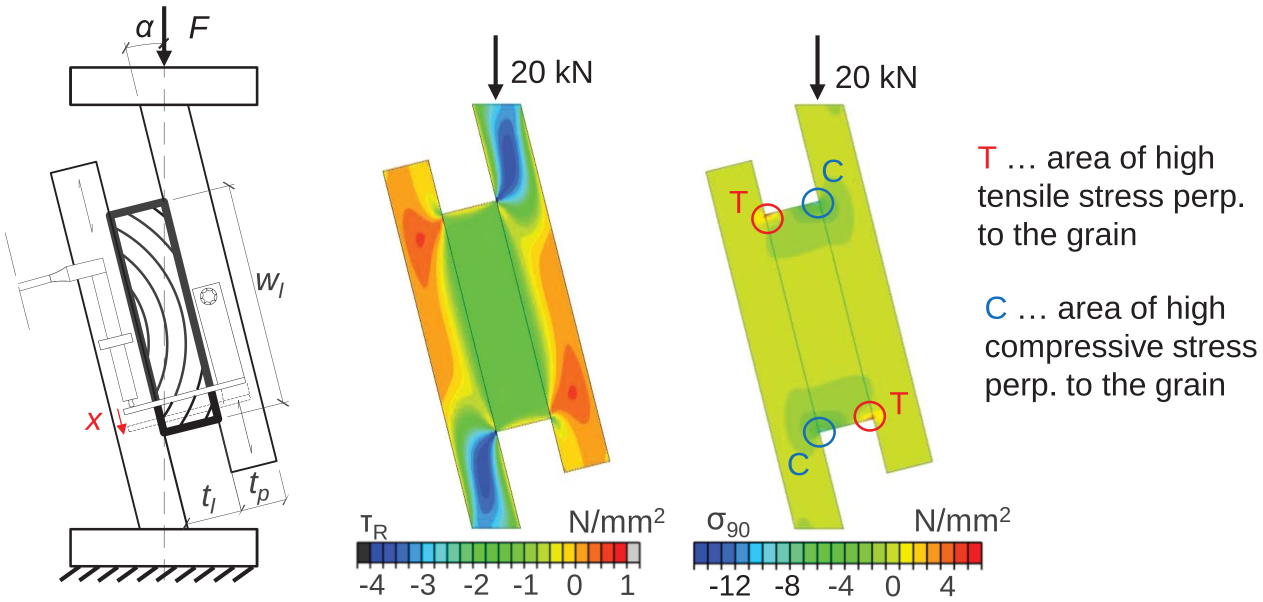

Figure 2.3 Test configuration, distribution of shear- and normal stresses (left to right)

The angle between shear plane and force direction (α) was 14° for all tests and the length of the board segment (l) was 100 mm.

$$f_R = \frac{F_{max} \cdot \cos\alpha}{l \cdot w_l} \quad (1)$$

$$G_R = \frac{\Delta\tau_R}{\Delta\gamma_R} = \frac{\Delta F \cdot \cos\alpha \cdot t_l}{l \cdot w_l \cdot \Delta x} \quad (2)$$

According to EN 408 (2010), G_R was calculated between 0.1 F_{max} and 0.4 F_{max}. Using vertical advancing rates of 0.4 up to 0.8 mm/min, F_{max} was almost always reached within 300 ± 120 s.

3 Results and discussion

Main results of this study are summarised in *Table 2*. It contains values for rolling shear modulus and strength as well as determined density and moisture content for all samples.

Table 2 Rolling shear properties by groups: main statistics

		$G_{R,12}$ [N/mm²]			$f_{R,12}$ [N/mm²]				ρ_{12} [kg/m³]		u [%]
group	*n*	*range*	$\bar{x}$	*COV* [%]	*range*	$\bar{x}$	*COV* [%]	*05*	*range*	$\bar{x}$	$\bar{x}$
1	36	52:158	100	27	1.41:2.34	1.88	13	1.51	367:544	439	11.0
2.1	19	138:247	188	19	2.92:4.07	3.45	10	2.91	548:668	612	11.5
2.2	14	299:508	401	14	4.46:6.35	5.57	12	4.54	708:875	798	11.0
2.3	16	93:159	127	15	2.49:3.23	2.88	8	2.51	393:523	463	10.2
2.4	16	258:410	357	12	4.61:6.13	5.37	9	4.64	663:766	720	10.0
2.5	19	101:210	158	19	1.94:2.69	2.29	10	1.95	441:570	521	10.7
3.1	25	89:207	143	19	1.24:2.53	1.88	22	1.30	361:573	442	11.0
3.2	23	30:87	56	26	1.34:2.45	1.84	16	1.40	408:568	480	11.6
4.1	23	43:96	65	21	0.83:1.70	1.16	20	0.82	382:556	459	11.4
4.2	20	100:224	148	21	1.66:2.99	2.28	14	1.80	401:527	459	11.4

3.1 Correlation between density and G_R resp. f_R

Considering all investigated timber species in the regression and correlation analysis on the relationship density vs. rolling shear properties (*Figure 3.1*), high correlation exists.

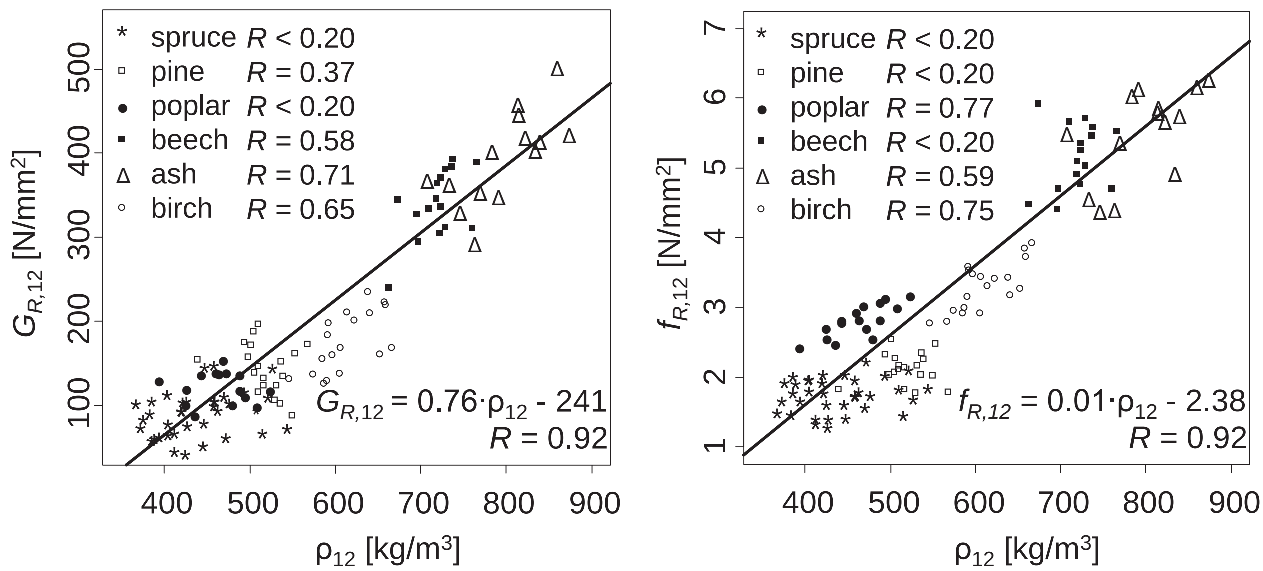

Figure 3.1 Density vs. rolling shear modulus (left) and strength (right)

Doing the same analysis for each timber species separately, for softwoods no significant correlation between density and the rolling shear properties is observed. A possible explanation for this might be found in the anatomy of coniferous wood species:

for example in Norway spruce, both, early- and latewood have quite constant densities of about 300 kg/m^3 and 900 to 1,000 kg/m^3, respectively. Since the thickness of latewood is relatively constant over the entire life of such a tree, the thickness of the earlywood zones varies with the yearly growth conditions and thus decisively influences the average density of a certain piece of wood. Following the circumstance, that rolling shear failure takes commonly place in the interface zone between early- and latewood of two subsequent years, the earlywood density may indicate the magnitude of shear properties.

By analysing the relationship between rolling shear properties and the density specific for each hardwood species high correlations are found (*Figure 3.1*). Compared to softwoods, in case of ring porous species the interface between the early- and latewood of two subsequent years may again act as the primary failure domain, however, because of a nearly constant thickness of earlywood over the years of tree's life, the average wood density becomes decisively affected by the thickness of the latewood. Considering diffuse porous species, a more or less homogeneous density profile over the entire thickness of annual rings can be assumed.

3.2 Correlation between G_R and f_R

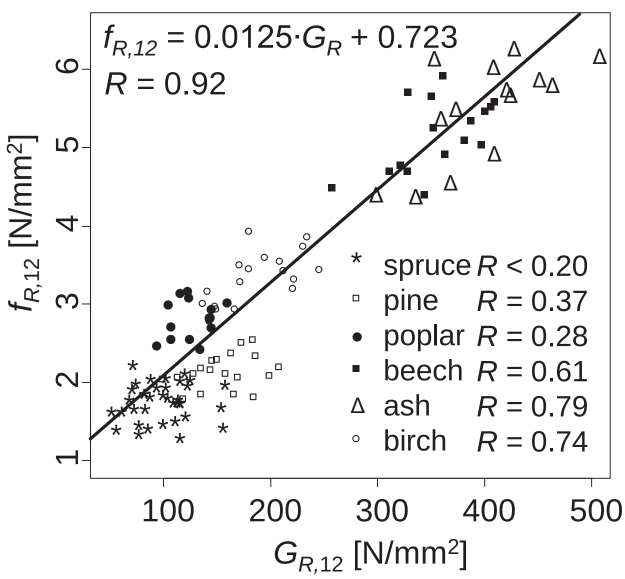

The regression analysis on rolling shear strength vs. modulus, done by comprising all investigated timber species, confirms the generally observed positive correlation between these two mechanical properties (*Figure 3.2*). By analysing the same relationship separately for each timber species, high correlation is found for ash, birch and beech, while low and debateable values are observed for spruce, pine and poplar.

Figure 3.2 Rolling shear modulus vs. strength

3.3 Influence of the sawing pattern on rolling shear properties

This and the next section discuss outcomes from a parameter study, which only comprises Norway spruce.

Boards with large distance to the pith generally tend to own lower ring widths and increasing amount of mature wood which both consequence higher densities. Therefore, given a positive correlation between rolling shear properties and density, higher strengths would be expected when increasing the radial distance to the pith r. However, a corresponding positive correlation between r and the rolling shear strength f_R was not observed (*Figure 3.3*). The mean values of 1.88, 1.88 and 1.84 N/mm^2 given for r = 30, 60 and 100 mm, respectively, are on equal basis. One possible explanation could be found in different sawing patterns causing different rolling shear modulus. Assuming that shear failure occurs under a certain distortion, lower G_R would cause lower strengths for outer boards. Thus, these two effects just seem to compensate each other.

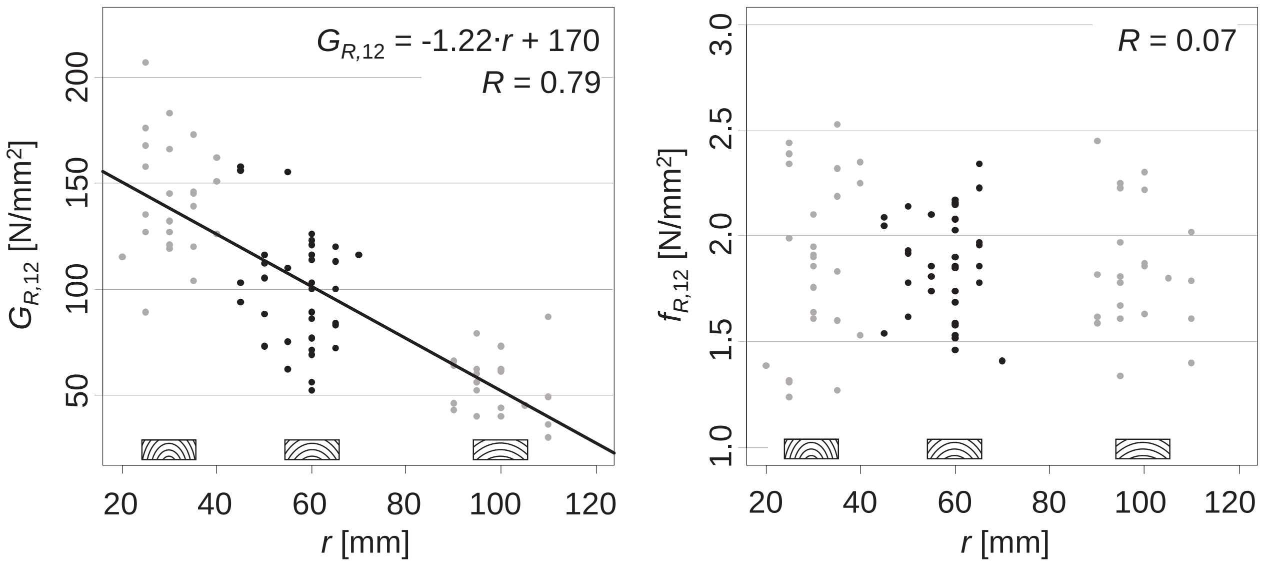

Figure 3.3 Relationship between the radial distance to the pith, indirectly causing changes in the sawing pattern and the rolling shear modulus (left) and strength (right); for Norway spruce

However and conform to previous studies by *Aicher & Dill-Langer* (2001), *Jakobs* (2005), *Görlacher* (2002) and *Feichter* (2013), a distinct relationship between the radial distance to the pith, indirectly causing changes in the sawing pattern from rift or half-rift gain to flat grain, and G_R is given. Although previous studies report a non-linear relationship between G_R and r, within the investigated range of sawing patterns, an almost linear reduction of G_R for increasing r is observed (*Figure 3.3*, left).

3.4 Influence of board geometry on rolling shear properties

The geometry of a board shows to have a strong influence on both, rolling shear strength and modulus.

Compared to the reference width of w_l = 120 mm, the average strength and modulus decrease by 40 % and 30 %, respectively, when w_l is reduced to 60 mm. However, they raise by approximately 20 % and 50 %, respectively, when w_l becomes 180 mm (*Figure 3.4*).

Distribution of shear stresses is not constant along the segment's cross section. In areas close to the edges, tensile stresses perpendicular to grain arise increasingly. The actual shear stress in these areas is lower than calculated using Eq. (1). However, in inner zones, actual stresses exceed those calculated. The lower the ratio w_l / t_l, the higher the stress peaks and the larger the gap between the actual and calculated stress (*Figure 3.5*). This causes lower determined rolling shear strengths for lower w_l / t_l ratios.

In our study only boards with negligible eccentricity to the pith, *e*, were used. Consequently, changes in width of the boards also lead to changes in the grain orientation at the board's edges, i.e. wider boards show an increasing amount of half-rift and flat grain oriented annual rings in their peripheral zones. As already discussed before (*3.3*), this leads to higher values of rolling shear modulus, which demonstrates the difficulty in separating the influences caused by the ratio w_l / t_l from that dedicated to the sawing pattern.

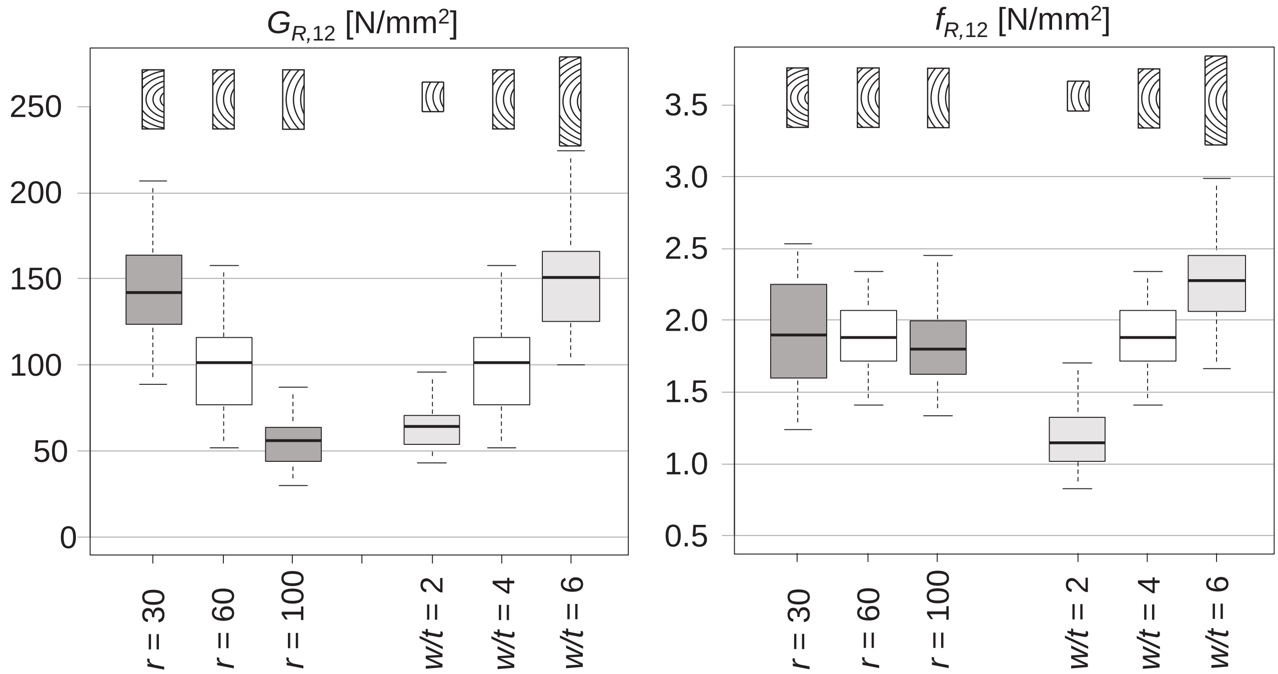

Figure 3.4 Rolling shear properties of Norway spruce: variation of the radial distance to the pith (indirectly sawing pattern) and w_l / t_l

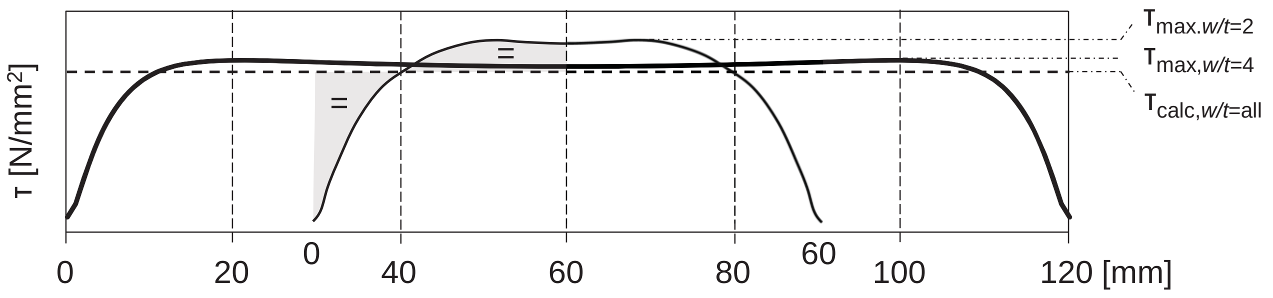

Figure 3.5 Qualitative distribution of shear stresses in boards with a w/t-ratio of two and four

3.5 Rolling shear properties of different timber species

The rolling shear properties of all tested timber species are overall very promising (*Figure 3.6*).

Strength and modulus determined for Norway spruce confirm and partly exceed values reported in previous studies. *Bendtsen* (1976) for example reported $f_{R,\text{mean}}$ of 1.79, 1.88 and 1.79 N/mm^2 for red, black and white spruce, respectively. Mean rolling shear modulus found was 68, 73 and 58 N/mm^2, however, no information about sawing pattern is provided. Nevertheless, in our comparative study for Norway spruce the lowest properties are observed. Properties of pine and poplar surpass those of spruce significantly. Pine particularly shows high rolling shear modulus and poplar a remarkable strength. Birch performs very well too with strength and modulus about double as high than for spruce. Beech and ash show outstanding rolling shear properties and reach values about three times higher than found for spruce (*Figure 3.6*).

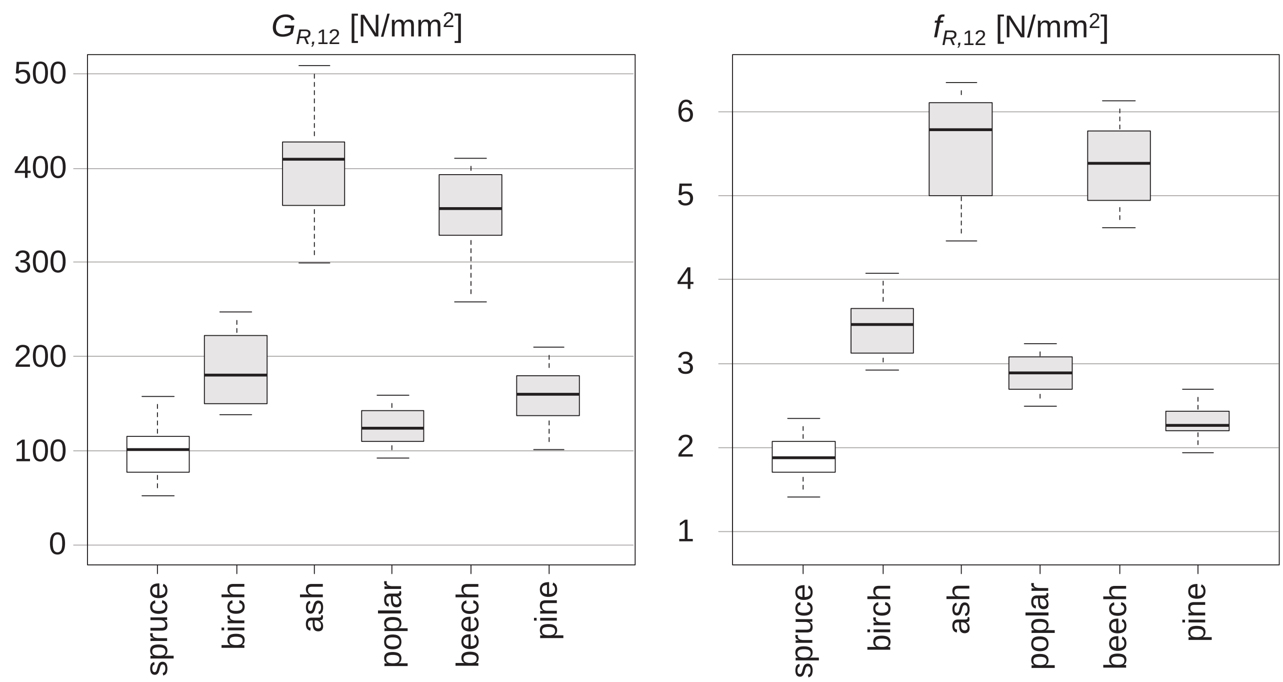

Figure 3.6 Rolling shear properties of different timber species: (left) modulus, (right) strength

4 Conclusion

4.1 Test configuration

Experiences made regarding the test configuration are very promising. Rolling shear failure along one or few annual rings was observed for most species (*Figure 4.1*), board-geometries and sawing patterns. Finite element (FE) analysis of the test configuration already showed local areas of stresses perpendicular to the grain. Small primary cracks were indeed observed during several tests in areas close to the edges (*Figure 4.2,* left). As they occurred exclusively after removing the displacement transducers, influence on measured rolling shear modulus can be excluded. Independent fracture pattern after failure indicates that the influence of small primary cracks is also negligible in calculating strengths.

In-depth investigations on the interaction between rolling shear and stresses perpendicular to the grain done by *Mestek* (2011) showed that compression tends to affect rolling shear strength positively. Following his model and due to the low angle between force direction and shear plane (α), negligible influence on the rolling shear behaviour can be assumed.

Investigation of the bonding surface after failure indicated that the bonded connection between the loading plates and specimen was sufficiently strong (*Figure 4.2*). However, the surfaces of a few birch and beech specimens were covered with wood fibres by less than 50 %.

Figure 4.1 Typical failures of specimens: spruce, pine, poplar, birch, beech and ash (from top left to bottom right)

Efforts and costs for preparation and conducting the tests were relatively low and geometrical variations of specimen easy to perform. Loading plates out of beech appear adequate for softwood species and poplar. We therefore propose to record the configuration described for the determination of rolling shear strength and modulus in EN 408 (2010).

Figure 4.2 Primary crack 1 and from that independent failure (left); bonding surface after failure of a spruce (middle) and birch (right) specimen

In a follow-up of this study, three-point bending tests using Norway spruce boards of the same population as base material were carried out, *Wilding et al.* (2014). Shear-field measurements on 5-layer beams featuring a standard CLT structure, i.e. subsequent orthogonal layering, and the structure suggested by *Gehri* (2011) – with only the outermost layers oriented parallel to the supporting direction (*Figure 1.2*) – led to $G_{R,app,\text{mean}}$ of 188 (apparent value because of the orthogonal middle layer) and $G_{R,\text{mean}}$ = 110 N/mm^2, respectively. Thus, results of bending tests using the structure suggested by Gehri agree very well with those obtained from single segment testing.

4.2 Rolling shear properties

Results of in total more than 200 tests confirm previous findings, extend knowledge on rolling shear behaviour and allow identifying sawing pattern and board geometry as the main parameters influencing the rolling shear properties G_R and f_R, respectively.

For Norway spruce, overall $G_{R,\mathrm{mean}}$ = 100 N/mm² and $f_{R,\mathrm{k}}$ = 1.4 N/mm² are found. Current values for $G_{R,\mathrm{mean}}$ and $f_{R,\mathrm{k}}$, given in European technical approvals of different CLT producers (e.g. *ETA-06/*0009, *ETA-06/0138* and *ETA-10/0241*), lie at about 50 N/mm² and 0.85 : 1.5 N/mm², respectively. As a minimal w_l / t_l-ratio of four is defined for boards in transverse layers in the same ETAs, it appears that the potential of timber is partly underestimated in the design process and for product characterisation. A circumstance which also frequently arises in comparisons of global (over the entire span) and local (only within area of constant moment) bending modulus, gained from four-point bending tests on CLT plates. Depending on the actual sawing patterns of the material used for CLT production, especially the values regulated currently for rolling shear modulus seem to be on a very conservative basis. This also by considering that boards within transverse layers commonly show varying sawing patterns.

Table 3 Proposed rolling shear characteristics for w_l / t_l ≥ 4

	$f_{R,\mathrm{k}}$ [N/mm²]	$G_{R,\mathrm{mean}}$ [N/mm²]
spruce	1.4	100
pine	1.7	150
poplar	2.2	120
birch	2.7	180
ash, beech	4.0	350

However, decreasing ratios of w_l / t_l distinctly decrease G_R and f_R. Comparable effects are assumed in boards with stress reliefs and comparable relief-distance vs. thickness ratios. As further differentiation in sawing patterns in CLT-production processes appears practicable questionable, representative values for all locations in the log – by taking into account preferable used board geometries and their relationship to radial positions due to the sawing process – are needed. A proposal for boards with a ratio w_l / t_l ≥ 4 is presented in *Table 3*. Eq. (3) and (4) are proposed to determine properties of spruce boards with a lower ratio.

$$f_{R,\mathrm{k}} = min\begin{cases} 0.2 + 0.3 \cdot \frac{w_l}{t_l} \\ 1.4 \end{cases} \quad (3) \qquad G_{R,\mathrm{mean}} = min\begin{cases} 30 + 17.5 \cdot \frac{w_l}{t_l} \\ 100 \end{cases} \quad (4)$$

In comparison to Norway spruce and the range of investigated timber species, the outstanding rolling shear properties of beech and ash are outlined which impose these species to be used in CLT. Pine, poplar and birch have also a great potential as base material for CLT.

Available information on rolling shear properties in international standards has yet been very limited. Results of this study therefore seem in particularly relevant for EN 338 (2009), where only values for shear strength and modulus parallel to the grain are listed. Findings of this study could also contribute to EN 14080 (2013) and prEN 16351 and have potential to supplement important points to these standards.

5 Acknowledgement

The holz.bau forschungs gmbh and the FFG COMET K-Project 'focus_sts' made this work possible and their support, including that of the funding agencies and company partners, is thankfully acknowledged. We would also like to express our gratitude to the entire team of the Institute of Timber Engineering and Wood Technology at Graz University of Technology for the valuable support during all stages of the project.

6 References

Aicher, S & Dill-Langer, G (2001): Basic Considerations to Rolling Shear Modulus in Wooden Boards. Otto-Graf-Journal, No. 11.

Bendsten, B A (1976): Rolling Shear Characteristics of Nine Structural Softwoods. Forest Products Journal, No. 11/1976.

Brandner, R et al. (2012): Determination of Shear Strength of Structural and Glued Laminated Timber. University of Technology, Graz.

Blass, H J & Görlacher, R (2001): Zum Trag- und Verformungsverhalten von LIGNOT-REND Decken- und Wandsystemen aus Nadelschnittholz (in German).

Dumail, J F et al. (2000): An Analysis of Rolling Shear of Spruce Wood by the Iosipescu Method. Holzforschung, No. 4/2000.

Ehrhart, T (2014): Material-Related Influential Parameters on Rolling Shear Behaviour Regarding Cross Laminated Timber (in German). University of Technology, Graz (Master Thesis).

ETA-06/0009 (2013): Multilayered timber elements for walls, ceilings, roofs and special construction components; Binderholz Brettsperrholz BBS.

ETA-06/0138 (2011): Solid wood slab elements to be used as structural elements in buildings; KLH-Massivholzplatten.

ETA-10/0241 (2013): Solid wood slab elements to be used as structural elements in buildings; Leno Brettsperrholz.

EN 338 (2009): Structural timber – Strength classes. European Committee for Standardization (CEN).

EN 384 (2010) Structural timber – Determination of characteristic values of mechanical properties and density. European Committee for Standardization (CEN).

EN 408 (2010): Timber structures – Structural timber and glued laminated timber - Determination of some physical and mechanical properties. European Committee for Standardization (CEN).

EN 14080 (2013): Timber structures – Glued laminated timber and glued solid timber – Requirements; European Committee for Standardization (CEN).

EN 13183-1 (2002): Moisture content of a piece of sawn timber – Part 1: Determination by oven dry method. European Committee for Standardization (CEN).

Feichter, I (2013): Stress – and ultimate load calculations for selected problems in solid timber constructions with cross laminated timber (CLT) (in German). University of Technology, Graz (Master Thesis).

Gehri, E (2011): Personal Correspondence on Rolling Shear Test Configurations and Properties.

Görlacher, R (2002): Ein Verfahren zur Ermittlung des Rollschubmoduls von Holz (in German). Holz als Roh und Werkstoff, No. 60.

Grosser, D & Teez, W (1985): Einheimische Nutzhölzer (in German). Informationsdienst Holz.

Hassel, B P et al. (2009): The Single Cube Apparatus for Shear Testing – Full-Field Strain and Finite Element Analysis of Wood in Transverse Shear. Composites Science and Technology, No. 69/2009.

Jakobs, A (2005): Zur Berechnung von Brettlagenholz mit starrem und nachgiebigem Verbund unter plattenartiger Belastung unter besonderer Berücksichtigung des Rollschubes und der Drillweichheit (in German). Universität der Bundeswehr, Munich (Doctoral Thesis).

Kollmann, F (1936): Technologie des Holzes und er Holzwerkstoffe (in German). Julius Springer Verlag, Berin.

Kreuzinger, H & Scholz, S (2001): Schubtragverhalten von Brettsperrholz (in German). Forschungsvorhaben-Schlussbericht. University of Technology, Munich.

Mestek, P (2011): Punktgestützte Flächentragwerke aus Brettsperrholz – Schubbemessung unter Berücksichtigung von Schubverstärkungen (in German). Technical University, Munich (Doctoral Thesis).

Neuhaus, F H (1981): Elastizitätszahlen von Fichtenholz in Abhängigkeit der Holzfeuchtigkeit (in German). Ruhr Universität, Bochum (Doctoral Thesis).

prEN 16351 (2012): Timber structures – Cross laminated timber – Requirements. European Committee for Standardization (CEN). Draft version.

Ringhofer, A et al. (2014): The influence of moisture content variation on the withdrawal capacity of self-tapping screws. Holztechnologie 55(3):33–40.

Wilding, B et al. (2014): Materialbezogene Einflussparameter auf die Rollschubeigenschaften in Hinblick auf Brettsperrholz. Präsentation im Rahmen der Beiratssitzung des COMET K-Projektes „focus_sts“ (in German). holz.bau forschungs gmbh, Graz.

Xavier, J et al. (2009): Measurement of the Shear Properties of Clear Wood by the Arcan Shear Test. Holzforschung, No. 63/2009.

Discussion

The paper was presented by T Ehrhart

S Franke commented that the test did not consider different laminate thicknesses but only focused on the increase of board width. He stated that Beech CLT showed influence of laminate thickness rather than the laminate thickness to width ratio. T Ehrhart asked whether the ratio was kept constant in the Beech CLT tests so that thickness effect could be isolated. S Franke said no. G Schickhofer added that in future standardized procedures for LCT, 20 30 and 40 mm thickness will be available; therefore, in this study 30 mm thickness was used.

H Blass asked about the low G value. G Schickhofer responded that higher G values up to 100 MPa can be used.

P Zarnani commented that the rolling shear test results using the two plate configuration are not pure shear as tension can play a role.

M Flaig commented that the work was well done and agreed with higher values of ~100 MPa for G values. The rolling shear strength of spruce of 1.4 MPa cannot be confirmed with bending test results. G Schickhofer discussed 3 layer CLT has lower strength values possibly due to rolling shear volume effect. Also rolling shear strength should be between 1.2 and 1.5 MPa.

F Lam commented that in CLT bending tests for rolling shear strength, a high speed camera was used to capture the actual failure mode confirming existing tension perpendicular to grain stresses causing cracks that preceded rolling shear like failure. The interaction is complicated and requires more attention. He also commented that the current study for basic rolling strength is valid.

A Universal Approach for Withdrawal Properties of Self-Tapping Screws in Solid Timber and Laminated Timber Products

Andreas Ringhofer*), Graz University of Technology, Institute of Timber Engineering and Wood Technology, www.lignum.at, Inffeldgasse 24, 8010 Graz, Austria

Reinhard Brandner, Graz University of Technology, Institute of Timber Engineering and Wood Technology, www.lignum.at, Inffeldgasse 24, 8010 Graz, Austria

Gerhard Schickhofer, Graz University of Technology, Institute of Timber Engineering and Wood Technology, www.lignum.at, Inffeldgasse 24, 8010 Graz, Austria

*) phone +43 316 873 4614, e-mail andreas.ringhofer@tugraz.at

Keywords: axially loaded self-tapping screws; withdrawal strength; stiffness; solid timber; glued laminated timber; cross laminated timber; universal approach

1 Introduction

Since 25 years modern self-tapping screws are frequently applied in timber engineered structures. Main reasons for their success are a flexible geometry enabling simple and economic installation without pre-drilling as well as a high load-bearing potential in terms of resistance and stiffness if stressed in axial direction. Consequently, they represent an efficient alternative to conventional laterally loaded fasteners such as nails, dowels and bolts.

In general, self-tapping screws are predominately used in solid timber (ST) and laminated timber products such as glued laminated timber (GLT, layers unidirectionally oriented) and cross laminated timber (CLT, layers orthogonally oriented). Their application can be classified as (a) fastener, i.e. transmitting loads in connections between elements, and (b) reinforcement of timber members, i.e. persisting exceedance of internal resistances in timber's weak directions, e. g. stresses perpendicular to grain or shear. In the design of primary axially loaded screws following failure scenarios have to be distinguished: (i) steel failure in tension and compression, (ii) pull-through failure of the screw head, (iii) withdrawal failure of the threaded part of the screw and (iv) block shear failure of a group of screws. Concentrating on single screw performance, we focus further on (iii) the withdrawal behaviour of self-tapping screws as design criteria influenced by the composite action between screw and timber and hence defined by timber properties and geometrical conditions.

Withdrawal properties were analysed so far e. g. in Blass et al. (2006), Frese and Blass (2009), Pirnbacher et al. (2009) or Hübner (2013). However, their main focus was rather on withdrawal strength f_{ax} than on stiffness, whereby investigations comprised primary solid timber and derived models constitute empirical regression functions considering a large number of influencing parameters. Even though their high predictive quality, these models are in general only applicable for the timber product tested and within the overall scope of their investigations. Transferring them to other timber products may cause unreliable results. Especially the complex lay-up of CLT as given in Fig. 1, including different layer orientations and the possibility of gaps, requires a comprehensive treatment and thus additional model parameters.

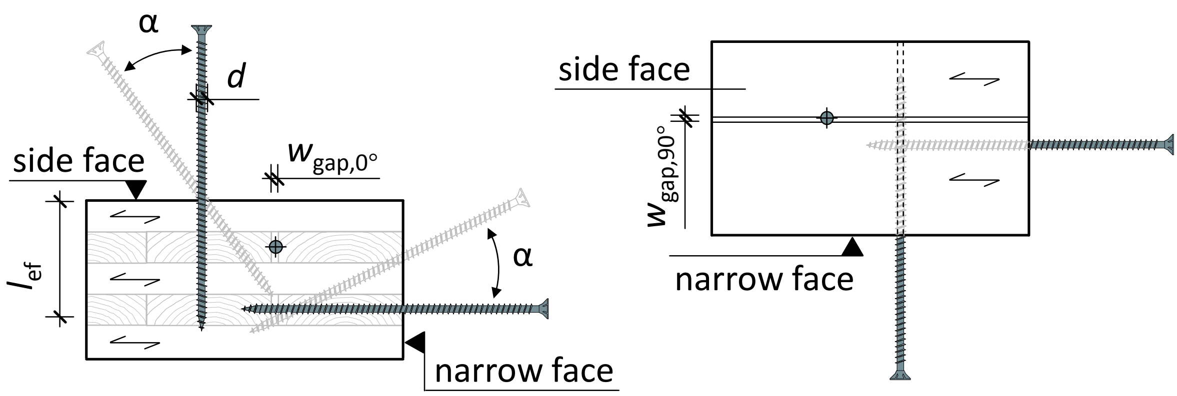

Figure 1. Essential influencing parameters of axially loaded screwed connections in CLT.

Uibel and Blass (2007) were the first who developed a prediction model for determining the withdrawal capacity R_{ax} of axially loaded screws situated in the side and narrow faces of CLT elements. Their function covers implicitly a reduction in strength caused by the possibility of screw insertion in gaps (gap width w_{gap}; average, unsystematic investigated range 0.5 to 2.0 mm) and intermediate zones of two layers with different axis-to-grain angles α. Although again a high agreement between model predictions and test results is given, two aspects concerning their approach are worth being discussed: first, α was limited to α_i = {0 °; 90 ° and 0|90 ° for intermediate zones} restricting the scope in applying the model to some extent. Second and as consequence of the aforementioned unsystematic variation in gap width, a direct relationship between f_{ax} and the type, number and width of gaps cannot be determined.

With regard to K_{ser} herein defined as the screw's withdrawal stiffness, only the prediction model published by Blass et al. (2006) and a further approach given e. g. in ETA-12/0062 (2012) have been found so far. In fact, both models differ regarding type and manipulation of input parameters. Based on them significantly different predictions for K_{ser} are observed. Furthermore, the aforementioned characteristics of laminated timber products with possible influence on K_{ser} are not considered.

Motivated by derived open questions and restricted parameter variation in previous studies, several additional investigations on the withdrawal behaviour of axially loaded self-tapping screws in laminated timber products within the last years, e.g. by Reichelt (2012), Bratulić (2012), Grabner (2013), Ringhofer et al. (2013,2014a,2015), Silva et al. (2014) and Plüss (2014) were made. These studies aimed additionally to explicitly determine and describe the specific impact of parameters on withdrawal properties in form of a systematic variation of parameter characteristics. Amongst others, the main parameters were the number of penetrated layers *N* and their orientation, the timber member's moisture content *u*, the axis-to-grain angle α as well as the number (n_{gap}), width and type of gaps (c. f. Fig. 5) in CLT side and narrow faces. Based on copious findings related, we propose determining withdrawal properties $X = \{f_{ax}; k_{ser}\}$ of self-tapping screws placed in layered timber products (and solid timber) with a new and universal approach conceptually presented in Ringhofer et al. (2014b), see Eq. (1) and (2).

$$X = k_{ax} \cdot k_{sys}(N) \cdot X_{ref} \cdot \left(\frac{\rho}{\rho_{ref}}\right)^{k_\rho}, \text{ with} \tag{1}$$

$$k_\rho = f(\alpha, d),\ k_{ax} = k_{90} f\left(\alpha, k_{gap}\right),\ k_{90} = \frac{X_{90}}{X_0},\ k_{gap} = \begin{cases} 1{,}00 & ST, GLT \\ f(d, w_{gap}) & CLT \end{cases}, \tag{2}$$

with ρ_{ref} and X_{ref} as reference values of density and the specific withdrawal property, the latter determined in one timber layer ($N = 1$, ST, with $\rho = \rho_{ref}$, $\alpha = 90$ ° and $u = 12$ %), k_ρ as power factor including the density influence on *X*, k_{ax} as function considering different α and gap insertion (k_{gap}) and k_{sys} as system value covering the effect of penetrated layers $N > 1$. Due to the withdrawal property's adaptability for the specific situation, Eq. (1) can be universally applied for axially loaded self-tapping screws, irrespective the timber product used and the position the screw is inserted.

In the frame of this paper, we show and discuss the background and derivation of these *k*-values (or *k*-functions). Consequently, we verify them in form of Eq. (1) with results from selected test series usually not applied for calibration of model parameters. Beside its general suitability for modelling of connections and reinforcements as well as for verification of experimental results, we apply Eq. (1) also for determining an equation for the characteristic withdrawal strength with the potential to be implemented in design standards.

2 Materials and Methods

2.1 Materials

Tab. 1 shows a brief overview of test series used for calibrating model parameters and verifying of the approach in Eq. (1). The whole database, classified into the varied timber products (all in Norway spruce, *Picea abies*) and parameters, comprises about 8,000 datasets (82 single test series) for withdrawal strength f_{ax} and about 5,500 datasets (107 single test series) for withdrawal stiffness k_{ser}. In addition, Tab. 2 shows the investigated parameters and their ranges.

Table 1. Overview of investigated timber products and parameters.

Material	Use	invest. Parameters	rounded Number of Tests n (before outlier treatment)	
			strength f_{ax}	stiffness k_{ser}
Solid timber (ST)	modelling	d, l_{ef}, α, ρ, u, l_{emb}	5,200	3,400
GLT	verification	d, l_{ef}, α, ρ, u, N	1,700	1,300
CLT side face	verification	d, l_{ef}, α, ρ, u, N, w_{gap}, n_{gap}	800	400
CLT narrow face	verification	d, α, ρ, w_{gap}	500	500

d … outer thread diameter of the screw, l_{ef} … length of inserted threaded part of the screw,
l_{emb} … embedment depth of the inserted threaded part of the screw

Further parameters possibly influencing withdrawal properties and not listed in Tab. 1, such as pre-drilling, different screw test configurations as well as deviating geometries of the fully and partially threaded screws applied, have also been varied within the experimental programme. Investigations done in Pirnbacher and Schickhofer (2007), Pirnbacher et al. (2009), Frese and Blaß (2009) and Ringhofer and Schickhofer (2014) outlined that there is no remarkable influence of these parameters on f_{ax}. Thus, in the analysis these data sets were combined. In case of withdrawal stiffness, results gained by Reichelt (2012) indicate also a negligible effect of pre-drilling on k_{ser}, while a possible influence caused by applying different test configurations has not been investigated so far. Consequently, only tests carried out with a standard push-pull configuration, as shown in Fig. 2, were considered for modelling this property.

Table 2. Investigated parameters (see Tab. 1) and their range.

Param.		Range	
		strength f_{ax}	stiffness k_{ser}
d	[mm]	4, 6, 8, 10, 12	6, 8, 10, 12
l_{ef}	[mm]	2.5d ÷ 15d	2.5d ÷ 39d
α	[°]	0, 12.5, 25, 30, 37.5, 45, 60, 72.5, 90, 45/45, 0/90	0, 30, 45, 60, 90, 45/45, 0/90
ρ_{12}*	[kg/m³]	310 ÷ 621	310 ÷ 621
u	[%]	8.20 ÷ 20.0	8.20 ÷ 20.0
N	[-]	1 ÷ 20	1 ÷ 20
w_{gap}	[mm]	0 | 2 | 4 | 6	0 | 2 | 4 | 6
n_{gap}	[-]	0 | 1 | 2 | 3	0 | 1 | 2 | 3

* density at u = 12 %

2.2 Methods

All experiments summarised in Tab. 1 were performed on two test rigs Dyna Z-25FS (concrete adhesion tester) and LIGNUM-UNI-275 (universal testing device, Zwick GmbH & Co. KG) in accordance to EN 1382 (1999). From each specimen and after testing (about) 4d x 4d x l_{ef} clear wood samples were cut centrically around the screw hole determining density and moisture content. After this specimen were split centrically to evaluate possible influences on the withdrawal properties caused by knots or other growth characteristics.

Deviating from EN 26891 (1991), withdrawal stiffness K_{ser}, as inclination coefficient shown in Fig. 2 (middle), has been determined by a simple regression analysis considering load and displacement recorded in the linear elastic part of the test curve. Following Brandner et al. (2015) and given in Fig. 2 (right), we localised this area by plotting the load increments $F_{i+1} - F_i$ against their related time steps i of our way-controlled loading protocol. Corresponding local displacement measurement has been determined according to Eq. (3):

$$w = \frac{\delta_1+\delta_2}{2} - w(l_{sh}) = \frac{\delta_1+\delta_2}{2} - \frac{\sigma_{ax}}{E} \cdot l_{sh}, \tag{3}$$

with δ_1 and δ_2 as displacements recorded by two LVDTs clamped on the screw shank, l_{sh} as distance between their clamping points and the timber surface, E as the screw's elastic modulus and σ_{ax} as axial stress in the screw's shank.

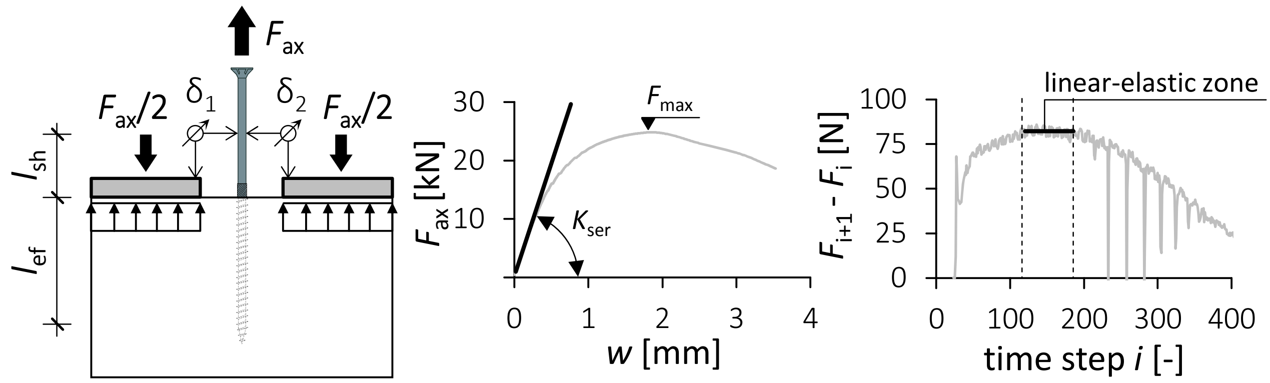

Figure 2. (left) push-pull test configuration including local displacment measurement; (middle) typical test curve of an axially loaded screw, including K_{ser}; (right) load increment vs. time step in accordance to Brandner et al. (2015).

Similar to withdrawal strength $f_{ax} = F_{ax} / (U \cdot l_{ef}) = F_{ax} / (d \cdot \pi \cdot l_{ef})$, with U as outer thread perimeter we determine k_{ser} as withdrawal stiffness per mm displacement and the effective lateral area, see Eq. (4):

$$k_{ser} = \frac{K_{ser}}{d \cdot \pi \cdot l_{ef}} \; [N/mm^3]. \tag{4}$$

Thereby and deviating from the regulations given in EN 1995-1-1 (2008), l_{ef} is defined as inserted threaded part of the screw without its tip, c. f. Fig. 2, i.e. only the effective anchoring length is considered. Withdrawal properties gained from tests with screw tips situated in timber specimen have thus been determined with $l_{ef} = l_p - 1.17d$ according to Pirnbacher et al. (2009) with l_p as the total inserted threaded part of the screw. As introduced in Section 1, our reference withdrawal property X_{ref} is referred to the reference moisture content u = 12 %. Consequently, test data X_u with u differing from 12 % has been corrected by an approach similar to that proposed in Ringhofer et al. (2014a), see Eq. (5):

$$\frac{X_u}{X_{ref}} = \begin{cases} 1.00 \\ 1.00 - k_{mc} \cdot (u - 12) \end{cases}, \text{ for } \begin{cases} 8\,\% \leq u \leq 12\,\% \\ u \geq 12\,\% \end{cases}, \text{ with} \tag{5}$$

k_{mc} = {0.034; 0.016} for {f_{ax}; k_{ser}} as inclination coefficient describing the decrease of withdrawal properties per increasing u. Pirnbacher et al. (2009) observed a positive effect of screw thread embedment on withdrawal strength, i.e. an increase of f_{ax} at α = 90 ° in cases l_{emb} exceeds 2d. Since further investigations carried out by Burgschwaiger (2010) indicate a minor benefit for screws when inserted parallel to grain, we assume that this effect decreases by decreasing α. Results from tests with embedded screw threads (all 2d) were thus corrected according to Eq. (6):

$$\frac{f_{ax,emb}}{f_{ax,ref}} = \begin{cases} 1.00 \\ 1.05 + 1.11 \cdot 10^{-3} \cdot \alpha \end{cases}, \text{ for } l_{emb} \begin{cases} 0\,mm \\ 2d \end{cases}. \tag{6}$$

As investigations on the effect of embedment depth comprised only the withdrawal strength, for k_{ser} a quantitative approach is missing. Consequently, related datasets of k_{ser} were left without correction and used only for relative comparisons in series with the same embedment configuration. Final outlier treatment was done in two steps: after excluding tests on screws penetrating or touching knots, we performed Tukey's criteria for statistical outliers (values outside the inter-quartil-range (IQR) ± 1.5-times the IQR) on logarithmised data sets and by means of box-plots.

3 Discussion of model components

3.1 General notes

Data analysis in Section 3 bases on the general hypothesis of lognormal-distributed (2pLND) densities and withdrawal properties. In fact, there are two reasons for this assumption: (i) 2pLND constraints only positive data values as they are common for physical and mechanical properties such as strength and stiffness (c. f. Brandner, 2012), (ii) standard EN 14358 (2006) as well as recently published investigations on screw withdrawal properties (c. f. Pirnbacher et al., 2009; Frese and Blaß, 2009 and Hübner, 2013) also assume 2pLND for data assessment. Consequently, statistical test procedures and characteristics such as the correlation coefficient according to Pearson, t-Test or confidence intervals of selected statistics were carried out (or determined) for logarithmised data and if required transformed to the linear domain (c. f. Olsson, 2005).

3.2 System factor k_{sys} considering the number of penetrated layers N

Currently, all mentioned regression models determining withdrawal strength consider the density as only material property indicating the fastener's anchoring capacity in timber members. Due to more homogeneous properties and higher 5 % values of density ρ_k in GLT compared to structural timber (ST, N = 1), according to EN 1995-1-1 (2008) and for screws penetrating more than one layer (N > 1), higher 5 %-characteristic withdrawal strengths $f_{ax,k}$ can be applied. Increasing homogenisation with increasing N is expressed by a reduced variability in density while expectation E[ρ] remains constant (c.f. Brandner, 2012; and Ringhofer et al.,2015).

Focusing on this topic, Reichelt (2012) carried out several test series in GLT and CLT specimen with identical lay-ups, varying N but constant E[ρ]. Therein, she not only observed the mentioned increase of $f_{ax,0.05}$ but also a similar behaviour for E[f_{ax}] at N = {3; 6; 20}. Since current regression models are not able to cover this effect, also proved later by Bratulić (2012), we apply a stochastic approach derived in Ringhofer et al. (2015) considering the increase of E[f_{ax}] with increasing N. Corresponding values $k_{sys,mean}$ and $k_{sys,k}$ (for 5 % quantiles) in dependence of N are given in Tab. 3.

Table 3. Values for $k_{sys,mean}$ and $k_{sys,k}$ in dependence of N; according to Ringhofer et al. (2015).

N	1	2	3	4	5	6	7	8	9	10
$k_{sys,mean}$	1.00	1.05	1.07	1.09	1.10	1.11	1.12	1.12	1.13	1.13
$k_{sys,k}$	1.00	1.06	1.10	1.12	1.13	1.14	1.15	1.16	1.17	1.17

Although the withdrawal stiffness is not part of the model in Ringhofer et al. (2015), we propose to apply the same values ($k_{sys,mean}$ in Tab. 1) for this property. Main reasons are: (i) the referenced stochastic approach only depends on density without exclusive calibration to withdrawal strength and (ii) mean values of withdrawal stiffness determined by Reichelt (2012) show a relationship with N similar to that observed for withdrawal strength.

3.3 Power value k_ρ considering the influence of density in case of N = 1

As declared in Eq. (1), we consider the influence of densities differing from ρ_{ref} on withdrawal properties by a power function. Thereby, k_ρ serves as power value determined as gradient of the linear regression model between ln(f_{ax}) vs. ln(ρ), see Eq. (7).

$$ln(X) = k_\rho \cdot ln(Y) + d \rightarrow X = Y^{k_\rho} \cdot exp(d). \tag{7}$$

Current model approaches discussed in Section 1 consider k_ρ as constant value varying from 0.75 to 1.60. This limits their ability covering explicitly influences from input parameters others than density on the relationship between ρ and withdrawal properties f_{ax} and k_{ser}. Ringhofer et al. (2014b) observed a significant impact of α and d on k_ρ for withdrawal strength f_{ax}. Following that we aim on deriving k_ρ as steady function in dependence of these two parameters. This was done by doing linear regression analysis according to Eq. (7) for all withdrawal tests in solid timber, see Tab. 1. After outlier treatment about 5,000 results (56 single test series) for withdrawal strength and about 3,000 results (71 single test series) for withdrawal stiffness remained. Blaß et al. (2006) and own data show, that withdrawal stiffness k_{ser} is also significantly governed by the screw's effective thread length. Consequently, test series were grouped according to their l_{ef}. Results of the regression analysis for withdrawal strength analysing k_ρ vs. α (left, for d = {8; 12 mm}) and d (right for α = {0; 90 °}) are shown in Fig. 3.

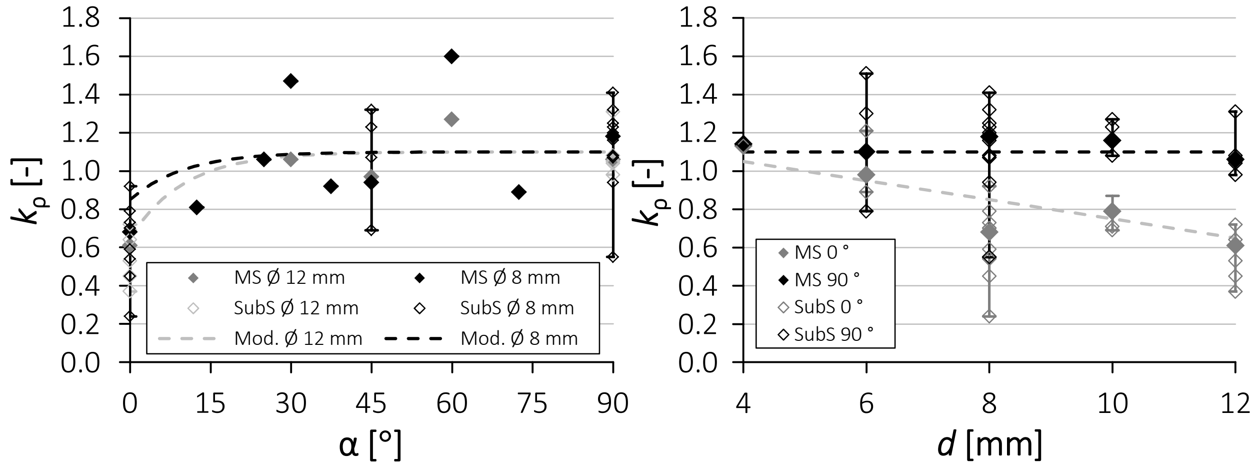

Figure 3. Power value k_ρ vs. insertion angle (left) and outer thread diameter (right) for withdrawal strength f_{ax}; MS = main dataset; SubS = single test series.

Values of k_ρ for main data set (MS) show a comparatively high variability. Nevertheless, decreasing k_ρ with decreasing α as well as a clear negative trend with increasing *d* for α = 0 ° can be observed. By considering the position of error bars, corresponding to the bandwidths of k_ρ and determined for related single test series (SubS), for simplification we conclude a constant behaviour of k_ρ between 30 ° ≤ α ≤ 90 ° followed by a decrease for α < 30 °. This is in fact quite similar to the behaviour of withdrawal strength vs. α as e. g. described in Hübner (2013). In analogy to that, Müller et al. (2015) observed decreasing correlation and inclination coefficient between shear modulus (as a potential indicator for withdrawal strength) and density with decreasing number of annual rings exposed to shear. With regard to the behaviour of k_ρ in Fig. 3, for modelling the relationship between density and withdrawal strength in dependence of α and *d* we apply Eq. (8),

$$f_{ax}: k_\rho = \frac{a \cdot d + b}{exp(\alpha/10)} + k_{\rho,90}, \text{ and } \{a; b; k_{\rho,90}\} = \{-0.05; 0.15; 1.10\}, \quad (8)$$

with $k_{\rho,90}$ as reference value at α = 90 ° and *a* and *b* as model parameters, determined by calibrating with least-squares method. For withdrawal stiffness k_{ser} and applying the same procedure, no clear trend between k_ρ and α, *d* or l_{ef}, but unexpectedly a high variability of the power factor were observed. Possible reasoning is the lower accuracy in measuring and examining k_{ser} compared to withdrawal strength. Consequently we treat k_ρ for withdrawal stiffness as constant value and ignore variation of the aforementioned parameters, see

$$k_{ser}: k_\rho = 0.75 \text{ for } 0\,° \leq \alpha \leq 90\,°, 6 \text{ mm} \leq d \leq 12 \text{ mm and } 10 \text{ mm} \leq l_{ef} \leq 310 \text{ mm}. \quad (9)$$

3.4 Function k_{ax} considering the influence of angle and gap variation

By inserting screws in CLT narrow faces, as illustrated in Fig. 1, a significant relationship between axis-to-grain angle α and the positioning relative to gaps is given. To account for both, we formulate $k_{ax} = f(\alpha, k_{gap})$. Consequently, we analysed the dependencies of withdrawal strength and stiffness on α for screw application in solid timber

(k_{gap} = 1.00 and N = 1). Therefore, both properties were normalised by applying Eq. (8) and (9), as discussed in Section 3.3. As local displacement measurements are not available for all tests, withdrawal stiffness of test series with varying angles were additionally referred to each $k_{ser,mean}$ at α = 90 °. Fig. 4 shows the relationship of both withdrawal properties and α, as combined scatter- and boxplot-graph (notches illustrate the 95 % confidence interval of each median). Values of $f_{ax,mean}$ are widely constant between 15 °≤ α ≤ 90 ° while at α = 0 °, $f_{ax,mean}$ is significantly lower. In analysing the same relationship but for the 5 %-quantiles of f_{ax} (empirically determined and with 2pLND assumption) already at α ≤ 45 ° a distinctive linear decrease in $f_{ax,05}$ is given. In case of withdrawal stiffness, the same but inverse relationship is observed for mean values, while 5 %-quantiles show a slight but steady increasing behaviour for α < 90 °.

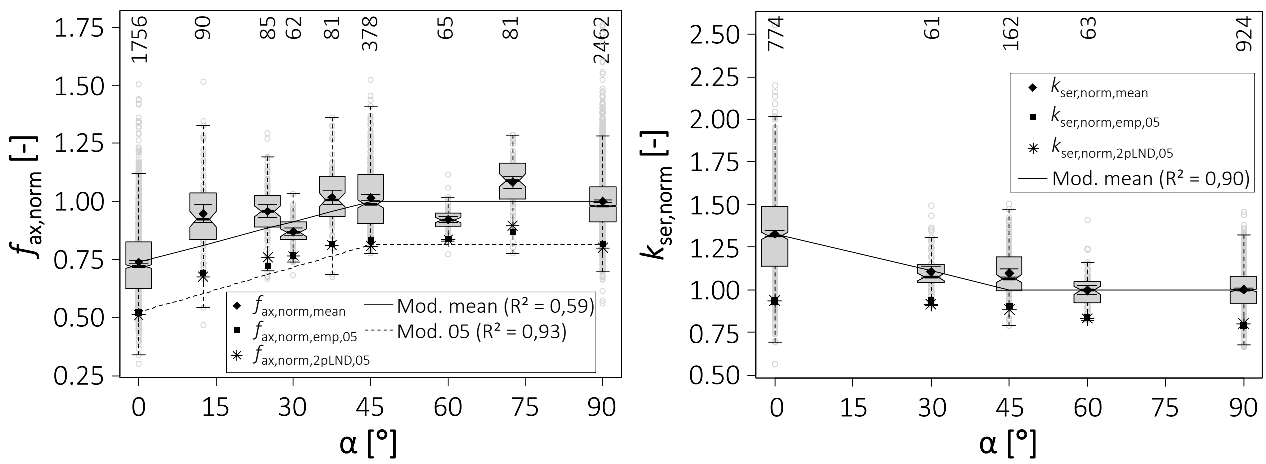

Figure 4. Normalised withdrawal properties (left: strength, right: stiffness) vs. insertion angle α.

Basing on these circumstances and similar to Hübner (2013), we decided to model the relationship between α and both withdrawal properties with a bilinear approach given in Eq. (10) and illustrated in Fig. (4):

$$k_{ax} = \begin{cases} 1.00 & for\ 45\,° \leq \alpha \leq 90\,° \\ c + \frac{1-c}{45} \cdot \alpha & for\ 0\,° \leq \alpha \leq 45\,° \end{cases}, \tag{10}$$

with $c = k_{90}^{-1} = X_0 / X_{90}$ and k_{90} = {1.35; 1.56 and 0.75} for {f_{ax}; $f_{ax,05}$ and k_{ser}}. Differences of k_{90} between withdrawal strength mean and 5 %-values can be explained by an increasing variability of f_{ax} with decreasing α.

3.5 Parameter k_{gap} considering the influence of gap insertion

As analysed in Brandner (2013), current technical assessments of CLT panels include gaps between two boards of one layer with w_{gap} up to 6 mm. In addition, withdrawal properties are also influenced by the gap type (butt joint, BuJ; T-joint, TJ; bed joint, BeJ; c. f. Fig. 5). Brandner et al. (2015) show that an observed loss of withdrawal strength and stiffness for screws inserted in gaps can be simply modelled by the corresponding reduction of the screw's effective lateral area $U_{ef} \cdot l_{ef}$. One possibility to quantify the gap related influence on withdrawal properties of screws randomly situated in CLT narrow faces (same approach also applicable on side face) is now introduced briefly.

We use a multi-modal density function $f_{X,\mathrm{CLT}}(x)$ of the property X, defined as sum of single density functions for specific axis-to-grain angles, gap types and widths. As shown in Eq. (11), they are weighted by their specific probabilities of occurrence p_i which correspond to area ratios A_i, see Fig. 5.

$$f_{X,CLT|w_{gap}}(x) = f_{X,0}(x) \cdot p_0 + f_{X,90}(x) \cdot p_{90} + f_{X,BuJ|w_{gap}}(x) \cdot p_{BuJ|w_{gap}} + f_{X,BeJ|w_{gap}}(x) \cdot p_{BeJ|w_{gap}} + f_{X,TJ|w_{gap}}(x) \cdot p_{TJ|w_{gap}}, \text{ with } \sum p_i = 1. \quad (11)$$

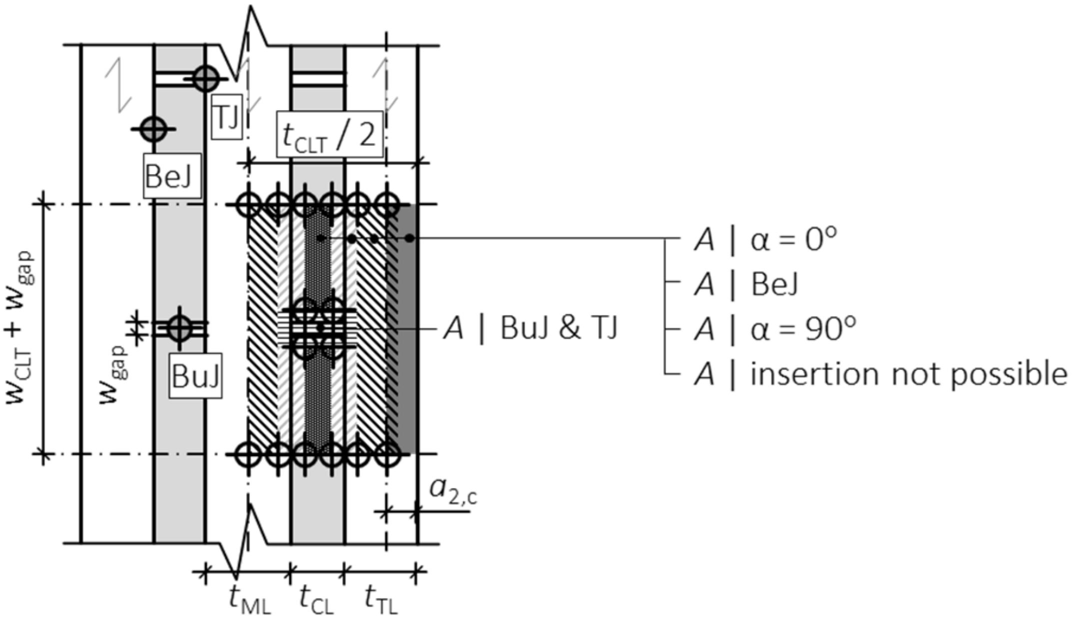

Figure 5. Definition of gap types and illustration of areas related to different axis-to-grain directions and gap types exemplarily for screw insertion normal to the CLT narrow face.

The possible cross-sectional area for screw insertion in CLT narrow face considers a thickness of the CLT-element which is on both sides reduced by the minimum spacing perpendicular to the panel's axis $a_{2,c}$ as determined in Uibel and Blaß (2007), see Fig. 5. All in all, related analysis comprised 16 different lay-ups (N = {3; 5}) of four leading European CLT manufacturers with standard board thicknesses t_l = {20; 30; 40 mm}, board widths w_l = {80; 160; 240 mm}, gap widths w_{gap} = {0; 2; 4; 6 mm} and screw diameters d = {8; 10; 12 mm}. Screw insertion in closed gaps (w_{gap} = 0 mm) was modelled without influence on withdrawal properties, c. f. Brandner et al. (2015). Since screw insertion in T-joints is hardly conceivable in practice, corresponding A_i are assigned to those of butt joints. In dependence of board and gap width, area ratios determined for screws positioned in open gaps (w_{gap} > 0 mm) with d = 8 to 12 mm vary between 12 to 21 % in case of w_l = 80 mm and between 4 to 7 % in case of w_l = 240 mm. Maxima were found for comparatively thin boards with high w_{gap} and d. Enabling practical applicability we thus consider a constant and conservative probability for gap insertion $p_{\mathrm{BuJ\ \&\ TJ}|w_{\mathrm{gap}}}$ of 25 %. With

$$f_{X,CLT|w_{gap}}(x) = f_{X,0}(x) \cdot 0.75 + f_{X,BuJ\&TJ|w_{gap}}(x) \cdot 0.25, \text{ and } CV\left[f_{ax,0}\right] \approx 16\ \%, \quad (12)$$

and a deterministic gap width, it can be shown that both withdrawal properties X should be reduced about 10 – 15 % if α = 0 ° and w_{gap} > 0 mm. For α > 0 °, the influence of k_{gap} on X soon converges to 1.00. Consequently, we propose to modify the parameter c introduced in Section 3.4 for CLT narrow face application as follows:

$c = k_{90}^{-1} \cdot k_{gap,0}$, with $k_{gap,0}$ = {0.85; 0.90; 0.85} for {$f_{ax,mean}$; $f_{ax,05}$; $k_{ser,mean}$}. (13)

4 Model verification

Verification of our model with test results is done in two steps. In the first step, we analyse the suitability of both isolated derived parameters k_ρ and k_{ax}, examined in Section 3 for solid timber, by using the complete model approach in Eq. (1) to estimate with the test results used for parameter determination. Applying Eq. (1), reference values for withdrawal properties and density (ρ_{ref} = {427; 428 kg/m³} for {f_{ax}; k_{ser}}) have thus to be specified. While withdrawal strength $f_{ax,ref}$ can in principle be determined according to one of the regression functions discussed in Section 1, measured withdrawal stiffness significantly deviates from both therein mentioned approaches. Consequently, we decided to use own regression models for $k_{ser,ref}$ and also for $f_{ax,ref}$ in order to minimise inaccuracies caused by reference value determination as far as possible. Justification of this procedure is also argued by conducting a second verification of our models on independent data sets, i.e. data sets not used for calibrating model parameters. Data sets (solid timber, α = 90 °) used for these regression models comprise about 2,500 results for withdrawal strength and about 600 results for withdrawal stiffness. For k_{ser} only tests with local displacement measurements were considered. In case of $f_{ax,ref}$, nonlinear regression analysis was carried out applying an approach similar to that presented in Frese and Blaß (2009), see Eq. (14):

$f_{ax,ref} = e \cdot \rho^f \cdot d^g$, R^2 = 0.57, (14)

with {e; f; g} = {0.014; 1.11; -0.33}. In case of $k_{ser,ref}$, the length of the inserted threaded part of the screw has a significant influence and had thus to be additionally considered, see Eq. (15):

$k_{ser,ref} = h \cdot \rho^i \cdot d^j \cdot l_{ef}^m$, R^2 = 0.85, (15)

with {h; i; j; m} = {24.7; 0.75; –1.70; –0.60}. Comparison of test data with values predicted by Eq. (1) and (2) (whole dataset for solid timber) is shown in Fig. 6. Following conclusions are made: Locations of data points as well as the course of the regression lines given in dependence of α indicate a high conformity (R^2 = {0.65; 0.73} for {f_{ax}; k_{ser}}) of test results with model predictions, especially for withdrawal strength f_{ax}. In case of withdrawal stiffness, we also observe a high accuracy for α = {0; 90 °}, while experimentally determined k_{ser} for α = 45 ° are slightly underestimated. This is in fact caused by the bilinear model considering angle influence on X, which estimates a smaller value for α = 45 °, c. f. Fig. 4.

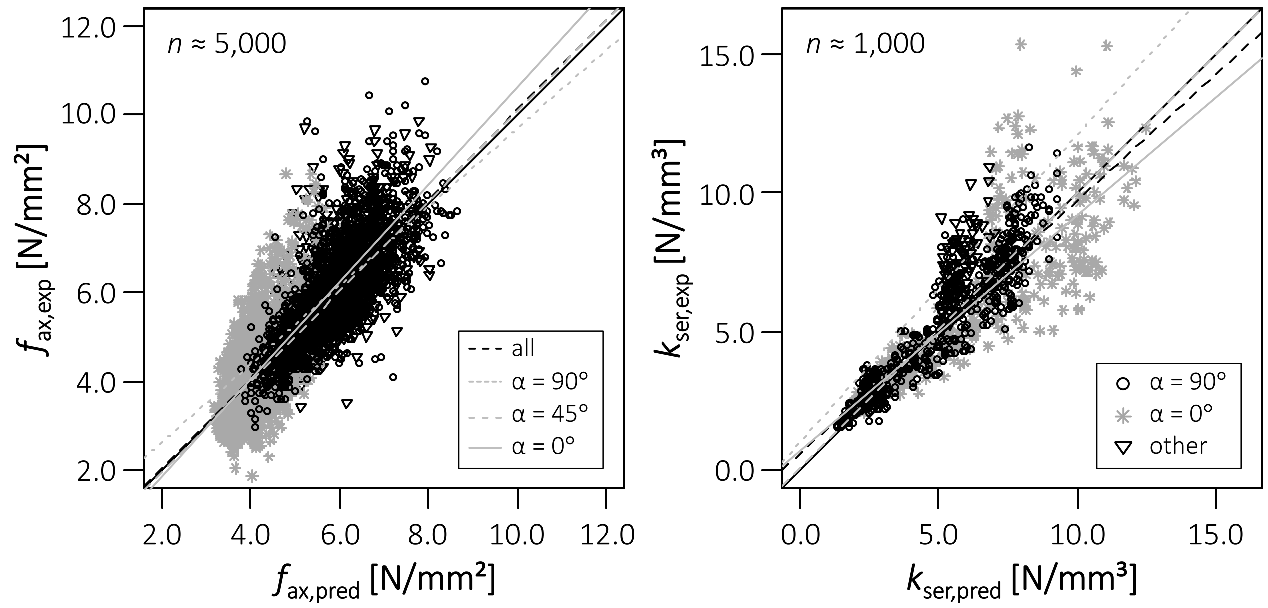

Figure 6. Comparison of test results with predicted values; left: strength; right: stiffness.

In the second step, we apply our universal approach given in Eq. (1) and (2) for estimating withdrawal strength and stiffness of self-tapping screws situated in both products GLT and CLT. Data used for comparison with experimental results was taken from the investigations mentioned in Section 1 and comprises after outlier treatment about 2,800 tests for withdrawal strength and about 1,300 tests for withdrawal stiffness. Since we know the number of layers penetrated by the screws as well as their position in gaps, we consider k_{sys} according to Tab. 3 and k_{gap} in form of the ratio between the effective and the total lateral area of the screw. Following the assumptions made in Section 3.5, T-joints were treated as butt joints while in case of bed joints the corresponding stiffness was averaged considering differences in interacting thread-grain angles.

Fig. 7 consequently compares model predictions with tests results for both properties f_{ax} and k_{ser}. Although the data sets applied for this verification were not used for calibrating the model parameters for Eq. (1), a high correspondence between observed and predicted withdrawal strengths is given ($R^2 = 0.66$). Furthermore, specific regression lines for α = {0; 90 °} indicate high conformity irrespective the position screws were inserted. With regard to withdrawal stiffness, we observe comparatively high deviations of test results from model predictions ($R^2 = 0.55$), especially for data sets with α = 0 ° and gap variation. This is mainly caused by underestimating the size of experimental values related (declared as “gap tests” in Fig. 7, right). Further deviations can be explained by inaccuracies in determining k_{ser} as well as by the constant value for k_ρ (c. f. Eq. (9)), aimed to be adapted in the frame of further considerations. In case of α = 90 °, our approach slightly overestimates measured stiffness but shows higher conformity if compared to α = 0 °.

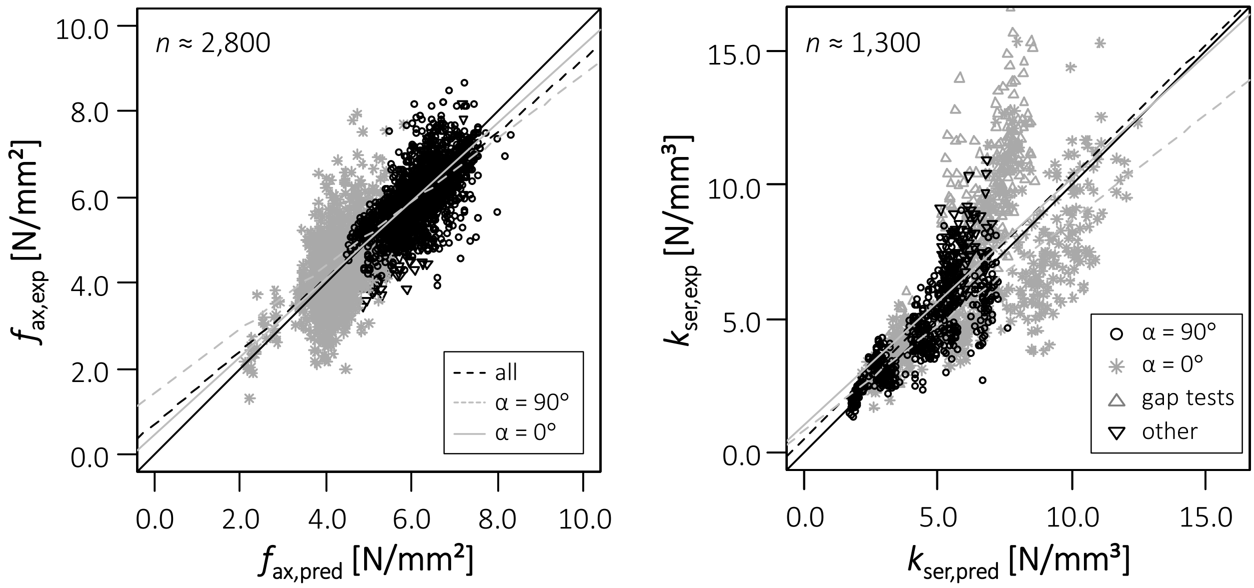

Figure 7. Comparison of test results in GLT and CLT with predicted values; left: strength; right: stiffness.

5 Derivation of a characteristic approach for withdrawal strength

According to the current semi-probabilistic design approach, the ultimate limit state (ULS) design considers characteristic properties of action and resistance. With regard to axially loaded screws, we thus apply Eq. (1) for deriving an approach determining the characteristic (5 %-) value of withdrawal strength in unidirectionally and orthogonally layered laminated timber products and solid timber. Eq. (16) includes the relationship between mean value, variability and 5 %-quantile of a 2pLND variable:

$$x_{0.05} = \exp(\mu_Y + \Phi^{-1}(0.05) \cdot \sigma_Y) = \xi \cdot \mu_X, \tag{16}$$

with μ_Y and σ_Y as mean value and standard deviation of $Y = \ln(X)$, $\Phi^{-1}(0.05)$ as inverse of standard ND for a given quantile p = 5 % and ξ as ratio between the mean value and 5 %-quantile of X. Assuming $[f_{ax}, \rho]$ ~ 2pLND and $\{CV[\rho]; CV[f_{ax}]\}$ = {8 %; 1.5·CV[ρ] = 12 %}, ξ results to {0.874; 0.816}. Consequently, the characteristic withdrawal strength (with model parameters for 5 %-quantile derived in Section 3) is determined according to Eq. (17) and (18):

$$f_{ax,k} = 0.816 \cdot k_{ax,k} \cdot k_{sys,k}(N) \cdot f_{ax,ref,mean} \cdot \left(\frac{\rho_k}{\rho_{ref,k}}\right)^{k_\rho} =$$

$$= k_{ax,k} \cdot k_{sys,k}(N) \cdot f_{ax,ref,k} \cdot \left(\frac{\rho_k}{\rho_{ref,k}}\right)^{k_\rho}, \text{ with} \tag{17}$$

$$f_{ax,ref,k} = 0.013 \cdot \rho_{ref,k}^{1.11} \cdot d^{-0.33},$$

$$k_{ax,k} = \begin{cases} 1.00 & 45° \leq \alpha \leq 90° \\ 0.64 \cdot k_{gap} + \frac{1-0.64 \cdot k_{gap}}{45} \cdot \alpha & 0° \leq \alpha \leq 45° \end{cases}, \tag{18}$$

and k_ρ and $k_{sys,k}$ according to Eq. (8) and Tab. 3. Fig. 8 compares characteristic withdrawal strengths $f_{ax,k}$ (k_{gap} was determined as described in Section 4) estimated by Eq. (17) with empirical 5 %-values of f_{ax} of all single test series the whole dataset ($n \approx 8{,}000$) consists of. Grey coloured data points illustrate test series in solid timber, black ones (symbols differ if N was known or estimated) those in GLT and CLT exclusively used for model verification. With regard to their locations and the course of corresponding regression lines, we can conclude high agreement between model predictions and test data ($R^2 = 0.78$), independent from the material used and further influencing parameters such as the axis-to-grain angle. Sole exceptions are four test series marked as outliers, which are significantly overestimated by our approach. In fact, all of them show unexpected high variabilities of withdrawal strength and density ($CV[X] \geq 20$ %). Since we considered usual variation of density by $CV[\rho] = 8$ % for determining $\rho_{k,i}$ of all test series, given difference between $f_{ax,05,exp}$ and $f_{ax,k}$ can be quantified.

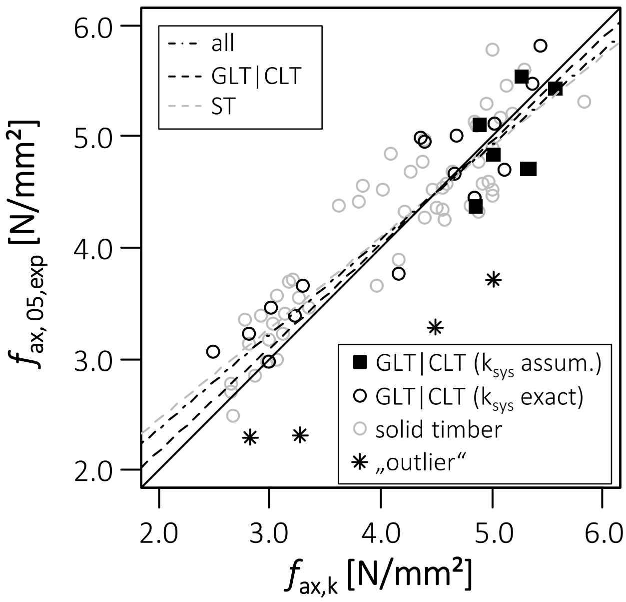

Figure 8. Comparison of empirical 5 %-quantiles of all test series with characteristic (5 %) withdrawal strengths determined according to Eq. (17).

6 Summary and conclusion

In the frame of this paper and basing on copious investigations concerning the axial load bearing behaviour of self-tapping screws placed in laminated timber products, we derived, discussed and verified a new universal approach estimating related withdrawal properties. Therein, multiplicative *k*-factors (or functions) enable the consideration of varying influencing parameters such as the density, the screw's outer thread diameter, the axis-to-grain angle, the number of penetrated layers as well as gap width and type. Consequently, we can estimate withdrawal strength and stiffness irrespective the timber product used and the position the screw is inserted. In addition, we used this model to derive a characteristic approach for withdrawal strength and verified it again with experimental data concluding high conformity. For practical application with random gap insertion we propose to determine $f_{ax,k}$ as given in Eq. (19) in simplified form:

$$f_{ax,k} = k_{ax,k} \cdot k_{sys,k}(N) \cdot f_{ax,ref,k} \cdot \left(\frac{\rho_k}{\rho_{ref,k}}\right)^{k_\rho}, \text{ with} \tag{19}$$

$$k_{ax,k} = \begin{cases} 1.00 & 45° \leq \alpha \leq 90° \\ 0.64 \cdot k_{gap} + \frac{1-0.64 \cdot k_{gap}}{45} \cdot \alpha & 0° \leq \alpha \leq 45° \end{cases}, \tag{20}$$

$$k_{gap,k} = \begin{cases} 0.90 & CLT\ narrow\ face \\ 1.00 & other \end{cases}, k_\rho = \begin{cases} 1.10 & 0° < \alpha \leq 90° \\ 1.25 - 0.05 \cdot d & \alpha = 0° \end{cases}, \tag{21}$$

$$k_{sys,k} = \begin{cases} 1.00 & solid\ timber \\ 1.10 & CLT \\ 1.13 & GLT \end{cases} \quad \text{if } N \geq 3, \tag{22}$$

and $f_{ax,ref,k}$ for α = 90 °, either determined according to Eq. (18), with one of the current existing models discussed in Section 1 or as given in screw manufacturers' European Technical Assessments (ETAs). Although, we implicitly consider gap influence in CLT narrow faces we still recommend to avoid corresponding screw insertion parallel to grain because of a questionable long-time behaviour which has not been conclusively investigated so far.

With regard to axial stiffness k_{ser} considering displacements of both timber and steel (the inserted threaded part) components, the specific approach derived also covers the effects mentioned before but shows more inaccuracy in prediction, especially in cases of α = 0 °. Consequently, we aim to increase its predictability in the frame of further investigations. Nevertheless, general suitability is given and thus also recommended for consideration in standardisation and assessments.

7 Acknowledgement

The research work within the project 'focus_sts' was financed by the competence centre holz.bau forschungs gmbh and performed in cooperation with the Graz University of Technology, Institute of Timber Engineering and Wood Technology. The project was financed by funds from the Federal Ministry of Economics, Family and Youth, the Federal Ministry of Transport, Innovation and Technology, the Styrian Business Promotion Agency Association and the Province of Styria (A12), the Carinthian Economic Promotion Fund (KWF), the Province of Lower Austria Department of Economy, Tourism and Technology as well as the Business Location Tirol.

8 References

Blaß, H-J, Bejtka, I, Uibel, T (2006) Tragfähigkeit von Verbindungen mit selbstbohrenden Holzschrauben (in German). Bd. 4, Karlsruher Berichte zum Ingenieurholzbau, Karlsruhe: KIT Scientific Publishing.

Brandner, R (2012) Stochastic system actions and effects in engineered timber products and structures. Dissertation, Graz University of Technology, Graz.

Brander, R (2013) Production and Technology of Cross Laminated Timber (CLT): A state-of-the-art report. In: Harris, R, Ringhofer, A, Schickhofer, G (Eds.) Focus Solid Timber Solutions – European Conference on Cross Laminated Timber (CLT), University of Bath, COST Action FP1004, ISBN 1-85790-181-9.

Brandner, R, Ringhofer, A, Grabner, M (2015) Probabilistic Models for the Withdrawal Behaviour of Single Self-Tapping Screws in the Narrow Face of Cross Laminated Timber. Wood Science and Technology (submitted).

Bratulić, K (2012) Alteration of the withdrawal strength of self-tapping screws along the board and over the varying GLT cross section. Master Thesis, Graz University of Technology, Graz.

Burgschwaiger, M (2010) Einfluss der Einbindelänge auf die Ausziehfestigkeit von Teilgewindeschrauben (in German). Bachelor Thesis, Graz University of Technology, Graz.

EN 26891 (1991) Timber structures – Joints made with mechanical fasteners - General principles for the determination of strength and deformation characteristics. (CEN).

EN 1382 (1999) Timber structures – Test methods – Withdrawal capacity of timber fasteners. (CEN).

EN 14358 (2006) Timber structures – Calculation of characteristic 5-percentile values and acceptance criteria for a sample. (CEN).

EN 1995-1-1+A1 (2008) Eurocode 5: Design of timber structures – Part 1-1: General – Common rules and rules for buildings. (CEN).

ETA-12/0062 (2012): SFS self-tapping screws WR. Austrian Institute of Construction Engineering (OIB).

Frese, M, Blaß, H-J (2009) Models for the calculation of the withdrawal capacity of self-tapping screws. Meeting 42 of the Working Commission W18-Timber Structures, CIB, Dübendorf (Switzerland), paper CIB-W18/42-7-3.

Grabner, M (2013) Einflussparameter auf den Ausziehwiderstand selbstbohrender Holzschrauben in BSP-Schmalflächen (in German). Master Thesis, Graz University of Technology, Graz.

Hübner, U (2013) Withdrawal strength of self-tapping screws in hardwoods. Meeting 46 of the Working Commission W18-Timber Structures, CIB, Vancouver (Canada), paper CIB-W18/46-7-4.

Müller, U, Ringhofer, A, Brandner, R, Schickhofer, G (2015) Homogeneous shear stress field of wood in an Arcan shear test configuration measured by means of electronic speckle pattern interferometry: description of the test setup. Wood Science and Technology, DOI 10.1007/s00226-015-0755-3, (in press).

Olsson, U (2005) Confidence Intervals for the Mean of a Log-Normal Distribution. Journal Statistics Education, Volume 13, Issue (1), pp. 1-8.

Pirnbacher, G, Schickhofer, G (2007) Schrauben im Vergleich – eine empirische Betrachtung (in German). 6. Grazer Holzbau-Fachtagung (6. GraHFT'07), Graz (Austria).

Pirnbacher, G, Brandner, R, Schickhofer, G (2009) Base parameters of self-tapping screws. Meeting 42 of the Working Commission W18-Timber Structures, CIB, Dübendorf (Switzerland), paper CIB-W18/42-7-1.

Plüss, Y (2014) Prüftechnische Ermittlung des Tragverhaltens von Schraubengruppen in der BSP-Schmalfläche (in German). Master Thesis, Graz University of Technology, Graz.

Reichelt, B (2012) Einfluss der Sperrwirkung auf den Ausziehwiderstand selbstbohrender Holzschrauben – Eine vergleichende Betrachtung zwischen BSP und BSH (in German). Master Thesis, Graz University of Technology, Graz.

Ringhofer, A, Ehrhart, T, Brandner, R, Schickhofer, G (2013) Prüftechnische Ermittlung weiterer Einflussparameter auf das Tragverhalten der Einzelschraube in der BSP-Seitenfläche (in German). Research Report, holz.bau forschungs gmbh, Graz University of Technology, Graz.

Ringhofer, A, Grabner, M, Silva, C, Branco, J, Schickhofer, G (2014a) The influence of moisture content variation on the withdrawal capacity of self-tapping screws. Holztechnologie, Volume 55, Issue (3), pp. 33-40.

Ringhofer, A, Grabner, M, Brandner, R, Schickhofer, G (2014b) Die Ausziehfestigkeit selbstbohrender Holzschrauben in geschichteten Holzprodukten (in German). Doktorandenkolloquium Holzbau "Forschung und Praxis", Stuttgart (Germany).

Ringhofer, A, Schickhofer, G (2014) Influencing parameters on the experimental determination of the withdrawal capacity of self-tapping screws. 13th World Conference on Timber Engineering (WCTE), Quebec (Canada).

Ringhofer, A, Brandner, R, Schickhofer, G (2015) Withdrawal resistance of self-tapping screws in unidirectional and orthogonal layered timber products. Materials and Structures, Volume 48, Issue (5), pp. 1435-1447.

Silva, C, Ringhofer, A, Branco, J, Lourenco, P-B, Schickhofer, G (2014) Influence of moisture content and gaps on the withdrawal resistance of self-tapping screws in CLT. 9th Congresso Nacional de Mecânica Experimental, Aveiro (Portugal).

Uibel, T, Blaß, H-J (2007) Edge joints with dowel type fasteners in cross laminated timber. Meeting 40 of the Working Commission W18-Timber Structures, CIB, Bled (Slovenia), paper CIB-W18/40-7-2.

Discussion

The paper was presented by G Schickhofer

H Blass commented and discussed about the usefulness of K_{ser} (screw's withdrawal stiffness) as K_{ser} is very much dependent on test configuration. G Schickhofer agreed as the test configuration dependency of stiffness is different from that of strength. R Jockwer commented that there are discussions in EC5 about test configuration. G Schickhofer agreed that the availability of a standardized test configuration would be good.

S Winter commented that he did not doubt the accuracy of the equations but they should be further simplified for practising engineers. G Schickhofer disagreed as there are so many products but the equation has three main variables for consideration.

H Stamatopoulos commented that withdrawal stiffness had more factors affecting the values.

P Zarnani asked about different screw manufacturers. G Schickhofer answered that different screws should have little effect in terms of the values. T Tannert commented that some believe in Canada that the design method for self-tapping wood screws should be extended to all types of screws. He asked whether the model fits to other data or other types of screws. G Schickhofer answered that this would be a good idea.

A Salenikovich agreed that diameter mattered and not the product type and that the difference between self-tapping and non self-tapping screws is small. H Blass stated that this would depend on density of the wood as some species would need predrilling.

K Malo supported that withdrawal stiffness would be important for vibration cases.

M Flaig commented that using a probabilistic approach about gap influence would be valuable. F Lam commented that angle application of screws would lessen the influence of gaps. G Schickhofer agreed.

Characteristic withdrawal capacity and stiffness of threaded rods

Haris Stamatopoulos and Kjell Arne Malo
Norwegian University of Science and Technology (NTNU), Trondheim, Norway

Keywords: Threaded rod, withdrawal capacity, withdrawal stiffness, embedment length, rod-to-grain angle, withdrawal strength parameter

1 Introduction

Long threaded rods show high withdrawal capacity and stiffness and thus they may be used in order to realize strong and stiff connections for timber structures. In comparison to dowel-type connectors, they have no initial soft response and no initial slip. In comparison to glued-in-rods they are less prone to construction quality issues, less brittle and offer greater protection against high temperatures (Mischler and Frangi 2001). Due to their length, their withdrawal capacity and stiffness are not significantly affected by local defects. Furthermore, a high degree of pre-fabrication is possible and hence easy and fast erection on site may be achieved.

Over the last years, the vast majority of the research effort has been devoted to the withdrawal capacity of screws with diameters up to 12 mm. The influence of parameters such as the embedment length and the angle between the screw axis and the grain direction has been investigated; see for example (Pirnbacher, Brandner and Schickhofer 2009, Frese and Blaß 2009). On the other hand, the research effort on the withdrawal capacity and also stiffness of threaded rods with diameters up to 20-25mm has not been so intensive and mostly it is limited to rods installed parallel and perpendicular to the grain (Jensen et al. 2011, Jensen et al. 2012, Nakatani and Komatsu 2004, Mori et al. 2008).

Eurocode 5, EC5 (CEN 2004) do not provide guidelines for the estimation of the withdrawal stiffness which is required for the evaluation of the stiffness of connections with threaded connectors (Tomasi, Crosatti and Piazza 2010, Malo and Ellingsbø

2010). Some expressions may be found in technical approvals of screws, but mostly these expressions are valid for screws with relatively small diameters. Moreover, EC5 does not allow the installation of rods in an angle to the grain less than 30° in order to eliminate the risk of splitting failure. However, in practice, it may be desired to install threaded rods in an angle to the grain smaller than 30° (in combination with some sort of reinforcement to prevent splitting failure).

In the present paper, an experimental study on withdrawal of threaded rods embedded in glue-laminated timber (abbr. glulam) elements is presented. The parameters of this study were the embedment length and the angle between the rod axis and the grain direction (with emphasis on angles which are smaller than 30°). Moreover, analytical expressions for the estimation of withdrawal capacity and stiffness are provided. The characteristic withdrawal capacity and the mean withdrawal stiffness were obtained by the experimental results and compared to the analytical estimations.

2 Experimental methods

2.1 Experimental set-up

The experimental set-up for the withdrawal tests is presented in Figure 1. As shown, the loading condition of the specimens was a 'remote' pull-push (i.e. the support was provided in the same plane surface as the entrance of the rod, but at a distance to the rod). A thin steel plate, as shown in Fig. 1d, was placed between the supports and the specimen. The plate was used to counteract bending stresses and prevent tensile splitting failure, while allowing local deformation on the surface of the specimen in the vicinity of the rod. Two displacement transducers were placed next to the supports of the specimen, measuring the relative displacement between the rod and support as shown in Figures 1a, 1c and 1e. The average of these two measurements was used for the displacement. Testing was performed using the loading protocol given in EN 26891:1991 (ISO6891:1983) (CEN 1991).

2.2 Materials

The specimens were cut from glulam beams of Scandinavian class L40c which corresponds to European strength class GL30c (CEN 2013). This type of glulam is fabricated with 45 mm thick lamellas, made of Norwegian spruce (*Picea Abies*). The mean and characteristic density of L40c is ρ_{mean} = 470 kg/m^3 and ρ_k = 400 kg/m^3 respectively. The mean moduli of elasticity, parallel and perpendicular to the grain, are $E_{0.mean}$ = 13000 MPa and $E_{90.mean}$ =410 MPa respectively, and the shear modulus is G= 760 MPa.

For increased homogeneity, all specimens were manufactured such that the rods were inserted in the inner, weaker lamellas of the beams. SFS WB-T-20 (DIBt 2010) steel threaded rods were used. These rods are made according to DIN7998 (DIN 1975). The outer-thread diameter d of the rods is 20 mm and the core diameter, d_c, is 15 mm. According to the manufacturer, the steel grade of the rods is 8.8 and their characteristic tensile capacity is 145 kN.

2.3 Specimens

Prior to rod installation, all specimens were pre-drilled with a diameter equal to d_c. All specimens were conditioned to standard temperature and relative humidity conditions (20°C / 65% R.H.), leading to approximately 12% moisture content in the wood. The parameters of the experimental investigation were the rod-to-grain angle, α, and the embedment length of the rod, l_{ef}. Specimens with 6 different rod-to-grain angles (α = 0, 10, 20, 30, 60 and 90°) and 4 different embedment lengths (l_{ef} = 100, 300, 450, 600 mm) were tested. The series of specimens are denoted Sα-l_{ef}, based on their rod-to-grain angle and embedment length. The width, b, of the glulam beams and consequently of all specimens was equal to 140 mm. A full description of the specimens' dimensions can be found in (Stamatopoulos and Malo 2015b).

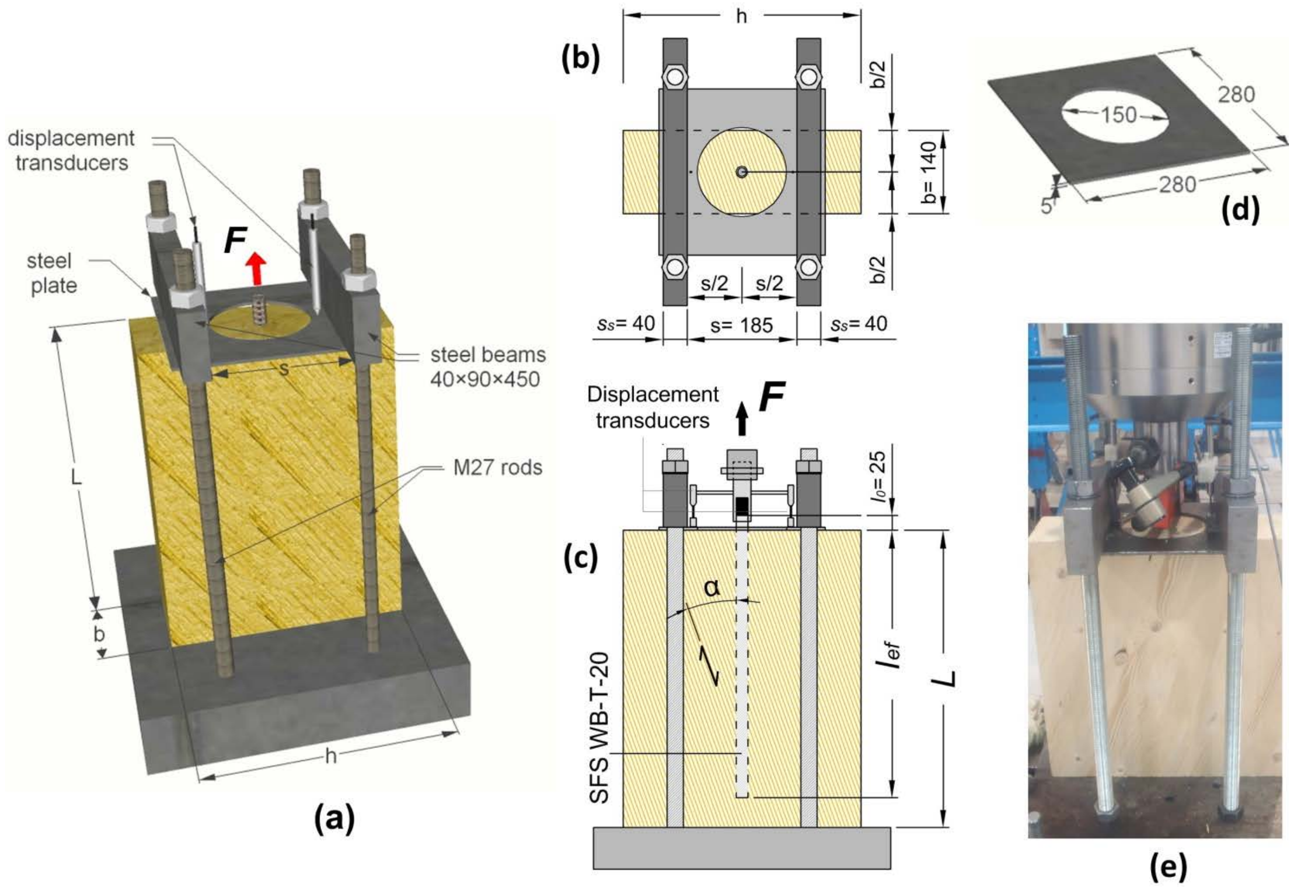

Figure 1. Experimental set-up: (a) 3D representation, (b) plan view, (c) side view, (d) steel plate and (e) photo

3 Eurocode 5

According to EC5 (for screws with d > 12 mm) the characteristic withdrawal capacity, $F_{ax.Rk}$, is given by (the expression is re-arranged):

$$F_{ax.Rk} = n_{ef} \cdot f_{ax.\alpha.k} \cdot d \cdot l_{ef} \tag{1}$$

The parameter n_{ef} is the effective number of screws and equal to $n_{ef} = n^{0.9}$, where n is the number of screws acting together in a connection. The withdrawal strength parameter, $f_{ax.\alpha.k}$, is given by:

$$f_{ax.\alpha.k} = \frac{f_{ax.90.k}}{1.2 \cdot \cos^2\alpha + \sin^2\alpha} \cdot \left(\frac{\rho_k}{\rho_a}\right)^{0.8} \quad (\alpha \geq 30°) \tag{2}$$

where $f_{ax.90.k}$ is the withdrawal strength parameter perpendicular to the grain which must be experimentally determined, for the associated density ρ_a. EC5 provides no guidelines for the estimation of withdrawal stiffness.

In the technical approval of WB-T-20 rods, Z-9.1-777 (DIBt 2010), the following expression is provided for the withdrawal strength parameter (unit MPa and kg/m^3):

$$f_{ax.k} = 70 \cdot 10^{-6} \cdot {\rho_k}^2 \quad (45° \leq \alpha \leq 90°) \tag{3}$$

4 Analytical model

Analytical estimations can be obtained by use of the concept of the classical Volkersen theory (Volkersen 1938), applied for axially loaded connectors (Jensen et al. 2001). This model has initially been developed assuming that all shear deformation occurs in an infinitely thin shear layer, while the connector and surrounding wood are assumed to be in states of pure axial stress. The shear stress-displacement behaviour (τ - δ) of the shear layer is approximated by a linear constitutive law, which is a reasonable approximation for glued-in-connectors.

In the case of screwed-in connectors, however, it is more convenient to assume a bi-linear constitutive law, because these connectors are by far less brittle than glued-in connectors and their post-elastic behaviour should not be omitted. The bi-linear constitutive law is presented in Figure 2. The bi-linear idealization separates the curve in two distinct domains; the linear elastic domain and the fracture domain. These domains are characterized by the equivalent shear stiffness parameters Γ_e and Γ_f, which are the slopes of the two branches of the bi-linear constitutive law. The advantage of this method is that, apart from the withdrawal capacity and stiffness, it also allows the estimation stress and displacement distributions for any given withdrawal force level. Thus, an analytical estimation of the force-displacement curve can be obtained. Note that all shear deformation is assumed to occur in a shear zone of finite dimensions. A full description of this method is given in (Stamatopoulos and Malo 2015a).

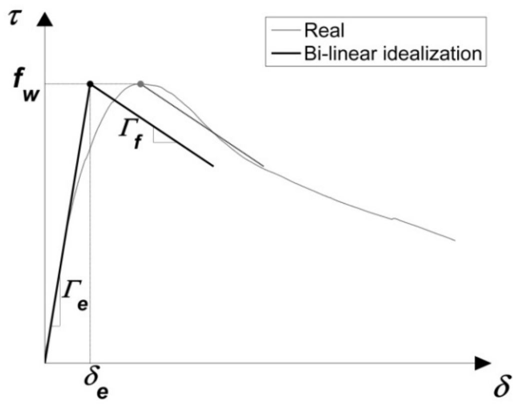

Figure 2. Bi-linear approximation of τ-δ curve

The withdrawal stiffness, K_w, and the characteristic withdrawal capacity, $F_{ax.Rk}$, are provided by the following expressions (Stamatopoulos and Malo 2015a, Jensen et al. 2001):

$$K_w = \pi \cdot d \cdot l_{ef} \cdot \Gamma_e \cdot \frac{\tanh\omega}{\omega} \tag{4}$$

$$\frac{F_{ax.\alpha.Rk}}{d \cdot l_{ef} \cdot f_{ax.\alpha.k}} = \frac{\sin(m \cdot \omega \cdot \lambda_u)}{\omega \cdot m} + \frac{\tanh\{(1-\lambda_u) \cdot \omega\} \cdot \cos(m \cdot \omega \cdot \lambda_u)}{\omega} \tag{5}$$

Note that these expressions are valid for pull-push or pull-shear loading conditions, but not for the pull-pull loading condition. The parameter *m* has been introduced as:

$$m = \sqrt{\Gamma_f / \Gamma_e} \tag{6}$$

This parameter is a measure of the brittleness of the shear zone. In the limits, $m \to 0$ indicates perfect plastic post-elastic behaviour, while $m \to \infty$ indicates totally brittle behaviour. The parameters ω and β have been defined as follows:

$$\omega = \sqrt{\pi \cdot d \cdot \Gamma_e \cdot \beta \cdot {l_{ef}}^2} \tag{7}$$

$$\beta = \frac{1}{A_s \cdot E_s} + \frac{1}{A_w \cdot E_{w.\alpha}} \tag{8}$$

where E_s and $E_{w.\alpha}$ are the moduli of elasticity of steel and wood (as function of α), respectively. The core cross-sectional area of the rod is $A_s = \pi \cdot d_c^2/4$ and A_w is the area of wood subjected to axial stress. $E_{w.\alpha}$ may be estimated by the Hankinson formula and A_w by an effective area, confer (Stamatopoulos and Malo 2015b). The parameter λ_u is a dimensionless length parameter which expresses the percentage of the embedment length (at failure), in which post-elastic behaviour takes place and it can be determined by the diagram in Figure 3.

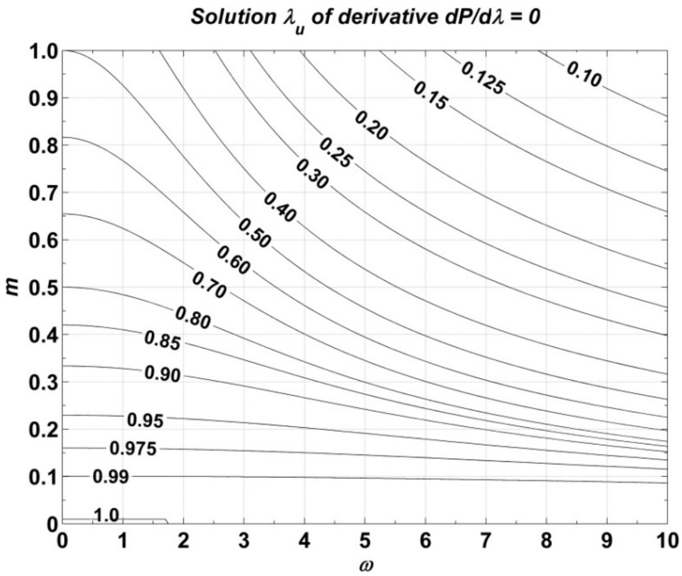

Figure 3. Diagram for the determination of parameter λ_u

The parameters Γ_e (in MPa/mm) and m are provided as functions of α, by the following expressions(Stamatopoulos and Malo 2015a):

$$\Gamma_{e.\alpha} = \frac{9.35}{1.5 \cdot \sin^{2.2}\alpha + \cos^{2.2}\alpha} \tag{9}$$

$$m_\alpha = \frac{m_0}{(m_0/m_{90}) \cdot \sin\alpha + \cos\alpha} = \frac{0.332}{1.73 \cdot \sin\alpha + \cos\alpha} \tag{10}$$

Finally, $f_{ax.\alpha.k}$ can be calculated by Equation (2).

5 Results and discussion

5.1 Withdrawal stiffness

The experimentally derived mean values of K_w and the coefficient of variation (abbr. C.o.V.) for all embedment lengths and rod-to-grain angles are summarized in Table 1. The sample size for each sub-set of parameters (l_{ef} and α) was 5 tests. The analytical estimations are compared to the experimental results in Figure 4, where K_w is plotted as function of l_{ef} for all rod-to-grain angles. Results from finite element simulations are also provided in Figure 4. The finite element model has been presented in detail in (Stamatopoulos and Malo 2015b).

Table 1. Experimentally recorded mean withdrawal stiffness (units kN/mm) and C.o.V.

	l_{ef} =100 mm	l_{ef} =300 mm	l_{ef} = 450 mm	l_{ef} = 600 mm
	$K_{w.mean}$ /C.o.V.	$K_{w.mean}$ /C.o.V.	$K_{w.mean}$ /C.o.V.	$K_{w.mean}$ /C.o.V.
$\alpha = 0^{\circ}$	54.6 / 0.16	121.0 / 0.30	121.8 / 0.13	128.6 / 0.17
$\alpha = 10^{\circ}$	56.0 / 0.27	137.3 / 0.19	132.8 / 0.22	131.1 / 0.05
$\alpha = 20^{\circ}$	53.8 / 0.23	125.9 / 0.20	121.7 / 0.16	128.0 / 0.14
$\alpha = 30^{\circ}$	42.6 / 0.27	111.2 / 0.11	100.3 / 0.10	114.8 / 0.11
$\alpha = 60^{\circ}$	36.6 / 0.33	73.5 / 0.17	90.1 / 0.09	(-)[1]
$\alpha = 90^{\circ}$	29.0 / 0.31	61.4 / 0.11	66.6 / 0.16	(-)[1]

[1] Experiments were not performed for l_{ef} = 600mm and $\alpha = 60^{\circ}, 90^{\circ}$

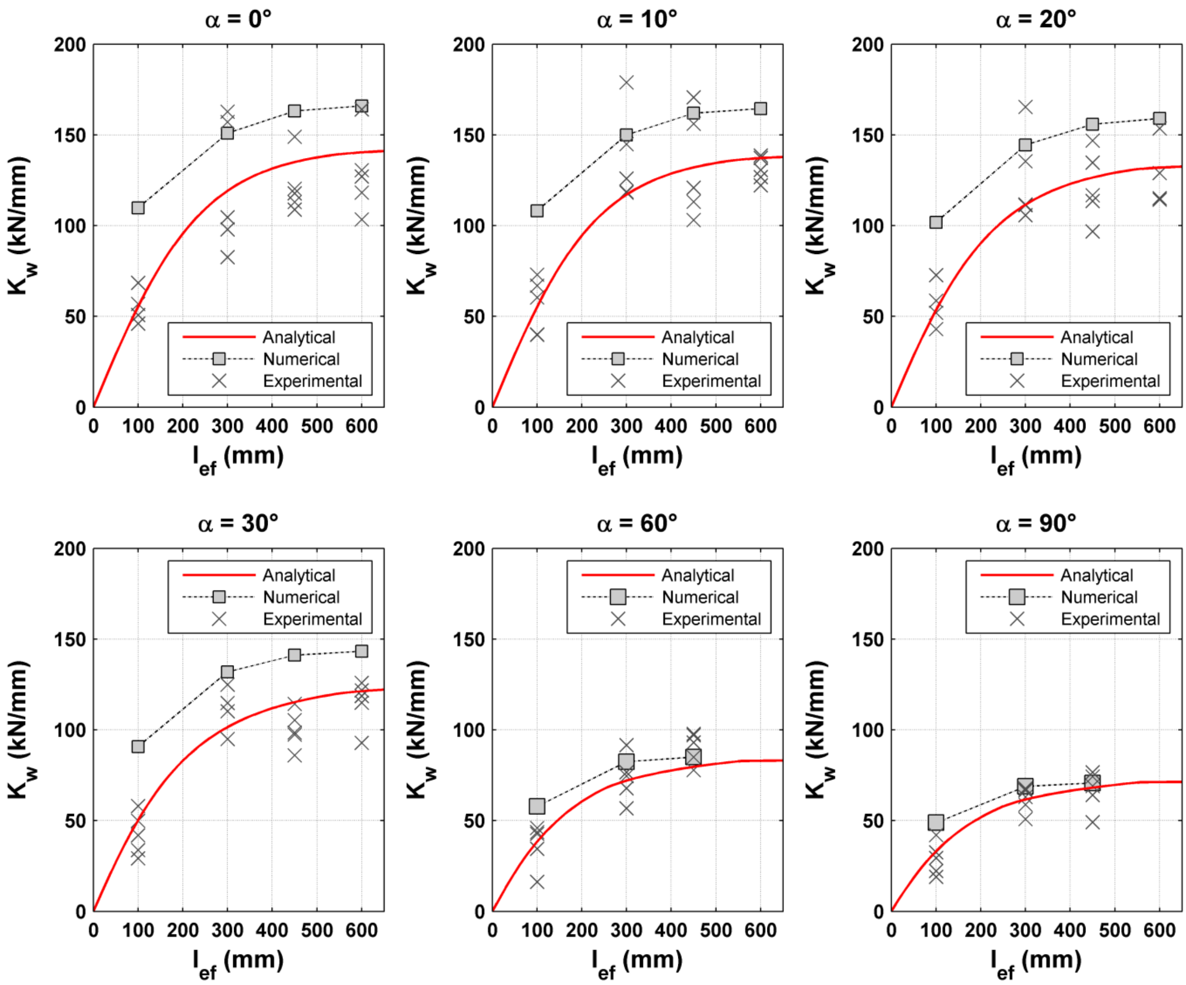

Figure 4. Withdrawal stiffness as function of l_{ef}

It is clear from the experimental results that the specimens exhibited high stiffness, especially for small rod-to-grain angles. As shown in Figure 4, the increase of withdrawal stiffness due to increasing embedment length becomes gradually smaller as the embedment length increases. This is estimated both analytically and by numerical results and validated experimentally. In fact, the experimental results for these threaded rods suggest that K_w has no correlation with the embedment length if $l_{ef} \geq$ 300 mm. This is especially true for small rod-to-grain angles. Finally, according to experimental observations, no initial slip occurred if the threaded steel coupling parts of the set-up were tightly fastened.

5.2 Withdrawal strength parameter

The withdrawal strength parameter was calculated for all angles from the experimental results for all specimens. The mean values, the C.o.V., the median and the 5%-fractile characteristic values are provided in Table 2. It should be noted that the requirements of EN1382 (CEN 1999) for the determination of $f_{ax.\alpha}$ have not been met with respect to the embedment length and the edge distances. The characteristic values are calculated according to EN14358 (CEN 2006). In comparison to the experimental results presented in the previous Section, some additional experimental results have been used in Sections 5.2 and 5.3.

Table 2. Values of the withdrawal strength parameter $f_{ax.\alpha}$

		$fax.\alpha = F_{max} / d \cdot l_{ef}$ (MPa)			
	Number of tests	*Mean*	*C.o.V.*	*Median*	*5% - fractile*
$\alpha = 0°$	25	13.81	0.152	13.79	10.19
$\alpha = 10°$	22	14.14	0.168	13.90	10.06
$\alpha = 20°$	20	15.70	0.145	16.05	11.46
$\alpha = 30°$	20	15.16	0.136	15.52	11.47
$\alpha = 60°$	16	15.17	0.124	15.75	11.50
$\alpha = 90°$	20	14.88	0.108	15.04	11.92

* Note: the requirements of EN 1382 with respect to l_{ef} and the edge distances were not met for all specimens

The variability decreases with increasing angle. The ratio $f_{ax.90.k} / f_{ax.0.k}$ is equal to 1.17 which is very close to the ratio 1.20 according to Equation (2). Moreover, the withdrawal strength for rod-to grain angles 0° and 10° is significantly smaller than the withdrawal strength for greater angles. The experimental results together with the estimations by Equations (2) and (3) are presented in Figure 5.

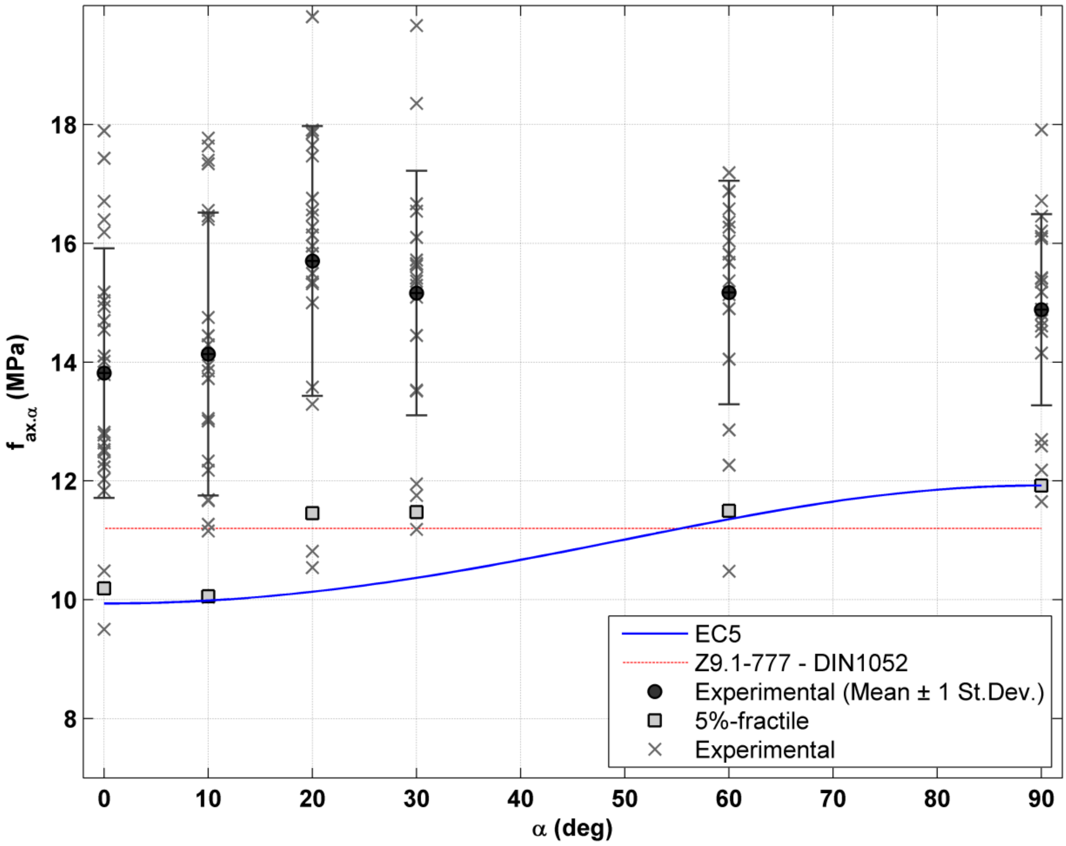

Figure 5. Withdrawal strength parameter as function of α

5.3 Withdrawal capacity

All specimens with $l_{ef} \leq 450$ mm failed due to withdrawal of the rod. In a few specimens with l_{ef} = 450 mm yielding of the rod was observed, however the increasing force due to steel hardening led to withdrawal failure prior to steel fracture. In the vast majority of the specimens with l_{ef} = 600 mm yielding of the rod was observed. All 5 specimens in S20-600 and S30-600 series and 3 out of 5 specimens in S10-600 series failed due to steel fracture (none in the S0-600 series). These values have been excluded from the calculation of $f_{ax.\alpha}$ in the previous Section. Yielding and steel fracture of the rods occurred at load levels which were significantly higher than those predicted by the nominal yield and ultimate strength properties of steel. The observed increase in strength of the steel can probably be attributed to steel hardening due to thread rolling.

The mean experimentally recorded capacities and their C.o.V. as well as the characteristic capacity for all embedment lengths and rod-to-grain angles are summarized in Table 3. The characteristic capacities have also been calculated according to EN 14358. A minimum C.o.V equal to 0.05 was used to calculate the characteristic capacities, in cases where C.o.V. was smaller.

The experimentally recorded capacities, together with the EC5 and the analytical estimations are plotted as function of the embedment length for all rod-to-grain angles in Figure 6. The withdrawal strength parameter was determined by Equation (2) and by setting $f_{ax.90.k}$ = 11.92 MPa (from Table 2). Note that Equation (2) has been used also outside its valid range for α.

Table 3. Experimentally recorded withdrawal capacity for all specimens (in kN)

	l_{ef} =100 mm (10 tests)	l_{ef} =300 mm (5 tests)	l_{ef} = 450 mm (5 tests)	l_{ef} = 600 mm (5 tests)
	$F_{ax.Rm}$ / C.o.V. / $F_{ax.Rk}$	$F_{ax.Rm}$ / C.o.V. / $F_{ax.Rk}$	$F_{ax.Rm}$ / C.o.V. / $F_{ax.Rk}$	$F_{ax.Rm}$ / C.o.V. / $F_{ax.Rk}$
α = 0°	26.2 / 0.14 / 19.6	89.7 / 0.12 / 66.8	130.2 / 0.24 / 66.7	161.6 / 0.05 / 141.8
α = 10°	25.8 / 0.18 / 17.9	99.8 / 0.10 / 76.9	127.5 / 0.14 / 88.7	173.1[1a] / (-) / (-)
α = 20°	30.2 / 0.19 / 19.5	98.7 / 0.11 / 74.3	145.8 / 0.06 / 124.7	175.7/0.01/155.3[1b]
α = 30°	27.9 / 0.13 / 20.9	99.9 / 0.11 / 77.4	144.6 / 0.09 / 115.5	176.7/0.01/156.2[1b]
α = 60°	28.7 / 0.17 / 18.3 [2]	93.6 / 0.12 / 66.9	141.7 / 0.03 / 125.2	(-) [3]
α = 90°	28.0 / 0.12 / 21.7	96.5 / 0.07 / 80.8	139.2 / 0.05 / 121.9	(-) [3]

[1a] Steel and withdrawal failures were observed and thus no characteristic capacity was calculated, [1b] Steel failure, characteristic value calculated with C.o.V = 0.05, [2] 6 tests (instead of 10), have been performed for l_{ef} = 100mm and α = 60°, [3] No experiments performed for l_{ef} = 600mm and α = 60°, 90.

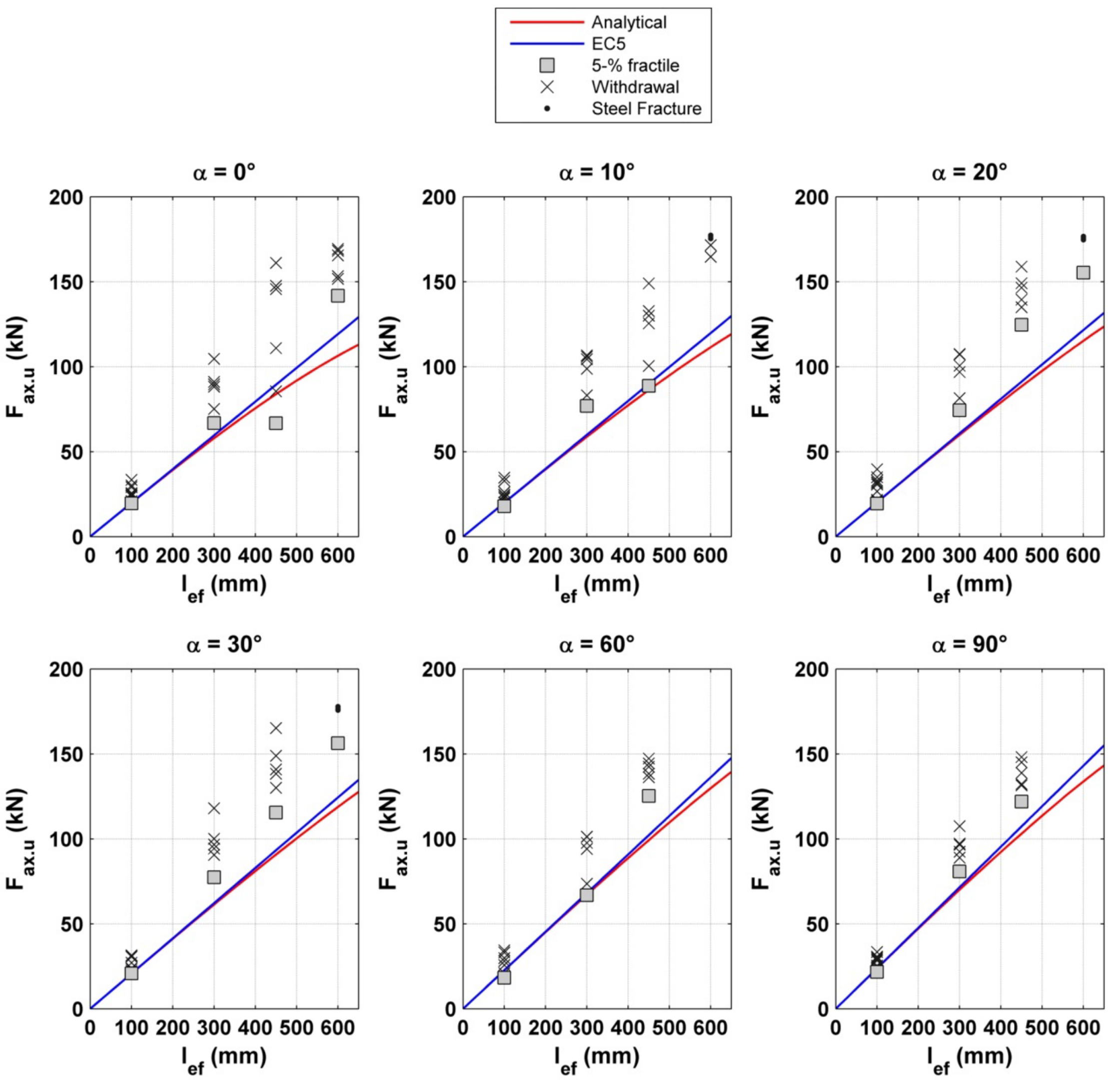

Figure 6. Withdrawal capacity as function of l_{ef}

As shown in Figure 6, Equation (5) results in a nearly linear relation between the capacity and the embedment length and thus the difference between Equations (1) and (5) is small. The estimations by Equations (1) and (5) are generally conservative, especially for $l_{ef} \geq 300$ mm and for $\alpha \geq 20°$. According to the experimental results, the withdrawal capacity of specimens with $\alpha = 20°$ was equally reliable as the capacity of specimens with greater angles. On the other hand, for $\alpha < 20°$ the capacity may be less reliable like in series S0-450 where the evaluated from experiments characteristic capacity was smaller than the analytical prediction.

Finally, it has been reported (Ringhofer and Schickhofer 2014) that the long-term behaviour of axially loaded screws inserted parallel to the grain is very poor. It follows that the long-term behaviour of threaded rods (as function of the rod-to-grain angle and the embedment length) should be further explored.

6 Conclusions

The withdrawal of axially loaded threaded rods with a diameter of 20 mm, screwed into glulam was studied using experimental and analytical methods. The following main conclusions are drawn:

- The withdrawal stiffness and capacity can be estimated by use of a simple analytical procedure, based on the principle of Volkersen model.
- The characteristic withdrawal strength, as estimated by EC5 expression, is on the safe side especially for rod-to grain angles 20° and 30°.
- The characteristic withdrawal strengths for rod-to grain angles 0° and 10° are significantly smaller than the strengths for greater angles.
- The capacity of specimens with a rod-to-grain angle equal to 20° was equally reliable as the capacity of specimens with greater angles.
- Experimental, analytical and numerical results suggest that the increase of withdrawal stiffness due to increasing embedment length becomes gradually smaller as the embedment length increases.
- According to experimental observation, initial slip did not occur when the steel coupling parts of the set-up were tightly fastened.
- Steel fracture of the rods occurred at load levels which were significantly higher than those predicted by the nominal yield and ultimate strength properties of steel.

7 Acknowledgements

The support by The Research Council of Norway (208052) and The Association of Norwegian Glulam Producers, Skogtiltaksfondet and the Norwegian Public Road Administration is gratefully acknowledged. The authors would like to acknowledge the contribution of students Joakim Troller and Roland Falk in the preparation of the experiments.

8 References

CEN, European committee for standardization. 1991. EN 26891:1991 (ISO 6891:1983): Timber structures- Joints made with mechanical fasteners-General principles for the determination of strength and deformation characteristics. Brussels, Belgium.

CEN, European committee for standardization. 1999. EN 1382-1999: Timber structures- - Tests methods - Withdrawal capacity of timber fasteners. Brussels, Belgium.

CEN, European committee for standardization. 2004. EN 1995-1-1:2004: Design of timber structures. Part 1-1: General-Common rules and rules for buildings. Brussels, Belgium.

CEN, European committee for standardization. 2006. EN 14358-2006: Timber structures- Calculation of characteristic 5-percentile values and acceptance criteria of a samle. Brussels, Belgium.

CEN, European committee for standardization. 2013. EN 14080-2013: Timber structures- Glued laminated timber and glued solid timber - Requirements. Brussels, Belgium.

DIBt, Deutsches Institut für Bautechnik. 2010. SFS intec, GmbH., Gewindestangen mit Holzgewinde als Holzverbindungsmittel, Allgemeine bauaufsichtliche Zulassung Z-9.1-777.

DIN, Deutsches Institut für Normung. 1975. DIN 7998:Gewinde und Schraubenenden für Holz-schrauben. Berlin, Germany.

Frese, M. & H. J. Blaß. 2009. Models for the calculation of the withdrawal capacity of self-tapping screws. In *Proceedings of the 42nd CIB-W18 meeting* Dübendorf, Switzerland.

Jensen, J. L., A. Koizumi, T. Sasaki, Y. Tamura & Y. Iijima (2001) Axially loaded glued-in hardwood dowels. *Wood Science and Technology,* 35, 73-83.

Jensen, J. L., M. Nakatani, P. Quenneville & B. Walford (2011) A simple unified model for withdrawal of lag screws and glued-in rods. *European Journal of Wood and Wood Products,* 69, 537-544.

Jensen, J. L., M. Nakatani, P. Quenneville & B. Walford (2012) A simplified model for withdrawal of screws from end-grain of timber. *Construction and Building Materials,* 29, 557-563.

Malo, K. A. & P. Ellingsbø. 2010. On connections for timber bridges. In *Proceedings of the International Conference Timber Bridges (ICTB)*, 297-312. Lillehammer, Norway.

Mischler, A. & A. Frangi. 2001. Pull-out tests on glued-in-rods at high temperatures. In *Proceedings of the 34th CIB-W18 meeting* Venice, Italy.

Mori, T., M. Nakatani, S. Kawahara, T. Shimizu & K. Komatsu. 2008. Influence of the number of fastener on tensile strength of lagscrewbolted glulam joint. In *10th World Conference on Timber Engineering*, 1100-1107.

Nakatani, M. & K. Komatsu. 2004. Development and verification of theory on pull-out properties of Lagscrewbolted timber joints. In *Proceedings of the 8th World Conference on Timber Engineering*, 95-99. Lahti, Finland.

Pirnbacher, G., R. Brandner & G. Schickhofer. 2009. Base parameters of self-tapping screws. In *Proceedings of the 42nd CIB-W18 meeting* Dübendorf, Switzerland.

Ringhofer, A. & G. Schickhofer. 2014. Influencing parameters on the experimental determination of the withdrawal capacity of self-tapping screws. In *Proceedings of the 13th World Conference on Timber Engineering*. Quebec City, Canada.

Stamatopoulos, H. & K. A. Malo (2015a) Withdrawal capacity of threaded rods embedded in timber elements. *Construction and Building Materials,* 94, 387-397.

Stamatopoulos, H. & K. A. Malo (2015b) Withdrawal stiffness of threaded rods embedded in timber elements. *Submitted to Construction and Building Materials*.

Tomasi, R., A. Crosatti & M. Piazza (2010) Theoretical and experimental analysis of timber-to-timber joints connected with inclined screws. *Construction and Building Materials,* 24, 1560-1571.

Volkersen, O. (1938) Die nietkraftverteilung in zugbeanspruchten nietverbindungen mit konstanten laschenquerschnitten. *Luftfahrtforschung,* 15, 41-47.

Discussion

The paper was presented by H Stamatopoulos

H Blass commented about the stiffness dependence on the embedment and asked why FEM predictions were higher than experimental values except for the 90 degrees case. H Stamatopoulos answered that the rod slipped with the interface more at 0 degrees than with 90 degrees. Therefore, with less relative slip at 90 degrees, there was better agreement.

S Franke asked how was the load slip evaluated in relation to the strength. H Stamatopoulos answered that small embedment length was used only. FEM calculation for strength would be more difficult as crack formation could be issues that needed to be considered; therefore, only used for stiffness prediction. S Franke stated that he has a student working on strength prediction.

P Zarnani and H Stamatopoulos discussed local shear failure mode such as block shear failure issues.

W Seim asked about the definition of fracture energy and from where these values were obtained. H Stamatopoulos clarified that he did not use fracture energy and just used a bilinear constitutive law. E Serrano commented that you needed f_w and two slopes for the bilinear constitutive law; therefore, you have defined the fracture energy. H Stamatopoulos agreed.

I Smith and H Stamatopoulos discussed progressive collapse and the use of a long rod to get steel yielding rather than withdrawal.

R Jockwer asked about pull-pull rather than push-pull test configuration. H Stamatopoulos responded that there was work done and support conditions played an important role in withdrawal stiffness.

Load-carrying capacity of dowelled connections

H.J. Blass, Karlsruhe Institute of Technology

F. Colling, Augsburg University of Applied Sciences

Keywords: Dowel, yield moment, connection

1 Introduction

The load-carrying capacity of joints with dowel-type fasteners in Eurocode 5 (2010) is mainly based on the Johansen theory (Johansen, 1949), later extended by Meyer (1957). Even though Johansen's model is based on plastic hinge formation in the dowel-type fasteners for some of the failure modes considered, the elastic bending moment capacity of the fasteners is used. Eurocode 5 contains an empirical equation to calculate the fastener yield moment which in many cases results in values between the elastic and full plastic fastener bending capacity. However, Sandhaas (2012) showed that for large diameter dowels of high steel grades the predicted yield moment according to Eurocode 5 is even lower than the elastic moment capacity.

The introduction of the Johansen theory in the German design code DIN 1052:2004, being very similar to Eurocode 5, in many cases led to a significant decrease of the calculated load-carrying capacity of dowelled joints with drift pins compared to the design according to the former version DIN 1052:1988. The reason for this apparent decrease in load-carrying-capacity is mainly due to the much more stringent consideration of the group effect in DIN 1052:2004 using n_{ef} for dowels in line with load and grain direction. A comparison between the 1988 and 2004 versions of DIN 1052 also revealed that the difference in calculated load-carrying-capacity increases with increasing dowel diameter. These differences motivated the studies described in the following.

In order to find a more realistic bending moment capacity of dowel-type fasteners, the load-carrying capacity of dowelled joints with drift pins was comprehensively studied and evaluated, based on 1588 tests with dowelled connections reported in seven different research studies (Brühl, 2010; Ehlbeck & Werner, 1989; Jorissen, 1998; Kneidl, 2009; Mischler, 1998; Sandhaas, 2012; Schmid, 2002). Additionally, bending and tensile tests with dowels sampled in companies during third party quality control visits formed the basis for a more realistic equation for the calculation of the yield moment $M_{y,k}$.

2 Eurocode 5 versus DIN 1052:1988

Calculated load-carrying capacities of dowelled connections with drift pins according to EN 1995-1-1:2010 (Eurocode 5, 2010) are in many cases significantly lower than the corresponding values according to the former German DIN 1052:1988. Consequently, structures comprising connections designed according to DIN 1052:1988 might be unsafe or the design according to Eurocode 5 might be overly conservative.

Figures 2.1 to 2.4 exemplarily show a comparison between the load-carrying-capacities according to Eurocode 5 and DIN 1052:1988, respectively. The two design codes are based on different safety concepts: Eurocode 5 uses partial safety factors for both, actions and resistances while DIN 1052:1988 uses permissible loads for connections. In order to compare the load-carrying-capacities, the following assumptions were made:

- Design actions are calculated by multiplying characteristic actions with a partial factor of 1.4;
- The design load-carrying-capacity of a dowelled joint is calculated for service class 1 or 2 and load-duration class medium-term.

Using these assumptions, the permissible load according to DIN 1052:1988 was compared with the design resistance of the connection, divided by the partial action factor of 1.4:

$$R_{comp} = \frac{k_{\mathrm{mod}}}{\gamma_M} \cdot \frac{F_{v,Rk}}{\gamma_{G/Q}} = 0.44 \cdot F_{v,Rk} \leftrightarrow zul\ N \qquad (1)$$

Here, k_{mod} = 0.8, γ_M = 1.3, $\gamma_{G/Q}$ = 1.4, $F_{v,Rk}$ is the characteristic load-carrying-capacity and *zul N* is the permissible load of a dowelled connection. In Figures 2.1 to 2.4, the dowel diameter d, the side and middle member's slenderness ratios λ_{sm} and λ_{mm} (timber member thickness over dowel diameter) as well as the number of fasteners n_h arranged parallel to the load and grain direction were varied.

If a single dowel is considered, Eurocode 5 results in higher load-carrying-capacities for small diameter dowels and low slenderness ratios (see Fig. 2.1). For larger diameters and slenderness ratios, Eurocode 5 shows lower load-carrying-capacities (see Fig. 2.2). For several dowels arranged in line with the load and grain direction (n_h > 1), the difference between Eurocode 5 and DIN 1052:1988 increases, especially for large diameter dowels and large slenderness ratios (see Fig. 2.3 and Fig. 2.4).

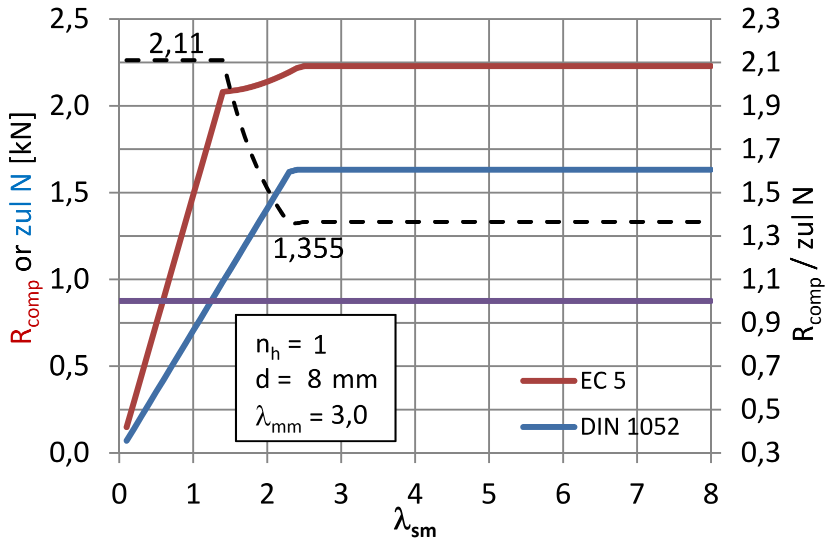

Figure 2.1. R_{comp} versus zul N; n_h = 1, d = 8 mm, middle member slenderness ratio λ_{mm} = 3,0

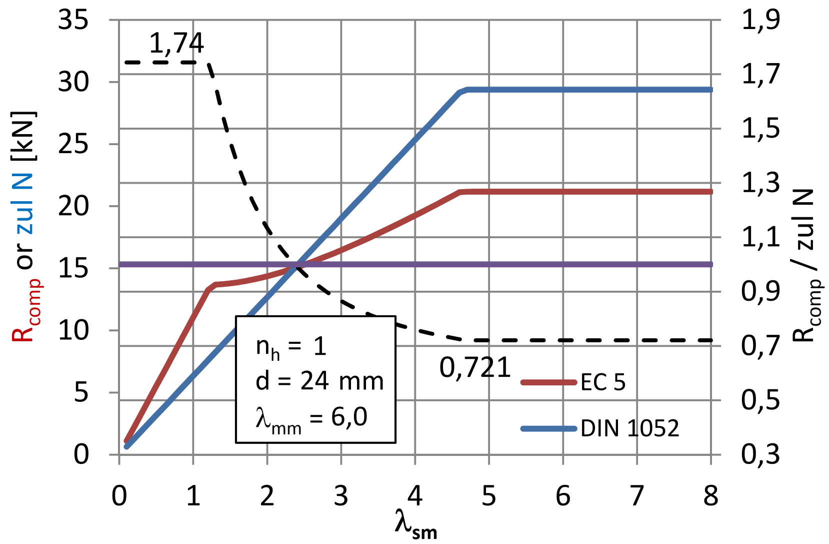

Figure 2.2. R_{comp} versus zul N; n_h = 1, d = 24 mm, middle member slenderness ratio λ_{mm} = 6,0

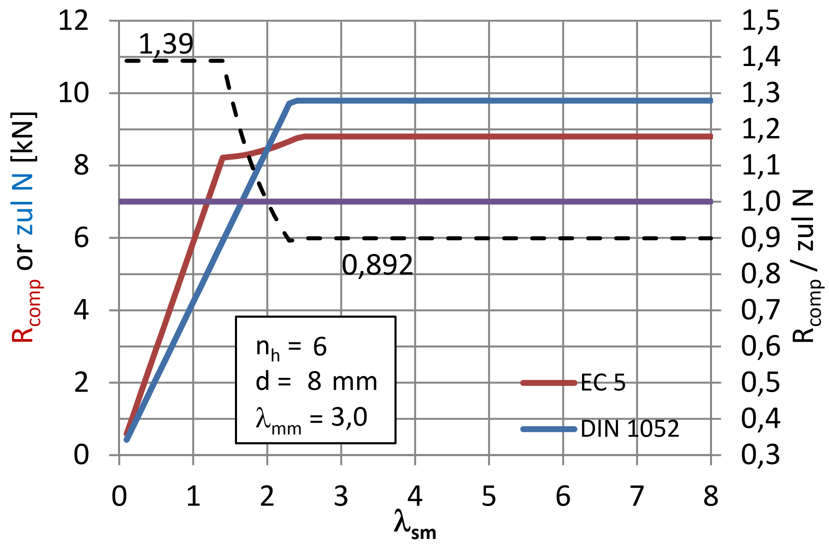

Figure 2.3. R_{comp} versus zul N; n_h = 6, d = 8 mm, middle member slenderness ratio λ_{mm} = 3,0

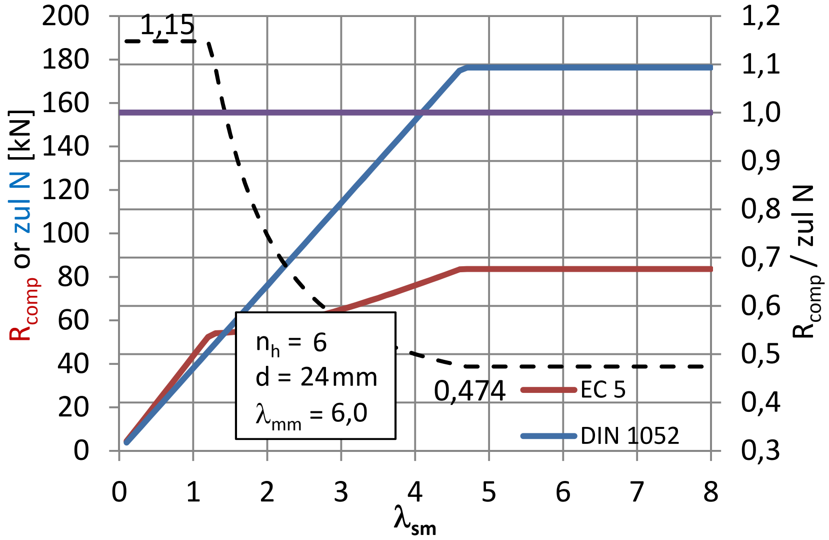

Figure 2.4. R_{comp} versus zul N; n_h = 6, d = 24 mm, middle member slenderness ratio λ_{mm} = 6,0

3 Connection test results

3.1 Test specimens

Altogether 1588 tests were evaluated, 1045 timber-to-timber and 543 steel-to-timber connections. The different sources yield the following tests with sufficient information regarding the test configuration, the timber members and the steel properties:

- Jorissen: 919 timber-to-timber connections, tension and compression;
- Ehlbeck and Werner: 126 timber-to-timber connections, tension and compression;
- Kneidl: 58 steel-to-timber connections, tension;
- Brühl: 22 steel-to-timber connections, tension;
- Mischler: 190 steel-to-timber connections, tension;
- Sandhaas: 179 steel-to-timber connections, tension;
- Schmid: 94 steel-to-timber connections, tension;

The side member slenderness ratios λ_{sm} varied between 1.0 and 7.5, for timber-to-timber connections most tests were performed with $\lambda_{sm} < 5$. Dowel spacing a_1 parallel to the grain ranged from 3 d to 11 d with most test specimens between 5 d and 7 d.

The predominant dowel diameter used in the tests was 12 mm (see Fig. 3.1 left). The majority of the dowels were made of steel with lower grades (see Fig. 3.1 right).

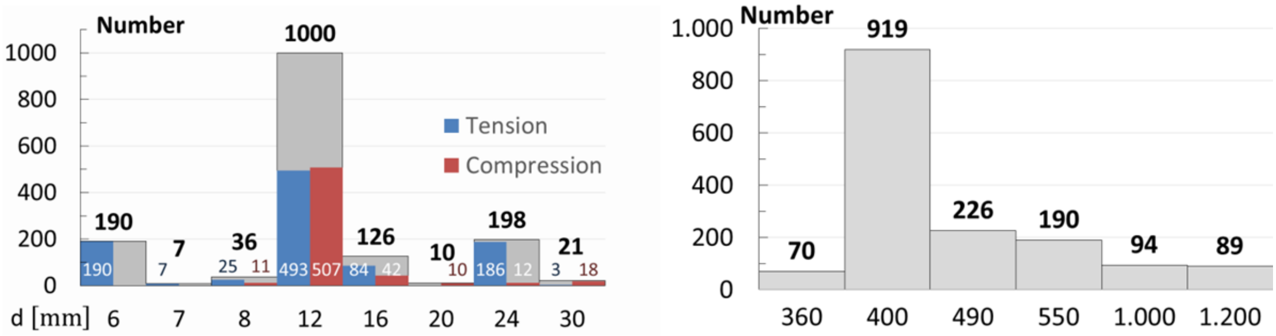

Figure 3.1. Used dowel diameters in the test specimens (left) and dowel steel tensile strength in N/mm² (right)

The arrangement of the dowels parallel (n_h) and perpendicular (n_n) to the load and grain direction is given in Fig. 3.2.

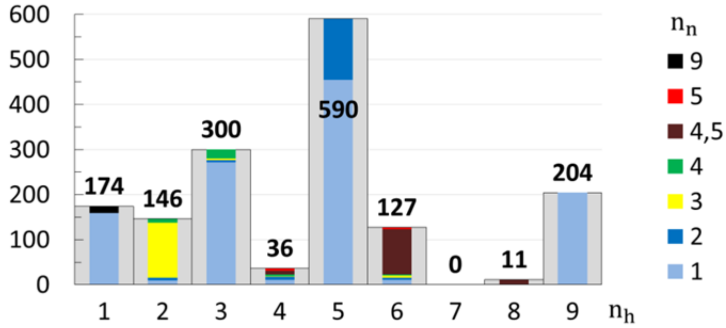

Figure 3.2. Number of dowels parallel (n_h) and perpendicular (n_n) to load and grain direction

Some of the tests were performed with parameters either outside the requirements of the design codes Eurocode 5 and DIN 1052:1988 or the parameters were quite exceptional for practical applications like side member slenderness ratio $\lambda_{sm} < 2$. Connection tests with hardwood showed significantly higher load-carrying-capacities compared to the expected values from the design codes. Therefore, test specimens fulfilling one of the following conditions were excluded from the evaluation:

- Spacing parallel to the grain $a_1 < 5$ d,
- Loaded end distance $a_{3,t} < 6$ d,
- Unloaded edge distance $a_{4,c} < 3$ d,
- Side member slenderness ratio $\lambda_{sm} < 2$,
- Density $\rho > 600$ kg/m³ (hardwood).

Discounting the excluded values, 561 test results with timber-to-timber and 325 with steel-to-timber connections remain for the following evaluation.

3.2 Test results versus calculated permissible load according to DIN 1052

This evaluation shows the ratio of the ultimate test load $F_{v,R}$ versus the calculated permissible load *zul N* according to DIN 1052:1988. In the calculation of *zul N* the dowel steel strength is not considered, only a minimum steel grade of S235 for dowels and 3.6 for bolts is required. Similarly, the strength class of solid or glued laminated softwood timber is not accounted for in the calculation. Only for more than six fasteners parallel to the load and grain direction a reduction of the effective number of fasteners, $n_{ef} < n_h$ is taken into account. Figures 3.3 and 3.4 show the ratios $F_{v,R}$/zul N for timber-to-timber and steel-to-timber connections, respectively. The ratios were calculated for every single test, the dark red triangles show the ratios for the excluded test results.

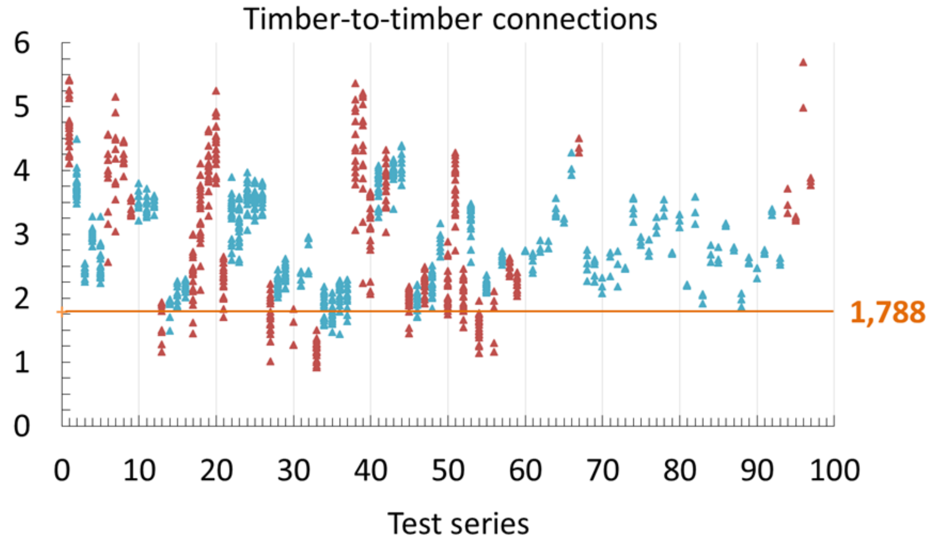

Figure 3.3. Ratios of the ultimate test load $F_{v,R}$ versus the calculated permissible load zul N according to DIN 1052:1988 for 1045 timber-to-timber connections

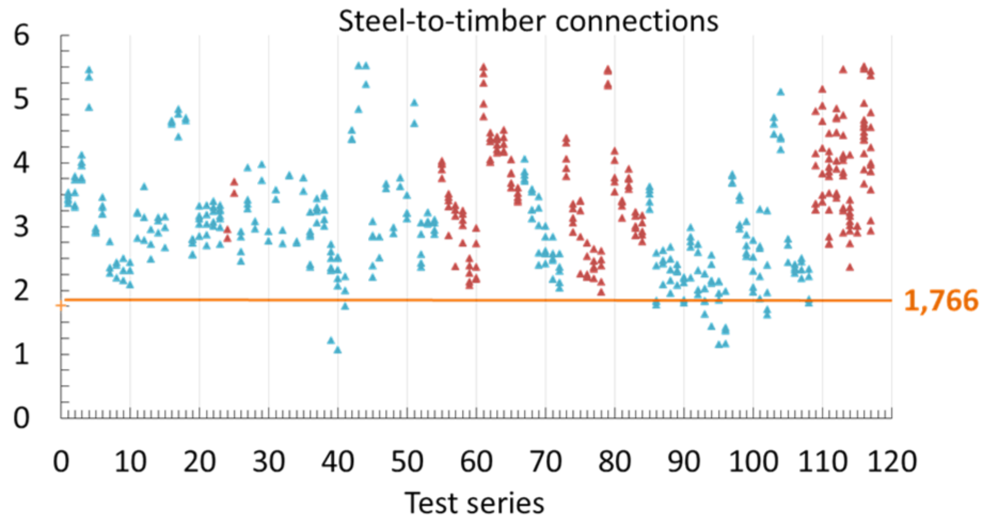

Figure 3.4. Ratios of the ultimate test load $F_{v,R}$ versus the calculated permissible load zul N according to DIN 1052:1988 for 543 steel-to-timber connections

The characteristic ratio calculated according to EN 14358 is 1.79 for timber-to-timber and 1.77 for steel-to-timber connections only calculated for the test results not excluded. The characteristic ratio corresponds to a global safety factor. Depending on the service and load-duration classes, it should be between 2.0 and 2.3. The results hence show a deficiency of 10% to 25% in the global safety factor for dowelled connections designed according to DIN 1052:1988.

3.3 Test results versus calculated characteristic load-carrying-capacity according to Eurocode 5

The second evaluation compares the ultimate loads $F_{v,R}$ in the connection tests to the calculated characteristic load-carrying-capacities $F_{v,Rk}$ according to Eurocode 5. When calculating the load-carrying-capacities, the factors 1.05 and 1.15 in sections 8.2.2 and 8.2.3 of Eurocode 5 are disregarded, since they only compensate the lower required partial factor and the use of the modification factor k_{mod} for the fastener's yield moment.

In order to determine the characteristic timber density, the mean density was determined for each test series and the associated characteristic density according to EN 338 or EN 14080 was assumed for the test series.

Similarly, a characteristic dowel tensile strength was assumed for dowels, where the tensile strengths were given in the test report. If only a steel grade of the dowels was given, corresponding characteristic tensile strength was used. If no information regarding the dowel steel grade was available, the characteristic tensile strength of steel grade S235 was assumed ($f_{u,k}$ = 360 N/mm²).

An effective number of dowels according to equation (8.34) of Eurocode 5 was used for connections with several dowels arranged parallel to load and grain direction.

Figures 3.5 and 3.6 show the ratios $F_{v,R}/F_{v,Rk}$ for timber-to-timber and steel-to-timber connections, respectively. The ratios were calculated for every single test, the dark red triangles show the ratios for the excluded test results. The characteristic ratio calculated according to EN 14358 is 1.074 for timber-to-timber and 1.073 for steel-to-timber connections only for the test results not excluded. Ideally, the characteristic ratio would be 1.0 for both cases. The calculation model according to Eurocode 5 is hence slightly conservative.

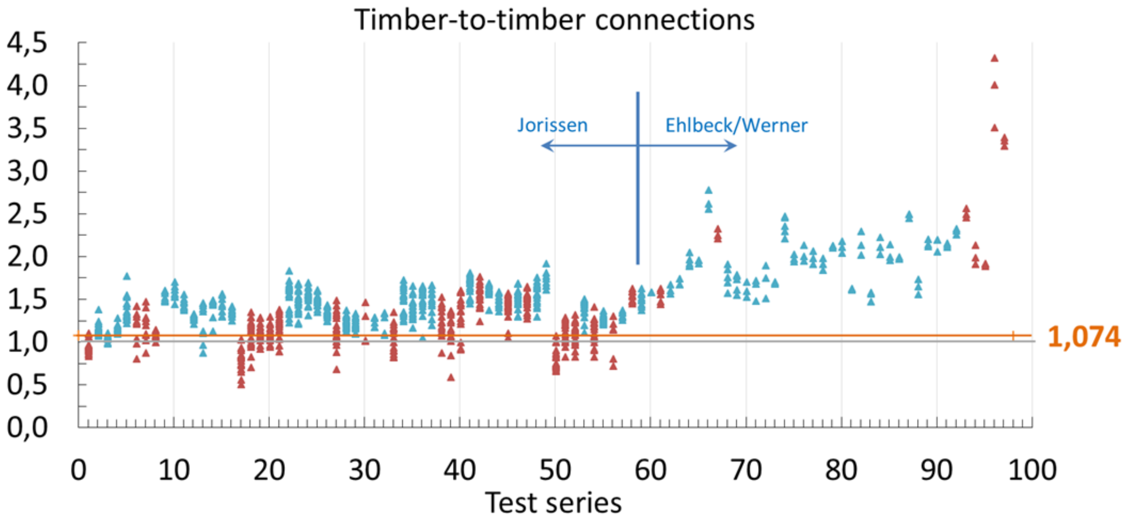

Figure 3.5. Ratios of the ultimate test load $F_{v,R}$ versus the calculated characteristic load-carrying-capacity $F_{v,Rk}$ according to Eurocode 5 for 1045 timber-to-timber connections

The ultimate test loads for timber-to-timber connections published by Ehlbeck and Werner (1989) are significantly higher than the calculated characteristic load-carrying-capacities (test series No. 59 and higher). The dowel slenderness ratios in the tests by Ehlbeck and Werner were significantly larger than those used by Jorissen (1998).

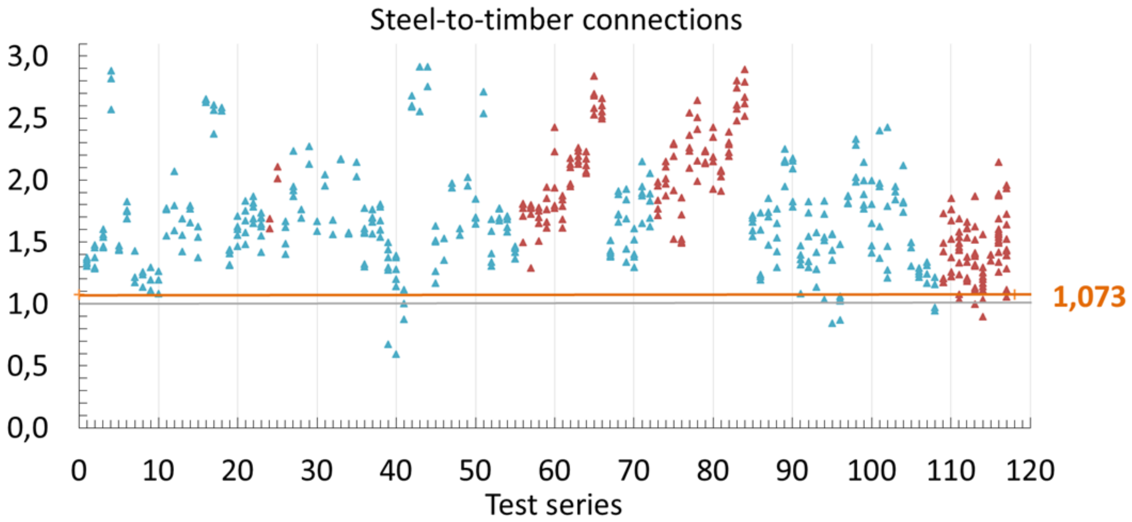

Figure 3.6. Ratios of the ultimate test load $F_{v,R}$ versus the calculated characteristic load-carrying-capacity $F_{v,Rk}$ according to Eurocode 5 for 543 steel-to-timber connections

Another tendency observed during the evaluation was that the difference between the ultimate test load and the calculated characteristic load-carrying-capacities increases with increasing dowel diameter. Obviously, the load-carrying-capacity of connections with large diameter dowels is underestimated by Eurocode 5.

4 Dowel test results

4.1 General

The evaluation of the connection tests in section 3 shows an increasing underestimation of the characteristic load-carrying-capacities for larger dowel diameters. The same holds for higher dowel slenderness ratios where failure modes including dowel bending occur and the yield moment of the dowel more and more influences the load-carrying-capacity. Therefore, dowel yield moments were experimentally determined for different dowel diameters and different steel grades. In order to check equation (8.30) of Eurocode 5, dowels were sampled in different timber construction companies as well as ordered from different suppliers. Altogether 159 dowel tensile tests in 31 series and 122 dowel bending tests in 38 series were carried out. If possible, part of each sample was tested in tension and another part in bending. Long dowels were cut in half and one half was tested in tension and the other in bending. Since the variation of test results within a test series was very low, the yield moments according to EN 409 could be compared to the calculated yield moments according to equation (8.30) of Eurocode 5 by directly using the tensile strength from the test. Figure 4.1 exemplarily shows dowels after tensile or bending tests.

Figure 4.1. 16 mm dowels after tensile tests (left) and 8 mm dowels after bending tests (right)

4.2 Yield moment M_y

The tests showed different moment-rotation behaviour of steel grades with low and high tensile strengths, respectively. For mild steel the bending moment still increased significantly after plastic deformation started. This increase is less pronounced for higher steel grades (see Fig. 4.2).

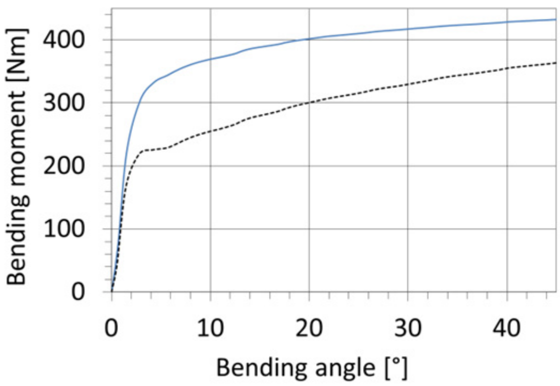

Figure 4.2. Bending moment – angle relation for 16 mm dowels made of mild steel (dotted line) and higher grade steel (solid line)

The yield moment was determined according to EN 409 at a bending angle α:

$$\alpha = \alpha_1 \cdot \left(\frac{2{,}78 \cdot \rho_k}{f_u} \right)^{0{,}44} \tag{2}$$

Here, ρ_k is the characteristic timber density and f_u the dowel tensile strength. Since the timber density is not known, ρ_k = 350 kg/m³ is assumed. Table 1 shows the yield moments M_y determined according to EN 409, and the steel tensile strengths f_u from the tensile tests. For comparison the yield moments M_y according to equation (8.30) of Eurocode 5 on the one hand using the tensile strength $R_{m,mean}$ of each test series and on the other hand on the basis of the nominal tensile strength of the dowel $f_{u,k}$. If $f_{u,k}$ was unknown, the tensile strength of S235 of 360 N/mm² was assumed.

Table 1. Results of dowel bending tests compared to calculated yield moments according to Eurocode 5.

Source	Diameter/Length [mm]	$R_{m,mean}$ [N/mm²]	$M_{y,EN409,mean}$ [Nm]	$M_{y,EC5,Rm,mean}$ [Nm]	$M_{y,EC5,fuk}$ [Nm]
SFS	7/233	584	32	28	26
GH	8/200	593	52	40	24
RB	8/140	662	59	44	24
Rög	8/160	634	56	42	24
Würth	8/115	687	60	46	24
Alberts	10/140	622	106	74	45
Murr	10/210	603	101	72	43
Rie	10/140	607	107	72	43
Würth	10/140	604	102	72	43
AHH	12/180	641	193	123	69
Alberts	12/220	631	184	121	73
Bsch	12/320	712	198	137	69
D	12/400	652	184	125	69
Gei	12/160	717	196	138	69
Gei	12/200	591	136	113	69
Gei	12/240	440	95	84	69
GH	12/200	604	174	116	69
RB	12/200	567	166	109	69
San	12/140	752	202	144	69
Würth	12/200	697	201	134	69
DX	16/200	397	198	161	146
Gei	16/240	535	377	217	146
GH	16/300	540	377	219	146
HO	16/140	446	257	181	146
RB	16/240	742	494	301	146
SF	16/220	542	349	220	146
VK	16/200	414	213	168	146
B	20/420	564	776	408	261
GH	20/300	572	759	414	261
RB	20/240	628	825	455	261
Rie	20/390	483	696	350	261

In order to enable a more realistic calculation of dowel yield moments, an alternative to equation (8.30) of Eurocode 5 is determined. Here, the different behaviour of steel dowels made of low or high grade steel (see Fig. 4.2) is taken into account. Those test results are used to derive an equation to determine the yield moment, where both tensile and bending tests were carried out with dowels from the same batch. The best agreement between test results and calculated values was found for the following expression, representing the mechanically correct full plastic bending moment of a circular cross-section:

$$M_y = \frac{f_{y,ef} \cdot d^3}{6} \tag{3}$$

$$f_{y,ef} = \begin{cases} \dfrac{0{,}9 \cdot (f_y + f_u)}{2} & \text{for } f_u < 450\,MPa \\ 0{,}9 \cdot f_u & \text{for } f_u > 450\,MPa \end{cases} \tag{4}$$

Here, d is the dowel diameter, f_y is the fastener yield strength and f_u is the fastener tensile strength.

Fig. 4.3 left shows the ratio between M_y according to EN 409 and the calculated value according to equation (3) for the 122 bending tests, on the one hand based on the mean tensile strength from the tests (diamonds) and on the other hand based on the nominal dowel tensile strength (squares). The ratio is independent of the dowel diameter. The average ratio for test based tensile strengths is 1.09, the characteristic ratio is 1.00. Equation (3) hence provides an excellent description of the dowel yield moments according to EN 409. Since in a real design situation nominal rather than real tensile strength values are applied, the proposed equation (3) is conservative in most cases due to the over-strength of the steel dowels.

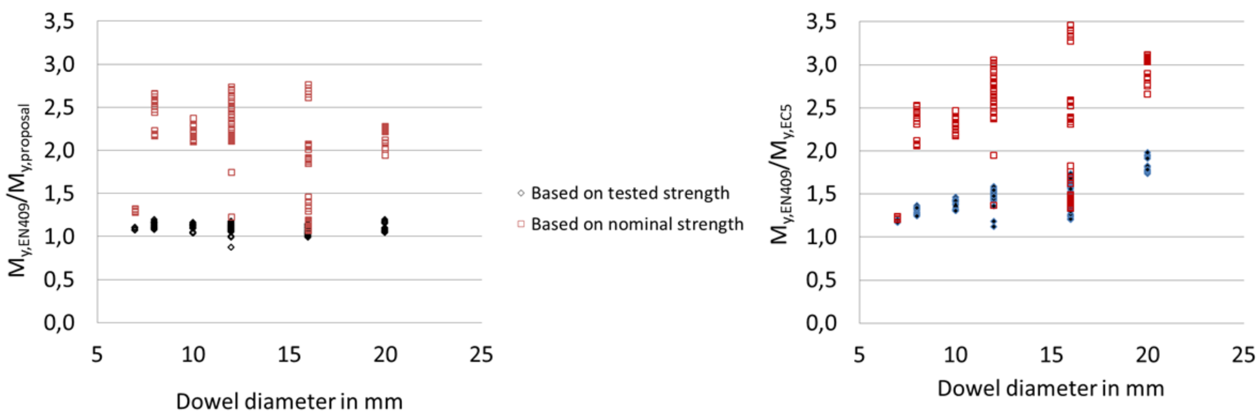

Figure 4.3. Ratio between M_y according to EN 409 and M_y according to equation (3) (left) or M_y according to Eurocode 5 (right)

For comparison the ratio between M_y according to EN 409 and the calculated value according to equation (8.30) of Eurocode 5 is shown in Figure 4.3 (right). It is obvious that Eurocode 5 is increasingly conservative for larger dowel diameters.

4.3 Influence of yield moment M_y on calculated results

Figures 4.4 and 4.5 again show the ratios $F_{v,R}/F_{v,Rk}$ for timber-to-timber and steel-to-timber connections, respectively. The ratios were calculated using equation (3) instead of equation (8.30) of Eurocode 5 to calculate the characteristic yield moment of the dowels. The characteristic ratio calculated according to EN 14358 decreases from 1.074 to 1.048 for timber-to-timber and from 1.073 to 1,001 for steel-to-timber connections, again only for the test results not excluded. The calculation model according to Eurocode 5 with the modified yield moment M_y hence is still slightly conservative for the tested timber-to-timber connections and appropriate for the tested steel-to-timber connections.

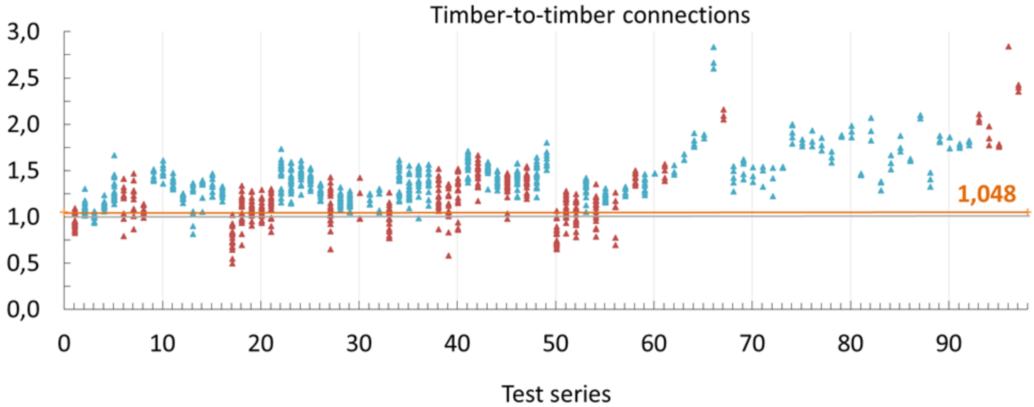

Figure 4.4. Ratios of the ultimate test load $F_{v,R}$ versus the calculated characteristic load-carrying-capacity $F_{v,Rk}$ taking into account My according to equation (3) for 1045 timber-to-timber connections

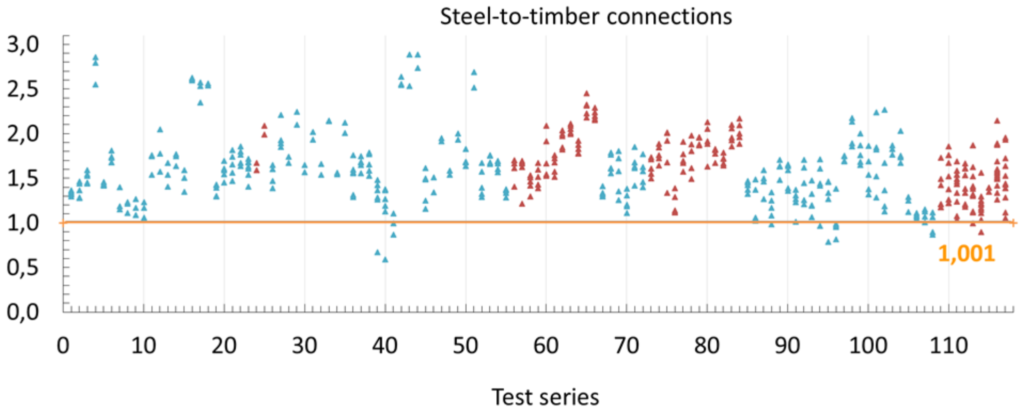

Figure 4.5. Ratios of the ultimate test load $F_{v,R}$ versus the calculated characteristic load-carrying-capacity $F_{v,Rk}$ taking into account My according to equation (3) for 543 steel-to-timber connections

In the average, the timber-to-timber connections tested by Ehlbeck and Werner (1989) still show higher ratios $F_{v,R}/F_{v,Rk}$ even with the modified equation for the dowel yield moment M_y (see test series 59 through 118 in Fig. 4.4). Apart from the plastic dowel bending capacity there seem to exist further causes for higher ratios with increasing dowel slenderness ratios. If a slenderness effect is taken into account for dowelled connections similar to the rope effect in Eurocode 5, leading to an increase of 25 % of the lateral load-carrying-capacity of dowels with a failure mode showing two plastic hinges per shear plane, the characteristic ratio for timber-to-timber connections would only drop to from 1,048 to 1,037, for steel-to-timber connections from 1,001 to 0,978.

Reasons for the additional safety margin for slender dowels could be friction between the dowel and the surrounding timber along the length of the dowel, especially in areas where the embedding strength is reached. This friction would create a withdrawal capacity leading to a twofold rope effect: friction between the timber or steel members and the fastener tensile component parallel to the shear plane. Further research is required to quantify this possible rope effect in dowelled connections with drift pins.

5 Conclusions

The load-carrying capacity of dowelled joints with drift pins was comprehensively studied and evaluated, based on 1588 tests with dowelled connections reported in seven different research studies (Brühl, 2010; Ehlbeck & Werner, 1989; Jorissen, 1998; Kneidl, 2009; Mischler, 1998; Sandhaas, 2012; Schmid, 2002).

The analysis of the short-term tests shows an overestimation of the load-carrying capacity according to DIN 1052:1988 by 10 – 25 %. Consequently, connections designed according to DIN 1052:1988 are below the reliability level required today. The evaluations also show that some load-carrying capacities according to Eurocode 5 are conservative and hence could be increased accordingly.

Based on bending and tensile tests with dowels sampled in companies during third party quality control visits, a modified equation for the calculation of the yield moment $M_{y,k}$ was derived, leading to higher calculated load-carrying capacities especially for large diameter dowels or higher steel grades. The dowel bending and tensile tests also revealed that actual steel strength values often show significant over-strength.

For dowelled connections with a failure mode showing two plastic hinges per shear plane, an additional slenderness effect was observed, increasing the load-carrying capacity of these connections in the order of 25 % compared to calculated values based on the Johansen model. This is surprising, since drift pins so far show no significant withdrawal capacity and hence a rope effect is hardly to be expected.

The design rules in DIN 1052:1988 were originally derived based on tests, where the dowel steel strength was not determined. This means that both effects mentioned above, namely the surplus strength of the steel dowels and the slenderness effect, were implicitly included in the permissible loads according to DIN 1052:1988.

Considering the consequences of these findings (modified equation for M_y, slenderness effect and steel over strength), the existing differences between the calculated load-carrying capacities according to DIN 1052:1988 and Eurocode 5, respectively, may be explained to a large extent.

A new equation for Eurocode 5 for calculating the characteristic yield moment of bolts and dowels is proposed.

6 References

Brühl, F (2010): Ductile timber connections (in German). Research report, Universität Stuttgart, Stuttgart.

Colling, F & Blass, HJ (2014): Load-carrying-capacity of dowelled connections (in German). In: Proceedings, Karlsruher Tage 2014 - Holzbau: Forschung für die Praxis. KIT Scientific Publishing, Karlsruhe.

Ehlbeck, J & Werner, H (1989): Load-slip behaviour of dowels in glued laminated timber and solid timber of different species considering different dowel arrangements (in German). Research report, Universität Fridericiana Karlsruhe, Karlsruhe.

Eurocode 5 (2004): Design of timber structures - Part 1-1: General and rules for buildings. CEN. (EN 1995-1-1).

Johansen, KW (1949): Theory of Timber Connections. IABSE publications 9 (1949), Zürich, Switzerland.

Jorissen, A (1998): Double shear timber connections with dowel type fasteners. Dissertation, Delft University Press, Delft.

Kneidl, R (2009): Final report regarding experimental studies of dowelled connections (in German). Bayrische Ingenieurkammer Bau, München.

Meyer, A (1957): Load-carrying-capacity of nailed joints under static load (in German). Holz als Roh- und Werkstoff 15 Heft 2.

Mischler, A (1998): Relevance of ductility for the load-slip behaviour of bolted steel-to-timber joints. Dissertation, ETH Zürich, Zürich.

Sandhaas, C (2012): Mechanical behaviour of timber joints with slotted-in steel plates. Dissertation, Delft University Press, Delft.

Schmid, M (2002): Application of fracture mechanics on timber connections. Dissertation (in German), Universität Fridericiana Karlsruhe, Karlsruhe.

Discussion

The paper was presented by H Blass

K Malo asked whether the approach is valid for stainless steel. H Blass responded yes. S Franke and H Blass discussed about the fitting process for screws are more difficult.

A Salenikovich asked for comments for multiple fasteners in a row. H Blass responded that EC5 equations were used.

S Franke commented that the attempt was to justify changes to EC5. H Blass responded that the old allowable values were not based on tests of steel strength, therefore over-strength situations were not correctly considered. Here the old code is still non-conservative by ~ 10% but not 25% as previously thought.

V Rajčić and H Blass discussed the lack of conservatism of the old code when different failure cases were considered.

R Jockwer commented the yield strength of the dowels were very important. H Blass responded that high strength steel dowel compared to mild steel would still be more beneficial although it would be dependent on cost and economics.

I Smith commented that this is a manifestation of system effect.

U Kuhlmann commented about target failure mode in relationship to the type steel used.

Evaluation of the reliability of design approaches for connections perpendicular to the grain

Robert Jockwer
ETH Zürich, Institute of Structural Engineering, Zurich, Switzerland

René Steiger
Empa, Swiss Federal Laboratories for Materials Science and Technology, Dübendorf, Switzerland

Andrea Frangi
ETH Zürich, Institute of Structural Engineering, Zurich, Switzerland

KEYWORDS: Connection perpendicular to grain, brittle failure, fasteners, partial safety factor

ABSTRACT: In this paper different design approaches for connections loaded perpendicular to the grain are evaluated with regard to their reliability. The structural behaviour of connections loaded perpendicular to the grain is described based on existing experimental and theoretical studies. The detailed failure behaviour of dowel connections loaded perpendicular to grain with slotted in steel plates is analysed in a recent test series. Based on these observations and on a large number of test results from literature different design approaches are benchmarked. The design and characteristic values of the relevant material parameters and the partial safety factors for the design of connections loaded perpendicular to grain are determined in a reliability analysis. As a result a much lower design value of the material parameter used in the EC5 design equation for connections loaded perpendicular to grain is proposed.

1 Introduction

1.1 General

In connections global failure can occur either due to local failure of the fastening elements and the timber surrounding the fasteners or due to failure in the timber next to the joints. Failure of the fasteners can be accounted for by designing them according to appropriate design rules, e.g. the so called European yield model (for dowel type fasteners). Design to prevent this failure mechanism includes prevention of embedment timber failure or of failure of the metallic fastener. However, sometimes such a design is not sufficient because splitting of the timber next to the joint might occur and hence design has also account for this failure. For timber members loaded parallel to the grain spacing requirements are specified in Eurocode 5 (2004) (EC5). In EC5 there is also a design approach for situations where connections are loaded perpendicular to the grain. It is independent from the load-carrying capacity of the fasteners. Alternative design approaches to be applied for the design of connections loaded perpendicular to grain are described in Chapter 2. The aim of this paper is to evaluate different approaches for the design of single connections in the span of beams loaded perpendicular to the grain with regard to their reliability and simplicity.

1.2 Geometrical properties of connections loaded perpendicular to the grain

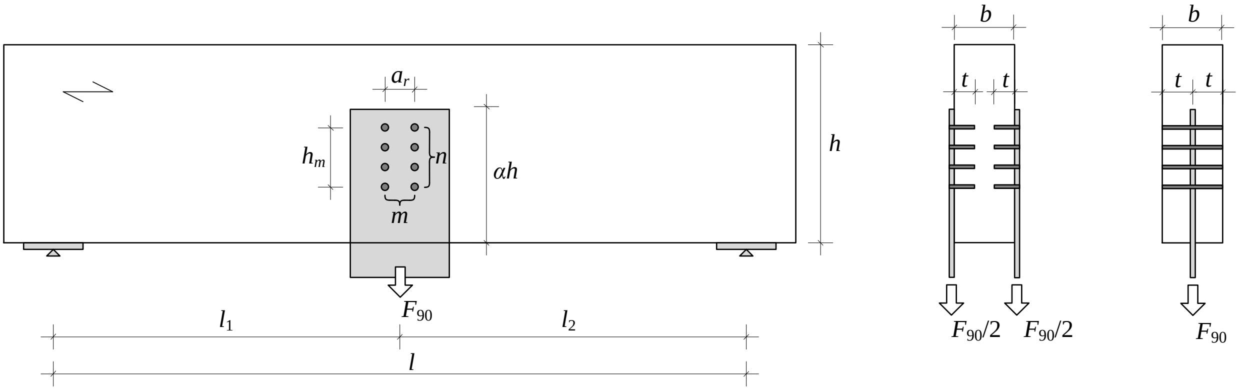

Figure 1: Definition at connections loaded perpendicular to grain.

The geometrical properties and definitions of a connection loaded perpendicular to the grain are depicted in Fig. 1. The level of tensile stresses perpendicular to the grain depends amongst others on the distance between loaded edge of the member and the top row of fasteners of the joint. This distance, expressed as a portion α of the full member height is one of the parameters with the highest impact on the reduction of the load-carrying capacity in connections loaded perpendicular to the grain. From fracture mechanics analysis (e.g. Leicester (1973)) and from Weibull's weakest link theory applied to tension perpendicular to grain (e.g. Mistler (1998)) it is known that the strength of the timber volume surrounding a connection loaded perpendicular to the grain decreases with increasing beam height h. The impact of the beam width b on the load-carrying capacity is often assumed to be linear. Additional geometrical parameters are h_n the distance between the n^{th}-row of fasteners to the loaded edge and l_l the distance between multiple connections along the beam axis.

1.3 Types of connections

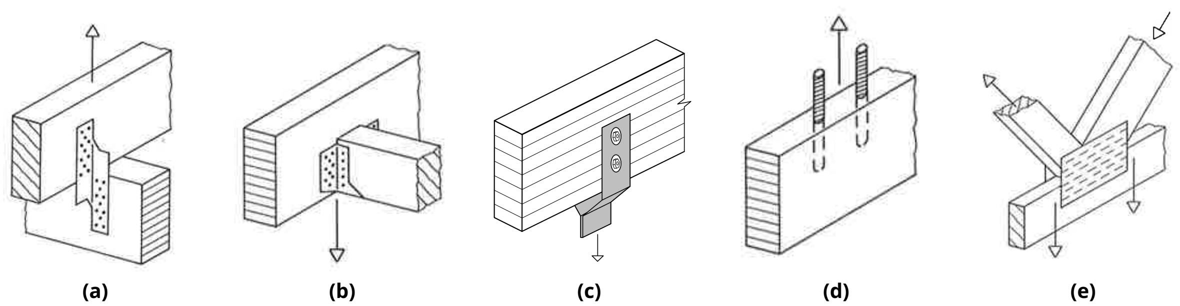

Figure 2: Examples for connections loaded perpendicular to grain: rafter to purlin connection (a), joist hanger (b), bolted steel-to-timber connection (c), glued in rods (d) and punched metal plate fasteners (e).

Due to the low strength and brittle failure mechanism of the timber, as a general rule situations where timber is subjected to tension perpendicular to the grain should be avoided in general. Hence, it is often poor design when connections transfer high tensile stresses perpendicular to the grain into timber elements. However, there are certain situations where this cannot be avoided. Examples of situations where connections introduce loads perpendicular to the grain are given in Fig. 2:

- Nailed connections with sheet metal plates for hold downs between rafter and perlins (Fig. 2 (a)) or for joist hangers for main and secondary beam connections (Fig. 2 (b)). These connections are often single sided with a large number of fasteners of relatively small diameter.
- Doweled or bolted connections between timber-to-timber or steel-to-timber connections (Fig. 2 (c)). Bolts are often used for external steel plates and dowels are used for internal slotted-in steel plates.
- Screwed or glued-in rod connections are used for hanging loads (Fig. 2 (d)). Screws are also used for steel-to-timber connections.
- Other examples are shear connections by means of ring connectors, punched in metal steel plates (Fig. 2 (e)) or special products like e.g. Sherpa® connectors.

2 Design approaches

Failure of connections loaded perpendicular to the grain due to splitting has often been discussed in literature. A comprehensive study with a review of various design approaches and test results was made by Schoenmakers (2010). Existing design approaches are based either on stress criteria like the approach in the former DIN 1052 (2008) as proposed by Ehlbeck et al. (1989) and the approach in Lignum (1990) or on fracture mechanics theory like e.g. the design approach in EC5 developed by van der Put (1990). The linear elastic fracture mechanics (LEFM) approach developed by van der Put (1990) was extended and adapted e.g. based on quasi-nonlinear fracture mechanics (Jensen et al., 2003) or semi-empirical theories (Ballerini, 2004). Mixed mode failure in tension perpendicular to the grain and shear was accounted for in the studies by Franke and Quenneville (2011). Empirical based design approaches are presented by Quenneville and Mohammad (2001) and Lehoux and Quenneville (2004) based on the design of rivet connections.
The impact of the parameters beam height h, relative connection height α, number of fastener columns m and number of fastener rows n is graphed in Fig. 3. Overall the approaches show a similar behaviour with different intensity of the specific impact of the parameters. The beam height h, the relative connection height α and the beam width b are accounted for by all approaches but not the geometry of the connections. The respective terms for the number of rows n and number of columns m of fasteners in a connection are summarized in Table 1.

Table 1: Terms accounting for the geometry of the connection.

Parameter	Ehlbeck et al. (1989)	Lignum (1990)	Ballerini (2004)	Franke & Quennev. 2011
m (width)	$max\left\{1; 0.7+1.6\frac{a_r}{h}\right\}$	$(1+a_r/(\alpha h))^{0.1}$	$min\left\{2.2; 1+0.75\left(\frac{a_r+l_l}{h}\right)\right\}$	✓
n (height)	$\frac{1}{n}\sum_{i=1}^{n}\left(\frac{h_1}{h_i}\right)^2$	$h_m^{0.4}$	$1+1.75\frac{\kappa}{1+\kappa}$ with $\kappa=\frac{nh_m}{1000}$	$0.1+\arctan(n)^{0.6}$ for $n>1$

As can be seen from Tab. 2 the type and diameter of the fasteners is only accounted for by the design approaches in former DIN 1052 based on Ehlbeck et al. (1989) and in Lignum (1990). The effective beam width b_{ef} is reduced in these approaches in order to account for early splitting in the vicinity of fasteners with small penetration depth t or high slenderness. Also Zarnani and Quenneville (2013) proposed to differentiate between full and partial splitting of the beam and account for the effective embedment depth of fasteners. For partial splitting the load-carrying capacity of the fasteners is relevant for the design whereas splitting failure of the surrounding timber is decisive for full splitting.

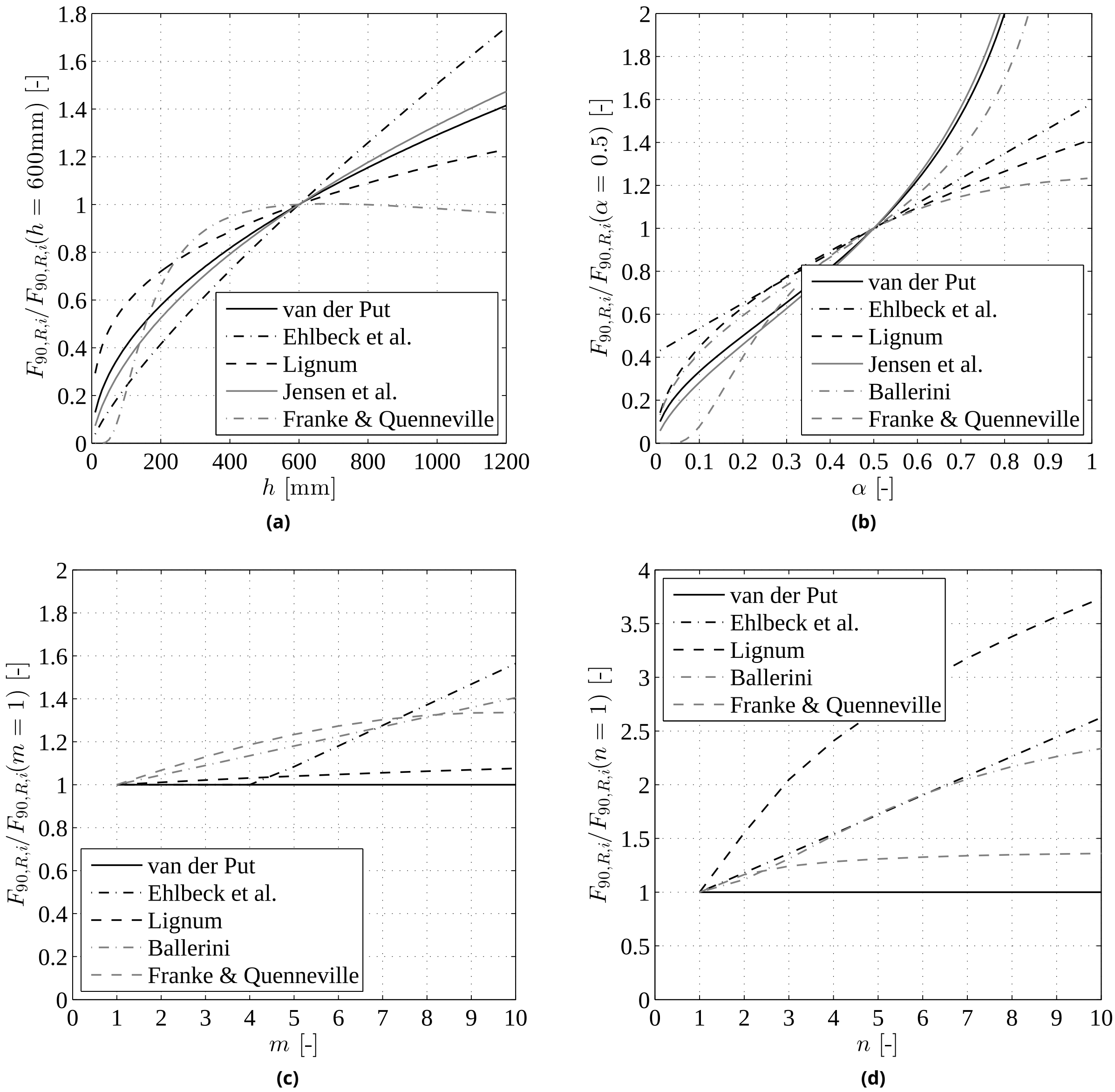

Figure 3: Impact of beam height h (a), relative connection height α (b), number of fastener columns m (c) and number of fastener rows n (d) on the relative load-carrying capacities $F_{90,R,i}/F_{90,R,i}(ref)$.

Table 2: Impact of the type and diameter of the fastener on the effective beam width b_{ef}.

two-sided connections	DIN 1052 (2008)	Lignum (1990)
Nails	$b_{ef} = min\{$ b ; $2t$; $24d$ (Timber / Timber) $\}$ $30d$ (Steel / Timber)	$b_{ef} = min\{$ b ; $2t$; $24d$ $\}$
Screws	$b_{ef} = min\{$ b ; $2t$; $24d$ (Timber / Timber) $\}$	
Dowels	$b_{ef} = min\{$ b ; $2t$; $12d$ $\}$	$b_{ef} = min\{$ b ; $6d$ $\}$
Shear connectors	$b_{ef} = min\{$ b ; 100 mm $\}$	$b_{ef} = 0.6d$ (ring connectors) d (toothed plate connector)
Glued in rods	$b_{ef} = min\{$ b ; $6d$ $\}$	

one-sided connections	DIN 1052 (2008)	Lignum (1990)
Nails	$b_{ef} = min\{$ b ; t ; $12d$ (Timber / Timber) $\}$ $15d$ (Steel / Timber) $\}$	$b_{ef} = min\{$ b ; t ; $12d$ $\}$
Screws	$b_{ef} = min\{$ b ; t ; $12d$ (Timber / Timber) $\}$	
Dowels	$b_{ef} = min\{$ b ; t ; $6d$ $\}$	
Shear connectors	$b_{ef} = min\{$ b ; 50 mm $\}$	$b_{ef} = 0.3d$ (ring connectors) $0.5d$ (toothed plate connector)

3 Experimental data

3.1 Experiments reported in literature

Test results from literature which were used in this paper to evaluate the design approaches for connections loaded perpendicular to the grain are summarized in Tab. 3. Only tests on glulam beams and with a single connection in the span were used in this evaluation. The most common type of connection exposed to experiments was a bolted or doweled connection with external steel plates.

Table 3: Experimental data from literature used for the evaluation of design approaches for connections loaded perpendicular to the grain

Literatur	Number	Species	Fastener type
Möhler and Siebert (1981)	28	Softwood	Nails, dowels, ring connectors
Ehlbeck and Görlacher (1983)	41	Softwood	Nails
Ballerini (1999)	49	Norway Spruce	Dowels
Ballerini and Giovanella (2003)	72	Norway Spruce	Dowels
Reshke (1999)	138	Spruce/Pine, GL 20f-E	Bolts
Kasim (2002)	90	Spruce/Pine & Douglas Fir	Bolts
Habkirk (2006)	50	Spruce/Pine & Douglas Fir	Bolts
Jensen and Quenneville (2011)	18	Douglas Fir, GL8 + GL15	Dowels
Schoenmakers (2010)	59	Spruce	Nails, dowels

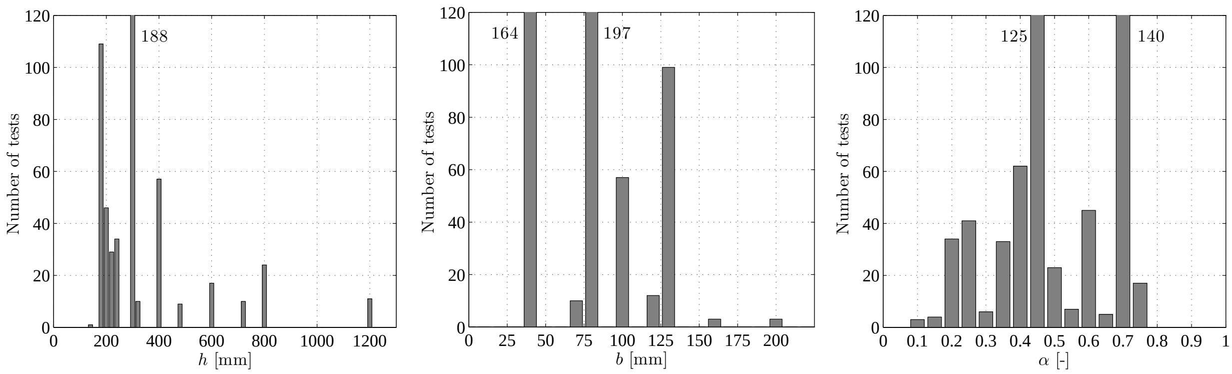

Figure 4: Histograms of beam and connection parameters height h, width b and relative connection height α as studied in the publications listed in Tab. 3.

Dimensions of the beams used in the tests and the geometry and relative connection height as studied in the publications listed in Tab. 3 are shown in Fig. 4. The suitability of the existing studies for the evaluation of the design of connections loaded perpendicular to the grain in practice can be summarized:

- The majority of the tests has been carried out on small sized specimen with small height and width (Fig. 4). This has to be accounted for when evaluating the size effects.
- A large number of tests has been performed on bolted steel-wood-steel connections. The reason for the choice of these connections might be the convenience in the experimental assembly.
- In many of the tests the diameter of the fastener was relatively large compared to the width of the beams. This very stiff configuration with thick fasteners allows for an uniform loading over the entire beam width. However, the load-carrying capacity of the fasteners was often much higher compared to the load observed at brittle failure of the timber. Due to economic reasons it should be aimed for an equal load-carrying capacity of the fasteners and the timber in practice .

3.2 Recent tests at ETH Zurich

A test series recently carried out at ETH Zurich was focused on the evaluation of the failure behaviour of connections loaded perpendicular to the grain and on the assessment of the crack growth. Doweled connections with slotted-in steel plates inserted at midspan position in glulam beams of grade GL 24h with $h = 440$ mm, $b = 140$ mm and a span of $l = 2$ m were tested. The thickness of the slotted-in steel plate was 10 mm. Smooth dowels with diameter $d = 12$ mm were used. The yield moment of the dowels was determined in 3-point bending tests with $M_{y,mean} \approx 190$ Nm. The estimated load-carrying capacity of connections loaded perpendicular to the grain consisting of 8 dowels is $F_{v,mean} \approx 114$ kN for the failure mode 2 according to the EYM.
In the test series three different relative connection heights $\alpha = 0.6,\ 0.7$ and 0.8 were studied. Width and height of the connection was chosen as $m \times n = 4 \times 2$ and 2×4. Six different configurations with 4 replicates each result in a total of 24 individual tests. 4 specimens with $\alpha = 0.6$ were reinforced against splitting by means of a total of 4 SFS WR-T 13 self-tapping fully threaded screws inserted 50 mm besides the external columns of fasteners.
The applied load was measured by means of oil pressure at the manually powered pump. The deflection in midspan of the beam, pull-out deformation of the steel plate and crack opening were measured by means of inductive measurements and LVDT. The deformation of the timber surface was determined by means of digital image correlation measurements.

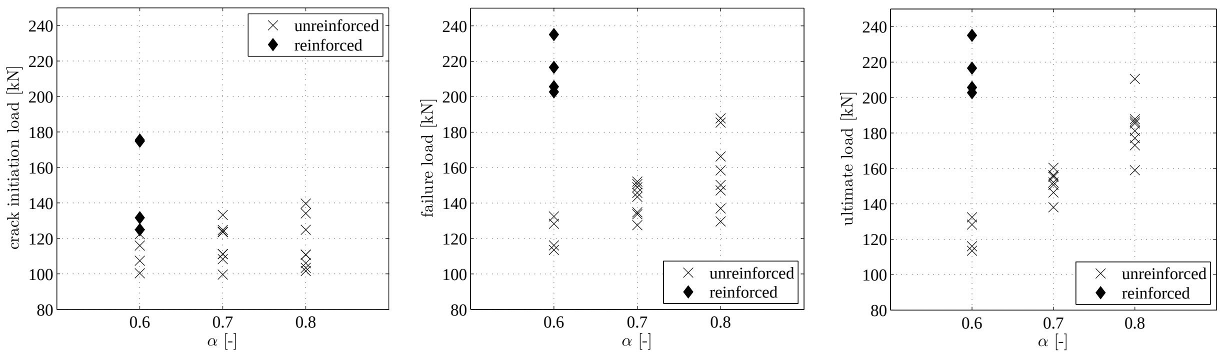

(a) (b) (c)

Figure 5: Loads at crack initiation (a), failure with unstable crack growth (b) and ultimate load (c) in the tests.

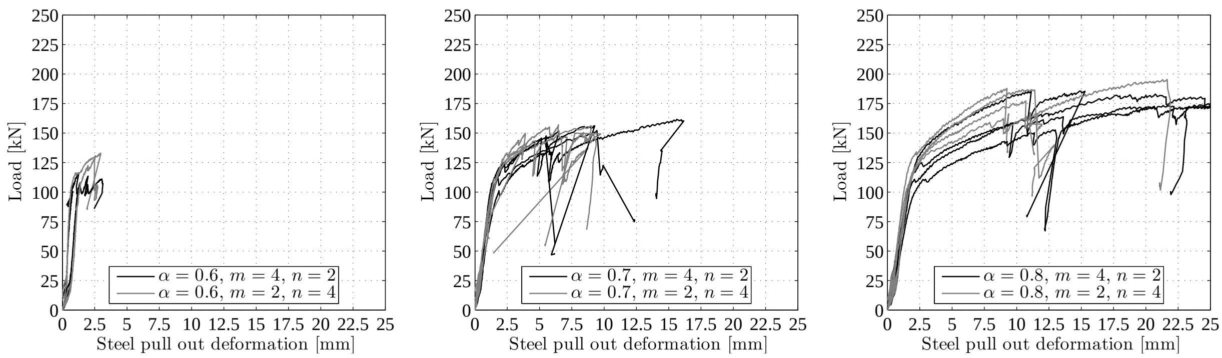

(a) (b) (c)

Figure 6: Pull-out deformation of the slotted-in steel plates for relative connection heights $\alpha = 0.6$ (a), $\alpha = 0.7$ (b) and $\alpha = 0.8$ (c).

In Fig. 5 the ultimate loads for specific failure events observed in the tests are given. It can be distinguished between load at crack initiation, unstable crack growth and ultimate load. Connections with a small relative connection height failed in a very brittle way. With increas-

ing relative connection height further loading after crack initiation was possible. Beams with $\alpha = 0.8$ showed a relatively stable crack growth and reached even higher capacities after separation of the upper and lower part of the beam.
The deformation of the slotted-in steel plates in relation to the timber is shown in Fig. 6. It can be seen that with increasing relative connection height a pronounced deformation of the connection occurs. Such ductile behaviour should be aimed at when designing connections loaded perpendicular to the grain for applications in practice. For $\alpha = 0.6$ failure occurs already at small relative deformations with a brittle failure behaviour. It can be concluded, that the load-carrying capacity of the fasteners is too high compared to the load-carrying capacity perpendicular to the grain of the timber in the vicinity of the connection.

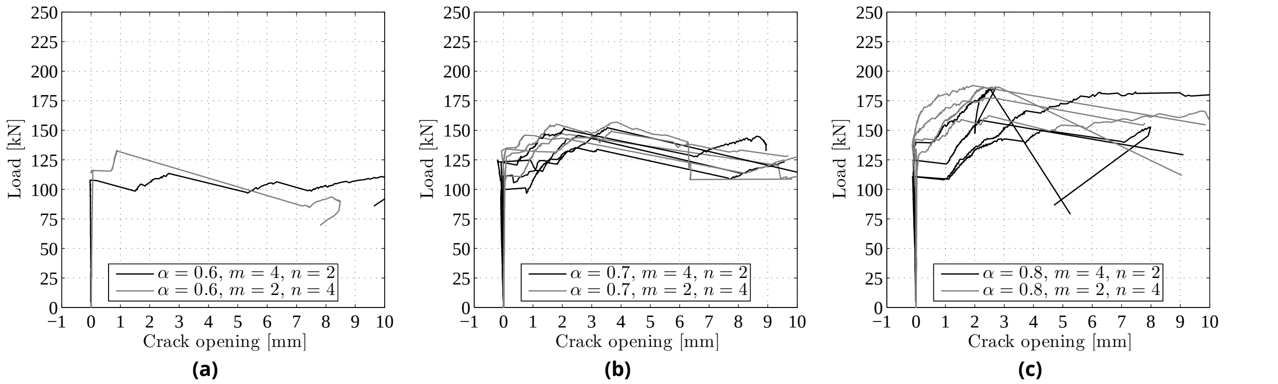

Figure 7: Crack opening in the center of the connection for relative connection heights $\alpha = 0.6$ (a), $\alpha = 0.7$ (b) and $\alpha = 0.8$ (c).

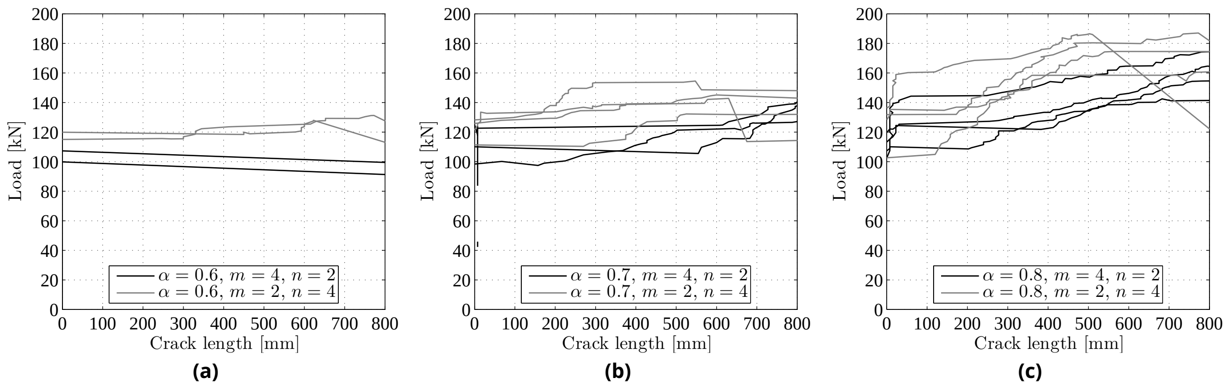

Figure 8: Development of the crack length in dependency of the applied load for relative connection heights $\alpha = 0.6$ (a), $\alpha = 0.7$ (b) and $\alpha = 0.8$ (c).

By evaluating the crack opening and crack length development (Fig. 7 and 8) a distinction between stable and unstable crack growth is possible. The crack opening was measured by means of LVDTs in the centre of the connection between two points approximately 25 mm above and below the top row of fasteners. The crack length was computed from the deformation measurements on the surface of the beam by means of 2D digital image correlation. It can be seen that crack initiation starts at a similar load level irrespective of the relative connection height. This load level corresponds approximately to the estimated load-carrying capacity of the fasteners according to EYM. Load levels for further crack growth and crack opening differ between the test series. For $\alpha = 0.6$ unstable crack growth occurs already at crack initiation with no potential of an increase in load. For $\alpha = 0.7$ and 0.8 continued loading is possible and a more stable crack growth can be observed before ultimate failure. The observed different degree in brittleness of the failure mechanism could serve as a basis for defining partial safety factors for design.

4 Evaluation of selected design approaches

Best fit between design approaches (Chapter 2) and test data (Tab. 3) is achieved when applying the approach by Ballerini (2004). The approach by Ehlbeck et al. (1989) shows a good match with test data as well. The relatively simple approach by van der Put (1990) exhibits a worse agreement with experimental data.
For a more detailed evalution of the design approaches the value of the material strength parameter $C_{1,i}$ can be back-calculated from the test results according to Eq. 1 and 2 for the design approaches by van der Put and Ballerini, respectively.

$$C_{1,vanderPut} = \frac{F_{90}}{2b\sqrt{\frac{\alpha h}{(1-\alpha)}}} \tag{1}$$

$$C_{1,Ballerini} = \frac{F_{90}}{2bf_w f_r\sqrt{\frac{\alpha h}{(1-\alpha^3)}}} \tag{2}$$

The theoretical value of C_1 can be calculated from the mode 1 fracture energy $G_{f,\mathrm{I}}$ and the shear modulus G_v according to Eq. 3.

$$C_{1,Theory} = \sqrt{\frac{3G_{f,I}G_v}{5}} \tag{3}$$

In this study the following values were used: mode 1 fracture energy $G_{f,\mathrm{I},mean} = 0.3$ N/mm with $CoV = 30\%$, shear modulus $G_{v,mean} = 650$ N/mm^2 with $CoV = 13\%$.
The approach by Ehlbeck et al. is evaluated with regard to the tensile strength perpendicular to the grain back-calculated according to Eq. 4.

$$f_{t,90,Ehlbeck} = \frac{F_{90}}{k_s k_r\left(6.5+18\alpha^2\right)\left(b_{ef}h\right)^{0.8}} \tag{4}$$

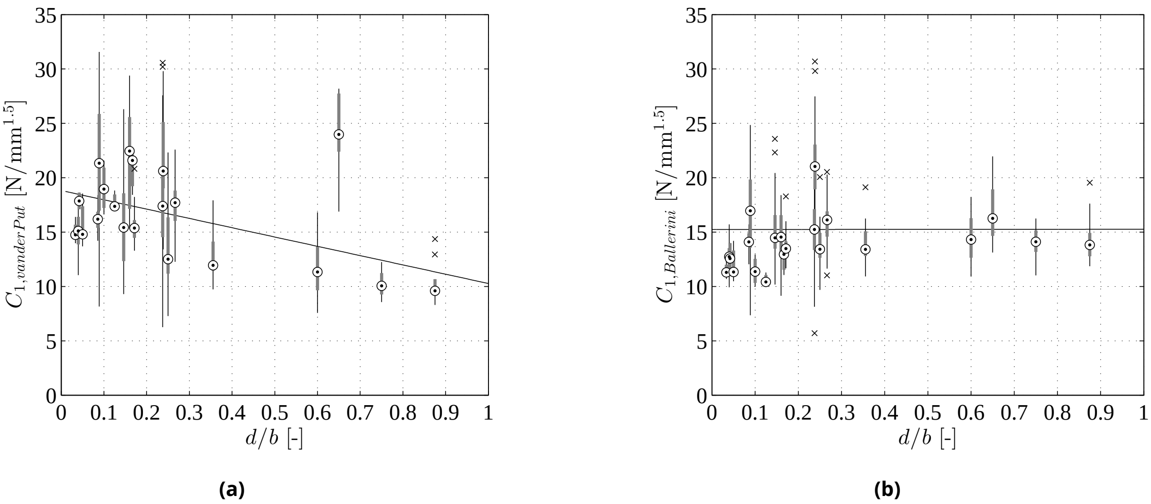

Figure 9: Dependency of $C_{1,i}$ on the relative fastener diameter d/b.

The mean coefficient of variation of the empirical value of material strength parameter $C_{1,i}$ and the tensile strength perpendicular to the grain $f_{t,90,Ehlbeck}$, respectively, are in the order of $CoV \approx 24\%$ (Ballerini), $CoV \approx 30\%$ (van der Put) and $CoV \approx 27\%$ (Ehlbeck et al.). The C_1 value back-calculated from the approach proposed by van der Put markedly depends on the relative fastener diameter d/b (Fig. 9 (a)). This approach is based on a situation represented by a beam with a crack over the entire beam width starting at a single dowel connection. For a larger number of dowels or nails with small diameter this approach leads to a conservative estimate. For the approach by Ballerini and by Ehlbeck et al. no such dependency can be found (Fig. 9 (b)). These approaches account for the effect of the geometry of the connection (Fig. 3 (c) and (d)).
The material parameter $C_{1,Theory}$ has a higher mean value and shows a lower variation than the values $C_{1,i}$ defined by Eqs. 1 and 2. The bias and increased variation of $C_{1,i}$ defined by Eqs. 1 and 2 can be accounted for by multiplying $C_{1,Theory}$ in Eq. 3 with a model uncertainty X with the distribution characteristics given in Tab. 4. It can be seen, that the model uncertainty $X_{Ballerini}$ according to the approach suggested by Ballerini is larger but the resulting coefficient of variation (CoV) of the model uncertainty is lower than according to the approach suggested by van der Put.

Table 4: Distribution characteristics of the model uncertainty X for multiplication with the theoretical value of material parameter $C_{1,Theory}$ to fit the back-calculated values from the approaches proposed by van der Put and Ballerini for the test data in Tab. 3.

Model uncertainty	Distribution	Mean	CoV
$X_{\text{van der Put}}$	Lognormal	0.94	29%
$X_{\text{Ballerini}}$	Lognormal	0.85	18%

5 Reliability of the evaluated design approaches

5.1 Actions and resistances

The reliability of the approaches for the design of connections loaded perpendicular to the grain can be evaluated as desribed in Kohler et al. (2012) or Jockwer et al. (2011). In the general design equation (Eq. 5) the characteristic values of resistance R and permanent (G) and variable (Q) actions are factored by partial safety factors γ_i in order to guarantee for the desired reliability of the design.

$$z\frac{k_{\text{mod}} \cdot R_{\text{k}}}{\gamma_{\text{m}}} - \gamma_{\text{G}} G_{\text{k}} - \gamma_{\text{Q}} Q_{\text{k}} = 0 \tag{5}$$

A modification factor $k_{mod} = 1$ is chosen in this study which should represent a short term action and a connection applied in service class 1 condition. Information about duration of load effects and influence of variations in moisture content can be found e.g. in Gustafsson and Larsen (2001) and Vesa and Kevarinmäki (2001). The parameter z is chosen during the design of the structure in order to fulfill Eq. 5.
The partial safety factors for permanent and variable loads are set as defined in EN 1990 (2005) $\gamma_{\text{G}} = 1.35$ and $\gamma_{\text{Q}} = 1.5$, respectively. The partial safety factor for the resistance of connections is suggested $\gamma_{\text{m}} = 1.3$ in EC5 (2004). This values is generally valid for all types of connections with brittle or ductile failure. The calibration of this factor has partly been based on studies of the bending capacity beams as described in (Sørensen, 2002). Other design situations, especially when being represented by different distribution functions or

exhibiting different variation, result in different partial safety factors. Kohler et al. (2012) suggest a considerably higher partial safety factors $\gamma_m \approx 3$ for the design situation of tension perpendicular to the grain. This supports the need for an evaluation of the reliability of the design of connections loaded perpendicular to the grain where high tensile stresses perpendicular to the grain occur. A careful evaluation of the adequacy of the 5^{th}-percentile value as the characteristic value of material strength or the proposal of new partial safety factors γ_m are necessary.
For the assessment of the reliability of the design approaches evaluated above the resistance R is represented by the material parameters C_1 and the tensile strength perpendicular to the grain $f_{t,90}$, respectively. In Fig. 10 (a) cumulative distributions of $C_{1,i}$ are given according to Eq. 1 and 2 based on the test results summarized in Tab. 3. In addition the tensile strength perpendicular to the grain according to Eq. 4 is graphed in Fig. 10 (b). A Lognormal distribution shows the best fit with the test results. However, the Weibull distribution is suggested by JCSS (2001) for the representation of tensile strength perpendicular to the grain. For the reliability study of the design approaches the parameters $C_{1,i}$ and $f_{t,90}$ were represented by distribution functions as given in Table 5. The distribution characteristics of permanent and variable loads are summarized in Tab. 6.

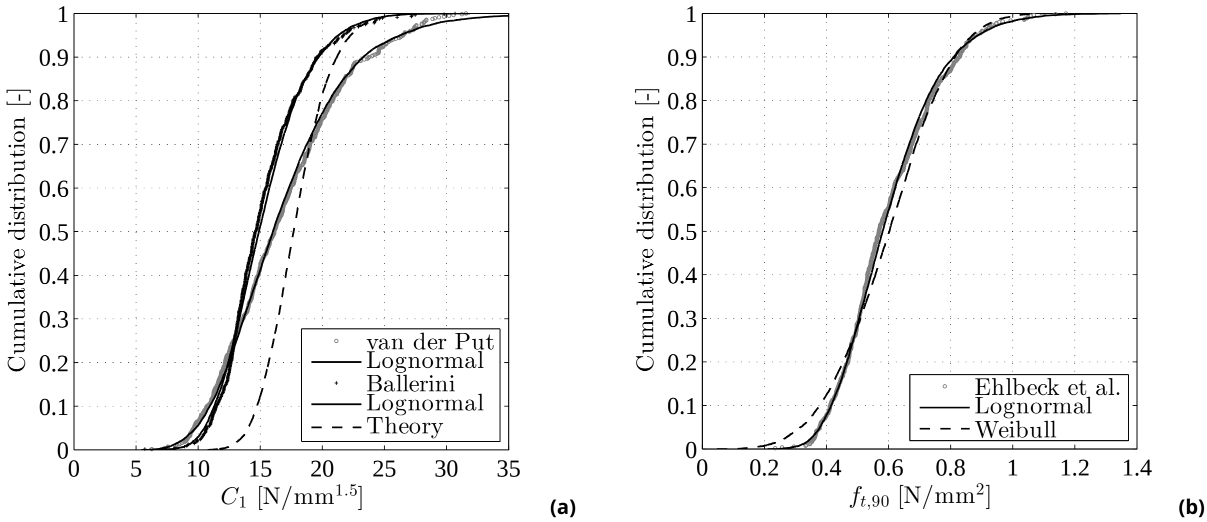

Figure 10: Cumulative distribution of the material parameters $C_{1,i}$ according to van der Put (Eq. 1) and Ballerini (Eq. 2) with the corresponding fitted Lognormal distributions and according to theory (Eq. 3) (a) and tensile strength perpendicular to the grain according to the approach by Ehlbeck et al. (Eq. 4) with fitted Lognormal and Weibull distribution (b).

Table 5: Distribution parameters and functions for material property value C_1 and $f_{t,90}$ determined from test data for the approaches by van der Put, Ballerini and Ehlbeck et al.

Approach	Parameter	Unit	Distr. function	Mean	CoV
van der Put	C_1	[N/mm$^{1.5}$]	Lognormal	16.7	30.6%
Ballerini	C_1	[N/mm$^{1.5}$]	Lognormal	15.2	21.8%
Ehlbeck et al.	$f_{t,90}$	[N/mm^2]	Lognormal	0.60	26.5%
Ehlbeck et al.	$f_{t,90}$	[N/mm^2]	Weibull	0.60	28.3%

Table 6: Distribution characteristics for loading types according to JCSS (2001) and partial factors.

Load type	Distribution	CoV	char. level	γ
Self weight	Normal	10%	50%	1.35
Live load	Gamma	53%	98%	1.5

5.2 Reliability analysis

The limit state function can be written as:

$$g = z \cdot \mathbf{R} - \mathbf{G} - \mathbf{Q} \tag{6}$$

In this function the resistance **R** can be represented by the random variables of the material parameters $\mathbf{C_1}$ and $\mathbf{f_{t,90}}$, respectively, with the distribution characteristics summarised in Tab. 5. The parameter z will be chosen in the design procedure such that the desired failure probability of $P_\text{f} \leq 10^{-5}$ ($\beta_r = 4.2$, for general situations) is not exceeded.

$$P_\text{f}(g \leq 0) = P_\text{f}(z \cdot R - G - Q \leq 0) \leq 10^{-5} \tag{7}$$

The fraction of variable load $Q_\text{mean}/(G_\text{mean} + Q_\text{mean})$ can cover a range between 0 and 1. For a value of 0.8 as proposed in (Kohler et al., 2012) the resulting design values of the material strength parameter $C_{1,d}$ and $f_{t,90,d}$, respectively, and the corresponding partial safety factors γ_m are listed in Tab. 7. Other values of the fraction of variable load lead to different reliability indices β_f (Fig. 11). Especially the design approach by Ballerini leads to considerably higher reliability indices for smaller fractions of variable loads compared to the desired value $\beta_r = 4.2$ corresponding to a probability of failure of $p_f = 10^{-5}$.

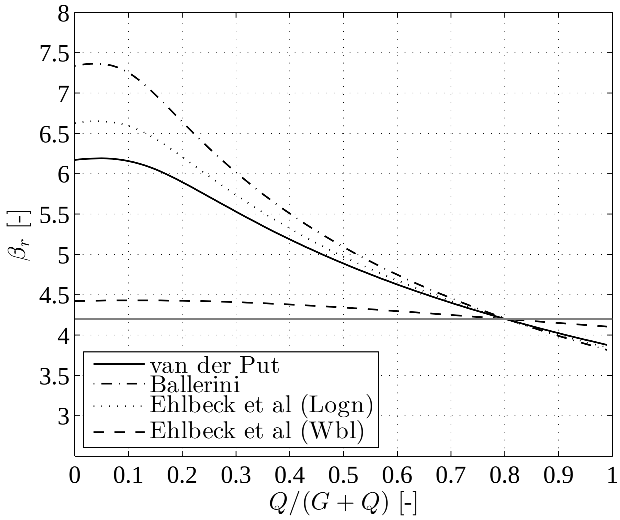

Figure 11: Reliability indices β_r in dependency of the fraction of variable load for the approaches suggested by van der Put, Ballerini and Ehlbeck.

Table 7: Mean, 5%-, and design values of the material parameter C_1 and $f_{t,90}$, respectively, and the corresponding partial safety factors γ_m for the design approaches suggested by van der Put, Ballerini and Ehlbeck for a fraction of variable load $Q_{mean}/(G_{mean} + Q_{mean})$ = 0.8.

Approach	Parameter	Unit	Mean	5%-value	design value	γ_m
van der Put	C_1	[N/mm$^{1.5}$]	16.7	9.8	7.19	1.36
Ballerini	C_1	[N/mm$^{1.5}$]	15.2	10.4	8.39	1.25
Ehlbeck et al. (Logn)	$f_{t,90}$	[N/mm^2]	0.60	0.38	0.292	1.30
Ehlbeck et al. (Wbl)	$f_{t,90}$	[N/mm^2]	0.60	0.31	0.12	3.27

5.3 Interpretation of the reliability study

When proposing design recommendations for connections loaded perpendicular to the grain, it has to be accounted for the different concepts behind design equations. A conservative design philosophy is to avoid design situations with loading in tension perpendicular to the grain and to avoid any possibility of crack initiation. Cracking is often considered as a diminution of esthetics though the load-carrying capacity might not be affected. The Swiss standard for timber structures SIA 265 (2012) is formulated based on the philosophy to give only low values of tensile strength perpendicular to the grain in order to make the designer not to calculate and verify the tensile stresses but either not to apply critical connections or to foresee strengthening elements.
The design value for tensile strength perpendicular to the grain $f_{t,90,d} = 0.15$ N/mm^2 for glulam and $f_{t,90,d} = 0.1$ N/mm^2 for solid timber given in SIA 265 (2012) is on the same level as the design value $f_{t,90,d} = 0.12$ N/mm^2 for connections loaded perpendicular to the grain determined for the approach by Ehlbeck et al. when using a Weibull distribution (Tab. 7). In contrast to that the characteristic value $f_{t,90,k}$ in EN 14080 (CEN, 2013) is even higher compared to the 5%-value determined for the approach by Ehlbeck et al. when using a Lognormal distribution. An increase of the partial safety factor γ_m for the tensile strength perpendicular to the grain or a reduction of the characteristic value $f_{t,90,k}$ seems necessary.
The material parameter C_1 in the approach by van der Put for the implementation in EC5 should be based on the design value $C_{1,d} = 7.2$ N/mm$^{1.5}$. This design values leads in combination with a general partial safety factor $\gamma_m = 1.3$ to a characteristic value $C_{1,k} = 9.3$ N/mm$^{1.5}$. A further reduction of the characteristic value based on the above discussion regarding tensile strength perpendicular to the grain or the implementation of the more sophisticated approach by Ballerini can be reasonable.

6 Reinforcement of connections

In the tests carried out at ETH Zurich also the effect of the reinforcement on the failure behaviour and the load-carrying capacity of connections loaded perpendicular to the grain was studied. A beneficial impact of the reinforcement on the load-carrying capacity could be confirmed, though crack initiation could not be avoided as shown in Fig. 12. After crack initiation the crack was stabilized approximately at the position of the reinforcement. The load at ultimate failure reaches the level of the bending capacity of the full cross-section.

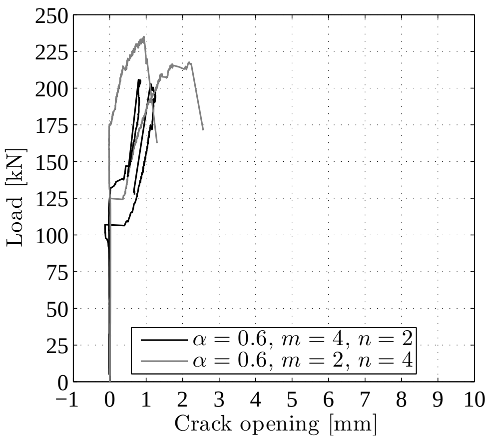

(a)

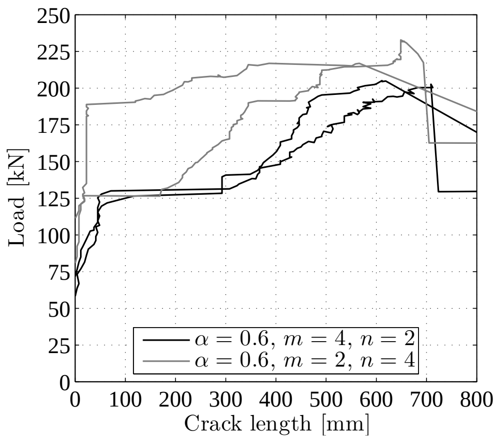

(b)

Figure 12: Crack opening in the center of the connection (a) and development of the crack length (b) in dependency of the applied load for reinforced connections loaded perpendicular to the grain with $\alpha = 0.6$.

7 Conclusion

From the study presented in this paper, the following conclusions can be drawn:

- The efficiency of the design approaches evaluated in this study depends on the degree of detailing of the approach. The relatively simple approach by van der Put forming the basis of the EC5 design equation requires a higher partial safety factor compared to the more detailed design approach by Ballerini. A characteristic value $C_{1,k} = 9.3$ N/mm$^{1.5}$ can be used in combination with a general partial safety factor $\gamma_m = 1.3$ for the approach by van der Put which is considerably lower than the current value in EC5.
- The design approach suggested by Ehlbeck et al. based on the tensile strength perpendicular to the grain requires a very low design value $f_{t,90,d}$ or a considerable high value of the partial safety factor $\gamma_m = 3.3$ compared to the current general value in order to achieve the desired reliability ($\beta_r = 4.2$). Duration of load effects and effects from moisture variations have to be accounted separately.
- Cracking at connections loaded perpendicular to the grain due to excessive tensile stresses perpendicular to the grain can occur also for relative connection heights $\alpha > 0.7$ exceeding the threshold currently given in EC5. Though crack growth becomes more stable with increasing relative connection height the separation of the beam into individual parts of small cross-section has to be accounted for in the design. Bending failure of the lower cross-section occurred in the tests carried out at ETH Zurich for $\alpha = 0.8$.
- Reinforcement is an easy and efficient measure to restore the load-carrying capacity of beams with connections loaded perpendicular to the grain. Nevertheless, initial cracking at a load level similar to the unreinforced beam will occur also when using reinforcement.

References

Ballerini M. (1999): A new set of experimental tests on beams loaded perpendicular-to-grain by dowel-type joints. In: Proc. of the CIB-W18 Meeting 32, Graz, Austria, Paper No. CIB-W18/32-7-2

Ballerini M. (2004): A new prediction formula for the splitting strength of beams loaded by dowel-type connections. In: Proc. of the CIB-W18 Meeting 37, Edingburgh, Scotland, Paper No. CIB-W18/37-7-5

Ballerini M., Giovanella A. (2003): Beams transversally loaded by dowel-type joints: influence on splitting strength of beam thickness and dowel size. In: Proc. of the CIB-W18 Meeting 36, Colorado, USA, Paper No. CIB-W18/36-7-7

CEN (2004): EN 1995-1-1: Eurocode 5: Design of timber structures - Part 1-1: General - Common rules and rules for buildings. European Committee for Standardization CEN, Bruxelles, Belgium

CEN (2005): EN 1990/A1: Eurocode - Basis of structural design. European Committee for Standardization CEN, Bruxelles, Belgium

CEN (2013): EN 14080: Timber structures - Glued laminated timber and glued solid timber - Requirement. European Committee for Standardization CEN, Bruxelles, Belgium

DIN (2008): DIN 1052: Entwurf, Berechnung und Bemessung von Holzbauwerken - Allgemeine Bemessungsregeln und Bemessungsregeln für den Hochbau. DIN 1052 (2008-12), DIN Deutsche Institut für Normung e.V., Berlin, Germany

Ehlbeck J., Görlacher R. (1983): Tragverhalten von Queranschlüssen mittels Stahlformteilen, insbesondere Balkenschuhen, im Holzbau. Tech. rep., Versuchsanstalt für Stahl, Holz und Steine, Abteilung Ingenieurholzbau, Universität Fridericiana Karlsruhe, Germany

Ehlbeck J., Görlacher R., Werner H. (1989): Determination of perpendicular to grain stresses in joints with dowel-type fasteners - a draft proposal for design rules. In: Proc. of the CIB-W18 Meeting 22, Berlin, Germany, Paper No. CIB-W18/22-7-2

Franke B., Quenneville P. (2011): Design approach for the splitting failure of dowel-type connections loaded perpendicular to grain. In: Proc. of the CIB-W18 Meeting 44, Vancouver, Canada, Paper No. CIB-W18/44-7-5

Gustafsson P., Larsen H. (2001): Dowel joints loaded perpendicular to grain. In: Proceedings of the Int. RILEM Symposium, Stuttgart, Germany, pp 577–586

Habkirk R. (2006): Bolted wood connections loaded perpendicular-to-grain - effect of wood species. Tech. rep., Department of Civil Engineering, Royal Military College of Canada, Kingston, Ontario, Canada, master thesis

JCSS (2001): Probabilistic Model Code. Joint Committee of Structural Safety, available online at: http://www.jcss.byg.dtu.dk/

Jensen J.L., Quenneville P. (2011): Splitting of beams loaded perpendicular to grain by connections–some issues with EC 5. In: Proc. of the CIB-W18 Meeting 44, Alghero, Italy, research note

Jensen J.L., Gustafsson P.J., Larsen H.J. (2003): A tension fracture model for joints with rods or dowels loaded perpendicular to grain. In: Proc. of the CIB-W18 Meeting 36, Colorado, USA, Paper No. CIB-W18/36-7-9

Jockwer R., Steiger R., Frangi A., Kohler J. (2011): Impact of material properties on the fracture mechanics design approach for notched beams in Eurocode 5. In: Proc. of the CIB-W18 Meeting 44, Alghero, Italy, Paper No. CIB-W18/44-6-1

Kasim M.H. (2002): Bolted timber connections loaded perpendicular-to-grain - effect of row spacing on resistance. Tech. rep., Department of Civil Engineering, Royal Military College of Canada, Kingston, Ontario, Canada, master thesis

Kohler J., Steiger R., Fink G., Jockwer R. (2012): Assessment of selected Eurocode based design equations in regard to structural reliability. In: Proc. of the CIB-W18 Meeting 45, Växjö, Sweden, Paper No. CIB-W18/45-102-1

Lehoux M.C.G., Quenneville J.H.P. (2004): Bolted wood connections loaded perpendicular-to-grain, a proposed design approach. In: Proc. of the CIB-W18 Meeting 37, Edinburgh, Schottland, Paper No. CIB-W18/37-7-4

Leicester R.H. (1973): Effect of size on the strength of structures. Commonwealth scientific and industrial research organization CSIRO, Melbourne, Australia

Lignum (1990): Holzbau-Tabellen HBT 2. Lignum, Zürich

Mistler H.L. (1998): Design of glulam beams according to EC 5 with regard to perpendicular-to-grain tensile strength - A comparison with research results. Holz als Roh - und Werkstoff 56(1):51–60

Möhler K., Siebert W. (1981): Queranschlüsse bei Brettschichtträgern oder Vollholzbalken. Bauen mit Holz 83:84–89

van der Put T.A.C.M. (1990): Tension perpendicular to the grain at notches and joints. In: Proc. of the CIB-W18 Meeting 23, Lisbon, Portugal, Paper No. CIB-W18/23-10-1

Quenneville J., Mohammad M. (2001): A proposed canadian design approach for bolted connections loaded perpendicular-to-grain. In: Proceedings of the Int. RILEM symposium on joints in timber structures, pp 61–70

Reshke R. (1999): Bolted timber connections loaded perpendicularto grain: influence of joint configuration parameters on strength. Tech. rep., Department of Civil Engineering, Royal Military College of Canada, Kingston, Ontario, master thesis

Schoenmakers J.C.M. (2010): Fracture and failure mechanisms in timber loaded perpendicular to the grain by mechanical connections. PhD thesis, Technische Universiteit Eindhoven

SIA (2012): Standard SIA 265 - Timber Structures. SIA Swiss Society of Engineers and Architects, Zurich, Switzerland

Sørensen J.D. (2002): Calibration of partial safety factors in Danish structural codes. In: Proc. of the JCSS Workshop on Reliability Based Code Calibration, Zurich, Switzerland

Vesa J., Kevarinmäki A. (2001): Long-term capacity of bolted joints loaded perpendicular to grain. In: Proceedings of the Int. RILEM Symposium, Stuttgart, Germany, pp 587–596

Zarnani P., Quenneville P. (2013): Wood splitting capacity in timber connections loaded transversely: Riveted joint strength for full and partial width failure modes. In: Proc. of the CIB-W18 Meeting 46, Vancouver, Kanada, Paper No. CIB-W18/46-7-5

Discussion

The paper was presented by R Jockwer

F Lam commented that 3 P Weibull distribution would provide a better fit for the distribution tails. R Jockwer agreed.

I Smith suggested use of reinforcement rather than depending on design approaches that rely on stable crack growth.

H Blass asked about reinforcement between the dowels. R Jockwer responded that they thought about this but did not use it because of the arrangement of steel plates and dowels were rather close. H Blass and R Jockwer further discussed the diameter of the dowel in relationship to the size of the potential reinforcement screws.

P Zarnani and R Jockwer discussed issues related to recording the crack opening.

P Gustafsson asked if this is only valid for symmetric test set up. R Jockwer answered that they had considered one sided loading and it seemed to be okay. However the experimental base for unsymmetrical loading is quite weak.

Simplified Fatigue Design of Typical Timber-Concrete Composite Road Bridges

Dipl.-Ing. Katrin Kudla, Scientific Researcher

Prof. Dr.-Ing. Ulrike Kuhlmann, Head of Institute

Institute of Structural Design, University of Stuttgart, Germany

Keywords: Timber-concrete composite, road bridge, notch connection, fatigue

1 Introduction

Timber-concrete composite (TCC) road bridges are an economical solution for one- or two-lane single span bridges with spans between 10 and 30 m. Approximately 50 % of all existing road bridges in Germany have spans ranging from 5 to 30 m (*Schmitt et al.*, 2003), which shows the big market. Because traffic is representing a variable cyclic load, fatigue verifications of all structural members including the shear connectors are required for the design.

Design rules for fatigue verifications of TCC bridges and of appropriate connectors are not given in the standards. That is why, based on an extensive parameter study and traffic simulations, fatigue verifications and possible simplifications for typical types of TCC bridges with notched shear connections have been investigated (*Kuhlmann & Kudla*, 2015). Notched connections are especially appropriate for bridges due to high stiffness, high strength values and the simplicity of construction. Thus a practice-oriented design proposal for simplified fatigue verifications of the structural members and the notched connection has been developed. The results are directly applicable also for the connector type described in *Müller* (2014). Other possible connection types for TCC road bridges, e.g. hbv system (*Bathon & Bletz-Mühldorfer*, 2014) or X-connectors (*Kuhlmann & Aldi,* 2009), were not considered, but studies could easily be extended.

2 Important parameters of the bridges

2.1 Geometry and material properties

For the improvement of the fatigue verifications given in *EN 1995-2* (2010) regarding TCC road bridges, simulations with two different fatigue load models according to *EN 1991-2* (2010) were carried out. Herein typical geometries, span lengths and material properties, which are relevant for practice, were taken into account. In Table 1 the most important conditions and parameters, the simulations were based on, are summarised.

In total 15 different TCC road bridges were investigated. The cross-sections of the bridges, given in Table 2, were calculated using two-dimensional framework models, as e.g. in Figure 5, under static loading conditions and with all relevant load cases. Time steps *t = 0*, *t = 3-7 years* and *t = ∞* were considered according to *Schänzlin & Fragiacomo* (2006).

Table 1. Parameters for the simulations with TCC bridges.

Parameter	Property
Structural system	Single span bridges
Span length	10 m, 15 m, 20 m, 25 m and 30 m
Bridge Type 1 (Figure 1)	Total width 4.5 m (single lane bridge), one block timber beam
Bridge Type 2 (Figure 2)	Total width 10.5 m (two lanes), two block timber beams
Bridge Type 3 (Figure 3)	Total width 10.5 m (two lanes), six timber beams
Shear connector	Notch, slip modulus $K_{ser} = K_u$ = 1,600 kN/mm per m beam width
Timber strength class	Glulam GL28c according to *EN 14080* (2013)
Concrete strength class	C 40/50 according to *EN 1992-1-1* (2011)

Table 2. Cross-sections for all bridge Types.

Bridge Type	Span length [m]	Width of timber beam [m]	Height of timber beam [m]	Effective width of concrete slab per beam [m]	Thickness of concrete slab [cm]
Type 1	10	2.52	0.6	4.5	22
	15	2.70	0.8	4.5	25
	20	3.06	0.9	4.5	28
	25	3.24	1.1	4.5	34
	30	3.60	1.2	4.5	40
Type 2	10	2 x 2.52	0.6	4.19	28
	15	2 x 2.70	0.8	4.76	28
	20	2 x 3.24	0.9	5.25	28
	25	2 x 3.42	1.1	5.25	32
	30	2 x 3.60	1.2	5.25	38
Type 3	10	6 x 0.90	0.7	1.60	22
	15	6 x 0.90	0.8	1.70	25
	20	6 x 1.08	0.9	1.78	28
	25	6 x 1.26	1.1	1.76	32
	30	6 x 1.26	1.2	1.76	36

For a span length of 20 m, bridge Types 1 to 3 are shown in Figures 1 to 3. Bridge Type 1 with only one lane could be built for agricultural or forestry use and low flow rates of lorries (see Table 4.5 in *EN 1991-2* (2010), traffic categories 3 or 4). In Germany, for this kind of bridges a total width of 4.5 m is recommended. Bridge Types 2 and 3 could be used for roads and motorways with up to 300 lorries per day. This restriction is not related to the fatigue failure, but to geometry specifications given in the German guideline for road construction (*Forschungsgesellschaft für Straßen- und Verkehrswesen*, 1996). Here the number of heavy vehicles per day is decisive for the choice of a standard cross-section for the bridge. For the project standard cross-section types *RQ 7.5* (width of one lane 2.75 m) or *RQ 9.5* (width of one lane 3.0 m) were chosen for bridge Types 2 and 3. Even though type *RQ 7.5* should be used for a maximum of 60 lorries per day and type *RQ 9.5* for a maximum of 300 lorries per day, for investigation of the fatigue verifications, traffic categories 3 to 1 according to Table 4.5 in *EN 1991-2* (2010) were considered. Traffic categories given in *EN 1991-2* (2010) indicate the number of heavy vehicles expected per year and per lane. Traffic category 3 stands for 343 lorries per day and traffic category 1 stands for 5480 lorries per day.

Standard cross-section type *RQ 7.5* with a total width of 10.0 m was chosen for bridge Type 2 with span lengths of 10 m and 15 m due to the long cantilever of the concrete slab. Also the thickness of the concrete slab was increased in these cases, see Table 2. In practice it might be a better solution to support the cantilevers with additional timber beams. In any other case of bridge Types 2 and 3 standard cross-section type *RQ 9.5* was used.

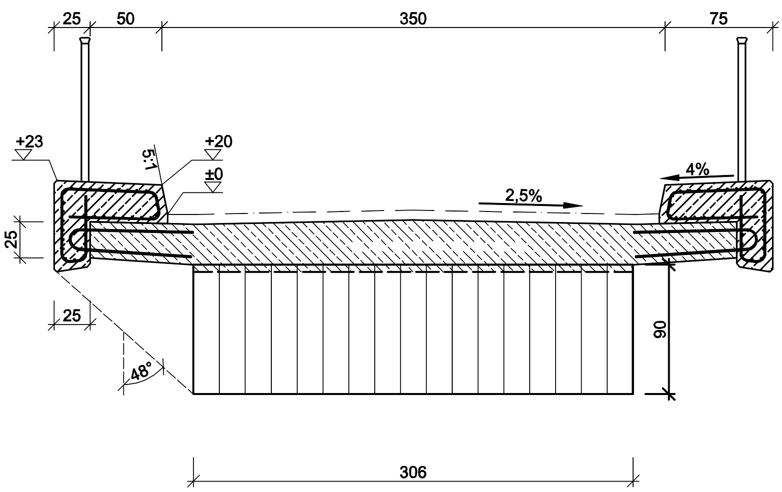

Figure 1. Type 1 - Cross-section for single lane bridge (span length 20 m), dimensions in cm.

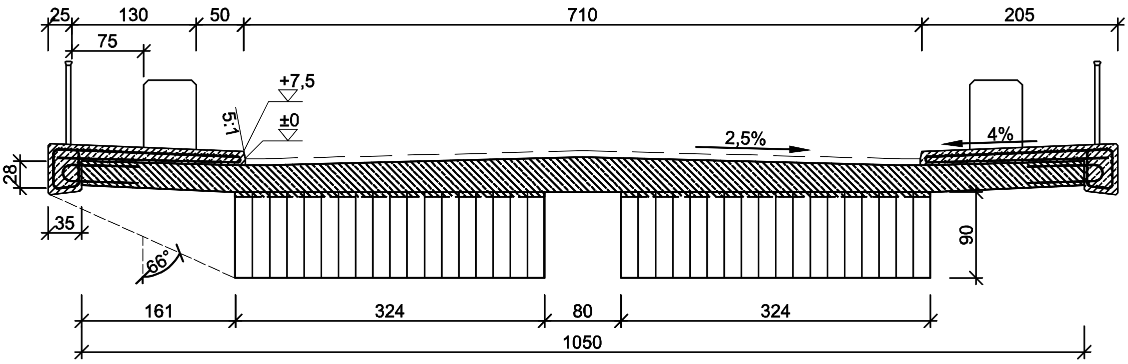

Figure 2. Type 2 - Standard cross-section for two lane bridge (span length 20 m), dimensions in cm.

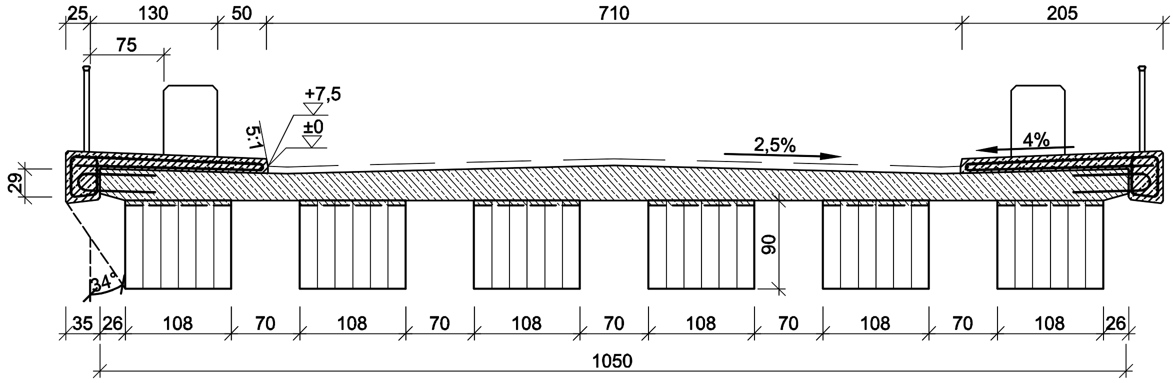

Figure 3. Type 3 - Standard cross-section for two lane bridge (span length 20 m), dimensions in cm.

2.2 Properties of the notched shear connection

2.2.1 Dimensions and slip modulus

In Figure 4 the functionality of a notched connection, where the shear force is transferred directly through the compression edge of the notch, is shown. Additionally a screw (not shown) is placed vertically in the notch for transferring lifting forces between timber and concrete. For the shear connection between timber and concrete 50 mm deep and 200 mm long notches were considered. The longitudinal distance between the notches was varied according to the shear force distribution for a uniformly distributed load.

The slip modulus of the connection of K_u = K_{ser} = 1,600 kN/mm per m beam width has been estimated according to former research works and experimental tests. In *Kuhlmann & Kudla* (2015) a summary of different values for the slip modulus based on various push-out tests is included. A relatively high slip modulus of 1,600 kN/mm represents a conservative assumption for the fatigue verification. A lower slip modulus would lead to a better load distribution between the notches and to a decreased shear force of the maximum loaded notch.

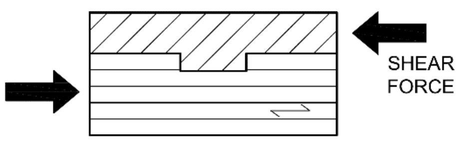

Figure 4. Notched connection within a TCC beam.

2.2.2 Fatigue strength

For an application to traffic loading conditions, the fatigue behaviour of the notch is needed. At the University of Stuttgart (Germany) experimental tests on push-out and beam specimens with notches have been carried out under static and fatigue loading (*Kuhlmann & Aldi*, 2010). All the tests showed a shear failure mechanism in the timber beam in front of the notch, which is more critical than a relatively ductile compression fatigue failure. Based on the test results from *Kuhlmann & Aldi* (2010) it was identified that the longitudinal shear strength of the notch and the corresponding number of load cycles to failure match the specifications given in *EN 1995-2* (2010), Annex A, § A3 (3) for timber elements under shear. At the University of Stuttgart the fatigue tests were carried out for a load ratio of $R = 0.1$. Based on the good accordance of tests and design code in this case, the values for strength reduction according to *EN 1995-2* (2010) were used for the traffic simulations in *Kuhlmann & Kudla* (2015). The reduction of strength with number of load cycles may be calculated depending on the type of action with Equation (1).

$$k_{fat} = 1 - \frac{1-R}{a \cdot (b-R)} \cdot \log(\beta \cdot N_{obs} \cdot t) \qquad (1)$$

where $R = F_{min} / F_{max}$, $N_{obs}\, t$ = number of constant amplitude load cycles in total, β = design fatigue factor based on the damage consequence for the actual structural component, a, b = coefficients representing the type of fatigue action. The value β has been chosen to 3 for substantial consequences in case of damage (*EN 1995-2*, 2010, Annex A, § A3 (3)). Corresponding to the dominating failure mechanism in the tests, the values of coefficients a and b have been chosen to $a = 6.7$ and $b = 1.3$ for shear, see Table A.1 in *EN 1995-2* (2010).

Using the factor representing the reduction of strength, the characteristic strength for static loading may be modified for the fatigue verification. The design fatigue strength for shear may be calculated according to Equation (2).

$$F_{fat,d} = k_{fat} \cdot \frac{F_{ult}}{\gamma_{M,fat}} \qquad (2)$$

where F_{ult} = characteristic shear strength for static loading, $\gamma_{M,fat} = 1.0$ = material safety factor for fatigue.

3 Traffic simulations

3.1 Fatigue load models (FLM) for the fatigue design

For the traffic simulations, two different fatigue load models (FLM 3 and FLM 4 according to *EN 1991-2*, 2010) were used. FLM 3 consists of a single vehicle load, whereas FLM 4 represents five different types of lorries. FLM 3 is a simplified model, which originally was derived through a comparison of the damage of different internal forces in a main girder due to FLM 3 and due to a more detailed load model. As common for other construction materials, the resulting internal forces due to FLM 3 may be modified with damage equivalent λ-factors corresponding to the geometry of the bridge and the real traffic load in order to simplify the fatigue verification. Without such a modification, only the total number of constant amplitude load cycles ΔF_{max} per year can be taken into account, see *EN 1995-2* (2010), Annex A, § A3 (1). The consequence is an overall conservative estimation of the damage due to traffic loads. A more precise and detailed possibility is the fatigue verification with FLM 4 and a damage accumulation according to Palmgren-Miner rule (*Miner*, 1945). It consists of five types of lorries that are typical for the European traffic. The standard lorries are defined by the number of axles, axle distances, axle load and wheel types. For FLM 4, the percentages of different lorry types in the sequence depend on the traffic type (long distance, medium distance or local traffic). For FLM 4 as well as for FLM 3, the total number of lorries expected per year and per lane depends on the traffic category (*EN 1991-2*, 2010). How the damages due to FLM 3 and FLM 4 have been calculated is shown in *Stephan & Kuhlmann* (2014).

3.2 Determination of internal forces due to fatigue loading with two-dimensional and three-dimensional models

To determine internal forces of a TCC bridge with notches due to fatigue loading, a two-dimensional framework model according to *Grosse et al.* (2003) may be used, see Figure 5. In the model, properties of the concrete slab are assigned to the upper chord and properties of the timber beam are assigned to the lower chord. The slip modulus of the connection is transformed into an effective bending stiffness of the vertical struts with hinges at the edges, connecting upper and lower chord and representing the notches.

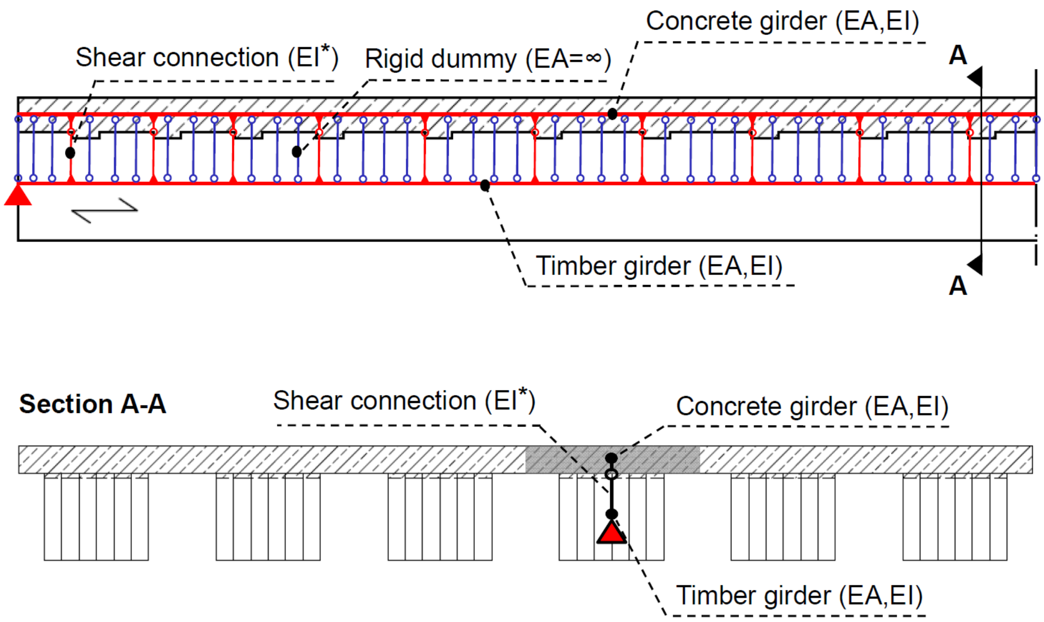

Figure 5. Framework model for a TCC bridge with notches (side view and cross-section Type 3).

With two-dimensional models, influence lines for a moving load of 1 kN in longitudinal direction were developed for all bridges and the governing internal forces. These influence lines were the basis for the calculation of load ranges due to the crossing of moving axle loads from fatigue load models FLM 3 and FLM 4.

For bridge Type 3, also influence lines for the transverse direction were calculated using three-dimensional models. With three-dimensional models the influence of the load distribution between the timber beams were analysed. Especially the influence of the load distribution on the maximum shear force at the notch was investigated with regard to the fatigue design. One of the results was that if the span length increases, the load distribution between the notches in longitudinal direction and also the distribution between adjacent beams in transverse direction are improved, because the overall stiffness of the system decreases. For the fatigue verification of the notch for bridge Type 3, the maximum load range could be calculated with a reduction factor depending on the span length (see Table 3), if the load distribution between the beams should be taken into account. The reduction factor corresponds to the maximum shear force at the outer beam, calculated with a three-dimensional model. To derive the shear force from a two-dimensional model, the maximum force from this model can be multiplied by the reduction factor given in Table 3.

Table 3. Reduction factor considering load distribution for bridge Type 3 (calculation of the shear force at the notch).

Span length [m]	Reduction factor
10	0.74
15	0.74
20	0.71
25	0.67
30	0.66

4 Summary of the numerical parameter studies

4.1 Conditions for the parameter studies

Within the parameter studies, three different bridge types with five different span lengths (see Table 2), four traffic categories, three traffic types and service lives between 80 and 140 years were considered. Damage effects of fatigue load models FLM 3 and the more detailed FLM 4 were compared to each other in order to identify critical cases for which fatigue verifications are required. A detailed description of the parameter studies and calculated damages may be found in *Kuhlmann & Kudla* (2015).

4.2 Results

- For a bridge with a span length of 25 m or more and a service life less than 140 years, there is no risk of a fatigue failure of any timber member or notch.
- A high traffic volume (traffic category 1 with 2 million lorries per year) leads to a greater fatigue damage than a low traffic volume (traffic category 4 with 50,000 lorries per year). This correlation is linked to the total number of load cycles during

service life. Therefore the fatigue damage also rises with longer service lives, but the influence of the traffic category is higher.

- Damages due to FLM 4 are significantly less than the damages due to FLM 3 with only a few exceptions.
- Based on investigations with the more detailed FLM 4, fatigue verifications of the notches are relevant for the design if all of the following conditions apply:
    - Design for traffic categories 1 or 2 according to *EN 1991-2* (2010) and span length smaller than 25 m
    - Traffic types of medium or long distance (a minimum distance of 50 km) according to *EN 1991-2* (2010), which is decisive for the amount of lorries
    - Bridge Type 3 (without consideration of the load distribution in transverse direction)
- In any other case strength verifications of the notch under static loading conditions are governing the design compared to fatigue verifications. Especially for local traffic and traffic categories 3 or 4 there is no risk of fatigue failure.
- Fatigue failures of the timber beams under bending moment and tension force at mid-span and under shear at the supports are not relevant.
- A fatigue verification of the concrete slab was not required in any case, because the concrete compression stresses for the characteristic combinations of actions were smaller than 60 % of the characteristic compression strengths.

5 Proposal for a simplified fatigue verification of TCC bridges with notches

5.1 Design steps

5.1.1 Overview

For the combination of bending moment and tension force in the timber beam as well as for the shear at the support fatigue verifications are not required, if the ratio κ between the stress range for fatigue loading $\Delta\sigma = |\sigma_{max} - \sigma_{min}|$ and the corresponding design strength $f_k/\gamma_{M,fat}$ is not higher than the following values (*EN 1995-2*, 2010, Annex A, § A1 (3)):

- Members in bending and tension: 0.2
- Members in shear: 0.15

Based on investigations in *Kuhlmann & Kudla* (2015) it is proposed that these threshold values should be checked, if the bridge is designed for traffic categories 1 or 2 and a span length smaller than 25 m. For any other case the fatigue verifications of these internal forces have proved to be not relevant. If the given threshold value for the combination of bending moment and tension force or shear at the support is exceeded, the fatigued design should follow the procedure given in *EN 1995-2* (2010), Annex A.3.

For the notched connection, the new design procedure for the fatigue verification is summarised in Figure 6. The chosen standard cross-sections of the bridges are primarily applicable for traffic categories 3 and 4 (see Chapter 2.1). For these traffic categories no fatigue verifications are required, because the strength verifications govern the design. In the following, results of further investigations with traffic categories 1 and 2 are given which show the chances in TCC road bridge construction regarding fatigue.

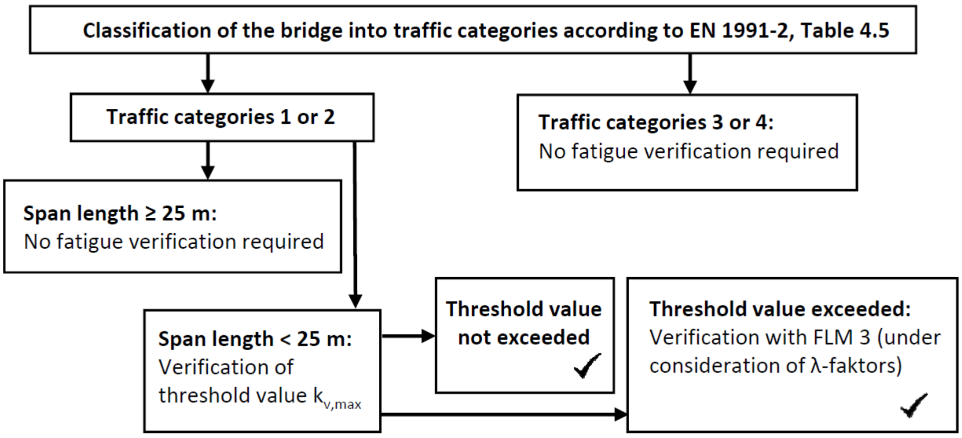

Figure 6. Proposed design steps for the simplified fatigue verification of the notched connection.

The threshold value for ratio κ given in *EN 1995-2* (2010) indicates that a fatigue verification of the notch (timber member in shear) is not required, if the stress due to FLM 3 is smaller than 15 % of the characteristic shear strength. It is not known on which tests or publications this assumption is based on. Using a threshold value for ratio κ implies the existence of a constant amplitude fatigue limit for each loading direction. If the maximum stress from fatigue loading is lower than this fatigue limit, an infinite number of load cycles would be bearable and no fatigue failure would occur. But the existence of constant amplitude fatigue limits similar to steel is not proven for timber. According to *Mohr* (2001) a bilinear S-N-curve with a smaller gradient of the curve for load cycles of more than 2 million might be possible for the shear fatigue strength. But the specifications for the threshold values given in *EN 1995-2* (2010), where no fatigue limit has to be considered, proved to be on the safe side for the cases considered in *Kuhlmann & Kudla* (2015) and should be applied.

Verifications with a threshold value for ratio κ do not include influences from the number of load cycles per year, the service life and load ratio R. There is no relation to the governing S-N-line or the reduction of strength with number of load cycles. Therefore a new design procedure is proposed to consider these influences within a simplified fatigue verification of the notched connection.

5.1.2 Step 1: Verification of the notch with a threshold value to check whether a detailed fatigue verification is needed

For traffic categories 1 and 2 and span lengths smaller than 25 m, a verification of ratio $k_{v,max}$, which is the ratio between the maximum shear force under fatigue loading and the shear strength, is recommended. Ratio $k_{v,max}$ is calculated according to Equation (3).

$$k_{v,\max} = \frac{F_{d,\min} + \Delta F_{FLM3}}{\dfrac{F_{ult}}{\gamma_{M,fat}}} = \frac{F_{d,\max}}{\dfrac{F_{ult}}{\gamma_{M,fat}}} \tag{3}$$

where F_{ult} = characteristic shear strength, $\gamma_{M,fat}$ = 1.0, $F_{d,min}$ = shear force due to permanent load and ΔF_{FLM3} = shear force due to FLM 3. The characteristic shear strength of the notch is determined according to Equation (4).

$$F_{ult} = 8 \cdot t_v \cdot b \cdot k_{cr} \cdot f_{v,k} \tag{4}$$

where t_v = notch depth, b = beam width, k_{cr} = 2.5 / $f_{v,k}$ according to German NA for *EN 1995-1-1* (2010) and $f_{v,k}$ = 3.5 N/mm² according to *EN 14080* (2013).

The verification for ratio $k_{v,max}$ is shown in Equation (5).

$$k_{v,\max} \le k_{fat} \tag{5}$$

The threshold value k_{fat} (reduction of strength with number of load cycles according to Equation (1)) for ratio $k_{v,max}$ can be calculated for traffic categories 1 and 2 separately. A diagram that shows the reduction of strength depending on the number of load cycles according to the traffic category (*TC 2* traffic category 2 and *TC 1* traffic category 1) and load ratio $R = F_{d,min} / F_{d,max}$ allows for a simple estimation of the fatigue strength of the notched connection, see Figure 7.

In Table 4 and Table 5 values for ratio $k_{v,max}$ and corresponding parameters for the considered bridges are summarised. In Table 5 it is distinguished whether the load distribution between the timber beams of bridge Type 3 is considered or not.

For example, a TCC bridge of Type 2 with a span length of 20 m gives a load ratio R of 0.691 (see Table 4). Looking at

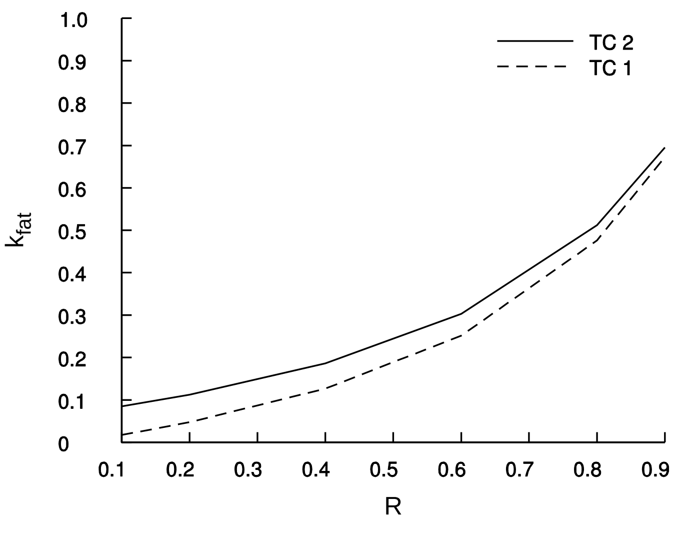

Figure 7. Reduction of shear strength for a service life of 100 years depending on traffic category (TC 2 traffic category 2 and TC 1 traffic category 1 according to EN 1991-2 (2010)).

the diagram in Figure 7, ratio $k_{v,max}$ for the notch has to be smaller than 0.4 (for $R = 0.7$), so that the road bridge may be built for traffic category 2 (*TC 2*). In this case $k_{v,max} = 0.266 < k_{fat} = 0.381$ (see Table 4) , so the fatigue resistance is verified.

Table 4. Shear forces at the notch due to permanent load and FLM 3 and values $k_{v,max}$ and k_{fat} for bridge Types 1 and 2.

Bridge Type	1	2	1	2	1	2	1	2	1	2
Span length [m]	10	10	15	15	20	20	25	25	30	30
F_{ult} [kN]	2520	2520	2700	2700	3060	3240	3240	3420	3600	3600
$F_{d,min}$ [kN]	288	340	364	443	515	595	615	689	772	852
ΔF_{FLM3} [kN]	238	238	260	260	266	266	234	234	223	223
$F_{d,max}$ [kN]	526	578	624	703	781	861	849	923	995	1075
R [-]	0.548	0.588	0.583	0.630	0.659	0.691	0.724	0.746	0.776	0.793
$k_{v,max}$ [-]	0.209	0.229	0.231	0.260	0.255	**0.266**	0.262	0.270	0.276	0.299
$k_{fat,TC\,1}$ [-]	0.212	0.242	0.238	0.277	0.303	0.335	0.373	0.400	0.440	0.464
$k_{fat,TC\,2}$ [-]	0.266	0.294	0.291	0.326	0.351	0.381	0.416	0.441	0.478	0.501

Table 5. Shear forces at the notch due to permanent load and FLM 3 and values $k_{v,max}$ and k_{fat} for bridge Type 3.

Bridge Type	Type 3 without load distribution					Type 3 with load distribution				
Span length [m]	10	15	20	25	30	10	15	20	25	30
F_{ult} [kN]	900	900	1080	1260	1260	900	900	1080	1260	1260
$F_{d,min}$ [kN]	67	109	154	176	225	72	107	144	181	204
ΔF_{FLM3} [kN]	103	130	133	117	112	76	91	95	79	74
$F_{d,max}$ [kN]	170	239	287	293	337	148	198	239	260	278
R [-]	0.394	0.456	0.537	0.601	0.669	0.486	0.540	0.603	0.696	0.734
$k_{v,max}$ [-]	**0.189**	**0.266**	**0.266**	0.233	0.267	**0.164**	**0.220**	0.221	0.206	0.221
$k_{fat,TC\,1}$ [-]	**0.124**	**0.156**	**0.205**	0.252	0.312	**0.173**	**0.207**	0.253	0.341	0.384
$k_{fat,TC\,2}$ [-]	0.184	**0.213**	0.259	0.303	0.360	0.230	0.262	0.305	0.386	0.426

In Table 5, cases for which a detailed fatigue verification is recommended (as the ratio $k_{v,max}$ exceeds k_{fat}) are printed in bold. If the load distribution is taken into account for bridge Type 3, values for ratio $k_{v,max}$ become smaller. Here only a fatigue verification for traffic category 1 and span lengths of 10 m and 15 m is necessary.

5.1.3 Step 2: Fatigue verification of the notch using a damage equivalent load

If ratio $k_{v,max}$, calculated in step 1, exceeds the threshold value k_{fat}, a more detailed fatigue verification is recommended. For the investigated types of TCC bridges, a fatigue verification with a damage equivalent force has been derived. This concept is applicable for the following cases:

- Traffic category 1 and long distance traffic: Bridge Type 2 with span length 10 m and Type 3 with span length 10 m, 15 m, 20 m and 25 m
- Traffic category 2 and medium or long distance traffic: Bridge Type 3 with span length 10 m, 15 m and 20 m

A verification with a damage equivalent force avoids a complex analysis with FLM 4 and damage accumulation according to Palmgren-Miner rule, but allows for the consideration of parameters like span length, service life, traffic volume or bridge type. Therefore damage equivalent factors (λ-factors) were derived for the modification of the shear force caused by FLM 3 in view of damage caused by FLM 4 (*Stephan & Kuhlmann*, 2014). For the verification, the maximum shear force at the notch has to be calculated with the sum of the force due to permanent load and the modified force due to FLM 3, see Equation (6).

$$F_{d,\max} = F_{d,\min} + \lambda \cdot \Delta F_{FLM\,3} \tag{6}$$

The maximum damage equivalent force according to Equation (6) has to be smaller than an equivalent fatigue strength given in Equations (7) and (8). The definition of an equivalent fatigue strength is similar to the simplified fatigue verification in steel construction, where a reference value of the fatigue strength at 2 million load cycles (= detail category) is used. The reduction factor k_{equ} is calculated according to Equation (1) with certain values for R, N_{obs} and t. Further information on the chosen parameters, which were applied to determine the equivalent shear strength reduction k_{equ} = 0.385, and on the calculation of λ-factors with the damage due to FLM 4 may be found in *Stephan & Kuhlmann* (2014) or *Kuhlmann & Kudla* (2015).

$$F_{d,\max} \le k_{equ} \cdot \frac{F_{ult}}{\gamma_{M,fat}} \tag{7}$$

$$F_{d,\max} \le 0.385 \cdot \frac{F_{ult}}{\gamma_{M,fat}} \tag{8}$$

Using a reference value for the fatigue strength means that a strength reduction k_{fat} does not have to be calculated for each case separately. Here the consideration of the effects caused by load ratio R, number of load cycles N_{obs} and service life t are included in the λ-factors. The calculated λ-factors, given in Table 6, are only applicable in combination with k_{equ} = 0.385 and for the chosen cross-sections. For other geometries or another number of beams for bridge Type 3, different λ- factors may occur.

For example, for bridge Type 3 and 15 m span length (load distribution in transverse direction is neglected), the simplified verification in step 1 is exceeded for traffic category 2, which means $k_{v,max} > k_{fat}$ (0.266 > 0.213, see Table 5). In this case, the λ-factor is 2.3 for a service life of 100 years and traffic type “medium distance”, see Table 6. In general, $\lambda > 1.0$ means that the force due to FLM 3 is increased and $0 < \lambda < 1.0$ means that it is decreased. Values $\lambda < 0$ are not permitted, because that would cause a reduction of the permanent load. Further λ-factors for traffic category 1 (medium and long distance traffic) are included in *Kuhlmann & Kudla (2015)*.

Table 6. λ-factors for bridge Type 3 and traffic category 2 for medium and long distance traffic.

Traffic Type	Medium distance			Long distance		
Span length [m]	**10**	**15**	**20**	**10**	**15**	**20**
80 a	0.9	1.6	-	1.3	3.0	0.4
100 a	1.2	**2.3**	0.1	1.8	3.9	0.8
120 a	1.6	2.9	0.3	2.3	4.9	1.2
140 a	2.0	3.5	0.6	2.8	5.8	1.6

6 Conclusions

Even though the preferred field of application for pilot projects with TCC bridges are road bridges for a low flow rate of heavy vehicles, the research project showed that high traffic categories and service lives of more than 100 years are realistic regarding fatigue. The dimensions of typical TCC bridges with spans up to 30 m are mainly defined by short-term and long-term strength verifications.

Fatigue verifications of the timber elements for the combination of bending moment and tension force at mid-span and shear force at the support can be calculated according to *EN 1995-2* (2010). In general, the parameter studies showed that fatigue verifications of TCC bridges with notches are not required for traffic categories 3 and 4 and for a span length of more than 25 m. In any other case, a simplified fatigue design procedure modifying the verification according to *EN 1995-2* (2010), is proposed for the verification of the notch. Thereby, a complex fatigue verification with FLM 4 and the linear damage accumulation method (Palmgren-Miner rule) is not necessary for typical TCC bridges.

Further parameter studies with other types of cross-sections and shear connectors are recommended in order to identify the importance and the verification of fatigue failures for these situations.

7 Acknowledgement

The research was financially supported by the international Association for Technical Issues related to Wood (iVTH) and by the German Federation of Industrial Research Associations (AiF). This support is gratefully acknowledged.

8 References

***Bathon, L. & Bletz-Mühldorfer, O.* (2014)**: Fatigue Design of Wood-Concrete-Composite System. In: World Conference on Timber Engineering (Québec City, Canada).

***EN 1991-2* (2010)**: Eurocode 1: Actions on structures – Part 2: Traffic loads on bridges. With German NA (2012). DIN – Deutsches Institut für Normung e.V.

***EN 1992-1-1* (2011)**: Eurocode 2: Design of concrete structures – Part 1-1: General rules and rules for buildings. With German NA (2013). DIN – Deutsches Institut für Normung e.V.

***EN 1995-1-1* (2010)**: Design of timber structures – Part 1-1: General – Common rules and rules for buildings. With German NA (2013). DIN – Deutsches Institut für Normung e.V.

***EN 1995-2* (2010)**: Eurocode 5: Design of timber structures – Part 2: Bridges. With German NA (2011). DIN – Deutsches Institut für Normung e.V.

***EN 14080* (2013)**: Timber structures – Glued laminated timber and glued solid timber – Requirements. DIN – Deutsches Institut für Normung e.V.

***Forschungsgesellschaft für Straßen- und Verkehrswesen – Arbeitsgruppe Straßenentwurf* (1996)**: Richtlinien für die Anlage von Straßen RAS Teil Querschnitte RAS-Q 96 (in German) / Bundesministerium für Verkehr.

Grosse, M. et al. (2003): Modellierung von diskontinuierlich verbundenen Holz-Beton-Verbundkonstruktionen, Teil 1: Kurzzeittragverhalten (in German). Bautechnik 80 (8), p. 534-541.

***Kuhlmann, U. & Aldi, P.* (2009)**: Prediction of the Fatigue Resistance of Timber-Concrete Composite Connections. In: International Council For Research And Innovation In Building And Construction. Meeting 42, CIB-W18/42-7-11, Dübendorf, Switzerland.

***Kuhlmann, U. & Aldi, P.* (2010)**: Research project DGfH/iVTH 15052 N Ermüdungfestigkeit von Holz-Beton-Verbundträgern im Straßenbrückenbau (in German). Universität Stuttgart, Institut für Konstruktion und Entwurf, No. 2010-60X, final report.

***Kuhlmann, U. & Kudla, K.* (2015)**: Research project AiF/iVTH 17070 N Vereinfachter Ermüdungsnachweis von Holzbauteilen in Holz- und Holz-Beton-Verbundstraßenbrücken (in German). Universität Stuttgart, Institut für Konstruktion und Entwurf, No. 2015-5X, final report.

***Miner, A.* (1945)**: Cumulative Damage in Fatigue. In: Journal of Applied Mechanics 12 p.159-164.

***Mohr, B.* (2001)**: Zur Interaktion der Einflüsse aus Dauerstands- und Ermüdungsbeanspruchung im Ingenieurholzbau (in German). Berichte aus dem Konstruktiven Ingenieurbau, Technische Universität München, Diss.

***Müller, J.* (2014)**: Trag- und Verformungsverhalten spezieller Verbundelemente für Holz-Beton-Verbundstraßenbrücken unter Kurzzeit-, Ermüdungs- und Langzeitbeanspruchung (in German), Institut für Konstruktiven Ingenieurbau, Bauhaus-Universität Weimar, Diss.

***Schänzlin, J. & Fragiacomo, M.* (2006)**: Extension of EC5 Annex B formulas for the design of timber-concrete composite structures. In: International Council For Research And Innovation In Building And Construction. Meeting 40, CIB W-18, Bled, Slovenia, pages 178-188.

***Schmitt, V. et al.* (2003)**: Statistische Grundlage zum Forschungsprojekt: Untersuchungen zum verstärkten Einsatz von Stahlverbundkonstruktionen bei Brücken kleiner und mittlerer Stützweiten (in German). Research project FOSTA P 629.

***Stephan, K. & Kuhlmann, U.* (2014)**: Determination of damage equivalent factors for the fatigue design of timber-concrete composite road bridges with notched connections. In: World Conference on Timber Engineering (Québec City, Canada).

Discussion

The paper was presented by K Kudla

I Smith commented that we do not really know what the damage accumulation rule should be. Creep rupture rather than cyclic load effect would be more important with the concept of killer load. He asked about the experimental verification of the work. K Kudla answered that experimental verification was not done. Miner's rule should be on the safe side.

W Seim received clarification that the S-N line results are conservative. U Kuhlmann commented that this is a typical approach.

P Zarnani asked about the geometry of the concrete slab compared to the beam. K Kudla answered that it would not make sense to change the geometry as they had aimed for optimal conditions.

K Malo asked if temperature rise was experienced during testing. U Kuhlmann responded yes, but that it should not be a big issue.

Concentrated load introduction in CLT elements perpendicular to plane

Bogensperger Thomas, Competence Center for Timber Engineering – holz.bau forschungs gmbh, A-8010 Graz, bogensperger@tugraz.at

Jöbstl Robert August, Haas Fertigbau Holzbauwerk GmbH & Co KG/Haas Holzprodukte GmbH, Radersdorf 62, A-8263 Großwilfersdorf /Industriestraße 8, D-84326 Falkenberg, robert.joebstl@haas-group.com

Keywords:

Cross laminated timber (CLT), concentrated load introduction, column supported CLT slab, punching strength

1 Introduction

Cross laminated Timber (CLT) – also known as X-lam – can be utilised as a plate-like element for loads in and/or out of plane. Under loads out of plane bending moment and shear force develop often in one direction. For this cases several methods for computation of internal section forces are available. For example the well known Timoshenko beam theory, which takes into account the high weakness of layers under rolling shear stresses is one commonly used representative. Other methods are e. g. the modified γ-method and the shear analogy method [8, 9]. A recently work out study [1] showed that differences in the calculation of stresses determined with higher theories and simple beam theories like Timoshenko's are negligible.

Modern challenging architecture is demanding solutions where CLT slabs activate two dimensional load carrying behaviour. Support by columns (e.g. see Fig. 1.1) is often needed for such solutions. For this purpose plate theories under consideration of shear effects (better known as Reissner-Mindlin-plate theory) are a de-facto standard for the computation of stresses. The mechanical stiffness properties for the Reissner-Mindlin plate theory can be found in [2]. Usually five stiffness values – two bending, one twist and two shear stiffness values – are necessary. Typically the distribution of internal section forces and moments of CLT elements under concentrated loads show high values in a small zone around the load. It this context it has to be mentioned that strength verifications for CLT elements are widely clear for internal section forces and moments except twisting moments [3].

Reissner-Mindlin plate theory corresponds to Timoshenko beam theory, but comparably 2D plate-theories on comparable level of modified γ-method or shear analogy method, implemented e.g. in FEM software for engineering applications, are still missing.

Figure 1.1. examples for CLT plates with column support.

This paper deals with bending and shear failure of cross laminated timber (CLT) plates under concentrated loads generated by e.g. columns as supports. Several verifications have to be performed for this cases: One is the verification of compression perpendicular to plane (presented by Bogensperger et. al at CIB meeting in 2011 [10]). In addition the bending and shear stresses in the CLT plate under high local loads (punching) have to be done which shall be presented in this paper.

2 State of the art

Bending verifications of CLT panels have to consider effective cross section properties due to the orthogonally layered cross-section the of CLT panels. A typical CLT cross section is shown in Fig. 2.1.(a) and has a typical stress distribution like a "saw blade". Strength properties are based on tension strength values of the graded timber boards used for the production. A model, which links tension strength values of graded timber boards to the CLT bending strength values was presented in [6]. For the application in practise the proposed formula is often simplified in a form $f_{mk,CLT}=\alpha \cdot f_{mk,g,0}$ with α = 1,1 to 1,2 and $f_{mk,g,0}$ as bending strength of comparable glulam. This formula can be found in most of the approvals of relevant CLT producers.

Typical shear stress distribution can be seen in Fig. 2.1.b. The maximum shear stress occurs at the centre of gravity of the underlying cross section. Shear verification has to consider the corresponding strength values of each layer. In layers where rolling shear stresses develop shear stress distribution is almost constant and the crucial location of the rolling shear verification can be found in that layer, which is next to the centre of gravity. The relevant rolling shear strength $f_{v,90,k,CLT}$ can be assumed with 1,25 N/mm² if grooves in the lamellas are absent and geometric ratio of used lamellas fulfils ratio of $b/t \geq 4$ (b ... width and t ... thickness of the board).

P. Mestek [5, 11] investigated shear respectively punching resistance of CLT elements under uniformly distributed and high concentrated loads. The used test configuration is shown in Fig. 2.2. The measurements of the tested CLT elements was chosen with 1380/1020 mm which were simple supported at all four sides. The CLT section was a 7-layered element with an overall thickness of 189 mm. Based on these geometrics a span to thickness ration of $L/t_{CLT} \approx \sqrt{a \cdot b}/t_{CLT} = \sqrt{1380 \cdot 1020}/189 = 6,28$ can be estimated. The work of Mestek focused on the improvement of shear and punching resistance by the application of self tapping screws drilled into the slab under 45° closed to the local load introduction. CLT panels were investigated which were built up with grooves in the lamellas. As a disadvantage of these grooves the rolling shear strength is significantly reduced. Therefore a reinforcement with self tapping screws is a meaningful approach for such CLT panels whereas the research presented in the following is concentrated on the resistance of CLT panels without screws in CLT panels (except for the local load introduction with screws under 90° of the layers).

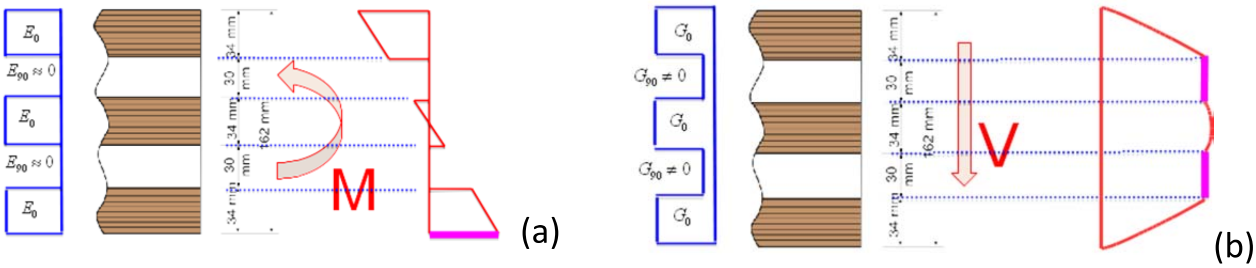

Figure 2.1. (a) typical bending stress distibution in CLT; (b) typical shear stress distibution in CLT

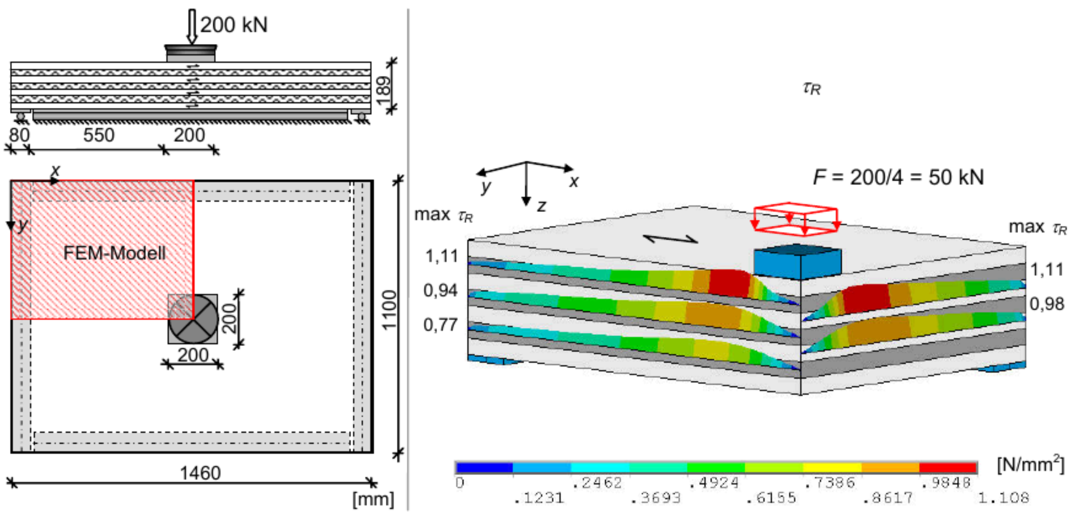

Figure 2.2. Test configuration used by Mestek [5, 11]

Although Mestek investigated primarily the effect of a reinforcement with screws in CLT elements, some tests without 45° screws were conducted (Fig. 2.3.a). CLT elements with grooves in lamellas were used. Additional tests were carried out which compare the rolling shear strength of lamellas with and without grooves. Based on these results a rolling shear strength for CLT panels built-up with lamellas without grooves could be estimated between 2,06 to 2,25 N/mm². It has to be mentioned that the verification of the rolling shear was performed along a controlling perimeter line or – written in terms of Mestek – along the intersection line (Fig. 2.3.b).

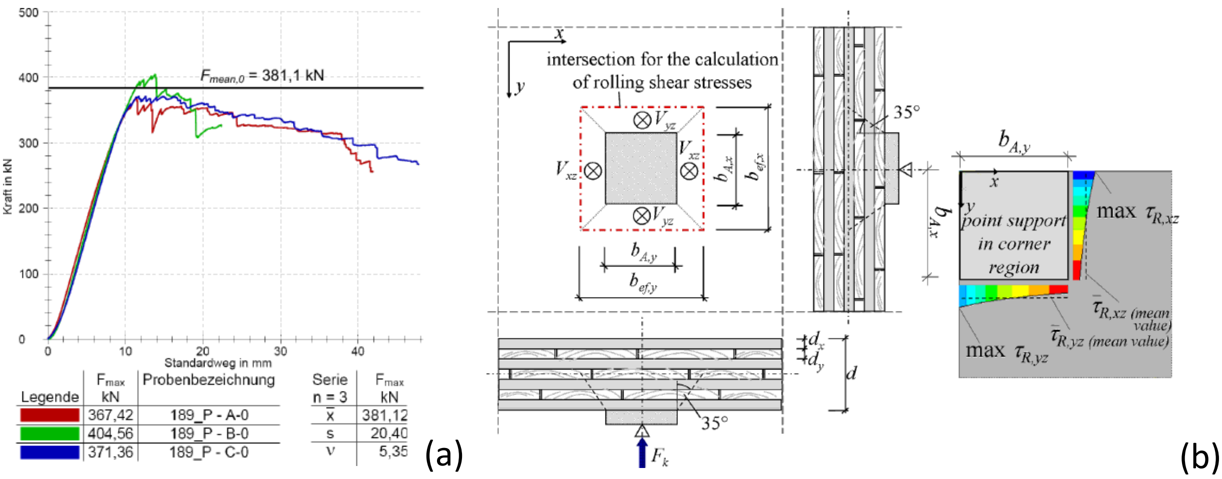

Figure 2.3. (a) Test results of Mestek without reinforcements with selftapping screws
(b) controlling perimeter for shear stresses [5, 11]

3 Numerical studies

The dominating failure mechanism (bending, shear) of CLT plates under a concentrated load depends primarily on the geometric dimensions of the CLT plate (mean span to thickness $\sqrt{(a \cdot b)}/t_{CLT}$, ratio a/b of spans in *x* and *y* direction and the number of layers and the relation of thickness of adjacent layers).

These parameters were investigated numerically by means of FEM in combination with strength verifications based on the findings mentioned in Cap. 2. In a first step the optimum a/*b* ratio (Fig. 3.1.a) was evaluated under the constraint condition that the total area of the CLT plate should remain $a \cdot b$=1 m² and under consideration that the rolling shear stresses should be the same for both directions *x* and *y*. The rolling shear verification was carried out in the controlling perimeter line around the load introduction. This controlling perimeter line was computed under an assumed load spreading angle of 35° according to Mestek (Fig 3.1).

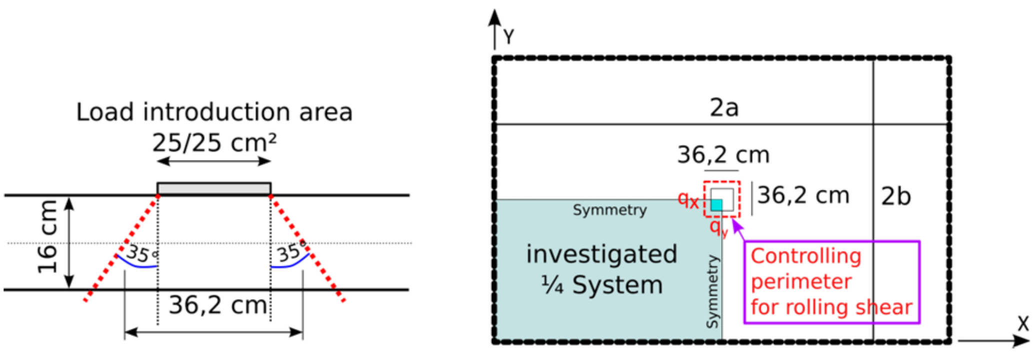

Figure 3.1. controlling perimeter line based on the findings of Mestek

This study was carried out with a 5- and 7- layered CLT cross section. The thickness ratio of adjacent layers was 1:1 and 2:1 respectively. Based on symmetry conditions only ¼ of the system was modelled as illustrated in Fig. 3.1 and Fig. 3.2.a (blue shadowed area). The overall thickness of the CLT panel was chosen with 160 mm (Fig. 3.2.b).

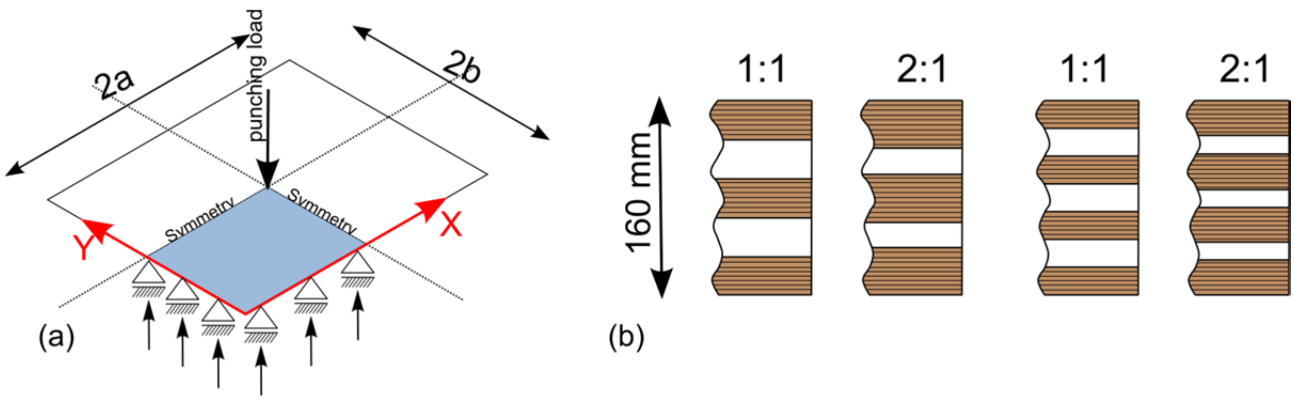

Figure 3.2. (a) variation of a/b *(b) investigated CLT sections worked-out FEM study*

The results with optimised 2·a and 2·b values are summarized in Table 1. One conclusion of the done study is that 5-layered CLT element with equal lamella thickness does not behave well under two dimensional load transfer as an extraordinary *a/b* ratio of 50,7/197,3 is the optimum with same rolling shear stress level in both directions. 7-layered CLT element behaves much better with the optimum *a/b* ratio of 105,6/94,7=1,11 which is close to a quadratic shape.

Table 1. optimum span length 2·a and 2·b

	2·a [cm]	2·b [cm]
BSP5s_160mm_1:1	50,7	197,3
BSP5s_160mm_2:1	106,1	94,3
BSP7s_160mm_1:1	105,6	94,7
BSP7s_160mm_2:1	161,1	62,1

The *a/b* ratio (Mestek chose 138/102=1,35 in his work) differs from results of this study. One important reason lies in the differences of the numerical model: In the present study a 2D shell model was used while Mestek used a 3D solid model.

An other approach for a further study is to investigate differences of expected load carrying capacities under deviating *a/b* ratios. Proposed *a/b* ratios for a second study are shown in Fig. 3.3.

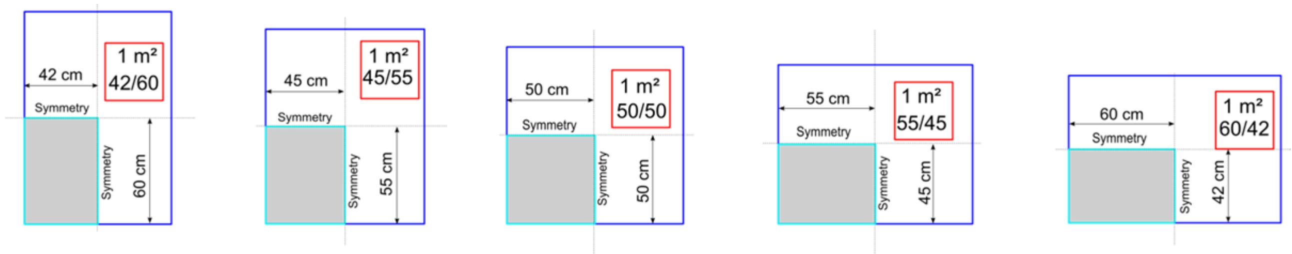

Figure 3.3. investigated a/b ratios

Results of computed FEM-load carrying capacities are illustrated in Fig. 3.4. Based on these it can be concluded, that the a/b ratio of the CLT elements is not as dominant as expected.

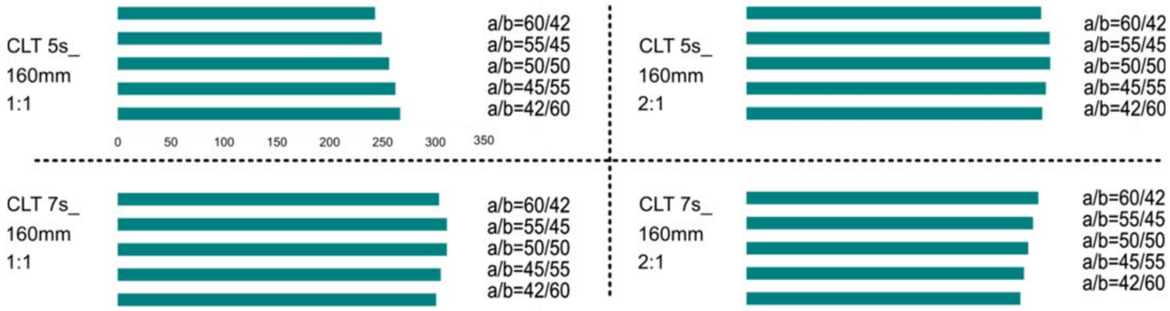

Figure 3.4. expected load carrying capacities for different a/b ratios based on a FEM-study

4 Development of test configuration

Test specimens for the tests presented in the following should contain 5- and 7-layered CLT elements. Furthermore the chosen cross sections should be available as industrially produced elements. The geometric as wells as stiffness values of the selected cross sections are summarized in table 2. Specimens denoted as “CLT 5s” and “CLT 7s” were delivered from producer 1 while the specimen of series “CLT 7s*” originated from a different producer 2.

Table 2. CLT cross sections used for experimental investigations

	E_0	E_{90}	G_0	G_{90}	#	t_1	t_2	t_3	t_4	t_5	t_6	t_7
	N/mm²	N/mm²	N/mm²	N/mm²		mm	mm	mm	mm	mm	Mm	mm
CLT 5s	11600	≈0	690	50	5	34	30	34	30	34		
CLT 7s	11600	≈0	690	50	7	19	30	19	30	19	30	19
CLT 7s*	11600	≈0	690	50	7	20	30	20	30	20	30	20

A graphical illustration of “CLT 5s” and “CLT 7s” and associated stress distributions for unit section moments and shear forces in longitudinal (0°) and in transverse direction (90°) (m_x=m_y=1 kN·cm/cm, q_x=q_y=1 kN/cm) is given in Fig 4.1.

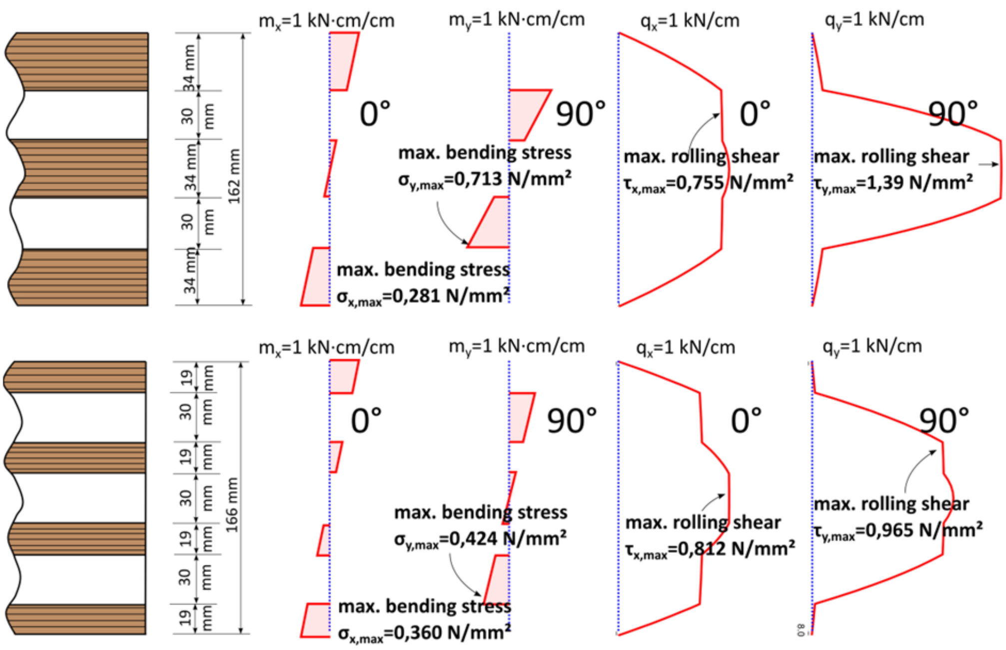

Figure 4.1. CLT cross sections used for experimental investigations and shear stress distributions

A sketch of the test configuration “punching” (test configuration 1) can be found in Fig. 4.2. Ratio of a/b was chosen with 1,0 (a = b = 1,0 m). The supports were implemented by means of tension rods which could be constraint within an existing grid of load introduction points with a distance of 50/50 cm in the laboratory. The span to thickness ratio varied between 6,17 and 5,88 depending on the cross-section. The geometric boundary conditions were thereby similar to the mean span to thickness ratio of Mestek configuration with 6,28. Three images of test configuration 1 are shown in Fig. 4.3.

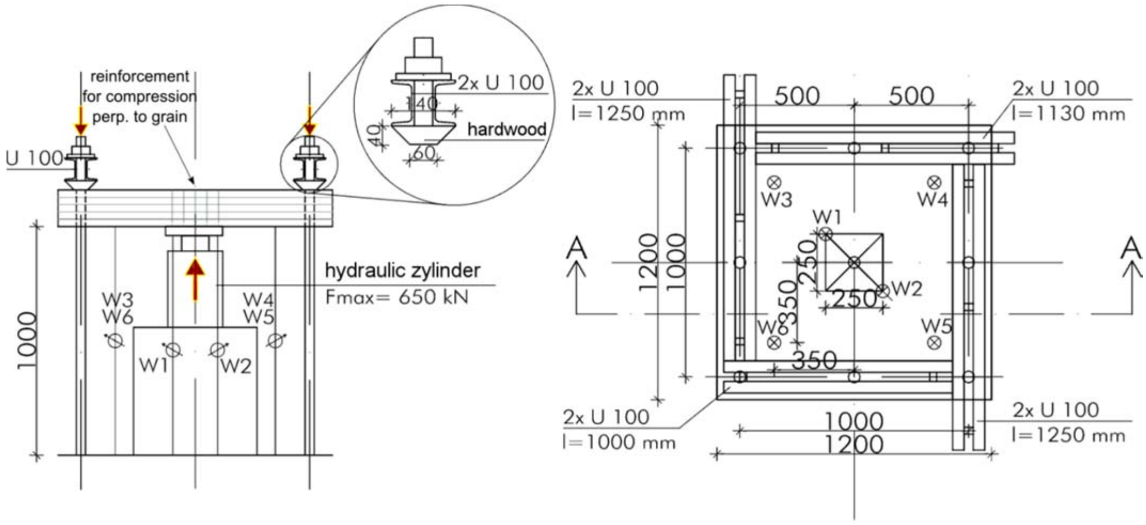

Figure 4.2. Test configuration for expected punching shear failure (test configuration 1)

Figure 4.3. Images of test configuration for expected punching shear failure (test configuration 1)

The test configuration “bending under concentrated loads” were designed with significant higher length to thickness ratio in order to achieve bending failure modes (test configuration 2). Restricted to the grid of load introduction points of the test field the longer span a was chosen with 4,0 m, the shorter span b with 2,5 m. Mean length to thickness ratios were between 19,5 and 18,6 depending on the used cross section. As the parameter study already showed that 5-layered CLT elements behave worse than 7-layered ones under all side support with global bidirectional bending behaviour. Therefore tests with one directional bending behaviour with support only along both shorter sides was proposed for 5-layered CLT elements while a two directional bending loading (with simple supports on all four sides) of the CLT elements was implemented for the 7-layered CLT element (Fig. 4.4).

Test specimens denoted with “A” are build up in the laboratory for series "CLT 5s" and "CLT 7s". The lamellas used were graded in respect to density of the boards within a range of 400 kg/m³ ± 20 kg/m³. Annual ring pattern was the second grading parameter. The allowance of knots was reduced in comparison to industrially graded boards. Test specimens with CLT elements from producer 1 are denoted with “B”. If they came from producer 2 they are denoted as series “C”.

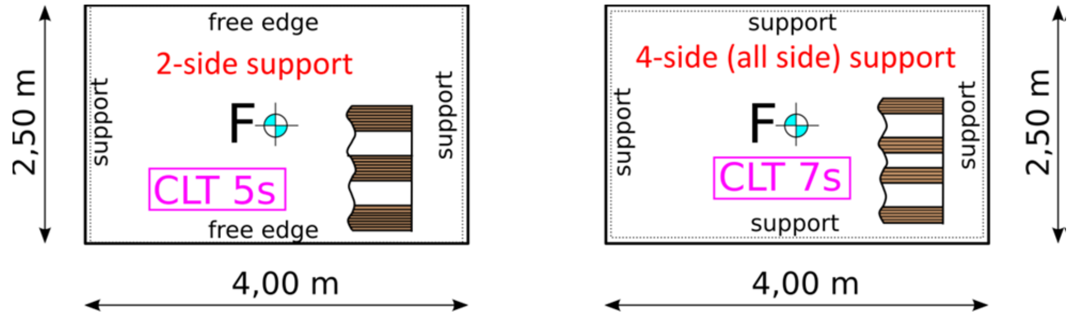

Figure 4.4. Test specimens for expected bending failure (test configuration 2)

Two images of test configuration 2 can be found in Fig. 4.5.

Figure 4.5. Images of test configuration 2 for test series with expected bending failure mode

5 Test results

The load-displacement curves of the tested showed a relative ductile behaviour for test configuration 1 (Fig 5.1) Different failure modes were observed. The non linear characteristic indicates an increasing loss of shear strength which is more or less a relative steady process. In some cases failure modes of lamellas in tension in conjunction with unsteady load-displacement curves was observed.

For specimens of test configuration 2 bending failure always occurred first. Subsequently rolling shear failures were observed. A ductile behaviour could be recognised also for test configuration 2 (Fig 5.2). As failure of several lamellas in tension leaded to an immediate load decrease discontinuities in the load displacement curve were developed more significant in configuration 2 than 1, especially in case of the tests with 5-layered CLT elements.

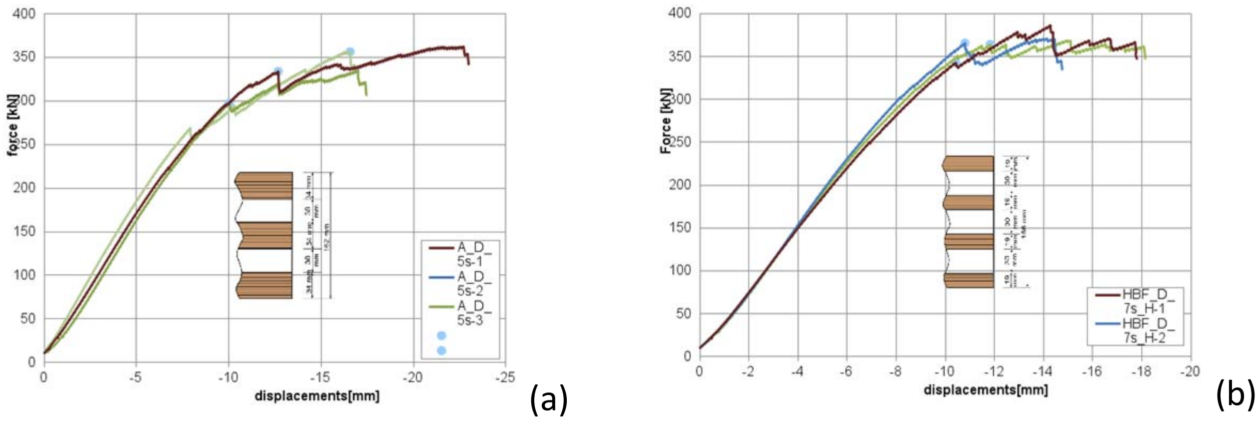

Figure 5.1. load displacement curves (a) 5-layered CLT; (b) 7-layered CLT in test configuration 1

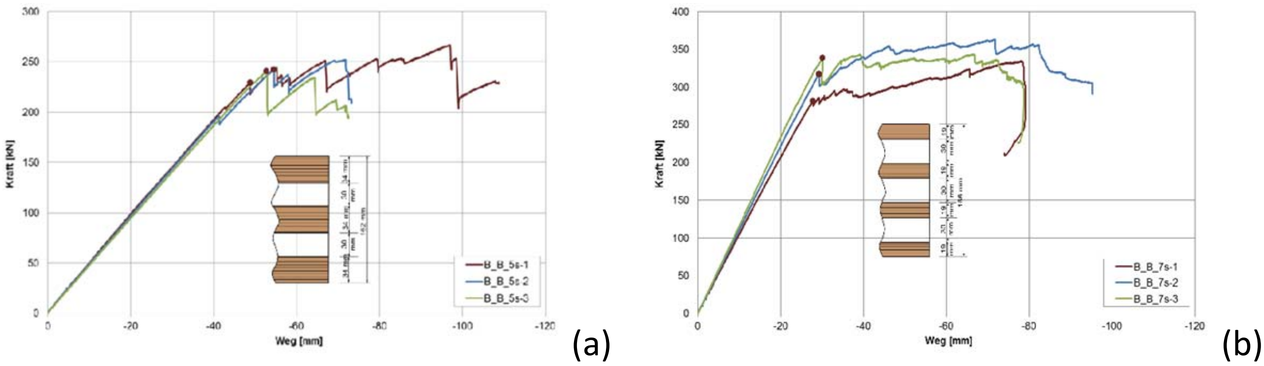

Figure 5.2. load displacement curves (a) 5-layered CLT; (b) 7-layered CLT in test configuration 2

Failure of lamellas under tension was also observed in configuration 1. But the already established non linear character of the load displacement curve indicates already existing failures due to shear, whereas in configuration 2 unsteadiness always finishes the linear load displacement behaviour.

Typical shear failures are shown in figure 5.3. These failures became visible by cuting the test elements along their axis of symmetry after the tests. In the area of the load introduction could be easily detected due to indentations of the steel plate and the used reinforcement screws.

Figure 5.2. observed typical failures in test configuration 1

Figure 5.4 shows typical failures observed in test configuration 2. In the first row failures of 5-layered bending under more or less one dimensional bending could be detected whereas the images in the second row show impressive destruction under pure two dimensional bending for the 7-layered CLT specimens.

Figure 5.3. observed typical failures in test configuration 2

All numerical results concerning test configuration 1 can be found in table 3, in an analogous manner table 4 contains the test data of test configuration 2.

Table 3. Test results of test configuration 1

Typ of CLT panel			5-layered CLT panels		7layered CLT panels		
Identification of test series			A_D-5s	B_D-5s	A_D-7s	B_D-7s	C_D-7s
Width of lamellas b	Longitudinal lay.	[mm]	235	230	235	230	181 (90)[1)]
	Cross layer	[mm]	120	190/120	120	190	184 (90)[1)]
Thickness of boards h	Longitudinal lay.	[mm]	34	34	19	19	20
	Cross layer	[mm]	30	30	30	30	30
ratio b/h	Longitudinal lay.	[-]	6,91	6,76	12,4	12,1	9,05 (4,50)[1)]
	Cross layer	[-]	4,00	6,33/4,00	4,00	6,33	6,13 (3,00)[1)]
Number of test specimens (in evaluation)		[-]	6	4	6	3	4
Moisture content u	Mean value	[%]	11,7	11,3	12,1	10,0	11,0
	COV	[%]	6,40	9,90	5,88	1,33	3,06
density ρ	Mean value	[kg/m³]	414	435	412	460	431
	COV	[%]	4,13	5,03	5,46	5,20	6,60

stiffness	Mean value	[kN/mm]	35,4	32,2	39,0	42,8	42,6
	COV	[%]	4,28	3,80	4,40	7,29	6,90
Force level at first crack $F_{1.\ crack}$	Mean value	[kN]	328	289	350	(400)[2)]	351
	COV	[%]	6,90	5,76	4,17	(7,08)[2)]	9,42
	5%-Quantile NV	[kN]	291	262	326	(353)[2)]	296
	charact. value acc. to EN 14358	[kN]	279	247	311	(320)[2)]	273
Maximum of load F_{max}	Mean value	[kN]	358	339	372	(408)[2)]	366
	COV	[%]	3,87	3,72	2,04	(4,70)[2)]	5,85
	5%-Quantile NV	[kN]	335	318	360	(376)[2)]	331
	charact. value acc. to EN 14358	[kN]	318	296	331	(348)[2)]	313

Remarks:
1) Values in brackets represent ratios of b/t under consideration of grooves.
2) Appropriate values of series B_D-7s represent bending failure.

Table 4. Test results of test configuration 2

Typ of CLT panel			5-layered CLT panels	7-layered CLT panels, support at all sides	
Identification of test series			B_B-5s	B_B-7s	C_B-7s
Number of test specimens		[-]	3	3	3
Moisture content u	Mean value	[%]	10,7	9,70	10,8
	COV	[%]	4,07	9,54	2,45
density ρ	Mean value	[kg/m³]	442	440	445
	COV	[%]	10,8	4,48	2,72
stiffness	Mean value	[kN/mm]	4,78	11,0	11,2
	COV	[%]	1,85	5,12	2,15
Force level at first crack $F_{1.crack}$	Mean value	[kN]	238	312	361
	COV	[%]	3,03	9,18	8,09
	5%-Quantile NV	[kN]	226	265	313
	charact. value acc. to EN 14358	[kN]	203	232	280
Maximum of load F_{max}	Mean value	[kN]	253	347	369
	COV	[%]	5,10	4,25	5,84
	5%-Quantile NV	[kN]	232	323	333
	charact. value acc. to EN 14358	[kN]	216	296	314

6 Recommendations for standardisation

The results of test configuration 1 serve as basis for punching shear strength values. Rolling shear strength values are evaluated with the maximum of elastic shear forces q_x and q_y along the controlling perimeter line (see Fig. 3.1). The test results of series C (producer 2) are exceptional as lamellas of this series contains grooves. These grooves are essentially smaller than those in [5]. A graphical comparison shows the differences of the grooves in [5] and the present study (Fig. 6.1).

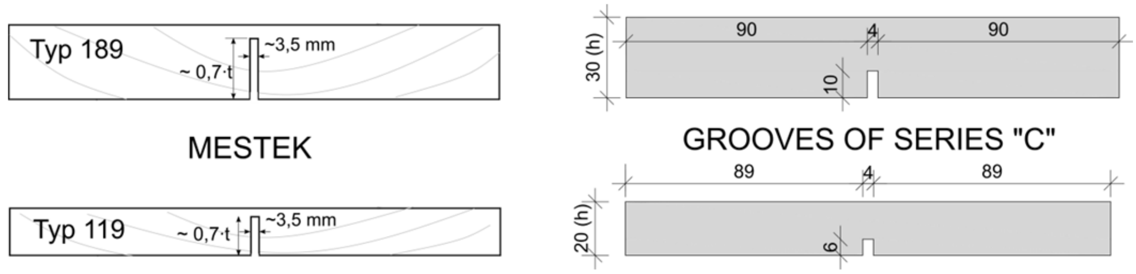

Figure 6.1. differences between grooves in Mestek [5] and test specimens of the presented tests

Based on forces defined at first crack level (see table 3) the associated stress values for rolling shear could be identified and values are summarized in table 5.

Table 5. rolling shear strength values (based on results of configuration 1)

Typ of panel	5-layered CLT panel		7-layered CLT panel		
Identification of test series	A_D_5s	B_D_5s	A_D_7s	B_D_7s	C_D_7s
charact. value (EN 14358)	279	247	311	320	273
$q_{x,max}$ [kN/cm]	2,74	2,43	2,37	2,44	2,08
$q_{y,max}$ [kN/cm]	1,59	1,41	2,40	2,47	2,10
rolling shear str. $\tau_{90,x}$ [N/mm²]	2,07	1,83	1,92	1,98	1,69
rolling shear str. $\tau_{90,y}$ [N/mm²]	**2,21**	**1,95** *)	**2,31**	**2,38** *)	**2,03**
*) elements with a width of lamellas b=230 mm in the longitudinal layers and b=115 mm in the cross layers; influence has to be evaluated					

A shear strength value of 2,21 N/mm² could be computed (mean strength value: 2,62 N/mm²; COV: 6%, see table 3) with bold values in table 5 for series A and B. Shear in y-direction was dominating, whereas a mean stress level of about 85% developed in x-direction. Test specimens acc. to series C had grooves similar to test specimens of Mestek, but in a less dominant implementation (see Fig. 6.1). As a consequence the strength reduction is quite moderate (9%).

The proposed strength value of 2,21 N/mm² - a similar value can be calculated with data from Mestek - is only valid if stress computation is based on a pure elastic method and rolling shear stresses have to be verified in the vicinity of concentrated load introduction. In bending test according to the usual standards (e.g. EN 16351) the characteristic rolling shear strength is significantly lower (for spruce: $f_{v,k,90}$=1,25

N/mm²). The differences can be explained by the definitely non-linear stress strain behaviour (see following chapter). Therefore the proposed strength values in combination with elastic stress calculation is a simplification for practice.

Bending strength can be checked similarly with forces defined at first crack level (see table 4). Results are summarized in table 6. Values for the specimens of series A are missing as only industrial fabricated panels were tested with test configuration 2.

Table 6. bending strength values (based on results of configuration 2)

Typ of panel	5-layered CLT panel		7-layered CLT panel		
Identification of test series	A_B_5s	B_B_5s	A_B_7s	B_B_7s	C_B_7s
charact. value (EN 14358)	—	203	—	232	280
$m_{x,max}$ [kN·cm/cm]		110,18		61,54	74,27
$m_{y,max}$ [kN·cm/cm]		31,21		69,37	83,72
bending stress σ_x [N/mm²]	—	**30,95**	—	22,17	24,99
bending stress σ_y [N/mm²]	—	22,25	—	**28,52**	**34,72**

Grooves do not influence bending strength significantly. Therefore no differences were made between series B and C. In case of 5-layered CLT element the dominating direction is longitudinal (x) whereas for 7-layered elements the crucial direction is the direction transverse (y). The test results showed that the limiting direction in case of the 7-layered CLT panels does not fit always with the numeric prediction. Mean value over these test results (bold values in table 6) delivers 31,4 N/mm² which is 9% higher than comparable bending strength values of CLT panels ($f_{m,k,CLT}$=1,2·24=28,8 N/mm²). An increase of bending strength can be expected because under a concentrated load only a small area is exposed to high bending moments (volume effect).

7 FE-model for punching shear configuration

It was already mentioned, that a numerical analysis with non-linear behaviour describes mechanical behaviour more precisely than a pure linear-elastic model can do. Such an analysis was carried out with the FE-Software ABAQUS. A solid 3D-model for the 5-layered punching shear configuration '1' was established for one quarter of the test specimen taking into account two planes of symmetry, as shown in fig. 7.1 (a). The numerical model was meshed with linear 3D solid elements 'C3D8'. The first axis of the material orientation denotes the orientation of the lamellas (longitudinal direction), whereas third axis is parallel to the normal direction of the CLT element. Axis 2 is perpendicular to axis 1 and 3 (see fig 7.1 (b)).

The orthotropic MOE parallel to grain was chosen with 12000 N/mm², perpendicular to grain with 370 N/mm². The value of the shear modulus was 690 N/mm² and the rolling shear value 50 N/mm². Stress-strain curves based on data in [12] are shown in fig 7.2 (a). The observed rolling shear behaviour is not ideal elastic-plastic, but this assumption can be seen as a simplification for the FE-model. The plastic plateau was assumed to be 1,5 N/mm² (see fig 7.2 (a)).

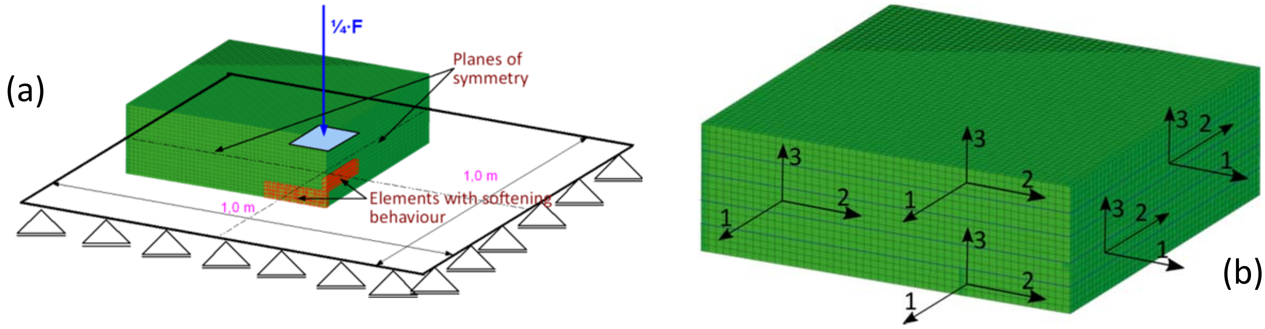

Figure 7.1 (a) FEM Model for punching shear configuration (b) orientations of layers

For simplification all stress-interactions between all stress components were neglected. The orthotropic elastic behaviour and the elastic-plastic behaviour for rolling shear were to be implemented in a user subroutine for ABAQUS. A comparison between computed and experimentally founded load displacement curves can be seen in fig 7.2 (b).

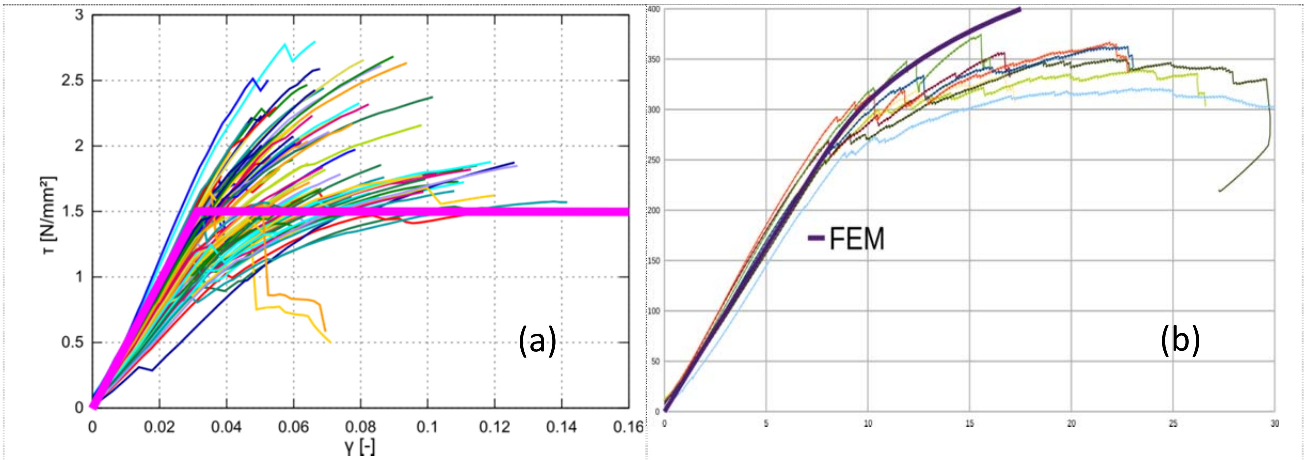

Figure 7.2 (a) stress strain behaviour for rolling shear, based on data of master thesis [12]
(b) FEM results with elastic-plastic behaviour for rolling shear

The agreement is quite pretty good at the beginning where linear elastic behaviour dominates. In the non-linear part (load above 250 kN) the computational model describes behaviour correctly in principal, but overestimates the mechanical strength and resistance of the test specimen. This leads to the conclusion, that another failure mechanism has to be implemented in the model. At the mentioned load level of 250 kN and above significant cracks can be seen in the experimental load displacement curves, which indicates, that softening due to tension in the outer lamellas is missing in the model. This softening behaviour was supplemented in a small domain of the numerical model in two outer lamellas. This domain is highlighted in a red colour and shown in fig 7.1 (a). The size of this selected domain is equal to the height of the outer lamella (34 mm), the width is set to 150 mm. Due to symmetry conditions two lamellas can fail now due to tension in the numeric model in both directions. The location of failure was chosen in the middle of the test specimen, where maximum bending stresses occur. The maximum tension stress, when softening starts, was introduced with $f_{t,mean}$ =39,0 N/mm². This value bases upon various CLT-bending tests in our laboratory as a mean value. Descend of stress-strain function during softening depends on size of mesh. The area under the stress-displacement curve equals to the fracture energy release rate for Mode I, which was introduced with a value of 1650 J/m², taken from [13]. The complete stress-strain curve with softening is shown in fig 7.3 (a) and added to the user subroutine for ABAQUS. The comparison between computed and experimentally measured load displacement curves is now much better than without softening. Two significant steps in the computed load displacement curve indicates failure in y (m_y) and x (m_x) direction (see fig. 7.3 (b)).

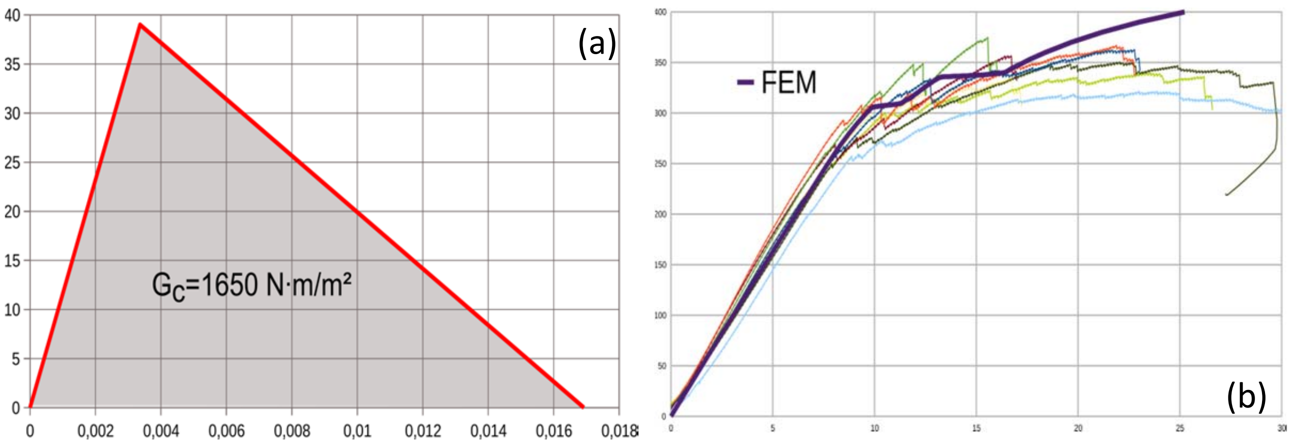

Figure 7.3 (a) stress strain behaviour with softening for outer lamellas under tension (b) FEM results with elastic-plastic behaviour for rolling shear and tension softening in outer lamella

Shown computational results show, that the proposed high strength value of 2,21 N/mm² for rolling shear can be explained by elastic plastic behaviour of rolling shear with some stress redistribution. Further improvements of the numerical simulation could be an implementation of a more precise stress-strain behaviour for rolling shear as well as an implementation of stress interactions, in particular rolling shear with compression stresses perpendicular to grain.

8 Acknowledgement

The research work within the project 'focus_sts' was financed by the competence centre holz.bau forschungs gmbh. The project was financed by funds from the Federal Ministry of Economics, Family and Youth, the Federal Ministry of Transport, Innovation and Technology, the Styrian Business Promotion Agency Association and the Province of Styria (A12), the Carinthian Economic Promotion Fund (KWF), the Province of Lower Austria Department of Economy, Tourism and Technology as well as the Business Location Tirol.

9 References

[1] Bogensperger T. , Silly G., Schickhofer G. (2012): Comparison of Methods of Approximate Verification Procedures for Cross Laminated Timber, Research Report,

holz.bau forschungs gmbh, Institute for Timber Engineering and Wood Technology, Graz University of Technology.

[2] Bogensperger T. , Silly G. (2014): Zweiachsige Lastabtragung von Brettsperrholzplatten, Ernst & Sohn publisher for architecture and technical science GmbH & Co. KG, Berlin. Bautechnik 91 issue 10.

[3] Silly G. (2010): Numerische Studien zur Drill- und Schubsteifigkeit von Brettsperrholz (BSP), diploma thesis, Graz University of Technology.

[4] Bogensperger T. , Wallner B., Augustin M. (2015): Durchstanzen von Brettsperrholzplatten, Research Report to project focus_sts 2.2.3_2, holz.bau forschungs gmbh Graz, (report in progress).

[5] Mestek P. (2011): Punktgestützte Flächentragwerke aus Brettsperrholz (BSP) – Schubbemessung unter Berücksichtigung von Schubverstärkungen, Ph.D., Munich University of Technology.

[6] Jöbstl R. A., Bogensperger T., Moosbrugger T., Schickhofer G. (2006): A Contribution to the Design of Cross Laminated Timber, CIB W18, 39th Meeting, Florence (I)

[7] Schickhofer G., Bogensperger T. , Moosbrugger T. (2009): BSPhandbuch Holz-Massivbauweise in Brettsperrholz Nachweise auf Basis des neuen europäischen Normenkonzepts, Graz University of Technology, 2011, ISBN 978-3-85125-109-8

[8] Peterson, L. A. (2008): Zum Tragverhalten nachgiebig verbundener Biegeträger aus Holz, Berichte des Instituts für Bauphysik der Leibniz Universität Hannover Herausgeber: Univ.-Prof. Dr.-Ing. Nabil A. Fouad; Leibniz Universität Hannover - Institut für Bauphysik Heft 1

[9] Schelling, W. (1982): Zur Berechnung nachgiebig zusammengesetzter Biegeträger aus beliebig vielen Einzelquerschnitten In: Ehlbeck, J. (publisher), Steck, G. (publisher): Ingenieurholzbau in Forschung und Praxis. Bruderverlag Karlsruhe.

[10] Bogensperger T, Augustin M, Schickhofer G. (2011): Properties of CLT-Panels Exposed to Compression Perpendicular to their Plane, CIB W18, 44th Meeting, Alghero , Italy

[11] Mestek P, Kreuzinger H, Winter S (2011): Design concept for CLT - reinforced with self tapping screws, CIB W18, 44th Meeting, Alghero, Italy

[12] Ehrhart T (2014): Materialbezogene Einflussparameter auf die Rollschubeigenschaften in Hinblick auf Brettsperrholz, Masterarbeit, Graz University of Technology.

[13] Mackenzie-Helnwein P. et al (2005): Analysis of layered wooden shells using an orthotropic elasto-plastic model for multi-axial loading of clear spruce wood, Computer methods in applied mechanics and engineering 194, p. 2661-2685

Discussion

The paper was presented by T Bogensperger

F Lam received confirmation that the equation involved $f_{r,90mean}$ *and the characteristic strength was incorrect and should be modified. F Lam asked about the softening procedure used in FEM analysis. T Bogensperger provided some explanation and agreed to add information in text of paper.*

H Blass received clarification for the justification of punching factor k of 1.75 as possible localized effect where rolling shear failure was assumed not to be brittle. F Lam asked about the deflection in compression perpendicular to grain. T Bogensperger stated that the deflection was small because reinforcement screws were used. These screws did not add to the shear strength.

INTER / 48 - 12 - 02

Shear Properties of Cross Laminated Timber (CLT) under in-plane load: Test Configuration and Experimental Study

Reinhard Brandner, Graz University of Technology *)

Philipp Dietsch, Technische Universität München *)

Julia Dröscher, Graz University of Technology

Michael Schulte-Wrede, Technische Universität München

Heinrich Kreuzinger, Technische Universität München

Mike Sieder, Technische Universität Braunschweig

Gerhard Schickhofer, Graz University of Technology

Stefan Winter, Technische Universität München

*) joint first authorship

Keywords: cross laminated timber; CLT; shear in-plane; diaphragm; test configuration; experimental study; parameter study; shear strength; shear modulus; failure mechanisms; characteristic properties; design concept

1 Introduction

Cross laminated timber (CLT) is a two-dimensional laminated engineered timber product, commonly composed of an uneven number of orthogonally and rigidly connected layers. High resistances in- and out-of-plane predestines it for numerous applications, e.g. for floor and wall elements, shear walls, folded panels and beams. With respect to its resistances and properties as a structural product, it is differentiated between out-of-plane and in-plane loading. For CLT under out-of-plane loading, test configurations and characteristic values are well agreed. For CLT under in-plane loading, some properties are still under discussion, presently resulting in conservative regulations, e.g. tension and compression in direction of the top layers. The same is valid for CLT under in-plane shear. To fully profit from the high capacities of CLT in-plane, a detailed knowledge of all relevant mechanical properties, which are dependent on the geometrical layup of the elements, as well as the development and verification of practicable test configurations to determine these properties are indispensable.

Consolidated knowledge of CLT properties under in-plane shear is crucial for typical structural applications such as wall and floor diaphragms, cantilevered CLT walls and CLT used as (deep) beams, in all cases potentially featuring holes or notches. The current technical approvals for CLT products contain differing regulations to determine their load-carrying capacities in-plane. Generally they imply a verification of the torsional stresses in the cross-section of the cross-wise glued elements as well as a verification of the shear stresses proportionally assigned to the boards of the top and cross layers. The basis of theoretical and practical considerations are the following three basic failure scenarios for a CLT-element under in-plane shear: (i) gross-shear (longitudinal shearing in all layers), (ii) net-shear (transverse shearing in all layers in weak direction), and (iii) torsion failure in the gluing interfaces between the layers (Bogensperger et al. 2007, 2010; Flaig and Blaß 2013; Brandner et al. 2013). All failure mechanisms can be achieved if a corresponding test configuration is applied.

Properties for the mechanism (iii) "torsion", based on Blaß and Görlacher (2002), Jeitler (2004) and Jöbstl et al. (2004) are well accepted (DIN EN 1995-1-1/NA). In contrast, the determination of the properties (i) gross-shear and (ii) net-shear by testing is challenging, as it is practically impossible to secure larger fields of pure shear. Up to now, the properties for in-plane shear provided in technical approvals are based on testing single nodes. The resulting strength values are partly seemingly high and feature a higher variability than expected for diaphragms. Associated investigations include Wallner (2004), Jöbstl et al. (2008) and Hirschmann (2011). After re-evaluating and summarizing previous findings Brandner et al. (2013) propose $f_{v,net,05}$ = 5.5 N/mm² as 5 %-quantile of net-shear strength for a reference CLT node in conjunction with the test configuration "EN" of Hirschmann (2011). Board thickness, gap width and annual ring pattern were identified as parameters with significant influence on shear resistance. Tests on single-nodes are able to produce separated stress conditions, hence all test configurations on single-nodes can represent and lead to separate failure mechanisms in CLT under in-plane shear. The full stress state within a full-scale CLT-element under in-plane shear, however, cannot be represented by them.

Several efforts were made to determine shear properties on full-scale CLT diaphragms, e.g. Bosl (2002), Bogensperger et al. (2007) and Andreolli et al. (2014). The main challenges within the tested configurations were – apart from their rather costly implementation – (i) to realize a continuous load introduction, (ii) to receive a field of pure shear and (iii) to achieve failure under in-plane shear. It is expected that these challenges are also encountered when applying the standardized test configuration which is used to determine the racking strength and stiffness of timber frame wall panels, see EN 594 (2011). The determination of shear strength based on four-point bending tests, e.g. given in FprEN 16351 (2015) (based on CUAP 03.04/06 2005) has to be critically analysed as well. Here, the determination of shear strength is based on beam theory considering the total thickness of all cross layers in the evaluation. The typical stress states within CLT diaphragms under in-plane shear are not represented by this approach.

In the context of an approval in the individual case, Kreuzinger and Sieder (2013) published a proposal for a test configuration and evaluation procedure for CLT diaphragms. The principle approach to determine shear strength from a combined stress state with transverse stresses can already be found in Szalai (1992). The approach proposed by Kreuzinger and Sieder (2013) is based on a simple compression test, the test results are evaluated using theoretical approaches from plate theory (in-plane stresses). The evaluation procedure is partly extended and specified in the frame of this paper.

2 Test configuration and evaluation procedure

2.1 Description of test configuration

In this configuration, column-shaped rectangular specimen, which are cut out under 45° rotated to the main orientation of CLT elements, are tested in compression, see Fig. 1.

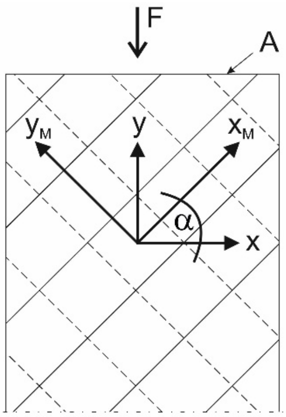

with:

x_M *direction of CLT top and middle layer (TL; ML)*

y_M *direction of CLT cross layer (CL)*

x *x-direction of the column*

y *y-direction of the column*

F *load*

A *column cross-section*

α 45°

Figure 1. System.

2.2 Determination of in-plane shear strength

The stresses on the column as well as on a differential CLT section are given in Fig. 2. Based on the Cartesian coordinate system of the column cross-section (*x*, *y*), the principal stresses are:

$$\sigma_x = 0; \qquad \sigma_{xM} = \sigma_{yM} = \frac{\sigma_y}{2}; \qquad \tau_{xM,yM} = \frac{\sigma_y}{2}$$

The shear stress at maximum load is determined according to Eq. (1), see Fig. 3.

$$\tau_{xM,yM} = \frac{1}{2} \cdot \frac{F_{max}}{A} = \frac{F_{max}}{2 \cdot w_{CLT} \cdot t_{CLT}} \tag{1}$$

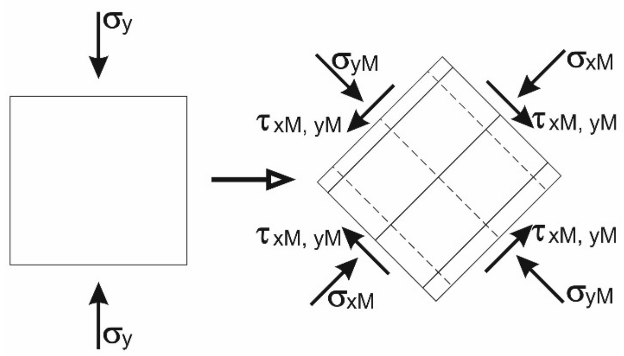

Figure 2. Stress states in column (left) and in differential CLT-section (right)

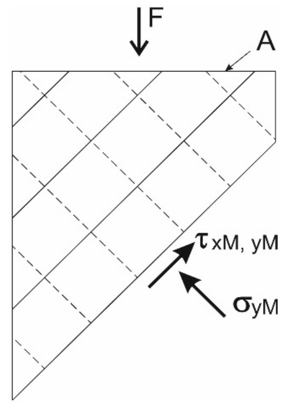

Figure 3. Internal stresses and external loading.

In general, the shear resistance is influenced by stresses perpendicular to the grain, see Spengler (1982) and Hemmer (1984). Compressive stresses perpendicular to the grain result in an increase of shear resistance. In the given test setup (see Fig. 1), the obtained shear stresses $\tau_{xM,yM}$ are higher than the actual shear strength f_v. The test setup leads to compressive stresses σ_{xM} and σ_{yM}, which equal the shear stresses $\tau_{xM,yM}$, see Fig. 3. In cases of gross shear failure, the compressive stresses σ_{yM} are primarily transferred by the layers featuring a board direction y_M. The compressive stresses perpendicular to the grain on the layers with a board direction x_M will feature a magnitude, which is reduced by the relationship

E_{90}/E_{yM} with:

- E_{yM} weighted modulus of elasticity in y_M-direction, CLT cross layer (value standardized or determined by testing (preferred))
- E_{90} modulus of elasticity perpendicular to the grain of the base material top layers (value standardized or determined by testing)

The approach

$$t_{CLT} \cdot E_{yM} = \sum t_{l,yM} \cdot E_0 + \sum t_{l,xM} \cdot E_{90} \tag{2}$$

with $t_{CLT} = \sum t_{l,xM} + \sum t_{l,yM}$ and $\sum t_{l,L} \geq \sum t_{l,T}$

and E_0 modulus of elasticity parallel to the grain of the base material

leads to

$$E_{yM} = \frac{\sum t_{l,yM} \cdot E_0 + \sum t_{l,xM} \cdot E_{90}}{t_{CLT}} \tag{3}$$

with the relationship

$$\sigma_{90} = \sigma_{yM} \cdot \frac{E_{90}}{E_{yM}} = \tau_{xM,yM} \cdot \frac{E_{90}}{E_{yM}} \tag{4}$$

Assuming softwood of typical strength classes according to EN 338 with (C16 to C30) and layup parameters (ratios between the sum of layer thicknesses in weak direction, $\sum t_{\ell,T}$, to that in the strong direction, $\sum t_{\ell,L}$) of $0.25 \leq \sum t_{\ell,T} / \sum t_{\ell,L} \leq 1.0$, this leads to values $\sigma_{90} = \tau_{xM,yM}$ (0.06 to 0.25) and to $\sigma_{90} = \tau_{xM,yM} \cdot$ (0.07 to 0.17) for C24.

Using the test results reported in Spengler (1982), an attempt to estimate this influence is given by the approach taken by Blaß & Krüger (2012), based on results of Spengler (1982), which can be modified as follows:

$$f_{v,gross} = \tau_{xM,yM} + 1.15 \cdot \sigma_{90} + 0.13 \cdot \sigma_{90}^2 \qquad (5)$$

whereby σ_{90} is negative if representing compression stresses.

To determine the shear strength $f_{v,gross}$, the obtained shear stresses $\tau_{xM,yM}$ should be reduced in the range of $f_{v,gross} = \tau_{xM,yM} \cdot$ (0.75 to 0.94) (C16 to C30) and $f_{v,gross} = \tau_{xM,yM}$ (0.83 to 0.93) (C24 only). The higher the layup parameters, $\sum t_{\ell,T} / \sum t_{\ell,L}$, the smaller the reduction.

In case of a net-shear failure in principle the same considerations can be made. In doing so the layers relevant for transferring compression perpendicular to grain stresses change and the number of layers which fail in transverse shear is equal to the number of layers in the weak direction of the CLT element. Consequently, the following relationships apply:

$$E_{xM} = \frac{\sum t_{l,xM} \cdot E_0 + \sum t_{l,yM} \cdot E_{90}}{t_{CLT}} \qquad (6)$$

with:

E_{xM} weighted modulus of elasticity in x_M-direction, CLT top layer (value standardized or determined by testing)

$$\sigma_{90} = \sigma_{xM} \cdot \frac{E_{90}}{E_{xM}} = \tau_{xM,yM} \cdot \frac{E_{90}}{E_{xM}} \qquad (7)$$

$$f_{v,net} = \tau_{xM,yM} \cdot \frac{t_{CLT}}{t_{net}} + 1.15 \cdot \sigma_{90} + 0.13 \cdot \sigma_{90}^2 \qquad \text{with: } t_{net} = \sum t_{l,T} \qquad (8)$$

The resistances in net- and gross-shear in case of gross- and net-shear failure, respectively, can be calculated by considering the relevant ratio between $\sum t_{l,T}$ and t_{CLT}.

2.3 Determination of in-plane shear stiffness

The shear modulus G can be determined using the flexibility matrix and its transformation. Using the constitutive Eq. $\varepsilon = S \cdot \sigma$, the flexibility matrix describing the state of plane stress

$$S_{xM,yM} = \begin{bmatrix} \frac{1}{E_{xM}} & 0 & 0 \\ 0 & \frac{1}{E_{yM}} & 0 \\ 0 & 0 & \frac{1}{G_{xM,yM}} \end{bmatrix} \tag{9}$$

can be transformed from the coordinates x_M, y_M to x, y by the angle 360° – α = 315°, see Eq. (10).

$$S_{x,y} = \begin{bmatrix} \frac{0.25}{E_{xM}} + \frac{0.25}{E_{yM}} + \frac{0.25}{G_{xM,yM}} & \frac{0.25}{E_{xM}} + \frac{0.25}{E_{yM}} - \frac{0.25}{G_{xM,yM}} & \frac{0.5}{E_{xM}} - \frac{0.5}{E_{yM}} \\ & \frac{0.25}{E_{xM}} + \frac{0.25}{E_{yM}} + \frac{0.25}{G_{xM,yM}} & \frac{0.5}{E_{xM}} - \frac{0.5}{E_{yM}} \\ symm. & & \frac{1}{E_{xM}} + \frac{1}{E_{yM}} \end{bmatrix} \tag{10}$$

From the load-deformation characteristics of the column-section, the load *F* and the modulus of elasticity E_y can be determined.

For a discrete stress state σ_y with associated strain ε and using the constitutive Eqs. $\varepsilon = S \cdot \sigma$ and $\sigma_y = E_y \cdot \varepsilon_y$, the following relationship, Eq. (11), can be found:

$$\frac{1}{E_y} = 0.25 \cdot \left(\frac{1}{E_{xM}} + \frac{1}{E_{yM}} + \frac{1}{G_{xM,yM}} \right) \tag{11}$$

with: E_y modulus of elasticity in y-direction of the column-section (determined by test)

E_{xM}, E_{yM} weighted modulus of elasticity in x_M- or y_M-direction, CLT top or cross layer

The shear modulus $G_{xM,yM}$ can then be determined according to Eq. (12).

$$G_{xM,yM} = \frac{1}{\left(\frac{4}{E_y} - \frac{1}{E_{xM}} - \frac{1}{E_{yM}} \right)} \tag{12}$$

First tests at the Technische Universität München (TUM) and Graz University of Technology (TU Graz) in 2013 indicated the functional and operational efficiency of the test configuration. Motivated by these promising results, a joint research project between TUM and TU Graz was initiated with the aim

- to prove the applicability and suitability of the test configuration for a wider range of parameter settings,
- to investigate and quantify possible influences on the shear properties, and
- to answer the open question on a possible transfer from single-node outcomes to CLT diaphragms.

3 Materials and methods

3.1 Test programme

The test programme was developed in consideration of all relevant product parameters and their range found in current European Technical Approvals (ETAs) of CLT products. Only CLT elements with glued surfaces were investigated. Tab. 1 contains an overview of the tested parameters and their range of values. The parameters of each series are given in Tab. 2. Fig. 4 shows the scheme of a specimen featuring 5 layers including a notation of some parameters used throughout the text.

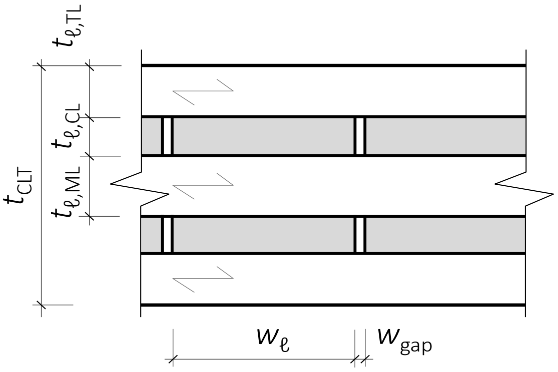

$$\sum t_{\ell,\mathrm{L}} = \sum t_{\ell,\mathrm{TL}} + t_{\ell,\mathrm{ML}}$$

$$\sum t_{\ell,\mathrm{T}} = \sum t_{\ell,\mathrm{CL}}$$

$$t_{\ell,\mathrm{fail}} = t_{\ell,\mathrm{CL}}$$

Fig. 4. Schematic drawing of a 5-layer CLT-element cross section and notation of some parameters.

Table 1. Overview of tested parameters and their values (range).

Parameter [-]	Values [-]
Gap execution	edge bonded (EB); not edge bonded, gap width w_{gap} = {0; 5} mm
Board width	w_ℓ = {80; 160; (230) 240} mm
Layer thickness	t_ℓ = {20; 30; 40} mm
Number of layers	{3; 5; 7} layers
Stress reliefs	{Yes; No}
Layup parameter	$\sum t_{\ell,\mathrm{T}} / \sum_{\ell,\mathrm{L}}$ = {0.32; 0.35; 0.46; 0.50; 0.68; 0.75; 0.86}, with $\sum t_{\ell,\mathrm{T}} \leq \sum t_{\ell,\mathrm{L}}$
Producer	{A; B; C}

Only CLT from Norway spruce (*Picea abies*) was used which was provided by three producers, leading to three groups of specimen, *A*, *B* and *C*. For the boards used for group *A*, strength class C24 according to EN 338 was agreed. The boards for all series within group *A* were delivered in one stack with the exception of the boards of series A4 and A5, which were delivered at a later stage. Due to production limits at the producer, series A1 and A3 were produced at the laboratories at TU Graz, see Dröscher (2014) for further details. All specimen within groups *B* and *C* were produced according to the specific Technical Approvals of the producers. These allow the use of boards of strength class C16 according to EN 338 at a share ≤ 10 %.

Table 2. Test programme; overview of test series including all necessary parameters

Institute		TU Graz									TUM								
Series		A1[1]	A2	A3[1]	A4[2]	A5[2]	A6	A7	A8	A9	B1	B2	B3	B4	B5	C1	C2	C3	C4
No. of specimen		6	6	6	6	6	6	6	6	6	6	6	6	6	6	7	7	7	7
Layers		3	3	3	5	5	5	5	5	7	3	3	3	3	3	3	3	3	3
Layup	TL	30	29	30	17/19	28/30	40	31	40	30	20	20	30	30	40	30	30	40	40
	CL	30	29	30	32	30	19	19	19	30	20	20	30	30	40	30	30	40	40
	ML	-	-	-	19	30	30	20	40	30	-	-	-	-	-	-	-	-	-
t_{CLT} [mm]		90	87	90	119	148	148	120	158	210	60	60	90	90	120	90	90	120	120
$\sum t_{\ell,T} / \sum t_{\ell,L}$ [-]		0.50	0.50	0.50	0.86	0.68	0.35	0.46	0.32	0.75	0.50	0.50	0.50	0.50	0.50	0.50	0.50	0.50	0.50
w_ℓ [mm]		160	160	160	160	160	160	160	160	160	80	160	160	160	240	230	230	230	230
Gap execution[3]		EB	0	5	0	0	0	0	0	0	0	0	0	0	0	0	0	0	0
Stress relief		N	N	N	N	N	N	N	N	N	N	N	N	Y	Y	N	Y	N	Y
$t_{\ell,fail}$ [mm]		90	29	30	17/19	30	19	19	19	30	20	20	30	30	40	30	30	40	40
Layer failing		All	CL	CL	LL	CL	CL	CL	CL	CL	CL	CL	CL	CL	CL	CL	CL	CL	CL

TL ... Top Layer, CL ... Cross Layer, ML ... Middle Layer, LL ... longitudinal layers (TL & ML);
$t_{\ell,fail}$ ... thickness of failed layer(s) where shear failure(s) was (were) observed;
[1] produced in laboratory;
[2] boards delivered at later stage;
[3] EB ... edge bonded, 0 resp. 5 ... gap width [mm]

The series in groups *A* and *B* consisted of 6, the series in group *C* of 7 specimen. The specimen were generally retrieved consecutively from one CLT plate. Thus it is expected that the variability of the parameters within one series is reduced due to partly the same base material within this series. To evaluate this influence, a stochastic simulation was conducted, see Section 4.1.

3.2 Test configuration

The test configuration was realized according to the configuration described in Section 2. The geometric relationship was set to h_{CLT} / w_{CLT} = 3 / 1, more specifically to h_{CLT} / w_{CLT} = 1,500 mm / 500 mm. This effectuated a field of pure shear outside the quadratic area potentially influenced by the support conditions while eliminating the potential for stability failure in most configurations. The assumption of a field of constant shear was verified by means of a Finite-Element (FE) study, in which geometric and stiffness parameters were varied in a practical range, see Silly (2014) for further details. The potential influence of friction between the support (surface of load application) and the test specimen was investigated by using (i) lubricated edges, (ii) teflon intermediate layers, (iii) roller bearing and (iv) blank steel to wood contact. The differences in determined transverse strains were evaluated by measurements of the horizontal deformation near the load application and found to be not of practical relevance. All tests within group *A* were realized using Teflon intermediate layers, all tests within groups *B* and *C* were conducted with a roller-bearing at the bottom support and steel plate to wood contact at the load introduction. In all cases, the load was applied at a constant rate to achieve failure within 300 ± 120 s according to EN 408 (2010). The tests within group *A* were realized in the 4 MN four-column test frame of the Laboratory for Structural Engineering (LKI) at TU Graz. All tests of groups *B* and *C* were conducted in the Zwick Z-600 testing machine at the MPA BAU at TUM. In case of very slender test specimen, one horizontal support was added to each side face of the specimen to prevent premature buckling. The deformation was determined on both side faces of the specimen using centrically placed measurement crosses featuring a measuring distance of h_0 = 400 mm. For this, the specimen of group *A* were equipped with DD1 strain transducers, which were removed at approximately 50 % of F_{max}. The specimen of groups *B* and *C* were equipped with rope extensometers on one side face. On the other side face, the contact-free optical measurement system GOM with software Pontos (2007) was used.

3.3 Determination of parameters

3.3.1 Moisture content and density

For each specimen, the mean density as well as the mean moisture content (group *A*: kiln drying, groups *B* and *C*: resistance method) were determined. In the case of moisture contents differing from the reference moisture content u_{ref} = 12 %, the mean density at 12 % moisture content, ρ_{12}, was determined according to EN 384 (2010).

3.3.2 Shear strength and torsional stresses

The shear strength in case of gross- and net-shear failure was determined according to Eq. (5) and (8), respectively. The (low) influence of compressive stresses perpendicular to the grain on shear strength was taken into account using the regression formula from Blaß & Krüger (2012), applying compressive stresses perpendicular to the grain determined with Eqs. (4) and (7).

The torsional stresses $\tau^*_{tor,i}$ at the time of failure in gross- or net-shear were determined on the basis of polar torsion, considering a finite number of layers *N* and a heterogeneous layup with thicknesses $t_{l,i}$ by establishing ideal layer thicknesses $t^*_{l,i}$ to take into account bonded areas in the outer and core region of the CLT-elements, with

$t^*_{l,1} = min(2 \cdot t_{l,1}; t_{l,2})$ resp. $t^*_{l,N-1} = min(t_{l,N-1};\ 2 \cdot t_{l,N})$ and $t^*_{l,2\leq i\leq N-1} = min(t_{l,i};\ t_{l,i+1})$ (13)

with: $t_{l,i}$ as thickness of the layer *i* = 1, 2, …, *N*, and the relationship

$$\tau^*_{tor,i} = 3 \cdot f_{v,gross} \cdot \left(\frac{t^*_{l,i}}{w_l}\right), \quad (14)$$

see Bogensperger et al. (2010). To determine the shear strength at the reference moisture content u_{ref} = 12 %, a relationship of 3 % per percent change in moisture content was applied.

3.3.3 In-plane shear stiffness of the CLT elements

The shear modulus $G_{090,CLT}$ of the CLT elements under in-plane shear was determined with two approaches. The first approach, described in Section 2, is based on the measured vertical deformation in the local measurement field and moduli of elasticity $E_{0,mean}$ and $E_{90,mean}$, standardized according to the strength class of the boards, considering a strength class of C24 according to EN 338 (2009), with $E_{0,mean}$ = 11,000 N/mm² and $E_{90,mean}$ = 370 N/mm². The shear modulus $G_{090,CLT,xM,yM,KS} = G_{090,KS}$ is determined according to Eq. (12).

The second approach applied is standardized in EN 408 (2010) with

$$G_{090,CLT,xM,yM,EN} = G_{090,EN} = \frac{h_0}{w_{CLT} \cdot t_{CLT}} \cdot \frac{\Delta F/2}{\Delta w_G} \quad (15)$$

with:

h_0 measurement length

$\Delta F/\Delta w_G$ relationship between load and shear deformation, determined in the linear elastic range between 0.1 and 0.4 F_{max}

With aid of a Finite-Element study it could be shown, that the differences between ideal and real stress distribution are negligible for given geometric and stiffness relationships (< 1 %), hence no correction factor α_G was applied, see Dröscher (2014) for further details. To determine the shear moduli at reference moisture content u_{ref} = 12 % a relationship of 2 % per percent change in moisture content was applied.

4 Results and Discussion

4.1 General

Three groups with a total of 18 series featuring different product configurations were tested. The statistics of the main parameters in each series are illustrated in Tab. 3. The statistical analysis as well as stochastic simulations were carried out in R (2015).

The moisture content *u* of all specimen was in the range of 12 ± 2 %. Regarding the density ρ_{12} it can be noted that it decreases from group *A* to *C* (*A*: 463, *B*: 437, *C*: 419 kg/m³). Only series B5 exhibited a density, which is below the expected range for series within group *B*. Deriving all specimen from the same CLT element was concluded to be the reason for low CVs in density.

The low CVs of the shear strength (2 % ≤ CV[$f_{v,net,12}$] ≤ 8 %) in combination with the very reliable failure in gross-shear respectively net-shear, independent of the multitude of parameters and their range, affirmed the very robust test configuration. No differences in results were identified between both test institutes as well as the utilized testing machines. However, as mentioned above, these low CVs are biased by the applied sampling approach. Based on a stochastic simulation, conducted by considering parallel and serial interaction of nodes and sections of lamellas in the test area, CV[$f_{v,net}$] is estimated to be approximately 6 %.

In contrast to common expectation, shear moduli feature higher CVs than the shear strength. This is attributed to the known difficulties in deriving distinct values from deformation curves, which are the result of measurements of very low deformations.

4.2 Shear modulus

A comparison of the shear moduli determined with above given approach Eq. (12) and the approach given in EN 408 (2010), Eq. (15), shows that the values determined with latter approach are on average about 10 % higher. The reason is the considerably higher vertical deformation in comparison to the horizontal deformation. The approach by Kreuzinger und Sieder (2013), Eq. (12), only takes into account the vertical deformation. Furthermore, the application of standardized values for $E_{0,mean}$ and $E_{90,mean}$ leads to higher CVs for shear moduli compared to shear moduli determined according to EN 408 (2010). It should be discussed how both approaches could be adapted to better eliminate the influence of deformations from other stresses than shear stresses. For the time being, the approach according to EN 408 (2010) is preferred as it returns more stable results.

Table 3. Statistics of tested series: moisture content, density, maximum load, apparent fracture deformation, shear strength, shear moduli, torsional stresses

Institute	TU Graz									TUM								
Statistics	A1	A2	A3	A4	A5	A6	A7	A8	A9	B1	B2	B3	B4	B5	C1	C2	C3	C4
No. of. specimens [-]	6	6	6	6	6	6	6	6	6	6	6	6	6	6	7	7	7	7
u_{mean} [%]	12.3	12.2	12.2	12.5	11.6	11.2	10.9	11.3	10.6	10.5	10.1	11.6	10.8	10.4	12.4	12.7	13.1	14.1
$\rho_{12,mean}$ [kg/m³]	470	478	461	472	459	455	461	445	471	434	450	443	445	414	423	411	410	433
CV[ρ_{12}] [%]	1.4	1.4	2.6	1.9	1.9	1.0	1.4	0.7	1.4	1.1	1.1	1.3	1.2	2.7	1.3	1.6	2.6	1.4
$F_{max,u,mean}$ [kN]	378	194	177	379	431	353	339	353	570	178	226	247	214	217	244	230	264	268
$w_{f,app,mean}$ [mm]	8.7	7.9	8.6	10.4	9.9	8.1	9.0	7.9	9.5	9.1	7.7	9.0	8.8	8.2	8.3	8.1	7.8	8.4
$f_{v,gross,mean,12}$ [N/mm²]	3.8	2.2	1.9	3.1	2.8	2.3	2.7	2.2	2.5	2.8	3.5	2.7	2.3	1.7	2.7	2.6	2.2	2.3
$f_{v,net,mean,12}$ [N/mm²]	11.5	6.6	5.8	6.8	6.9	8.9	8.5	9.0	5.9	8.4	10.5	8.0	6.7	5.1	8.1	7.7	6.7	7.0
CV[$f_{v,net,12}$] [%]	7.4	5.3	3.3	4.1	3.2	3.5	6.3	7.1	7.7	1.8	4.1	5.2	2.1	5.5	6.1	4.7	2.3	4.3
$f_{v,net,12,05,LND}$ [N/mm²]	10.1	6.0	5.5	6.3	6.6	8.4	7.6	8.0	5.2	8.1	9.8	7.3	6.5	4.6	7.3	7.1	6.5	6.5
$G_{090,KS,12,mean}$ [N/mm²]	640	460	300	520	510	460	490	410	460	500	600	420	430	310	480	470	450	440
CV[$G_{090,KS,12}$] [%]	11.0	11.8	5.8	4.8	6.3	4.0	13.3	9.1	6.6	7.7	12.2	7.2	12.3	12.4	14.2	9.9	10.8	11.8
$G_{090,EN,12,mean}$ [N/mm²]	650	490	320	540	550	490	540	460	510	500	590	490	480	380	560	520	530	510
CV[$G_{090,EN,12}$] [%]	7.5	10.0	5.8	6.9	5.9	2.6	10.0	12.4	5.3	8.1	9.7	5.5	10.0	4.8	10.8	6.2	7.3	10.7
$G_{090,CLT,mean,est}$ [N/mm²]	-	460	460	540	490	540	540	540	500	410	520	460	460	480	510	510	470	470
$\tau_{tor,12,mean}$ [N/mm²]	2.2	1.2	1.1	1.9	1.6	0.8	1.0	0.8	1.4	2.1	1.3	1.5	2.5	0.9	1.1	2.0	1.2	2.4

$w_{f,app,mean}$ ... apparent fracture deformation corresponding to maximum load, based on measurement from the testing device

Table 3 contains also values $G_{090,CLT,mean,est}$ calculated with the formalism given in Bogensperger et al. (2010), see Eq. (16)

$$G_{090,CLT,mean,est} = \frac{G_{0,l,mean}}{1+6\cdot\alpha_T\cdot\left(\frac{t_{l,mean}}{w_l}\right)^2}, \text{ with } \alpha_T = p\cdot\left(\frac{t_{l,mean}}{w_l}\right)^q \text{ and } t_{l,mean} = \frac{t_{CLT}}{N}, \tag{16}$$

with $G_{0,l,mean}$ as average shear modulus of the lamellas, p and q as parameters of function α_T, see Tab. 4. Compared to $G_{090,EN,12,mean}$ overall congruent shear module, with deviations within ± 10 % and only for some series of ± 20 %, are found, apart from A3.

Table 4. Parameters p and q for α_T from Dröscher (2014).

No. of layers N [-]	p [-]	q [-]
3	0.53	–0.79
5	0.43	–0.79
7	0.39	–0.79

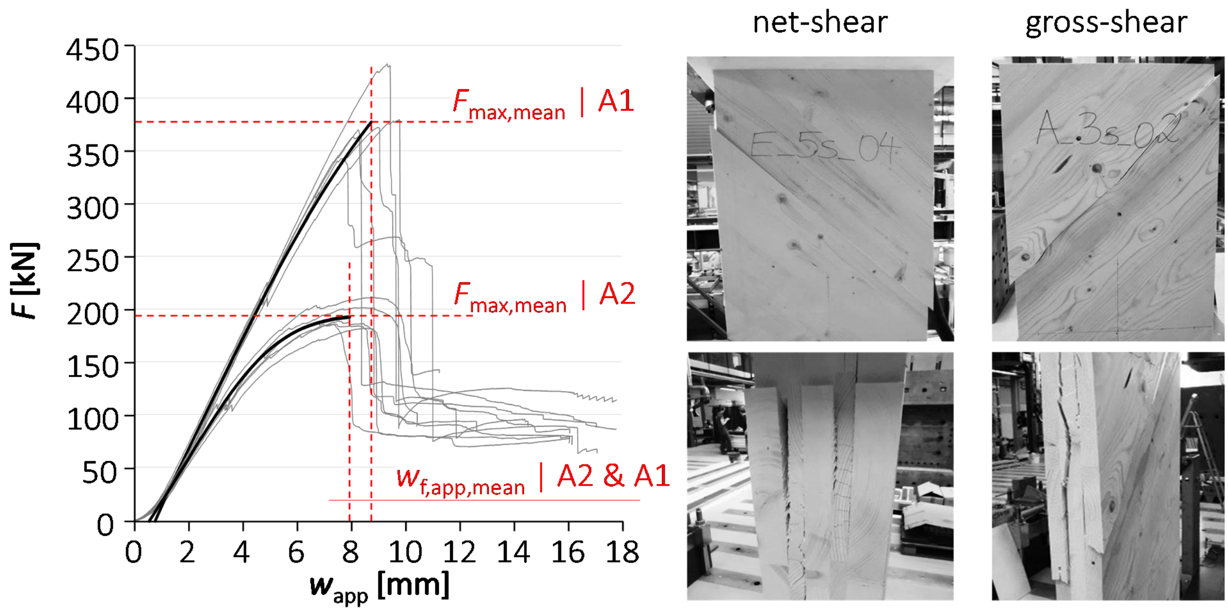

Figure 5. (left) load-displacement curves of series A1 (with) & A2 (without edge bonding); (right) typical impressions of net- and gross-shear failure mode.

4.3 Shear strength

All specimen within series A1, featuring edge bonded boards, failed in gross-shear. All specimen without edge bonding failed in net-shear. The failure in gross-shear was followed by a failure in net-shear and corresponding softening to a plateau of about 30 – 60 % of net-shear strength, see Fig. 5. In contrast to gross-shear failure, net-shear failure exhibited a considerable proportion of non-linear deformation. All series without edge bonded boards failed due to a net-shear failure in the cross layer(s) with the exception of series A4 in which most specimen exhibited a failure in direction of the top layer. The mean vertical deformations at time of failure feature, independent of the type of failure, a low range (7.7 mm ≤ $w_{f,app,mean}$ ≤ 9.5 mm). Two specimen within series B1 experienced a stability failure (second eigenmode due to horizontal support) before net-shear failure. A comparison to the strength values of the other specimen within that series did not show any influence of stability failure on shear properties. Fig. 6 shows the net-shear strength of individual series arranged by certain parameters to enable examination of parameters relevant for shear strength. In the following sub-sections, these parameters will be discussed with respect to their influence on shear strength.

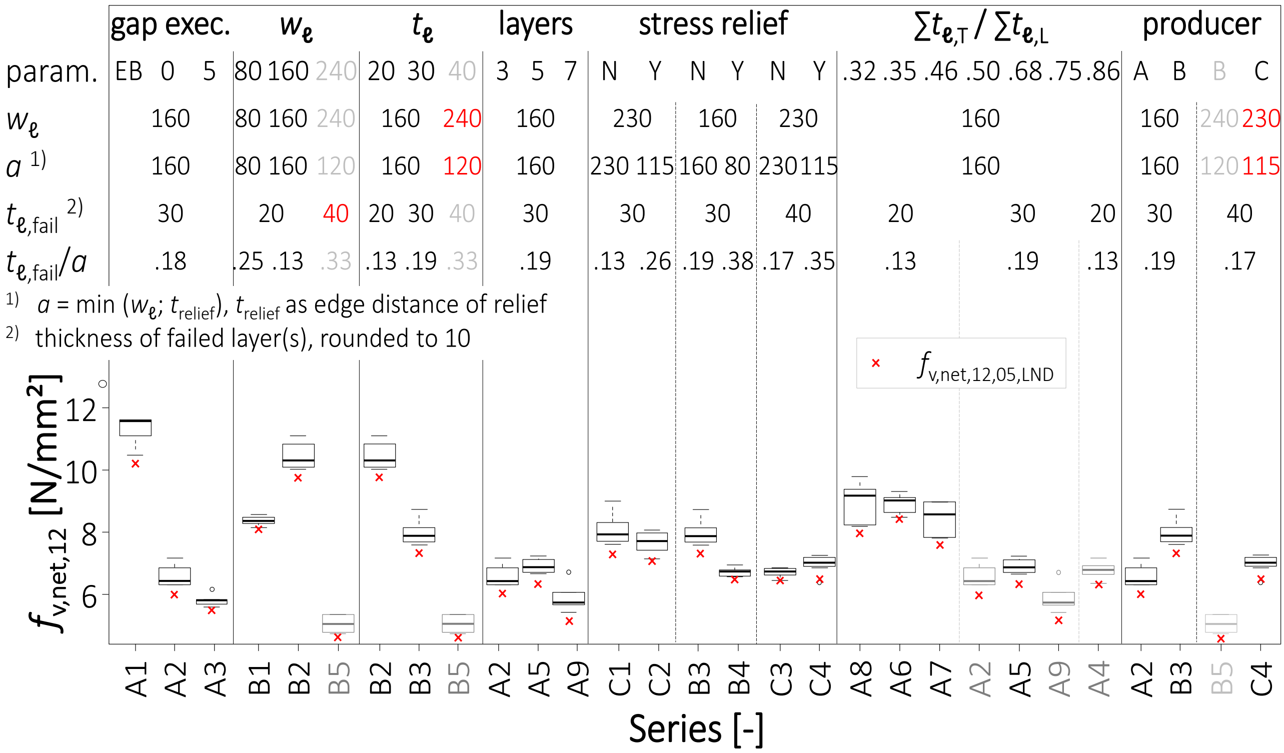

Figure 6. Box-plots of net-shear strength for identification of relevant parameters.

4.3.1 Gap execution

Series A1, A2 and A3 were used to analyse the influence of gap execution. The edge bonded specimen A1 exhibited increased stiffness and a failure in gross-shear, followed by failure in net-shear. The parameters determined for series A1 $f_{v,gross,12,05}$ = 3.8 N/mm^2 and $G_{090,EN,12,mean}$ = 650 N/mm^2 are comparable to those of glulam GL24h with, according to EN 14080 (2013), $f_{v,g,k}$ = 3.5 N/mm^2 and $G_{g,mean}$ = 650 N/mm^2. Series A2 and A3, without edge bonding, like all other remaining series, failed in net-shear. The shear strength of series A2 and A3, compared to the edge bonded series A1, is almost halved. The lower shear parameters of series A3 in comparison to series A2 can mainly be attributed to the unintended but common edge bonding of CLT with closed gaps due to the penetration of glue from the side faces into the gaps between the boards during the production process. Another effect is the activation of friction between the boards in contact. Current technical approvals allow for gaps between 4 and 6 mm. The resulting reduction in cross-section is, however, negligible for practical applications (< 5 %). Higher shear properties could be attributed to CLT elements with closed gaps and/or edge bonding. This implies however that the closed gap is preserved throughout the lifetime of the structure. Cracks due to climatic changes are at least to be expected in the top layers.

4.3.2 Board width

To analyse the parameter board width w_ℓ respectively gap or relief distance *a*, the results of series B1 and B2 were used directly; series B5, due to its board thickness and stress relief, could be used to a limited extent. Taking into account the pronounced influence of the parameter board thickness (see Section 4.3.3), the results given in Fig. 6 and Tab. 3 indicate a regressive relation between board width and shear parameters.

Jöbstl et al. (2008), Hirschmann (2013) and Brandner et al. (2013) state that the failure in net-shear happens as a result of a local interaction of torsional and longitudinal shear failure at the board edges. From this it can be expected that increasing board width and hence decreasing torsional stresses due to a decreasing relation (t_ℓ / a) has a positive effect on shear strength. On the other hand, wider boards are usually cut close to the core of the log, leading to an increased proportion of rift or half-rift cuts. The shear strength in the longitudinal-tangential plane, $f_{v,LR}$, is lower than in the longitudinal-radial plane, $f_{v,LT}$ (see e.g. Keenan et al. 1985, Denzler & Glos 2007, Brandner et al. 2012). With respect to knots and checks, a reciprocal relation is expected. Due to the very local formation of failure, the influence of these timber characteristics is expected to be low. Taking into account the very heterogeneous densities of the series compared and the comparable outcomes of C1 vs. C3 and C2 vs. C4, both pairs without and with reliefs, no clear influence of the board width can be derived. In accordance with the results from tests on single CLT nodes (Brandner et al. 2013), the influence of board width on the shear parameters is evaluated as low, thus it is proposed to disregard this parameter for practical applications.

4.3.3 Board (layer) thickness

This parameter was evaluated by comparison of series B2 & B3 (to a limited extent also B5) as well as C1 & C3 and C2 & C4. With increasing layer thickness, a distinct decrease in net-shear strength could be identified. This is in accordance with results from tests on single CLT nodes (Brandner et al. 2013). This result can be attributed to the locking effect due to the orthogonal arrangement of layers as well as the tendency of thicker boards to feature an increased proportion of wood prone to fail in the longitudinal-tangential plane, featuring a lower shear strength, $f_{v,LR}$, see Section 4.3.2. Another potential effect is the size effect of wood under shear, i.e. area available in which shear failure (e.g. cracking) can develop. The shear properties of the series within group *A* were lower compared to the results of series within groups *B* and *C*. However, the relative differences between series featuring board thicknesses t_ℓ = 20 mm and 30 mm were comparable. A comparison of the series within group *B* showed that the shear strength of series B5 is unexpectedly low, accompanied by very low densities and unexpectedly high CV. This series is therefore disregarded when determining characteristic shear strength.

4.3.4 Number of layers

A comparison of series A2 (3 layers), A5 (5 layers) and A9 (7 layers) showed, inversed to the density, a slightly concave relationship between the shear strength, $f_{v,net,12}$, and the number of layers *N*. It should be noted that the boards used within series A5 were delivered at a later stage, a corresponding influence cannot be excluded. Due to the relative small differences between the series, the parameter number of layers is evaluated negligible for practical applications.

4.3.5 Stress relief

For an assessment of this parameter, three pairs of series with / without stress relief were available. Due to the local interaction of shear and torsional stresses in the case of net-shear failure, it was expected that higher relationships of (t_ℓ / a) lead to lower shear properties. Apart from one exception, only small differences could be found in this comparison. With respect to building practice and regarding the potential question of how to define individual shear parameters for CLT with stress reliefs, it is proposed to disregard this parameter.

4.3.6 Layup parameter

The layup parameter (ratio between the sum of layer thicknesses in weak direction to that in the strong direction) of all tested series featuring layer thicknesses t_ℓ = 20, 30 and 40 mm was in the range of 0.25 to 1.00. The results of the series of group *A*, grouped according to the thickness of the failing layer, $t_{\ell,fail}$, show a progressive trend of gross-shear strength $f_{v,gross,12}$ while the net-shear strengths, $f_{v,net,12}$, were rather constant for given layer thickness, $t_{\ell,fail}$. Series A4 exhibited comparatively low net-shear strengths. In this series, not the cross but the top and middle layers failed. CLT elements with ratios close to 1.0 can exhibit failure of the top and middle layers, series A4 featured a comparatively high ratio of 0.86. It is expected that the missing locking effect at the outer side of the top layers leads to a decreasing shear strength in the magnitude of about one thickness class.

5 Design proposal

The results of the test series described in the preceding sections show that the main parameters influencing the shear properties are the layer thickness (decreasing properties with increasing thickness) and the gap execution (edge bonded, not edge bonded and without / with gaps, with decreasing properties in mentioned order). The distinct relation between layer thickness and net-shear strength leads to a dependency of the gross-shear strength on the layup parameter (ratio between sums of layer thickness). Therefore the most practical approach would be to define a verification concept based on the net-shear strength and the associated layers prone to fail. Such a concept would allow for a design independent of the above mentioned layup parameter. In addition, it would mirror the approach applied for the verification of longitudinal stresses in CLT elements under in-plane loads. In case of

CLT-elements with a layup parameter ≥ 0.8, indicating a potential failure of the top and middle layer(s), verification of net-shear has to be met for both diaphragm directions. In doing so, a reduced shear strength of the top layers, following the approach in Section 4.3.6, shall be considered.

For CLT elements with expected gross-shear failure, a verification on the basis of gross-shear strength and assuming the full element width is feasible. Due to the longitudinal shear failure of all layers in edge bonded CLT elements, the dependency on the layup parameter is expected to be low and not of practical relevance. This implies however that the closed gap is preserved throughout the lifetime of the structure. Cracks due to climatic changes are at least to be expected in the top layers. The approach given in EN 1995-1-1+A1 (2008), implying the reduction factor k_{cr} to take into account shrinkage cracks in glulam, could be translated to edge bonded CLT elements. Following this approach, the cross-section utilized for verification would be reduced by a certain proportion of the top layer thickness, hence by considering only 30 to 50 % of $t_{\ell,TL}$. However, additional investigations to better quantify this approach are required. Securing the full potential utilization of the core layers over the lifetime of the structure implies as well, that the load-carrying capacity of the edge bond, i.e. the certified applicability of the utilized glue and the correct execution of the bond, is ensured and controlled.

For CLT-elements that are expected to fail in net-shear, the verification of torsional stresses, i.e. the potential failure between two layers in the vicinity of the glued bond, has to be met, in addition to the verification of net-shear. Following Schickhofer et al. (2010), i.e. considering a characteristic torsional strength $f_{v,tor,k}$ = 2.5 N/mm², in combination with the values for $f_{v,net,k}$ presented in this paper, it can be concluded that the torsional failure mechanism can potentially govern only in cases of CLT diaphragms featuring a ratio between board thickness to board width / distance of reliefs, t_l / a or t_l / w_l, exceeding 0.25.

6 Conclusions

The new shear test configuration was successfully applied to the full spectrum of tested configurations, demonstrating its functional and operational efficiency and reliable shear failures of all tested CLT diaphragms. Consequently, we propose this test configuration for implementation in EN 16351. Regarding the investigated parameters, qualitatively congruent results to experiences made on single node tests were achieved. This comprises the influence of gap width and board or layer thickness. All specimen without layers of edge bonded boards failed in net-shear. For CLT-elements that are expected to fail in net-shear, a design concept based on the net-shear strength of the layers in the weaker direction is proposed in combination with a net-shear strength $f_{v,net,k,ref}$ = 5.5 N/mm^2. Here, layer thicknesses up to 40 mm and gap widths up to 6 mm are taken into account. For layers in weak direction with thicknesses between 20 mm ≤ $t_{l,fail}$ < 40 mm and without gaps or reliefs higher strength values are expected. Also taking into account the results from single CLT nodes (Brandner et al. 2013), a relationship $f_{v,net,k} = f_{v,net,k,ref} \cdot \min\{(40 / t_{\ell,fail})^{0.30}; 1.20\}$ is proposed. The shear modulus can be determined according to Eq. (16) (Bogensperger et al. 2010). For simplification a value of $G_{090,mean}$ = 450 N/mm^2 is proposed. In case of CLT elements with a layup parameter ≥ 0.8, the net-shear strength of both directions of layers has to be verified. The reason is the potential failure of the weaker top layers. The lower shear strength of the top layers can be taken into account using the approach given in Section 4.3.6.

In case of edge bonded specimen, gross-shear failure, followed by net-shear failure was observed together with significantly higher resistances and shear moduli. For such elements, the shear properties known from glulam, $f_{v,gross,k}$ = 3.5 N/mm^2 and G_{0mean} = 650 N/mm^2 are proposed. This necessitates, however, the consideration of potential influences during the lifetime of the structure, e.g. crack formation and delamination, in the design and production process, see Section 5. Further research could include a comparison of shear properties of intact edge bonded specimen to edge bonded specimen featuring pronounced shrinkage cracking. In addition to the verification of CLT diaphragms in gross- or net-shear, the verification of the torsional stresses, as third potential failure mechanism, is required in cases of CLT diaphragms prone to fail in net-shear and featuring a ratio t_l / a or t_l / w_l, exceeding 0.25.

7 Acknowledgement

This research project originated from a cooperation project between the holz.bau forschungs gmbh, in the frame of the FFG COMET K-Project „focus_sts“, the Graz University of Technology, Institute of Timber Engineering and Wood Technology and the Technische Universität München (TUM), Chair of Timber Structures and Building Construction, in cooperation with the Glued Laminated Timber Research Association inc., Wuppertal. The support by the funding bodies and project partners as well as the funding of a short-term scientific mission in the frame of COST Action FP1402 is gratefully acknowledged.

8 References

Andreolli, M, Rigamonti, M, A Tomasi, R (2014) Diagonal compression test on cross laminated timber panels. WCTE, Quebec, Canada.

Blaß, H-J, Görlacher, R (2002) Zum Trag- und Verformungsverhalten von Brettsperrholz-Elementen bei Beanspruchung in Plattenebene: Teil 2 (in German). Bauen mit Holz, 12:30–34.

Blaß, H-J, Krüger, O (2010) Schubverstärkung von Holz mit Holzschrauben und Gewindestangen, Karlsruher Berichte zum Ingenieurholzbau, Band 15, Universitätsverlag Karlsruhe.

Bogensperger, T, Moosbrugger, T, Schickhofer, G (2007) New test configuration for CLT-wall-elements under shear load. CIBW18/40-21-2, Bled, Slovenia.

Bogensperger, T (2008) A contribution to the characteristic shear strength of a CLT wall under shear. 3rd Workshop, COST E55, Espoo, Finland.

Bogensperger, T, Moosbrugger, T, Silly, G (2010) Verification of CLT-plates under loads in plane. WCTE, Riva del Garda, Italy.

Bosl, R (2002) Zum Nachweis des Trag- und Verformungsverhaltens von Wandscheiben aus Brettsperrholz (in German). Military University Munich, Munich.

Brandner R, Gatternig W, Schickhofer G (2012) Determination of Shear Strength of Structural and Glued Laminated Timber. CIB-W18/45-12-2, Växjö, Sweden.

Brandner, R, Bogensperger, T, Schickhofer, G (2013) In plane Shear Strength of Cross Laminated Timber (CLT): Test Configuration, Quantification and influencing Parameters. CIB-W18/46-12-2, Vancouver, Canada.

CUAP 03.04/06 (2005) Common Understanding of Assessment Procedure: Solid wood slab element to be used as a structural element in buildings. OIB, Wien.

DIN EN 1995-1-1/NA (2013) National Annex – Nationally determined parameters – Eurocode 5: Design of timber structures – Part 1-1: General – Common rules and rules for buildings. (DIN).

Dröscher, J (2014) Prüftechnische Ermittlung der Schubkenngrößen von BSP-Scheibenelementen und Studie ausgewählter Parameter (in German). Master Thesis, Graz University of Technology, Graz.

EN 338 (2009) Structural timber – Strength classes. (CEN).

EN 384 (2010) Structural timber – Determination of characteristic values of mechanical properties and density. (CEN).

EN 408+A1 (2010) Timber structures – Structural timber and glued laminated timber – Determination of some physical and mechanical properties. (CEN).

EN 594 (2011) Timber structures – Test methods – Racking strength and stiffness of timber frame wall panels. (CEN).

EN 1995-1-1+A1 (2008) Eurocode 5: Design of timber structures — Part 1-1: General — Common rules and rules for buildings. (CEN)

EN 14080 (2013) Timber structures – Glued laminated timber and glued solid timber – Requirements. (CEN).

Flaig, M, Blaß, H J (2013) Shear strength and shear stiffness of CLT-beams loaded in plane. CIB-W18/46-12-3, Vancouver, Canada.

FprEN 16351 (2015) Timber structures - Cross laminated timber – Requirements. CEN.

Hemmer, K (1984) Versagensarten des Holzes der Weißtanne (Abies Alba) unter mehrachsiger Beanspruchung, Dissertation, TH Karlsruhe.

Hirschmann, B (2011) Ein Beitrag zur Bestimmung der Scheibenschubfestigkeit von Brettsperrholz (in German). Master Thesis, Graz University of Technology, Graz.

Jeitler, G (2004) Versuchstechnische Ermittlung der Verdrehungskenngrößen von orthogonal verklebten Brettlamellen (in German). Master Thesis, Graz University of Technology, Graz.

Jöbstl, R A, Bogensperger, T, Schickhofer, G, Jeitler, G (2004) Mechanical Behaviour of Two Orthogonally Glued Boards. WCTE, Lahti, Finland.

Jöbstl, R A, Bogensperger, T, Schickhofer, G (2008) In-plane shear strength of cross laminated timber. CIB-W18/41-12-3, St. Andrews, Canada.

Kreuzinger, H, Sieder, M (2013) Einfaches Prüfverfahren zur Bewertung der Schubfestigkeit von Kreuzlagenholz / Brettsperrholz (in German). Bautechnik, Volume 90, Issue (5), pp. 314–316.

PONTOS (2007) Benutzerhandbuch. GOM – Gesellschaft für optische Messtechnik, Braun-schweig.

R CORE TEAM (2015) R: A language and environment for statistical computing. R Foundation for Statistical Computing, Vienna, Austria, http://www.R-project.org.

Schickhofer, G, Bogensperger, T, Moosbrugger, T (eds., 2010) BSPhandbuch: Holz-Massivbauweise in Brettsperrholz – Nachweise auf Basis des neuen europäischen Normenkonzepts. Verlag der Technischen Universität Graz, ISBN 978-3-85125-109-8.

Silly, G (2014) Schubfestigkeit der BSP-Scheibe – numerische Untersuchung einer Prüfkonfiguration (in German). Research Report, holz.bau forschungs gmbh, Graz University of Technology, Graz.

Spengler, R (1982) Festigkeitsverhalten von Brettschichtholz unter zweiachsiger Beanspruchung, Teil 1, Ermittlung des Festigkeitsverhaltens von Brettlamellen aus Fichte durch Versuche (in German). Technische Universität München, München (Berichte zur Zuverlässigkeitstheorie der Bauwerke, Heft 62).

Szalai, J (1992) Indirekte Bestimmung der Scherfestigkeit des Holzes mit Hilfe der anisotropen Festigkeitstheorie. Holz als Roh- und Werkstoff, Volume 50, Issue 6, pp. 233 238.

Wallner, G (2004) Versuchstechnische Ermittlung der Verschiebungskenngrößen von orthogonal verklebten Brettlamellen (in German). Master Thesis, Graz University of Technology, Graz.

Discussion

The paper was presented by P Dietsch

F Lam received clarification that the effect of compressive stresses on rolling shear strength was taken into considered using adjustment factors.

H Blass and P Dietsch discussed the roller bearing details and member under pure shear such as the case of shear wall. They also discussed the case of CLT as bending members on edge where standard bending test would be available but difficult to achieve shear failure of the members. Here torsional shear and rolling shear would coexist. A Ceccotti stated that in a 3x3 m wall in shear connection design would be more critical.

I Smith asked how the specimen size was selected. P Dietsch responded that they were chosen to avoid localized stresses therefore a ratio of 1:3 for width to height was chosen. G Schickhofer added that the tests are good for wall and diaphragm cases but beam solutions would need more work.

P Zarnani asked whether mechanistic modelling approach would be used. P Dietsch answered that the model is already mechanics based.

Advanced modelling for design helping of heterogeneous CLT panels in bending

L. Franzoni – Laboratoire Navier (ENPC/IFSTTAR/CNRS) – Université Paris Est

A. Lebée – Laboratoire Navier (ENPC/IFSTTAR/CNRS) – Université Paris Est

F. Lyon – Centre Scientifique et Technique du Bâtiment (CSTB)

G. Foret – Laboratoire Navier (ENPC/IFSTTAR/CNRS) – Université Paris Est

Keywords: Cross Laminated Timber, bending, modelling, heterogeneities, bending tests, innovative floors

1 Introduction

Cross Laminated Timber panels are gaining importance in timber construction, due to their advantages coming from their crosswise lay-up. However the heterogeneities affecting their bending behaviour still require advanced tools for being taken into account.

In the first part of the present paper the “low” heterogeneities are mainly represented by gaps between narrow boards of each layer and CLT transverse shear weakness. The suggested equivalent-layer model at the layer scale combined with the 3D exact structure solution (Pagano, 1969 – 1970) and a failure criterion for wood (van der Put, 1982) provide a good comparison with a reference test (Hochreiner, 2013). Then, parameter studies are performed with the validated model in order to quantify shear effects and the influence of varying layers’ number and orientation.

The second part of this paper deals with stronger CLT heterogeneities, namely regularly spaced voids within the panel. The results of an experimental campaign are presented. The experimental behaviour is therefore compared with the behaviour predicted with the equivalent-layer model and design methods for CLT (Eurocode 5, 2004, Kreuzinger, 1999). The input mechanical properties are reduced by wood volume fractions. The results of this comparison shows the need of a more accurate modelling which is currently in development. The first results of such a new modelling procedure are presented as well.

2 Low heterogeneities

A previous study (Franzoni et al, 2015) identified the gaps between lateral boards of each layer and CLT transverse shear weakness as the main "low heterogeneities" affecting their bending behaviour. In the following, the modelling procedure and main results are briefly summarized.

2.1 Modelling

CLT heterogeneities are taken into account with a combined equivalent layer-based mechanical model at the layer scale (Fig. 1) and the exact 3D solution at the structure scale (Pagano, 1969 – 1970). The equivalent layer model takes into account the edge-gluing or not of lateral boards by means of simplified hypotheses on layer's mechanical behaviour (Tab. 1). A failure criterion for wood (van der Put, 1982) is implemented in order to include a failure analysis. The reference bending behaviour (Hochreiner, 2013) documents well the elastic and failure response of CLT, highlighting the edge-gluing detachment as a firs failure mode. The comparison is made in terms of panel's global stiffness and failure stages within the apparent elastic regime.

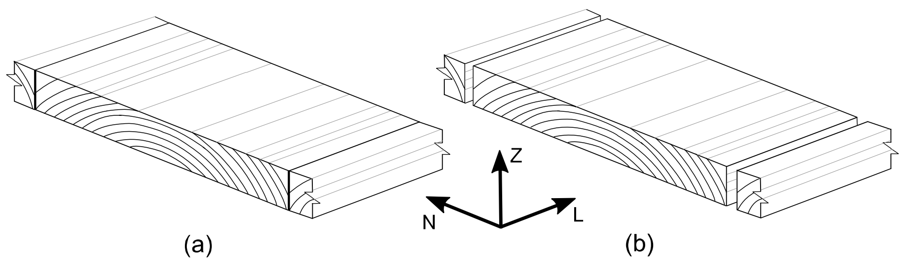

Figure 1 Schematic representation of continuous (a) and discontinuous (b) equivalent layer with the layer's reference frame

Table1 Elastic and strength properties of continuous and discontinuous equivalent layers [Mpa]

Elasticity (Keunecke et al, 2008)	E_L	E_N	E_Z	G_{LZ}	G_{LN}	G_{ZN}	ν_{LZ}	ν_{LN}	ν_{ZN}
Continuous	12800	511	511	602	602	53	0.41	0.41	0.21
Discontinuous	12800	0.0	511	602	602	53	0.41	0.0	0.0

Failure (Dahl, 2009)	$f_{L,t}$	$f_{L,c}$	$f_{N,t}$	$f_{N,c}$	$f_{Z,t}$	$f_{Z,c}$	f_{LZ}	f_{LN}	f_{ZN}
Continuous	63.4	28.9	2.8	3.6	2.8	3.6	4.8	4.8	2.0
Discontinuous	63.4	28.9	-	-	2.8	3.6	4.8	4.8	2.0

2.2 Results

<u>*Comparison / edge-gluing.*</u> Each equivalent-layer model turns out to fit well the reference behaviour within the corresponding edge-gluing regime. It appears that edge-glued layers increase CLT panel's stiffness of about 8% but introduces also an additional failure mode. Indeed, the edge-gluing detachment is one of the first failure modes, and therefore the discontinuous model gives a better prediction of

global load-carrying capacity in terms of failure modes (see Franzoni et al, 2015 for further details). The discontinuous model is then used to perform parameter studies on CLT properties. For all parameter studies the bending configuration is a panel supported on two sides and submitted to an evenly distributed load.

Shear effects. The slope variation of failure load trend as a function of panel's slenderness ratio (Fig. 1a) clearly separates the bending failure regime and the rolling-shear one. This leads to the identification of a transition slenderness of 15 for a 5-ply CLT and 19 for a 3-ply. The normalized difference between the predicted mid-span deflection and the one using the thin-plates theory quantifies the shear part in deflection as a function of slenderness ratio (Fig. 1b).

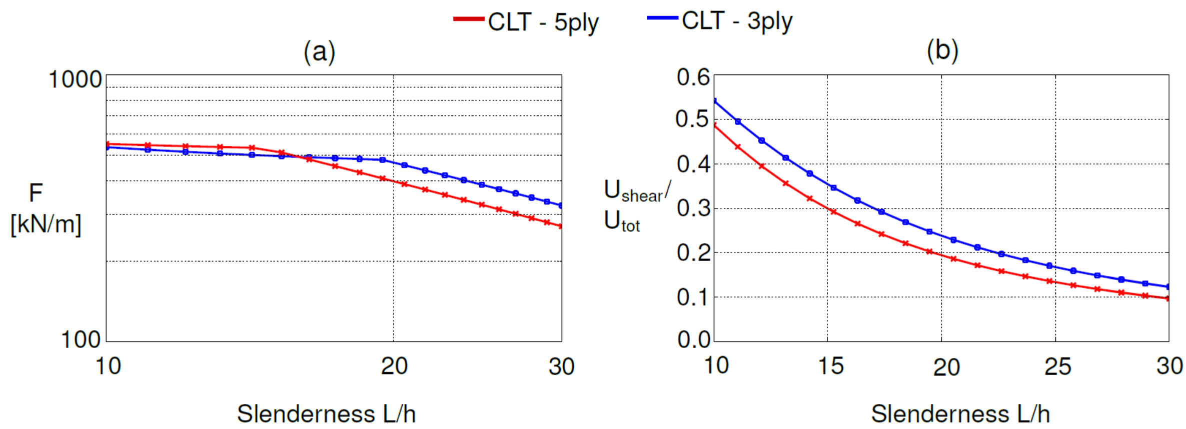

Figure 2 Shear effects on CLT in bending. Failure load trend (a) and shear contribution to mid-span deflection (b) as a function of panel's slenderness ratio

Number of layers. Figure 2 shows that, from a deterministic point of view, increasing layers' number for a fixed CLT total thickness yields lower failure load (Fig. 2a) and higher mid-span deflection (Fig. 2b). Both cases when the panel is thick and slender are presented. The oscillations in shear failure load trend (blue line in Fig. 2a) derive from the position of shear-compliant cross layers, which change with the lay-up.

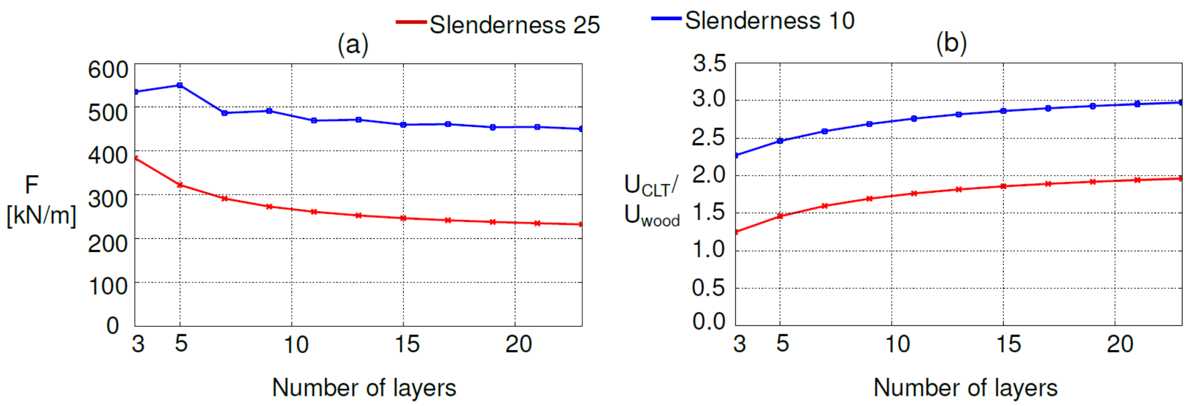

Figure 3 Decreasing CLT bending performance while enlarging the number of layers. Failure load (a) and normalized mid-span deflection (b)

Transverse layers' orientation. Intuitively, intermediate orientations of transverse layers between 90° and 0° may mitigate CLT shear weakness. Figure 3 presents the variation of mid-span deflection and failure load as a function of the varying orientation of 5-ply CLT transverse layers. Similar results are obtained for three or seven layers configurations. The favourable effects of rotating transverse layers are significant only for thick CLT panels, while for slender ones the gains are lower. Moreover, for both cases, the failure load trend shows a drastic drop at several lamination angles due to high in-plane shear stresses related to the torsion moment coming from the non-orthotropic configuration of the plate.

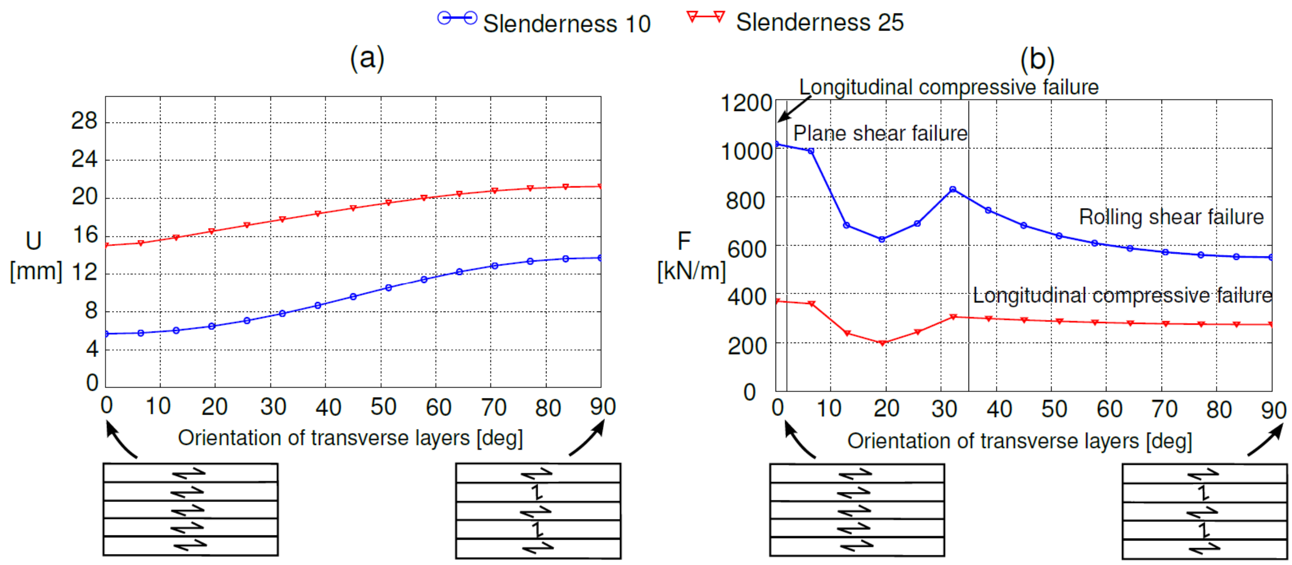

Figure 4 Mid-span deflection (a) and failure load (b) as a function of the varying orientation of transverse layers

3 Strong heterogeneities

Cross Laminated Timber panels having periodic spacing within each layer are already in production. The challenge is to assess the bending efficiency of these lighter and more acoustically efficient floors. Since they are innovative products and the knowledge about them is limited, an experimental campaign has been carried out. A modelling procedure in order to predict their bending behaviour, and especially transverse shear effects, is in development. In this section, the main results of the experiments and the first results of the modelling are presented and discussed.

3.1 Experimental campaign

3.1.1 Four-points bending tests on classical and innovative timber floors

The experimental campaign was based on four-points bending tests on classic and aerated CLT floors. The distance between the supports and the loading points was L/3 (where L is the span). The spaced floors had the same regular spacing between boards along both direction and for all layers. The voids were filled with an insulating material (glass wool), having no mechanical properties. The wood species was Norway spruce of strength class S10 (DIN 4074) for the CLT panels and C24 (EN 338) for the spaced floors. Figure 5 and Table 2 present the geometry of the tested specimens as well as the main results.

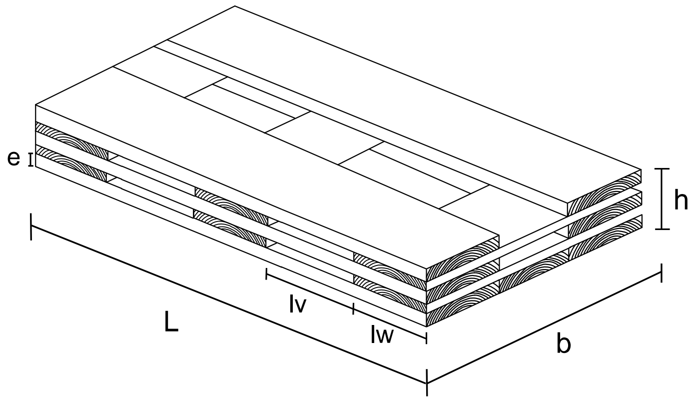

Figure 5 and Table 2 Geometry of the tested panels in four-points bending and main results

Configuration	**CLT**	**Panel-1**	**Panel-2**
Number of specimens	2	2	2
L (m)	4.65	5.88	5.88
b (m)	1.25	1.31	1.26
e (mm)	20	30	30
Number of layers	5	7	7
h (mm)	100	210	210
Voids length - lv (mm)	-	150	300
Wood length - lw (mm)	-	100	100
Wood volume (%)	100	40	25
Failure load (kN)	75	68	34
Failure mode	CL	TL	RS
Global stiffness (kN/m)	470	765	390
Bending stiffness (kN·m^2)	870	3100	1700
Shear / bending deflection (%)	3.5	15	25

Failure modes: RS = rolling shear; CL = longitudinal compressive; TL = longitudinal tensile

The measuring system was mainly based on linear variable differential transformers (LVDTs) for displacement measurement. For all specimens the global mid-span deflection (U) and the bending deflection (u) were measured. For some specimen, the absolute rotation (φ) of the plate's cross section was also measured. Then, the effective plate bending stiffness can be computed using the following equations:

$$(EI)_{flex} = \frac{F \cdot L_b^2 \cdot L}{48 \cdot u} \quad (1) \qquad\qquad (EI)_{flex} = \frac{F \cdot L^2 \cdot \varphi}{18} \quad (2)$$

where F is the load and L_b is the distance between the LVDTs used to measure the bending deflection u. Once the bending stiffness is determined, panel's shear stiffness and shear contribution to deflection can be estimated by means of equations (3) and (4):

$$GA = \frac{F}{U} \cdot (EI)_{flex} \cdot \frac{216 \cdot L}{1296 \cdot (EI)_{flex} - 23 \cdot {}^{F}/_{U} \cdot L^3} \qquad (3)$$

$$\frac{Shear\ deflection}{Bending\ deflection} = \frac{216 \cdot (EI)_{flex}}{23 \cdot GA \cdot L^2} \qquad (4)$$

Additionally, the panel's failure load and failure mode were monitored. Table 2 shows the main results of the bending tests

Due to its high slenderness, the classical CLT floor failed in bending, with several ductile compressive cracks appearing in the upper layer before the brittle tensile failure of bottom layer. Both specimens of Panel-2 failed in rolling shear, with a significant rotation of transverse boards (Fig. 6), while the other configuration of spaced floors failed in tension in the bottom layer.

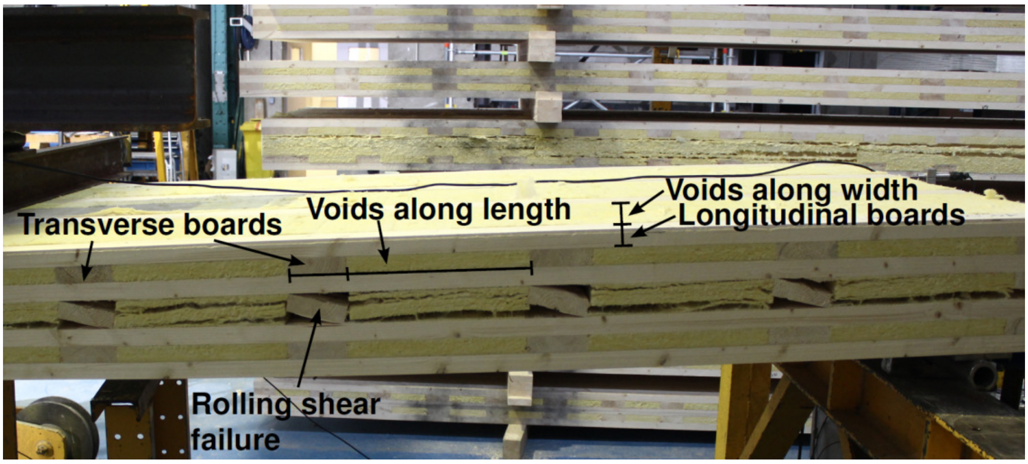

Figure 6 Rolling shear failure of transverse boards of spaced timber floors (Panel-2) in bending

3.1.2 Small-scale tests on clear raw timber

In order to mitigate the uncertainity on the mechanical properties for the subsequent modelling procedure, tests for the identification of elastic and strength properties of the raw timber are currently in progress. Axial-parallel to the grain (E_L, $f_{L,t}$, $f_{L,c}$) and rolling shear (G_{ZN}, f_{ZN}) tests have been carried out. The previous study (Franzoni et al, 2015) identified such mechanical properties as the dominant ones when dealing with bending behaviour of crosslams. Moreover, the mechanical properties of *clear* spruce have been found to be adequate to reproduce CLT bending response. Fig. 7-Table 4 and Fig. 8-Table 5 show the axial and shear tests on clear specimens of timber. The remaining elastic and strength properties for the modelling are taken from Table 1. Classic crosslam floors and spaced ones have been supplied from two different producers; hence all results on the respective lumber boards are presented separately.

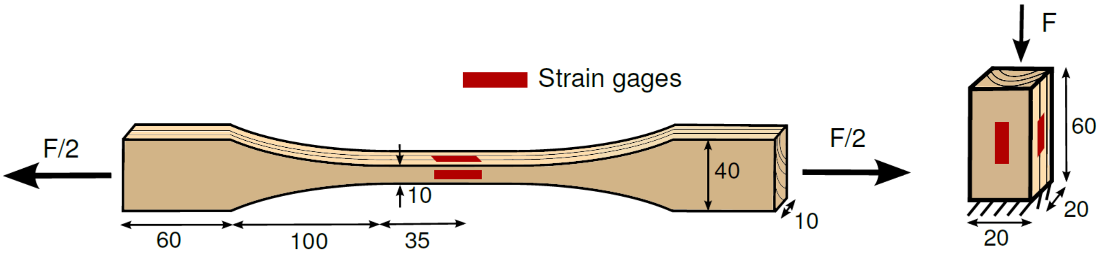

Axial Tests – Parallel to grain (L)	n	$\bar{x}$ (MPa)	COV (%)
Spaced floors-Norway spruce C24 (EN 338)			
E_L (tension + compression)	21	12700	17.2
$f_{L,t}$	10	85	17.3
$f_{L,c}$	8	51	6.4
CLT floors-Norway spruce S10 (DIN 4074)			
E_L (tension + compression)	17	9850	11.8
$f_{L,t}$	7	77	13.7
$f_{L,c}$	8	38	4.1

Figure 7 and Table 4 Geometry and results of the axial tests on clear wood. Dimensions in mm

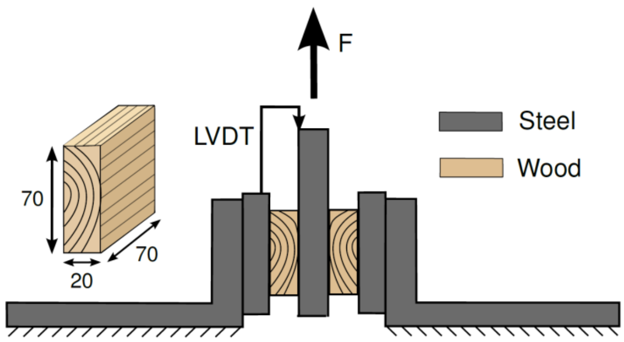

Rolling Shear Tests (ZN)	n	$\bar{x}$ (MPa)	COV (%)
Spaced floors-Norway spruce C24 (EN 338)			
G_{ZN}	10	110	25
f_{ZN}	12	1.6	18
CLT floors-Norway spruce S10 (DIN 4074)			
G_{ZN}	8	70	25
f_{ZN}	8	1.3	9

Figure 8 and Table 5 Geometry and results of the shear tests on clear wood. Dimensions in mm

3.2 Advanced modelling and existing design methods

The bending tests on CLT panels allowed a further validation of the previously described equivalent-layer model. The deflections predicted at the same points of LVDTs lead to the identification of structure's elastic moduli using equations (1), (3) and (4). Two existing design methods for CLT which allow the direct estimation of the bending stiffness are applied: the gamma-method (Eurocode 5, 2004) and the shear analogy method (Kreuzinger, 1999). Both of them are implemented following the instructions found in Gagnon & Pirvu, 2013. Table 6 shows the relative difference between the actual and predicted bending behaviour f CLT panels.

Table 6 Relative distances between the actual and predicted bending behaviour of CLT

Comparison - CLT	Gamma Method	Shear Analogy	Equivalent layer - discontinuous
Failure load	-	-	**+5%**
Failure mode	-	-	**CL**
Global stiffness	**-5%**	**-4%**	**-4%**
Bending stiffness	**-8%**	**-4.5%**	**-4.5%**
Shear / bending deflection	**-8.5%**	**+8%**	**-5.5%**

From Table 6 it is clear how both the suggested advanced model of equivalent-layer and design methods can reproduce well CLT bending response.

A starting point for analysing more heterogeneous CLT floors could be using the methods presented above and reducing wood mechanical properties by the wood volume fractions. This approach has been already used in Blass & Gorelacher, 2000 for the rolling shear modulus and is common in engineering practice.

A more accurate model for periodically spaced CLT panels is currently in development. This model is based on a homogenization scheme handled by a high-order plate theory (Lebée & Sab, 2012). Basically it enforces membrane, bending and shear strains on an elementary unit cell of the spaced crosslam panel (Fig. 9) and equalizes the elastic energy of such an unit cell to the elastic energy of the whole panel. This homogenization approach leads to the identification of panel's bending and shear moduli, which will be used by the plate theory for computing the stresses and displacements.

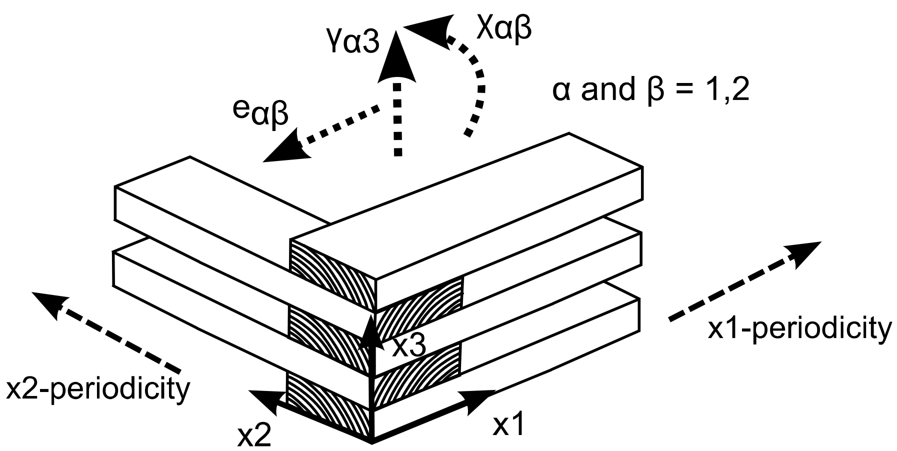

Figure 9 Unit cell of spaced CLT floors and imposed membrane (e), bending (χ) and shear (γ) strains

At present, only the membrane-bending step was conducted and therefore only the effective bending stiffness can be computed. Tables 7 and 8 present the distances between the actual and predicted behaviour of spaced floors. The equivalent-layer model predicts plate's moduli by means of equations (1), (3) and (4) using the predicted deflections, while the shear analogy method and the homogenization scheme compute directly the plate bending and shear stiffnesses. Due to the significant distance from the reference and from the other models, the gamma method is not presented and it is replaced by the periodic homogenization model.

Table 7 Relative distances between the actual and predicted bending behaviour of Panel-1

Comparison – Panel-1: wood volume = 40%	Shear Analogy*	Equivalent layer - discontinuous*	Periodic homogenization
Failure load	-	**+40%**	in progress
Failure mode	-	**RS**	in progress
Global stiffness	**+25%**	**+23%**	in progress
Bending stiffness	**+18%**	**+16%**	**-9.5%**
Shear / bending deflection	**-73%**	**-60%**	in progress

* Mechanical properties reduced by wood volume fraction

Table 8 Relative distances between actual and predicted bending behaviour of Panel-2

Comparison – Panel-2: wood volume = 25%	Shear Analogy*	Equivalent layer - discontinuous*	Periodic homogenization
Failure load	-	**+34%**	in progress
Failure mode	-	**RS**	in progress
Global stiffness	**+32%**	**+28%**	in progress
Bending stiffness	**+31%**	**+28%**	**+2%**
Shear / bending deflection	**-84%**	**-76%**	in progress

* Mechanical properties reduced by wood volume fraction

Table 7 and 8 shows that the wood volume fractions approach fails the more the panel becomes heterogeneous. The equivalent-layer model returns less margin of error than the design method. The advanced model based on periodic homogenization gives a good prediction of the effective bending stiffness of strongly heterogeneous panels.

4 Conclusion and outlooks

Low heterogeneities. The developed equivalent-layer model turned out to be appropriate to reproduce elastic and strength bending response of CLT panels. The edge-gluing of lateral boards does not contribute very much to the bending performance, introducing an additional failure mode. The discontinuous layer model gives a better prediction of CLT load-carrying capacity than the continuous layer. Moreover, mechanical properties of clear wood lead to a good comparison with a reference specimen having knots. This suggests the “system effect” when assembling lumber boards in a CLT configuration, which effect is to regularize the presence of knots and increase boards stiffness and strength. The parameter studies performed with the validated model quantified shear effects in CLT in bending and showed the loss and low gains while enlarging the number of layers or the orientation of transverse layers.

Stronger heterogeneities. Reducing wood mechanical properties by wood volume fractions is not sufficient for a reliable design of spaced timber floors, especially with respect to transverse shear effects. This means that such a simplified approach cannot take into account the complexity of stress and strains distribution within these strongly heterogeneous panels. Therefore a more accurate model based on a homogenization scheme is currently in development. First results show that such an advanced model can precisely predict the bending stiffness of spaced floors. Therefore the following steps of this advanced modelling are the prediction of the panel’s shear modulus, deflection and failure load/mode. The final aim is to develop a simplified calculation tool for the design of heterogeneous CLT floors in order to encourage their safe application in timber construction.

5 References

Blass, H. Gorlacher, R. (2000) Rolling shear in structural bonded timber elements. International conference on wood and wood fiber composites, Stuttgart, Germany.

Dahl, K. (2009) Mechanical properties of clear wood from Norway spruce. PhD thesis, Norwegian University of science and technology

DIN 4074-1:2012-06 Sortierung von Holz nach der Tragfahigkeit, Nadelschnittholz.

EN 338:2010 Structural timber—strength classes

Eurocode 5 (2004): Design of timber structures - Part 1-1: General and rules for buildings, CEN (EN 1995-1-1)

Franzoni, L. Lebée A., Lyon, F. Foret, G. (2015) Cross Laminated Timber panels in bending: an equivalent-layer approach (submitted)

Gagnon, S. Pirvu, C. (2013) CLT handbook: Cross Laminated Timber. FPInnovations, Quebec, Canada

Hochreiner, G. Fussl, J. Eberhardsteiner, J. (2013) Cross Laminated Timber plates subjected to concentrated loading. Experimental identification of failure mechanisms. Strain, 50(1):68-71

Keunecke, D. Hering, S. Niemz, P. (2008) Three-dimensional elastic behaviour of common yew and Norway spruce. Wood Science and Technology, 42: 633-647

Kreuzinger, H. (1999) Platten, Scheiben und Schalen. Ein Berechnungsmodell fur gangige Statikprogramme (German). Bauen mit Holz, 1:34-39

Lebée, A. Sab, K (2012) Homogenization of thick periodic plates: application of the Bending-Gradient plate theory to a folded core sandwich panel. International journal of solids and structures, 49: 2778-2792

Pagano, N.J. (1969) Exact solutions for rectangular bidirectional composites and sandwich plates. Journal of composite materials, 4:20-34

Pagano, N.J. (1970) Influence of shear coupling in cylindrical bending of anisotropic laminates. Journal of composite materials, 4:330-343

Van der Put, TACM (1982) A general failure criterion for wood. In Proceedings of 15th Union of Forest Research Organizations Meeting, Boras, Sweden

Discussion

The paper was presented by L Franzoni

H Blass asked if the effect of board width was considered. L Franzoni said not yet and 3.5 is the ratio between boards. H Blass asked why were tension and compression properties established using small clear tests. L Franzoni answered that they tried to be consistent with modelling approach using clear properties and agreed that the material in reality has defects.

K Malo asked why there were sharp changes shown in the curves in slide 9 where with in-plane shear failure one would expected smooth rather than sharp changes. L Franzoni said that this could be caused by numerical issues

G Fink received clarification that the model was based on small clear properties.

K Malo and L Franzoni further discussed sharp changes were due to change in failure mode because the model could not determine mixed failure mode and therefore sharp changes were seen.

G Schickhofer asked whether the end goal should be aimed towards design code. L Franzoni said that this was not their goal at this moment.

Performance of Canadian glulam columns with new laminae E requirements

Frank Lam, University British Columbia

Jung Kwon Oh, Seoul National University (formerly Post Doc University of B.C.)

B.J. Yeh, APA – The Engineered Wood Association

Jun-Jae Lee, Seoul National University

Keywords: Glulam column, Reliability index, Cubic Rankine Gordon curve

1 Introduction

It is well-known that glulam column performance depends on its length and the strength properties of the laminae (Blass 1987, John 1991). When the column height is short, its design is governed by the compression strength parallel to grain. When the column height is long, its design is governed by Euler buckling (hence modulus of elasticity (MOE)). As intermediate columns, the design is governed by both compression strength parallel to grain and MOE. The traditional approach recognized three different categories of columns: short, intermediate and long, representing a transition from short column plastic failure to elastic buckling failure modes. In Canada, the Code on Engineering Design in Wood CSA O86 adopted a column design equation based on the Cubic Rankine Gordon (CRG) curve which was originally proposed by Neubauer and Tekinel (1966). The CRG formula is continuous over all slenderness ratios, and is more conservative than the traditional column formula in the intermediate slenderness range. In the US, Ylinen's buckling equation is used in column design. The equation is based on an empirically fitted fourth power parabolic function (Newlin and Gahagan, 1930) and a nonlinear function representing the compressive stress-strain relation of wood (Ylinen 1956). Zahn and Rammer (1995) and Rammer and Zahn (1997) provided a detailed database and an evaluation of the Ylinen equation for glulam and parallel strand lumber columns, respectively.

The strength properties of the laminae are influenced by the grading rules of the laminae that control the quality of the wood. For Canadian 16c-E grade glulam, CSA O122 requires that Douglas fir laminae have a minimum MOE of 12,400 MPa and minimum visual C-grade. These rules were established several decades ago based primarily on common practice of the time, industry experience, and product performance record. As the characteristics of the timber resources evolve through time, these rules may no longer be suitable in terms of resource utilization. The competitive position of glulam can be improved if modifications to the grading rules of glulam laminae can be considered to fit closer to the characteristics of the current resource with technical evidence that the final product can still meet the target level of performance of Canadian wood products.

This paper presents the results of an experimental program to address the impact of modifying the laminae MOE requirements on the strength properties of glulam columns. Glulam specimens manufactured with laminae having a MOE range of 11,000 MPa and 13,100 MPa were considered. The performance of the glulam columns was quantified by reliability analysis to study their safety level per Canadian Design code provisions.

2 Materials and Methods

2.1 Test set-up for full-size intermediate-length column

Full size glulam column testing is challenging because it involves high axial forces. Since the behaviour of columns depends on the boundary condition, such high forces can create problems because there could be unintended restrains at the column ends. Neubauer (1972) carried out column tests with pointed end steel supports and reported that these supports appeared to be unsatisfactory for stronger and short column under heavy load. Zahn and Rammer (1995) used roller supports (pinned end) for full-size intermediate-length glulam column tests. They also indicated that rollers in the end supports sometimes locked up under the heavy axial load. This is because rolling friction could be high enough to make the test behave like a test of members with square ends on rigid platens rather than a test of members with simple supports. Therefore, as a solution he applied dithers (vibrators that supply the energy needed to break the static friction) to make “pinned end” boundary condition. If rotation is restrained by friction, the effective length would decrease significantly, which would cause overestimation of the column performance. In practice, it is very difficult to create pure frictionless pinned end supports or to estimate the amount of rotational restraints contributed by friction. In this study, an alternative conservative approach using fixed support conditions was chosen.

A total of 90 glulam specimens were prepared for the full-size glulam test. All glulam specimens were made with four C grade Douglas fir laminae with a minimum and maximum MOE of 11,000 MPa and 13,100 MPa, respectively. The test material was produced by Western Archrib following CSA O122 and shipped to the Timber Engineering and Applied Mechanics (TEAM) Laboratory at the University of British Columbia for testing. The cross section of the glulam test columns was 79 mm by 150 mm. The size of the test columns was chosen based on the capacity of the test actuators in the TEAM laboratory.

Three slenderness ratios (Sr=Le/d) were chosen in the range of intermediate length. For the full-size compressive test, both ends of the specimens were carefully sawn off square. Table 1 shows the final length of the three slenderness ratio groups.

Table 1. Test specimens.

Group	*Slenderness ratio *1 (Sr=Le/d)*	*No. of specimen*	*Cross section*	*Length (mm)*	*Effective length*1 (Le in mm)*	*Visual Grade of lamination*	*Species*
A	*25.1*	*30*	*79mm x 150mm*	*3,657*	*1,986*	*C*	*Douglas-fir*
B	*20.1*	*30*		*3,048*	*1,590*		
C	*15.1*	*30*		*2,439*	*1,194*		

**1 Effective factor = 0.65 (CSA O86); Total reaction support length (602 mm); Le=0.65*(Length-602mm)*

MOE of each specimen was measured by the Metriguard E computer. Hand-tapping initiated vibration of the simple-supported glulam specimen to make it vibrated in the same direction as it would be buckled in full-size column test.

In a companion test program, APA-The Engineered Wood Association carried out short column tests (381 mm in length). The glulam specimens were made with the same C-grade laminae and cross section as the UBC test specimen. The test results show that the compressive strength in current Canadian design code seemed to be slightly conservative. Table 2 shows the statistics of short column compressive strength parallel to grain.

Table 2. Short column test results performed by APA.

	Compressive strength parallel to grain (MPa)
Average	*42.9*
COV (%)	*5.1*
N	*30*
Max	*47.5*
Min	*40.0*
5% tolerance	*38.8*

** NOTE - The laminating lumbers of this glulam were visual C grade satisfying the requirements for 16c-E grade of CSA O122.*

Fig. 1 shows a schematic drawing for the full-scale compression test. The fixed supports were designed and custom built as shown in Figs. 2a and 2b. At one end, the fixed support composed of a steel shoe and a set of steel roller guide to allow axial movement while preventing rotation. At the other end, the support did not have to move axially; hence, it consisted of a steel shoe only to restrain rotation.

Glulam specimens were placed into these supports with the narrow face of the specimen oriented parallel to the ground. At one end, the MTS hydraulic actuator pushed the steel shoe in the fixed support transferring the axial force to the glulam column with rotational restraint about the vertical axis (Fig. 2a). The other end was also placed in a custom-made fixed support (Fig. 2b) with the fixed-support attached to a strong steel column. To prevent unexpected buckling in strong axis, two lateral supports were installed between a fixed support and mid-point. In this test setup, buckling occurred only in weak axis and horizontal direction (Fig. 3). To create a small load eccentricity to initiate lateral deformation, a lateral load of 68 kg (150lb, Group B and C) and 45 kg (100 lb, Group A) was applied at the mid-point (Fig. 4b). This small lateral load was less than 0.022% of peak axial load.

Axial force was applied at the displacement controlled speed of 2.5 mm/min for this testing and all specimens reached to maximum load in 10 min. The test continued until the load dropped below 50% of the maximum load. Axial load and test machine stroke were recorded. Lateral displacements resulting from column buckling were measured at mid-span by linear voltage displacement transducers (LVDT).

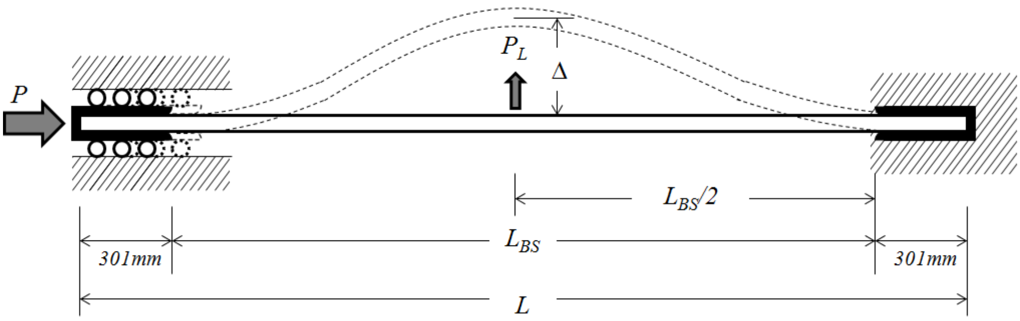

Figure 1. Schematic drawing for full size column test set-up (Top view)

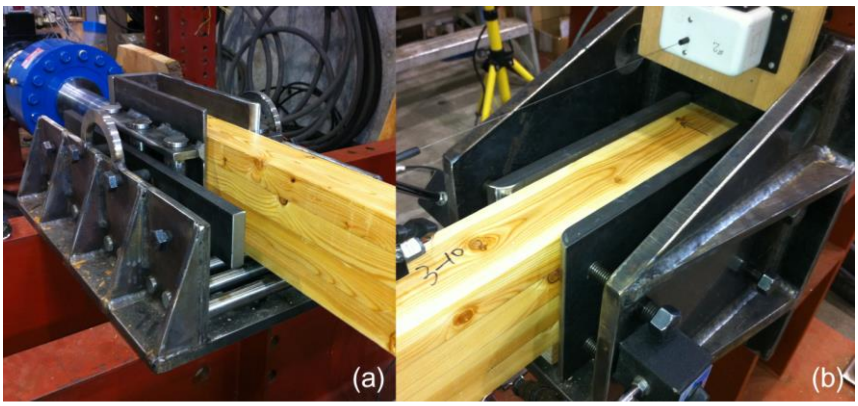

Figure 2. Picture of custom-made fixed support. (a: Support at the hydraulic actuator side. b: Support at the other side.)

Figure 3. Picture of full-size column test set-up. (a) Vertical movement were restrained by two supports to prevent buckling in strong axis. (b) Pulley system applied small lateral load.

2.2 Test observations and results

In this study, transverse vibration technique was applied to measure the vibration MOE for each glulam pieces. Table 3 shows the statistics of the MOE measurements. Normal distribution was used to estimate the 5th percentile MOE. The 5 % parametric tolerance limit with a 75% confidence level (E_{05}) was 11,561 MPa.

The glulam specimens of this study were manufactured with laminae having a minimum MOE of 11,000 MPa and a maximum MOE of 13,100 MPa. For 16c-E grade glulam, CSA O122 requires that laminating lumber to have a minimum MOE of 12,400 MPa and minimum visual C-grade. For the 16c-E grade glulam, the CSA O86 specifies 12,400 MPa as average MOE value and 10,788 MPa as 5th percentile value.

Although the glulam in this study was made with lower MOE rated laminations than the CSA requirements, the average and 5th percentile MOE of the glulam were higher than the values specified by CSA O86 (Table 4). This comparison means that the specified MOE value for glulam columns in CSA O86 may be conservative.

Table 3. Statistics of vibration MOE for each group

Group	*Length (mm)*	*MOE (MPa)*		
		Average	*St. dev.*	*COV (%)*
A	*3,657*	*12,299*	*748.8*	*6.1*
B	*3,048*	*13,126*	*579.8*	*4.4*
C	*2,439*	*13,259*	*543.7*	*4.1*
Total		*12,895*	*755.7*	*5.9*

Three different glulam column lengths were considered in full scale column tests. For the three groups, non-parametric 5th percentile tolerance of maximum axial load was calculated. Table 5 shows the statistics of maximum axial load for each group.

Table 4. Comparison between test specimen and 16c-E grade glulam. (Unit : MPa)

	Test	CSA
Lamination		
- Min. Visual grade	C-grade	C-grade
- Min. MOE	11,000	12,400
Glulam		
- Compression parallel, fc	38.8	30.2 (Specified Strength)
- Average MOE, E	12,895	12,400
- 5th percentile MOE, E_{05}	11,561	10,788

Table 5. Statistics of maximum axial load for each group.

	Group A	Group B	Group C
Average (N)	230,992	314,211	414,823
St. dev. (N)	10,150	20,650	27,463
COV (%)	4.4	6.6	6.6
5th Percentile tolerance (N)	208,274	275,563	373,465

2.2.1 Determination of actual effective length factor

The custom-made support was intended to restrain rotation to create a sufficiently strong and stiff steel assembly for this support. However, it is practically difficult to make a pure fixed support because the steel can deform elastically and there can be some free play in the system (albeit very small). Therefore, for the purpose of the analysis the custom-made support was assumed to be represented by a very stiff elastic rotational spring. The spring constant was calibrated by measurements in the test. To calibrate the spring constant, the graph of PΔ versus angle (Θ, $2\Delta/L_{BS}$ in Fig. 1) was drawn. The slope in this graph is governed by spring constant as shown in Fig. 4.

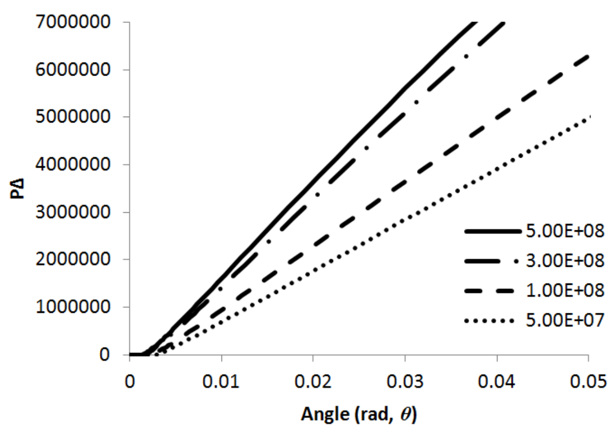

Figure 4. Estimated slope change for different spring constants predicted by SATA.

All specimens of Group A did not show any compressive failure until peak load. But in Groups B and C, compressive wrinkles were found before peak load. Therefore, only Group A specimens were used to calibrate the spring constant. The spring constant of other groups was assumed to be the same as the constant of Group A, because the same support was used for all test groups.

The spring constant was calibrated by least square method where the spring constant yielding the minimized sum of square error (Eq. 1) was determined as the spring constant of the support.

$$S = \sum_{i=1}^{n} \left[K_i - K_i^*(k) \right]^2 \tag{1}$$

where K_i is the actual slope from the test and $K_i^*(k)$ is the predicted slope from the FEM program SATA (Song 2009), of the ith specimen with a specific spring constant, k.

Here K_i=∂(PΔ)/∂Θ and K_i *=∂(PΔ)*/∂Θ*. The spring constant to minimize the sum of square error was determined by Eq. 2.

$$\frac{\partial S}{\partial k} = 0 \tag{2}$$

In SATA, a polynomial model was assumed to represent the non-linear parallel-to-wood-grain stress-strain relationship (Eq. 3).

$$\sigma = \begin{cases} E_0 \varepsilon & f_t / E_0 > \varepsilon > 0 \\ (r-2) f_c (\frac{\varepsilon}{\varepsilon_p})^3 + (3-2r) f_c (\frac{\varepsilon}{\varepsilon_p})^2 + E_0 \varepsilon & 0 \geq \varepsilon \geq \varepsilon_p \\ E_d(\varepsilon - \varepsilon_p) + f_c & \varepsilon_u \leq \varepsilon < \varepsilon_p \end{cases} \tag{3}$$

where σ and ε are the stress and strain, respectively; f_t and f_c are the tensile and compressive strengths, respectively; E_0 and E_d are the initial modulus of elasticity and the slope of the falling branch of the stress strain curve, respectively; ε_p is the strain corresponding to the compression strength, f_c; $r= \varepsilon_p E_0 / f_c$ defines the nonlinearity of the model.; and ε_u and f_t/E_0 are the maximum compressive and tensile strains, respectively. The model is shown schematically in Fig. 5.

In the spring constant calibration, nonlinearity was assumed to be represented by the equation ε_p = 1.250 f_c/E (Blass, 1987). Because the other properties were not sensitive in this spring constant calibration, specified design values in CSA O86 for 16c-E glulam were used for the other properties.

Before calibrating the spring constant, the effect of initial lateral deflection on this slope was investigated. In this analysis, initial deflected shape was assumed to be sinusoidal with maximum values at the mid-span. From the comparison of slope with changing initial deflection up to 3.0 mm (l/1000), it was found that maximum difference from the case of l/2000 (1.5 mm) was only 2.6% and it was small enough to disregard. The measured initial deflection was less than 3 mm.

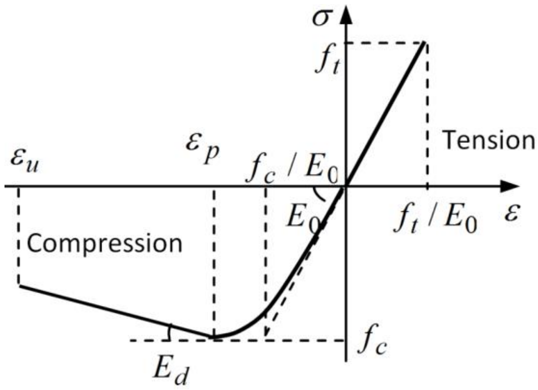

Figure 5. Polynomial model of the parallel-to-wood-grain stress-strain relationship (Song, 2009).

From the linear elastic range of the test data, the slope (K_i) in the graph of PΔ versus angle was calculated. In SATA, the assumed sinusoidal initial lateral deflection was assumed to be l/2000 at mid-point. Also for all specimens, average compressive strength from APA and as-measure MOE for each specimen were used as input f_c and E_0 to SATA. Based on these inputs the slope (K_i *) was obtained from SATA analysis with spring constant varying from 1.0×10^8 Nmm/rad to 5.0×10^8 Nmm/rad. The best-fit spring constant was calibrated as 2.3×10^8 Nmm/rad.

Effective length factor can be determined from the best-fit spring constant at the end. Effective length can be expressed by

$$L_e = \beta L \tag{4}$$

where β is the effective length (or buckling length) factor and $L=L_{BS}$ is length of the member.

Exact elastic effective length factors were determined by the zero determinant condition of the stiffness matrix of the restrained compression member, as expressed by the well-known transcendental equations (Eq. 6, Hellesland, 2007).

$$\frac{\left(\frac{\pi}{\beta}\right)^2}{H^2} + \left(\frac{2}{H}\right)\left(1 - \frac{\frac{\pi}{\beta}}{\tan\left(\frac{\pi}{\beta}\right)}\right) + \frac{\tan\left(\frac{\pi}{2\beta}\right)}{\frac{\pi}{2\beta}} = 1 \tag{5}$$

$$H = \frac{kL}{EI} \tag{6}$$

where, k is spring constant, E is modulus of elasticity and I is moment of inertia. By this equation, the effective length factor was calculated for the spring constant of 2.3×10^8 Nmm/rad where the length of specimen is different according to the length group. Therefore, actual effective length factor was calculated for each length group. The actual effective length factor for each length group was 0.60 (Group A), 0.62 (Group B) and 0.65 (Group C). This value is between the theoretical effective length factor (0.5) and the factor for fixed support specified by CSA O86 (0.65). For subsequent analysis 0.65 was used.

3 Reliability Analysis

The CSA O86 code provides the CRG formula (Eq. 8) as the slenderness factor the for column design.

$$K_c = \left[1.0 + \frac{F_c {C_c}^3}{N E_{05}}\right]^{-1} \tag{7}$$

where, K_c is slenderness factor and C_c is slenderness ratio as the effective length divided by the member's smaller cross sectional dimension. F_c and E_{05} are the short-column compressive strength and fifth percentile MOE, respectively (see Table 4). N is a calibration factor taken as 35 based on compression behaviour of dimension lumber.

The factored column resistance P_r can be estimated as:

$$P_r = \phi F_c \, A K_c \tag{8}$$

where A is the cross section area (mm)and ϕ is the performance factor. It is noted that other adjustment factors for volume, treatment, and serviceability effects are taken as unity. This is appropriate considering the size of the columns tested and the test condition.

Furthermore to allow direct comparison with test results, the specified compressive strength F_c needs to be increased by a factor of 1.25 to convert load duration adjusted specified strength from the standard load term of 3 months to short term test duration as F_C' = 30.2*1.25 MPa =37.75 MPa.

Reliability analyses were conducted to evaluate the performance of the glulam members under dead and snow load conditions for six Canadian cities (Arvida, Halifax, Ottawa, Saskatoon, Quebec City and Vancouver) following the procedures outlined by Foschi et al. (1989).

The limit state design equation for glulam column short term compressive resistance parallel to grain can be expressed as

$$\alpha_D G_D D_N + \alpha_L G_L L_N = \phi F_c' A K_c \tag{9}$$

where α_D and α_L are the load factors for dead (1.25) and live (1.5) loads, respectively; G_D and G_L are the dead and live load geometric factors which convert the applied loads to compression capacity; D_N and L_N are the nominal design dead load and nominal design total roof snow and rain load, respectively.

The failure function developed to relate the compression resistance and the effect of loads for reliability analyses is as follows:

$$G = P - (G_D D + G_L L) \tag{10}$$

where P, D, and L are random variables representing the compression capacity, dead load, and live snow load, respectively. G=0 => limit state; G>0 => safe and G<0 => failure. Statistical distributions and parameters for the snow load for the six Canadian cities were described in detail in past studies (Foschi et al. 1989).

The failure function can be rewritten as:

$$G = P - \frac{\phi F_c' A}{\alpha_D \varepsilon \gamma + \alpha_L} \left(1.0 + \frac{F_c' C_c^{\,3}}{N E_{05}} \right)^{-1} (\varepsilon \delta \gamma + \iota) \tag{11}$$

where $\gamma = D_N/L_N$; $\delta = D/D_N$; $\iota = L/L_N$; and $\varepsilon = G_D/G_L$. The variables ε and γ were taken as 1.0 and 0.25, respectively. The random variable δ was assumed to be normal with mean of 1.0 and standard deviation of 0.1.

The compressive resistance P was considered using two approaches: 1) log- normal distributions fitted to the test data and 2) calibrated CRG curve considering compression strength σ_c of short glulam column and modulus of elasticity E^* as correlated random variables.

The lognormal distribution parameters fitted to the three sets of intermediate column compressive capacity data are given in Table 6 and the comparison between fitted distribution and test data is shown in Figure 6.

Table 6. Lognormal distribution parameters of column capacity for each group.

	Group A	Group B	Group C
Average (kN)	231.001	314.240	414.848
St. dev. (kN)	10.182	20.912	27.258
COV (%)	4.41	6.65	6.57

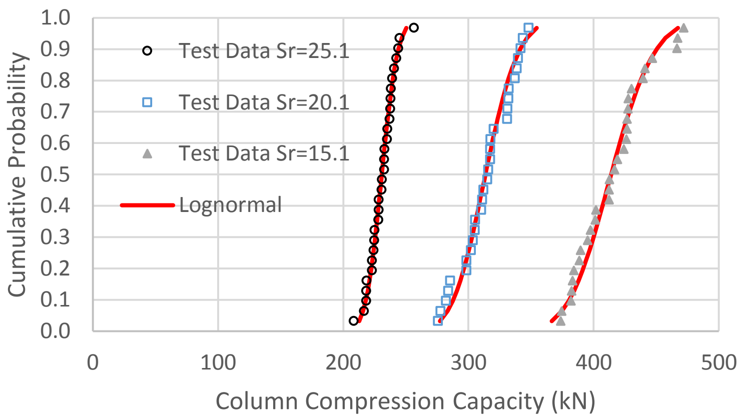

Figure 6. Comparison between lognormal fitted distribution and test data.

Alternatively the input strength properties parameters of the CRG Curve were considered as random. The modulus of elasticity E^* was assumed to be normally distributed with mean of 12895 MPa and coefficient of variation of 5.8% (based on modulus of elasticity test data). The short column compressive strength σ_c was assumed lognormally distributed and calibrated to have a mean of 46.5 MPa and a coefficient of variation of 7.8%. The calibrated σ_c is higher than the measured results from APA. However the "short" column strength in the CRG curve is referenced to columns with very short length whereas the APA short column specimens had lengths of 0.381 m; hence, the higher calibrated σ_c is justifiable.

The short column compressive strength and the modulus of elasticity were also assumed correlated with a coefficient of correlation of 0.525. This relatively weak correlation can be justified because of the narrow range of modulus of elasticity values. Finally the parameter N was also calibrated to be 38.

$$P = \sigma_c A \left[1.0 + \frac{\sigma_c C_c^{\ 3}}{38 E^*} \right]^{-1} \tag{12}$$

Comparisons between simulation results from the fitted random Cubic Rankine Gordon Curve and test data are shown in Figure 7. It can be seen that the fit was quite reasonable. The errors of the mean values were -4.3%, -0.6 % and 0.6% for the three slenderness ratios of 25.1, 20.1 and 15.1, respectively. The errors of the fifth percentile values were -6.0%, 1.5 % and -0.9% for the three slenderness ratios of 25.1, 20.1 and 15.1, respectively. Negative values imply conservatism. It may be possible to achieve better fit but in this process we tried to keep the positive errors as small as possible without excessive conservatism on the negative errors.

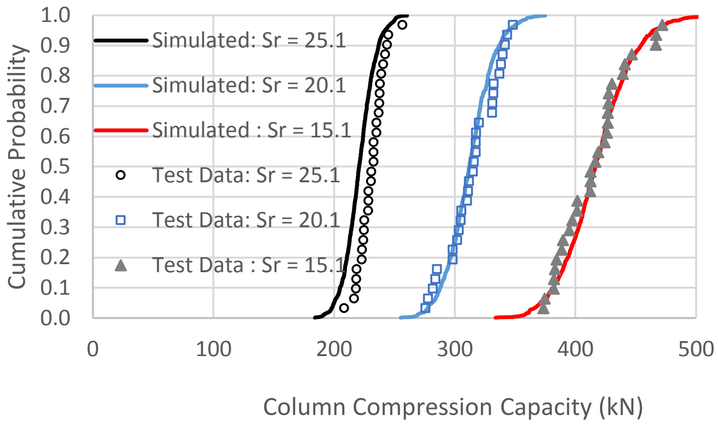

Figure 7. Comparison between Cubic Rankine Gordon Curves with random parameters and test data.

First-order second-moment reliability analyses were performed considering both approaches to represent *P* for dead load and live load of snow plus rain for the six Canadian cities. A 30 year return period of the live load is considered with a probability of non-exceedance of 29/30. Results of the reliability analyses are shown in Figs 8 and 9.

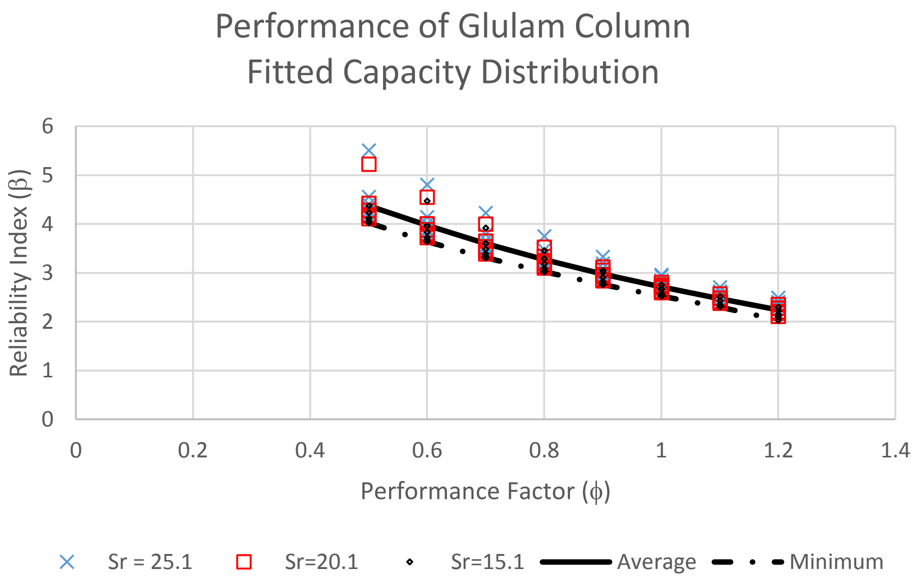

Figure 8. Reliability index versus performance factor relationship of column resistance (based on fitted column resistance distribution).

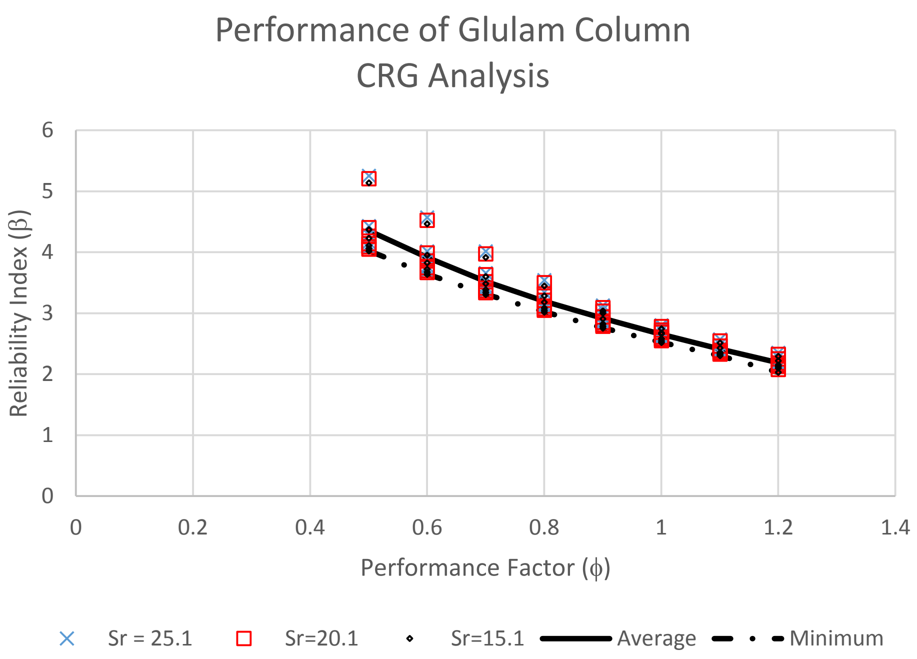

Figure 9. Reliability index versus performance factor relationship of column resistance (based on fitted random Cubic Rankine Gordon Curve).

In the Canadian Code CSA O86 a performance factor ϕ of 0.8 was used in the design provision of compressive resistance parallel to grain for glulam columns. At ϕ=0.8, the associated mean reliability index is 3.267 and 3.195 for the fitted capacity distribution and the fitted random CRG Curve approach, respectively. Similarly at ϕ=0.8, the associated minimum reliability index is 3.019 and 3.020 for the fitted capacity distribution and the fitted random CRG Curve approach, respectively. Considering the target mean reliability index adopted in the Canadian Code CSA O86 is between 2.6 and 2.7 for a ϕ=0.8, the new laminae of glulam columns evaluated in this study exceeded the target safety level. A higher ϕ value in the range of 0.9 for the new glulam column can be justified.

4 Conclusions

This paper presented the results of an experimental program to address the impact of modifying the laminae MOE requirements on the strength properties of glulam columns. Glulam specimens manufactured with laminae having a MOE range of 11,000 MPa and 13,100 MPa were considered. The measured MOE of the glulam specimens was slightly higher than the code specified value even though the tested glulam was made with laminate having lower MOE than the requirements of CSA O122.

A framework for reliability analysis of Canadian glulam columns has been formulated. The procedures take into consideration the randomness of the effects of applied loads and the column resistance. Two approaches were used to model the randomness of the column capacity. The calibrated CRG approach with random representation of σ_c and E^* is more flexible than the direct fitting of the column capacity distribution because it can be applied to various slenderness ratios. Evaluations of the performance of glulam made with new laminae grading rules show that these columns exceeded the target reliability for structural wood products in Canada.

5 References

Canadian Standards Association (2014). Engineering design in wood. CAN/CSA-086-14, Canadian Standards Association, Rexdale, Ontario, Canada.

Canadian Standards Association (2011). Structural glued-laminated timber. CAN/CSA-O122-06, Canadian Standards Association, Rexdale, Ontario, Canada.

Blass, H.J. (1987). Design of Timber Columns. CIB W18A – Timber Structures Meeting 20, Dublin, Ireland.

Foschi, R.O., Folz, B.R., and Yao, F.Z. (1989). Reliability-based Design of Wood Structures. Structural Research Series, Report No. 34, Dept. of Civil Engrg., University of British Columbia, Vancouver, Canada.

Hellesland, J. (2007). Mechanics and effective lengths of columns with positive and negative end restraints. Engrg. Structures 29: 3464-3474.

Johns, K.C. (1991). A continuous design formula for timber column. Canadian J.of Civil Engrg. 18:617-623.

Neubauer L.W. and Tekinel O. (1966). A more efficient column formula for the design of wooden posts and studs. Transactions of the ASAE 9(6):816-817.

Neubauer L.W. (1972). Full-size stud tests confirm superior strength of square-end wood columns. Transactions of the ASAE 15(2):346-349.

Newlin J.A. and Gahagan J.M. (1930). Test o large timber columns and prsenation of the forest products laboratory column formula. Tech. Bull. No.167. USDA FPL. Washington, D.C.

Rammer D.R. and Zahn J.J. (1997) Determination of Ylinen's parameter for parallel strand lumber. J. of Struct. Engrg. 123(10):1409-1411.

Song, X. (2009). Stability and reliability analysis of metal plate connected wood truss assemblies. Ph.D. thesis, University of British Columbia, Vancouver, Canada.

Ylinen A. (1956). A method of determining the buckling stress and the required cross-sectional area for centrally loaded straight columns in elastic and inelastic range. Int. Assoc. for Bridge and Struct. Engrg. Zurich Switzerland. 16:529-550.

Zahn J.J., and Rammer D.R. (1995). Design of glued laminated timber columns. J. of Struct. Engrg. 121(12):1789-1974.

Discussion

The paper was presented by F Lam

T Bogensperger received clarification of the definition of column length being the total length of the column minus the length of the supporting shoes.

H Blass asked about the orientation of the column in relation to the buckling direction. Since the columns buckled in the direction parallel to the glue-line of the laminae, would the bending strength of the column be different if the columns buckled in the other direction. F Lam responded the "bending" strength is governed by the compression strength of the laminae when maximum load was reached. The final failure of tension occurred at a lower load level; therefore, orientation should not matter.

I Smith asked whether pin-pin conditions were tried. F Lam said that it was considered but not adopted given that the literature reported friction issues from pin-ended cases. H Blass commented that in reality pin-ended conditions do not exist so the code would be conservative if one assumed pin-ended case. F Lam agreed especially at high load levels.

A Salenikovich received clarification that the laminae were sampled from a mixed pool with MOE ranged of 11 to 13.1 GPa.

Design of CLT beams with large finger joints at different angles

M. Flaig, Blaß & Eberhart GmbH, Germany

Keywords: long span CLT beams, double pitched CLT beams, CLT frame corners, large finger joints, bending strength under an angle to the grain

1 Introduction

Despite the good mechanical properties and the increasing availability of the material, CLT beams are used for a limited number of applications only. Two of the main reasons for the rare use are the limitation of the overall length of CLT members to about 18 m and the lack of production methods for CLT beams with special shape.

Large finger joints (LFJ) offer the possibility to connect prismatic or tapered CLT members to form, e.g. double pitched CLT beams or CLT frame corners (Figure 1). Compared to glulam members with similar shapes, finger jointed CLT beams with kinked axis provide appreciable advantages, since stresses perpendicular to the beam axis can be absorbed by the transverse layers included in the material. In the present paper the results of tests with different types of finger jointed CLT beams loaded in plane direction and a proposal for the design of LFJ in CLT members are presented.

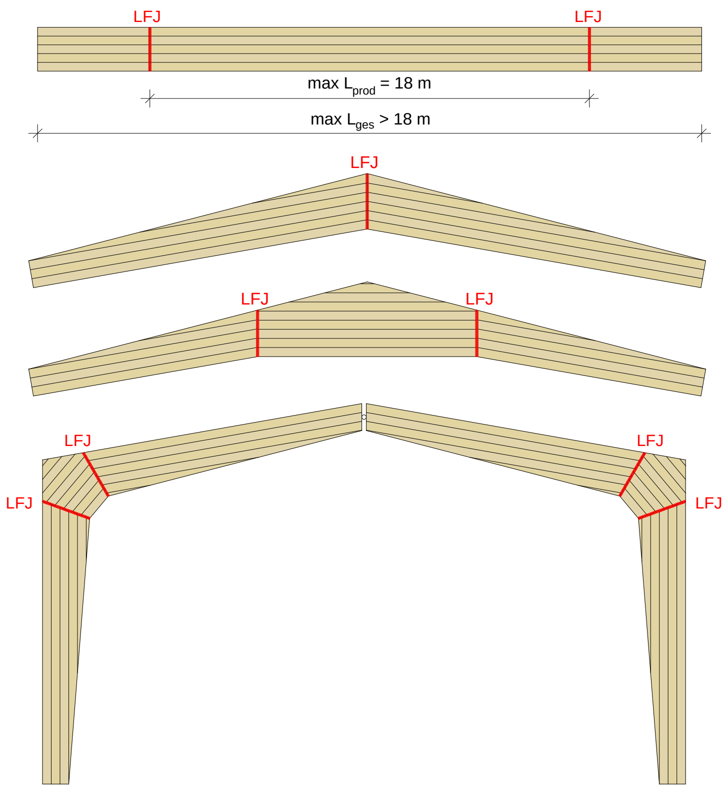

Figure 1. Possible dimensions and shapes of CLT members with large finger joints (LFJ)

2 Large finger joints in CLT

2.1 Finger joint profile

In finger jointed CLT elements, the position of fingers in individual layers and hence, also the number of finger tips within a layer depends on the ratio between the pitch p of the finger joint profile and the layer thicknesses. To ensure an equal reduction of the cross section in all layers of finger jointed CLT elements, the finger joint profile shown in Figure 2 was developed. The geometry of the new profile is based on the profile 50 – 12 – 2 which is specified as a suitable profile for LFJ in EN 387. It features a finger length ℓ_j of 40 mm, a pitch p of 10 mm and a tip width b_t of 1.4 mm. In combination with layer thicknesses that are integer multiples of 5 mm, the pitch p of 10 mm entails a constant nominal reduction v_{nom} of 0.14 for all layers within a CLT element.

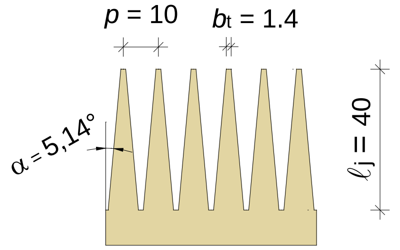

ℓ_j finger length

p pitch

b_t tip width

α finger slope

Figure 2. Finger joint profile 40 – 10 – 1.4

2.2 Effective reduction of the cross section

Besides the chosen profile, the design of edge fingers and the production process have significant influence on the residual cross section of a finger-jointed connection. To avoid fraying at the flat ends of the outermost fingers, LFJ are often produced with a shoulder perpendicular to the beam surface. In the tested CLT beams, the tip of the outermost fingers was enlarged by e = 2.5 mm resulting in shoulders with a width of 3.2 mm (Figure 3, left). The tip gap s (see Figure 3, right) also influences the residual cross section of a finger jointed connection. The size of tip gap mainly depends on the type of adhesive, the applied pressure and the pressing time.

Figure 3. left: broadened finger tip of edge finger
right: production tolerance in thickness direction Δt and tip gap s

A further reduction of the cross section can be caused by production tolerances Δ in thickness direction resulting from a deviation of the finger joint profile from the planned position. In CLT beams the thickness of every block of longitudinal layers, arranged at the surface or between two cross layers, is reduced by the production tolerance Δ in thickness direction. Consequently, the total reduction of the load carrying cross section amounts to (n_{cross} + 1) times the tolerance Δ. Taking into account the above-mentioned factors - the nominal reduction ν_{nom} of the finger joint profile, the enlarged tip of edge fingers, the tip gap s and the production tolerance Δ in thickness direction – the effective reduction of the cross section in finger-jointed connections in CLT members can be calculated according Eq. (1).

$$\nu_{eff,CLT} = (1-\nu_{eff}) \cdot \frac{(n_{cross}+1)\cdot\Delta + e}{t_{net,long}} + \nu_{eff} \qquad (1)$$

with $\nu_{eff} = \dfrac{b_t + 2\cdot s\cdot \tan\alpha}{p}$

n_{cross} number of cross layers within the element thickness

$t_{net,long}$ sum of thicknesses of longitudinal layers

3 Experimental work

3.1 General

CLT beams with LFJ were tested to determine the bending capacity of the finger-jointed connections under varying angles. The test series comprised tests with straight CLT beams, double pitched CLT beams and CLT corner frames. In addition, tests with straight CLT beams without LFJ were performed to determine the in-plane bending strength of CLT as a reference value.

Throughout all series, the tested CLT beams had a total thickness t_{gross} of 200 mm and a height h of 600 mm. The layup of the beams was symmetric to the centre plane and consisted of four longitudinal layers with a thickness of 40 mm and two transversal layers with a thickness 20 mm (Figure 4). The individual layers consisted of softwood lamellae with a width of 150 mm made of strength graded boards of strength class C24 / T14 according to EN 338 / EN 14080. Wood species of longitudinal layers was exclusively northern spruce (Picea abies). The transversal layers, too, mainly consisted of northern spruce, but also contained some lamellae made of pine wood.

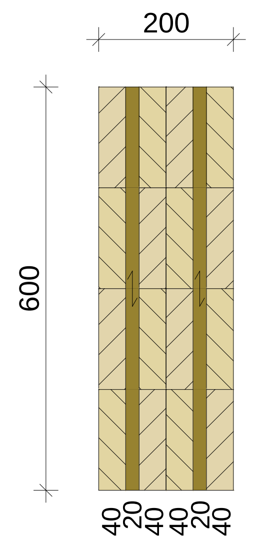

Figure 4. Cross section of tested CLT beams

Before the tests, the production tolerance Δ in thickness direction of each finger jointed connection was measured at four different points near the corners of the cross section. The tip gap *s* was also measured, but only in two points per connection in the middle of the beam height. After the tests, the density and the moisture content were determined from 20 to 30 mm thick samples taken over the complete cross section. An overview of the test series and the dimensions and the properties of the specimens are given in Table 1.

Table 1. CLT beams with and without LFJ; Test series and selected properties

beam type	LFJ	series	number	span	joint angle	density	moisture content	thickness tolerance	tip gap
			n	ℓ	α	ρ_{mean}	u_{mean}	Δ_{mean}	s_{mean}
				in mm	in °	in kg/m³	in %	in mm	in mm
straight	none	S-REF	15	10,800	-	442	10.5	-	-
	1	S-LFJ	15	9,000	0	436	10.7	2.2	4.9
double pitched	1	PI-05	5	9,000	5	451	11.0	0.9	5.0
	1	PI-15	5	9,000	15	447	10.7	1.5	6.0
	1	PI-25	5	9,000	25	448	11.1	1.4	5.5
frame corner	2	CO-90	5	4,500	22.5	458	11.8	3.0	6.0
	2	CO-105	5	4,500	18.75	463	11.6	3.2	5.4
	2	CO-115	5	4,500	16.25	469	11.2	2.9	5.3

3.2 Testing

In the first two test series, 30 four-point bending tests were performed to determine the in-plane bending strength and the MOE of straight CLT beams with and without LFJ. The beams without LFJ had a span ℓ of 18 times the beam height. For the beams with finger joints, the span was reduced to 15 times the beam height. During the tests, the local deflection between the load application points was measured within a length of (ℓ/3 – *h*) to determine the MOE of the beams. In Figure 5 and Figure 6 the test setup and the dimensions of the straight CLT beams are illustrated.

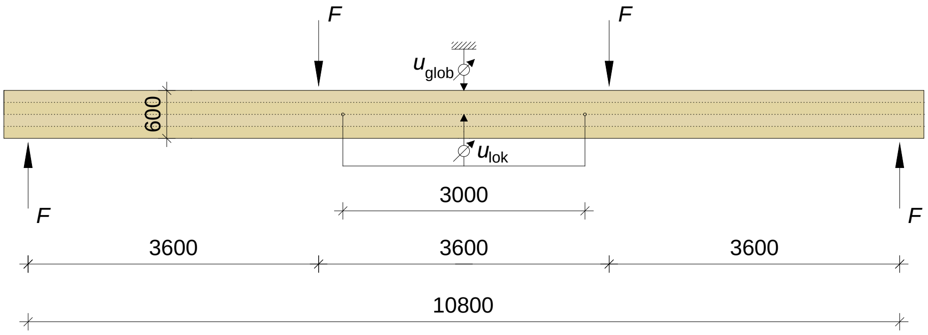

Figure 5. Test setup for straight CLT beams without LFJ (series S-REF)

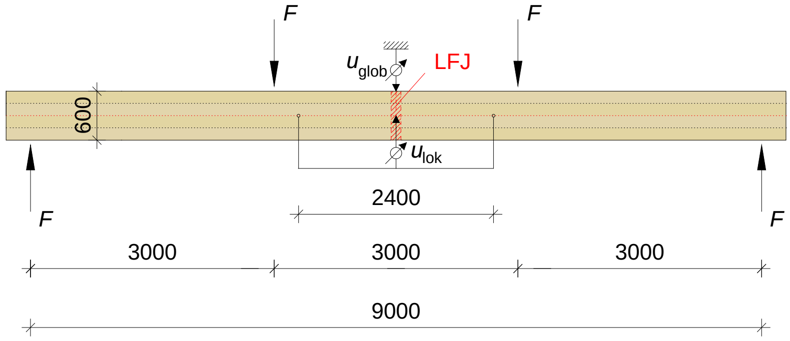

Figure 6. Test setup for straight CLT beams with LFJ (series S-LFJ)

Tests with double pitched CLT beams were performed to determine the in-plane bending strength of LFJ in kinked CLT-beams subjected to opening moments. The tested beams had three different slopes of 5°, 15° and 25°. The specimens were symmetric about the plane of the finger joints, resulting in cutting angles α of the finger joints that were equal to the slope of the beams. Like the straight beams, the double pitched beams were tested in four-point bending tests. The vertical component of the local deflection between the load application points was measured within a length of 2.4 m. The dimensions of the tested double-pitched CLT beams and the test setup are shown in Figure 7.

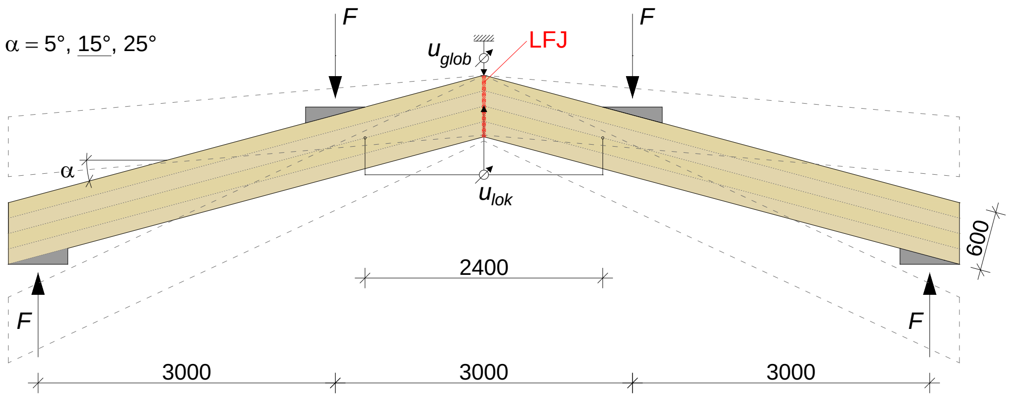

Figure 7. Test setup for double pitched CLT beams (series PI-05, PI-15 and PI-25)

In three test series CLT frame corners with opening angles β of 90°, 105° and 115° were tested. Each corner frame contained two finger-jointed connections with cutting angles α of 22.5°, 18.75° and 16.25°. To induce a closing moment in the finger-jointed connections in the corner a compressive force was applied to the ends of the legs of the specimens. During the tests the overall deformation in the line of action of the compressive forces and the local deformation at the finger-jointed connections were measured. The dimensions of the corner frames and the test setup are illustrated in Figure 8. The arrangement of displacement transducers in the corners is shown in Figure 9.

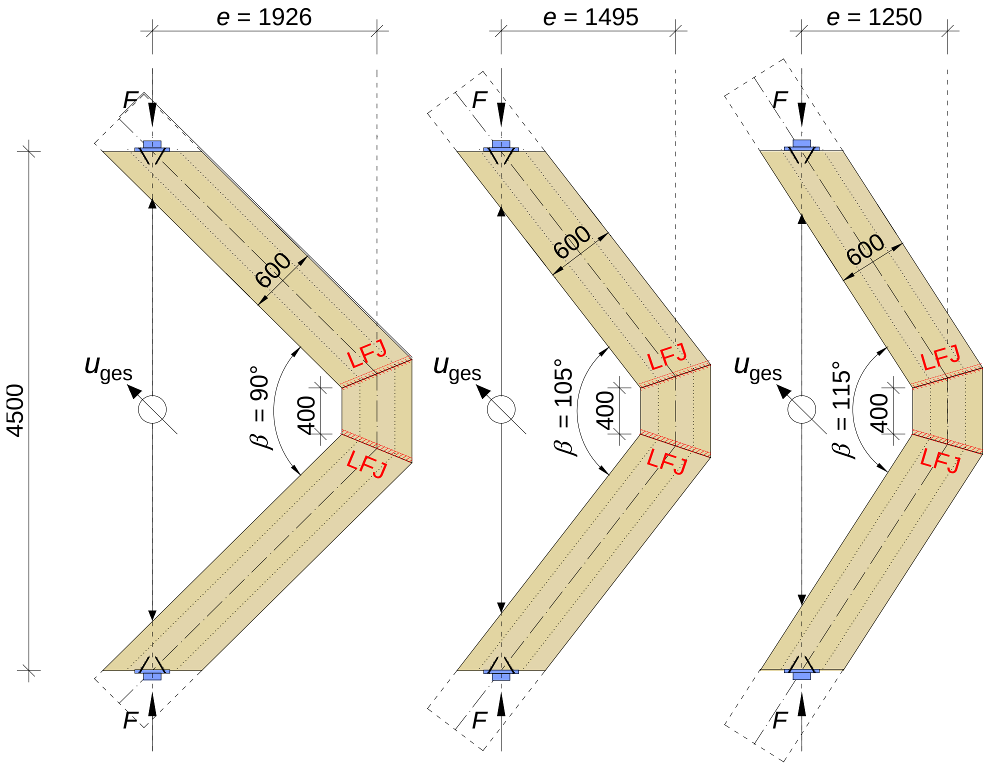

Figure 8. Test setup and dimensions of CLT frame corners (series CO-90, CO-105 and CO-115)

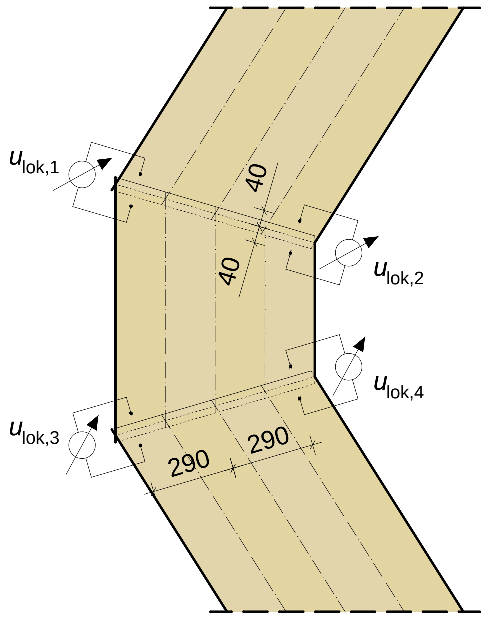

Figure 9. Measurement of local deformation in LFJ of tested frame corners

3.3 Results

3.3.1 Load carrying capacity of LFJ in CLT

In all test specimens with LFJ failure occurred due to bending stresses in the tension zone of the finger jointed connection. In the test series with straight beams and double pitched beams the failure was brittle and occurred abruptly without prior indication. In the test series with frame corners compressive wrinkles were observed in nearly all specimens before the ultimate load was reached. Figure 10 through Figure 12 show examples of the observed failures.

Figure 10. Typical failure in straight CLT beams with LFJ (left) and in CLT beams without LFJ (right)

Figure 11. Typical failure in double pitched CLT beams

Figure 12. Typical failure in CLT frame corners

From the ultimate loads of the individual tests the normal stresses parallel to the grain in the extreme fibre of longitudinal layers were calculated for all tests series. For straight beams and double pitched beams the stresses were calculated as $M/W_{\text{net,long}}$, for the corner frames the normal stresses at the inward corner resulting from combined bending and compression were calculated as ($M/W_{\text{net,long}} + N/A_{\text{net,long}}$). The section modulus $W_{\text{net,long}}$ and the area $A_{\text{net,long}}$ used for the calculation of stresses are the section properties of longitudinal layers in a cross sections perpendicular to the beam axis. For all test series the obtained values are summarized in Table 2. In addition to the stresses the effective reduction of the cross section v_{eff} was calculated for every failed LFJ according Eq. (1) using the measured values of the tip gap s and the production tolerance Δ in thickness direction. In the last row of Table 2 the values of (1-v_{eff}) are given, that represent the proportion of the remaining cross section in the tested finger-jointed connections.

For the tested straight CLT beams the ratio 20.3/29.2 = 0.698 between the mean values of the bending strength determined for beams with and without LFJ is almost equal to the value of (1-$\nu_{eff,mean}$) = 0.726 that was determined for LFJ in straight CLT beams in test series S-LFJ. Consequently, the bending strength of LFJ can be calculated by multiplication of the in-plane bending strength of the CLT member with the factor (1-ν_{eff}).

Table 2. Bending strength of LFJ related to the net cross section of longitudinal layers

series	n	α	$f^{LFJ}_{m,mean}$	$f^{LFJ\ 1)}_{m,k}$	1-$v_{eff,mean}$
	-	in °	in N/mm²	in N/mm²	-
S-REF	15	0	29.2	23.0	
S-LFJ	15	0	20.3	17.1	0.726
PI-05	5	5	17.7	14.3	0.747
PI-15	5	15	11.8	9.8	0.719
PI-25	5	25	10.3	9.0	0.730
CO-90	5	16.25	-24.8	-21.9	0.694
CO-105	5	18.75	-24.1	-19.1	0.697
CO-115	5	22.50	-23.7	-22.2	0.693

1) determined according EN 14358

The test results for the double pitched CLT beams show that for LFJ subjected to opening moments the bending strength strongly decreases with increasing angle α. For LFJ subjected to closing moments, in contrast, the bending strength is significantly larger than the bending strength of LFJ in straight beams and more or less independent of the angle α. To find an analytical solution for the calculation of the bending strength of LFJ in dependence of the cutting angle α the approaches of Norris Eq. (2) and Hankinson Eq. (3) for the calculation of the strength reduction factor k_α were used. In both equations factors ***a*** and ***b*** were introduced to be able to adapt the analytical solutions to test results.

$$k_{\alpha}^{LFJ} = \frac{1}{\sqrt{\left(\frac{(1-v_{eff})\cdot f_{m,k}^{CLT}}{\boldsymbol{a}\cdot f_{t,90,k}^{CLT}}\cdot\sin^2\alpha\right)^2 + \left(\frac{(1-v_{eff})\cdot f_{m,k}^{CLT}}{\boldsymbol{b}\cdot f_{v,k}^{BSP}}\cdot\sin\alpha\cdot\cos\alpha\right)^2 + \cos^4\alpha}} \tag{2}$$

$$k_{\alpha}^{\mathrm{LFJ}}=\frac{1}{\left(\frac{(1-v_{\mathrm{eff}})\cdot f_{\mathrm{m,k}}^{\mathrm{CLT}}}{\boldsymbol{a}\cdot f_{\mathrm{t,90,k}}^{\mathrm{CLT}}}\cdot\sin^{2}\alpha\right)+\left(\frac{(1-v_{\mathrm{eff}})\cdot f_{\mathrm{m,k}}^{\mathrm{CLT}}}{\boldsymbol{b}\cdot f_{\mathrm{v,k}}^{\mathrm{CLT}}}\cdot\sin\alpha\cdot\cos\alpha\right)+\cos^{2}\alpha} \tag{3}$$

The strength reduction factors for the tested LFJ were calculated with the bending strength $f_{\mathrm{m,k}}^{\mathrm{LFJ}}=(1-v_{\mathrm{eff}})\cdot f_{\mathrm{m,k}}^{\mathrm{CLT}}=17.1\ \mathrm{N/mm^2}$ obtained from test series S600LFJ for straight CLT beams with LFJ. The effective tensile strength perpendicular to the grain and the effective shear strength were calculated according Eq. (4) and Eq. (5), given in Blaß and Flaig (2013) and in Blaß and Flaig (2014), respectively.

$$f_{\mathrm{t,90,k}}^{\mathrm{CLT}}=\min\begin{Bmatrix}\dfrac{t_{\mathrm{net,cross}}}{t_{\mathrm{net,long}}}\cdot f_{\mathrm{t,0,k}}^{\mathrm{lam}}\\[2ex]\dfrac{n_{\mathrm{CA}}\cdot b}{t_{\mathrm{net,long}}}\cdot f_{\mathrm{R,k}}^{\mathrm{lam}}\end{Bmatrix} \tag{4}$$

$$f_{\mathrm{v,k}}^{\mathrm{CLT}}=\min\begin{Bmatrix}\dfrac{t_{\mathrm{gross}}}{t_{\mathrm{net,long}}}\cdot f_{\mathrm{v,k}}^{\mathrm{lam}}\\[2ex]\dfrac{n_{\mathrm{CA}}\cdot b}{2\cdot t_{\mathrm{net,long}}}\cdot\dfrac{1}{\dfrac{1}{f_{\mathrm{v,tor,k}}^{\mathrm{lam}}}\cdot\left(1-\dfrac{1}{m^{2}}\right)+\dfrac{2}{f_{\mathrm{R,k}}^{\mathrm{lam}}}\cdot\left(\dfrac{1}{m}-\dfrac{1}{m^{2}}\right)}\end{Bmatrix} \tag{5}$$

For the calculation of the effective strength properties of the tested double pitched beams with m = 4 lamellae in direction of the beam height and n_{CA} = 4 crossing areas in thickness direction the strength properties given in Table 3 were assumed for the lamellae.

Table 3. Assumed strength properties of lamellae

$f_{\mathrm{t,0,k}}^{\mathrm{lam}}$ in N/mm²	$f_{\mathrm{v,k}}^{\mathrm{lam}}$ in N/mm²	$f_{\mathrm{R,k}}^{\mathrm{lam}}$ in N/mm²	$f_{\mathrm{v,tor,k}}^{\mathrm{lam}}$ in N/mm²
14.0	4.0	1.1	2.75

By substituting the given values in Eq. (4) and Eq. (5) an effective tensile strength perpendicular to the beam axis of $f_{\mathrm{t,90,k}}^{\mathrm{CLT}}$ = 3,5 N/mm² and an effective shear strength of $f_{\mathrm{v,k}}^{\mathrm{CLT}}$ = 2,75 N/mm² were calculated.

The strength properties were then used to calculate strength reduction factors according Eq. (2) and Eq. (3). The best agreement with the test results was found for the modified Hankinson's equation with factors $\boldsymbol{a}$ = 2.5 and $\boldsymbol{b}$ = 2.5. The bending strength $f_{\mathrm{m},\alpha}^{\mathrm{LFJ}}$ calculated from Eq. (3) and the respective values obtained from test results are illustrated in Figure 13. Since the experimentally obtained values of $f_{\mathrm{m},\alpha}^{\mathrm{LFJ}}$ include different values of (1-ν_{eff}) the bending strengths in the diagram are related to the residual thickness in the finger jointed connection $t_{eff,LFJ} = t_{net,long} \cdot (1-\nu_{eff})$.

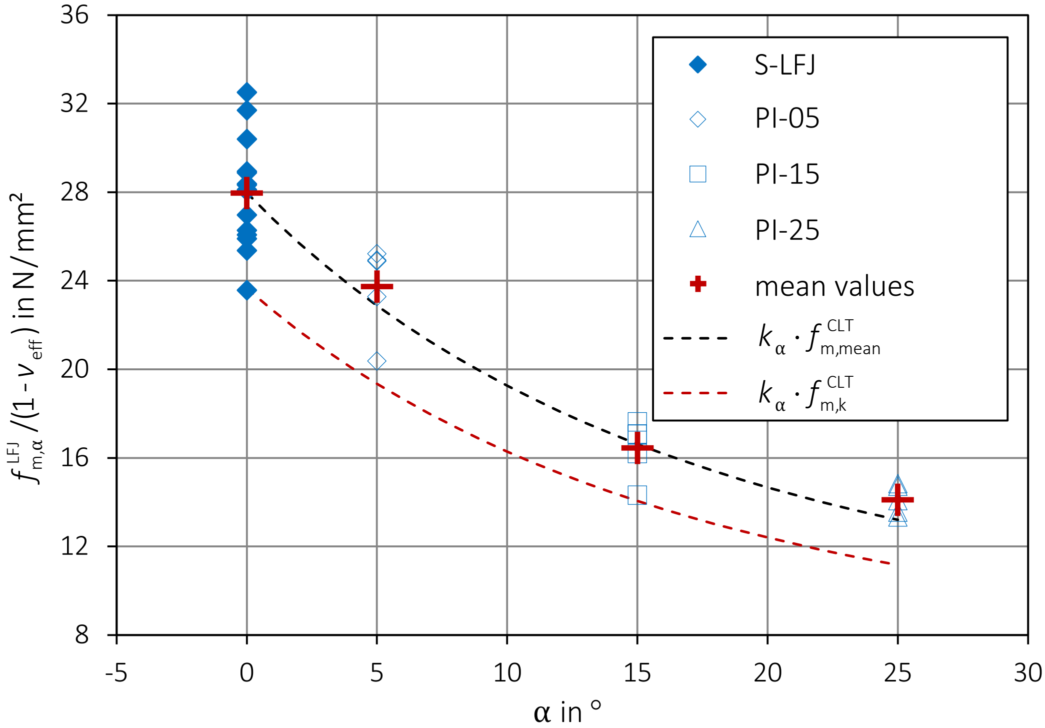

Figure 13. Experimentally and analyticly obtained bending strength $f_{m,\alpha,LFJ}$ of LFJ in CLT beams subjected to opening moments

3.3.2 Stiffness of LFJ in CLT

From the measured deflection, the local MOE of the tested straight and double pitched CLT beams was evaluated according to Eq. (6). In the evaluation of the tests with double pitched CLT beams, the influence of the larger length and the direction of the measured deflection were taken into account by the factor $\cos\alpha$ in the denominator. For the straight beams, in addition, the dynamic MOE was determined from the eigenfrequencies of the longitudinal vibration of the beams according Eq.(7). The obtained mean values of the MOE for the different test series are summarized in Table 4. The values are related to the net cross section of longitudinal layers.

$$E_{loc,net} = \frac{2}{16} \cdot \frac{\Delta M_{10-40}}{\Delta u_{10-40} \cdot \cos\alpha} \cdot \frac{\ell_m^2}{I_{net,long}} \qquad (6)$$

where ℓ_m is the measuring length (3,000 mm or 2,400 mm)

$$E_{dyn,net} = 4 \cdot f^2 \cdot L^2 \cdot \rho \cdot \frac{t_{gross}}{t_{net,long}} \qquad (7)$$

Table 4. MOE of the tested straight and double pitched CLT beams

Series	$E_{loc,net,mean}$ in N/mm²	COV -	$E_{dyn,net,mean}$ in N/mm²	COV -	E_{loc}/E_{dyn} -
S-REF	12,385	0.085	12,203	0.054	1.015
S-LFJ	11,283	0.045	11,884	0.035	0.949
PI-05	11,488	0.050	-	-	-
PI-15	10,642	0.031	-	-	-
PI-25	9,432	0.030	-	-	-

The decreasing values in the second column of Table 4 indicate that LFJs have significant influence on the overall deformation of finger jointed CLT beams. For straight beams with LFJ the additional deformation in the LFJ results in about 9% decreased values of the MOE compared to CLT beams without LFJ. In the tested double pitched CLT beams, the influence of the LFJ on the deflection strongly increases with increasing cutting angle α. To determine the stiffness of LFJ in CLT beams in dependence of the cutting angle α, the mutual displacement between the joined parts was measured in the test series with CLT frame corners (cf. Figure 9). Figure 14 shows an example of the obtained load displacement curves. The two curves in the third quadrant of the diagram clearly show that in the compression zone of the tested LFJ the strength was reached well before the ultimate load and that considerable non-elastic deformation occurred.

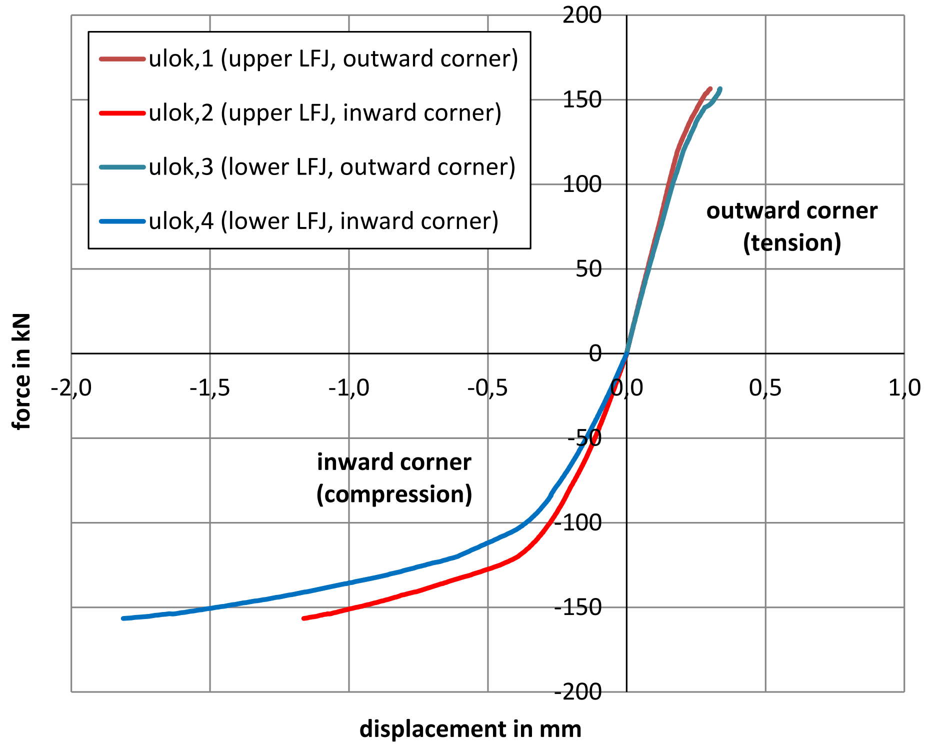

Figure 14. local displacements $u_{lok,i}$ in the LFJ in tested CLT frame corner CO105-05

The stiffness of the tested LFJ was evaluated on the assumption that the measured displacements are composed of two parts resulting from the bending moment and the normal force acting in the corner.

$$u_{\mathrm{loc,i}} = u_{\mathrm{N,i}} + u_{\mathrm{M,i}} \tag{8}$$

The two components u_{N} and u_{M} of the displacement were calculated according to Eq. (9) and Eq. (10) where k is a bedding factor describing the stiffness of the LFJ in dependence of the cross sectional area $A_{\mathrm{net,LFJ}}$ and the second moment of inertia $I_{\mathrm{net,LFJ}}$. The cross sectional values $A_{\mathrm{net,LFJ}}$ and $I_{\mathrm{net,LFJ}}$ were calculated using the net thickness of longitudinal layers and the height of the LFJ $h_{\mathrm{net,LFJ}} = h/\cos\alpha$.
In Eq. (10) e is the distance between the line of action of the applied force F and the center line of the vertical part of CLT frame corner (cf. Figure 8) and 290 mm is the distance of the displacement transducers from the center line of the CLT beams measured in direction of the LFJ (cf. Figure 9).

$$u_{\mathrm{N}} = \frac{F \cdot \cos\alpha}{k \cdot A_{\mathrm{net,LFJ}}} \tag{9}$$

$$u_{\mathrm{M}} = \pm \frac{F \cdot e \cdot 290\mathrm{mm}}{k \cdot I_{\mathrm{y,net,LFJ}}} \tag{10}$$

Substituting Eq. (9) and Eq. (10) into Eq. (8) and solving the equation for the bedding factor k yields the expression in Eq. (11).

$$k = \frac{F}{u_{\mathrm{lok}}} \cdot \left(\frac{\cos\alpha}{A_{\mathrm{net,LFJ}}} \pm \frac{e \cdot 290\mathrm{mm}}{I_{\mathrm{y,net,LFJ}}} \right) \tag{11}$$

In Table 5 minimum, mean and maximum values of the bedding factor k evaluated for the three test series with CLT frame corners are summarized.

Table 5. Bedding factors k of LFJ evaluated from local displacements in CLT frame corners

series	k_{min} in N/mm³	k_{mean} in N/mm³	k_{max} in N/mm³
CO-90	54,4	65,2	71,5
CO-105	64,6	76,3	88,1
CO-115	75,1	84,2	108

By means of a linear regression the relationship given in Eq. (12) was found between the bedding factor k and the cutting angle α.

$$k = 133 - 3{,}01 \cdot \alpha \qquad \text{with } k \text{ in N/mm}^3 \text{ and } \alpha \text{ in }^\circ$$
$$r = 0{,}425 \qquad s_R = 9{,}38 \qquad n = 15 \qquad (12)$$

In Figure 15 the bedding factor k evaluated from the test results are plotted against the cutting angle α. In the diagram, the linear regression according Eq. (12) is illustrated by a dotted line that was extrapolated to $\alpha = 0°$.

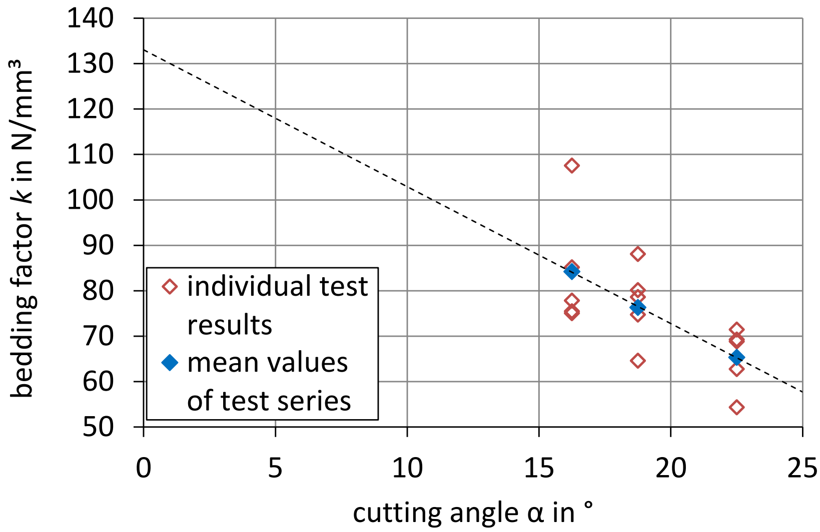

Figure 15. Bedding factor k of LFJ plotted against the cutting angle α

Bedding factors k calculated according Eq. (12) were used to determine the MOE of the tested straight and double pitched CLT beams in account of the stiffness of the LFJ. The resulting values of $E^{k}_{loc,mean}$ are summarized in Table 6. Although, the bedding factors used for the new evaluation had to be extrapolated far beyond the tested cutting angles, the values $E^{k}_{loc,mean}$ determined for straight CLT beams with LFJ differ only slightly from the value $E^{REF}_{loc,mean}$ = 12,385 N/mm² that was determined for straight CLT beams without LFJ. For the double pitched CLT beams of series, PI-05 and PI-15 with cutting angles of 5° and 15° the agreement is also very good. For the double pitched beams of series PI-25, the obtained values of the MOE still differ significantly.

Table 6. MOE of the tested straight and double pitched CLT beams evaluated with and without consideration of the bedding factor k of LFJ

Reihe	k in N/mm³	$E_{loc,mean}$ in N/mm²	$E^{k}_{loc,mean} / E^{REF}_{loc,mean}$ -
S-REF	-	12385	1
S-LFJ	133	12.104	0.98
PI-05	118	12.417	1.00
PI-15	88	11.665	0.94
PI-25	58	10.529	0.85

4 Design proposal

4.1 LFJ in straight CLT beams

The comparison of the values in the first two lines of Table 2 shows that there is good agreement between the value (1-v_{eff}) = 0.726 for straight beams and the ratio of 20.3/29.2 = 0.70 between the bending strength of straight beams with and without LFJ. It is therefore suggested to calculate the bending strength of LFJ in straight CLT beams loaded in plane direction by multiplying bending strength of CLT member with the value (1-v_{eff}). In general cases it is recommended to use a value of v_{eff} = 0.30 to take into account the effective reduction of the cross section.

$$f_{m,k}^{LFJ} = (1 - v_{eff}) \cdot f_{m,k}^{CLT} \tag{13}$$

For the design in the ultimate limit state, the bending stresses should be calculated according Eq. (14) using the section modulus $W_{net,long}$ of longitudinal layers and satisfy the condition given in Eq. (15).

$$\sigma_{m,net} = \frac{M}{W_{net,long}} \tag{14}$$

$$\frac{\sigma_{m,net,d}}{f_{m,d}^{LFJ}} \leq 1 \tag{15}$$

4.2 LFJ in CLT beams with kinked axis

For LFJ in CLT beams subjected to opening moments the bending strength can be calculated from the modified Hankinson's relation given in Eq. (16) that was derived from the test results by customizing the factors for shear strength and the tensile strength perpendicular to beam axis. The equation is valid for angles 0 < α ≤ 25°.

$$f_{m,\alpha,k}^{LFJ} = \frac{(1 - v_{eff}) \cdot f_{m,k}^{CLT}}{\left(\frac{(1 - v_{eff}) \cdot f_{m,k}^{CLT}}{2,5 \cdot f_{t,90,k}^{CLT}} \cdot \sin^2\alpha\right) + \left(\frac{(1 - v_{eff}) \cdot f_{m,k}^{CLT}}{2,5 \cdot f_{v,k}^{CLT}} \cdot \sin\alpha \cdot \cos\alpha\right) + \cos^2\alpha} \tag{16}$$

For the design of LFJ in CLT beams subjected to closing moments, in general, the bending strength of straight CLT beams with LFJ can be used.

$$f_{m,\alpha,k}^{LFJ} = (1 - v_{eff}) \cdot f_{m,k}^{CLT} \tag{17}$$

For the design in service class 1 according to EC 5, the bending strength according Eq. (17) can be increased by 50 %. Due to the strong influence of the moisture content on the compressive strength of softwood, the higher bending strength should not be used in service class 2.

Stresses in LFJ in kinked CLT beams should be calculated using the section modulus $W_{net,long}$ and the area $A_{net,long}$ of longitudinal layers in a cross section perpendicular to the beam axis. For the verification of stresses resulting from combined bending and tension or from combined bending and compression, the following procedure is suggested.

- Calculation of normal stresses $\sigma_m = M/W_{net,long}$ and $\sigma_N = N/A_{net,long}$ related to the net cross section of longitudinal layers.
- Calculation of the maximum normal stress by linear superposition of σ_m and σ_N
- Calculation of the bending strength $f_{m,\alpha}^{LFJ}$ according Eq. (16) or Eq. (17) in dependence of the cutting angle and verification by comparison of the maximum normal stress and the bending strength

In the diagram in Figure 16 the characteristic values $f_{m,\alpha,k}^{LFJ}$ according Eq. (16) and Eq. (17) are depicted by the red curve. The values were calculated using a characteristic bending strength $f_{m,\alpha,k}^{CLT}$ of 24 N/mm² and an effective reduction of the cross section of $v_{eff} = 0.30$. The results of all test series are also given in the diagram. On the abscissa the cutting angle α is given. Positive values of α indicate opening moments whereas negative angles stand for closing moments.

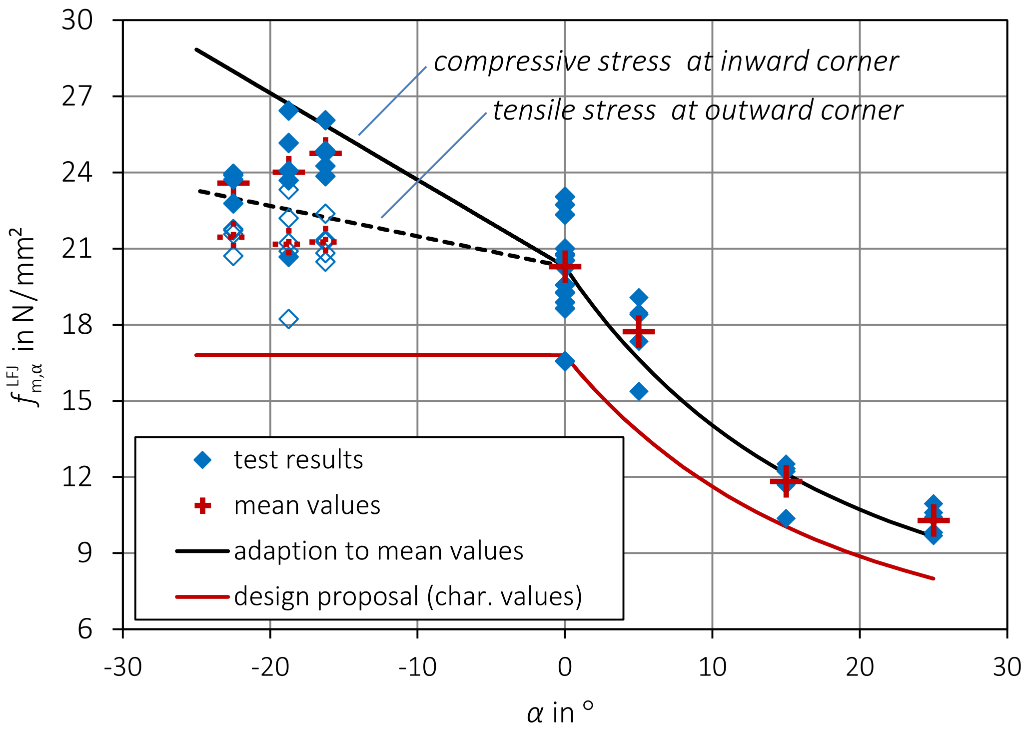

Figure 16. Bending strength $f_{m,\alpha}^{LFJ}$ in dependence of the angle α

5 Summary and Conclusions

A new finger joint profile, developed for LFJ in CLT beams, is presented. To determine the reduction of the bending strength resulting from LFJ, tests with straight CLT beams with and without LFJ were performed. Based on the test results a reduction factor of (1 – 0.30) = 0.70 is proposed for the bending strength of LFJ in straight beams. The factor includes the nominal reduction resulting from the finger joint profile and further reduction due to production tolerances and manufacturing processes.

For LFJ in CLT beams jointed under varying angles the influence of the cutting angle α on the bending strength was determined from tests with double pitched CLT beams and CLT frame corners. The results of tests show that the bending strength of LFJ in CLT is far less dependent on the cutting angle than the bending strength of LFJ in glulam. For LFJ subjected to opening moments the reduction of the bending strength for angles up to 25° is less than 50 %. For LFJ subjected to closing moments even a greater bending strength was found than for straight beams. Based on the test results a design proposal for LFJ in CLT beams is made, taking into account the strength reduction resulting from the LFJ and the influence of the cutting angle α.

6 References

Aicher S (2003): Structural Adhesive Joints Including Glued-In Bolts. In: Timber Engineering, Chapter 18, pp 333 – 363, Jon Wiley and Son LTD, Chichester

Flaig M, Blaß H J (2015): Keilgezinkte Rahmenecken und Satteldachträger aus Brettsperrholz. Karlsruher Berichte zum Ingenieurholzbau Band 29, KIT Scientific Publishing, Karlsruhe

Flaig M., Blaß H.J. (2014): Tapered beams made of cross laminated timber. In: Materials and Joints in Timber Structures. Springer, Berlin

Flaig M., Blaß H.J. (2013): Shear Strength and Shear Stiffness of CLT beams Loaded in Plane. In: Proceedings. CIB-W18 Meeting 46, Vancouver, Canada, Paper 46-12-3

Hankinson R L (1921): Investigation of crushing strength of spruce at varying angles of grain. Air service Information Circular III, No. 259, US Air Service

Heimeshoff B (1976): Berechnung von Rahmenecken mit Keilzinkenverbindungen. In: Holzbau Statik Aktuell, Folge 1, S. 7-8

Heimeshoff B, Seuß R (1982) Berechnung von Rahmenecken mit Keilzinkenverbindungen. Forschungsbericht, Universität München

Kolb H (1966): Versuche zur Ermittlung der Tragfähigkeit geleimter Rahmenecken. In: Bauen mit Holz, Heft 8, S. 363-369, Bruderverlag, Karlsruhe

Komatsu K et. al (2001): Moment-resisting performance of glulam beam to column joints composed of various types of large finger joints. In: Proceedings of the International RILEM Symposium, Stuttgart, Germany, pp. 520-530

Discussion

The paper was presented by M Flaig

G Schickhofer asked about the 0.3 reduction factor as a constant and suggested it would be better to have this as a function.

S Winter asked why there was a nominal reduction of 14% but found a 30% reduction for the profile. M Flaig responded that these specimens were from industry and they did not have control over the production accuracy. Here, optimized production of CLT as beams was not yet available.

W Seim received clarification that E_{local} as shear free MOE. He asked for examples of where these members could replace glulam. M Flaig responded that CLT beam has higher strengths in the perpendicular to grain direction therefore, these members could be suitable for cases where higher stress in perpendicular to grain directions as well as cases where cracks might be important.

L Franzoni asked given a straight beam why were those dimensions given. M Flaig said that bending strength of straight beams would depend on the specimen size; so standardized test span to depth ratio of 18 to 25 are typically used. In the current tests finger joint governed so the specimen length did not matter.

G Fink commented that based a sample size of 5 to get a characteristic strength might be too low. M Flaig agreed but stated that it would be too expensive to test many beams and that they relied on prior knowledge about CLT as beam element and used this information as guidance. G Fink commented they could consider different models to estimate characteristic properties.

T Bogensperger was surprised by the large stiffness degradation and asked if the strength depended on the glue. M Flaig stated that they did not know whether different glue would affect the strength but did not expect so. He also did not expect the large stiffness degradation at first but the test results clearly showed this.

T Bogensperger also asked about gluing large finger joint on site. M Flaig stated that it could be done but would not be recommended.

Performance-based seismic design of light-frame structures – Proposed values for equivalent damping

Johannes Hummel

Werner Seim

University of Kassel, Department of Structural Engineering,
Kurt-Wolters-Straße 3, 34125 Kassel, Germany.

Keywords: light-frame, cyclic behaviour, dynamic behaviour, seismic design

1 Summary

This paper discusses different methods for performance-based design. In this context, damped and inelastic spectra will be addressed as demand spectra. How to create demand spectra within the capacity spectrum method and the N2 method will be explained. The challenges which occur for timber structures in performance-based design with the capacity spectrum method and the N2 method will be identified.

A constant approach for equivalent damping will be proposed for light-frame structures for application within the capacity spectrum method. Values for equivalent damping can be derived directly from cyclic testing. A fairly constant progression of the values was observed here over increasing wall drift.

The constant approach for equivalent damping is applied to validate results from dynamic testing. Test results will be presented for two dynamic tests. The capacity spectrum method, according to ATC 40, and the N2 method, according to Eurocode 8 (2010), will also be applied for comparison.

2 Introduction

There are basically three design methods for buildings under earthquake impact which are introduced with Eurocode 8 (2010). The most common method for engineers in practice is the so-called force-based design. This method uses elastic response spectra scaled by a behaviour factor q to calculate the base shear, which is equivalent to the total of seismic forces. In addition, the time history analysis is used as the most comprehensive calculation method. The time history analysis needs accelerograms of real earthquakes or synthetically generated accelerograms, a definition of nonlinear hysteretic material behaviour and a powerful computer programme to determine displacements and stresses for the structure over time history. Performance-based design procedures can be classified more or less between force-based design and time history analyses.

Different performance-based design procedures have been developed in the last five decades. The most relevant procedures in Europe are the capacity spectrum method (*Freeman*, 1998) and the N2 method (*Fajfar*, 1999), which have been critically discussed by *Chopra & Goel* (1999) and *Freeman* (2004). The direct-displacement method (*Priestley & Kowalsky*, 2000) is also common in North America. These methods differ slightly in the analysis steps and mainly in the definition of seismic action. Whereas the capacity spectrum method and the direct-displacement method use elastic response spectra, which are scaled by equivalent damping $\acute{\xi}_{eq}$, the N2 method makes use of inelastic spectra.

Two formats of the response spectrum are commonly applied within performance-based design procedures: acceleration over displacement (S_a-S_d format) and displacement over period (S_d-T format). The spectrum in the S_a-S_d format is especially convenient for a graphical solution (see Figure 1a). Since the various codes usually provide elastic response spectra in the format elastic spectral acceleration S_e over period T, the spectral values for the displacement should be determined with equation (1).

$$S_d = \frac{T^2}{4 \cdot \pi^2} \cdot S_a \qquad \text{with } S_a = S_e(T) \tag{1}$$

Code spectra usually consider a proportion of 5 % viscous damping. For other values of viscous damping, the spectra can be adapted by the damping correction factor η, see equation (2), according to Eurocode 8.

$$\eta = \sqrt{\frac{10}{5+\xi}} \geq 0.55 \tag{2}$$

Inelastic spectra can be generated according to equation (3)

$$S_a = \frac{S_e(T)}{R_\mu} \quad \text{and} \quad S_d = \frac{\mu}{R_\mu} \cdot \frac{T^2}{4 \cdot \pi^2} \cdot S_e(T) \tag{3}$$

with the reduction factor R_μ depending on ductility μ.

A bilinear R_μ-μ-T relationship was proposed for the N2 method by *Vidic et al.* (1994). Here, the reduction factor R_μ increases linearly with period T up to the "corner period" T_C (see Eurocode 8 and Figure 1a), and from that point the reduction factor remains constant and is equal to the ductility μ:

$$R_\mu = (\mu - 1)\cdot\frac{T}{T_C} + 1 \qquad \text{for } T \leq T_C$$
$$R_\mu = \mu \qquad \text{for } T > T_C \qquad (4)$$

Here, ductility μ is defined as the ratio between ultimate displacement u_u and the yield displacement u_y (see Figure 1b). The R_μ-μ-T relationship according to equation (4) is based on a hysteretic model – the Q-model – which is representative for reinforced concrete frame constructions (*Saidi & Sozen*, 1979).

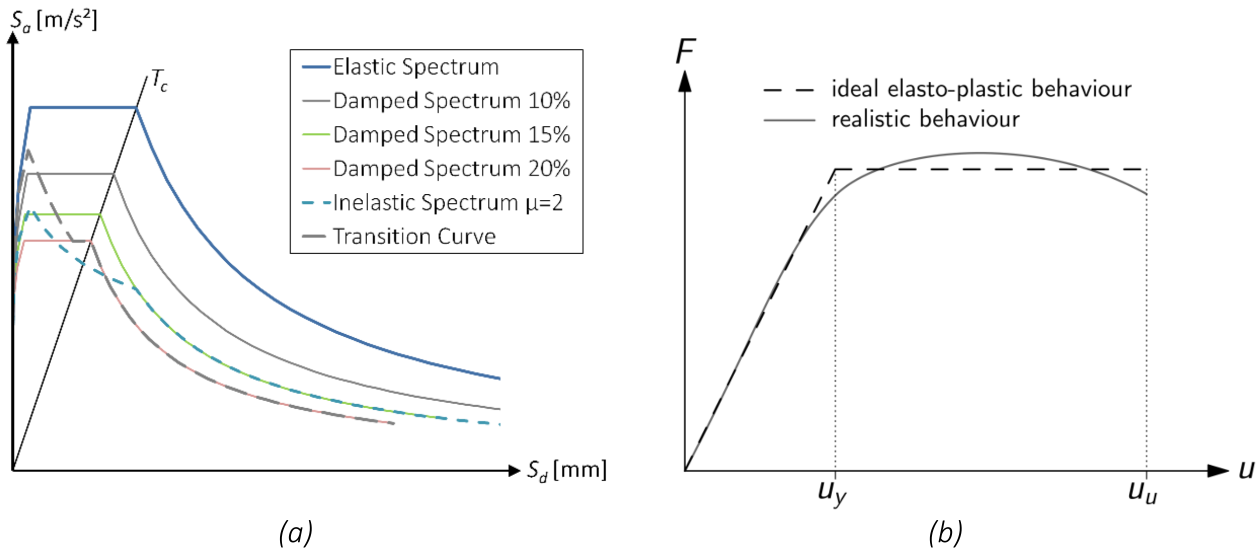

Figure 1. (a) Comparison of inelastic and damped spectra; (b) bilinear idealisation of the load-diplacement curve of the structure.

It must be noted that the Q-model does not necessarily match the hysteretic behaviour of timber structures, since it does not capture pinching effects. This issue was also addressed by *Fragiacomo et al.* (2011) with reference to CLT buildings. Consideration of the realistic hysteretic behaviour seems to be indispensable, because it accounts for the energy dissipation.

Another way to consider energy dissipation is to describe the hysteretic behaviour by equivalent damping. ATC 40 (1996) provides an approach for equivalent damping depending on the associated displacement, respectively, the related ductility, and hysteretic behaviour based on a bilinear idealisation of the load-displacement curve (see Figure 1b). Furthermore, *Filiatrault et al.* (2002) proposed an equivalent damping approach for light-frame structures focused on an application with the direct-displacement method. A bilinear relationship for equivalent damping over building drift was found by applying the CASHEW hysteretic model (*Folz & Filiatrault,* 2001).

In contrast to the inelastic spectrum, which can be determined directly with equation (3), there are always series of damped spectra for different values of ξ_{eq}' if equivalent damping depends on the building drift. A transition curve (see Figure 1a) might be found if a formulation for damping as a function of displacement is available (*Kawai*, 1999).

Applying the N2 method, according to Eurocode 8, to timber structures without further considerations seems to be questionable. There are certainly a number of other R_{μ}-μ-T relationships (e.g. *Miranda & Bertero*, 1994), but none of these approaches were validated for timber structures. The hysteretic behaviour can differ significantly between the various construction types, even for timber structures, such as light-frame, cross laminated timber, moment resisting frames and others (see *Seim & Hummel*, 2013; *Seim & Vogt*, 2013; *Seim & Schick*, 2013).

On the other hand, different hysteretic behaviour can be considered comparatively simply by equivalent damping. The hysteretic behaviour can be determined by standardised experimental investigations (see section 3) and approaches for equivalent damping can be derived directly from test results (see section 4). Anyway, experimental investigations – cyclic and dynamic tests – are necessary for any structural material or construction type to get basic information about the characteristics under earthquake impact and to validate design procedures.

Thus, in the author's opinion, it seems to be more promising to utilise equivalent damping to determine demand spectra with reference to performance-based design of timber structures. The adverse iteration process, which comes with the capacity spectrum method to obtain the effective damping value for defining the demand spectrum, can be avoided by means of a simplified formulation of equivalent damping (see section 4).

3 Experimental Investigations

Extensive experimental investigations on wall elements – light-frame and cross laminated timber – were carried out at the University of Kassel within the research project Optimberquake. The wall elements were tested under cyclic and dynamic loading.

3.1 Programme and Test Set-up

A total of 18 cyclic tests were performed with light-frame wall elements (see Table 1). Each of these elements had the dimensions 2.50 m × 2.50 m. A horizontal load was applied by a horizontal actuator on the top of the wall element. The vertical load was applied by two vertical actuators (see Figure 2a). The horizontal load and the corresponding horizontal displacement were measured on the top of the wall. Details concerning the cyclic tests can be found in the documentation (*Seim & Hummel*, 2013; *Seim & Vogt*, 2013).

(a) (b)

Figure 2. Test set-ups: (a) cyclic testing; (b) uniaxial shaking table.

Table 1. Cyclic tests on light-frame wall elements.

Test	Sheathing[1)]	Fasteners			Loading protocol	Anchoring	Vert. Load [kN/m]
		Type	ø - ℓ [mm]	Spacing[3)] [mm]			
WL-1.2	2×OSB 18 mm	Nail	2.8 - 65	75/150	ISO21581	symmetric	10
WL-1.3							
WL-1.4					CUREE		
WL-2.2	2×GFB 18 mm	Staple	1.53 – 55[2)]	75/150	ISO21581	symmetric	10
WL-2.3							
WL-2.4					CUREE		
WL-3.1	1×OSB 10 mm	Nail	2.8 - 65	75/150	ISO21581	symmetric	10
WL-3.2					CUREE		
WL-3.3	1×OSB 18 mm				ISO21581		
WL-3.4					CUREE		
WL-4.1	2×OSB 18 mm	Nail	2.8 - 65	75/150	ISO21581	asymmetric	10
WL-4.2	2×GFB	Staple	1.53 – 55[2)]				
WL-4.3	1×OSB	Nail	2.8 - 65				
WL-4.4	1×GFB	Staple	1.53 – 55[2)]				
WL-5.1	1×GFB 10 mm	Staple	1.53 – 55[2)]	75/150	ISO21581	symmetric	10
WL-5.2					CUREE		
WL-5.3	1×GFB 18 mm				ISO21581		
WL-5.4					CUREE		

1) "1" indicates sheathing at one side, "2" indicates sheathing at two sides
2) The thickness of the wire is 1.53 mm and length of the staple from the crown to the tip is 55 mm.
3) First value along the edge of the sheathing board, second value along the intermediate studs.

Furthermore, five light-frame elements were tested under dynamic loading (see Table 2) on the uniaxial shaking table of the University of Kassel (see Figure 2b).
The configuration of the light-frame wall elements for dynamic testing was chosen according to the test set-up of the cyclic tests. Two different materials – OSB and GFB (gypsum fibre board) – were used for the sheathing with thicknesses of 18 mm and 10 mm, respectively. Dimensions of the sheathing boards are 1.25 m by 2.50 m. The spacing of the studs (C24, 140 mm × 60 mm) was 625 mm. Four specimens had the same dimensions as in the cyclic tests. The half wall length (ℓ = 1.25 m) was chosen for one element. The wall elements were anchored with hold-downs at both ends against uplift. Shear steel plates were used as end stops (block shear connectors) to take the horizontal force. Hold-downs and steel plates were fixed to the base plate of the shaking table. Each hold-down (Type HTT 22 *SIMPSON*, 2011) was connected to the outer stud by means of 18 annular ring shank nails (ø4 - 60 mm). The load-bearing capacity of the anchoring amounts to 50 kN at the minimum which was obtained by monotonic and cyclic testing (*Seim, Hummel & Vogt*, 2013).

Table 2. Specimen and loading for dynamic tests.

Test	Dimensions [m] × [m]	Sheathing[1)]	Fasteners			Time history	Vert. Load [kN/m]
			Type	ø - ℓ [mm]	Spacing[3)] [mm]		
WL-dyn-1	2.50 × 2.50	1×OSB 18 mm	Nail	2.8 - 65	75/150	synthetic earthquake	9.5
WL-dyn-2	2.50 × 2.50	1×OSB 18 mm	Nail	2.8 - 65	75/150	El Centro, 1940	9.5
WL-dyn-3	2.50 × 2.50	1×OSB 10 mm	Nail	2.8 - 65	75/150	synthetic earthquake	9.5
WL-dyn-4	1.25 × 2.50	1×OSB 10 mm	Nail	2.8 - 65	75/150	synthetic earthquake	9.5
WL-dyn-7	2.50 × 2.50	1×GFB 18 mm	Staple	1.53 – 55[2)]	75/150	synthetic earthquake	9.5

1) "1" indicates sheathing at one side
2) The thickness of the wire is 1.53 mm and length of the staple from the crown to the tip is 55 mm.
3) First value along the edge of the sheathing board, second value along the intermediate studs.

The vertical load was applied by means of steel plates fixed on the top of the wall element. The shaking table uses a displacement-controlled regulation where the displacement capacity is ± 200 mm. The signal for the displacement is calculated from the acceleration time history (see Figure 3). The target acceleration is measured directly on the shaking table. In addition, reaction force (H-Load), top displacement, relative displacement between the top and bottom of the wall element, and the acceleration on the top of the wall were recorded.

An artificial time history compatible with the elastic response spectrum with ground conditions A-R, according to Eurocode 8/NA (see Figure 3), and the north-south component of the El Centro earthquake (1940) were used as input data for the target signal (acceleration). The time histories were scaled to 1 g in order to reach the load-bearing capacity of the wall elements and to remain in the displacement range of the shaking table.

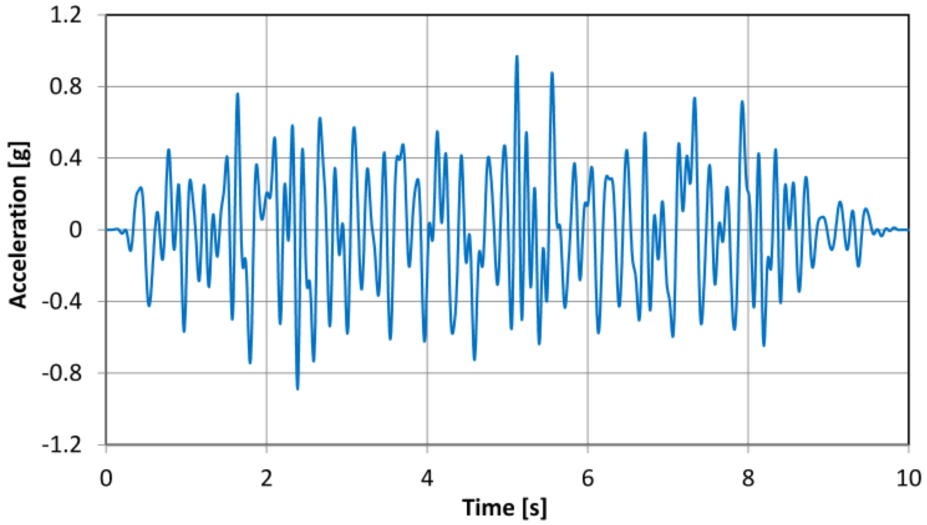

Figure 3. Artificial time history compatible to the elastic response spectrum with ground conditions A-R, according to Eurocode 8/NA (synthetic earthquake).

3.2 Test Results

Test results of the cyclic tests have already been published (*Seim et al.*, 2014) and are fully documented in test reports (*Seim & Hummel*, 2013; *Seim & Vogt*, 2013).

The dynamic test was initially started with a smaller earthquake, where the peak ground acceleration was 0.5 g to 0.6 g. This step was necessary to figure out the interaction between the shaking table and wall element. The peak ground acceleration was then increased to 1 g in order to reach the load-bearing capacity of the element.

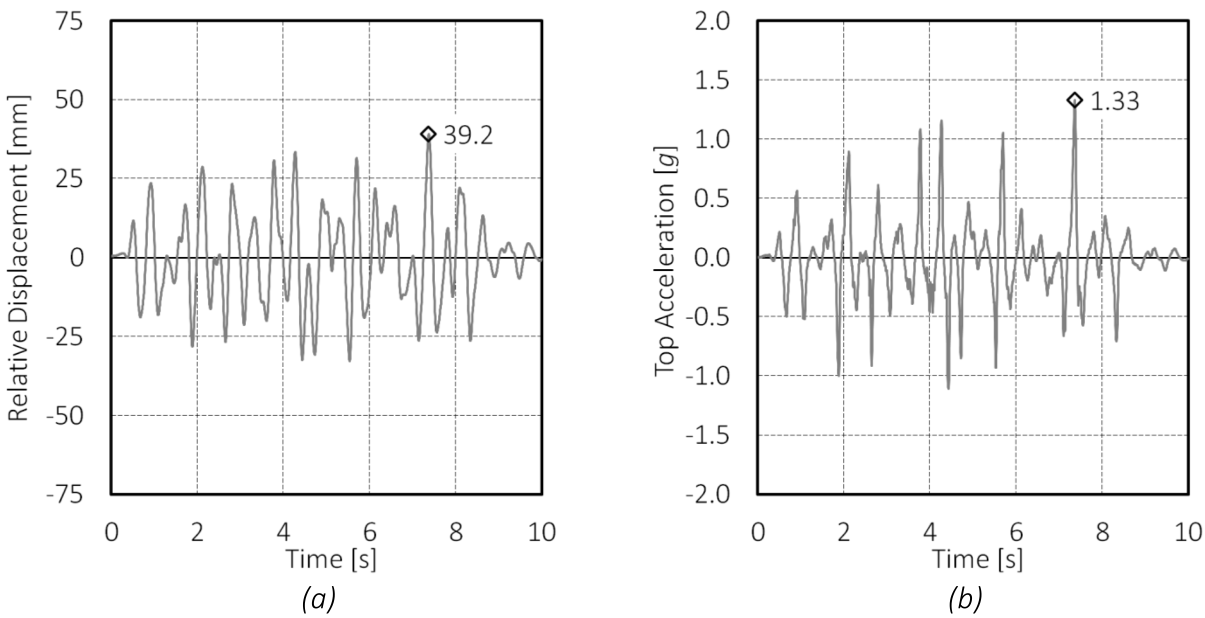

Figure 4. Results of test WL-dyn-1: (a) relative displacement over time and (b) top acceleration over time.

Figures 4 and 5 present the test results of the relative displacement and top acceleration for the two tests WL-dyn-1 and WL-dyn-3. The relative displacement is the difference between the top displacement and the displacement of the shaking table ("table displacement"), see Figure 2b.

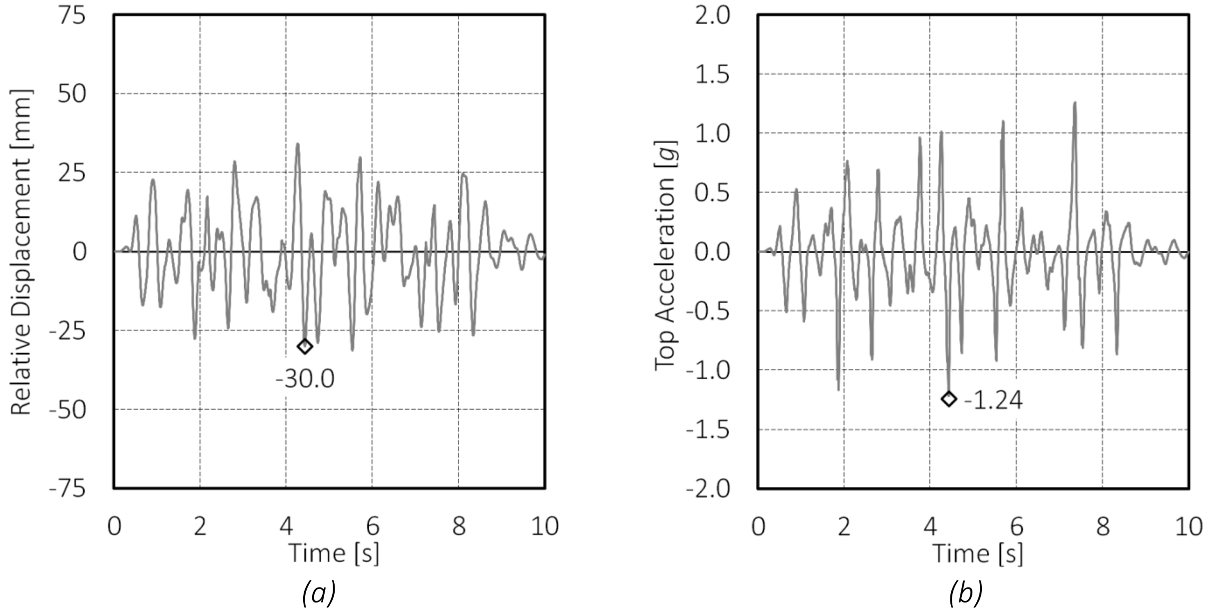

Figure 5. Results of test WL-dyn-3: (a) relative displacement over time and (b) top acceleration over time.

WL-dyn-1 and WL-dyn-3 show a similar behaviour with respect to the progression of the top acceleration (see Figures 4b and 5b). However, the relative displacements exhibit a slightly different characteristic (see Figures 4a and 5a). A completely different behaviour was obtained in test WL-dyn-2, where a real earthquake (El Centro, see Table 2) was applied. Obviously, significantly higher relative displacements occurred. The maximum acceleration is also higher.

Table 3. Results of dynamic tests, absolute values

Test	H-Load [kN]	Table disp. [mm]	Top disp. [mm]	Top acc. [*g*]
WL-dyn-1	40.3	87.7	106.2	1.3
WL-dyn-2	45.5	153.8	236.4	1.8
WL-dyn-3	37.9	88.2	121.4	1.2
WL-dyn-4	25.3	86.4	125.7	1.4
WL-dyn-7	50.5	103.8	138.5	1.8

The absolute values of top acceleration, top displacement, table displacement and H-Load (reaction force) for the dynamic test are summarised in Table 3.

An amplification of the acceleration from the bottom to the top can be noticed, since the maximum acceleration of the shaking table is 1 g (see section 3.1) and the top acceleration goes up to 1.8 g (see Table 3).

4 Equivalent damping approach

4.1 Definition

Equivalent damping $\xi_{eq}^{'}$ is defined in the following as a superposition of viscous damping ξ_0 and equivalent viscous damping ξ_{eq}:

$$\xi_{eq}^{'} = \xi_0 + \xi_{eq} \tag{5}$$

The nominal damping ratio ξ_0 accounts for energy dissipation within linear elastic behaviour and considers, for example, damping effects which are caused by friction. The damping value ξ_0 is typically determined by means of experimental tests and approaches are available in the literature (e.g. *Petersen*, 1996). Nominal damping ratios between 2% and 3% of critical damping are given for timber structures.

The equivalent viscous damping value ξ_{eq} represents energy dissipation which appears due to nonlinear hysteretic behaviour. Equivalent viscous damping was first defined by *Chopra* (1995) as an approximation to be compared to linear viscous damping. The values of equivalent viscous damping can be derived from data for load and displacement from cyclic testing (see section 3.2).

Values of equivalent viscous damping can be determined as

$$\xi_{eq} = \nu_{eq} = \frac{E_d}{4\pi \cdot E_p}, \tag{6}$$

where E_d is the dissipated energy for one cycle – enclosed area of one hysteresis loop – and E_p is the potential energy determined from the current stiffness corresponding to the maximum amplitude u per cycle (see Figure 6a).

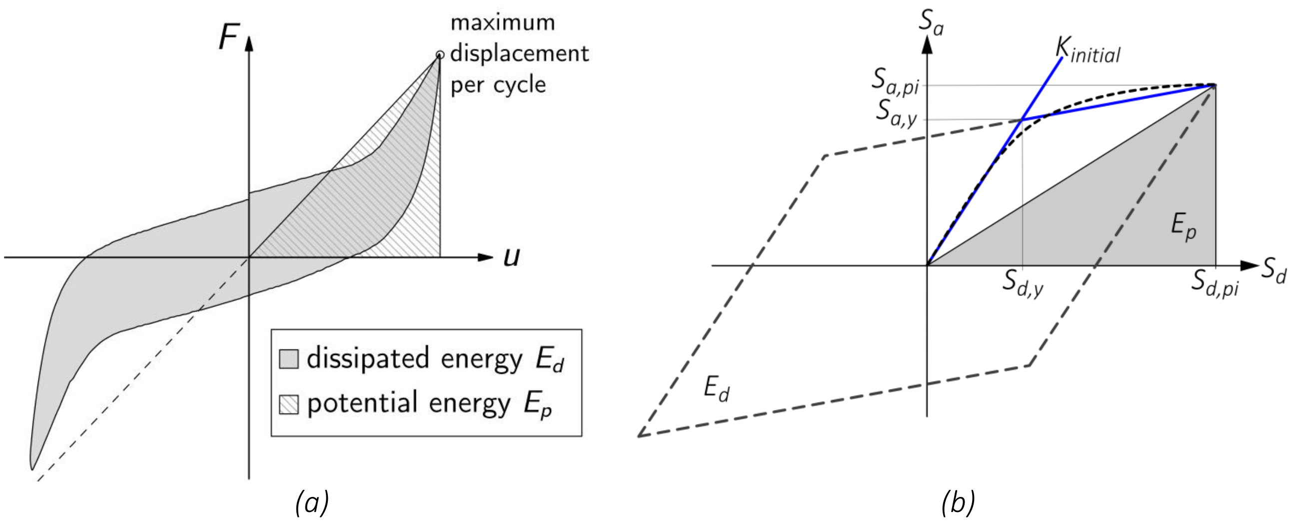

Figure 6. Definition of equivalent viscous damping: (a) according to Chopra (1995) and (b) according to ATC (1996).

4.2 Test Results

Data from a total of 18 cyclic tests on light-frame wall elements were evaluated for equivalent viscous damping. The damping values ξ_{eq} calculated from the first and the third cycle of the hysteresis are summarised in Table 4. Minimum, maximum, mean and median values are specifically reported. The damping values for the second cycle differ only slightly from those of the third cycle, therefore, the results of the second cycle are omitted.

Table 4. Values of equivalent viscous damping for light-frame elements.

Test	First Cycle				Third Cycle			
	Min	Max	Mean	Median	Min	Max	Mean	Median
WL-1.2	0.106	0.143	0.127	0.132	0.094	0.132	0.112	0.111
WL-1.3	0.126	0.168	0.146	0.143	0.115	0.131	0.122	0.123
WL-1.4	0.149	0.167	0.161	0.162	0.131	0.227	0.160	0.142
WL-2.2	0.161	0.207	0.185	0.185	0.153	0.174	0.162	0.161
WL-2.3	0.155	0.263	0.196	0.181	0.161	0.197	0.176	0.169
WL-2.4	0.161	0.188	0.174	0.173	0.167	0.254	0.203	0.191
WL-3.1	0.172	0.240	0.199	0.194	0.165	0.200	0.176	0.169
WL-3.2	0.172	0.198	0.187	0.188	0.178	0.246	0.214	0.215
WL-3.3	0.195	0.278	0.226	0.220	0.164	0.209	0.189	0.190
WL-3.4	0.209	0.248	0.219	0.215	0.186	0.297	0.236	0.233
WL-4.1	0.153	0.167	0.160	0.160	0.122	0.159	0.135	0.130
WL-4.2	0.143	0.292	0.185	0.164	0.095	0.189	0.135	0.131
WL-4.3	0.161	0.174	0.168	0.168	0.124	0.168	0.138	0.131
WL-4.4	0.137	0.216	0.164	0.148	0.123	0.164	0.134	0.127
WL-5.1	0.194	0.332	0.256	0.241	0.144	0.175	0.159	0.159
WL-5.2	0.144	0.162	0.150	0.145	0.113	0.133	0.122	0.122
WL-5.3	0.149	0.228	0.182	0.165	0.160	0.185	0.168	0.163
WL-5.4	0.153	0.307	0.202	0.190	0.134	0.273	0.203	0.207

It becomes clear from Table 4 that the damping values are scattered, even for wall elements with the same assembly. The influences are the loading protocol, sheathing material, and anchoring and support conditions (see Table 1). However, if one looks at the progression of equivalent viscous damping with the increasing deformation, the damping value remains approximately constant until the drift limit is reached (see Figure 7). This applies especially to the damping values of the third cycle. The drift limit was defined as $0.02 \cdot h$ with a wall height of 2.50 m (see Table 2).

Nevertheless, in some cases, outliers also exist for specific amplitudes and certain cycles. For that reason, the median value seems to be more descriptive than the mean value. The median value mostly coincides with the mean value.

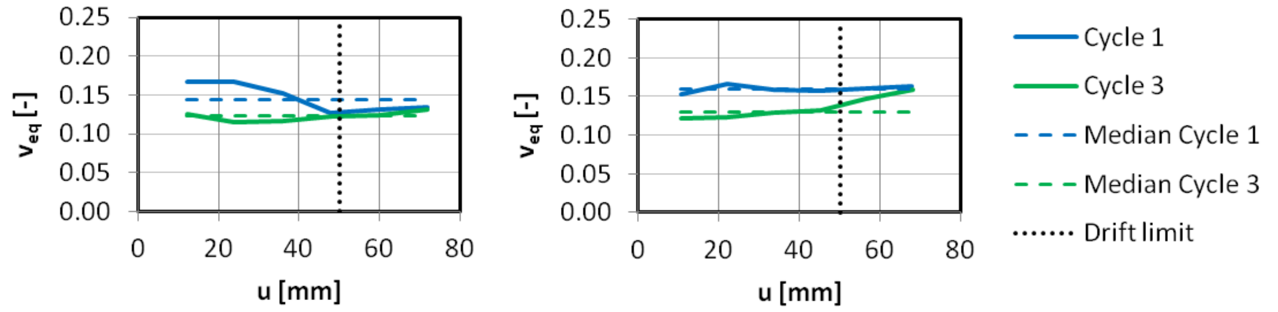

(a) (b)

Figure 7. Equivalent viscous damping over displacement amplitude for light-frame wall elements: (a) WL-1.3, (b) WL-4.1.

4.3 Proposal

As a result of the findings in the previous section, constant values for equivalent viscous damping are regarded as suitable for transferring elastic spectra into damped spectra for light-frame timber structures. In order to derive constant damping values, all equivalent viscous damping values were summarised in one statistical population, separately for the first and the third cycle. The values derived are reported in Table 5 and the summary of the equivalent viscous damping values is shown in Figure 8.

Table 5. Summary of equivalent viscous damping for light-frame timber structures.

First Cycle				Third Cycle			
Min	Max	Mean	Median	Min	Max	Mean	Median
0.106	0.332	0.182	0.172	0.094	0.297	0.167	0.164

The histogram in Figure 8 emphasises a strong concentration of the equivalent viscous damping values in the range of the constant values derived.

The use of constant values for equivalent damping will simplify the capacity spectrum method significantly, since a relationship between equivalent damping and displacement is no longer required. The design procedure will be demonstrated in section 5.

Based on Table 5 and Figure 8, a constant value between 0.16 (third cycle) and 0.18 (first cycle) for equivalent viscous damping might be suitable. However, the more conservative value 0.16 is proposed for light-frame constructions, since recurrent loading can lead to a reduction of equivalent viscous damping. Equivalent viscous damping can be affected by the assembly (e.g. sheathing material, sheathing thickness). If the assembly of the light-frame element is not clear, 10% equivalent viscous damping can be taken into account in any case.
A constant equivalent damping value of 0.21 can be derived for light-frame structures from the equivalent viscous damping values (0.16) proposed and 5% viscous damping, as considered in code spectra.

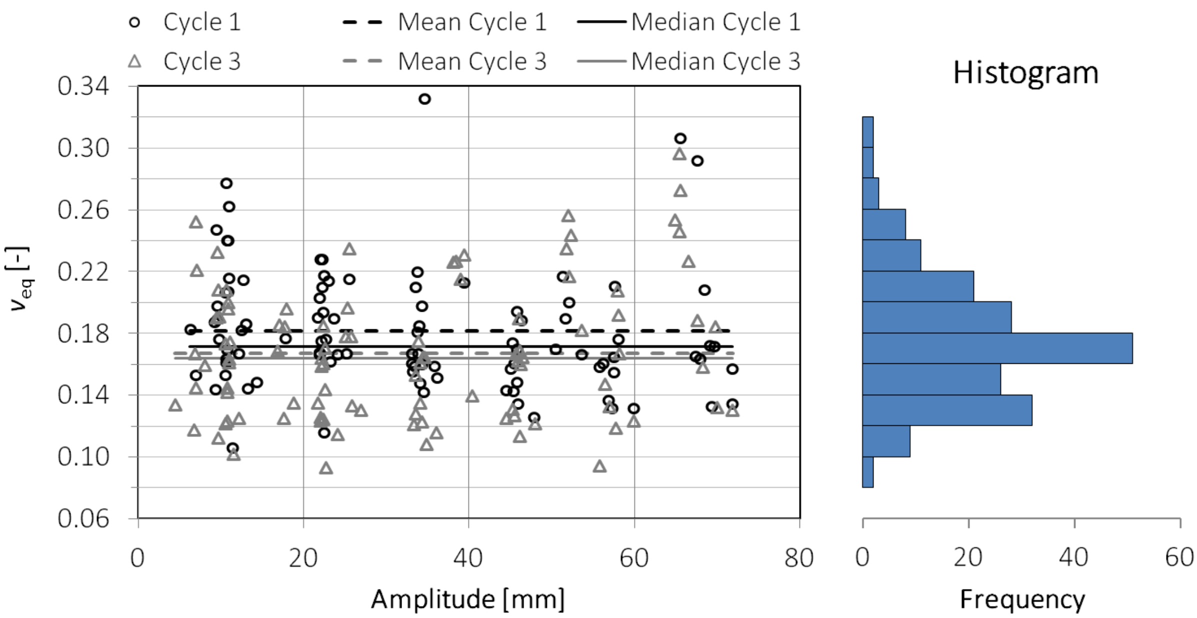

Figure 8. Summary of equivalent viscous damping for light-frame wall elements and overall distribution of equivalent viscous damping for cycle 1 and cycle 3.

5 Comparative Study and Validation

The application of performance-based design by means of the capacity spectrum method in combination with the values for equivalent damping proposed is illustrated in this section. The N2 method is used for comparison. Furthermore, the approaches for equivalent damping according to ATC 40 (1996) will be considered.

Exemplarily, two load displacement curves obtained by cyclic testing are used to carry out performance-based design. The backbone curves of WL-3.1 and WL-3.3 (see Table 1) were chosen here, since these cyclic tests are comparable to the dynamic tests WL-dyn-3 and WL-dyn-1. The results of the calculation will be compared with the results of the dynamic test.

The load displacement curve – also called the capacity curve – has to be transformed into the S_a-S_d format for the sake of consistency. The acceleration S_a is calculated with equation (7):

$$S_a = \frac{F}{m} \qquad (7)$$

The cyclic tests were performed with a vertical of 10 kN/m (see Table 1). That leads to a mass of 2.5 t for a wall length of 2.5 m. It must be noted that the light-frame wall elements tested are understood as a single degree-of-freedom system. For that reason, the relative displacements of the wall element are the same for the spectral displacements S_d.

The spectrum according to Eurocode 8/NA ground type A-R was chosen as the elastic response spectrum, which was scaled by 1.2 to match the spectrum of the time history applied (see Figure 9). The demand spectra were gained from the elastic response spectrum. The value 0.21 is used for the constant damping approach, as proposed in section 4.3.

The elastic response spectrum was transferred with equation (2) to generate the damped spectrum. Similarly, the demand spectrum, according to ATC 40 (1996), was created. Therefore, the effective damping for several steps of spectral displacement of the capacity spectrum has to be calculated following the procedure proposed in ATC 40. Consequently, effective damping can be determined with equation (8), see Figure 6b.

$$\xi_{eff} = \xi_0 + \kappa \cdot \xi_{eq} \qquad \text{with } \xi_{eq} = \frac{2}{\pi} \cdot \frac{S_{a,y} \cdot S_{d,pi} - S_{d,y} \cdot S_{a,pi}}{S_{a,pi} \cdot S_{d,pi}} \tag{8}$$

The modification factor κ was set to 0.33 in order to consider the hysteretic behaviour for light-frame elements (pinched shape). The definition of ISO 21581 (2010) was used as initial stiffness. Equal energy under the nonlinear and the bilinear capacity curve was considered.

The inelastic spectrum was created by following the N2 method proposed in annex B of Eurocode 8 (2010). A bilinear idealisation of the nonlinear capacity curve is required to determine the reduction factor R_μ, respectively, the ductility μ (see section 2). The capacity curve of WL-3.1 or WL-3.3 (backbone) was taken here and was idealised into a bilinear curve. In order to define the bilinear capacity curve, firstly, the maximum displacement was chosen and then the yield displacement was calculated by considering the energy equivalency between the nonlinear and bilinear curve. Regarding the bilinear capacity curve, the reduction factor R_μ and the ductility μ were determined, and the spectral values for the inelastic spectrum could be calculated with equation (3).

The spectra and capacity curves obtained were drawn into the S_a-S_d diagram (see Figure 9 and 10). The intersection between the demand spectrum and the capacity curve defines the performance point.

Figures 9 and 10 depict that reasonable performance points could be found for the two different wall configurations. The displacement demand ranges from 23 mm to 31 mm for WL 3.3 and from 27 mm to 41 mm for WL 3.1. In both cases, the performance points using the constantly damped spectrum provide the lower values and the performance points with the inelastic spectrum define the upper limit, while the performance point with the spectrum according to ATC 40 (1996) lies in between these two limits.

The hysteretic behaviour under realistic dynamic impact was used for a direct evaluation of inelastic and damped spectra for both wall configurations. In both cases, the S_a values and the related S_d value, which could be interpreted as one point of the damped or inelastic spectra, confirm basically the level of the transformation.

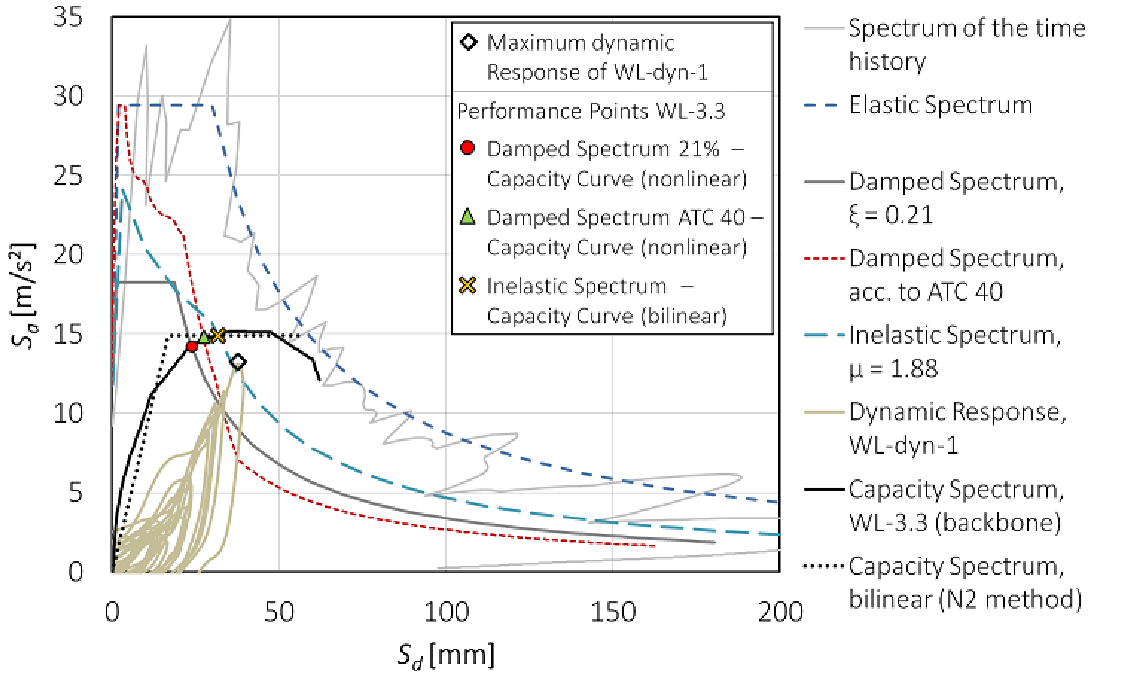

Figure 9. Seimic performance of dynamic test WL-dyn-1 compared with the results of performance-based design from different methods for WL-3.3 (graphical solution).

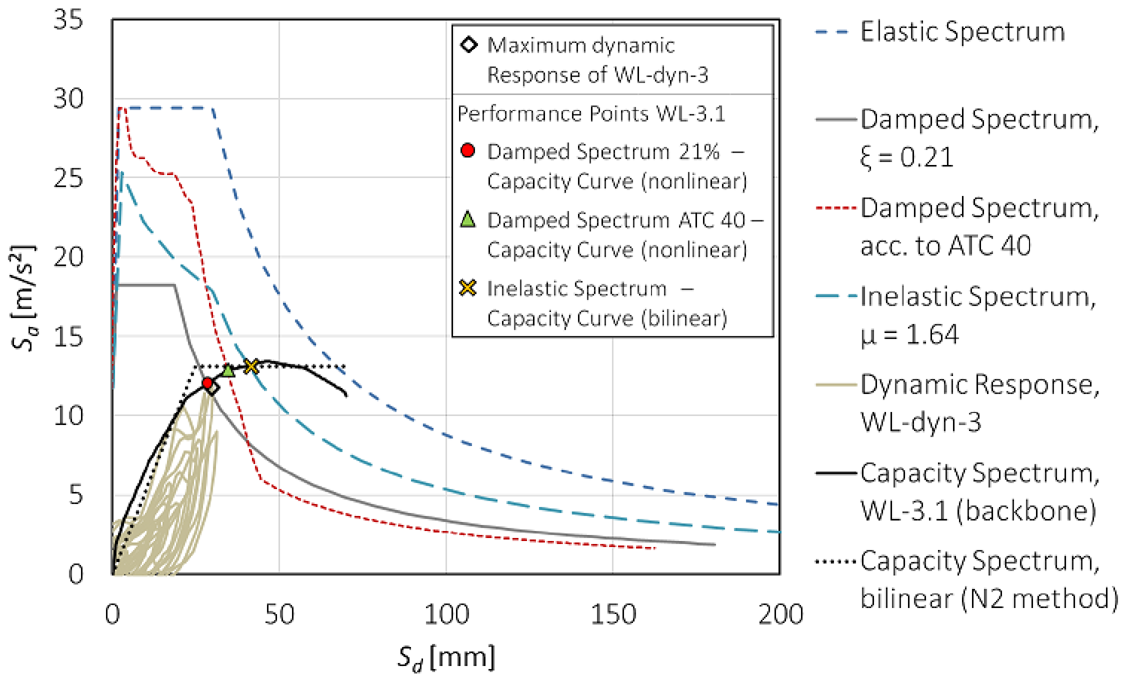

Figure 10. Seimic performance of dynamic test WL-dyn-3 compared with the results of performance-based design from different methods for WL-3.1 (graphical solution).

6 Conclusion

It was found that the values of equivalent viscous damping which are obtained from cyclic testing of light-frame elements do not depend on the displacement amplitude, since they remain fairly constant with increasing deformations. A constant value of equivalent viscous damping for light-frame elements of 0.21 was proposed. The use of constant values for equivalent damping to create damped spectra simplifies the transformation significantly.

Different performance-based design methods were applied to light-frame elements and the results were compared. It was confirmed that performance-based design with constant equivalent damping can lead to suitable results. Different results, especially in respect of the maximum relative displacement, were obtained with the N2 method. The comparison of results from performance-based design with results from dynamic tests exhibits a good agreement with the maximum acceleration, but sometimes deviations in the maximum relative displacement occurred.

It must be noted that the performance-based design with constant equivalent damping seems to underestimate the seismic performance slightly. A better agreement with the performance from dynamic testing can be achieved if a value of 2 % for viscous damping – as proposed by *Filiatrault et al.* (2002) – is considered for the constant damping approach (see section 4.3).

The N2 method is also possibly applicable to timber structures. An adaption of the N2 method is needed in order to consider the typical hysteretic for timber structures.

7 References

ATC-40 (1996): Seismic evaluation and retrofit of concrete buildings. Applied Technology Council. California Seismic Safety Commission. Volume 1.

Chopra, AK (1995): Dynamics of structures (Vol. 3). New Jersey: Prentice Hall.

Chopra, AK & Goel, RK (1999): Capacity-demand-diagram methods for estimating seismic deformation of inelastic structures: SDF systems. Civil and Environmental Engineering, 53.

Eurocode 5 (2004): Design of timber structures - Part 1-1: General and rules for buildings. CEN. (EN 1995-1-1).

Eurocode 8 (2010): Design of structures for earthquake resistance – Part 1: General rules, seismic actions and rules for buildings. CEN. (DIN EN 1998-1).

Eurocode 8/NA (2011): National Annex – Nationally determined parameters – Eurocode 8: Design of structures for earthquake resistance – Part 1: General rules, Seismic actions and rules for buildings CEN. (DIN EN 1998-1/NA).

Fajfar, P (1999): Capacity spectrum method based on inelastic demand spectra. Earthquake Engineering and Structural Dynamics, 28, 979-993.

Fajfar, P (2000): A nonlinear analysis method for performance-based seismic design. Earthquake Spectra, 16, 573-592.

Filiatrault, A & Folz, B (2002): Performance-based seismic design of wood framed buildings. Journal of Structural Engineering, 128(1), 39-47.

Filiatrault, A, Isoda, H & Folz, B (2003): Hysteretic damping of wood framed buildings. Engineering Structures, 25, 461-471.

Fragiacomo, M, Dujic, B & Sustersic, I (2011): Elastic and ductile design of multi-storey crosslam massive wooden buildings under seismic actions, Engineering Structures, 33, 3043-3053.

Freeman, SA (1998): The capacity spectrum method as a tool for seismic design Proceedings of the 11th European Conference on Earthquake Engineering, pp. 6-11.

Freeman, SA (2004): Review of the development of the capacity spectrum method. ISET Journal of Earthquake Technology, 41, 1-13.

ISO 21581 (2010): Timber structures – Static and cyclic lateral load test method for shear walls.

Kawai, N (1999): Application of capacity spectrum method to timber houses. CIB-W18 Graz, Austria.

Miranda, E & Bertero, VV (1994): Evaluation of strength reduction factors for earthquake-resistant design. Earthquake Spectra, 10, 357-379.

Petersen, C (1996): Dynamik der Baukonstruktionen, Vieweg Verlagsgesellschaft.

Priestley, MJN & Kowalsky, MJ (2000): Direct displacement-based seismic design of concrete buildings. Bulletin of the New Zealand National Society for Earthquake Engineering, 33(4), 421-444.

Saiidi, M & Sozen, MA (1979): Simple and complex models for nonlinear seismic response of reinforced concrete structures. University of Illinois Engineering Experiment Station. College of Engineering. University of Illinois at Urbana-Champaign.

Seim, W, Hummel, J & Vogt, T (2014): Earthquake design of timber structures – Remarks on force-based design procedures for different wall systems. Engineering Structures, 76, 124-137.

Seim, W & Hummel, J (2103): Deliverable 2D: CLT wall elements – monotonic and cyclic testing. Technical Report, Department of Structural Engineering, Building Rehabilitation and Timber Engineering, University of Kassel.

Seim, W, Hummel, J & Vogt, T (2013): Deliverable 2C: Anchoring units – monotonic and cyclic testing. Technical Report, Department of Structural Engineering, Building Rehabilitation and Timber Engineering, University of Kassel.

Seim, W & Vogt, T (2013): Deliverable 2B: Timber framed wall elements – monotonic and cyclic testing. Technical Report, Department of Structural Engineering, Building Rehabilitation and Timber Engineering, University of Kassel.

Seim, W & Schick, M (2013): Deliverable 2E: Moment resisting frames – monotonic and cyclic testing. Technical Report, Department of Structural Engineering, Building Rehabilitation and Timber Engineering, University of Kassel.

SIMPSON STRONG-TIE (2011): Qualitätsverbinder für Holzkonstruktionen – Charakteristische Werte nach EC5 und DIN1052.

Vidic, T, Fajfar, P & Fischinger, M (1994): Consistent inelastic design spectra: strength and displacement. Earthquake Engineering and Structural Dynamics, 23, 507-521.

Discussion

The paper was presented by J Hummel

M Popovski received confirmation that light frame and not CLT was shown in slide 7; also 2.8 mm diameter nails 65 mm in length and 75 mm spacing were used in the test. M Popovski commented that μ=1.64 from the data seemed too low.

D Moroder and J Hummel discussed the use of elastic spectrum and equal displacement approach. J Hummel also clarified issues related to rocking in the steel plate and the provision of ball bearing guides.

M Yasumura commented that in Japan a similar approach is available via the BSL using equivalent single mass. Here, long wall would depend on the joint at the end of the panel. Also in multi-story cases, different rotations of wall exist in each story. He asked how one would handle these cases. J Hummel answered that long walls were not considered yet. This could be considered in a model. Also multi-story cases need hold down to confine rotation such that shear would govern. M Yasumura commented that one would need a load displacement relationship and one should model the structure not just the wall. J Hummel agreed.

A Ceccotti stated that the CLT hysteresis loops would depend on different boundary conditions and the vertical load and paper reference on the topic is available.

B Dujič asked if this method would be applicable to timber structures. J Hummel responded that it has the potential to, but they would still need to work on inelastic spectrum for timber structures.

S Winter commented on editorial issues where details about the test specimens should be added. He also questioned the test with gypsum fibre boards and what would be the difference. J Hummel has the gypsum results where higher but similar load characteristics were observed. Also fatigue failures of staples and nails were observed.

WS Chang and J Hummel discussed about the flag shape hysteresis loops for CLT and the real building would behaviour differently because of centring effect. Also shear walls have relatively high equivalent viscous damping and the issue of building information from a wall to the whole structure.

F Lam received clarification the PGA used was 1g and it was chosen to drive the walls into the inelastic range. He commented that the spectrum of time histories looked strange. I Smith discussed about missing wood based material with other material.

B Dujič commented about viscous damping issues. D Moroder and J Hummel discussed the spectrum, time history shifting and scaling procedures.

Simplified Wall Bracing Using Wood Structural Panel Continuous Sheathing

Thomas D. Skaggs, APA – The Engineered Wood Association

Borjen Yeh, APA – The Engineered Wood Association

Edward L. Keith, APA – The Engineered Wood Association (Retired)

Keywords: International Residential Code, Prescriptive Lateral Design, Wall Bracing

1 Introduction

Before the introduction to the inaugural version of the *International Residential Code* (IRC) in 2000, code conforming wall bracing was poorly understood with marginal code compliance in some areas of the United States. The first version of the IRC provided a comprehensive methodology for providing prescriptive wall bracing, including expanding the methods of bracing, and expanding the applicability of the prescriptive provisions. With each triannual update of the IRC, the prescriptive bracing provisions have continued to evolve into very complicated solutions to prescriptively brace walls for wind and seismic loads.

The IRC provisions have raised the awareness to code officials; thus strict compliance to the building code is now being required by jurisdictions throughout the United States. However, the complexity of the residential code makes it difficult for designers and builders to navigate the various options of the IRC. The IRC attempted to address this issue by introducing a simplified wall bracing method in 2012, though this simplified method was still fairly complicated.

Based on a multi-year research and testing initiative carried out by APA, the *APA Simplified Wall Bracing Method* expands on the IRC Simplified Bracing Method to provide an approach to bracing that is even more valuable to builders and building officials by, in many cases, decreasing the amount of required wall bracing and the minimum length of braced wall panels. In addition, the APA Simplified Wall Bracing Method increases the applicability of the IRC simplified wall bracing provisions to as much as 4 times as many house plans, including those with multiple window and door openings on the front and rear elevations.

The Simplified Wall Bracing Method described in this paper is based on APA System Report SR-102 (2015). This methodology provides building officials, builders and designers with an approach and the supporting technical information to meet the requirements of the 2015 IRC Wall Bracing (Section R602.10). The IRC Simplified Wall Bracing has been modified to increase its applicability to a greater percentage of home designs. To achieve broad applicability and acceptance, the system uses the most common type of wall sheathing, wood structural panels, based on their superior structural performance. To provide the user with the greatest possible architectural latitude, SR-102 only covers continuously sheathed wood structural panel bracing (IRC Method CS-WSP) with an increased sheathing thickness (called "Performance Category" in product standards) and a closer nailing schedule on the first story of a two-story structure. This approach increases the performance of the bracing panels on the first story due to the additional restraint provided by the mass and stiffness of the structure above, through strength from increased fastening and with the use of thicker wood structural panel continuous sheathing. This enhanced performance on the bottom story of multi-story structures leads to reduced length of required bracing in these areas, allowing for the method to be used on homes with abundant window and door openings typically found on the front and back elevations. These decreases in the required bracing of multi-story structures are reflected in Table 3.

Design simplification and flexibility are achieved through the enhanced sheathing thickness and nailing described in this paper. Intermittent wood structural panel (Method WSP) and other bracing methods, except as discussed in Section 2.1 of this paper, are outside the scope. Like the IRC simplified bracing method, the APA Simplified Wall Bracing Method may be used for houses located in areas of low to moderate wind and seismicity. To increase the usability of the method, SR-102 includes additional details to augment IRC simplified bracing provisions. Also included are references to specific areas of the IRC and other publications when additional information is required.

Buildings meeting the requirements of SR-102 meet all of the bracing requirements of the 2015 Section R602.10 Wall Bracing with the enhancements discussed in Section 2 of this paper.

2 Methodology

2.1 Applicability

Residential structures must meet all of the following conditions when using this method:

1. The entire building should be continuously sheathed with wood structural panels in accordance with the requirements specified in this section.
2. Other bracing provisions of the 2015 IRC Section R602.10, except as specified herein, are outside the scope of this method.
3. The foundation or basement walls are concrete or masonry, or concrete slab; and the structure above should be 3 stories or less. Permanent wood foundations are beyond the scope of this methodology.
4. Floor cantilevers are not more than 0.61 m (24 inches) beyond the foundation or bearing wall below.
5. Stud wall height is 3.0 m (10 feet) or less when using the minimum required bracing lengths specified in Table 3 of this paper unless adjustments are made for other wall heights up to 3.7 m (12 feet) in accordance with Footnote c to Table 3 in this paper.
6. Roof eave-to-ridge height is 4.6 m (15 feet) or less.
7. Interior finish of exterior walls consist of minimum 12 mm (1/2-inch) gypsum boards installed on the interior side fastened in accordance with IRC Table R702.3.5. Interior gypsum finish is not required on continuously sheathed wood structural panels adjacent to garage openings (Method CS-G) and continuously sheathed portal frame (Method CS-PF) bracing panels (see Section 2.5 of this paper).
8. Design wind speed is 58 m/s (130 mph, Ultimate Design Wind Speed in the 2015 IRC) or less and the Wind Exposure Category is either B or C.
9. Seismic Design Category is either A, B or C for detached one- and two-family dwellings or Seismic Design Category A or B for townhouses.
10. Cripple walls, if present, is considered as the first story of the structure when using this method unless they are designed in accordance with 2015 Section R301.1.2. When the foundation has been engineered/designed to support all of the loads from the structure above, the method described in this paper is appropriate. Such foundation systems may include cripple walls, daylight and pile foundations, and permanent-wood and insulated-concrete-form foundations.
11. Horizontal joint blocking of the bracing panels may be omitted if the amount of bracing on a given wall is 2 times or more than the minimum required amount of bracing derived from Table 3 of this paper after adjustment by the relevant footnotes.

2.2 Circumscribed Rectangle

Traditional wall bracing following the IRC must consider many wall lines, wall line spacing, off-sets in wall lines, lengths of each wall line, and many various multipliers and bracing methods. Figure 1a demonstrates the plan view of a traditional home in North America with the initial layout for resolving the lateral loads. Figure 1b demonstrates the methodology described in this paper using a circumscribed rectangle. The rectangle surrounds all enclosed offsets and projections, such as sunrooms and attached garages, unless an attached garage or portion of the building is to be designed as a separate structure in accordance with IRC Section R301.1.3 or a separate element. SR-102 shows a detailed design example for designing a home in parts of circumscribed rectangles. Open structures, such as attached carports and decks, may be excluded from the rectangle. The rectangle should have no side longer than 18 m (60 feet) and the ratio between the long side and the short side should not exceed 3:1.

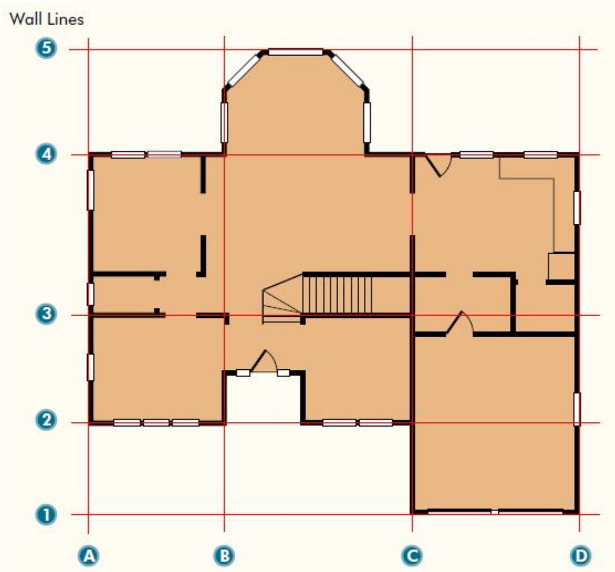

(a)

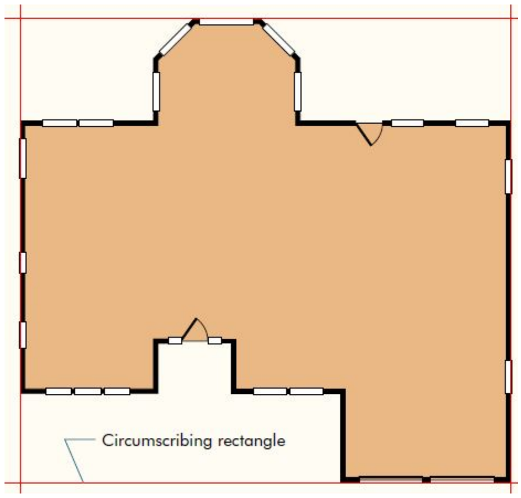

(b)

Figure 1. a.) Traditional wall bracing, b.) simplifed wall bracing.

2.3 Wood Structural Panel Materials

The wood structural panel sheathing is either Rated Sheathing or siding with a minimum 11 mm (7/16 Performance Category), meeting the requirements of DOC PS1 or PS2.

2.4 Wood Structural Panel Attachment

The wood structural panel sheathing is attached to framing in accordance with the following requirements:

1. The wood structural panels should be installed with minimum 8d common nails, 3.3 x 65 mm (0.131 x 2-1/2 inches), spaced at 100 mm (4 inches) on center at panel edges and at 300 mm (12 inches) on center over intermediate

supports. For single-story or the top story of two- or three-story buildings, the panels may be installed with 8d common nails spaced at 150 mm (6 inches) on center at panel edges and 300 mm (12 inches) at intermediate supports.

2. The wood structural panels are applied continuously over all areas of the exterior walls except windows and doors, and including gable ends; and may be installed either vertically or horizontally.
3. All horizontal panel joints should occur over and be nailed to common framing or blocking with an appropriate panel edge-nailing schedule in accordance with IRC Section R602.10.10.
4. Each end of a continuously sheathed braced wall line should have a 0.61 m (24-inch) return corner as defined in IRC Section R602.10.7 or a 3.6-kN (800-lbf) hold-down attached to the end stud of the braced wall panel closest to the corner.
    - If a continuously sheathed braced wall line contains an opening greater than 6 m (20 feet), each end of each resulting braced wall line segment/section should have one of the conditions described above.
    - If a continuously sheathed braced wall line contains two or more offset braced wall line segments/sections as permitted in Section R602.10.1.2, each end of each braced wall line segment/section should have one of the conditions described above.
5. Gypsum wallboard is installed on the opposite side of wall bracing panels. Gypsum wallboard is a minimum of 12 mm (1/2-inch) thick and is fastened with nails or screws in accordance with IRC Table R702.3.5. Exception: Gypsum wallboard may be omitted if the amount of bracing on a given wall is equal to or greater than 1.4 times the minimum required amount of bracing derived from Table 3 of this paper after adjustment by the relevant footnotes.

2.5 "Qualified" Bracing Panel

A single "qualified" bracing panel consist of a full-height portion of an exterior wall continuously sheathed with wood structural panels with a minimum length as shown in Tables 1 and 2 of this paper. The bracing panel should have no openings, except that small drilled holes in the wall sheathing and not penetrating the wall framing up to 38 mm (1-1/2 inches) for the passage of wiring and utilities. When using narrow wall bracing methods, CS-G and CS-PF, the minimum permissible lengths and contributing lengths for computing available bracing is shown in Table 1 of this paper. When using Method CS-WSP, Table 1 provides the minimum permissible lengths and contributing lengths based on both the wall height and the adjacent clear opening height. If an 2.4- or 2.7- m (8-, or 9-foot) tall wall line is present, Method CS-WSP braced wall segments less than the Table 1 minimum length may be used but with a corresponding reduction in contributing lengths for computing available bracing in accordance with Table 2 of this paper.

Table 1. Minimum length of braced wall lines (excerpt from 2015 IRC Table R602.10.5, modified in accordance with R602.12.3).

Method	Adjacent clear opening height (m)	Minimum length (m) Wall height 2.4 m	2.7 m	3.1 m	Contributing length (m)
CS-G	--	0.61	0.69	0.76	actual length[(a)]
CS-PF[(c)]	--	0.41[(b)]	0.46[(b)]	0.51[(b)]	1.5 x actual length[(a)]
CS-WSP	≤ 1.63	0.61	0.69	0.76	Actual length[(a)]
	1.73	0.66	0.69	0.76	
	1.83	0.69	0.69	0.76	
	1.93	0.76	0.74	0.76	
	2.03	0.81	0.76	0.76	
	2.13	0.89	0.81	0.81	
	2.24	0.91	0.89	0.84	
	2.34	0.91	0.91	0.89	
	2.44	0.91	0.91	0.91	
	2.54 – 2.74	--	0.91	0.91	
	2.84 – 3.05	--	--	0.91	

(39.4 in. = 1 m)

(a) Use the actual length when it is greater than or equal to the minimum length

(b) The wall height for CS-PF is based on the height of the portal frame, as documented in Keith (2014). The height of the portal frame is measured from the bottom plate to the top of the portal frame header.

(c) See IRC Figure R602.10.6.4.

2.5.1 Partial Credit for CS-WSP Panels

CS-WSP panels in 2.4- or 2.7-m (8- or 9-foot) tall walls between 0.51 and 0.61 m (20 and 24 inches) in length that do not meet the minimum length requirements of Table 1 may be used as bracing units at a full or reduced contributing length (depending on the adjacent opening height), as shown in Table 2 of this paper based on the latest APA research results, as documented in Keith (2012a and 2012b).

Table 2. Partial credit for CS-WSP less than full length with 2.4- or 2.7-m (8- or 9-foot) tall walls[(a)].

Wall Height (m)	Length of full height Method CS-WSP Panel (m)	Adjacent to a clear opening height (m) or less	Contributing length of braced wall panels (m)
2.4 or 2.7	0.61	≤ 1.55	0.61
		1.63	0.56
		1.73	0.51
		1.83	0.46
		1.93	0.41
		2.03	0.36
	0.51	≤ 1.55	0.51
		1.63	0.46
		1.73	0.41
		1.83	0.38
		1.93	0.33
		2.03	0.28

(39.4 in. = 1 m)

(a) Linear interpolation may be used

2.6 Computing “Qualified” Wall Bracing Length

Within an exterior wall, only those full-height wall panels with a length greater than or equal to the lengths specified in Tables 1 and 2 of this paper is deemed to contribute to resisting lateral load, and counted toward the required bracing length. The total bracing length contributing to the side of a rectangle is equal to the sum of the contributing lengths of each “qualified” wall panel. Any length of a “qualified” bracing panel over the minimum bracing length required in Table 1 of this paper may be used toward the total bracing length required for that side of the rectangle. Thus, if the minimum requirement for a specific method is 0.61 m (24 inches) in accordance with Table 1 of this paper and two such panels with lengths of 0.66 and 0.86 m (26 and 34 inches) are present, (0.66 + 0.86 =) 1.5m (60 inches) of bracing are present and should be used in determining the total bracing length for that wall.

For Methods CS-G and CS-PF, the bracing length on either side of the opening is considered a “qualified” bracing panel and contributes to bracing lengths for meeting the minimum length requirements of Table 1 of this paper. Examples of utilizing this simplified approach are demonstrated in the Appendix to SR-102 (APA, 2015).

2.7 Length of Bracing Required

Determining the minimum bracing length required is relatively straightforward:

1. Circumscribe the building with a rectangle. The rectangle encloses the maximum building length and width dimensions as described in Section 2.2.

2. Ensure that the long side of the rectangle is not greater than 3 times the short side of the rectangle or greater than 18 m (60 feet). If it is greater, consider using the multiple rectangle method covered in Appendix A of SR-102. The alternatives are to:
   - Use the "legacy" bracing provisions of IRC Section R602.10,
   - Use the multiple rectangle method in conjunction with the APA Simplified Wall Bracing Method (see Appendix A or SR-102), or
   - Have the structure designed in accordance with IRC Section R301.1.3 and the International Building Code (IBC).
3. With the dimensions of this circumscribed rectangle, use Table 3 of this paper to determine the bracing length that is required on each rectangle side *perpendicular to the side used to enter the table*. Note that interpolation may be used. Either value, the rounded or interpolated value, is multiplied by a wall height adjustment factor in accordance with Footnotes (c) and (d) to Table 3 of this paper, as applicable.
4. Parallel wall lines within 1.2 m (4-feet) of each other are considered the same wall line when following the Distribution Rules of Section 2.8 of this paper.

2.8 "Distribution Rules" for Bracing Panels

Once the required minimum bracing length has been determined for each side of the circumscribed rectangle using Table 3 of this paper, this bracing length is distributed along the actual exterior walls of the structure. In distributing these bracing panels, all of the following "Distribution Rules" should be met:

1. The first "qualified" bracing panel on each side of the rectangle begins within 3.7 m (12 feet) of the wall corner. The 3.7 m is measured between the wall corner and closest edge of the first full-height "qualified" bracing panel.
2. The distance between the closest edges of adjacent full-height "qualified" bracing panels is 6.1 m (20 feet) or less.
3. Any exterior wall with a length of 2.4 m (8 feet) or greater, when used as bracing, should have a minimum of 0.91 m (3 feet) of bracing.

In some cases, a greater bracing length is required to meet the Distribution Rules than is required by Table 3. In this case, the greater bracing length required by the Distribution Rules governs. In any cases, the bracing length required by Table 3 or the Distribution Rules, whichever is greater, should be met.

If the upper and lower stories share common exterior wall lines and the amount of bracing on the second floor equals or exceeds the amount of bracing located on the story immediately below, and the distribution rules of Section 2.8 for all such stories are met, only the bracing in the bottom story must be checked. If the bottom story checks out, the upper stories will be acceptable as well.

Table 3. Minimum required bracing length on each side of the circumscribed rectangle for wind exposure B [(a)(b)(c)(d)]. (Table provides required bracing amount for walls perpendicular to the maximum bracing length used to enter the table.)

Wind Speed	Story Level	Eave-to Ridge Height (m)	Minimum required bracing length on each long/short side (m) – Length of short/long side (m): 3.0	6.1	9.1	12.2	15.2	18.3
51 m/s (115 mph) ultimate based on 2015 IRC		3.0	0.61	1.07	1.52	1.83	2.29	2.74
	 (e)		0.88	1.65	2.26	3.02	3.66	4.27
	 (e)		1.25	2.41	3.41	4.42	5.43	6.40
		4.6	0.79	1.40	1.98	2.38	2.99	3.57
	 (e)		1.01	1.89	2.59	3.47	4.21	4.91
	 (e)		1.37	2.65	3.75	4.88	5.97	7.04
58 m/s (130 mph) ultimate based on 2015 IRC		3.0	0.76	1.22	1.83	2.29	2.90	3.35
	 (e)		1.13	2.01	2.77	3.66	4.54	5.33
	 (e)		1.52	2.90	4.15	5.43	6.68	7.80
		4.6	1.01	1.58	2.38	2.99	3.78	4.36
	 (e)		1.31	2.32	3.20	4.21	5.21	6.13
	 (e)		1.68	3.20	4.57	5.97	7.35	8.60

(39.4 in. = 1 m)

(a) Based on IRC Table R602.10.3(1) and modified in accordance with Keith (2011).

(b) Interpolation may be used.

(c) The Wall Height Adjustment Factor, as shown below, is used to multiply the minimum bracing lengths listed in the table above to accommodate wall heights from 2.4 to 3.7 m (8 to 12) feet based on IRC Table R602.10.3(2). Interpolation may be used.

	Wall Height (m)	Wall Height Adjustment factor
Any Story	2.4	0.90
	2.7	0.95
	3.0	1.00
	3.4	1.05
	3.7	1.10

(d) For Wind Exposure Category C, multiply length required from table above by 1.2 for single-story buildings, 1.3 for two-story buildings and 1.4 for three-story structures.

(e) The first story of two stories and the first and second of three stories should be continuously sheathed with wood structural panels attached with 8d common nails, 3.3 x 65 mm, (0.131 x 2-1/2 inches) spaced 100 mm (4 inches) on center around the panel perimeter and at 300 mm (12 inches) on center over intermediate supports.

3 Lateral Support

For bracing panels in exterior walls located along eaves where the distance between the top of the top plates to the underside of the roof sheathing is 0.23 m (9-1/4 inches) or less, blocking between the rafters or trusses is not required. When the distance between the top of the top plates to the underside of the roof sheathing above braced walls is greater than 0.24 m (9-1/4 inches) and less than 0.39 m (15-1/4 inches), attachment should be in accordance with IRC Section R602.10.8.2, item 1. These details are not duplicated here because they vary slightly between different editions of the IRC and because the 0.39 m (15-1/4 inches) limitation is not commonly exceeded.

If the vertical distance between the underside of the roof sheathing and the top of the top plate is greater than 0.39 m (15-1/4 inches), or if the user wants to use the wall sheathing to block raised-heel trusses to meet the wind uplift and lateral load requirements of IRC sections R602.3.5 and R602.10.2.1, see APA System Report SR-103, for more information.

4 Limitations

Recommendations provided in this paper are subject to the following conditions:

1. The exterior walls of the structure is continuously sheathed with a minimum 11 mm (7/16 Performance Category) wood structural panel sheathing or siding meeting the requirements of DOC PS1 or PS2 and is attached to framing with 8d common nails, 3.3 x 65 mm, (0.131 x 2-1/2 inches) at 100 mm (4 inches) on center around the panel perimeter and at 300 mm (12 inches) on center over intermediate supports. For exterior walls in single story structures or in the top story of multi-story structures the 8d common nails are spaced at 150 mm (6 inches) on center around the panel perimeter and at 300 mm (12 inches) on center over intermediate supports.
2. The APA Simplified Wall Bracing Method is applicable to buildings of no more than three stories, subject to the applicability listed in Section 2.1 of this paper.
3. When placed over masonry or concrete stem walls, wall bracing panels used in the APA Simplified Wall Bracing Method must meet the requirements of IRC Section R602.10.9.
4. While the APA Simplified Wall Bracing Method is not part of the code, it is based on the code and other modifications permitted by IRC Sections R301.1.3 Engineering Design. Further modifications to the APA Simplified Wall Bracing Method by the user of this paper are beyond the scope of this paper.
5. The basis for this paper, APA System Report SR-102 is subject to periodic review. The latest copy of SR-102, in imperial units, is available for download at www.apawood.org/resource-library.

5 References

APA. 2015. APA simplified wall bracing method using wood structural panel continuous sheathing, APA System Report – SR-102C, APA – The Engineered Wood Association, Tacoma, WA

APA. 2014. Use of wood structural panels for energy-hell trusses, APA System Report – SR-103A, APA – The Engineered Wood Association, Tacoma, WA

AWC. 2015. Wood frame construction manual for one and two family dwellings (WFCM), American Wood Council, Leesburg, VA.

ICC. 2015a. International building code (IBC), International Code Council, Falls Church, VA.

ICC. 2015b. International residential code (IRC), International Code Council, Falls Church, VA.

Keith, E. L. 2011. Wall bracing capacity enhanced due to partial restraint, APA Report T2011L-33, APA – The Engineered Wood Association, Tacoma, WA

Keith, E. L. 2012a. Narrow wall bracing. APA Report T2012L-16, APA – The Engineered Wood Association, Tacoma, WA

Keith, E. L. 2012b. Narrow wall bracing – eight-foot tall walls, APA Report T2012L-16, APA – The Engineered Wood Association, Tacoma, WA

Keith, E. L. 2014. Portal frame aspect ratio, APA Report T2014L-39, APA – The Engineered Wood Association, Tacoma, WA

Discussion

The paper was presented by T Skaggs

I Smith received confirmation that there are plan limitations for diaphragm and wall to match each other.

G Schickhofer asked if it would be possible to introduce CLT with this approach. T Skaggs responded yes and that it could be possible although the market demand in N America for CLT in residential construction is low.

A Salenikovich asked if calculation tools would be available. T Skaggs said yes but the calculations are so simple that the tools would not really be needed.

W Seim and T Skaggs discussed how to deal with symmetrical and asymmetrical cases where location of the bracing elements would have to be within certain distance of the centre of the building plan.

F Lam and T Skaggs discussed consideration of CLT for tornado resistance structures although tornado forces are not considered in N American codes. Here, CLT for safe room tornado has been considered.

Structural characterization of multi-storey CLT buildings braced with cores and additional shear walls

Andrea Polastri, Research Associate, Trees and Timber Institute - National Research Council of Italy (CNR IVALSA), Via Biasi 75, 38010 San Michele all'Adige (TN), Italy

Luca Pozza, Ph.D., Department of Civil, Environmental and Architectural Engineering, University of Padova, via Marzolo, 9, 35131 Padova, Italy

Cristiano Loss, Research Fellow, Department of Civil, Environmental and Mechanical Engineering, University of Trento, via Mesiano 77, I-38123 Trento

Ian Smith, Professor Emeritus, Faculty of Forestry & Environmental Management, University of New Brunswick, Canada

Keywords: CLT structures, core structures, seismic design, shear walls

1 Introduction

In last twenty years the CLT panels have become widely employed to build multi-storey residential and mercantile buildings. These buildings are often characterised by the presence of many internal and perimeter shear walls. Such structures have been widely studied through experimental and numerical simulation methods. The most comprehensive experimental investigation to date on seismic behaviour of CLT buildings was carried out by CNR–IVALSA, Italy, under the SOFIE Project (Ceccotti 2008, Ceccotti et al. 2013). Other important investigations have been conducted at the University of Trento, Italy (Tomasi and Smith 2015). European seismic performance related tests have also been conducted at the University of Ljubljana, Slovenia where the behaviour of 2-D CLT shear walls with various load and boundary conditions were assessed (Dujic et al. 2005). FPInnovations in Canada has undertaken tests to determine the structural properties and seismic resistance of CLT shear walls and small-scale 3-D structures (Popovski et al. 2014). Those and other studies have enabled characterisation failure mechanisms in large shear wall systems (Pozza et al. 2013). Multi-storey building superstructures in which beam-and-column frameworks resist effects of gravity loads and cross-braced or core substructures and exterior CLT shear walls resist effects of lateral forces from earthquakes or wind have been found structurally effective, and fail in predictable stable ways if overloaded (Smith et al. 2009). Advantages of such systems can include creation of large open interior spaces, high structural efficiency, and material economies.

Recently innovative connection solutions that create discrete panel-to-panel, or panel-to-other material joints have been developed in Italy (Polastri and Angeli 2014). The method results in point-to-point mechanical connections that only connect corners of individual CLT panels in ways that fulfil hold-down and lateral shear resistance functions (Gavric et al. 2013). This has the advantage of making the load paths within superstructures unambiguous. Different connectors have also been tested to find the best ways to make point-to-point connections between CLT panels and steel structures (Loss et al. 2014).

During recent years connector designs had evolved considerably making them suitable for much large systems that place high capacity demands on connections, with emphasis on requirements for high seismicity areas (Polastri et al. 2014). During such development attention was paid to avoiding the possibility of brittle behaviour of joints to CLT panels having many nails.

Structural performance issues not fully studied are those related to using CLT building cores as replacements for one constructed from reinforced concrete or masonry. Pertinent issues relate to vertical continuity between storeys, connections between building core elements and elevated floors, and building core-to-foundation connections.

2 Mechanical characterization of the connectors

2.1 Experimental studies

The mechanical behaviour of connection systems for CLT structures that employ thin metal elements fastened to panels with nails or other slender metal fasteners is well known, as demonstrated by numerous scientific papers (Ceccotti et al. 2008, Pozza et al. 2013). The behaviour of such connectors is determined largely by the elastoplastic response of the fasteners, and to a lesser extent by the response of steel elements. Stiffness and capacity values implemented into the numerical models described in Section 4 were calculated directly from experimental data.

The first study was carried out at CNR-IVALSA (Gavric et al 2011), the second study at the University of Trento (Tomasi and Smith 2015). In both cases tests were conducted according to the European standard EN 12512 (CEN 2006). The CEN 2006 protocol provides a load history characterized by load cycles of increasing intensity and is intended to apply to structures in seismic regions. As suggested by the standard, a preliminary monotonic test was undertaken to define the magnitudes of cyclic load excursions, Figure 1.

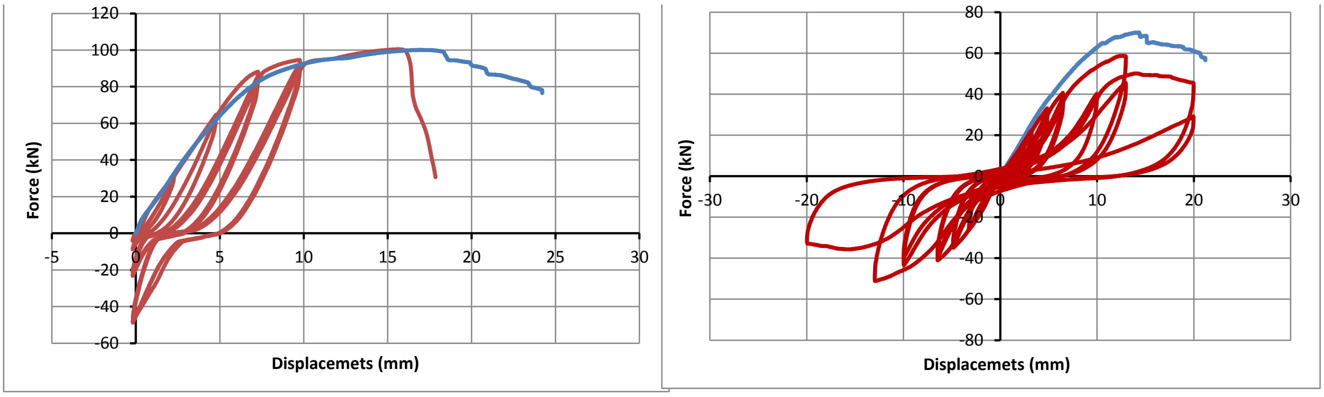

Figure 1. Typical tests results: hold-down (left) and angle bracket (right)

Initial stiffness was calculated according to 'method b' specified by EN 12512 that permits description of the mechanical behaviour of trends representing elastic phase and post-elastic phase responses (Piazza et al. 2011). However, as this paper deals with Linear Dynamics Analysis of superstructure systems only the parameters that characterize the elastic properties of connections (k_{test}) and the maximum load at failure (F_{max}) are reported here, Table 1.

2.2 Analytical definition of stiffness according to Eurocode 5

The Finite Element (FE) model presented in Section 4 implements hold-down Rothoblaas WHT 620 (EOTA 2011) and angle brackets TITAN TTF200 (EOTA 2012) connectors joined to CLT panels manufactured from class C24 wood boards using 32 4x60 or 30 4x60 Anker nails. The initial stiffness of connectors was calculated taking into account the stiffness of the steel-to-timber nailed joints in shear and hold-down connections. Deformation of steel parts within the connections are very small, compared deformation of nailed joints, and was therefore neglected. Characteristic load-carrying capacities, $F_{v,Rk}$, and slip moduli, k_{ser}, were calculated based on Eurocode 5 (CEN 2014), Table 1.

Table 1. Experimental and Eurocode 5 derived connection properties

Connection type	Elastic stiffness (kN/mm)		Capacity (kN)	
	Test (k_{test})	EC5 (k_{ser})	Test (F_{max})	EC5 ($F_{y,Rk}$)
TITAN TTF 200	8.2	23.1	70.1	35.5
WHT 620	12.1	24.8	100.1	85.2

3 Estimation of T_1 and design of connections

A crucial issue in the design of a CLT building under horizontal seismic action, is the definition of the principal elastic vibration period (T_1) of an entire superstructure (CEN 2013). Such vibration period depends on the mass distribution and on the global stiffness of the buildings. In a CLT structure the global stiffness of the buildings is highly sensitive to deformability of the connection elements (Pozza et al. 2013). Consequently for a precise control of the vibration period of the building it is crucial to define the stiffness of each connections used to assemble a superstructure. During design engineers are required to solve iteratively to find the principal natural frequency ($f_1 = 1/T_1$) using a scheme such as that in Figure 2. Under the shown scheme: (1) the stiffness of the connections influences the global stiffness of the building and therefore its principal elastic period; (2) the external force induced by earthquake in each connection is a function of the principal vibration period; (3) the load bearing capacity of the connection must be compatible with the external force; (4) the strength and the stiffness of the connection are linked through the effective number of fasteners.

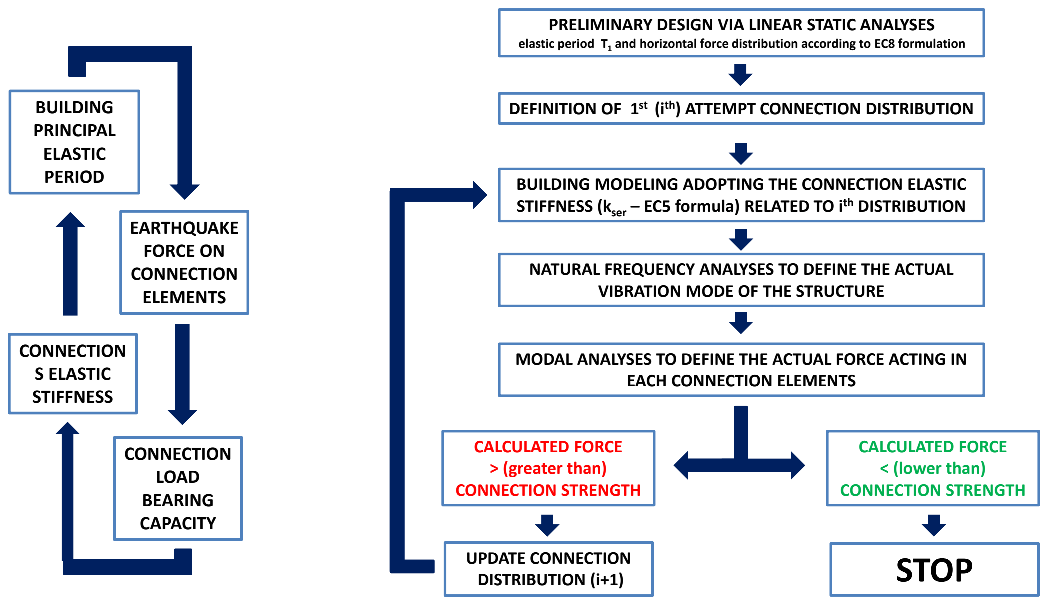

Figure 2. Calculation process for design of connections

An efficient approach to design a CLT structure is to start from a preliminary definition of the external force induced by earthquake in each wall panel according to the common equivalent static force linear static analysis approach (CEN 2013). This does not involve the definition of T_1 accounting for effects of connection stiffness. Once static forces on each CLT wall panel are defined connection capacities can be designed to be compatible with external static forces. This allows estimation of the connection elastic stiffness (k_{test} or k_{ser}), and therefore realistic preliminary estimation of T_1. Then T_1 can be in modal analyses to calculate the effective forces induced in connections by earthquakes. Obtained connection forces may or may not be compatible with the connection strength, and if not it is necessary to redesign connections. Afterward it is possible to perform a more iterative precise frequency analyses until solutions, including connection designs, are convergent.

4 Numerical analysis of core tall buildings

The behaviour of multi-storey buildings braced with cores and CLT shear walls is examined using numerical modal response spectrum analyses, with connection properties calibrated based Eurocode 5 (CEN 2014) and experimental test discussed in Section 2. Analyses followed the scheme in Figure 2 and are presented in terms of principal elastic periods, base shear and up-lift forces, and inter-storey drift.

4.1 Case study buildings

The aim is to characterize behaviour of multi-storey CLT buildings braced with cores and additional shear walls from the seismic design perspective based on effects of varying design parameters. Varied design parameters are: number of storey (3-5-8), lateral shear wall panels width, construction methodology, and regularity of connectors as a function of the height within a superstructure, Table 2.

Table 2. Examined building configuration

Case study ID	3(5-8) A R	3(5-8) A I	3(5-8) B R	3(5-8) B I	3(5-8) C R
Graphical schematization of building cores (ex. 3-storey case)	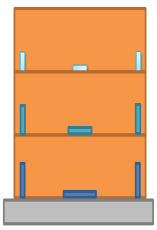	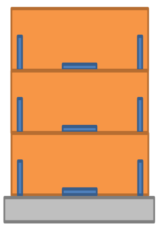	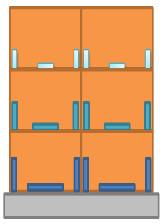	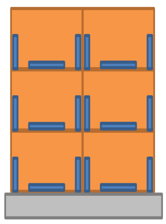	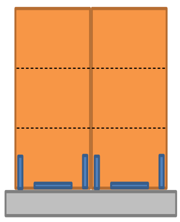
Panel assembly	Joint free wall panels		Jointed wall panels		Joint free wall panels
Elevation regularity	Regular	Irregular	Regular	Irregular	Regular
Construction methodology	Platform System				-

4.1.1 Geometric configurations

Examined case-study building superstructures have footprint dimensions of 17.1m (direction X) by 15.5m (direction Y). Seismic Force Resistant Systems (SFRS) include a building core that is 5.5m by 5.5m on plan, and partial perimeter shear walls constructed from CLT panels with a total base length of 6m, Figure 3. Storey height is 3m in all cases, resulting in total superstructure heights of 9m, 15m and 24m respectively. All CLT panels in the core walls have a thickness of 200mm. CLT panels in perimeter shear walls are 154mm thick, except for those in the lowest four storeys of the 8-storey SFRS which are 170mm thick. Floor diaphragms are composed of 154mm CLT panels in all cases.

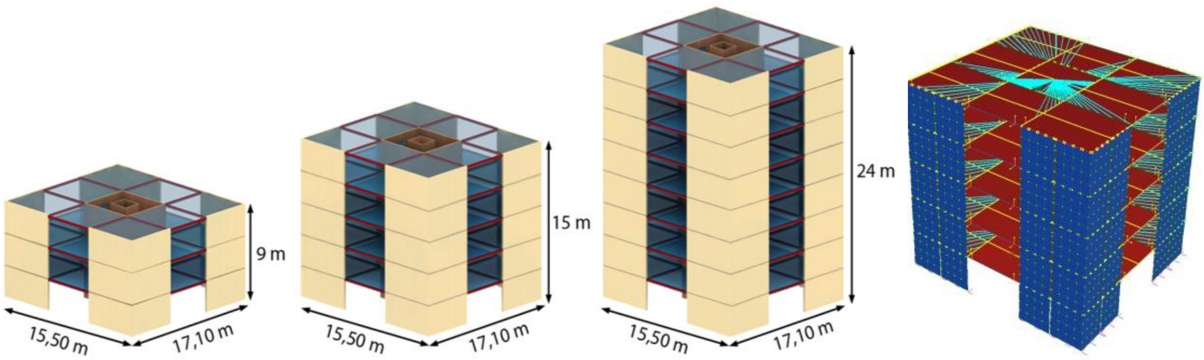

Figure 3. SFRS wall configurations of case study buildings (left) and typical FE model (right)

4.1.2 Design method

The earthquake action for these case study buildings was calculated according to Eurocode 8 (CEN 2013) and the associated Italian regulations (MIT 2008) using design response spectra for building foundations resting on ground type C*, assuming the PGA equal to 0.35g (the highest value for Italy) with a building importance factor of $\lambda = 0.85$. [*Deep deposits of dense or medium dense sand, gravel or stiff clay with thickness from several tens to many hundreds of meters]. The seismic action was calculated starting from the elastic spectra and applying an initial q-reduction factor of 2 (CEN 2014). The coefficient k_r was taken equal to 1.0 for regular configurations and 0.8 for non-regular configurations. Figure 4 shows the adopted design spectra and other relevant design parameters. The figure shows T_1 values determined by simplified formula and numerical frequency analyses methods for configurations A R 3-5- 8.

Connections were first designed using the force pattern obtained applying linear elastic static analysis (CEN 2013) and the seismic action defined by taking $T_1 = T_{1\_EC8}$. Connection designs were then refined using the rotation and translation force equilibrium approach described by Gavric et al. (2011) and Pozza and Scotta (2014) and the iterative design process in Figure 2.

seismic area	zone 1
soil type	C
Peak Ground Acceleration	0.35 g
q_0 (behaviour factor)	2
k_R (regular configuration)	1
λ (importance factor)	0.85

	3 A R	5 A R	8 A R
H [m]	9	15	24
$T_{1\_EC8} = 0.05\ H^{3/4}$ [s]	0.26	0.38	0.54
M [t]	276	482	800
$S_{d\text{-}el\,(T1)}$ [ag/g] *	0.82	0.82	0.78
$q = k_R\ q_0$	2	2	2
$S_{d\,(T1)}$ [ag/g] *	0.41	0.41	0.39

**using elastic period evaluated via code (CEN 2013)*

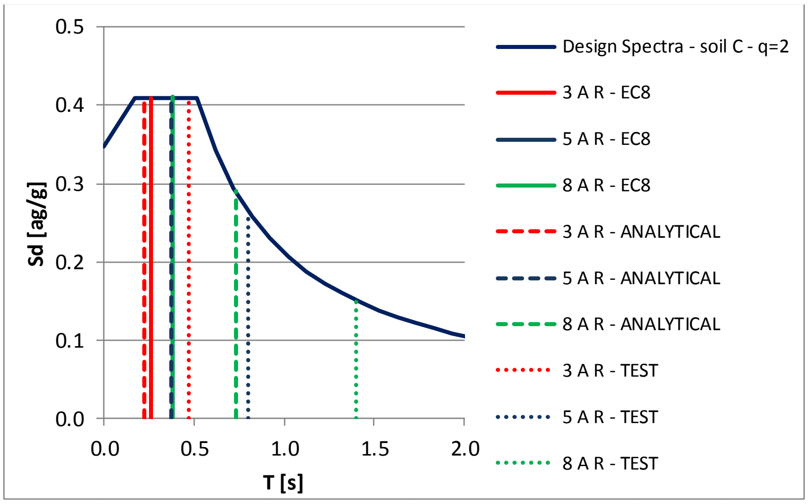

Figure 4. Input data for seismic analysy (left); design spectra and calculated periods (right)

4.1.3 Finite element (FE) models

Numerical models of the investigated building were realized using the finite-element code Strand 7 (2005). The illustrative FE model in Figure 3 (right) uses linear elastic shell elements to represent CLT panels and link elements to simulate the elastic stiffnesses of connectors. Beam elements with pinned end conditions were used to represent beam members interconnecting perimeter shear walls and shear walls in the building core at the top of each storey. Horizontal slabs elements in floor and roof diaphragms were assumed to be rigid in-plane.

All the 15 building configurations have been modelled respecting the geometrical features and connection stiffnesses in Tables 1 and 2.

4.2 Analysis results

Results presented here were obtained by modal response spectrum analyses of case study buildings, Tables 3 to 6 and Figure 5. Those tables and figure show calculated building principal elastic periods (T_1), base shear forces (v) on angle brackets at the Ultimate Limit State (ULS), uplift forces on base hold-down anchors at ULS (N), and the maximum inter-storey drift values (δ) at Damage Limitation State (DLS). The alternative values given represent effects of taking connection stiffnesses (k_{conn}) equal to values derived from Eurocode 5 (k_{ser}) versus values derived from experiments (k_{test}). Plus in the case of T_1, the simple formula value T_{1_EC8} is included (CEN 2013). Inter-storey drift was calculated for each case study building using the Modal Response Spectrum Analyses and the DLS design spectrum.

Table 3. Predicted principal elastic periods (T_1)

[s]	3AR	3AI	3BR	3BI	3CR	5AR	5AI	5BR	5BI	5CR	8AR	8AI	8BR	8BI	8CR
T_{1_EC8}	0.26	0.26	0.26	0.26	0.26	0.38	0.38	0.38	0.38	0.38	0.54	0.54	0.54	0.54	0.54
$T_{1\_kconn.\ =\ kser}$	0.22	0.19	0.22	0.20	0.18	0.37	0.34	0.38	0.35	0.30	0.73	0.69	0.73	0.68	0.50
$T_{1\_kconn.\ =\ ktest}$	0.47	0.39	0.44	0.37	0.33	0.80	0.61	0.73	0.57	0.45	1.40	1.14	1.30	1.08	0.66

Table 4. Predicted base shear per unit of length (v)

[kN/m]	3AR	3AI	3BR	3BI	3CR	5AR	5AI	5BR	5BI	5CR	8AR	8AI	8BR	8BI	8CR
$v_{\_kconn.\ =\ kser}$	28.2	33.2	32.7	40.3	35.8	42.3	51.7	51.8	64.2	50.4	50.2	64.6	61.6	82.6	79.7
$v_{\_kconn.\ =\ ktest}$	28.1	34.9	33.4	36.4	29.2	29.7	49.3	38.4	58.4	50.5	34.0	47.4	42.7	76.3	61.6

Table 5. Predicted free edge base uplift forces (N)

[kN]	3AR	3AI	3BR	3BI	3CR	5AR	5AI	5BR	5BI	5CR	8AR	8AI	8BR	8BI	8CR
$N_{\_kconn.\ =\ kser}$	128.1	170.9	152.0	178.1	161.3	316.0	420.6	355.4	447.3	373.2	511.6	884.1	559.5	759.7	897.0
$N_{\_kconn.\ =\ ktest}$	138.5	185.7	149.4	232.1	138.5	246.2	403.8	260.1	455.7	366.9	334.4	527.3	339.5	516.1	678.8

Table 6. Predicted maximum inter-storey drift (δ)

[mm]	3AR	3AI	3BR	3BI	3CR	5AR	5AI	5BR	5BI	5CR	8AR	8AI	8BR	8BI	8CR
$\delta_{\_kconn.\ =\ kser}$	2.9	1.8	2.5	1.9	1.4	5.6	4.4	5.1	4.3	2.6	9.9	8.8	8.8	7.8	4.7
$\delta_{\_kconn.\ =\ ktest}$	12.3	7.8	10.9	6.8	3.8	15.6	9.7	14.0	8.8	5.1	21.3	13.9	18.5	12.4	5.6

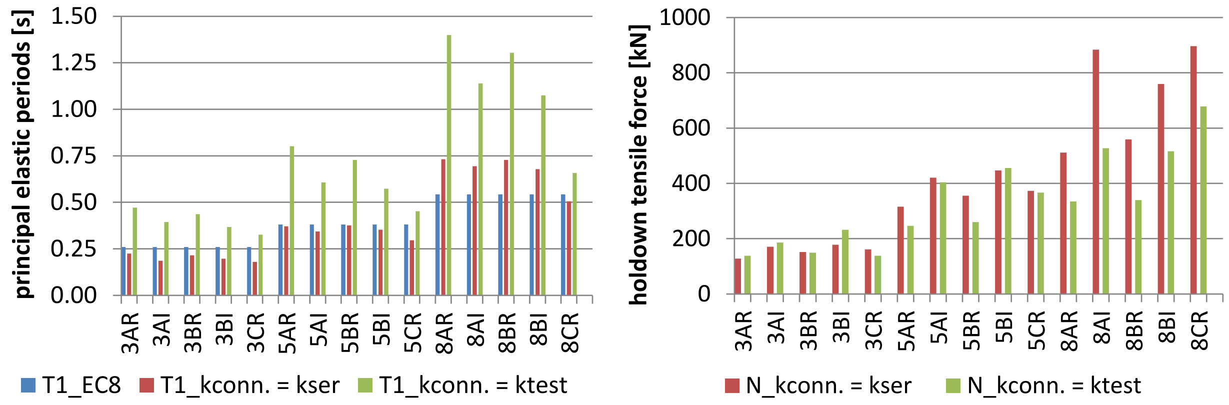

Figure 5. Comparison of estimates of principal elastic periods and base free edge uplift forces

Observing Figure 5 it is apparent that can be seen that in most cases use of experimental connection stiffnesses (k_{conn} = k_{test}) leads to much larger T_1 values than those predicted based Eurocode 5 based estimates of connection stiffnesses (k_{conn} = k_{ser}). Similarly using the simple formula given by Eurocode 8 leads to low estimates of T_1 values. Interestingly use of Eurocode 5 based estimates of k_{conn} results is estimates of

T_1 relatively close to simple formula values. However results suggest that neither of those approaches are reliable ways of estimating principal natural periods of buildings having SFRS consisting of CLT cores and perimeter shear walls. Consequences of discrepancies in k_{conn} values from those found by testing varied in their effects on v, N and δ values, but in general results show that how connection stiffnesses are estimated can alter design force and lateral drift estimates by substantial amounts. For example, estimates of δ were especially sensitive for eight-storey buildings.

It is important to underline that the adopted FE model is a limiting condition representing the maximum deformability of the system since the interaction between the orthogonal walls and the out of plane stiffness, provided by the interposed floor slabs, are neglected. On the other hand, FE models did not take into account nonlinear deformability or large displacements effects.

It is possible to achieve large vertical reaction forces using a group of hold-down anchors working “in parallel”. To obtain the required uplift force resistances, that can be greater than 600kN (configuration 8CR), it is necessary to use more than eight hold-down anchors; however it is not demonstrated that the hold downs, disposed in the aforementioned group configuration, are able to spread the total force between the different reaction elements.

5 Connection solutions for innovative diaphragms

Diaphragms are an integral part of the building any SFRS and if they have high stiffness and capacity any non-linear behaviour of the entire structure is primarily defined by the response of the vertical bracing elements and complexity of the seismic analysis is reduced. CLT multi-storey buildings are erected using panels with limited dimensions because of production and transportation limitations (FPInnovations 2011). In floors and roofs, the different CLT panels are commonly joined together at the edges using dowel-type mechanical fasteners like self-tapping screws, Figure 6 (left).

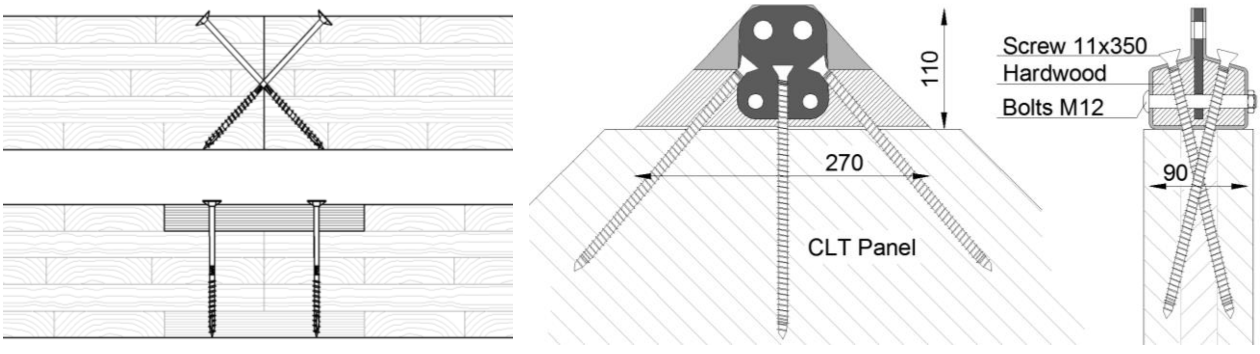

Figure 6. Typically floor-floor panel connections (left) and new X-RAD connector (right)

The in-plane behaviour of the horizontal floors constructed from CLT panels and connections is mainly affected by the response of panel-to-panel connections, with the overall length-to-width ratio of the floor and aspect ratio of the CLT panels playing primary role (Ashtari et al. 2014). More generally, the in-plane behaviour of CLT floors depends on the building system, the location of the bracing walls and their stiffnesses (Loss et al. 2015). For multi-storey CLT buildings with cores and additional perimeter shear walls the construction system varies significantly compared to other common CLT structures. In such cases the mechanism of deformation of the floors under in-plane actions can increase the level of shear forces in the connections, due to the distance between the supports and the number and placement of shear walls around the perimeter of the building. Consequently standard connection techniques for CLT elements can be inadequate in terms of capacity and special high performance connections are then required, e.g. Figure 6 (right). Discussion here addresses use of two innovative high-capacity connection technologies suitable for the purpose.

Figure 7 (left) shows a slab made of CLT panels joined together by steel beams, with the beam-to-panel connections designed and engineered from the perspectives of mechanical behaviours of the materials, installation tolerances, feasibility of on-site assembly, and cost. The load-slip curve (F-δ) for these connections measured by tests is shown in Figure 7 (right) based on Loss et al. (2014). The operating principle of such floors is similar to a truss system in which each pair of steel beams is braced by the CLT panel and related to characteristics of the beam-to-panel connections. In Figure 7 it is presented a beam-to-panel connection solution obtained by the use of steel plates welded to the beam and glued to the CLT panel.

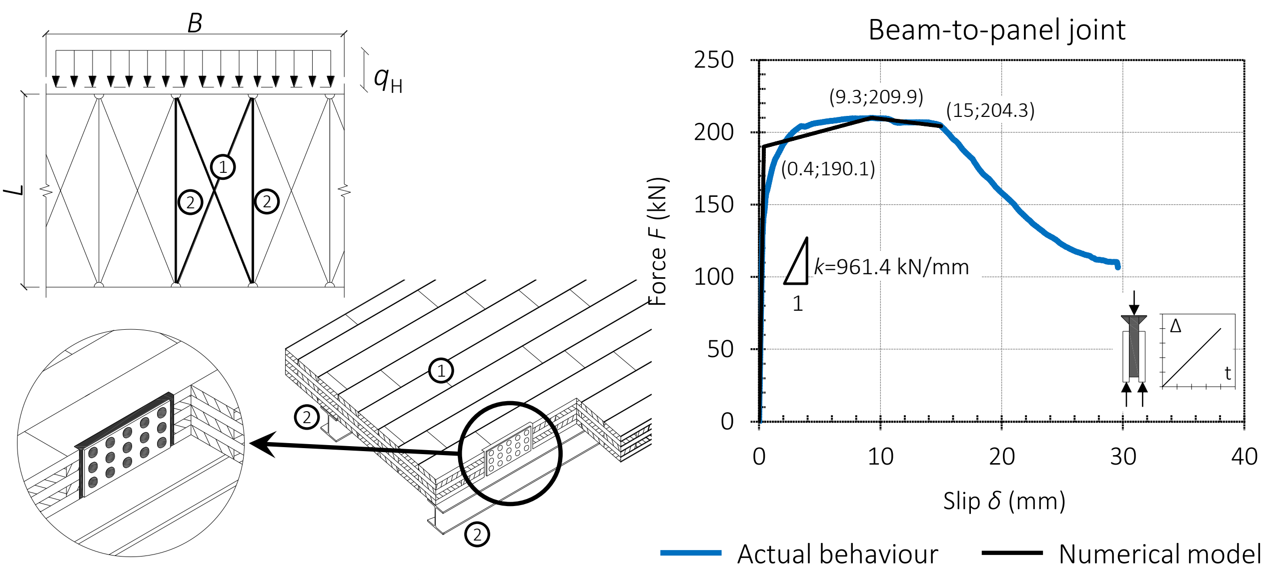

Figure 7. Innovative hybrid floor system (left) and tests results (right)

The second innovative connection method discussed here employs X-RAD connectors, Figure 6 (right) that create discrete panel-to-panel joints. This method results in point-to-point mechanical connections in ways that fulfil hold-down and lateral shear resistance functions (Polastri and Angeli 2014). As for shear walls, making point-to-point interconnections lessens the chances that structural systems will fail in unintended ways if overloaded. Figure 8 (left) shows use of X-RAD connectors in a floor diaphragm with the result being ability to transfer very large forces and achieve very high stiffness (Polastri and Angeli 2014). As shown in Figure 8 (right) the load capacity was 171kN and the elastic stiffness 23.6kN/mm.

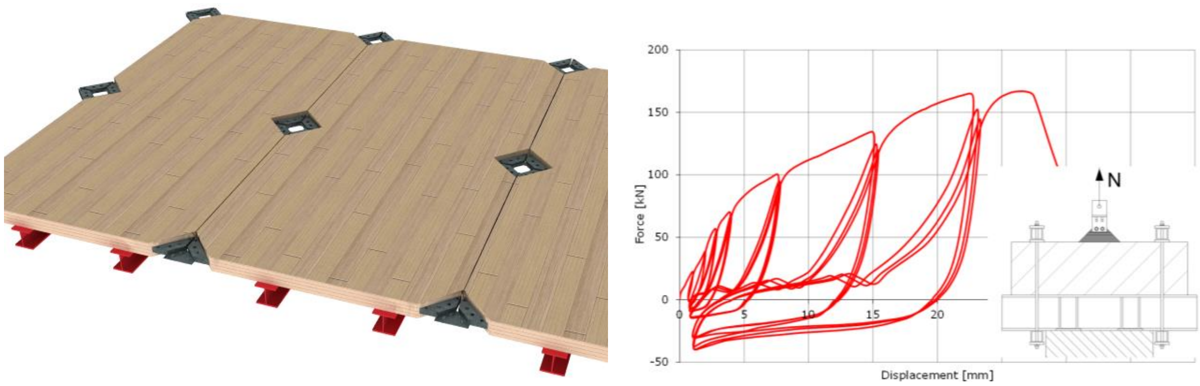

Figure 8. Innovative hybrid floor system (left); tests setup and test results (right)

Although results are not reported here it is to be mentioned that the authors are currently studying use on the described innovative connectors as ways of creating next generation of CLT floor diaphragms. It is anticipated this will enable new applications of CLT like construction of tall building having large footprints and braced by one or more building cores and perimeter shear walls.

6 Discussion and Implications for Design Practice

As the case studies demonstrate, hold-down and shear connections at the bases of CLT wall panels largely determine the behaviors of SFRS. It is therefore crucial to properly represent the stiffnesses of connections during structural analyses from which T_1, peak dynamic forces flowing through wall and connection elements and inter-storey drift are estimated.

For buildings having three to eight storeys T_1 estimates, shear and uplift forces at bases of wall panels, and inter-storey drift can all be miscalculated by substantial margins, Tables 3 to 6. The remainder of this discussion assumes connection stiffnesses derived from test data ($k_{conn} = k_{test}$) are the most accurate and therefore correct estimates of how connections embedded within SFRS actually behave. Although designers could also estimate connection stiffnesses in many other ways, the authors believe it reasonable to suppose that estimating stiffnesses will often be based on information in Eurocode 5 and similar international codes (i.e. $k_{conn} = k_{EC5}$ in case studies).

Case studies suggest T_1 values being underestimated by up to 50 percent is a realistic scenario unless designers use test data to estimate connection stiffnesses. Large errors occurring during subsequent calculation of shear and hold-down forces and inter-storey drift is also highly feasible. In capacities terms estimation of design forces and sizing shear and hold-down connection the likely consequences of how connection stiffnesses are characterized are lesser, with connections being somewhat overdesigned being normal (i.e. based on assuming $k_{conn} = k_{EC5}$). However, errors in estimation of inter-storey drift are likely to be much greater. As results in Table 6 show, interstorey-drift was estimated to be up to four times larger assuming $k_{conn} = k_{test}$ than assuming $k_{conn} = k_{EC5}$.

Based on findings here it suggested that design standards require testing of all connections intended to be used in SFRS constructed partially or completely from CLT wall panels. Furthermore, it is recommended that testing be required to characterize both initial stiffness and capacities of such connections. Also highly desirable is that engineers be given explicit guidance about what constitute appropriate structural model representations of SFRS and appropriate Modal Response Spectrum Analyses. The calculation process for design of connections in Figure 2 is believed suitable as the basis for such guidance.

7 Conclusions

The primary finding of work reported here is that estimates of the principal vibration periods of buildings with Seismic Force Resisting Systems containing CLT wall panels can be grossly inaccurate if proper attention is not paid to accurate representation of connection stiffnesses. Estimates of T_1 obtained using the simple formula in Eurocode 8 can deviate greatly from values found using finite element models employing connection stiffnesses test data. Similarly finite element model predictions of T_1 in which connection stiffnesses are estimated from information in Eurocode 5 can differ greatly from values obtained using connection test data. Inaccurate representation of connection stiffnesses can also result in incorrect sizing of elements in SFRS, and gross inaccurate in predictions of inter-storey drift. For these reasons it is important that design standards give specific guidance related to determination of initial stiffnesses as well as capacities of connections. A suitable calculation process for design of connections is required based on proposals here dealing with the structural analyses of CLT shear wall systems.

8 Acknowledgement

The authors wish to thank Eng. Davide Trutalli, student Matteo Pasin of University of Padua and Arch. Francesca Paoloni trainee at CNR-IVALSA.

9 References

Ashtari S., Haukaas T. and Lam F. (2014): In-plane stiffness of cross-laminated timber floors, Proceedings 13th World Conference on Timber Engineering, Quebec City, Canada.

Ceccotti A. (2008): New technologies for construction of medium-rise buildings in seismic regions: the XLAM case. Structural Engineering International, 18(2):156-165.

Ceccotti A., Sandhaas C., Okabe M., Yasumura M., Minowa C. and Kawai, N. (2013): SOFIE project – 3D shaking table test on a seven-storey full-scale cross-laminated timber building. Earthquake EngStruct. Dyn.,42: 2003-2021.

Comité Européen de Normalisation (CEN) (2006): EN 12512 - Timber structures – test methods – cyclic testing of joints made with mechanical fasteners, CEN, Brussels, Belgium.

Comité Européen de Normalisation (CEN) (2013): Eurocode 8 - design of structures for earthquake resistance, part 1: General rules, seismic actions and rules, CEN, Brussels, Belgium.

Comité Européen de Normalisation (CEN) (2014): Eurocode 5 - design of timber structures, Part 1-1, General - Common rules and rules for buildings, CEN, Brussels, Belgium.

Dujic B., Aicher S. and Zarnic R. (2005): Investigation on in-plane loaded wooden elements – influence of loading on boundary conditions, Otto Graf Journal, Materialprüfungsanstalt Universität, Otto-Graf-Institut, Stuttgart, Germany, Vol. 16.

European Organisation for Technical Assessment (EOTA) (2011), Rotho Blaas WHT hold-downs, European Technical Approval ETA-11/0086, Charlottenlund, Denmark.

European Organisation for Technical Assessment (EOTA) (2011), Rotho Blaas TITAN Angle Brackets, European Technical Approval ETA-11/0496, Charlottenlund, Denmark.

Gavric I., Ceccotti A. and Fragiacomo M. (2011): Experimental cyclic tests on cross-laminated timber panels and typical connections. In: Proceeding of ANIDIS, Bari, Italy.

Loss C., Piazza M. and Zandonini A. (2014): Experimental tests of cross-laminated timber Floors to be used in Timber-Steel Hybrid Structures, Proceedings 13th World Conference on Timber Engineering, Quebec City, Canada.

Loss C., Piazza M. and Zandonini R. (2015-in press): Innovative construction system for sustainable buildings, IABSE Conference on Providing Solutions to Global Challenges, September 23-25, 2015, Geneva, Switzerland.

Ministero delle Infrastrutture e dei Trasporti (MIT) (2008): DM Infrastrutture 14 gennaio 2008 - Norme tecniche per le costruzioni - NTC (Italian national regulation for construction), MIT, Rome, Italy.

Piazza M., Polastri A., Tomasi R., (2011): Ductility of Joints in Timber Structures, Special Issue in Timber Engineering, Proceedings of the Institution of Civil Engineers: Structures and Buildings, 164 (2): 79-90.

Polastri A. and Angeli A. (2014): An innovative connection system for CL T structures: experimental - numerical analysis, 13th World Conference on Timber Engineering 2014, WCTE 2014, Quebek City, Canada.

Polastri A., Pozza L., Trutalli D., Scotta R., Smith I., (2014): Structural characterization of multistory buildings with CLT cores, Proceedings 13th World Conference on Timber Engineering, Quebec City, Canada.

Popovski M., Pei S., van de Lindt J.W. and Karacabeyli E. (2014): Force modification factors for CLT structures for NBCC, Materials and Joints in Timber Structures, RILEM Book Series, 9:543-553, RILEM, Bagneux, France.

Pozza L. and Scotta R. (2014): Influence of wall assembly on q-factor of XLam buildings, Proceedings of the Institution of Civil Engineers Journal Structures and Buildings, ISSN: 0965-0911 E-ISSN: 1751-7702 – DOI:10.1680/stbu.13.00081.

Pozza L., Trutalli D., Polastri A. and Ceccotti A., (2013): Seismic design of CLT Buildings: Definition of the suitable q-factor by numerical and experimental procedures, Proceedings 2nd International conference on Structures and architecture, Guimarães, Portugal: 90 – 97.

Smith T., Fragiacomo M., Pampanin S. and Buchanan A. H. (2009): Construction time and cost for post-tensioned timber buildings. Proceedings of the Institution of Civil Engineers: Construction Materials, 162:141-149.

Strand 7 (2005): Theoretical Manual – Theoretical background to the Strand 7 finite element analysis system, http//www.strand7.com/html/docu_theoretical.htm.

FPInnovations (2011): CLT Handbook: cross-laminated timber, Eds. Gagnon S. and Pirvu C., FPInnovation, Quebec City, Canada.

Tomasi R. and Smith I. (2015): Experimental characterization of monotonic and cyclic loading responses of CLT panel-to-foundation and angle bracket connections, Journal of Materials in Civil Engineering, 27(6), 04014189.

Discussion

The paper was presented by A Polastri

D Moroder commented that the proposed interactive effort for design included FEM model for tall building but no practicing engineers are doing this. A Polastri agreed but stated that the FEM model is important and needed for tall buildings. D Moroder asked about higher mode effect. A Polastri said that only regular buildings were considered so there was no higher mode effect. D Moroder commented that higher mode was observed even in three story buildings but perhaps not in those made of CLT.

M Follesa asked about the bonding connection to the foundation. A Polastri responded that they did not consider the difference of the behaviour of hold down between wood elements and between wood wall and concrete foundation elements.

P Zarnani asked about the coupling issues between CLT panels at the corner of a building. A Polastri agreed that this would be important; here, crossed screws would be used to connect the corner panels to achieve high stiffness.

S Winter commented about the use of FEM for tall buildings. This type of study would not only be needed for earthquake, but wind issues would also need consideration. Also non-standardized hold downs should be considered. X Rad connectors have to be considered beyond strength including issues with fire, sound, airtightness etc.

A Polastri responded that they are looking at different covers to address these issues. In traditional steel plate solutions with the steel exposed, poor fire resistance would also be expected.

A Salenikovich received clarification about comparison between balloon and platform construction.

I Smith commented in Canada, a related study was done with taller buildings and wind forces tended to govern the design above 8 stories.

Dissipative connections for squat or scarcely jointed CLT buildings. Experimental tests and numerical validation

Roberto Scotta, Luca Pozza, Davide Trutalli, Luca Marchi, University of Padova, Italy

Ario Ceccotti, University IUAV of Venezia, Italy

Keywords: CLT; X-Lam; dissipative connection; numerical model; experimental tests.

1 Introduction

The seismic behaviour of CLT system has been studied by numerous researchers from various countries. Quasi-static tests on shear-wall systems and shake-table tests on full-scale buildings showed that CLT structures are characterized by high strength and stiffness with respect to seismic actions but might have low ductility and dissipative capacity if not correctly designed (e.g., *Ceccotti et al.,* 2013; *Gavric et al.,* 2015; *Popovski & Gavric,* 2015).

In particular, squat and scarcely jointed buildings realized with large horizontal panels show limited dissipative capacity due to their prevailing sliding behaviour. However, in the constructive practice these structures are largely preferred, because adoption of large panels with few joints allows the reduction of time and cost for on-site assembling, despite more shear-resistant connectors are needed to resist to earthquake forces because of the low dissipative capacity of such buildings. According to such practice, Eurocode 8 (2013) suggests a quite prudential behaviour factor for seismic design of CLT buildings: q=2. Recent studies demonstrated that the seismic response of CLT system is affected by the building geometry (e.g., slenderness) and by the number, type, arrangement and design of joints used to assemble the timber panels. Slender or highly jointed buildings have much more dissipative and ductility capacities than squat and scarcely jointed buildings. Such dependency was demonstrated by experimental tests on different shear walls (e.g., *Gavric et al.,* 2015) and by numerical simulations on different building systems (*Pozza et al.,* 2013; *Pozza & Scotta,* 2014). According to these researchers more generous values of the behaviour q-factor have been suggested, depending on building geometry and panel arrangement.

Seismic performance of CLT buildings is mainly related to the capability of connections to do plastic work if loaded over yielding, whereas timber elements have limited capability to deform inelastically (*Smith et al.,* 2003). Nowadays in CLT buildings, hold-down and angle-bracket connections, which were developed for platform-frame constructions, are typically employed. However, the dissipative capacity of light-frame buildings is mainly concentrated in nailing between frames and panels, while in CLT buildings dissipative contribution is demanded exclusively to the connections between wall panels, floor panels and foundation. Actually, hold-downs and angle brackets subjected to cyclic loading show a marked pinching behaviour due to wood-embedment phenomenon, which reduces the energy dissipation capability of connections. Moreover, they are optimized and certified for uniaxial loading (i.e., only tension or only shear) while they may show undesired brittle behaviour if subjected to combined loading and a rigorous capacity design is not applied (*Gavric et al.,* 2013).

The aim of this work is to demonstrate how the adoption of innovative dissipative connections, specifically developed to be adopted in CLT buildings, can improve the intrinsic ductility of stocky and scarcely jointed CLT buildings and the cyclic behaviour assured by standard hold-downs and angle brackets when used in CLT buildings.

Several of such innovative connections have already been proposed and tested (*Latour & Rizzano,* 2015; *Loo et al.,* 2014; *Polastri et al.,* 2014; *Sarti et al.,* 2015). In this work first the design phase of a newly developed joint is proposed. The mechanical behaviour of this innovative connection element has been validated by means of experimental tests and numerical models. Then numerical simulations of quasi-static cyclic-loading tests were used to demonstrate the increased seismic performances of shear walls using the proposed connection.

2 Design process

2.1 Design criteria

Currently adopted connectors for CLT panels are differentiated to prevent sliding (angle brackets) or rocking movements (hold-downs). Instead, the connection proposed in this work operates properly in both circumstances and can be subjected to mixed axial and shear forces. It assures high ductility before failure and has a negligible pinching behaviour to empathise dissipative capacity under cyclic loading. Criteria fixed in the design of the connection were: displacement capacity not less than 30 mm according to EN 12512 (2006a); high ductility class according to Eurocode 8 (2013); resistance comparable to the traditional connectors (*Gavric et al.,* 2011); optimized shape to reduce production costs with minimum scarf production.

The core of the proposed connection is constituted by a “X” shaped plate obtained by cutting of a flat steel sheet. Grade S275 steel was found to be the more appropriate to achieve adequate ductile hysteretic behaviour without excessive decay of the strength capacity. The “X” shape is optimized in order to prevent localized yielding of material and then to assure diffuse yielding and emphasize ductility and energy dissipation capacity. The chosen shape assures low production costs and minimal scarf production.

2.2 Parametric design assisted by numerical modelling

Once decided the tentative “X” shape, a parametric FE model was used to find the optimal one fulfilling the design criteria. A 2D FE model of the “X” shaped plate using shell elements was implemented into ANSYS Workbench (*ANSYS Inc.,* 2012). An elasto-plastic constitutive law combined with a kinematic hardening model was adopted for steel. Non-linear geometrical analysis option was activated to account for possible buckling phenomenon under high displacements.

To minimize failure risk due to oligocyclic fatigue, a limit to the maximum strain of steel was imposed (Priestley et al., 1996). Accordingly maximum axial deformation of the “X” plate was limited between -2% and +10% (small compression was accounted for), while its allowable shear strain was set in the range ±6%.

For the shape optimization of the “X” plate, a parametric FE model with modifiable geometries was employed. The geometrical parameters chosen as variable in the model are evidenced with letters in Figure 1a. To enable a single-cut production as shown in Figure 1b other geometrical parameters are dependent on these.

Numerical simulations were conducted for pure tension and pure shear cyclic loading. A total of 70 different combinations of the variable parameters led to the definition of the optimal final shape. Figure 2 shows the deformation at maximum imposed displacements, in pure tension and pure shear loading. The darkest contour shows plastic regions in which the yield strength (275 MPa) has been exceeded. Position and extension of yielded zone vary with the loading type, but spreading of yielding is well evident in both tests. Figure 3 shows the force-displacement hysteresis cycles obtained with the optimal combination of parameters, compared with experimental results.

2.3 Anchoring to the timber panel

In order to ensure the localization of deformations in the dissipative X plate, a proper design of fixing details to the timber panel is required. Connection has to guarantee a suitable over-resistance with respect to the X plate, while remaining elastic and rigid with limitation of wood embedment. An effective semi-rigid solution could be the use of dowel-type fasteners coupled with punched metal plates fixed to the timber panel (*Blass et al.,* 2000). An alternative method to reduce the wood embedment is the use of toothed-plate connectors (e.g., Bulldog or Geka).

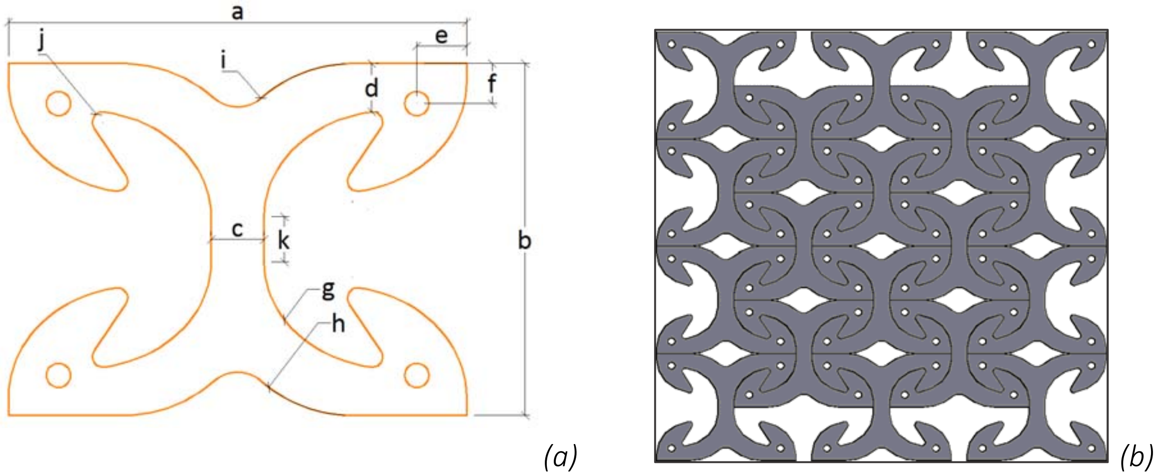

Figure 1. (a) Geometrical parameters of connectors; (b) demonstration of single-cut production.

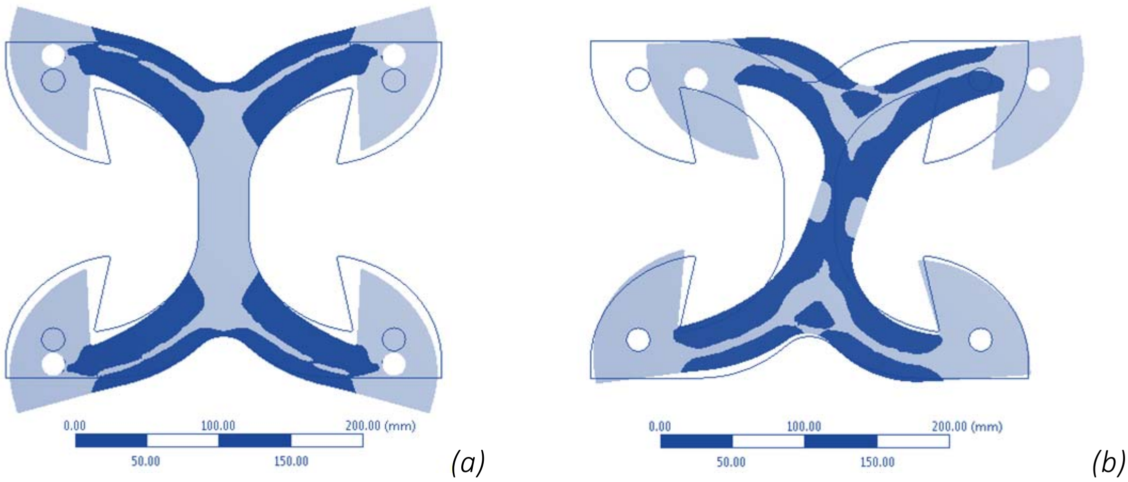

Figure 2. Numerical output: deformation and plastic zones. (a) Tension test; (b) Shear test.

3 Experimental tests

Once concluded the design and optimization phases, experimental tests on prototypes have been conducted to obtain actual cyclic behaviour of the X brackets. Three pairs of X brackets were tested in pure tension and as many in pure shear, for a total of 12 specimens. Tests were performed at the Laboratory of Construction and Materials of the University of Padova.

3.1 Test setup

Two different setups were designed for tension and shear tests. In order to evaluate exclusively the behaviour of the X plate, suitable rigid steel frames were realized to transmit load from actuators. The couple of X brackets were fixed externally on both sides of the supporting frame without any buckling restraining elements.

In the tension test, the two lowest fixing points were connected to a 20-mm thick steel plate rigidly fixed to the portal. The two upper fixing points were connected to another 20-mm thick plate fixed to the hydraulic jack with an eyebolt mechanism. The pure shear loading was obtained with an unbraced steel truss, in which the X brackets operated as cross-bracing element. 15-mm thick steel plates were used for the steel truss. PTFE sheets were interposed between each contact surface to minimize friction. The whole assembly was positioned in a rotated configuration, in order to keep loading direction as close as possible to the virtual diagonal line. It was fixed at the bottom to the portal with 2 M20 steel bolts and at the top to the hydraulic jack with an M45 eyebolt.

3.2 Test procedure

Tests were performed according to quasi-static cyclic-loading protocol recommended by EN 12512 (2006a). The cyclic procedure was stopped after reaching a relative displacement of 30 mm, then the specimens were loaded until their failure. Tests were conducted under displacement control with a deformation rate of 0,02 mm/s.

3.3 Test results

Figure 3 illustrates the results of the experimental tests and the comparison with those from numerical analyses. The good matching of the experimental curves with the numerical models is clearly shown. It was possible thanks to the well predictable behaviour of the steel used for the realization of the X brackets.

On 30-mm cycle of the tension test (Figure 3a), the reloading path decreased gradually due to instability phenomenon. For the same reason the maximum compression force measured during unloading was lower than the tension one, but still maintaining a wide area and, consequently, an appropriate dissipative capacity. Lastly, the numerical model tolerably underestimated force and stiffness for the unloading sequences. For the shear test the progressive rotation of the steel frame was taken into account to correctly evaluate shear force plotted in the force-displacement curves in Figure 3b. The experimental hysteresis loops are perfectly centred on the origin of the axis thus demonstrating the suitability of the setup configuration. The experimental results are in good agreement with expectation, even if the numerical prediction slightly over estimates shear force at high displacements. In general, no noticeable strength degradation was observed in experimental tests and no cracks induced by fatigue were observed.

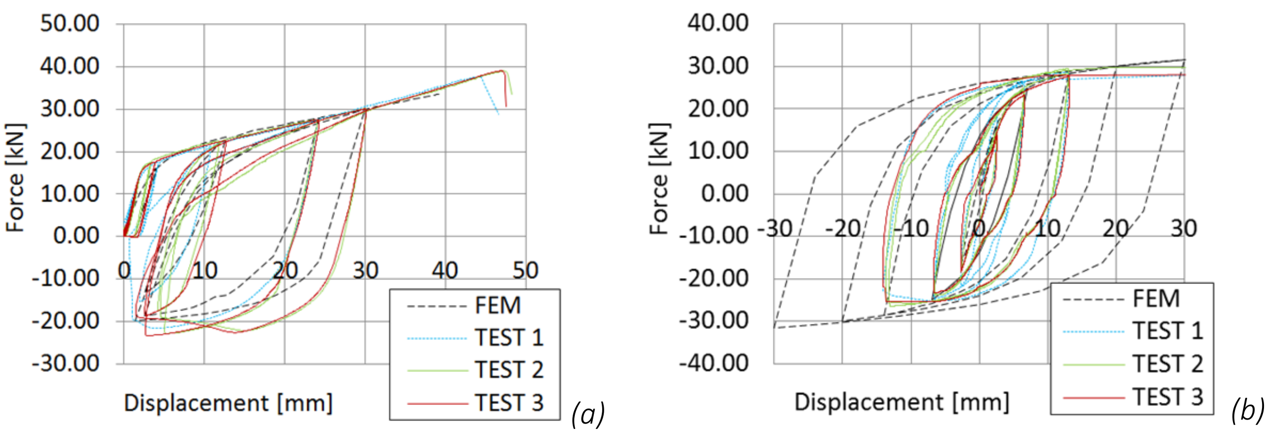

Figure 3. Experimental cycles in comparison with FEM results. (a) Tension tests; (b) Shear tests.

Figure 4 shows the tested specimens at maximum deformation. The main evidence is that X brackets are able to experience large plastic deformations before failure, in both loading configurations. Instability phenomena of limited parts of the connection occurred during both shear and axial tests without impairing significantly the mechanical performance of the connections. Failure occurred for very large displacements due to stress concentration for a not correct realization of fillet “j” in Figure 1.a. Therefore, ductility of X brackets could be further improved by modifying this detail.

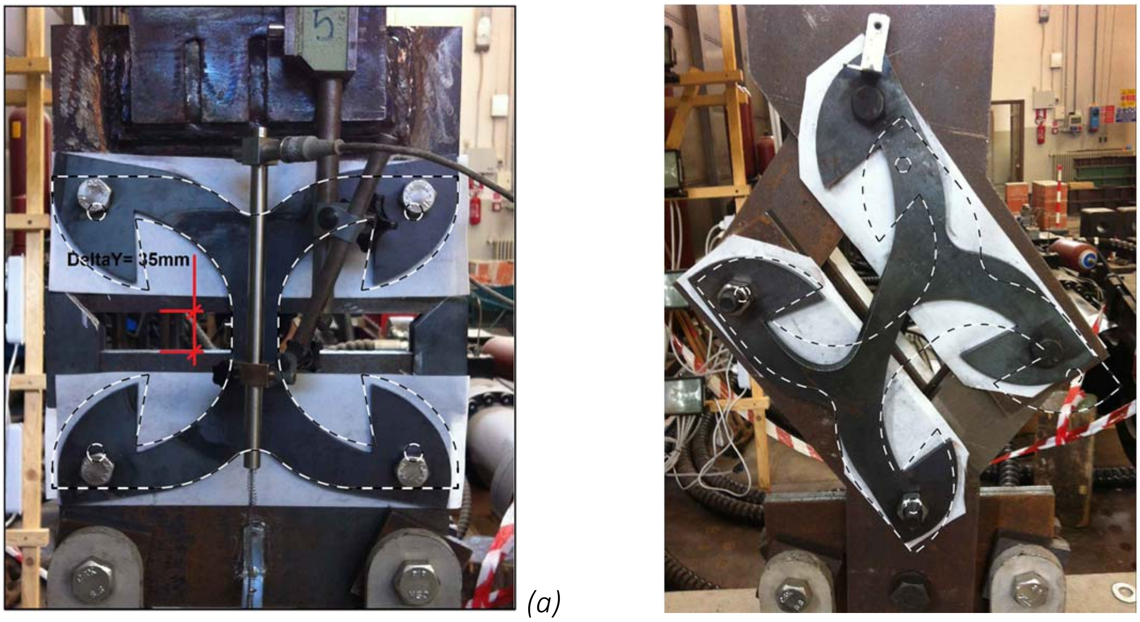

(a) *(b)*

Figure 4. Deformed specimens: (a) Axial test (b) Shear test. In dashed white line the original shape.

3.3.1 Analysis of test results

The performed cyclic-loading tests allow to define the main mechanical parameters for a proper characterization of the tested elements according to EN 12512 (2006a): elastic and post-elastic stiffness (k_{el}, k_{pl}), yielding point (V_y, F_y), failure condition (V_u, F_u), and ductility ratio μ. From these data it is possible to classify the proposed connection into the appropriate ductility class, according to Eurocode 8 (2013), i.e., low (L), medium (M) or high (H) ductility class. Various methods were proposed to compute these parameters (*EN 12512*; *Muñoz et al.,* 2008). In this work, the envelope of the hysteresis curves was fitted using the analytical formulation proposed by *Foschi & Bonac* (1977). Then, method (a) of EN 12512 was chosen for both axial and shear tests, in order to obtain the best linear fitting of the envelope curve. This method is adequate for curves with two well-defined linear branches and the yielding point is defined by the intersection of these two lines. Moreover, also the equivalent Elastic–Plastic Energy (EEEP) method (*Foliente,* 1996) was used to analyse the results of the shear test, because of the elastic perfectly-plastic behaviour shown. Tables 1 and 2 list the obtained values from the three tests referred to a single plate of the couple. Average value, standard deviation (SD) and 5% characteristic value according to EN 1990 (2006b), were computed considering a sample of six elements.

Table 1. Analysis of tension test (EN 12512 method).

	Test 1	Test 2	Test 3	Average	SD
F_y [kN]	17.55	18.37	17.99	17.97	0.36
V_y [mm]	1.89	2.01	1.98	1.96	0.06
F_u [kN]	37.18	37.84	38.25	37.76	0.48
V_u [mm]	44.30	47.30	47.00	46.20	1.48
k_{el} [kN/mm]	9.31	9.12	9.08	9.17	0.11
k_{pl} [kN/mm]	0.46	0.43	0.45	0.45	0.01
$\mu(V_u)$ [-]	23.49	23.49	23.72	23.57	0.12
Ductility Class	H	H	H	H	-

Table 2. Analysis of shear test (EN 12512 method and EEEP method).

	Test 1		Test 2		Test 3		Average		SD	
	EN	EEEP	EN	EEEP	EN	EEEP	EN	EEEP	EN	EEEP
F_y [kN]	26.71	27.41	29.41	28.88	28.14	27.83	28.09	28.04	1.21	0.68
V_y [mm]	2.38	2.60	4.00	4.45	4.02	4.53	3.46	3.86	0.84	0.98
F_u [kN]	29.00	27.41	29.70	28.88	28.40	27.83	29.03	28.04	0.58	0.68
V_u [mm]	50.00*	50.00*	58.00*	58.00*	80.00	80.00	-	-	-	-
k_{el} [kN/mm]	11.24	10.55	7.36	6.49	7.00	6.14	8.53	7.73	2.10	2.19
k_{pl} [kN/mm]	0.05	0.00	0.01	0.00	0.00	0.00	0.02	0.00	0.02	0.00
μ (V_u=50mm)	21.04	19.24	12.51	11.24	12.44	11.03	15.33	13.84	4.42	4.19
Ductility Class	H	H	H	H	H	H	H	H	-	-

* Tests 1 and 2 were stopped before the ultimate displacement.

Results show that the proposed connection is characterized by an high initial stiffness and adequate resistance both for tension and shear loads. However, the most valuable result is the very high value of ductility obtained, coupled with almost null strength degradation and pinching effect. The highest values of ductility were obtained for the axial configuration. However, ductility for the shear configuration was computed assuming V_u as 50 mm, even if in test 3 failure of the specimen was reached for a displacement equal to 80 mm, whereas tests 1 and 2 were stopped before failure. If the ultimate displacements of 80 mm were assumed, ductility values in shear tests would become higher and comparable with those from axial tests. Comparing values of initial stiffness and of yielding and ultimate forces from the two configurations, it can be observed that the connection shows an almost uniform response when subjected to shear or axial loads.

Table 3 lists the 5th and the 95th percentile of the ultimate force ($F_{0.05}$ and $F_{0.95}$). According to *Fragiacomo et al.* (2011) the ratio $F_{0.95}$ / $F_{0.05}$ is fundamental for the estimation of the overstrength factor to be used in a capacity design approach. Since only a single type of steel has been used the obtained values should be amplified to account for the typical variation of steel yielding stress. The limited values $F_{0.95}$ / $F_{0.05}$ assured by the proposed connection, which are much lower than those shown by standard ductile connections failing on the timber side, suggest that the adoption of capacity design rules would become feasible if the proposed connection were employed.

Table 3. Characteristic values and overstrength ratio.

	Tension test			Shear test (EN method)			Shear test (EEEP method)		
	$F_{0.05}$	$F_{0.95}$	γ_{ov}	$F_{0.05}$	$F_{0.95}$	γ_{ov}	$F_{0.05}$	$F_{0.95}$	γ_{ov}
F_y [kN]	17.18	18.76	1.09	25.46	30.71	1.21	26.56	29.52	1.11
F_u [kN]	36.70	38.81	1.06	27.76	30.30	1.09	26.56	29.52	1.11

3.3.2 Comparison with typical connections for CLT walls

Values of mechanical parameters obtained for the proposed connection can be compared with analogous quantities assured by angle brackets and hold-downs typically used in CLT buildings. Comparative values are reported in *Gavric et al.* (2011) for hold-downs and angle brackets loaded respectively in tension and in shear.

In comparison with a commercial hold-down having almost the same strength and stiffness, the proposed connection assures, on average, an approximately twice ultimate displacement and a ductility value about eight times larger. In comparison with a commercial angle bracket having similar strength, the proposed X shaped connection assures, on average, an ultimate displacement two times larger, a ductility value nine times larger and an elastic stiffness about 4 times larger.

The proposed connection element shows performances much higher than traditional ones, in particular when loaded in shear. This evidence testifies that this element can be properly used to improve the ductility and seismic performances of intrinsically fragile buildings, such as squat CLT buildings realised with large horizontal panels. Moreover, the proposed connection makes more feasible the introduction of capacity criteria in design of timber buildings limiting value of overstrength factor.

4 Numerical modelling of CLT shear walls

The FE models of three CLT shear walls (wall A, wall B and wall C) were implemented into ANSYS Workbench (*ANSYS Inc.* 2012). Quasi-static cyclic-loading tests were simulated according to EN 12512 (2006a) protocol. Wall A and wall B have the same geometry (dimension of 2.95 x 2.95 m, aspect ratio 1:1) and vertical distributed load (18.5 kN/m) of CLT specimens I.1 and I.2, tested by *Gavric et al.* (2015). These configurations were chosen in order to allow a direct comparison with true panels anchored using traditional connection system. Wall I.1 is anchored with two hold-downs and two angle brackets; wall I.2 with two hold-downs and four angle brackets. Wall C, representing a squat and scarcely jointed CLT wall, has dimensions equal to 5.90 x 2.95 m (aspect ratio 2:1) and the same vertical distributed load of the other two walls. Figure 5 shows the geometry and fastener arrangement of the modelled

CLT shear walls. Wall A is anchored with four X brackets (two per each side), whereas wall B and C with six X brackets (three per side).

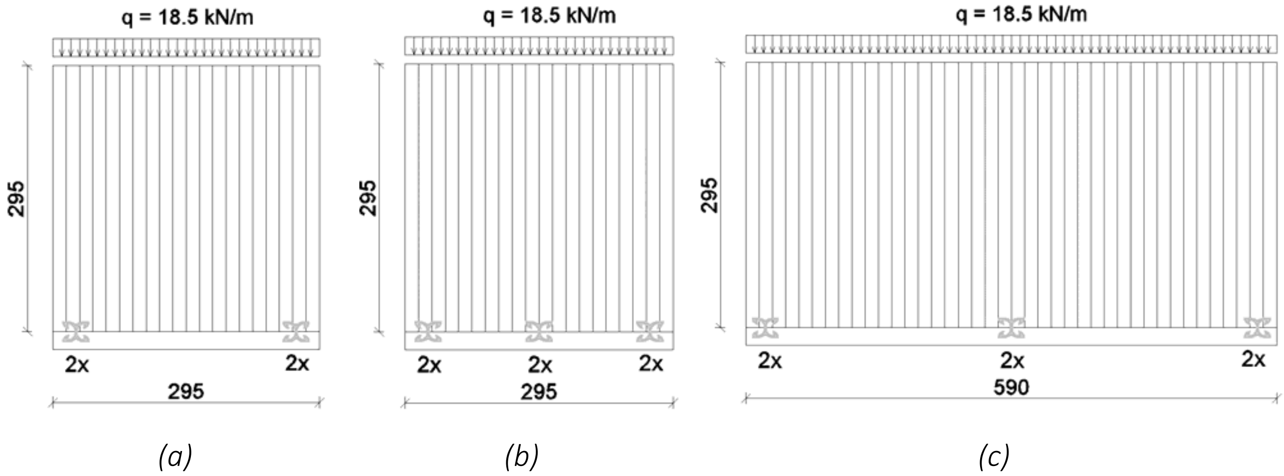

Figure 5. Shear walls: (a)Wall A; (b) Wall B; (c) Wall C. (dimensions are in cm)

4.1 Numerical models of timber walls

Linear elastic shell was used to simulate the timber panels (Figure 6), whereas the connectors were modelled with the same FE non-linear models previously described in section 2. Coupling constraint equations were applied in correspondence of the fixing points to avoid relative displacements between panels and X brackets and permit exclusively the relative rotation (hinge connections). The supporting curb was modelled with only-compression frictionless rigid springs. Large deformations were enabled to allow out-of-plane buckling of the X brackets, well simulated by the model, as shown in Figure 7. It has to be stressed that in these analyses X brackets are subjected to mixed loadings.

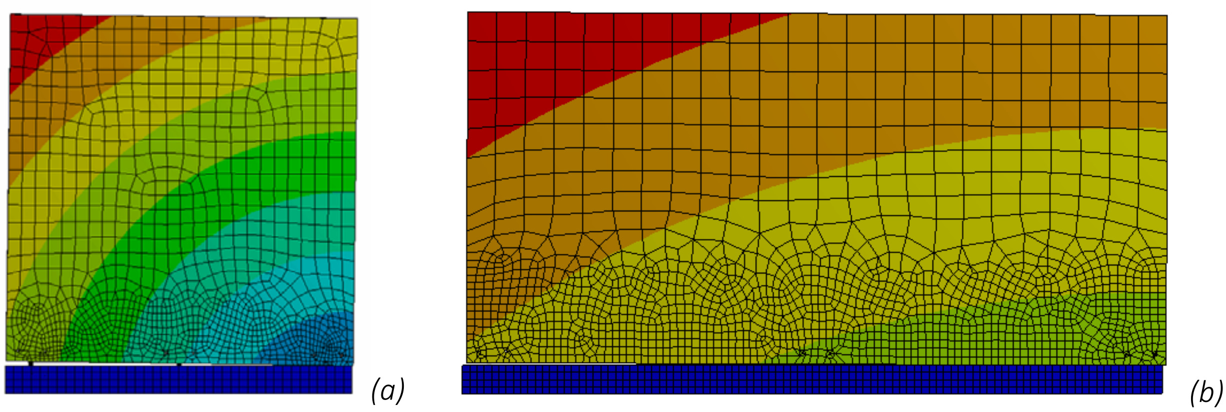

Figure 6. Deformed geometries at maximum top displacement: (a) Wall B ; (b) Wall C .

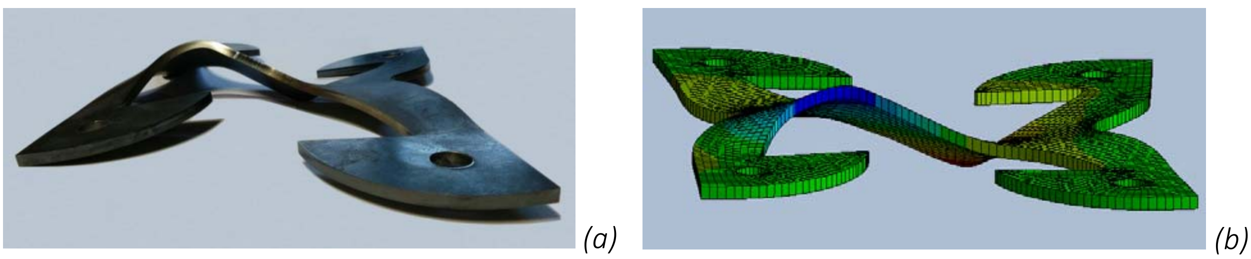

Figure 7. Plate buckling under shear loading. (a) Experimental evidence; (b) Numerical prediction.

4.2 Analysis of results

This section reports a comparison between numerical results on walls A and B with experimental ones on walls I.1 and I.2 respectively. Moreover, the predicted behaviour of wall C is presented.

4.2.1 Comparison with CLT walls anchored with traditional connections

Figure 8 shows the predicted base shear force vs. applied top displacement (i.e., hysteresis cycles) for wall A and wall B specimens. The main evidence is the different behaviour of these walls in terms of strength, displacement and cycle amplitude (i.e., dissipated energy capacity). It can be seen that wall B (with 6 X brackets) reaches an higher base shear force than wall A (with 4 X brackets), even if they both fail with a combined rocking-sliding behaviour. In wall A connectors are subjected to combined shear-tension load. However wall A shows a good seismic response: it reaches an ultimate displacement of 60 mm (drift 2%) without exhibiting strength degradation and demonstrating good dissipative capability. The two additional connectors placed in the middle, whose shear resistance is less weakened by contemporary traction due to rocking, are responsible of the increased ultimate load of wall B. Wall B fails at 60 mm after three fully reversed cycles and with slight strength degradation due to buckling of X brackets, which however does not compromise the overall behaviour of the wall.

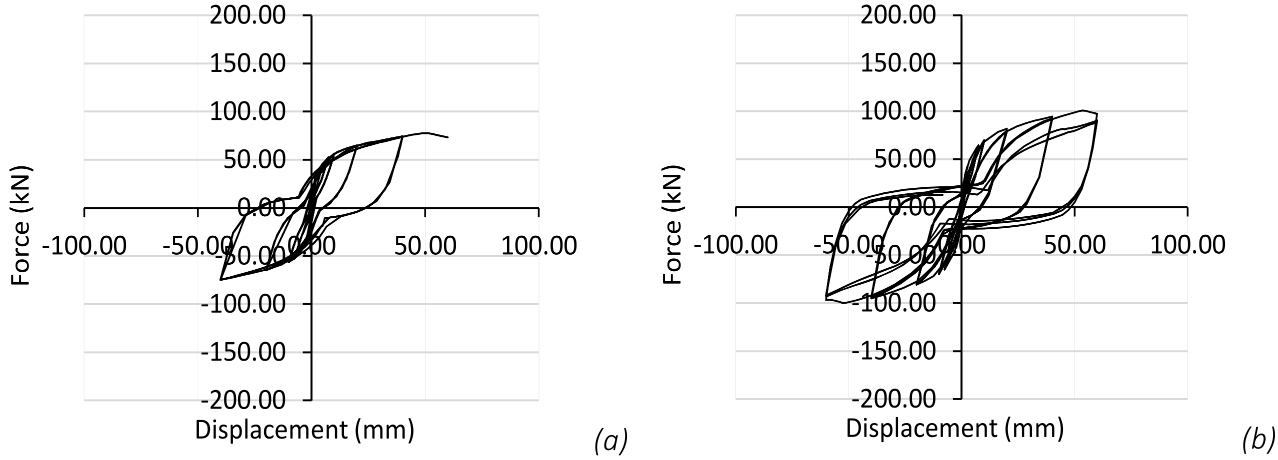

Figure 8. Hysteresis cycles: (a) Wall A; (b) Wall B.

The similitude in terms of geometry, test configuration and loading protocol between walls A and B and walls I.1 and I.2 tested by *Gavric et al.* (2015), allows a direct comparison in terms of ductility (μ), viscous damping ratio (ν), strength degradation (ΔF) and strength (F_y, F_{max}). These parameters were evaluated according to EN 12512 provisions. Figure 9 resumes such comparison. It can be seen that the yielding loads for the CLT walls with the proposed connection system remains similar to that of the walls with traditional connections, whereas ductility, strength degradation and pinching effect are strongly improved. The limited strength degradation and the higher and stable equivalent viscous damping ratio lead to a strongly increased dissipative capacity of the walls.

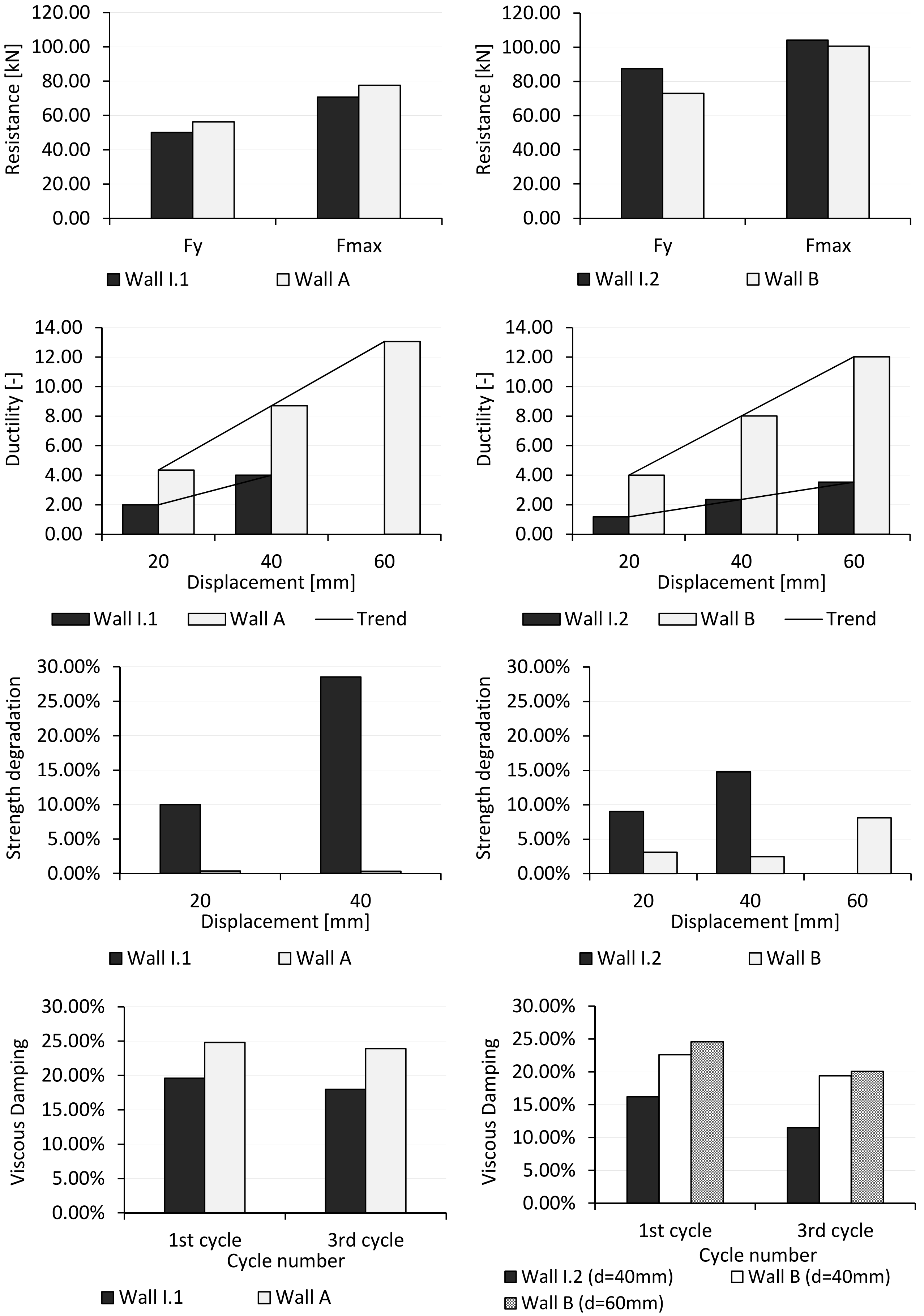

Figure 9. Comparison of seismic performace parameters between CLT walls anchored with traditional (I.1 and I.2) and proposed (A and B) connections.

4.2.2 Analysis of squat CLT wall

The analysis of wall C was performed in order to provide a comparative application test on a squat wall realized with a unique horizontal CLT panel. Such constructive methodology is normally adopted in practice and ductility and dissipation capacity of such walls are mainly demanded to the shear behaviour of traditional angle brackets. The use of the proposed connection assures adequate ductile seismic response also for these buildings, as illustrated in Figure 10.

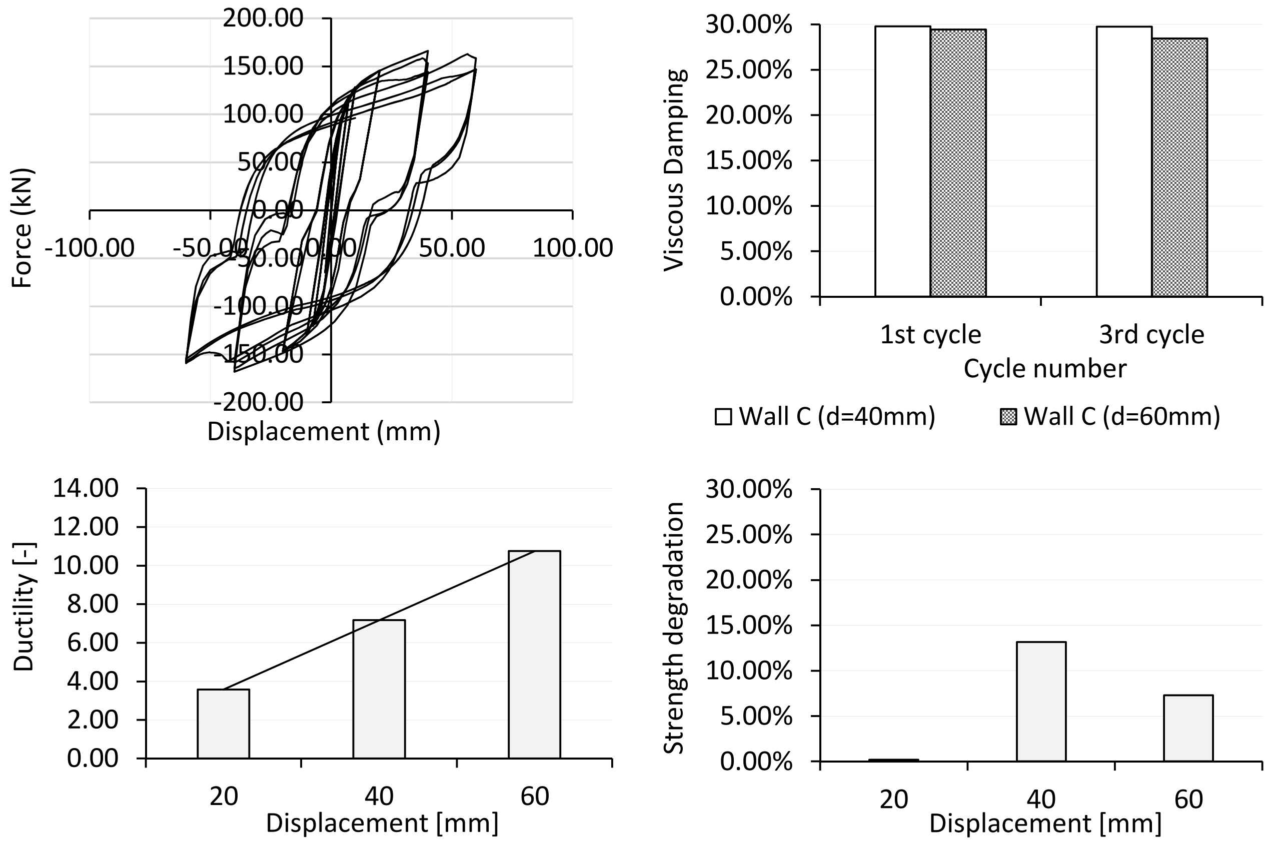

Figure 10. Hysteresis cycles and analysis of wall C.

It can be seen that wall C reaches the highest value of resistance (166.0 kN) and of viscous damping ratio (about 30.0%). This is mainly due to the pure shear behaviour of the connection element (i.e., shear strength is not impaired by the traction forces). At the 40-mm cycles the out-of-plane buckling of X brackets causes a slight strength degradation, but the connection still maintains its capacity and the strength degradation decreases for higher displacements (60 mm).

5 Conclusions

The adoption of newly developed dissipative connections in substitution of traditional anchoring systems allows to strongly increase the seismic response of CLT buildings, in terms of ductility and energy dissipation capacity.

The design and optimization phases of a newly developed X shaped dissipative bracket has been described in the paper, together with following experimental validation and interpretation of obtained results. It has been demonstrated that such innovative devices, specifically developed to be used in CLT structures, assure several times larger ductility and dissipative capacity than standard connections of comparable yielding strength and elastic stiffness. The assessment of the mixed shear-tension behaviour (i.e., definition of the strength domain), keeping into account for local buckling phenomenon, is fundamental to correctly assess the actual dissipative properties of such devices. The procedure adopted in this paper could serve as a reference for the due certification of dissipative connections by means of testing and/or numerical modelling.

Effects of utilization of the proposed X brackets to fasten CLT shear walls have been simulated numerically. Obtained results confirm that obtained CLT shear walls are classifiable into High Ductility Class according to Eurocode 8. Even shear walls realized with large horizontal CLT panels show a favourable highly dissipative behaviour.

In view of a code implementation, increased q-factor should be allowed when dissipative connection elements are employed for the realization of massive shear walls or shear frames. It has to be highlighted also that the utilization of dissipative connections with limited controlled overstrength makes the utilization of a capacity design approach more realistically affordable in designing of timber structures.

6 References

ANSYS Mechanical Workbench R14 (2012).

Blass, HJ, Schmid, M, Litze, H, Wagner, B (2000): Nail plate reinforced joints with dowel-type fasteners. In Proceedings of the 6th World Conference on Timber Engineering

Ceccotti, A, Sandhaas, C, Okabe, M, Yasumura, M, Minowa, C, Kawai, N (2013): SOFIE project – 3D shaking table test on a seven-storey full-scale cross-laminated timber building. Earthquake Engineering & Structural Dynamics, 42(13):2003-2021.

EN 12512 (2006a): Timber structures—test methods—cyclic testing of joints made with mechanical fasteners. CEN. Brussels, Belgium.

EN 1990 – Eurocode (2006b): Basis of structural design. CEN. Brussels, Belgium.

Eurocode 8 (2013): Design of structures for earthquake resistance, part 1: general rules, seismic actions and rules for buildings. CEN. (EN 1998-1-1). Brussels, Belgium.

Foliente, GC (1996): Issues in seismic performance testing and evaluation of timber structural systems. Proceedings of the International Wood Engineering Conference, New Orleans, USA.

Foschi, RO, Bonac, T (1977): Load slip characteristic for connections with common nails. Wood Science and Technologly, 9(3): 118-123.

Fragiacomo, M, Dujic, B, Sustersic, I (2011): Elastic and ductile design of multi-storey crosslam massive wooden buildings under seismic actions. Engineering Structures, 33(11):3043-3053.

Gavric, I, Ceccotti, A, Fragiacomo, M (2011): Experimental cyclic tests on cross-laminated timber panels and typical connections. Proceedings of ANIDIS, Bari, Italy.

Gavric, I, Fragiacomo, M, Ceccotti, A (2013): Capacity seismic design of X-LAM wall system based on connection mechanical properties. Meeting 46 of the Working Commission W18-Timber Structures, CIB, Vancouver, Canada, paper CIB-W18/46-15-2.

Gavric, I, Fragiacomo, M, Ceccotti, A (2015): Cyclic behaviour of CLT wall systems: experimental tests and analytical prediction models. ASCE Journal of Structural Engineering, DOI: 10.1061/(ASCE)ST.1943-541X.0001246.

Latour, M, Rizzano, G (2015): Cyclic Behavior and Modeling of a Dissipative Connector for Cross-Laminated Timber Panel Buildings. Journal of Earthquake Engineering, 19(1): 137-171, DOI: 10.1080/13632469.2014.948645.

Priestley, M J N, Seible, F, Calvi, G M (1996): Seismic design and retrofit of bridges, Wiley, New York.

Loo, WY, Kun, C, Quenneville, P, Chouw, N (2014): Experimental testing of a rocking timber shear wall with slip-friction connectors. Earthquake Engineering and Structural Dynamics, 43(11):1621-1639.

Muñoz, W, Mohammad, M, Salenikovich, A, Quenneville, P (2008): Need for a harmonized approach for calculations of ductility of timber assemblies. Proceedings of the Meeting 41 of the Working Commission W18-Timber Structures, CIB, Saint Andrews, Canada.

Polastri, A, Angeli, A, Dal Ri, G (2014): A new construction system for CLT structures. Proceedings of World Conference on Timber Engineering WCTE, Quebec City, Canada.

Popovski, M, Gavric, I (2015): Performance of a 2-story CLT house subjected to lateral loads. ASCE Journal of Structural Engineering, DOI: 10.1061/(ASCE)ST.1943-541X.0001315.

Pozza, L, Scotta, R, Trutalli, D, Ceccotti, A, Polastri, A (2013): Analytical formulation based on extensive numerical simulations of behavior factor q for CLT buildings. Meeting 46 of the Working Commission W18-Timber Structures, CIB, Vancouver, Canada, paper CIB-W18/46-15-5.

Pozza, L, Scotta, R (2014): Influence of wall assembly on q-factor of XLam buildings. Institution of Civil Engineers Journal Structures and Buildings. DOI:10.1680/stbu.13.00081.

Sarti, F, Palermo, A, Pampanin, S (2015): Quasi-Static Cyclic Testing of Two-Thirds Scale Unbonded Posttensioned Rocking Dissipative Timber Walls. ASCE Journal of Structural Engineering, DOI: 10.1061/(ASCE)ST.1943-541X.0001291.

Smith, I, Landis, E, Gong, M (2003): Fracture and fatigue in wood. John Wiley and Sons, Chichester, UK.

Discussion

The paper was presented by R Scotta

F Sarti asked whether the differential movement between the wall and the connector was considered. R Scotta said the connector was assumed to be well connected to the wall and the differential movement was not considered. F Sarti discussed about vertical load that could help the self-centring in rocking systems. R Scotta responded that in squat systems, shear deformation is more important and has to be considered first.

T Tannert asked about the fancy shape of the connector. R Scotta said that this was made for production efficiency and consideration to use less material.

H Blass asked whether a steel angle type connector would be needed for the wall to floor connection. R Scotta said yes especially in wall to concrete foundation some steel plates would be needed to help transfer the high forces.

F Sarti asked about buckling and low cycle fatigue issues. R Scotta responded that when designing the connector, limiting the maximum strain would be needed to take low cycle fatigue into consideration. Buckling was observed and modelled, but did not influence the strength much.

B Dujič and R Scotta discussed that friction needed to be considered.

Z Li commented that the buckling would change the force distribution and one might need to avoid this failure mode. He received confirmation that mild steel with 275 MPa yield strength was used.

W Seim commented that this component test was a steel to steel connection but in buildings this would be steel to wood connection. R Scotta agreed and will use model to take this aspect into consideration.

U Kuhlmann stated that when using mild steel one must consider the over strength in the steel.

I Smith commented about practicality and tolerance, and whether the potential users have any opinions. R Scotta stated that the study mainly focused on the structural performance issues first.

Analysis of fire resistance tests on timber column buckling with respect to the Reduced Cross-Section Method

Joachim Schmid, SP Wood Building Technology and LTU, Sweden

Michael Klippel, ETH Zurich, Institute of Structural Engineering, Switzerland

Andrew Liew, ETH Zurich, Institute of Structural Engineering, Switzerland

Alar Just, SP Wood Building Technology and TUT, Sweden and Estonia

Andrea Frangi, ETH Zurich, Institute of Structural Engineering, Switzerland

Keywords: Fire design model, Reduced Cross-Section Method, Buckling, Timber, Standard fire, Fire resistance, Fire testing

1 Abstract

The Reduced Cross-Section Method (RCSM) is a popular method for the design of timber members exposed to fire, which uses an effective cross-section and mechanical properties at normal temperature. The RCSM was adopted from publication that was originally developed for single-span beams subjected to bending (Schaffer 1984).It has been introduced in EN 1995-1-2 (Eurocode 5) (CEN 2004) for a large range of timber members, including columns under compression and members under tension. Recently, the applicability of the method and its extended applications has been questioned with respect to the basis of limitations and contradictions found by advanced simulations (Klippel et al. 2012) and a comprehensive review (Schmid et al. 2014) of fire resistance test results for members in bending, tension and compression. In the present paper, results of a review of buckling members exposed to fire are presented. This paper analyses a total of 126 full-scale fire resistance tests of members subjected to buckling and using the RCSM. The analysis shows that (i) most of the literatures are of too poor quality, or incomplete, to be used for developing or verifying a design model, and (ii) considering the variability of input data, a significant scatter implies that the RCSM in its present form is not able to describe sufficiently the behaviour of timber columns exposed to fire. It is therefore recommended that the existing design approach in Eurocode 5 should be revised and further work initiated.

2 Introduction

The RCSM in EN 1995-1-2 can be used to verify the load-bearing capacity of a large number of timber member in a fire situation, e.g. bending, compression buckling or lateral torsional buckling. Although no limitations are explicitly given on the use of the RCSM, it is assumed that any verification calculation described in EN 1995-1-1 (CEN 2004) can be performed using the effective cross-section. This is in contradiction to the different properties governing the mechanical response of structural timber members and the different reduction curves for specific properties of timber with increasing temperature also given in Annex B of EN 1995-1-2. The RCSM was originally proposed for simply-supported glued-laminated (glulam) beams by Schaffer (1984). For its implementation in EN 1995-1-2, the method was further simplified and its use extended to other members, e.g. members influenced by buckling. A systematic comparison of the RCSM and fire test results was never published when drafting EN 1995-1-2. Recently, this RCSM specifying a general zero-strength layer d_0 of 7 mm was discussed in some papers (Klippel, Schmid et al. (2012), Schmid et al. (2014)). A comparison of fire test results with the RCSM of members in bending, tension and compression was presented by Schmid, Klippel et al. (2014). It was shown that the scatter of results is significant and that most reports are of such poor quality that it is not recommended to use them to verify a calculation model. Simulation results from Klippel, Schmid et al. (2012) showed that the RCSM appears to be appropriate for members in tension, but my lead to non-conservative results for members in compression.

The aim of this paper is to compare the RCSM specified in EN 1995-1-2 with actual fire test results. Test results presented here range from fire tests performed in the 1960s to recent tests performed in 2005. This paper compares fire test results in terms of the determined zero-strength layer d_0. It was focused on analysing fire tests for members in buckling, excluding members with failure in pure compression. Since the main design procedure in EN 1995-1-2 is based on the standard fire exposure EN 1363-1 (CEN 2012), only fire tests following the standard time-temperature fire curve were evaluated.

3 Analysis procedure

The large variety of available literature from different authors, fire test standards and technical setup possibilities results in a large spectrum of reports and papers to analyse. To overcome a subjective judgement of data, a procedure to classify results was followed, as described in this section. The procedure for the suitability, classification and extension of data is described in detail by Schmid, Klippel et al. (2014).

3.1 Suitability and classification of references

In the first step, the available literature was analysed, reports and papers had been classified as primary or secondary. Secondary references were considered as those where test reports were used to determine or improve a design method instead of reporting test results. These are often referred to when the reliability of today's design models is discussed (Lie 1977, Scheer 1994). Only primary references give details of conducted tests, but do not contain necessary design recommendations and design rules. For the quantitative analysis of the zero-strength layer, mainly primary references were used.

In the second step, the suitability of the references was evaluated before further analysis. Although very ambitious and costly, some test series are not suitable for further analysis with respect to the assessment of the RCSM and determination of the zero-strength layer respectively, since serious mistakes and wrong assumptions were made. Sometimes the results of such studies are misinterpreted to prove agreement with today's calculation methods. Although these references were summarised, and errors highlighted in this study, in order to point out the unsuitability of the references with respect to the RCSM and to identify the mistakes which can be avoided in future test series. The data from these references were not analysed further.

When a reference was found to be suitable for further analysis, the reported data sets were classified as (i) certain data, (ii) uncertain data, and (iii) very uncertain data, depending on the availability of fire test details and the characterisation of the materials tested.

To classify the references, the test characteristics reported as data sets were evaluated in terms of the feasibility of performing backwards calculation of a corresponding zero-strength layer. The requirements to consider a data set as complete, and the calculated results for the zero-strength layer as certain, call for the following test details in the references: (i) standard fire exposure during loaded tests with (ii) well-defined support conditions, (iii) documentation of the failure time, (iv) appropriate definition of the timber at normal temperature to allow a prediction of the load-bearing capacity, (v) adequate initial moisture content (MC) of the timber member before the fire test and (vi) documentation of the residual cross-section by means of appropriate measurements. Only determined values for the zero-strength layer based on data sets fulfilling all these obligatory requirements are classified as certain. If one requirement was not fulfilled, the result was classified as uncertain. If more than one compulsory requirement was not fulfilled, the result was classed as very uncertain.

3.2 Extension of the data sets

Available reports describe fire tests with varying degree of completeness. To extend incomplete data sets, different procedures were used to allow further analysis of the test reports. Two major problems were observed when analysing the available literature. (i) the poor quality of the material determination allowing a prediction of the load-bearing capacity at normal temperature and (b) the inadequate description of the boundary conditions for the buckling tests considering the support conditions.

3.2.1 Estimation of the support conditions

3.2.1.1 General

In general, the buckling behaviour of structural members is complex. The mechanical performance of timber members was investigated in many studies at normal temperature (Theiler et al. 2012). For the fire situation, different models are available, e.g. the model of (Lie 1977, APA 2009) where the residual cross-section is considered alongside a reduction of the strength and stiffness by 20%.

In EN 1995-1-1 (CEN 2004), the concept of the Effective Length Method (ELM) is given for the calculation of the load-bearing capacity of timber columns at normal temperature. Using this method the buckling problem can be reduced to the structural system of a simply supported column. Non-linear effects are taken into account by means of a buckling factor k_c. Alternative to the ELM, according to EN 1995-1-1 a second order analysis may be performed which tends to deliver non-conservative results compared to the ELM when using mean values for the MOE in bending (Theiler, Frangi et al. 2012). For the fire design, EN 1995-1-2 specifies the RCSM which is also valid for buckling members.

In the present investigation, the zero-strength layer for the buckling situation was determined using the ELM: (i) due to the intention to use mean values for strength and stiffness properties, and (ii) due to the fact that the RCSM should be capable to be used together with the ELM as intended by designers.

To estimate the buckling conditions typical for fire testing frames a Finite Element Analysis (FEA) was conducted. Results were used to perform appropriate backwards calculation of the load-bearing performance of the columns tested in fire.

3.2.1.2 Buckling lengths in fire testing frames

The support conditions are important for the analysis of tests at normal temperature as well as for fire resistance tests. In some of the literature, timber columns were placed between horizontal supports at both ends, e.g. a horizontal moving but not rotating top support (e.g. a spreader beam).

The shape influence of the column end surface in buckling was analytically and experimentally investigated by König (1988).The effective length is dependent on the radius r of the contact surface. The two limiting cases can be described by the Euler mode 2 with pin jointed ends and an effective length $l_k = l$ (buckling factor 1.0) and at the other extreme where $r = \infty$ corresponding to Euler mode 4 with fixity (clamped support) at both ends and an effective length $l_k = 0{,}5 \cdot l$ (buckling factor 0.5), see *Figure 1*. Timber specimens exposed to fire keep often the curvature after the test developed during the fire test under loaded conditions. This can be used to evaluate support conditions with respect to their mechanical boundary conditions, see *Figure 2*. The cross laminated timber (CLT) wall element was placed on the bottom to a horizontal CLT to reflect building practice. The top support was free to rotate. It can be observed that the horizontal support at the bottom end (r = ∞) corresponds to restraint conditions (clamped support) while for the top end the pinned support is clearly visible in *Figure 2*.

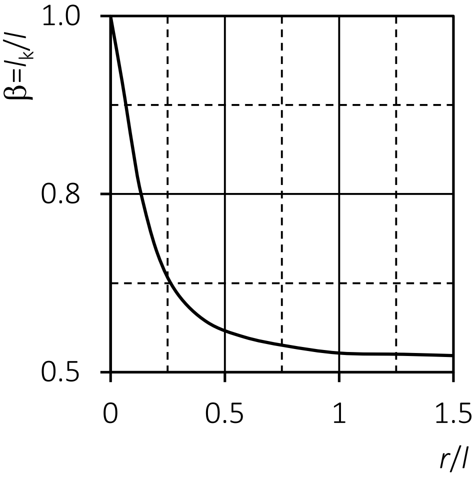

Figure 1. Effective length, expressed as $l_k = \beta \cdot l$ *as function of the end surface radius* (König 1988).

Figure 2. Buckling shape of a CLT element after the fire resistance test with an elastic clamping at the bottom end and pinned at the top end (Schmid et al. 2015).

3.2.1.3 Finite Element analysis to investigate the support conditions

In the past, many fire testing frames did not use well defined support conditions. The influence of the actual support conditions on the load-bearing behaviour of timber columns in buckling subjected to compression was studied with non-linear Finite Element Analyses (FEA). These simulations used test data obtained from the tests at normal temperature (Theiler, Frangi et al. 2012) to verify the model. A three-dimensional FE model was implemented in Abaqus using a phyton script to control a variety of input parameters. The analyses were performed to show the influence of a non-rotating and horizontal support on the buckling behaviour of timber columns loaded in compression. Three-dimensional solid brick elements were used with the "Concrete Damaged Plasticity" (CDP)-model provided by the Abaqus material library to describe the material behaviour. The CDP-model is able to model both the linear elastic brittle behaviour of timber in tension and the linear elastic plastic behaviour under compression. The developed Abaqus model was first verified by comparing the results from the simulations with the test results of Theiler, Frangi et al. (2012), who investigated the behaviour of 50 columns (constant $w = 140$ mm , $h = 160$ mm, and varying $l =$1400, 2300, 3200 mm) under compression load.

Prior to testing, the lamellas of each column were thoroughly inspected for knots and the dynamic modulus of elasticity was measured. Based on this information, Theiler, Frangi et al. (2012) estimated the strength and stiffness of each lamella. This information for the material properties of each lamella was introduced in the Abaqus model. Simulations and tests were in good agreement with regard to both the initial stiffness and ultimate strength of the columns. Both pinned and fixed support conditions were modelled and showed that a horizontal support, i.e. a stiff steel beam, coincides with the behaviour of fixed support conditions for a timber column. Further, mixed support conditions (FP) typically used in fire resistance tests were investigated. Results for a comparison of the support conditions are given in EN 1995-1-2. The FEA results were used to determine appropriate buckling lengths for the buckling model given in EN 1995-1-2. This assumption is supported by König (1988). For mixed support conditions (FP) with a pinned support and a horizontal support, a conservative buckling factor (slightly lower value than following the FEA) of 0.7 was used in the analysis. For support on horizontal and non-rotating surfaces (elastic clamping) the buckling factor 0.5 was used.

3.2.2 Estimation of the material properties

It is self-evident that the timber quality of members tested in fire has a large influence on the load-bearing capacity. In most of the literature, timber is graded using different philosophies either related to the bending strength at normal temperature, visual grading or distinction in solid or glulam timber only. The lack of thorough investigations into the material properties, and the less than satisfactory prediction methods used by many authors in the references, lead to significantly high uncertainties in the conclusions regarding the load-bearing capacity and subsequently in the results of the zero-strength layer depth based on these tests. Any underestimation of the strength at normal temperature leads obviously to unacceptable general conclusions and to unusable data for the development of any calculation method. Results in this paper that show negative values for the zero-strength layer imply either (i) a contribution of the char layer to the load-bearing capacity, (ii) an improvement in strengths of the heated cross-section or (iii) an underestimation of the strengths at normal temperature. Since (i) and (ii) can be excluded, the error source is the limited information describing the material tested in the fire situation.

Reference tests at normal temperature are considered as a reliable method for the prediction of the load-bearing capacity of the specimens. As no buckling tests were performed in the literature analysed, the determined material properties, e.g. density, were used to predict the load-bearing capacity of the columns and determine the input data for a backwards calculation of the zero-strength layer. Details of the procedure are given in Section 4 and in (Schmid, Klippel et al. 2014).

4 Fire test results and analysis

In total, 126 fire test results were collected and reviewed, with 84 tests suitable for further analysis to perform a backwards calculation to determine the zero strength layer depth. Details are given in Table 1 specifying the test program, standard and parameters as well as the number of performed tests. Report summaries in Sections 4.1

to 4.7 are needed, since the testing procedures vary significantly and make it impossible to compare all details in the tables. Furthermore, many of the references are literature published in languages other than English.

Table 2. Overview of the references available and further analysed.

Author	Title and Classification of results	No. of fire tests*	Test program and test parameters and Determined resistance
Fackler (1961)	Essais de résistance au feu (Fire resistance tests)	5 (2)	Geometry
	Not Suitable		41 to 72 min
Malhotra and Rogowski (1967)	Fire-Resistance of Laminated Timber Columns	26 (16)	Grade, adhesive, geometry, species, load level, fire retardant treatment, fire protection system
	Very Uncertain		23 to 77 min
Klement et al. (1972)	Das Brandverhalten von Holzstützen unter Druck-beanspruchung (The fire behaviour of timber columns exposed to compression load)	72 (68)	Monolithic and segmented, grade, solid and glulam timber, resorcinol and urea adhesives, geometry, load ratio
	Uncertain		20 to 114 min
Haksever (1976)	Untersuchungsbericht zum Brandverhalten von brettschichtverleimten Holzstützen mit Rechteck-querschnitt (Report on the fire behaviour of glue laminated timber columns with rectangular cross-section)	17 (15)	Glulam columns, geometry, support condition (elastic clamped and simply supported)
	Uncertain		22 to 96 min
Ali and Kavanagh (2005)	Fire resistance of timber columns	6 (6)	Geometry
	Not Suitable		6 to 20 min

* number in brackets specifies the no. of fire tests with rectangular cross-sections which are considered in this study if found Suitable

4.1......Fackler, 1961

The oldest reference available presents results from a larger study on the fire resistance including different kind of building products. Two rectangular loaded glulam columns were tested with a fire resistance of about 48 minutes. Since neither the support conditions nor the timber grade is specified nor reference tests reported, no further evaluation of these fire tests was performed in this study.

4.2......Malhotra and Rogowski (1967)

26 full-scale tests with glued laminated timber columns were performed of different squared and rectangular cross-sections of approximate constant area equal to the squared 230 mm x 230 mm. The grade was UK grade LB and four different adhesives were used to produce the columns. Tests with different load-levels were performed in a loading frame with restrained support conditions and with constant loading. Some tests were performed with applied fire protection or fire-retardant treatments, 16 tests were evaluated further in the present investigation. For the analysis, the specific strength and MOE in bending was determined by means of the density. Thus, the results are classed as very uncertain although an exponential regression show limited deviations, see *Figure 3*. Further results are given in Table 2. The exponential behaviour of timber members in fire was earlier observed (König 1995).

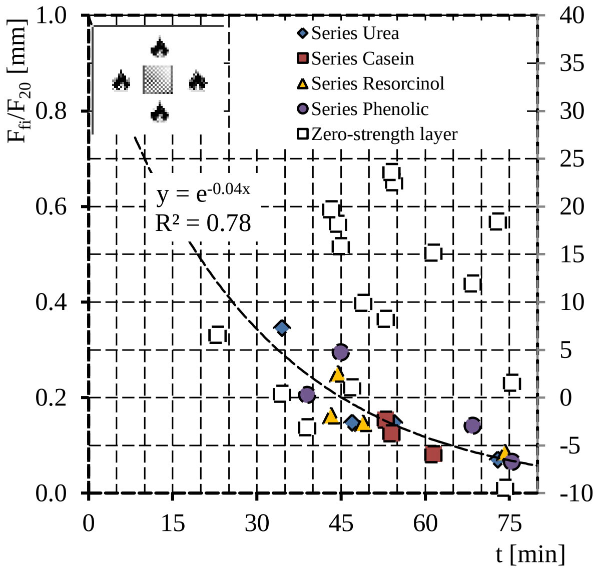

Figure 3. The load-ratio and failure time of the test results (coloured markers) including an exponential regression line and the corresponding zero-strength layer depths (white squares).

4.3 Klement et al. (1972), Stanke et al. (1973), Seekamp (1969), and Rudolphi (1979)

A comprehensive test program was performed to investigate the fire performance of timber members in buckling by Stanke et al. (1973). A different selection of tests and different details are given in different reports with the intention to develop national verification models, e.g. the German F60 criterion (Seekamp and Stanke 1969). Thus, a large number of parameters was varied, see Table 2. Segmented cross-sections were not further analysed in this review. The fire tests came along with an investigation of the source material comprising the moisture content, the density (all columns), the compression strength and stiffness (cubes 20 mm x 20 mm x 60 or 120 mm; ca. every third column), the MOE in bending (static; three columns) and the dynamic MOE using ultrasonic sound transmission.

The length of the tested members was 3650 mm while the fire exposed length was 3000 mm (non-centric). In some fire tests the oxygen content of the exhaust gases was measured (around 5%) to control the completeness of the combustion. Fire tests lasted from 10 min to 114 min and were terminated after buckling failure of the member.

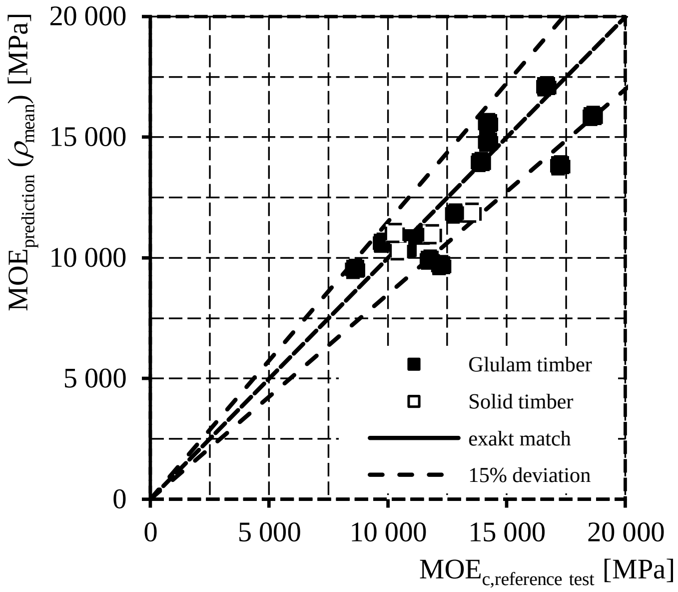

Figure 4. The predicted values for the modulus of elasticity in compression based on the reference tests.

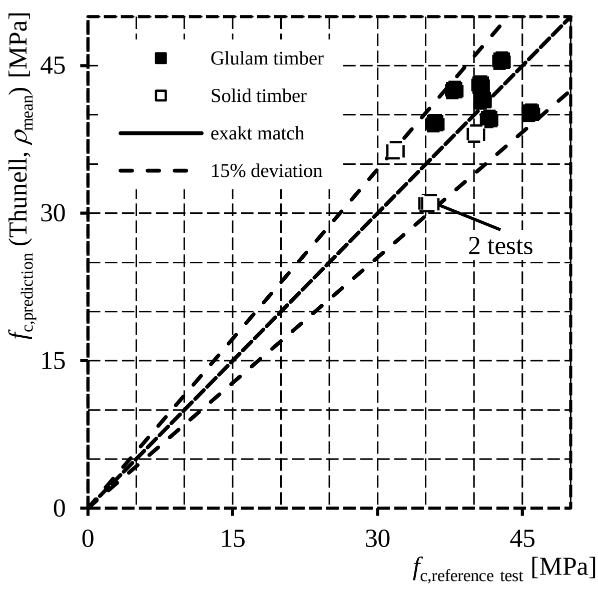

Figure 5. The predicted values for the compression strength using the model of Thunell (1971) based on the density of the specimens.

The charring depth and the geometry of the residual cross-section were evaluated on the basis of unloaded, 500 mm long reference specimens exposed in the same fire test. One residual cross-section was used to determine the notional charring depth (rectangle with corresponding area) which is in-line with the actual design model (CEN 2004). The moisture content of the columns at the beginning of the fire test was not specified. Deviating from the verification model presented in (Stanke, Klement et al. 1973), the buckling length for the actual testing frame with a horizontal, non-rotating top support and a hydraulic jack was estimated to $0{,}75l$ following Section 3.2.1.3. As the density is the only material characteristic available for all columns it was used to estimate the compression strength f_c and the modulus of elasticity in compression for the analysis presented this study. To use the buckling model given in EN 1995-1-2 the MOE in bending was determined by means of the density using the technique presented by Schmid, Klippel et al. (2014) based on the relationship between compression strength and MOE in bending given in EN 1194 (CEN 1999), EN 338 (CEN 2009) and JCSS (JCSS 2007).

A comparison of the prediction of the MOE by using the density and results of the reference tests is given in *Figure 4*. A comparison of the prediction of the compression strength using the density and results of reference tests prediction is given in *Figure 5*. In both figures it is shown that the error of prediction is about 15%. The span of ±15% for the strength and stiffness was later used to estimate the influence on the zero-strength layer depth. When the strength or the MOE in compression was available, this value was used for further calculations.

The residual cross-section for glulam members was determined for this study using the specified linear equation by Stanke, Klement et al. (1973) while for solid members no equation was available a 10% increased value was used for further calculations in this study. Using the assumptions for the estimation of the material properties the results are evaluated as Uncertain, results are given in *Figure 6* and Table 2. The variation of the strength and stiffness would result in 2,7 mm lower and 2 mm higher values respectively (maximum deviation values).

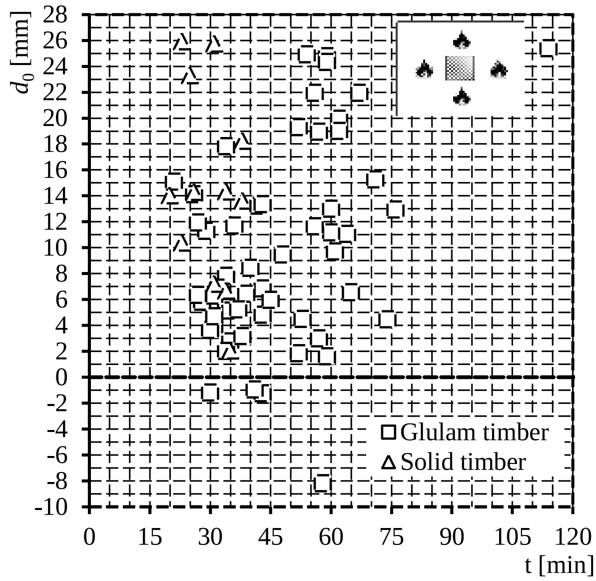

Figure 6. Calculated zero-strength layer for glulam and solid timber columns.

4.4......Haksever (1976)

The report contained the imprecise support conditions of earlier fire tests (Stanke, Klement et al. 1973), thus simply supported (PP) soft wood (GK1, German grading class 1) and glulam columns (glued with resorcinol adhesive) were tested and compared to the elastic climbed condition (four tests). To define the material properties, the strength f_c and the stiffness E_c under compression (parallel to grain) were determined by means of eight specimens (areas 140 mm x 140 mm and 280 mm x 280 mm; lengths 600 or 900 mm) produced from the same materials as the columns. The charring rate was determined to 0,7 mm/min by means of unloaded specimens placed at the bottom of the furnace. The residual cross-sections and the charring depths specified in the report were estimated using the middle section of the specimens.

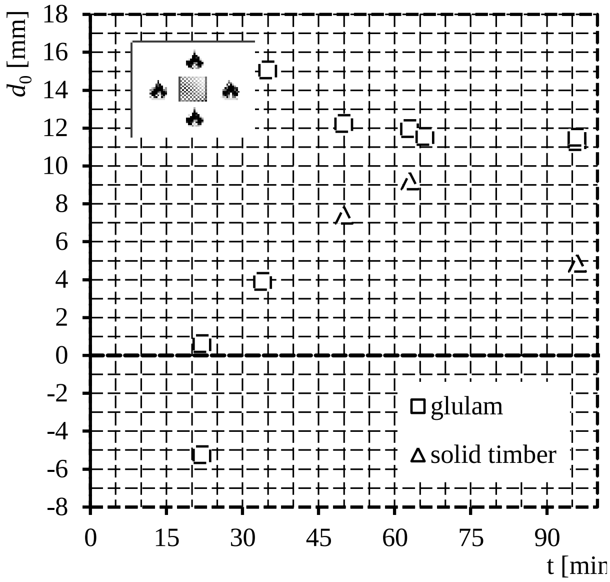

Figure 7. Calculated zero-strength layer for glulam and solid timber columns.

In the analysis for this study, the results for the reference tests were used for all columns with the particular cross-section. The MOE in bending was determined by means of the compression strength f_c using the technique presented in (Schmid, Klippel et al. 2014) based on the relationship between compression strength and MOE in bending given in EN 1194, EN 338 and JCSS. Due to the weak material prediction as well as the limited information on the residual cross-sections the results are considered as Very Uncertain. Results are shown in *Figure 7* and given in Table 2.

4.5 Lie (1977)

The work is used in literature as reference for design models for timber columns in buckling although it is a secondary source where 67 fire tests in buckling and bending were evaluated. However, it is not further specified which fire test results of columns were evaluated. References lead back to fire tests with members in bending and buckling reporting beam tests and 88 column tests (Malhotra and Rogowski 1967, Klement, Rudolphi et al. 1972). It remains unknown which selection criteria were used and which tests were further used to develop the model. Further, in (Lie 1977) test loads are described using the indication “allowable load” which indicates national regulation systems that are not further specified. It is mentioned that the actual safety factors was not known. In this study, this reference was not used any further.

4.6 Rudolphi (1978)

The doctoral thesis deals with the fire design of steel and timber members in general and the validity of fire resistance tests performed at different labs in specific. No fire resistance tests were conducted in this study but results reported by Klement, Rudolphi et al. (1972) leading back to tests of Stanke, Klement et al. (1973). This secondary source is referenced in literature to verify calculation models, e.g. Schnabl et al. (2011) gives interesting details about the fire tests performed earlier. Whereas for steel columns tested in the same fire testing frame the buckling factor was assumed to be $0{,}7\mathrm{l}$ the buckling length of timber columns were assumed equal to the column length. The support conditions and effects of an elastic clamping were discussed but rejected later. The author estimated the charring depth at the failure time for all fire tests and presented linear regression functions for all results of Klement, Rudolphi et al. (1972). Since the curves for a reduced buckling length of $0{,}7\mathrm{l}$ and $0{,}5\mathrm{l}$ would intersect at about 10 and 20 mm at $\mathrm{t} = 0$ min respectively it was concluded that the support conditions were pinned on both ends (PP) instead of ascribing the increase to losses in strength and stiffness. With this observation, it can be concluded that the author was the first observing and quantifying a zero-strength layer. Based on his observations a very rough estimation of the value can be estimated up to 20 mm. As the report is a secondary source, this study was not further evaluated in this paper.

4.7 Ali and Kavanagh (2005)

The authors performed six fire resistance tests with timber columns of 1800 mm length to determine failure temperatures depending on the load level and slenderness as available for steel structures. Two different cross-sections (100 mm x 100 mm and 75 mm x 75 mm) of solid timber columns (C24) were tested as buckling members in normal temperature (reference test) and in the fire situation. No information on the support condition is found in the reference but according to personal author information the columns were simply supported on the top and bottom using half spherical steel supports (Ali, Faris, personal communication, 20th May, 2015) representing pinned supports on both ends. Fire tests were terminated at buckling failure between 6 and 20 minutes. The charring layer depth was evaluated but the shape of the residual cross-section was not further investigated. Failure loads are given in ratio to the design model of EN 1995-1-1 (402 kN and 106 kN) and reference tests (446 kN and 127 kN). All values deviate considerably from a correct estimation of the buckling failure load at normal condition (164 kN and 68 kN disregarding safety factors) and were not considered for further estimation in this paper.

5 Results and discussion

The evaluation of buckling members required specific effort since the support conditions are crucial and standard testing has experienced significant changes since beginning of fire testing. Early design models assumed simply supported columns while later tests showed significant influence of the support conditions even in fire tests.

The results of the comprehensive analysis of performed fire tests support the concerns raised recently. In this paper, on the basis of extensive experimental investigations supported by FEA it could be shown that the zero-strength layer d_0 for timber members subjected to compression is different to the constant value currently used in EN 1995-1-2. This paper extends the analysis of the zero-strength layer significantly by a comprehensive evaluation of 126 fire tests under ISO-fire exposure. The mean value for the zero-strength layer of all results is about 11 mm for members in buckling (S.D. about 8 mm). Further details are given in Table 2. In general, results show that no significant difference between glulam and solid timber members was found but a considerable scatter of results indicate severe problems to describe the complex processes of fire exposed timber members in buckling with a single value.

Table 2. Minimum, mean and maximum values for the zero-strength layer of the analysed fire test results for buckling members (values in mm), number or results and classification of sources.

	Malhotra, 1967 (glulam timber)	Haksever, 1976 (glulam timber)	Haksever, 1976 (solid timber)	Stanke et. al, 1973 (glulam timber)	Stanke et. al, 1973 (solid timber)
min	-9.4	0.7	4.9	-8.2	2.0
mean	10.0	12.5	6.6	9.9	14.1
max	23.6	27.2	9.2	25.4	25.9
No. of results	16	11	4	53	12
Classification	Very Uncertain	Very Uncertain	Very Uncertain	Uncertain	Uncertain

6 Conclusions

In general, the analysis of fire tests is complex since the references give only limited information regarding the material tested. Where information was lacking, the data sets were extended and results classified in Certain, Uncertain and Very Uncertain. None of the tests performed meet today's requirements of verification tests and none of the reports meet the requirements to perform a backwards calculation of the zero-strength layer depth without appropriate assumptions. Thus, not a single reference is classified Certain.

Today, in EN 1995-1-2 (Eurocode 5) (CEN 2004) the complex behaviour of timber members in fire is described by a single constant value of d_0 = 7 mm developed originally for bending members. When the design model was presented a further verification of the design model using the zero-strength layer was proposed (Schaffer 1984), however this was not performed. In this paper it is shown that the available full-scale fire tests cannot be used to verify the design model introduced also for buckling members. The scatter of results indicates either that the uncertainties regarding the material tested cannot be controlled easily or that the zero-strength layer may be depending on several parameters.

As the EN 1995-1-2 is under revision, it is recommended to consider the modification of the existing design model with respect to the different mechanical models for bending and buckling since earlier investigations showed different results for members in tension, compression and bending (Klippel, Schmid et al. 2012, Schmid, Just et al. 2014). Based on the analysis of all test results presented in this paper a mean value for the zero-strength layer depth for buckling members in the range of about 11 mm has been obtained.

For further investigations a combined approach of simulations and verification tests in model and full-scale is recommended. Simulations should cover the variation of the material properties as well as the change of stiffness when the member is reduced by char.

7 References

Ali, F. and S. Kavanagh (2005). "Fire resistance of timber columns." Journal of the Institute of Wood Science 17(2): 85-93.

APA (2009) "Calculating Fire Resistance of Glulam Beams and Columns."

CEN (1999). EN 1194: Timber structures — Glued laminated timber — Strength classes and determination of characteristic values. European Standard. Brussels, European Committee for Standardization.

CEN (2004). EN 1995-1-1: Design of timber structures - Part 1-1: General - Common rules and rules for buildings. Brussels, European Committee for Standardization.

CEN (2004). EN 1995-1-2 Design of timber structures – Part 1-2: General – Structural fire design. Brussels, European Committee for Standardization.

CEN (2009). EN 338: Structural timber – Strength classes. Brussels, European Committee for Standardization.

CEN (2012). EN 1363-1: Fire resistance tests - Part 1: General requirements. Brussels, European Committee for Standardization.

Fackler, J. P. (1961). Essais de résistance au feu. Paris, Centre Scintifique et Technique du Bâtiment, Paris, France.

Haksever, A. (1976). Untersuchungsbericht zum Brandverhalten von brettschichtverleimten Holzstützen mit Rechteckquerschnitt. Technische Universität Braunschweig, Berlin, Germany.

JCSS (2007). Probabilistic Model Code. (http://www.jcss.byg.dtu.dk), Joint Committee on Structural Safety, Danmark.

Klement, E., R. Rudolphi and J. Stanke (1972). Das Brandverhalten von Holzstützen unter Druckbeanspruchung (in German), Germany.

Klippel, M., J. Schmid and A. Frangi (2012). The Reduced Cross-section Method for timber members subjected to compression, tension and bending in fire. International Council for Research and Innovation in Building and Construction, Working Commission W18 – Timber Structures, Meeting 45 (CIB-W18 Meeting 2012). Växjö, Sweden, CIB-W18 Meeting 2012. 45: CIB-W18/45-16-11.

König, J. (1988). The structural behaviour of axially Loaded Wood Studs Exposed to Fire on one Side. Report I8808057. Stockholm, Sweden, TräteknikCentrum.

König, J. (1995). Fire Resistance of Timber Joists and Load Bearing Wall Frames. Stockholm, Trätek, Institutet för träteknisk forskning: 102.

Lie, T. T. (1977). "A method for assessing the fire resistance of laminated timber beams and columns." Canadian Journal of Civil Engineering 4(2): 161-169.

Malhotra, H. L. and B. F. W. Rogowski (1967). Fire Resistance of Laminated Timber Columns. Fire and Structural Use of Timber in Buildings, HMSO.

Schaffer, E. (1984). "Structural Fire Design: Wood, Research Paper FPL 450." US Department of Agriculture, Forest Service, Forests Products Laboratory, Madison, WI.

Schaffer, E. L. (1984). Structural fire design: wood. Madison, Wis., U.S. Dept. of Agriculture.

Scheer, C. K., Thorsten (1994). "Brandschutz unbekleideter Holzbauteile - Mindestquerschnitte, die einer Feuerwiderstandsklasse F30 genügen." Bautechnik 71(4): 6.

Schmid, J., A. Just, M. Klippel and M. Fragiacomo (2014). "The Reduced Cross-Section Method for Evaluation of the Fire Resistance of Timber Members: Discussion and Determination of the Zero-Strength Layer." Fire Technology.

Schmid, J., M. Klippel, A. Just and A. Frangi (2014). "Review and analysis of fire resistance tests of timber members in bending, tension and compression with respect to the Reduced Cross-Section Method." Fire Safety Journal Fire Safety Journal, 68, 81 - 99.

Schmid, J., A. Menis, M. Fragiacomo and G. Bochicchio (2015). "Behaviour of loaded cross-lamnated timber wall elements in fire conditions." Fire Technology.

Schnabl, S., G. Turk and I. Planinc (2011). "Buckling of timber columns exposed to fire." Fire Safety Journal 46(7): 431-439.

Seekamp, H. and J. Stanke (1969). "Das Brandverhalten von belasteten Holzstützen. (In German)." Bauen mit Holz 5, Germany.

Stanke, J., E. Klement and R. Rudolphi (1973). Das Brandverhalten von Holzstützen unter Druckbeanspruchung. Bundesanstalt für Materialprüfung: 37, BAM-BR 024, Berlin, Germany.

Theiler, M., A. Frangi and R. Steiger (2012). Design of timber columns based on 2nd order structural analysis. International Council for Research and Innovation in Building and Construction, Working Commission W18 – Timber Structures, Meeting 45 (CIB-W18 Meeting 2012). Växjö, Sweden.

Thunell (1971). "Grading and Strength of Timber." Holz als Roh- und Werkstoff 9(29): 4.

Discussion

The paper was presented by J Schmid

H Blass commented that if these values could be trusted would you use the mean value or 5th percentile values. J Schmid responded that he would use the mean values and that there would be many other areas where safety could be added.

K Ranasinghe commented that in the UK they have huge difficulties in accepting the concept that 7 mm is too high. He asked if J Schmid would be insisting to increase 7 mm in the next EC5 revision. J Schmid responded that they are aiming to build a model to reduce the variability in the data to establish a better value. He stated that the starting value should be ~14 mm and then one can reduce it later as variability in the data base is reduced.

S Winter agreed that more investigation would be needed and that the old data base has limitations. He stated that the problem of zero strength layer concept as the actual reduction curve is questionable. Comparison with FEM is very difficult as exact properties with increase in temperature are not available. The use of 7 mm has worked well for more than 20 years and worked well all over the world. S Winter commented that he has never heard of a collapse before expected time of fire resistance in a real fire. We need to oppose making changes to the current rules now. J Schmid related to the example of weakness of steel connection in fire design and that the old standard was built on one unreliable database. The main problem is missing information on influence of temperature on timber properties if we want to replace fire testing with models.

BJ Yeh commented on the use of 7 mm for CLT and increase of char rate to account for falling off of the char layer. J Schmid responded that CLT is more complicated with many producers and issues with loading directions.

A beam theory fracture mechanics approach for strength analysis of beams with a hole

Henrik Danielsson, Division of Structural Mechanics, Lund University, Sweden

Per Johan Gustafsson, Division of Structural Mechanics, Lund University, Sweden

Keywords: Glulam, Hole, Fracture Mechanics, Strength Analysis.

1 Introduction

A hole in a member constitutes a sudden change in the cross section and concentrated perpendicular to grain tensile stress and shear stress appear in the vicinity of the hole, see Figure 1.1. This stress situation may for relatively low external loads lead to crack propagation in the fiber direction. Looking at the design approaches for beams with a hole in timber engineering design codes over the last decades, it can be seen that the issue has been treated in many different ways. The theoretical backgrounds on which the design approaches are based show fundamental differences and there are also major discrepancies between the strength predictions according to the different codes as well as between tests and predictions according to codes (Aicher & Höfflin 2004, Höfflin 2005, Danielsson & Gustafsson 2008, Danielsson & Gustafsson 2011).

There is at the moment no fully accepted design method based on a completely rational mechanical background. There are for example no design equations for beams with a hole in the contemporary version of Eurocode 5 (2004). However, design equations are found in the German and Austrian National Annexes to EC 5. This design approach originates from the work presented by Kolb and Epple (1985), although simplifications and empirical modifications have been added over time.

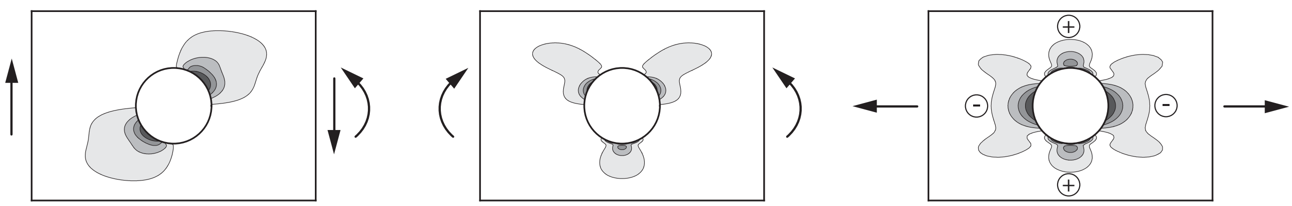

Figure 1.1. Schematic illustration of perpendicular to grain tensile stress distribution; hole placed in shear force dominated region (left), pure bending (middle) and axially loaded member (right).

For applications with concentrated perpendicular to grain tensile stress and shear stress, conventional maximum stress failure criteria are seldom of any use but instead strength analysis by means of fracture mechanics is more relevant. The EC 5 design equations for end-notched beams and dowel-type connections loaded at an angle to grain are examples of fracture mechanics based design equations.

Concerning the case of end-notched beams, an equation for the energy release rate during crack extension and the corresponding beam strength was derived by compliance analysis using beam theory almost 30 years ago (Gustafsson 1988). In its EC 5 implementation, the Gustafsson design criterion is expressed as a comparison of a nominal shear stress and the reduced shear strength, although the decisive material properties from the fracture mechanics approach are fracture energy and stiffness.

Inspired by the relative simplicity of the design equation for end-notched beams, a similar but generalized method was outlined by Gustafsson (2005). This generalized method is in the present paper in detail developed and presented for the case of beams with a hole. The application of a beam theory fracture mechanics approach for beams with a hole is more complex than for end-notched beams due to:

- the significant influence of shear makes it necessary to consider the respective contributions of modes I and II to the total energy release rate,
- the normal force acting on the cross section parts above and below the hole must be considered and
- the cross section forces and moments acting on the parts above and below the hole are statically indeterminate.

In this paper, a beam theory fracture mechanics approach for strength analysis of beams with a hole is presented. This approach is based on assumptions of an orthotropic material behavior, a beam model according to Timoshenko beam theory and a mixed mode fracture criterion based on Linear Elastic Fracture Mechanics (LEFM).

The strength analysis approach is evaluated by means of a comparison between theoretically predicted beam strengths and strengths found from experimental tests. For this purpose, test results for beams with circular holes (Höfflin 2005, Aicher & Höfflin 2006) are used as well as test results of beams with square holes (Danielsson 2008). The tests of beams with square holes are further also presented and discussed in (Danielsson & Gustafsson 2008) and (Danielsson & Gustafsson 2011).

Further evaluation is carried out by means of comparison to other strength analysis methods, including both code type methods and more general methods based on linear and nonlinear fracture mechanics approaches carried out using 2D and 3D finite element (FE) analysis.

2 Theory and model formulation

The basic concept of the present approach for analysis of beams with a hole relates to rectangular/square holes and by assumption also circular holes are analyzed. Cross section forces and moments in the beam parts above and below the hole are determined by equilibrium considering kinematic assumptions according to Timoshenko beam theory. An infinitesimally short part of the beam at the end of the hole is then considered. The forces and moment acting across a horizontal section of the infinitesimally short part of the beam, dividing it into one part above and one part below an assumed crack, are determined by equilibrium. The energy release rates for modes I and II are then obtained by using the method of work of crack closure with consideration to the deformations of the infinitesimal parts above and below the assumed crack. The beam strength with respect to cracking is then found by using a mixed mode fracture criterion.

In order to facilitate a convenient formulation, which is consistent for circular and rectangular/square holes with or without rounded corners, a number of assumptions and simplifications are introduced. These are partly based on engineering approximations and partly based on experience from experimental tests.

2.1 Basic assumptions and definition of geometry

Definitions and notation for the parameters used to describe the beam and the hole geometry are found in Figure 2.1. A circular hole with diameter 2*r* may formally be regarded as a rectangular/square hole with $a = h_d = 2r$. The parameter *s* defines the hole placement with respect to beam height and is given by the *y*-coordinate of the centre of the hole. *N*, *V* and *M* refer to values at the edge of the hole on its right hand side, although the figure below may seem to indicate another location.

The formulation of the present approach is general in the sense that it allows for any combination of cross sectional forces *N*, *V* and *M*. Depending on loading conditions and the signs of *N*, *V* and *M*, different areas in the hole vicinity are exposed to perpendicular to grain tensile stress and may experience cracking, see Figure 1.1. The most common case for practical engineering purposes is however believed to be transversal loading giving a combination of shear force and bending moment only.

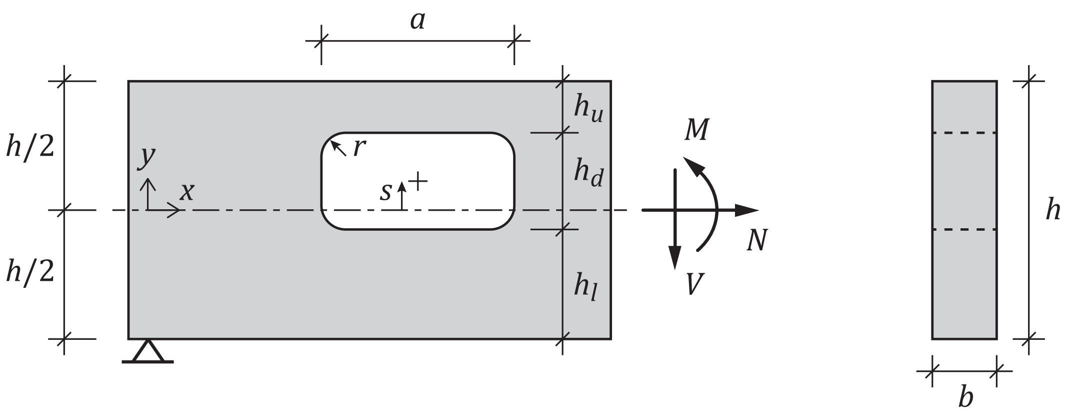

Figure 2.1. Definition of beam and hole geometry.

The location of the point of crack initiation is assumed to be known a priori and crack propagation is assumed to occur in the parallel to grain direction, which is assumed to be aligned with the beam length direction (the *x*-direction). The chosen predefined crack location is based on results from the experimental tests mentioned above of beams loaded in bending, having either a circular or a square hole. The tests with square holes having rounded corners ($r \approx 0.12h_d$) showed that cracking commonly started at the top right corner of the hole. Crack initiation commonly occurred within the rounded part of the hole corner. The tests with circular holes showed crack initiation at the hole periphery at an angle of approximately 45° with respect to the beam central axis, for holes placed centrically with respect to the beam height. Based on these findings from experimental tests, the location of the crack is in the present approach assumed to be at an angle of 45° from the beam length direction according to Figure 2.2 a), yielding a distance from the upper horizontal hole edge to the crack plane of $0.3r$.

The geometry of the beam parts above and below the hole are in the calculations simplified in the sense that these are assumed to be prismatic. As illustrated in Figure 2.2 b)-e), there are a number of feasible interpretations of the hole geometry which result in this simplification. The interpretation used for all analyses presented here is according to Figure 2.2 b). Interpretation of hole geometry according to Figures 2.2 c)-d) or some other simplification may however possibly yield equal or better agreement between model strength predictions and experimentally found beam strength.

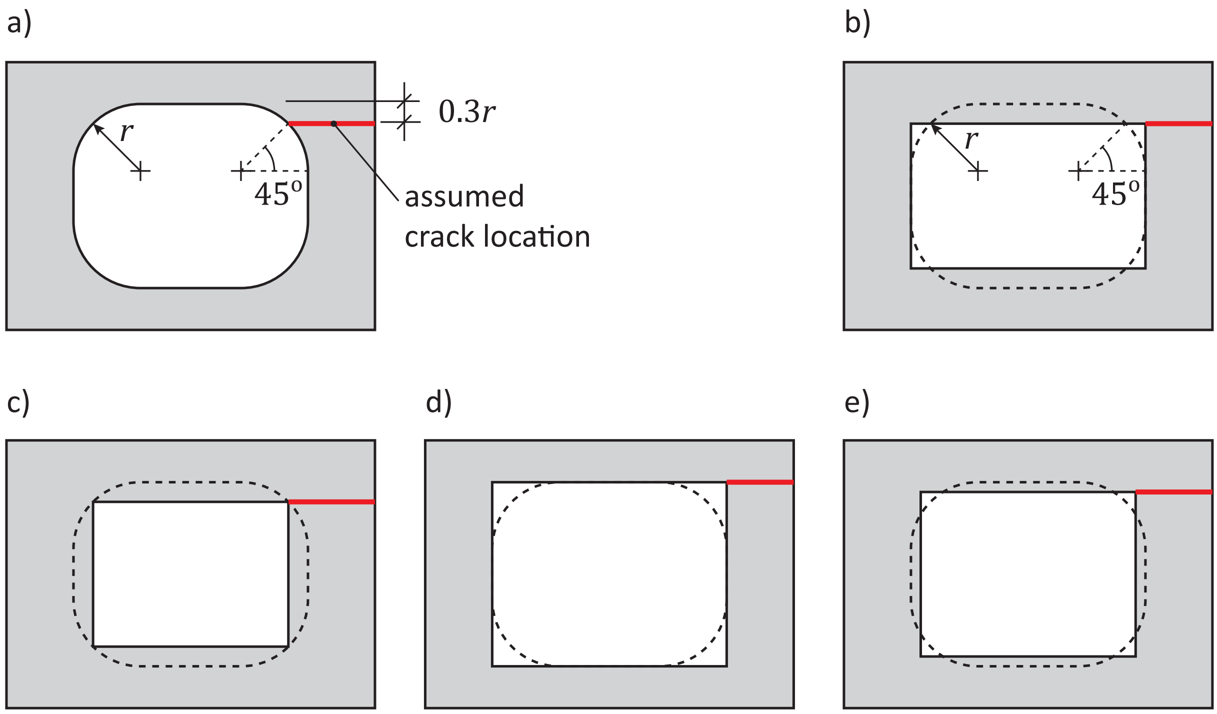

Figure 2.2. Location of crack plane and possible simplifications of the hole geometry.

2.2 Element cross sectional forces and moments

The cross sectional forces N_i, V_i and M_i (i = 1, 2) in the beam parts above (1) and below (2) the hole are determined by equilibrium considerations of the statically indeterminate system shown in Figure 2.3. Kinematic assumptions according to Timoshenko beam theory are used for beam elements 1 and 2. The vertical cross sections on the two sides of the hole are assumed to remain plane at loading. With the simplification given in Figure 2.2 b), the beam parts above and below the hole are assumed to have constant heights according to

$$h_1 = h_u + 0.3r \tag{1}$$

$$h_2 = h_l + 0.3r \tag{2}$$

To account for the elastic clamping of the beam elements in an approximate way, these are in the calculations given a length slightly longer than the actual length of the hole, $L = a + 0.5h_1$, based on numerical results presented by Petersson (1974).

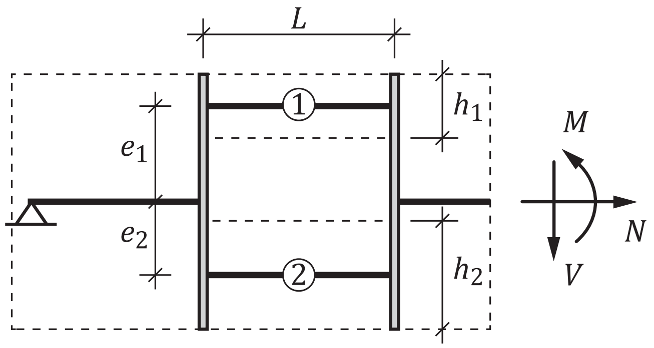

Figure 2.3. Definition of subelements 1 and 2 for beam parts above and below the hole respectively.

According to the kinematic assumptions, the infinitesimally thin cross section to the right of the hole remains plane prior to crack initiation and propagation. At crack propagation however, it is split into two cross sections according to Figure 2.4. The cross section sectional forces N_s, V_s and M_s – forcing the cross section to remain plane in the uncracked state – may be determined from equilibrium giving

$$V_s = N_1 - N_{res} \tag{3}$$

$$N_s = V_1 - V_{res} \tag{4}$$

$$M_s = M_1 - M_{res} - N_1 \frac{h_1}{2} + N_{res} \frac{h_1}{2} \tag{5}$$

where V_{res}, N_{res} and M_{res} are the resulting forces and the moment from the normal- and shear stresses acting on the right side of the cross section part above the crack plane according to

$$V_{res} = \int \tau_{xy}(y) dA = V \frac{h_1^2(3h - 2h_1)}{h^3} \tag{6}$$

$$N_{res} = \int \sigma_x(y) dA = (Nh^2 - 6Mh + 6Mh_1) \frac{h_1}{h^3} \tag{7}$$

$$M_{res} = \int \sigma_x(\bar{y}) \bar{y} dA = M \frac{h_1^3}{h^3} \tag{8}$$

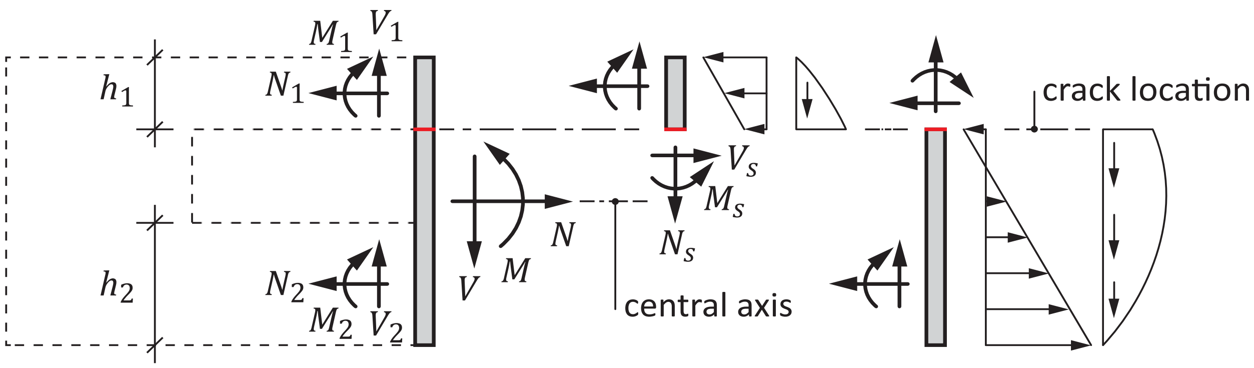

Figure 2.4. Illustration of cross section sectional forces N_s, V_s and M_s.

2.3 Relative displacements at crack propagation

At crack initiation and propagation in the beam length direction, the original beam cross section is split into two separate cross sections. The two respective cross sections are still assumed to remain plane but since they are separated, they may be deformed in different ways. The relative displacements *u* and *v* and the relative rotation θ of the two cross sections, above and below the crack plane, are illustrated in Figure 2.5. The relative displacement *v*, related to N_s, corresponds to mode I crack deformation. The relative displacement *u* and the relative rotation θ are influenced by both V_s and M_s with *u* corresponding to mode II crack deformation and θ assumed to contribute to mode I crack deformation.

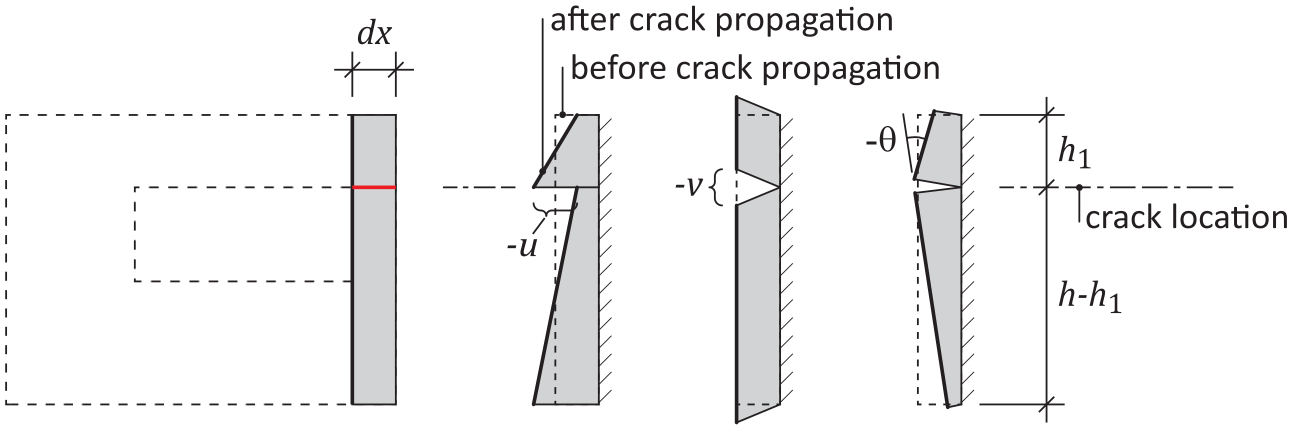

Figure 2.5. Cross section relative displacements at crack propagation.

The relations between the relative displacements *u* and *v* and the relative rotation θ and the cross section sectional forces and moment N_s, V_s and M_s may be expressed as

$$\boldsymbol{u} = \boldsymbol{C}\,\boldsymbol{F}_s \tag{9}$$

where the displacement and force vectors are given by

$$\boldsymbol{u} = [u \quad v \quad \theta]^T \tag{10}$$

$$\boldsymbol{F}_s = [V_s \quad N_s \quad M_s]^T \tag{11}$$

and the compliance matrix is given by

$$\boldsymbol{C} = \begin{bmatrix} C_{11} & 0 & C_{13} \\ 0 & C_{22} & 0 \\ C_{31} & 0 & C_{33} \end{bmatrix} \tag{12}$$

The components of the compliance matrix are determined based on the compliance of the cross sections of infinitesimal length above and below the crack plane. Considering kinematic assumptions according to Timoshenko beam theory gives

$$C_{11} = \frac{4}{E_x b}\left(\frac{1}{h_1} + \frac{1}{h-h_1}\right) dx \tag{13}$$

$$C_{22} = \frac{1}{G_{xy} b}\left(\frac{1}{h_1} + \frac{1}{h-h_1}\right) dx \tag{14}$$

$$C_{33} = \frac{12}{E_x b}\left(\frac{1}{h_1^3} + \frac{1}{(h-h_1)^3}\right) dx \tag{15}$$

$$C_{13} = C_{31} = \frac{6}{E_x b}\left(\frac{1}{h_1^2} + \frac{1}{(h-h_1)^2}\right) dx \tag{16}$$

where E_x is the parallel to grain stiffness and G_{xy} is the shear stiffness.

2.4 Crack closure work, energy release rate and fracture criterion

According to LEFM, see e.g. textbook (Hellan 1985), crack propagation is governed by crack propagation criteria which may be formulated based on, for example, the concept of strain energy release rate or stress intensity factors. The strain energy release rate G can, according to LEFM, also be calculated in terms of *crack closure work*, i.e. the work required to completely close a propagated crack. The crack closure work W may for the present application be expressed as

$$W = \frac{1}{2}\boldsymbol{F}_s^T\boldsymbol{u} = \frac{1}{2}\boldsymbol{F}_s^T\boldsymbol{C}\boldsymbol{F}_s =$$

$$= \underbrace{\frac{1}{2}(C_{11}V_s + C_{13}M_s)V_s}_{W_{II,u}} + \underbrace{\frac{1}{2}C_{22}N_s^2}_{W_{I,v}} + \underbrace{\frac{1}{2}(C_{31}V_s + C_{33}M_s)M_s}_{W_{I,\theta}} \tag{17}$$

where W_I and W_{II} refer to the crack closure work related to mode I and II respectively. Indices u, v and θ refer to the relative displacements and the rotation illustrated in Figure 2.5 above. According to LEFM, the stress intensity factors K_I and K_{II} are proportional to the applied load. The principle of superposition may be used for multiple load cases giving contributions in the same mode of deformation. For the present application this means that the mode I stress intensity factor may be expressed as

$$K_I = K_{I,v} + K_{I,\theta} \tag{18}$$

The relationship between the mode I and mode II stress intensity factors K_i and the corresponding energy release rates G_i (i = I, II) is given by

$$K_i = \sqrt{E_i G_i} \tag{19}$$

where E_i (i = I, II) is a measure of the stiffness of the material with respect to the corresponding mode of deformation (Gustafsson 2002).

The energy release rate at crack extension over an area $dA = bdx$ is equal to the corresponding crack closure work giving for the present case

$$G_{I,v} bdx = W_{I,v} \quad (20)$$

$$G_{I,\theta} bdx = W_{I,\theta} \quad (21)$$

$$G_{II,u} bdx = W_{II,u} \quad (22)$$

and

$$G_I = \left(\sqrt{G_{I,v}} + \sqrt{G_{I,\theta}}\right)^2 = \frac{\left(\sqrt{W_{I,v}} + \sqrt{W_{I,\theta}}\right)^2}{bdx} \quad (23)$$

$$G_{II} = \frac{W_{II,u}}{bdx} \quad (24)$$

In order to determine the beam strength with respect to cracking, a crack propagation criterion needs to be chosen. In the present applications, with in general mixed mode of loading, the following interaction criterion has been used

$$\left(\frac{G_I}{G_{Ic}}\right)^m + \left(\frac{G_{II}}{G_{IIc}}\right)^n = 1.0 \quad (25)$$

where G_I and G_{II} are the energy release rates in mode I and II given above and where G_{Ic} and G_{IIc} are the corresponding critical energy release rates (or fracture energies). Results presented in Sections 4 and 5, relating to analysis of beams with a hole using the present approach, are based on $m = n = 0.5$ and material property parameters according to Table 1. The choice of crack propagation criterion is not obvious, and other criteria could possibly be more suitable. In case of negative values of G_I and/or G_{II}, the negative contribution is ignored and fracture in pure mode I or II is considered.

Table 1. Material property parameters used for strength analysis.

Parameter	Notation	Value
Parallel to grain stiffness	E_x	12 000 MPa
Shear stiffness	G_{xy}	600 MPa
Fracture energy, mode I	G_{Ic}	300 Nm/m^2
Fracture energy, mode II	G_{IIc}	900 Nm/m^2

3 Comparison to end-notch beam equation

The present analysis approach for beams with a hole has many features in common with the LEFM-based design approach for notched beams, originally presented by Gustafsson (1988) and with modifications included in EC 5. The present approach for strength analysis of beams with a hole may also be used for analysis of notched beams, since this is essentially only a special case in terms of the general geometry illustrated in Figure 2.1.

As mentioned in the introduction, there are however some differences in the general formulation between the two approaches. For the end-notched beam approach, no distinction between modes I and II is made in terms of the crack propagation criterion and the material is characterized by the mode I fracture energy only. Another difference relates to the effect of elastic clamping of the reduced beam parts at the section where the notch or hole corner is located, which is considered partly different in the two approaches. The expression for the nominal beam strength with respect to cracking at a right angled notch derived by Gustafsson (1988) reads

$$\frac{V_c}{A_{net}} = \frac{V_c}{b\alpha h} = \frac{\sqrt{G_c/h}}{\sqrt{0.6(\alpha-\alpha^2)/G_{xy}+\beta\sqrt{6(1/\alpha-\alpha^2)/E_x}}} \tag{26}$$

where V_c is the crack shear force, A_{net} is the net cross section area at the reduced cross section and where α and β are defined in Figure 3.1.

Illustrations of the predicted beam strengths as influenced by the normalized beam height α and the normalized notch length β according to the two approaches are shown in Figure 3.1. The comparison is based on a beam of height h = 500 mm, with $G_{Ic} = G_{IIc}$ = 300 Nm/m^2 and values of the exponent in Equation 25 as $m = n = 1$. For this choice, i.e. for $G_{Ic} = G_{IIc}$ and $m = n = 1$, is the mixed mode crack propagation criterion the same for both calculations. More or less slight differences in predicted strengths are to be expected due to the differences in the model formulations with respect to the influence of the elastic clamping of the reduced cross section.

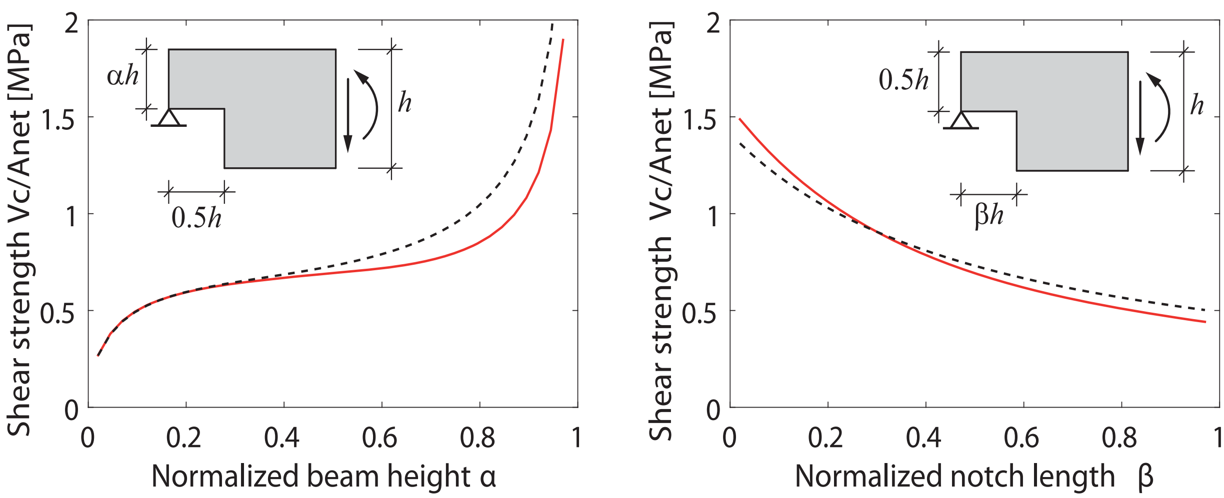

Figure 3.1. Strength according to Equation 26 (dashed black) and present approach (solid red).

4 Comparison to experimental tests

Examples of theoretically predicted strengths for beams with a hole are presented in Figures 4.1 and 4.2, where also results of experimental tests on beams with circular holes (Höfflin 2005, Aicher and Höfflin 2006) and with square holes (Danielsson 2008) are shown. Theoretical beam strengths refer to the crack propagation load predicted according the theory presented in Section 2, using Equation 25 with $m = n = 0.5$ and with material data according to Table 1. The net cross section area is defined as $A_{net} = b(h-h_d)$ and the strength from experimental tests corresponds to the load at the instant of crack propagation across the entire beam width b.

Beam and hole geometries are for these illustrations chosen based on availability of test results, yielding partly different geometries for the case of circular and square holes respectively. Results presented in Figure 4.1 relate to the influence of beam height, hole size and bending moment to shear force ratio for holes centrically placed with respect to beam height (s = 0). Results presented in Figure 4.2 relate to the influence of hole corner radius and hole placement with respect to beam height.

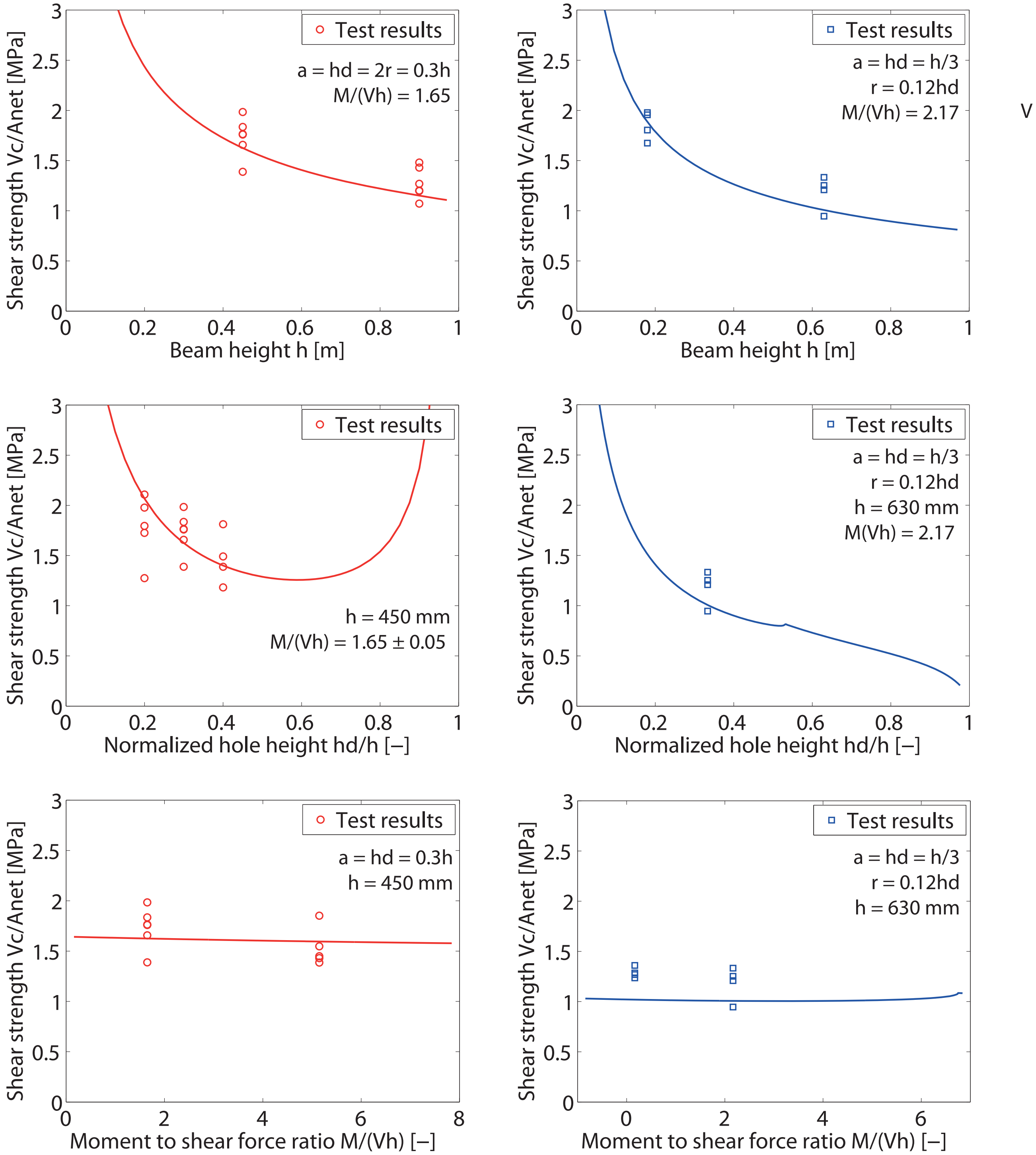

Figure 4.1. Experimentally found strength and theoretically predicted strength as influenced by beam height, hole size and bending moment to shear force ratio. Left (in red): Circular holes (Höfflin 2005, Aicher & Höfflin 2006). Right (in blue): Square holes (Danielsson 2008).

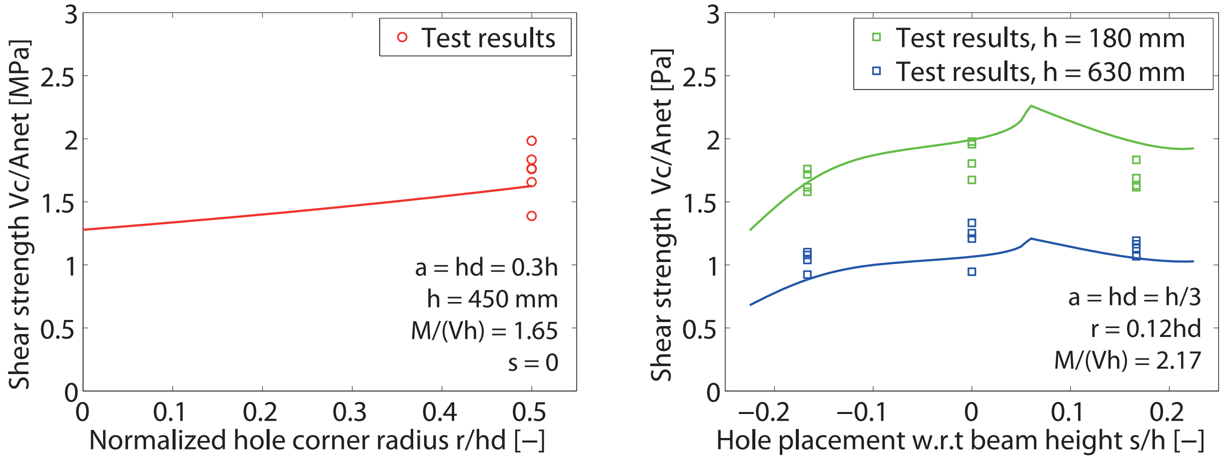

Figure 4.2. Experimentally found strength and theoretically predicted strength as influenced by hole corner radius and hole placement with respect to beam height. Left (in red): Circular holes (Höfflin 2005, Aicher & Höfflin 2006). Right (in green/blue): Square holes (Danielsson 2008).

5 Comparison of strength analysis approaches

An overview of the ratio between experimentally found beam capacity and theoretically predicted capacity according to some different approaches for strength analysis is given in Figure 5.1. The experimental tests used for this comparison consist of beams with either circular holes (Höfflin 2005, Aicher & Höfflin 2006) or square holes (Danielsson 2008) also used for comparison in Section 4.

The strength analysis methods included are:

1. PFM – A Probabilistic Fracture Mechanics method based on 2D FE-analysis and consideration of fracture ductility according to a generalized LEFM approach in combination with consideration of material variability according to Weibull theory (Danielsson & Gustafsson 2011).
2. Weibull – Classical Weibull theory based on 2D FE-analysis (Danielsson & Gustafsson 2011).
3. NLFM – A nonlinear fracture mechanics approach (a cohesive zone model) based on 3D FE-analysis (Danielsson & Gustafsson 2014).
4. Present approach – see previous sections.
5. Glulam Handbook – end-notched beam analogy approach for beams with a hole found in the old version of the Swedish Glulam Handbook (Carling 2001) and also included in a draft version of EC 5 (2002).
6. DIN EN 1995-1-1/NA – Semi-empirical approach found in German and Austrian National Annexes to EC5.
7. Aicher et al – Design approach based on Weibull theory presented by Aicher, Höfflin and Reinhardt (2007). Originally suggested to be used for circular holes only but here used also for square holes assuming $a = h_d = 2r$.

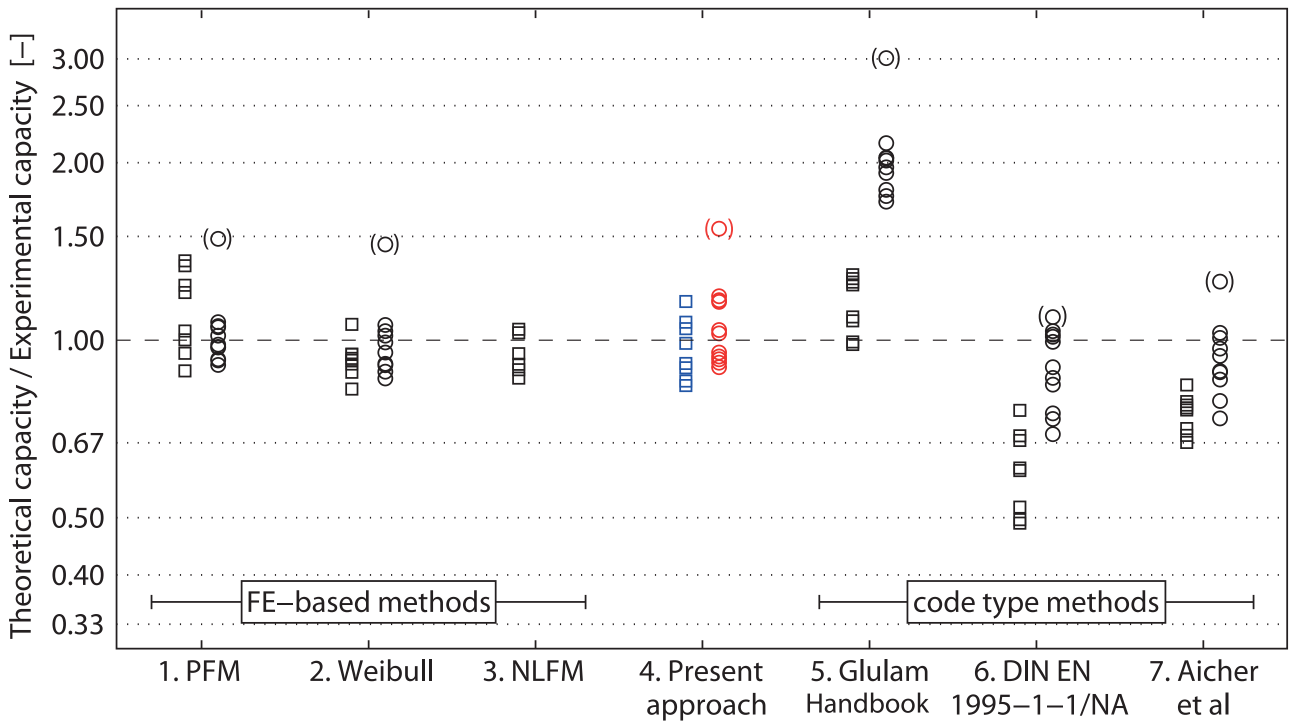

Figure 5.1. Comparison of experimentally found strengths and theoretically predicted strengths according to some different approaches for strenth analysis of beams with a hole. The test result indicated as (o) appears abnormal without known cause; see further comments in (Danielsson & Gustafsson 2011).

For the general approaches (items 1-4 above), experimentally found mean values are compared to predicted strength based on assumed mean values of material property parameters. For the NLFM approach (item 3 above), only results for the beams with square holes are presented since analysis of beams with circular holes were not included in the work presented in (Danielsson and Gustafsson 2014).

The strength according to the three code type approaches (items 5-7 above) are based on characteristic material strength values f_{vk} = 3.5 MPa and f_{t90k} = 0.5 MPa, valid for strength class GL 32h according to SS-EN 14080:2013. The predicted strengths are for these methods compared to characteristic values of the experimentally found strengths; see (Danielsson & Gustafsson 2011) for further information.

All test results included in the comparison relate to holes with larger height h_d than allowed to be used without reinforcement according to the German and Austrian National Annexes to EC 5.

6 Discussion

The presented approach is general in the sense that it allows for strength analysis including not only loading in terms of shear force and bending moment, but also axial force. Depending on relative load levels and the sign of the axial force, the assumed location of the crack (see Figure 2.2) may however need to be adjusted.

Beams with holes are in practical design situations often reinforced. The reason for this is likely related to two different factors: (i) the actual strength reduction due to the hole and (ii) the uncertainty and lack of knowledge related to strength analysis and design of beams with a hole. The cross section sectional forces N_s, V_s and M_s (see Equations 3-5) could possibly be of interest in relation to design of internal or external beam reinforcement in terms of fully threaded screws, glued-in rods or glued-on panels.

A new version of the Swedish Glulam Handbook is planned to be released during 2015, within which the end-notch beam analogy approach for beams with a hole will be removed in favour of the design approached found in the German and Austrian National Annexes to EC 5.

7 Conclusions

From the work presented in this paper, the following conclusions are drawn:

- The present approach is consistent with the LEFM-based design approach for end-notched beams found in EC 5.
- The present approach appears to be able to capture the strong beam size influence found from experimental tests of beams with a hole fairly well.
- The present approach appears fairly accurate in capturing the absolute values of the beam strength for both circular and square holes of various sizes and locations.

Although based on beam theory analysis, the present approach is not suitable for direct incorporation into timber engineering design codes of practice in its current form, because of rather complex equations. For certain applications and load configurations, more user-friendly design expressions may possibly be derived and could then serve as a base for improved design recommendations. Further work regarding verification and calibration is however needed before this can be realized.

8 References

Aicher S, Höfflin L (2004): New design model for round holes in glulam beams. In: Proceedings of 8th World Conference on Timber Engineering, vol 1, Lahti, Finland.

Aicher S, Höfflin L (2006): Tragfähigkeit und Bemessung von Brettschichtholzträgern mit runden Durchbrüchen – Sicherheitsrelevante Modifikationen der Bemessungsverfahren nach Eurocode 5 und DIN 1052. Materialprüfungsanstalt (Otto-Graf-Institute), University of Stuttgart, Germany.

Aicher S, Höfflin L, Reinhardt HW (2007): Runde Durchbrüche in Biegeträgern aus Brettschichtholz. Teil 2. Tragfähigkeit und Bemessung. Bautechnik 84(12):867-880.

Carling O (2001): Limträhandbok (Glulam handbook). Svenskt Limträ AB, Print & Media Center i Sundsvall AB, Sweden.

Danielsson H (2008): Strength tests of glulam beams with quadratic holes – Test report. Report TVSM-7153, Structural Mechanics, Lund University, Sweden

Danielsson H, Gustafsson PJ (2008): Strength of glulam beams with holes – Test of quadratic holes and literature test result compilation. In: Proceedings of CIB-W18 Meeting 41, St Andrews, Canada, Paper no. CIB-W18/41-12-4.

Danielsson H, Gustafsson PJ (2011): A probabilistic fracture mechanics approach and strength analysis of glulam beams with holes. Eur J Wood Prod 69:407-419.

Danielsson H, Gustafsson PJ (2014): Fracture analysis of glued laminated timber beams with a hole using a 3D cohesive zone model. Engng Fract Mech 124-125:182-195.

DIN EN 1995-1-1/NA:2013-08 (2013): German National Annex to EC 5

EN 14080:2013 (2013): Timber structures – Glued laminated timber and glued timber – Requirements. CEN.

Eurocode 5 (2004): Design of timber structures - Part 1-1: General – Common rules and rules for buildings. CEN. (EN 1995-1-1).

Eurocode 5 (2002): Design of timber structures - Part 1-1: General – Common rules and rules for buildings. Final draft 2002-10-09. (prEN 1995-1-1).

Gustafsson PJ (1988): A study of strength of notched beams. In: Proceedings of CIB-W18 Meeting 21, Parksville, Canada, Paper no. CIB-W18/21-10-1.

Gustafsson PJ (2002): Mean stress approach and initial crack approach. In: Aicher S, Gustafsson PJ (ed) Haller P, Petersson H: Fracture mechanics models for strength analysis of timber beams with a hole or a notch – a report of RILEM TC-133. Report TVSM-7134, Structural Mechanics, Lund University, Sweden.

Gustafsson PJ (2005): Mixed mode energy release rate by a beam theory applied to timber beams with a hole. In: Abstract Book of 11th International Conference on Fracture, Turin, Italy.

Hellan K (1985): Introduction to fracture mechanics. International Edition. McGraw-Hill.

Höfflin L (2005): Runde Durchbrüche in Brettschichtholzträger – Experimentelle und theoretische Untersuchungen. PhD thesis, Materialprüfungsanstalt (Otto-Graf-Institute), University of Stuttgart, Germany.

Kolb H, Epple A (1985): Verstärkung von durchbrochenen Brettschichtholzbindern. Vorschungsvorhaben I.4-34810, Forschungs- und Materialprüfungsanstalt Baden-Württemberg, Germany.

Petersson H (1974): Analysis of loadbearing walls in multistorey buildings: stresses and displacements calculated by a continuum method. PhD thesis, Chalmers University of Technology, Sweden.

ÖNORM B 1995-1-1:2014 (2014): Austrian National Annex to EC 5.

Discussion

The paper was presented by H Danielsson

H Blass commented that the stress distribution shown in slide 8 close to the hole is very different from reality. He questioned why the results are so good. H Danielsson agreed but stated that the beam theory is exact for normal stresses but might be different for shear stresses. PJ Gustafsson added that the solution should be exact in terms of energy release rate. As the crack propagated, the normal forces due to the moment should be exact but shear would not be true.

BJ Yeh asked how close the hole can be to the support and if there were two holes, how close can they be. H Danielsson responded the distances should be such that the support would not influence the hole. This would also apply to the multiple holes cases.

K Malo asked if there would be a limitation to the hole size. H Danielsson said that there would be no limit and the analysis would also work for notched beams.

I Smith commented that good results need accurate analysis, real structure, and accurate material properties; when results do not agree, maybe some of these are not working.

P Dietsch and H Danielsson discussed the cases of round and square holes and limitations to the model.

R Jockwer received clarifications that at this moment there is no recommendation for the size of the hole without reinforcement.

A strongest link model applied to fracture propagating along grain

Per Johan Gustafsson, Division of Structural Mechanics, Lund University, Sweden
Robert Jockwer, Institute of Structural Engineering, ETH Zurich, Switzerland
Erik Serrano, Division of Structural Mechanics, Lund University, Sweden
René Steiger, Swiss Federal Laboratories for Materials Science and Technology EMPA, Dübendorf, Switzerland

Keywords: Fracture, perpendicular to grain, knot, heterogeneity, notch, modelling, size effect

Abstract: The impact of knots and grain deviations on the perpendicular to grain strength of wood was studied by computational models and test results from literature. It was found that knots in general seem to have a positive influence on the perpendicular to grain fracture strength. A strongest link model for strength analysis relating to failure due crack propagation along grain is discussed, taking into account the influence of random strong spots along the crack path.

1 Introduction

Wood is a markedly heterogeneous material containing knots and grain deviations that strongly affect structural strength (Jockwer, 2014). This heterogeneity is the reason for the interest in application of strength models like the weakest link model (Weibull, 1939) and for the discussion in this paper about a strongest link model. One of the most important implications of the heterogeneities in wood is the size effect in load-carrying capacity as limited by tensile and/or shear failure perpendicular to grain. The influence of heterogeneities on this kind of fracture is the topic of this paper, in particular in relation to fracture starting at a local high stress region.

For cases of uniform or fairly uniform stress distribution in brittle materials it is reasonable to assume that structural failure is governed by the weakest part or link of the material. The weakest link concept agrees well with compilations of test results found in literature showing a significant size effect in strength of wood loaded in homogenous tension perpendicular to grain, see e.g. (Barret, 1974), (Barett et al. 1975), (Ehlbeck and Kürth, 1991), (Mistler, 1998), (Aicher et al., 2002) and (Gustafsson, 2003).

The situation may however be very different for materials with significant fracture toughness and for non-homogeneously stressed and/or statically indeterminate structures. In these cases failure typically involves progressive damage or crack propagation and one or many stress redistributions during the course of fracture events before the situation corresponding to maximum load-carrying capacity of the structure is reached. This may imply a better structural robustness since the ultimate load-carrying capacity is instead determined by the strongest link in a chain of states and stress distributions before complete structural damage. This general type of analysis is in the present study applied to beam failure caused by crack propagation along grain, taking into account random variation of the fracture toughness in the wood along the crack propagation path. As an introduction to the analysis of crack propagation failure, this paper also aims at investigating the impact of some different growth characteristics and heterogeneities on the fracture behavior of timber.

2 Impact of growth characteristics – some numerical and experimental results

2.1 Impact of a knot oriented out of the plane of fracture

A knot which is oriented out of the plane of fracture can give a very significant local contribution to the perpendicular to grain strength and fracture energy. This is illustrated in Figure 1 by a test result from (Jockwer, 2014) showing recorded load vs displacement for Single Edge Notched Beam specimens (SENB, (Larsen and Gustafsson, 1990), (Nordtest, 1993)) without a knot and for a specimen with a knot. The specimen with a knot has about twice the bending moment capacity and the fracture energy is increased by a factor of ten or more.

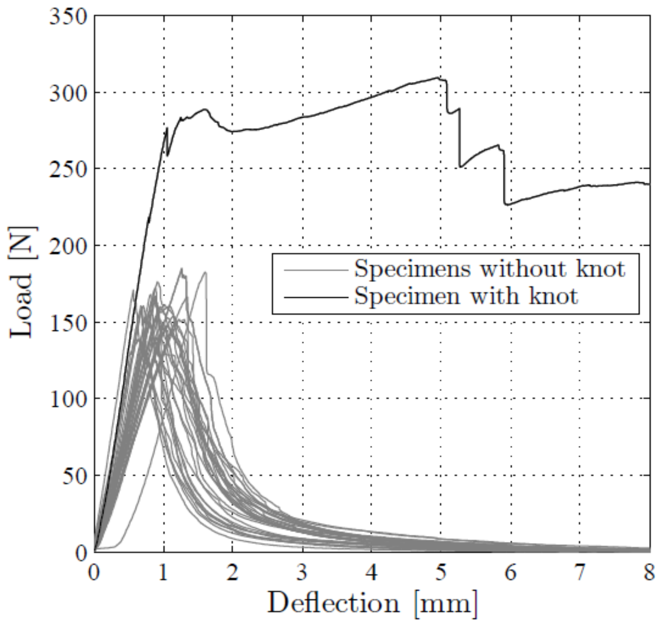

Figure 1. Load vs displacement for SENB specimens without and with a knot.

2.2 Impact of grain deviations around a knot on fracture energy

The deviation in crack propagation path in the vicinity of a knot causes an influence of a knot also when its axis lies within the fracture plane. Such a grain deviation is illustrated in Figure 2. The impact of this grain deviation on the load-deflection behavior and fracture energy was analyzed numerically for a SENB specimen by means of the FE-software Abaqus, using linear elastic fracture mechanics and an enriched FE-method, xFEM, described in (Qiu et al., 2014). The calculated apparent fracture energy versus knot size is shown in Figure 2.

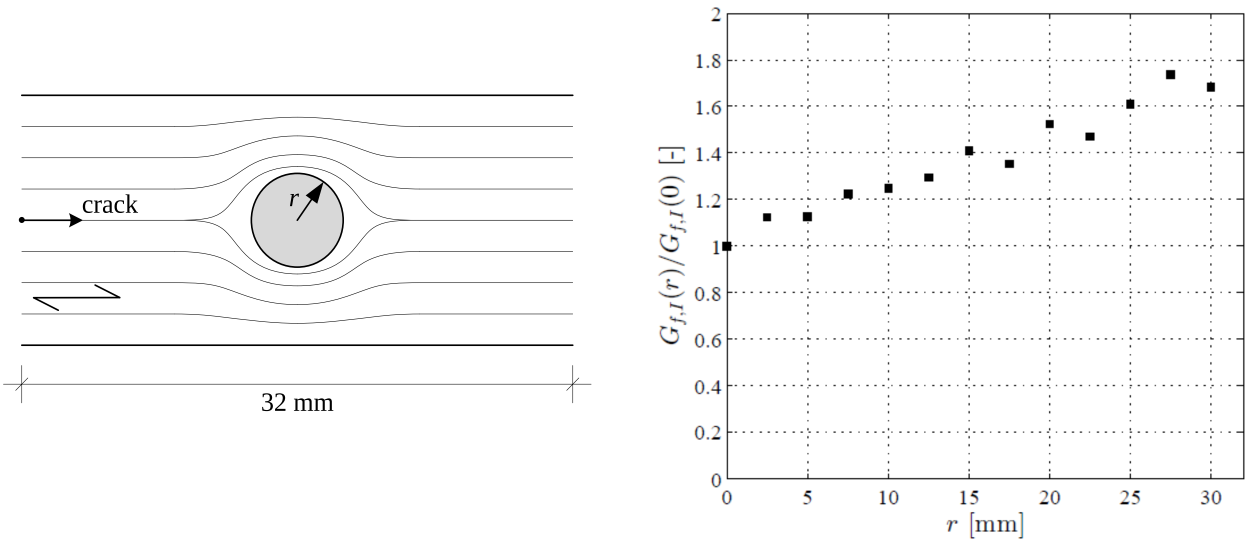

Figure 2. Impact of grain deviation at a knot on fracture energy $G_{f,I}$.

2.3 Impact of cross grain

The magnitude of the cross grain (see Figure 3) was quantified by means of the results from fiber orientation scanning of 450 laminations reported by Oscarsson et al. (2014). The median of the nominal grain direction on the edges of the laminations was used as a measure in order not to have the data corrupted by the local grain deviation close to knots. A median deviation from perfectly aligned grain in the range of up to 2 degrees was found to be quite common and the 10% fractile values of the median included deviations of approximately 4-6 degrees.

Figure 3 shows the influence of grain orientation in an end-notched beam as found by means of linear elastic fracture mechanics applied by the compliance method, using Matlab for plane stress FE-calculations. From the results it is evident that even a small grain inclination may strongly affect both the maximum load-carrying capacity and the development of the load causing crack propagation.

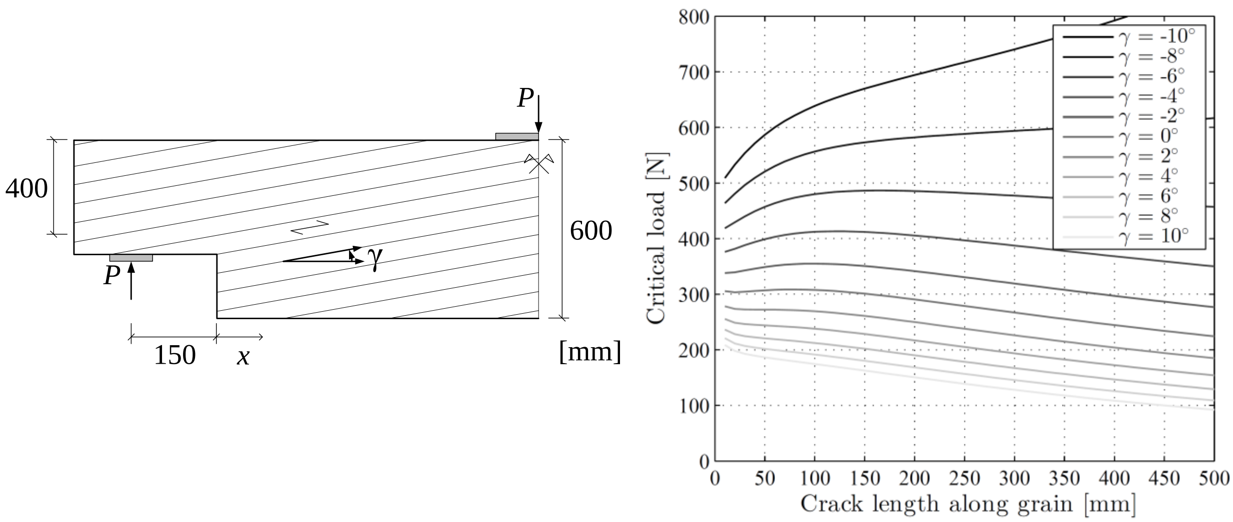

Figure 3. Beam cross grain and development of load causing crack propagation.

3 End-notched beam with random knots analyzed by means of Monte Carlo simulations

The strength of end-notched beams with geometrical shaping according to Figure 3 and with horizontal grain orientation was studied with regard to the influence of random material properties and knots. Monte Carlo simulations using an explicit strength equation for end-notched beams were carried out. The strength equation is based on linear elastic fracture mechanics and beam theory (Gustafsson, 1988) and for the present application is written as (Jockwer, 2014):

$$\frac{3V_f}{2b\alpha b} = \frac{\sqrt{3.75\,G_f G_V}}{\sqrt{h}\left(\sqrt{\alpha-\alpha^2} + \beta\sqrt{10\,G_V/E_0}\sqrt{1/\alpha-\alpha^2}\right)} \qquad (1)$$

The left hand term of the equation represents the shear stress in the net beam cross-section at start of crack propagation, where b is the beam width and V_f is the shear force. G_v and E_o is the shear stiffness and the modulus of elasticity parallel to the grain, respectively, and G_f is the fracture energy for the current mixed mode state of stress at the tip of the notch. A reasonable approximation is to assign G_f the mode 1 fracture energy. In the Monte Carlo calculations, stochastic values of G_v, E_o and $G_f = G_{f,I}$ according to Table 1 were used, unless otherwise specified. It is to be noted that the fracture energy values indicated in Table 1 relate to clear wood while the stiffness parameters relate to glulam including growth characteristics and inhomogeneities.

Eq. (1) was used also to evaluate the wood fracture mechanics strength parameter $(3.75\,G_f G_v)^{0.5}$ for a large number of end-notched beam strength test results compiled from literature (Jockwer, 2014). The result of this compilation of test results is indicated by circles in Figure 4. The numbers for $(3.75\,G_f G_v)^{0.5}$ given in the figure are thus a kind of normalized value of the failure load V_f of the notched beams assuming that G_v/E_0=650/11500≈1/18 and that Eq. (1) is valid.

Table 1. Distribution parameters of material properties relating to glulam equivalent to strength class GL24h at MC = 12% *acc. to EN 14080, (JCSS, 2001) and (Jockwer, 2014).*

Parameter	Unit	Symbol	Mean	5th perc.	CoV	PDF
MOE II to the grain	[N/mm²]	$E_{0,mean}$	11'500	9'600	13 %	Lognormal
MOE ⊥ to the grain	[N/mm²]	$E_{90,mean}$	300	250	13 %	Lognormal
Shear modulus	[N/mm²]	$G_{v,mean}$	650	540	13 %	Lognormal
Fracture energy Mode 1 *	[N/mm]	$G_{f,I,mean}$	0.3	0.218	20 %	Lognormal
Fracture energy Mode 2 *	[N/mm]	$G_{f,II,mean}$	1.15	0.695	30 %	lognormal

** clear wood*

In a first Monte Carlo simulation it was assumed that (1) the stochastic values of the fracture energy were equal to those for clear wood, see Table 1, and (2) that the ultimate failure load equaled the load at the beginning of crack propagation. The result from this simulation is depicted with a dash-dotted curve in Figure 4.

The simulation was then improved by considering the influence of knots and the variation in fracture resistance along the crack propagation path. In these calculations clear wood sections along the crack propagation path were assumed to be enclosed by intermediate knot or knot cluster sections. Values for the lengths of clear wood parts and knot parts were taken from (Fink et al., 2013). Hence, for Norway spruce (*picea abies*) wood the knot parts were assigned a constant length of 150 mm and the clear wood parts a stochastic length following a Gamma-distribution with a mean value 530 mm and a standard deviation 250 mm. The end-notch was assigned a random location along the wood member. Within each clear wood part, the fracture energy was assigned a constant value taken from a lognormal distribution with CoV 20%. A bias of the mean value was used to fit the test results. Within each knot part, the fracture energy was assigned a constant value taken as the mean value of the fracture energy for the clear wood times a lognormal distributed stochastic knot factor F_{knot}. The best fit to the test results was found by reducing the mean fracture energy of the clear wood, as compared to the value used in the reference calculation from 0.3 N/mm to about 0.2 N/mm (corresponding to a 20% reduction in the strength parameter $(3.75\ G_f\, G_v)^{0.5}$ for the clear wood from 27 N/mm$^{3/2}$ to 22 N/mm$^{3/2}$) and at the same time setting the mean value and CoV of F_{knot} equal to 2.0 and 40 %, respectively. The 20% strength reduction is in line with studies of e.g. Franke (2008) and Jockwer (2014). The resulting failure probability of this Monte Carlo simulation is depicted with the solid line in Figure 4.

Additional simulations showed that the mean value of the distance between knots has a strong impact on the distribution and magnitude of beam strength, while the

CoV of the inter knot distance is of minor importance. It was also found that the value of F_{knot} has a strong impact on beam strength.

The general trend found in the simulations is that the presence of knots leads to an increase in load-carrying capacity of notched beams. This is in contradiction to codes and procedures where only weakening effects of knot sections are accounted for, e.g. with respect to bending strength.

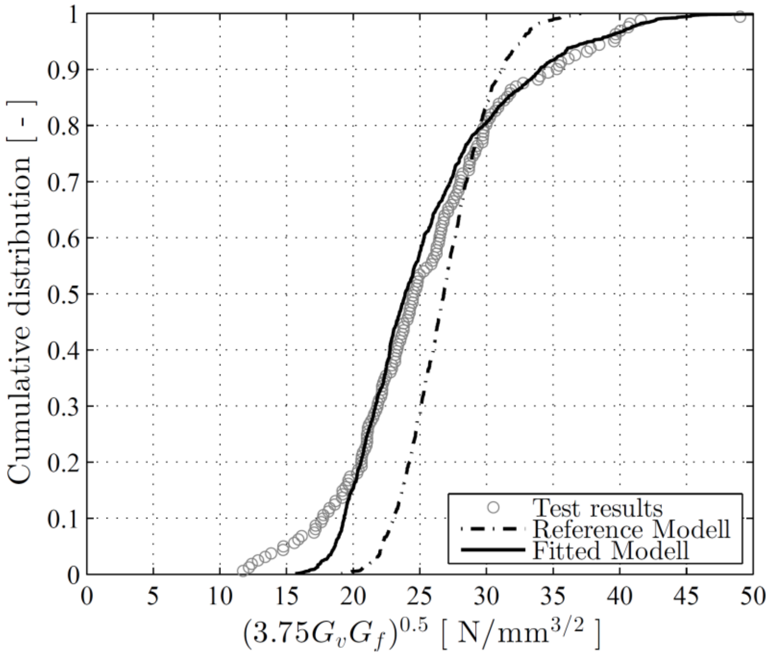

Figure 4. Cumulative strength distribution of test results compared to numerical calculations accounting for different growth characteristics.

4 End-notched beam with knots – additional observations

Early experimental research on the impact of knots on the perpendicular to grain fracture strength of timber was conducted by Larsen and Riberholt (1972). 200 end-notched solid softwood beams of quality "ungraded" and with varying height of the reduced cross-section αh were subjected to 3-point bending tests. Beam cross section height was h = 125 mm and the beams failed due to crack propagation starting at the notch. The recorded failure loads are summarized in Table 2. The failure load of the beams with one or more knots in the failure region of the beam was for all three αh tested found to be higher both at the mean value level and at the 10^{th}– and 5^{th}– percentile levels compared to beams lacking of knots. The CoV in strength for beams with knots was in general not higher than for those without knots.

About 20 years later, Riberholt et al. (1991) tested a large series of end-notched beams in order to study the influence of various geometrical parameters. A crack retarding effect of knots was again observed and specimens with knots showed higher load-carrying capacities. To determine fracture energy also small SENB specimens were tested and it was noted that a specimen with a knot had a considerably higher fracture energy than the clear wood specimens.

Table 2. Shear stresses at failure τ_u in the reduced cross-section of beams with variable notch height tested in 3-point bending, separated into samples with and without knots (Larsen and Riberholt, 1972).

	α [-]	$\tau_{u,mean}$ (CoV) [N/mm^2] (%)	$\tau_{u,0.05}$ [N/mm^2]	$\tau_{u,0.10}$ [N/mm^2]
With knots	0.75	3.63 (30.6)	1.78	2.04
	0.5	2.41 (20.9)	1.55	1.71
	0.25	2.77 (31.6)	1.47	1.70
Without knots	0.75	2.72 (24.1)	1.75	1.92
	0.5	2.12 (27.9)	1.32	1.45
	0.25	1.78 (31.8)	1.02	1.15
All	0.75	2.93 (29.6)	1.70	1.90
	0.5	2.19 (26.5)	1.36	1.51
	0.25	2.00 (38.0)	1.02	1.17

Similar impacts of knots on the load-carrying capacity of end-notched beams were detected in tests reported by Möhler and Mistler (1978). A reduction of the load-carrying capacity was on the other hand observed for beams with checks along the crack propagation path.

Jockwer (2014) showed that the large variation in load-carrying capacity of end-notched beams cannot be explained only by the variation of the elastic stiffness properties and fracture energy of timber and clear wood, respectively. The high level of variation could be explained by the presence of knots along the crack path. The crack retarding effect of knots was studied by means of optical measurement systems.

5 Strongest link model

5.1 Background

Perpendicular to grain failure of a structural element is initiated at some location and then followed by crack propagation along a potential fracture surface ending in ultimate failure. To analyse the load-carrying capacity of the structural element, in principle all possible fracture initiation locations and their corresponding crack paths must be investigated with respect to the load which initiates fracture and the load needed to propagate the crack along the fracture surface. For each initiation point, the maximum load required for assuring crack propagation until final failure must be determined. For all these maximum loads their stochastic character has to be identified and the minimum of these maxima must be determined. A complete analysis is demanding and probably is rarely needed. Instead special cases can be defined and analysed.

Such a special case is at hand if the fracture initiation load is greater or equal to the maximum of the load needed for crack propagation along the crack path. In that case the weakest link analysis of Weibull (1939) illustrated in Figure 5a) can be applied, the links in the chain representing the different possible locations of the failure initiation point.

Another special case is the situation where only one fracture initiation point together with the corresponding crack path needs to be considered. This is typically the case for failure initiated at a notch and can be analysed by means of a strongest link model. In this case the links represents the chain of crack tip locations along the crack propagation path. Strongest link modelling is illustrated in Figure 5b): the links are not loaded at the same time and they must all fail before global failure occurs. It is thus neither parallel coupling nor series coupling. One may instead compare the crack propagation with opening a zipper: the zipper link which provides the highest resistance is decisive.

In order to enable comparisons first some relations of the weakest link model shall be summarised. The probability of material failure of a "small" unit volume ΔV or dV of material is in Weibull weakest link model commonly described by the 2-parameter Weibull distribution:

$$p_f(\sigma) = 1 - e^{-(\sigma/f_c)^m} \qquad (2)$$

p_f is the probability that failure will occur at some stress lower than σ. σ is the magnitude of stress in the homogeneously stressed unit volume and f_c and m are material parameters which define magnitude and scatter in strength. If not uniaxial stressed, then σ and f_c represent an effective stress and strength, respectively, for the state of stress under consideration. f_c can be determined as the 0.63 fractile value of tested failure values of σ and m is uniquely related to the CoV.

From Eq. 2 it is evident that the probability that the unit volume does not fail is $\exp(-(\sigma/f_c)^m)$. The probability that no link in a chain made up of n links fails is then $(\exp(-(\sigma/f_c)^m))^n = \exp(-n(\sigma/f_c)^m)$ and accordingly the probability of failure of the chain is

$$p_f(\sigma) = 1 - e^{-n(\sigma/f_c)^m} \qquad (3)$$

This relation also estimates the probably of failure initiation in a structure made up of n equally stressed unit volumes. If the unit volumes are not equally stressed, then

$$p_f(P) = 1 - \prod_{i=1}^{n} e^{-(P\sigma_{0i}/f_c)^m} = 1 - e^{-\sum_{i=1}^{n}(P\sigma_{0i}/f_c)^m} \qquad (4)$$

P is the load and σ_{0i} is the stress in unit volume i when P = 1. The basic strength distribution Eq. 2 and the corresponding lowest-value extreme value distribution Eq. 3 or 4 exhibit the same curve shape and the same CoV. This is a very convenient feature of the 2-parameter Weibull distribution. The sum in Eq. 4 can be replaced by an integral if the "small" unit material volume is taken as dV. Some finite volume V_o must then be introduced as reference volume for the material parameters f_c and m.

The conventional Weibull weakest link theory with volume-integration is not applicable to structural elements with a sharp notch, crack or other shaping that reveals a stress singularity since the theory for such situations in general predicts either zero strength or no failure at the crack tip, no matter the magnitude of load (Gustafsson and Enquist, 1988). Mistler (1998) did, however, combine a previously developed wire-model for analysis of crack growth starting from the tip of a notch in wood (Mistler, 1979) with weakest link analysis in order to analyse the size effect in the perpendicular to grain tensile strength of structural elements like curved and tapered beams.

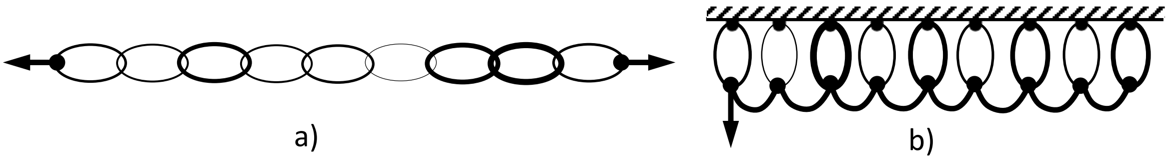

Figure 5. a) Weakest link model. b) Strongest link model.

5.2 A strongest link model

A strongest link model for crack propagation along grain and other progressive failure is considered (Gustafsson, 2014). The model is schematically illustrated in Figure 5b). If as an example the strength distribution of a single link can be described with a 2-parameter Weibull distribution according to Eq. 2, then, - since failure of the zipper in Figure 5 b) requires failure of all links -, the strongest link strength distribution of a zipper with n links is

$$p_f(\sigma) = \left(1 - e^{-(\sigma/f_c)^m}\right)^n \qquad (5)$$

The weakest link correspondence to Eq. 5 is Eq. 3. Commonly the first link would correspond to fracture initiation and the following links to crack propagation. If fracture starts at a crack or a notch, then both initiation and propagation can be analyzed applying fracture mechanics theory. If there is no initial crack or notch, then the strength of the first link may be determined by a conventional stress based criterion.

In crack propagation analysis the strength f_c of a link is replaced by the fracture toughness K_c of the link, being a measure of the magnitude of the fracture toughness of the material as determined for crack propagation along a "short" reference length

Δx. The parameter m is a measure of the scatter in fracture toughness. The numerical values of the material parameters K_c and m corresponding to reference length Δx can be determined experimentally by fitting experimental and theoretical strength distribution curves. σ in the ratio σ/f_c represents the stress intensity K. $K = PK_0(x)$ can be determined by conventional linear elastic fracture mechanics analysis, P being the external load, K_0 the stress intensity when $P = 1$ and x the length of the crack. If K is constant along the crack path and if the length of the path is $L = n\,\Delta x$, then:

$$p_f(P) = \left(1 - e^{-(PK_0/K_c)^m}\right)^n \qquad (6)$$

If the stress intensity PK_0 varies with the location x along the crack propagation length L, then

$$p_f(P) = \prod_{i=1}^{n}\left(1 - e^{-((PK_0)_i/K_c)^m}\right) \qquad (7)$$

where $(PK_0)_i = PK_0(x_i)$ and $x_i = (i-0.5)\Delta x$.

The fracture toughness of a material can be represented by the square root of a measure of the elastic stiffness times the critical energy release rate G_c or fracture energy G_f, e.g. by $K_c = (G_vG_f)^{0.5}$. Similarly, PK_0 is represented by $(G_vG)^{0.5}$. The calculation of G is simplified if all variation in K_c along the crack path is attributed to variation in G_f and thus taking G_v as constant. With fracture toughness replaced by fracture energy, Eq. 7 can be written

$$p_f(P) = \prod_{i=1}^{n}\left(1 - e^{-(G_i/G_f)^{m/2}}\right) \qquad (8)$$

In the above quasi-static loading conditions have tacitly been assumed. In more accurate analysis the possibility of accumulation of kinetic energy during crack propagation should be considered.

5.3 Application to end-notched beams

Failure probability results from an application of the strongest link model to end-notched beams are shown in Figure 6, also showing a comparison with test data from literature (Jockwer, 2014). The calculation of G for different loads $P = V$ and crack propagation lengths x were carried out by Eq. 1, giving

$$G(P,x) = \frac{0.6}{G_V}\left[\frac{P\sqrt{h}}{b\alpha h}\left(\sqrt{\alpha-\alpha^2} + \left(\beta + \frac{x}{h}\right)\sqrt{\frac{10G_V}{E_0}}\sqrt{1/\alpha-\alpha^2}\right)\right]^2 \qquad (9)$$

Knowing $G(P,x)$, Eq. 8 was used, thus assuming a stochastic distribution of fracture energy according to the 2-parameter distribution of Weibull. This makes the calculations simple, but some other distribution that would imply more comprehensive numerical calculations would probably give a better representation of the stochastic distribution due to presence of knots. The calculations were carried out for a beam with notch geometry α = 0.6, βh = 120 mm and h = 600 mm as defined in Figure 3, while the test results used for comparison relate to beams with different size and shape, assuming that Eq. 1 properly corrects for different geometrical shaping of the end-notch. The material parameters from Table 1 were used with deterministic E_0 = 11500 N/mm^2 and G_v = 650 N/mm^2, and stochastic $G_c = G_{f,I}$ with magnitude parameter G_f in Eq. 8 made equal to 0.3 N/mm and with different values of scatter parameter m. The total crack propagation length studied was throughout L = 1000 mm.

A good fit of the model with the test data was achieved for $m = 3.5$ and $n = 8$ links. This corresponds to a crack propagation length of each link of $\Delta x = 125$ mm. For an increasing number of links at a constant total crack length both the 5th– and the 50th–percentile values increase, see Figure 6a). In contrast, the model parameter m has a major impact on the progress of the upper tail of the probability density, see Figure 6b). The validity of Δx as a reference length for other fracture mechanics problems has to be evaluated more extensively. Basically Δx should be taken as the reference length for which the material parameters for stiffness and fracture energy (i.e. the fracture toughness) were determined.

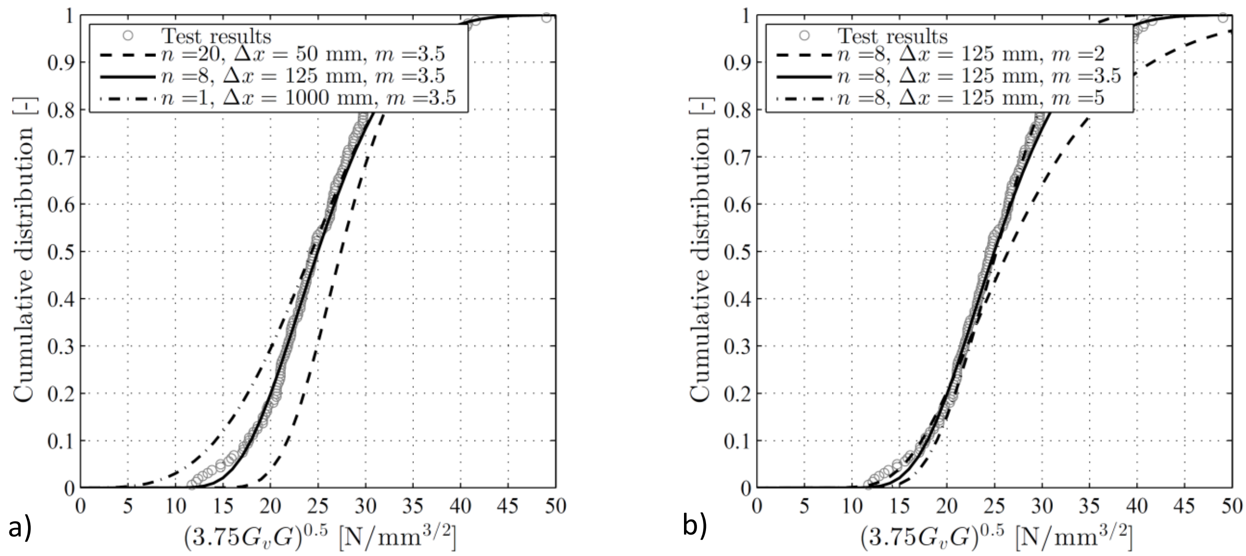

Figure 6. Cumulative probability of failure of end-notched beam strength: numerical predictions and test results.

5.4 Application to connections loaded perpendicular to grain

A further application example relates to a beam with a dowel loaded perpendicular to the beam, creating a risk for cracking along the beam, see Figure 7. For this situation, according to Jensen (2003) the energy release rate during crack propagation is:

$$G(P,x)=\frac{0.6}{G_V\alpha h}\left(\frac{P}{2b}\right)^2\left((1-\alpha)+2.5\frac{G_V}{E_0}\left(\frac{x}{\alpha h}\right)^2(1-\alpha^3)\right) \tag{10}$$

The result of application of Eq. 8 with *G* from Eq. 10 and a comparison with test data from literature (Jockwer et al., 2015) is shown in Figure 7. The same material data as for the application in Section 5.3 were used. The crack propagation length analysed was *L* = 1800 mm. A good fit between the theoretical result and the test data was found for *m* = 3 and with *n* = 3 links, shown by the solid line in Figure 7.

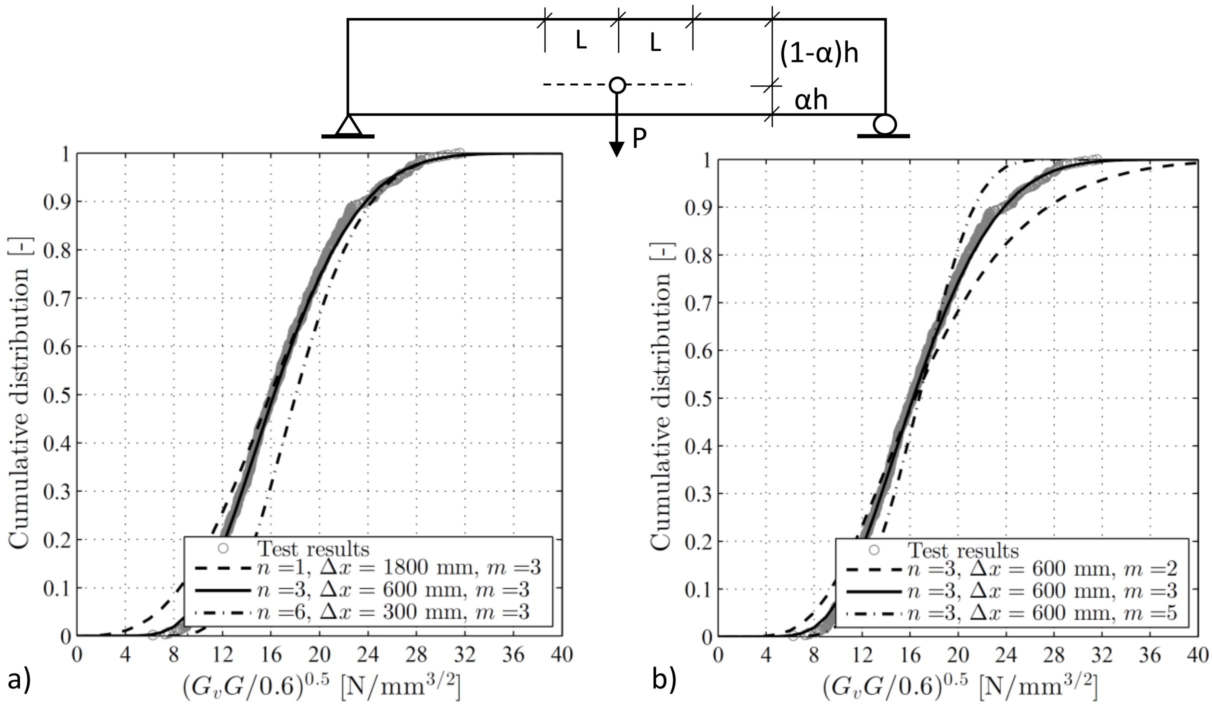

Figure 7. Cumulative probability of failure of test results for a beam with a connection perpendicular to the grain compared with numerical results for various numbers of links in a) and for various scatter in fracture energy in b).

5.5 A size effect comparison between the strongest and weakest link models

The strongest link model predicts *increased or constant* structural strength with increased crack propagation length and with increased scatter in material fracture toughness. The weakest link model predicts on the contrary *decreased* structural strength with increased volume and with increased scatter in material strength.

The magnitude of these influences of size and scatter is different for different probability distribution functions. Here the effects obtained when using the 2-parameter Weibull distribution are studied. The volume and scatter effects predicted by conventional Weibull analysis, see e.g. (Danielsson, 2013), is

$$\frac{f_A}{f_B}=\left(\frac{\Omega_A}{\Omega_B}\right)^{-1/m} \tag{11}$$

f_A and f_B is the stress in some reference point in equally shaped specimens A and B at loads corresponding to failure, e.g. the median failure loads. Ω indicates volume and m is the measure of scatter in strength. Theoretically m is related to CoV, but is often determined by fitting of Eq. 11 to the size effect test results. For wood in homogeneous tension perpendicular to grain and using size effect tests, m is typically found to be about 5, theoretically corresponding to CoV of about 20-25 %.

The crack propagation length effect predicted by the strongest link model is more complex and here studied for the case illustrated in Figure 8. For this geometry and loading the stress intensity K is constant along the crack path. Parameters K_c, m and Δx are assumed to be equal for specimens A and B. Eq. 6 gives

$$\frac{M_A}{M_B} = \left(\frac{ln(1 - p_f^{1/n_A})}{ln(1 - p_f^{1/n_B})} \right)^{1/m} \tag{12}$$

The length effect is thus different for different failure fractiles, p_f. A numerical example: for $p_f = 0.5$, $n_A = 4$, $n_B = 2$ and $m = 5$ is found that $M_A/M_B = 1.08$ while for $p_f = 0.05$, $n_A = 4$, $n_B = 2$ and $m = 5$ is found that $M_A/M_B = 1.20$. If the scatter is increased to the equivalent of $m = 3$ all other conditions being unchanged then is found $M_A/M_B = 1.14$ and 1.36 for $p_f = 0.5$ and $p_f = 0.05$, respectively. The weakest link model gives with $\Omega_A/\Omega_B = 2$ that $f_A/f_B = 0.87$ for $m = 5$ and that $f_A/f_B = 0.79$ for $m = 3$.

With respect to the influence of the height h of the specimen in Figure 8 is an effect found according to fracture mechanics theory. Analysis of the influence of beam width does not enter the present 2D analysis. 3D analysis would presumably indicate some decrease in beam strength with increased width due to less scatter in the fracture toughness along the beam.

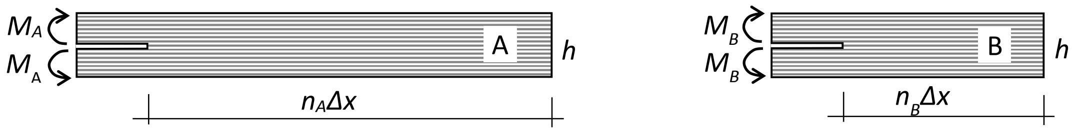

Figure 8. DCB-specimens with different crack path length.

6 Summary with remarks relating to design

The impact of some heterogeneities in wood from growth characteristics of the tree on the strength of timber in structural size was studied by computational models and test results from literature. It was found that the heterogeneities in timber due to knots and associated grain orientation disturbances in general seem to have a positive influence on the perpendicular to grain fracture strength.

The strongest link model discussed relates to fracture propagation along a crack path starting at a given point or, more generally, to the sequence of events for a given failure mode. The weakest link model relates to analysis of different possible fracture locations or, more generally, to different possible modes of failure.

Contemporary grading specifications relate primarily to loading situations resulting in stress parallel to the grain, e.g. bending of a beam. It is then tacitly assumed that the strength perpendicular to the grain correlates with the strength parallel to grain. This assumption is questionable. An example: a knot commonly gives a weak spot with respect to bending, but as discussed in the above, commonly a reinforcing spot with respect to fracture perpendicular to grain. Another example: a resin pocket or a check along grain may be devastating with respect to tensile strength perpendicular to grain, but may hardly have any significant influence on the bending strength. It can thus be difficult to find a reliable strength grading correlation, neither positive nor negative. It might therefore be appropriate to consider the development of a 2-parameter grading system. And the more so as fracture perpendicular to grain seems to be one of the more frequent causes of structural failure (Frühwald et al., 2007).

Research efforts on size effects have so far mainly been dealing with the influence of random weak spots in the wood. The more or less random presence of strong spots such as knots may, however, also be of matter in some cases, both in relation to size effects and to magnitude of structural strength. A strong spot effect may be found for crack propagation along grain and analyzed by a strongest link model. Such modelling might be useful also more generally in relation to analysis of robustness and failure mechanisms involving a sequence of events.

7 References

Aicher S, Dill-Langer G, Klöck W (2002): Evaluation of different size effect models for tension perpendicular to grain strength of glulam”. Proc. of CIB-W18 Meeting 35, Paper 35-6-1.

Barrett JD (1974): Effect of size on tension perpendicular-to-grain strength of Douglas-fir. Wood and Fiber Science, 6(2), 126-143.

Barrett JD, Foschi RO, Fox SP (1975): Perpendicular-to-grain strength of Douglas-fir. Canadian Journal of Civil Engineering, 2(1), 50-57.

Danielsson H (2013): Perpendicular to grain fracture analysis of wooden structural elements – models and applications. PhD thesis, TVSM-1024, Div. of Struct. Mech., Lund University, Sweden.

Ehlbeck J, Kürth J (1991): Influence of perpendicular to grain stressed volume on the load-carrying capacity of curved and tapered glulam beams. Proc. of CIB-W18 Meeting 24, Paper 24-12-2.

Fink G, Frangi A, Kohler J (2013): Modelling the bending strength of glued laminated timber – considering the natural growth characteristics of timber. Proc. of CIBW18 Meeting 46, Paper 46-12-6.

Franke B (2008): Zur Bewertung der Tragfähigkeit von Trägerausklinkungen in Nadelholz. PhD thesis, Bauhaus-Universität, Weimar, Germany.

Frühwald E, Serrano E, Toratti T, Emilsson A, Thelandersson S (2007): Design of safe timber structures – How can we learn from structural failuresin concrete, steel and timber?. Report TVBK-3053, Div. of Struct. Eng. Lund University, Sweden

Gustafsson PJ (1988): A study of strength of notched beams. Proc. of CIB-W18 Meeting 21, Paper 21-10-1.

Gustafsson PJ, Enquist B (1988): Träbalks hållfasthet vid rätvinklig urtagning. Report TVSM-7042, Div. of Struct. Mech., Lund University, Sweden.

Gustafsson PJ (2003): Fracture perpendicular to grain – structural applications. In: Timber Engineering, ed:s Thelandersson S, Larsen HJ. Wiley.

Gustafsson PJ (2014): Lecture notes on some probabilistic strength calculation models. Report TVSM-7161, Div. of Struct. Mech., Lund University, Sweden

JCSS (2001): Probabilistic Model Code. Joint Committee on Structural Safety. URL: http://www.jcss.byg.dtu.dk/.

Jensen JL (2003): Splitting strength of beams loaded by connections. Proc. of CIB-W18 Meeting 36, Paper 36-7-8.

Jockwer R (2014): Structural behaviour of glued laminated timber beams with unreinforced and reinforced notches. Ph.D. thesis, Inst. of Struct. Eng., ETH Zurich, Switzerland.

Jockwer R, Steiger R, Frangi A (2015): Evaluation of the reliability of design approaches for connections perpendicular to grain, Submitted to INTER Meeting 2, Sibenik, Croatia.

Larsen H, Gustafsson PJ (1990): The fracture energy of wood in tension perpendicular to the grain. Proc. of CIB-W18 Meeting 23, Paper 23-19-2.

Larsen, HJ, Riberholt H (1972): Forsøg med uklassificeret konstruktionstræ. Rapport R 31, Afd. for Bærende Konstruktioner, Danmarks Tekniske Højskole.

Mistler HL (1979): Die Tragfähigkeit des am Endauflager unten rechtwinklig ausgeklinkten Brettschichtträgers. PhD thesis, Technischen Hochschule Karlsruhe, Karlsruhe, Germany

Mistler HL (1998): Design of glulam beams according to EC 5 with regard to perpendicular-to-grain tensile strength - A comparison with research results. Holz als Roh – und Werkstoff, 56(1), 51–60.

Möhler K, Mistler HL (1978): Untersuchungen über den Einfluss von Ausklinkungen im Auflagerbereich von Holzbiegeträgern auf die Tragfestigkeit, Vol. F 1504.

Nordtest (1993): Wood: Fracture energy in tension perpendicular to the grain, Vol. NT Build 422. Nordtest.

Oscarsson J, Serrano E, Olsson A, Enquist B (2014): Identification of weak sections in gulam beams using calculated stiffness profiles based on lamination surface scanning. Proc. of WCTE 2014, Quebec, Canada.

Qiu L, Zhu E, Van De Kuilen J (2014): Modeling crack propagation in wood by extended finite element method. European J. of Wood and Wood Products, 72(2), 273–283.

Riberholt H, Enquist B, Gustafsson PJ, Jensen RB (1991): Timber beams notched at the support. Afd. for Baerende Konstruktioner, Danmarks Tekniske Højskole, Denmark.

Weibull W (1939): A statistical theory of the strength of materials. Proceedings no 151, Royal Swedish Institute for Engineering Research, Sweden.

Discussion

The paper was presented by R Jockwer

F Lam and R Jockwer discussed the factor K_{knot} as being established based on judgement with LN(2,0.8). F Lam commented that the fitting at the tail of the distribution was not very good. R Jockwer responded that there could be other factors such as influence of slope of grain involved.

I Smith commented about the load control testing situation versus displacement control and received information that this case related to crack arrest. He commented that how a dynamically developing crack growth could be handled with Weibull approach where Weibull did not consider stability issues. P Gustafsson responded that quasi static for dynamic loading was considered here and one could integrate the energy release rate as the crack propagates.

P Dietsch questioned if one applied the information from 48-7-4 in this situation what would happen. R Jockwer responded that one would expect little difference if the height adjustment model was applied as it might fit better than the volume adjustment model. With strongest link approach better fit could result.

T Tannert questioned the situation where the predefined failure plane in the FEM was the weak plane but failure could occur in the strong plane and how strongest link approach could consider the case with failure in the strong plane. R Jockwer responded that one could lower the fracture energy of a predefined strong crack plane so that the crack could develop along the strong plane.

A proposal for a new Background Document of Chapter 8 of Eurocode 8

Maurizio Follesa, Massimo Fragiacomo, Davide Vassallo - Department of Architecture, Design and Urban Planning, University of Sassari, Palazzo del Pou Salit, Piazza Duomo 6 07041 – Alghero – Italy / dedaLEGNO, Via Masaccio 252, 50132 – Firenze - Italy

Maurizio Piazza, Roberto Tomasi, Simone Rossi, Daniele Casagrande - Department of Civil, Environmental and Mechanical Engineering, University of Trento, Via Mesiano 77 - I 38123 Trento - Italy

Keywords: Eurocode 8, Multi-storey timber buildings, Background document

1 Introduction

Timber systems are becoming more and more popular in the construction of medium to high rise buildings in many European regions with different levels of seismicity, replacing day by day other materials like reinforced concrete, masonry or steel. Only considering the last decade, more than 20 buildings with a number of storeys ranging from 6 to 14 have been built in low to high seismicity areas.

Sustainability, energy efficiency and speed of construction together with the consequent costs reductions, and above all the excellent seismic performance demonstrated by recent research results based on extensive numerical simulations and full-scale tests on multi-storey buildings are just some of the advantages which explain this growing success.

However this progress and the growing diffusion have not been followed by a corresponding update of the provisions to be used in the seismic design, which for the case of timber buildings are included within Chapter 8 of Eurocode 8. This chapter, published in 2004, is very short and incomplete in many parts, especially when considering design provisions for modern construction systems that are nowadays widely used, thus causing real difficulties to structural engineers who have to apply these rules in the seismic design of timber buildings.

2 Seismic design according to Eurocode 8

The seismic design of structures according to Eurocode 8 (CEN, 2004) is founded on a force-based approach, according to which the energy dissipation capacity of the whole structure is implicitly taken into account by dividing the seismic forces obtained from a linear (static or dynamic) analysis by the behaviour factor q associated to the relevant ductility classification, which, according to the definition of Eurocode 8 “*accounts for the non-linear response of a structure, associated with the material, the structural system and the design procedures*”.

Therefore, in order to reach the desired means of ductility and energy dissipation capacity, (i) the structural system should be clearly identified, (ii) capacity design provisions should be given so as to address without any possible misinterpretation the components of the structural system devoted to the ductile behaviour and on the other hand the parts of the structure which should be over-designed to avoid any possible anticipated brittle failures and (iii) ductility rules for the dissipative zones should be given.

This could be achieved by designing the brittle elements for a force equal to the strength of the ductile elements multiplied by the over-strength factor. Summarizing, according to the Capacity Based Design philosophy, the design procedure of a structure should be based on the following method:

1. Clearly identify the structural type and the associated behaviour factor q.
2. Follow the Capacity Based Design rules and the detailing provisions for dissipative zones defined for the corresponding structural type.
3. Adopt the over-strength factors defined for the design of the brittle elements.

The current version of Chapter 8 of Eurocode 8 (CEN, 2004) is partially or totally missing the above mentioned conditions for most of the structural types currently used in the construction practice. Therefore is almost inapplicable for the seismic design of most of the structural systems nowadays used, forcing the structural designer to make assumptions which could be not necessarily conservative.

3 A critical analysis of the current version

The current provisions for timber buildings included in Chapter 8 of Eurocode 8 consist of only 5 pages and present some critical aspects partly already addressed in Follesa et al. (2011), which cause difficulties to structural engineers who have to apply these rules in the seismic design of timber buildings. More specifically, there are some clauses which should be improved and some others which deserve further explanations in order to give a correct guidance to the structural designers, as listed in the following.

- The structural types should be clearly identified, without any possible misinterpretation and should be all referred to lateral load resisting systems for buildings. Furthermore the current list of structural types should be completely reviewed and updated to the current construction practice.
- Capacity based design rules and detailing provisions for dissipative zones are totally missing for most of the structural types thus making the choice of the

correct value of the behaviour factor to be applied in the design difficult. Like for other building materials, these provisions should be given for each structural type and for each Ductility Class in order to address the choice of the correct behaviour factor q to be adopted in the seismic design (Casagrande et al., 2014).

- The definition of static ductility should be clarified. Furthermore, the requirements currently given for DCM and DCH are not always reached by some structural elements (e.g. nailed wall panels) and connections for timber structures (e.g. hold-downs and angle brackets in X-Lam structures).
- The ductility rules currently given for dissipative zones, i.e. mechanical joints in the case of timber structures, are “prescriptive” and not “performance based” as in the basic philosophy of Eurocodes.
- New provisions for materials and properties of dissipative zones should be added, including new wood-based materials recently developed such as X-Lam panels, and the existing provisions for wood-based panels used as sheathing material should be updated to incorporate, for example, oriented strand board (OSB).
- The values of the over-strength factors γ_{Rd}, to be used to design the non-dissipative parts of the structure in order to avoid anticipated brittle failure mechanisms, are not provided for the different structural types. These values should be included (Gavric et al. 2014, 2015).
- The partial safety factors γ_M for fundamental and accidental load combinations for the ultimate limit state verifications in case of dissipative and non-dissipative structural behaviour should be reviewed and corrected.
- Inter-storey drift limits for the Damage Limit State verifications should be provided.

4 Background Document for a new version of Chapter 8 of Eurocode 8

The proposal for the revision of Chapter 8 of Eurocode 8 presented herein is based both on the results of research projects conducted on the seismic behaviour of timber buildings through tests and numerical simulations on full-scale buildings, structural components and single joints, and on the technical development reached in the field of timber construction in the last years. In the following paragraphs all the proposed modifications to the code text will be referenced and the motivation as well as the scientific background behind each proposal will be given, together with the corresponding literature references.

4.1 Materials and properties of dissipative zones

New types of wood-based and other type of panels largely used in construction practice should be added to the existing ones. These are:

- Oriented Strand Board sheathing (OSB) type 2, 3 or 4 according to EN 300, with a minimum thickness of 12 mm.
- Gypsum Fibre boards (GF) sheathing according to EN 15283-2, with a minimum thickness of 12 mm.
- X-Lam panels according to prEN 16351 used in shear walls and diaphragms of solid construction, with a minimum thickness of 60 mm for shear walls and of 18 mm for floor and roof diaphragms.

OSB is probably the most used wood-based sheathing material in Light-Frame construction. There are a large number of experimental results about the good dissipation properties of Light-Frame shear walls sheathed with OSB panels (e.g., Sartori & Tomasi, 2013).

Light-Frame buildings sheathed with Gypsum Fibre boards (GF) sheathing and stapled connections are becoming more and more used in the current construction practice. Moreover recent research conducted at the University of Trento, Italy (Sartori and Tomasi, 2013) and within the SERIES Project (Piazza et al., 2013) have proved the suitability of Gypsum Fibre Panels (PF-GF) connected to the timber framing with staples as a sheathing material for shear walls in Light-Frame construction.

Cross Laminated Timber (X-Lam) buildings are widely used all over Europe for the construction of medium to high-rise buildings in seismic areas. Currently the qualification process of the structural panels is made by CE marking each panel according to European Technical Approvals (ETA) which are specific of each single producer and are generally based on the procedure described in CUAP 03.04/06. At present a European Standard for X-Lam (prEN 16351 Timber structures — Cross Laminated Timber — Requirements) is under formal vote and will be published soon. After the publication, the CE marking of X-Lam panels will be possible only according to the procedure established in this standard and all the single ETA’s will expire. The limitation of 60 and 18 mm of panel thickness is given according to current production specification of most of the European producers.

4.2 Structural types

Similarly to the chapters related to other materials included in Eurocode 8, a clear definition of the different structural types should be provided, possibly with the inclusion of graphical sketches in order to ease the understanding. A possible proposal including new structural types and the re-definition of the existing ones is given in Table 1.

Table 1. Structural types for timber buildings.

Structural type	Example of structure
1. Cross Laminated Timber (X-Lam) system, i.e. buildings comprised of X-Lam shear walls according to XX (reference to the Material Properties section) with the specifications given in YY (reference to the Capacity Design Rules section).	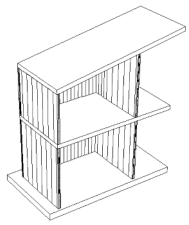
2. Light wood-frame system, i.e. structures in which shear walls are made of timber frames to which a wood-based panel or other type of sheathing material according to XX (reference to the Material Properties section) are connected according to the specifications given in YY (reference to the Capacity Design Rules section).	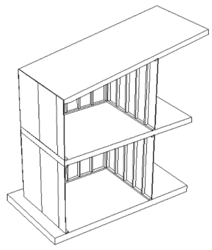
3. Log House building system, i.e. structures in which walls are made by the superposition of rectangular or round solid or glulam timber elements, prefabricated with carpentry joints at their ends and with upper and lower grooves according to specifications given in YY (reference to the Capacity Design Rules section).	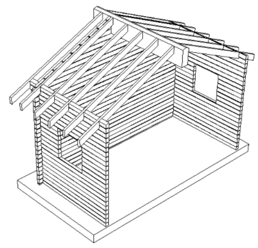
4. Moment-resisting frames, i.e. frames composed of timber elements with semi-rigid joints between the members - made with mechanical fasteners according to the specifications given in YY (reference to the Capacity Design Rules section).	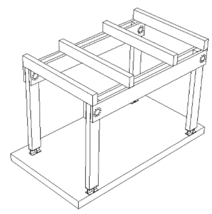
5. Post and beam timber systems, namely systems of timber columns and beams pinned-connected, with vertical bracings made of timber trusses according to the specifications given in YY (reference to the Capacity Design Rules section).	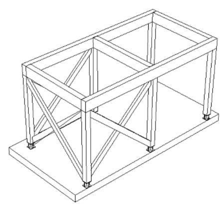
6. Mixed structures made of timber framing and masonry infill resisting to the horizontal forces.	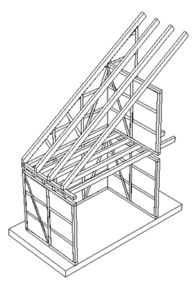

Structural type	Example of structure
7. Large span arches with two or three hinged joints according to the specifications given in YY (reference to the Capacity Design Rules section).	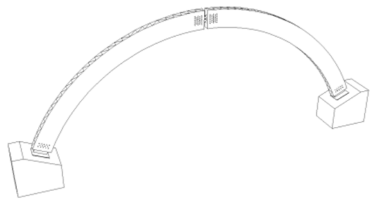
8. Large span trusses with nailed, screwed, doweled and bolted joints according to the specifications given in YY (reference to the Capacity Design Rules section).	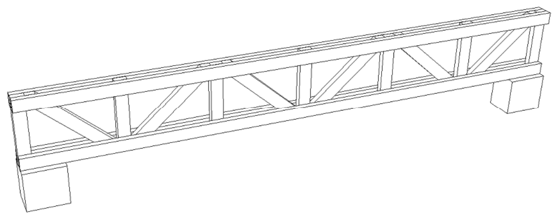
9. Vertical cantilever systems made with glulam or X-Lam wall elements according to the specifications given in YY (reference to the Capacity Design Rules section).	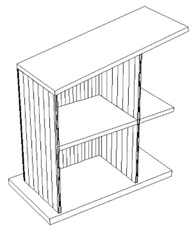

New structural systems for timber buildings already widely used in seismic regions such as the Cross Laminated Timber (X-Lam) system and the Log House system are introduced. With respect to the current 2004 version, all the structural types referred to structural assemblies for building roofs like trusses with nailed, doweled or bolted joints or with connectors were removed. The reason for this change is that the timber trusses were introduced in the 2004 edition probably overlooking the meaning of timber trusses given in the previous 1995 ENV edition where this system referred to vertical bracing systems used in buildings (or even large span glulam roofs, where the timber elements are directly connected to the foundation and resist vertical and horizontal loads). As this chapter refers to lateral load resisting systems in timber building, there is no reason to refer to structural assemblies used for roofs. The structural type referenced in 2004 edition as “Hyperstatic portal frames” is here referenced with the most common definition of “Moment resisting frames”. Also the vertical cantilever system is a new structural type not referenced in the 2004 edition which is nevertheless widely used in seismic regions.

4.3 Behaviour factors

Similarly to the chapters related to other materials included in Eurocode 8, also for timber structures two different values should be defined, if applicable, for DCM and DCH ductility classes, according to the ductility provisions given for the dissipative zones and specified in the Capacity Design Rules which should be provided for each structural type. For structures designed in accordance with the concept of low-dissipative structural behaviour (DCL) the behaviour factor q should not be taken greater than 1.5. A possible proposal is given in Table 2.

Table 2. Structural types and upper limit values of the behaviour factors for buildings regular in elevation

Structural type	DCM	DCH
X-Lam buildings	2.0	3.0
Light-Frame buildings	2.5	4.0
Log House buildings	2.0	-
Moment resisting frames	2.5	4.0
Post and beam timber buildings	2.0	-
Mixed structures made of timber framing and masonry infill resisting to the horizontal forces.	2.0	-
Large span arches with two or three hinged joints	-	-
Large span trusses with nailed, screwed, doweled and bolted joints	-	-
Vertical cantilever systems made with glulam or X-Lam wall elements	2.0	-

The values given for X-Lam structures are based on research results and numerical investigations conducted within the Sofie Project and referenced in Ceccotti & Follesa, (2006), Ceccotti et al. (2007), Fragiacomo et al. (2011), Pozza et al. (2013).

For Light-Frame structures two different values of the behaviour factor q are given for DCM and DCH. The highest values of 5.0 given in the 2004 edition, even if provided also in the National Building Code of Canada (NBCC, 2010) is not confirmed by other international codes (e.g. New Zealand, NZS 3603, 1993) and by numerical investigations (Follesa, 2015). Therefore a more conservative value of 4.0 is proposed. For the seismic design according to DCM a value of 2.5, given in Campos Costa et al., 2013, is proposed in order to include Light-Frame buildings sheathed with gypsum fibre boards and stapled connections. Unlike the 2004 edition, and according to the provisions given in the previous 1995 ENV edition, no distinction is made between glued and nailed diaphragms.

For Log House buildings no reference could be found on behaviour factor proposals; however studies are in progress (Bedon et al. 2014, 2015). Therefore the proposal is to use a value of 2.0 for DCM in order to take into account the dissipative contribution of frictions between logs, anyway further research is needed to confirm this value.

For moment resisting frames the lower q value (2.5) is confirmed for DCM. For DCH a value of 4.0 is confirmed, according to recent research results based on extensive numerical investigations on moment resisting frames with densified veneer wood reinforced joints with expanded tube fasteners (Wrzesniak et al., 2013).

4.4 General rules and capacity design rules

In order to allow the correct choice of the behaviour factor q to be used in the seismic design for the reference Ductility Class, for each structural type a hierarchy of resistance among the different structural components should be established. The whole structure should have an adequate capacity to develop plastic deformations without substantial reduction in the overall resistance against horizontal and vertical loads. Furthermore any possible anticipated brittle failure mechanism in the elements devoted to the energy dissipations, i.e. mechanical joints, should be avoided.

This could be achieved, as mentioned earlier, by over-designing the brittle elements with respect to the ductile elements, so as to ensure with a reasonable reliability that ductile failure modes occur before any possible failure in the brittle structural elements. Furthermore any possible global instability mechanism or soft-story mechanism should be avoided at a global level, as well as any possible brittle failure in the ductile structural elements should be prevented at a local level.

For this reason, capacity design rules should be provided for each structural type both at building level and at connection level. Seismic design rules should be divided for the different structural types into General Rules (where the above defined structural types should be further detailed, even by means of detailing drawings, in order to avoid any possible misinterpretations) and Capacity Design Rules, both at global and local level for the different Ductility Classes.

As an example, a proposal of possible General Rules and Capacity Design Rules for X-Lam buildings is presented. Due to length limitations it is not possible to provide the same provisions for all the above defined structural types in this paper. For further details see Follesa, 2015.

1 -Rules for X-Lam buildings

1.1 – General rules

(1) Cross laminated (X-Lam) timber buildings are structures in which walls are composed of cross laminated timber panels according to XX.

(2) The connection of the walls to the foundation should be made by means of mechanical fasteners (hold-down anchors, steel brackets, anchoring bolts, nails and screws) and shall adequately restrain the wall against uplift and sliding. Uplift connections should be placed at wall ends and at opening ends, while shear connections should be distributed uniformly along the wall length (Figure 1).

(3) Walls shall have heights at least equal to the inter-storey height and may be made of a unique element up to the maximum transportable length or may be composed of more than one panel ("segmented wall"). Each segment shall have width not lower than 0,25 h, h signifying the inter-storey height, and shall be connected to the other segments by means of vertical joints made with mechanical fasteners such as screws or nails. Individual wall-panels with a width of less than 0,25 h

shall not be regarded as a seismic resistant shear wall. Perpendicular walls are connected by means of joints made with mechanical fasteners (usually screws). Horizontal joints between walls should be avoided unless special provisions are taken to ensure adequate out- of- plane restraint (e.g. properly connected to perpendicular stabilizing walls, timber studs, etc.).

(4) Floor and roof diaphragms are made of X-Lam timber panels connected together by means of horizontal joints made with mechanical fasteners (screws or nails). The floor panels bear on the wall panels and on timber beams if present, to which they are connected with mechanical fasteners (screws or nails).

(5) Other types of horizontal diaphragms may be used, provided that their in-plane rigidity is ensured by means of wood-based sheathing panels according to XX (reference to the Material Properties section). Timber-concrete composite floors may be used provided that they are adequately connected to the lower and upper walls by means of mechanical fasteners. The concrete topping, in particular, shall be connected to the vertical panels to ensure the in-plane shear due to the diaphragm action is transferred to the walls and down to the foundations.

(6) The upper walls bear on the floor panels (platform construction), and are connected to the lower walls using mechanical fasteners similar to those used for the wall-foundation connection. Tie-down connections nailed to the X-Lam walls may be used for the external walls uplift restraint.

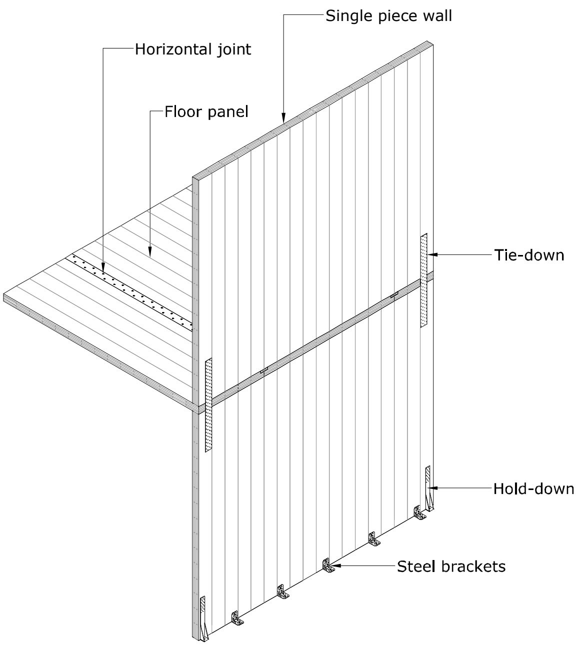

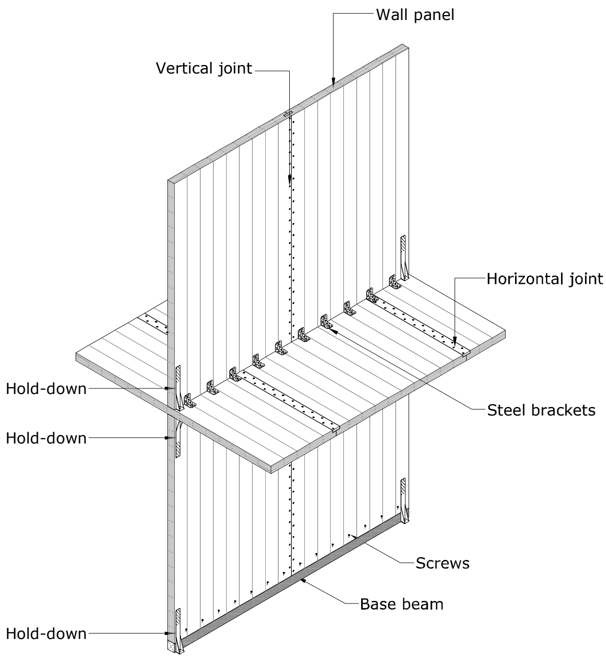

Figure 1. Walls and floors in monolithic, left and segmented, right Cross Laminated Timber buildings (after Follesa et al., 2011).

1.2 – Capacity design rules for DCM

(1) In X-Lam buildings designed for DCM, each wall may be composed either by only one X-Lam panel or by more than one panel connected with rigid vertical joints.

1.2.1 – Capacity design rules at building level

(1)P X-Lam buildings should be regarded as box-type structures. In order to achieve this behaviour some structural components should be considered as dissipative zones and some other should be

considered as non-dissipative and properly designed with sufficient overstrength to avoid any possible brittle failure mechanism. The dissipative connections will use dowel-type fasteners inserted perpendicular to the shear direction. Connections with dowel-type fasteners inclined in the shear direction (e.g. screws inclined in the shear direction) are allowed only in non-dissipative connections. The structural elements which should be designed with sufficient overstrength, according to Equation (1), in order to ensure the development of cyclic yielding in the dissipative zones, shall be (Figure 2):

- *all X-Lam wall and floor panels;*
- *connections between adjacent floor panels (or connection of other type of sheathing material like in XX (reference to the Material Properties section)) in order to limit at the greater possible extent the relative slip and to assure a sufficiently rigid in-plane behaviour;*
- *connections between floors and the underneath walls thus assuring that at each storey there is a sufficiently rigid floor to which the walls are rigidly connected;*
- *connections between perpendicular walls, particularly at the building corners, so that the stability of the walls themselves and of the structural box is always ensured.*

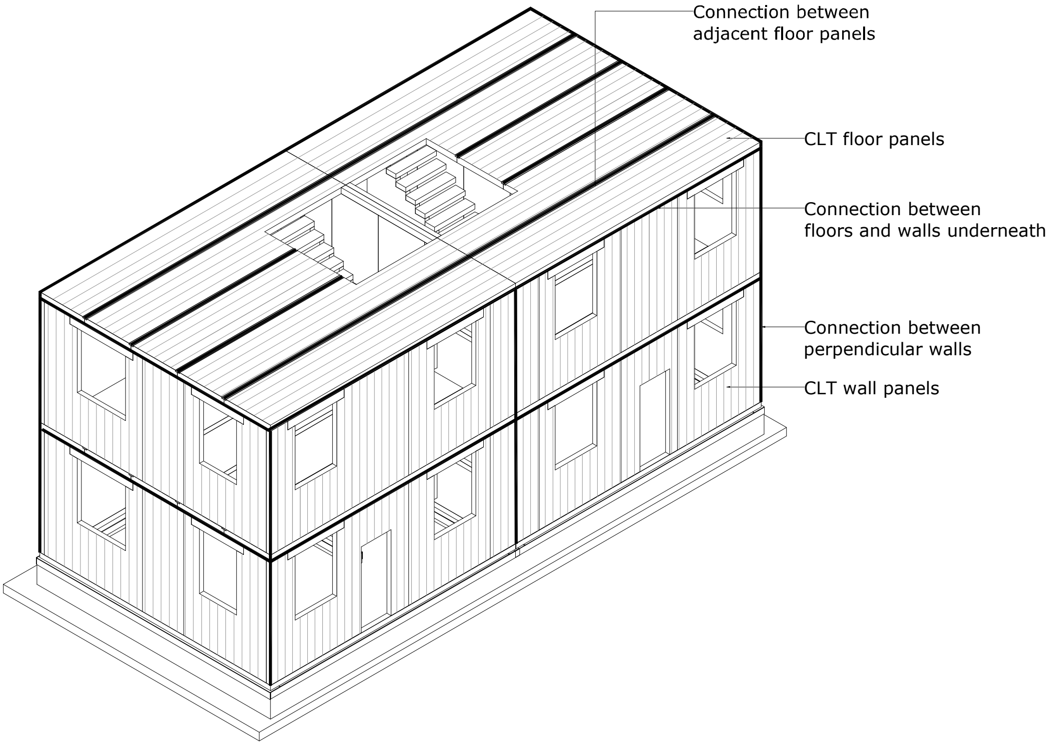

Figure 2. Connections designed with overstrength in order to fulfil the capacity design criteria in Cross Laminated Timber buildings in DCM. (after Follesa et al., 2011, modified).

(2)P The connections devoted to the dissipative behaviour in a X-Lam building should be:

- *shear connections between walls and the underneath floor, and between walls and foundation (usually steel brackets or screwed connections);*
- *anchoring connections against uplift placed at wall ends and at wall openings (usually hold-down anchors).*

1.2.2 – Capacity design rules at connection level

(1)P When designing connections as defined in 1.2.1(2)P a ductile failure mode characterized by yielding of fasteners (nails or screws) in steel-to-timber or timber-to-timber connections should be achieved and brittle failure mechanisms should be avoided according to overstrength rules. Specifically the following failure mechanisms shall be avoided:

- *tensile and pull-through failure of anchor bolts and screws*;
- *steel plate tensile and shear failure in the weakest section of hold-down and angle brackets connections.*

Other brittle failures such as splitting, shear plug, tear-out and tensile fracture of wood in the connection regions should be always avoided.

1.3 – Capacity design rules for DCH

(1) In X-Lam buildings designed for DCH, in each perpendicular direction, at least 50% in length of the seismic resistant shear walls shall be segmented. Segmented walls shall be composed by more than one panel, each one of width not lower than 0,25h, h signifying the inter-storey height, and not greater than h, connected with joints made with mechanical fasteners (screws or nails) inserted in a horizontal plane.

1.3.1 – Capacity design rules at building level

(1)P The same provisions of 1.2.1(1)P apply.

(2)P In addition to the provisions of 1.2.1(2)P the following connections should be considered and designed for dissipative behaviour:

- *vertical screwed or nailed step joints between adjacent parallel wall panels within the segmented shear walls.*

1.3.2 – Capacity design rules at connection level

(1)P The provisions of 1.2.2 apply.

4.5 Ductility rules for dissipative zones

A modification of the provisions currently included in Chapter 8 of Eurocode 8 in order to assign the dissipative zones of timber structures to a Medium or High Ductility Class is proposed as in the following:

(3)P In order to ensure that the given values of the behaviour factor may be used, the dissipative zones, specified in the capacity design rules for each structural type, shall be able to deform plastically for at least three fully reversed cycles at a static ductility ratio reported in Table 3, without more than a 20% reduction of their resistance between the first and third cycles backbone curve.

Table 3. Static ductility values of dissipative zones tested according to EN12512 without more than a 20% reduction of their resistance between the first and third cycles envelope backbone curve for all structural types.

Structural type	*Dissipative sub-assembly/element*	*DCM*	*DCH*
X-Lam buildings	*Shear wall*	*3.0*	*4.0*
X-Lam buildings	*Hold-downs, angle brackets, screws*	*3.0**	*4.0**

Light-Frame buildings	*Shear wall*	*3.0*	*5.0*
Light-Frame buildings	*Fastener (nail/screw)***	*4.0**	*6.0**
Log House buildings	*Shear wall*	*2.0*	-
Moment resisting frames	*Portal Frame*	*2.0*	*3.0*
Moment resisting frames	*Beam-column joint*	*6.0*	*10.0*
Post and beam timber buildings	*Braced Frame*	*2.0*	-
Mixed structures made of timber framing and masonry infill resisting to the horizontal forces	*Shear wall*	*2.0*	-
Vertical cantilever systems made with glulam or X-Lam wall elements	*Shear wall*	*2.5*	-

(4) The provisions of (3)P of this sub clause may be regarded as satisfied in the dissipative zones of all structural types classified in DCH if the following provisions are met:

a) in doweled, bolted and nailed timber-to-timber and steel-to-timber joints with fasteners inserted perpendicular to the shear plane, the minimum thickness of the timber connected members is 10d and the fastener-diameter d does not exceed 12 mm;
b) In shear walls and diaphragms of Light-Frame construction, the sheathing material is wood-based with a minimum thickness of 4d, where the nail diameter d inserted perpendicular to the sheathing plane does not exceed 3,1 mm.

If the above requirements are not met, but the minimum member thickness of 8d and 3d for case a) and case b), respectively, is assured, the dissipative zones of all structural types can be regarded as ductility class M.

As an alternative, the above provisions may be regarded as satisfied:

- *for the dissipative zones of all DCM structural types and of the ductility class H X-Lam system with segmented wall according to 1.3., if a ductile failure mechanism characterized by the formation of at least one plastic hinge in the mechanical fasteners inserted perpendicular to the shear plane is attained for the seismic design load condition;*
- *for the dissipative zones of all DCH structural types, if a ductile failure mechanism characterized by the formation of two plastic hinges in the mechanical fasteners inserted perpendicular to the shear plane is attained for the seismic design load condition.*

Referring to 8.2.2 of EN 1995-1-1 for timber-to-timber and panel-to-timber connections, failure modes a, b and c for fasteners in single shear, and g and h for fasteners in double shear should be avoided. Referring to 8.2.3 of EN 1995-1-1 for steel-to-timber connections, failure modes a, c for fasteners in single shear, and f, j and l for fasteners in double shear should be avoided. Special care should be taken in avoiding brittle failures characterized by splitting, shear plug, tear out and tensile *fracture of wood in the connection regions. In the case of connections with multiple fasteners in dissipative zones, adequate reinforcement should be added to avoid the aforementioned brittle failure mechanisms.*

The value marked with asterisk (*) in Table 3 have been calculated according to Casagrande et al. 2015.

For Light-Frame buildings with nailed/screwed connections (**) different values should be provided for the case of nailed or screwed sheathing-to-frame connections. However, since researches on Light-Frame buildings with screwed sheathing-to-frame connections are still ongoing, conservative values to be considered valid for both cases are provided.

There are a number of recent scientific experiences which demonstrate that the current provisions in order to classify timber structures in Medium and High ductility class (i.e. *the dissipative zones shall be able to deform plastically for at least three fully reversed cycles at a static ductility ratio of 4 for ductility class M structures and at a static ductility ratio of 6 for ductility class H structures, without more than a 20% reduction of their resistance*) are not always met both for Light-Frame (Boudaud et al, 2010; Vogt et al., 2012; Sartori and Tomasi, 2013; Tomasi and Sartori, 2013) and X-Lam (Gavric et al., 2011, Gavric et al., 2014, Gavric et al., 2015) shear walls and connections both in terms of values of static ductility and/or strength degradation.

Also regarding moment-resisting frames, Wrzesniak et al., 2013, by performing Incremental Dynamic Analysis (IDA) on an industrial portal frame and a three-story, five-bay frame, found that for a joint ductility of at least 6 and 4, q-factors of respectively 2 and 1.5 could be suggested for the portal frame, while the recommended q-factor values could be 2.5 and 2 for the 3-storey, 5-bay frame, which are markedly different for the q values suggested by the current version of Eurocode 8.

Thus the code proposal is to specify different minimum values of static ductility in order to attain a certain behaviour factor q depending upon the scale of the dissipative component being considered. More specifically, two levels are considered: (i) connection (single fastener in Light-Frame systems; hold-down/angle bracket and screw connection in X-Lam systems; beam-column joint in moment-resisting frames) or (ii) sub-assembly (e.g. shear walls, portal frames or single span trusses according to the structural type).

Also a new formulation of the detailing rules for dissipative zones is proposed, integrating the existing "prescriptive" philosophy of 2004 and previous editions with a new alternative provision towards “performance based” design rules. The new provisions are intended to require the attainment of a certain ductile failure mode (one or two plastic hinge formation in the fastener) according to the Johansen theory as given in Eurocode 5 independently of the fastener diameter and the member thickness.

4.6 Over-strength factors and safety verifications

As already discussed above, in order to achieve the desired ductile behaviour for the whole building and fulfil the capacity based provisions given for the specified structural system and material, the overstrength factors to be used in the design of the brittle elements should be defined.

A possible proposal could be the following.

(2)P In order to achieve the attainment of the capacity design rules defined in the following sub clauses for all the structural types listed in Table 1, the design strength of the brittle parts $F_{Rd,b}$ should be greater than or equal to the design strength of the ductile parts $F_{Rd,d}$ multiplied by an overstrength factor γ_{Rd} and divided by a reduction factor for strength degradation β_{sd} due to cyclic loading according to the following equation:

$$\frac{\gamma_{Rd}}{\beta_{sd}} \cdot F_{Rd,d} \leq F_{Rd,b} \qquad (1)$$

where the values of γ_{Rd} are provided in Table 4, and the value of β_{sd} is defined in XXX (reference to the Safety Verifications section) and assumes the values given in Table 5.

Lower values of the overstrength factor γ_{Rd} can be used only if supported by experimental tests.

Table 4. Values of the over-strength factor γ_{Rd}.

Structural type	*Overstrength factor γ_{Rd}*
X-Lam buildings	*1.3*
Light-Frame buildings	*1.3*
Log House buildings	*1.3*
Moment resisting frames	*1.6*
Post and beam timber buildings	*1.6*
Mixed structures made of timber framing and masonry infill resisting to the horizontal forces	*1.3*
Vertical cantilever systems made with glulam or X-Lam wall elements	*1.6*

The proposed value of over-strength factors are referenced in Casagrande et al. (2014), Schick et al. (2013), Jorissen & Fragiacomo, (2011) and Follesa et al., (2011).

The definition and the proposed values of the reduction factor for strength degradation due to cyclic loading β_{sd} is given later in the Safety Verification section as follows:

(2)P The partial factors for material properties γ_M for accidental load combinations in accordance with EN 1995-1-1 apply.

(3)P For ultimate limit state verifications of structures designed in accordance with the concept of dissipative structural behaviour (Ductility classes M or H), the strength degradation of the dissipative

zones shall be taken into account by multiplying the characteristic strength in static conditions by a reduction factor β_{sd} given in Table 5. The strength degradation of the non-dissipative zones may not be taken into account. Values of the reduction factor β_{sd} higher than in Table 5 may be used if the actual strength degradation due to cyclic loading is appropriately derived from experimental tests; the strength degradation shall be evaluated at the static ductility ratio shown in Table 3.

(4)P For ultimate limit state verifications of structures designed in accordance with the concept of low dissipative structural behaviour (Ductility class L), no strength degradation will be considered.

(5)P In order to ensure the development of cyclic yielding in the dissipative zones, all other structural members and connections shall be designed with sufficient overstrength.

Table 5 Values of the reduction factor β_{sd} for strength degradation due to cyclic loading

Structural type	*Reduction factor β_{sd}*
X-Lam buildings	*0.8*
Light-Frame buildings with stapled sheathing-to-frame connections	*0.7*
Light-Frame buildings with nailed and screwed sheathing-to-frame connections	*0.8*
Log House buildings	*0.8*
Moment resisting frames	*0.8*
Post and beam timber buildings	*0.8*
Mixed structures made of timber framing and masonry infill resisting to the horizontal forces	*0.8*
Vertical cantilever systems made with glulam or X-Lam wall elements	*0.8*

As already mentioned earlier, the partial safety factors γ_M for fundamental and accidental load combinations for the ultimate limit state verifications in case of dissipative and non-dissipative structural behaviour were inverted in the current 2004 edition with respect to the previous 1995 ENV version, where they were partly consistent with the same provisions given for other materials, like RC, steel or masonry.

In seismic design the partial safety factor γ_M=1.0 given for the accidental load combination should be used, as seismic actions should be regarded as an accidental load case. However, the reference strength considered for the dissipative zones, when designing according to the dissipative behaviour concept, should be adequately reduced to take into account the strength degradation due to cyclic loading. For timber structures, the dissipative elements are mechanical connections, whose strength is calculated according to Eurocode 5 (EN 1995-1, CEN, 2009) using the Johansen theory. This strength is calculated for monotonic loading and no allowance for degradation due to cyclic loading is made. Therefore the proposal is to consider the strength degradation by multiplying the characteristic strength in static conditions by a reduction factor β_{sd} given in Table 5. If the strength degradation is appropriately accounted for by means of experimental evaluation at the static ductility values given in Table 3, higher values of β_{sd} may be used. This proposal is in accordance with the other materials chapters, where it is therefore prescribed that the partial safety factor γ_M=1.0 given for the accidental load combination could be used only if the strength degradation due to cyclic loading is appropriately accounted for in the evaluation of the connection resistance.

For structures designed in accordance with the concept of low dissipative structural behaviour (Ductility class L), and for the non-dissipative zones of structures designed in accordance with the concept of dissipative structural behaviour, no strength degradation should be taken into account.

5 Conclusions

The current provisions for timber buildings included in Section 8 of Eurocode 8 seem not sufficient and adequate to guarantee a correct design of timber buildings according to the general principles of seismic design included in the common sections of Eurocode 8. This is demonstrated by the absence of specific provisions for new structural types currently widely used such as the X-Lam system and the lack of capacity based design criteria and over-strength factors to be used in the design in order to ensure the desired dissipative behaviour for the whole structure.

For these reasons in this paper a proposal for a new “Background Document” useful for a revision of Chapter 8 of Eurocode 8 is presented, based on recent research results and literature review.

The proposal is formulated in terms of revision and addition of some specific parts such as: (i) materials and properties of dissipative zones, (ii) structural types, (iii) behaviour factors, (iv) general rules and capacity based design rules and (v) ductility rules for dissipative zones and safety verification.

Given the length limitation of this paper, it is not possible to provide a comprehensive overview of the full proposal which includes also some provisions for (i) buildings with different lateral load resisting systems, (ii) the design of new structural elements and systems not listed in the structural types included in this proposal, (iii) inter-storey drift limits, and (iv) other minor changes and additions to the existing provisions.

Although the suggested additions are not sufficient to define a complete document according to the general principles of Eurocode 8, the proposal is still under discussion and provides a fundamental update of the code provisions for the seismic design of timber structures. This proposal could therefore represent a useful tool, updated to the recent technical and scientific developments for the future revision of Chapter 8 of Eurocode 8.

6 References

Becker K. et al. (1993): Eurocode 8 – Part 1.3 – Chapter 5 – Specific rules for timber buildings in seismic region. Proceedings of the 26th CIB W18, Athens, Georgia. (paper 26-15-2).

Bedon, C. et al. (2014): Experimental study and numerical investigation of “Blockhaus” shear walls subjected to in-plane seismic loads. ASCE Journal of Structural Engineering. (ASCE published online, doi: 10.1061/(ASCE)ST.1943-541X.0001065).

Bedon, C. et al. (2015): Non-linear modelling of the seismic behaviour of 'Blockhaus' structures. Engineering Structures, in print.

Bratulic, K. et al. (2014): Monotonic and cyclic behaviour of joints with self-tapping screws in CLT structures. Cost Action FP 1004. Experimental Research with Timber, University of Bath, Prague, Czech Republic (pages 1-8).

Boudaud, C. et al. (2010): European seismic design of shear walls: experimental and numerical tests and observations. Proceedings of the 11th World Conference on Timber Engineering, Riva del Garda (TN), Italy.

Campos Costa, A. et al. (2013): Seismic performance of multi-storey timber buildings - RubnerHaus building - Final Report. SERIES. (Work Package [WP9-TA5 LNEC]).

Casagrande, D. et al. (2014): Capacity design approach for multi-storey timber-frame buildings. Proc. of the International Network on Timber Engineering Research meeting INTER, Bath, United Kingdom. (paper 47-15-3).

Casagrande, D. et al.: (2015) A predictive analytical model for the elasto-plastic behaviour of a light timber-frame shear-wall. Construction and Building Materials, (Special Issue “SHATIS 2013”, 10.1016/j.conbuildmat.2015.06.025)

Ceccotti, A. & Follesa, M. (2006): Seismic Behaviour of Multi-Storey X-Lam Buildings. Proceedings of 426 COST E29 International Workshop on Earthquake Engineering on Timber Structures, Coimbra, Portugal. (pages 81-95).

Ceccotti, A. et al. (2007): Quale fattore di struttura per gli edifici multipiano a struttura di legno con pannelli a strati incrociati? (in Italian). Proceedings of the 12th ANIDIS Conference, Pisa (Italy).

Ceccotti, A. & Larsen, H.J. (1988): Background document for specific rules for timber structures in Eurocode 8. Report EUR 12266 EN for the Commission of the European Communities, Brussels, Belgium

EN12512 (2001): Timber structures- Test methods. Cyclic testing of joints made with mechanical fasteners. CEN.

Eurocode 5 (2009): Design of timber structures - Part 1-1: General and rules for buildings. CEN. (EN 1995-1-1).

Eurocode 8 (2004): Design of structures for earthquake resistance, Part 1: General rules, seismic actions and rules for buildings. CEN. (EN 1998-1-1).

Follesa, M. (2015): Seismic design of timber structures - A proposal for the revision of Chapter 8 of Eurocode 8. Phd Thesis, Università degli Studi di Cagliari, Italy.

Follesa, M. et al. (2011): A proposal for revision of the current timber part (Section 8) of Eurocode 8 Part 1. Proceedings of the 44th CIB W18 Meeting, Alghero, Italy. (paper 44-15-1).

Flatscher, G. et al. (2014a): Experimental tests on cross-laminated timber joints and walls. ICE Journal Structures and Buildings. (http://dx.doi.org/10.1680/stbu.13.00085).

Flatscher, G. et al. (2014b): Screwed joints in Cross-Laminated timber structures. Proceedings of the 13th World Conference on Timber Engineering WCTE 2014, Quebec City, Canada.

Flatscher, G. & Schickhofer, G. (2015): Shaking table test on a cross-laminated timber structure. ICE Journal Structures and Buildings. (http://dx.doi.org/10.1680/stbu.13.000856).

Fragiacomo, M. et al. (2011): Elastic and ductile design of multi-storey crosslam massive wooden buildings under seismic actions. Engineering Structures, Special Issue on Timber Structures. (Vol. 33 No. 11, pp. 3043-3053).

Gavric, I. et al. (2011): Experimental cyclic tests on cross-laminated timber panels and typical connections. Proceedings of the 14th ANIDIS Conference, Bari (Italy).

Gavric, I. et al. (2014): Cyclic behaviour of typical metal connectors for cross-laminated (CLT) structures. RILEM Materials and Structures. (Vol. 48 No. 3, pp. 1841-1857, doi: 10.1617/s11527-014-0278-7).

Gavric, I. et al. (2015): Cyclic behaviour of typical screwed connections for cross-laminated (CLT) structures. European Journal of Wood and Wood Products. (Vol. 73 No. 2, pp. 179-191, doi: 10.1007/s00107-014-0877-6).

Hummel, J. et al. (2013): CLT wall elements under cyclic loading – details of anchorage and connection. Cost Action FP1004, Focus Solid Timber Solutions – European Conference on Cross Laminated Timber (CLT), The University of Bath, Graz. (R.Harris, A. Ringhofer and G. Shickhofer eds., pp. 152-165).

Jorissen, A. & Fragiacomo, M. (2011): General notes on ductility in timber structures. Engineering Structures. (Vol. 33, N. 11, pp. 2987-2997).

Norme Tecniche delle Costruzioni NTC 2015 (in Italian) – Draft Nov. 4, 2014.

NRC (2010): National Building Code of Canada. Canadian Commission on Building and Fire Code, National Research Council of Canada, Ottawa, Ont.

NZS 3603 (1993): Timber structures standard. Wellington, New Zealand.

Piazza, M. et al. (2013): Seismic performance of multi-storey timber buildings - RubnerHaus building – Final Report. Seismic Engineering Research Infrastructures For European Synergies (SERIES). (Work package [WP9 – TA5 LNEC]).

Pozza, L. et al. (2013): A non-linear numerical model for the assessment of the seismic behaviour and ductility factor of X-Lam timber structures. Proceedings of the 46th CIB-W18-Meeting, Vancouver, Canada. (paper 46-15-5).

Sartori, T. & Tomasi, R. (2013): Experimental investigation on sheathing-to-framing connections in wood shear walls. Engineering Structures. (Vol. 56, pp. 2197- 2205).

Schick, M. et al. (2013): Connection and anchoring for wall and slab elements in seismic design. Proceedings of the 46th CIB-W18-Meeting, Vancouver, Canada. (paper 46-15-4).

Tomasi, R. & Sartori, T. (2013): Mechanical behaviour of connections between wood framed shear walls and foundations under monotonic and cyclic load. Construction and Building Materials. (Vol. 44, pp. 682-690).

Vogt, T et al., (2012): Timber framed wall elements under cyclic loading. Proceedings of the 12th World Conference on Timber Engineering, Auckland, New Zealand

Wrzesniak, D. et al. (2013): Proposal for the q-factor of moment-resisting timber frames with high ductility dowel connectors. Proceedings of the 46th CIB-W18-Meeting, Vancouver, Canada. (paper 46-15-6).

Discussion

The paper was presented by M Follesa

G Schickhofer stated that many structural types were considered here and that some should be considered only in the national annex such as log houses. M Follesa said that log houses would be interesting for Italy.

T Toratti commented that the two floor diaphragm cases where the floor went through the whole building would result in acoustic issues

F Lam commented that the ductility factor for screws connected light wood frame walls is too high. M Follesa agreed.

D Moroder discussed the information in slide 28 where β to reduce over-strength also has a β reduction; it seemed double reduction.

A Ceccotti commented that slide 7 stated that the current provisions are not always met. He asked whether the provisions are on the safe side. M Follesa said no and commented that for example some Xlam connectors have lower ductility ratio.

G Schickhofer and M Follesa discussed the definition of ductility as some of these are not consistent.

S Winter stated that the production of background documents is good; he asked about time schedule and finalization. M Follesa said that the proposal would be finalized by 2016. S Winter commented that the document should be circulated as soon as possible even as a draft.

Aspects of Code Based Design of Timber Structures[1]

Jochen Kohler
Dept. of Structural Engineering, Norwegian University of Science and Technology (NTNU), Trondheim, Norway

Gerhard Fink
Empa, Swiss Federal Laboratories for Material Science and Technology, Dübendorf, Switzerland

KEYWORDS: Code calibration, Structural reliability, Load and resistance factor design, European timber design standards

ABSTRACT: The European timber design standard is under development and a new version will be issued at the end of this decade. In this paper the present design standard is critically assessed in regard to its ability to identify design solutions with a consistent level of reliability. The main issues to enhance the current standards are identified and discussed. Thereunder, the influence of different material properties in different load directions, the quality of the grading process, the application of the current safety concept on non-linear design equations, duration of load effects, effects due to moisture induced stresses, volume and length effects, reliable and uniform design equations for joints and the adoption of consequence classes for associated situations are considered.

1 INTRODUCTION

Sustainable development is the important requirement and goal for modern society and the international research community is in demand to find solutions that provide the foundation for this aim. The role of structural engineering research is thereby of significant importance. The development of methodologies and principles that allows for the optimal allocation of resources into the structural performance and their implementation into the daily engineering practice constitute the major challenge for ongoing and future research in the field of structural engineering.

The broad implementation of newly developed principles requires their proper transition into rules and regulations that constitute the basis for the daily work of practicing engineers. Thus, rules and regulations as structural design codes constitute the mayor interface between structural engineering research and practical application and it is of utmost importance that structural design codes are up to date with the best scientific information available and, at the same time, are simple enough for straight forward application.

This challenge outlined above is general for the entire structural engineering research and professional community. Here, timber and timber based materials might be attributed

[1] The work is based on an article published at the 12th International Conference on Applications of Statistics and Probability in Civil Engineering (Kohler and Fink, 2015) including some adoptions after discussions at the conference.

with a special status since timber as a natural grown material plays an important role in the safe, cost efficient and sustainable development of our future build environment because of its beneficial properties. Timber is an efficient building material, not least in regard to its mechanical properties but also because it is a highly sustainable material considering all phases of the life cycle of timber structures: production, use and decommissioning.

Timber is a widely available natural resource; e.g. with proper management, there is a potential for a continuous and sustainable supply of raw timber material in the future. Because of the low energy use and the low level of pollution associated with the manufacturing of timber structures the environmental impact is much smaller than for structures built in other materials.

However, besides the beneficial properties of timber the confident use of timber as a load-bearing material is particularly challenging compared to other common structural materials as steel and concrete. One of the main reasons for this is that timber is a highly complex material; the proper use in structures actually requires a significant amount of expertise in structural detailing.

Another main reason is that any prediction of the structural performance of timber is associated with large uncertainties. Timber is by nature a very inhomogeneous material. The material properties depend on the specific wood species, the geographical location and furthermore on the local growing conditions over the entire lifetime of the tree. Timber is an orthotropic material, i.e. it consists of “high strength” fibres/grains which are predominantly orientated along the longitudinal axis of a timber log/ tree and packed together within a “low strength” matrix. After a log is sawn into pieces of structural timber, irregularities, such as grain direction or knots, become, in addition to the orthotropic characteristics mentioned above, highly decisive for the load-bearing capacity of a timber structural element. Consequently, the properties of solid timber cannot be designed or produced by means of some recipe but may be ensured to fulfil given requirements only by quality control procedures implemented during the production process for sawn timber. Timber material for structural purpose is generally associated to a certain grade or strength class. However, there are various different ways how quality control is implemented in the production process and the properties of timber of a certain strength class are highly sensitive to the quality control scheme applied to the timber.

Timber is a viscoelastic and hygroscopic material. When using timber as a load-bearing element in a structure it is of high interest how the load-bearing performance is developing over time, i.e. how the building environment with its variable loads, temperature and moisture is influencing the timber structural element.

The high importance of structural timber and timber products for the sustainable development of our build infrastructure together with the fact that many features of the structural behaviour of timber are not known with accurate precision underlines the urgent need for extensive and coordinated research in this field. Furthermore it is necessary that current and future knowledge about timber and timber based materials load- bearing behaviour is represented in the current design standards in a sensible way.

In Europe the design of structures is regulated by the Eurocodes, a suite of consistent standards for structural design covering all relevant load scenarios and building materials. They were developed under the supervision of the European Committee of Standardization (CEN) and regulate to a large extent the performance criteria of the build environment being reliability, serviceability and safety of structures. The Eurocodes had been introduced in the 1980s and are by now compulsory for structural engineering design in most European countries. Until 2020 a revision and update of the Eurocodes is planned. Thus, this constitutes an excellent opportunity to critically reflect the design procedures prescribed in the Eurocode 5 – “Design of Timber Structures” in the light of recent scientific developments.

Motivated by the ongoing revision and of the current version of Eurocodes a COST Action, entitled *Basis of Structural Timber Design – from research to standards*[2], was initiated. The presented paper represents a summary of tasks planned to work on during this COST Action.

2 BASIC PRINCIPLES OF RELIABILITY BASED CODE CALIBRATION

Modern design codes, such as the Eurocodes (2002), are based on the so-called load and resistance factor design (LRFD) format. Next, the principle of LRFD is explained for the case of two loads; one that is constant and one that is variable over time. The LRFD equation is given in Eq. (1). Here R_k, G_k and Q_k are the characteristic values of the resistance R, the permanent load G, and the time variable load Q. γ_m, γ_G and γ_Q are the corresponding partial safety factors. z is the so-called design variable, which is defined by the chosen dimensions of the structural component.

$$z\frac{R_\mathrm{k}}{\gamma_m} - \gamma_G G_\mathrm{k} - \gamma_Q Q_\mathrm{k} = 0 \tag{1}$$

The characteristic values for both load and resistance are in general defined as fractile values of the corresponding probability distributions. In Eurocode 5 (2004) the following characteristic values are defined: R_k is the 5% fractile value of a Lognormal distributed resistance, G_k is the 50% fractile value (mean value) of the Normal distributed load (constant in time), and Q_k is the 98% fractile value of the Gumbel distributed yearly maxima of the load (variable in time).

The corresponding partial safety factors can be calibrated to provide design solutions (z) with an acceptable failure probability P_f (Eq. 2). Here R, G, and Q are resistance and loads represented as random variables, $z^* = z(\gamma_m, \gamma_G, \gamma_Q)$ is the design solution identified with Eq. (1) as a function of the selected partial safety factors, and X is the model uncertainty.

$$\begin{aligned} &P_f = P\{g(X,R,G,Q) < 0\} \\ &\text{with} \quad g(X,R,G,Q) = z^* XR - G - Q = 0 \end{aligned} \tag{2}$$

Often the structural reliability is expressed with the so-called *reliability index* β (Eq. 3). A common value for the target reliability index is $\beta \approx 4.2$ which corresponds to a probability of failure $P_f \approx 10^{-5}$ (JCSS, 2001).

$$\beta = -\Phi^{-1}(P_f) \tag{3}$$

In general, different design situations are relevant; i.e. different ratios between G and Q. This can be considered using a modification of Eq. (1)–(2) into Eq. (4)–(5). α_i might take values between 0 and 1, representing different ratios of G and Q. $\hat{R}$, $\hat{G}$, and $\hat{Q}$ are normalized to a mean value of 1. For each α_i one design equations exists, thus altogether n different design equations have to be considered.

[2] `http://www.costfp1402.tum.de`

Table 1: Chosen representation of the model uncertainty X, the bending strength R, the permanent load G and the variable load Q.

	X	R	G	Q
Mean value	1	1	1	1
Standard deviation	0.1	0.25	0.1	0.4
Distribution type	Lognormal	Lognormal	Normal	Gumbel
Fractile	-	0.05	0.5	0.98
Characteristic value	-	0.647	1	2.037

$$z_i \frac{\hat{R}_\mathrm{k}}{\gamma_m} - \gamma_G \alpha_i \hat{G}_\mathrm{k} - \gamma_Q (1-\alpha_i) \hat{Q}_\mathrm{k} = 0 \tag{4}$$

$$g_i(X, \hat{R}, \hat{G}, \hat{Q}) = z_i^* X \hat{R} - \alpha_i \hat{G} - (1-\alpha_i)\hat{Q} = 0 \tag{5}$$

Afterwards, the partial safety factors ($\gamma_m, \gamma_G,$ and γ_Q) can be calibrated by solving the optimisation problem give in Eq. (6).

$$\min_{\gamma} \left[\sum_{j=1}^{n} \left(\beta_\mathrm{target} - \beta_j \right)^2 \right] \tag{6}$$

The reliability based code calibration is briefly introduced to illustrate the influence of uncertainties (load and resistance), in respect to codes. Please find more information in (e.g. JCSS, 2001; Faber and Sørensen, 2003).

The application of the above sketched framework constitutes the basis for reliability based calibration of the partial safety factors of a load and resistance factor design format. And it entirely depends on a realistic representation of loads, resistances and model accuracy by the random variables R, Q, G, and X.

2.1 Example

The design equation for a structural component can be calibrated according to the procedure described in above. The chosen variables of Eq. (4) and Eq. (5) are summarized in Table 1. Using this values the situation could represent a solid timber bending beam loaded by constant (e.g. self-weight of beam and installations) and variable (e.g. live load).

In the presented example, which is explained in more detail in Kohler and Fink (2012), the range $\alpha = [0.1, 0.2, ..., 0.8]$ is chosen, to exclude rather unrealistic design situations. The calculations was performed with the software CodeCal (JCSS, 2001). In Figure 1 the chosen target reliability index of $\beta = 4.2$ (red line) is compared with the design solutions for the structural component obtained according to the current version of the Eurocode ($\gamma_m = 1.3, \gamma_G = 1.5, \gamma_Q = 1.5$); represented by the line with squares. The reliability indices of the design solutions according to the Eurocode tend to be too low compared to the target reliability index, especially for small α. The line with the diamonds is obtained when all partial safety factors are subject to optimization: $\gamma_m = 1.29, \gamma_G = 1.30, \gamma_Q = 1.57$. However, it is the philosophy of the Eurocodes that the partial safety factors for the loads are material independent. Thus, γ_G and γ_Q are fixed and the optimization is performed only subject to γ_m. The line with the circles in Figure 1 is representing the corresponding result ($\gamma_m = 1.33$).

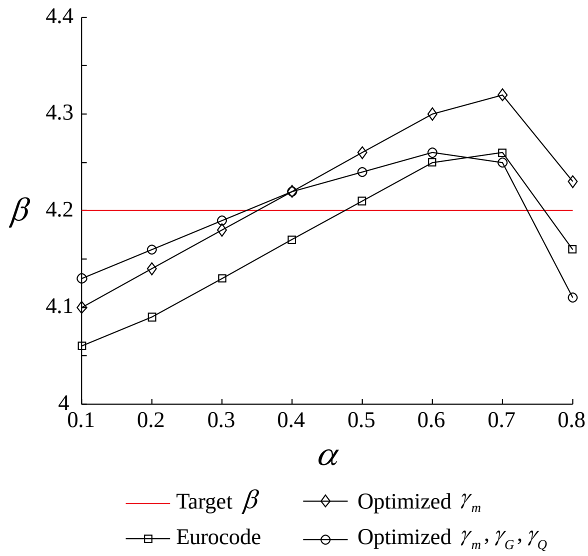

Figure 1: Reliability Index over different design situations alpha for solid timber in bending. The different lines represent different sets of partial safety factors (Kohler and Fink, 2012).

The above example demonstrates the validity of the Eurocode 5 (2004) design safety concept for timber load-bearing elements under the assumption that the parameters given in Figure 1 represent the real situation with sufficient accuracy. In the following it will be discussed in which ways the actual load load-bearing behavior derivate from the assumptions in Table 1. It is demonstrated and quantified how the corresponding deviation affects the reliability of design situations and it is discussed how recent research results might integrated in the further developed issue of Eurocode 5 (2004).

3 PARTICULARITIES IN TIMBER MATERIAL MODELLING

In the following section the main issues to enhance the current standards are identified and discussed. That includes the influence of different material properties in different load directions, the quality of the grading process, the application of the current safety concept on non-linear design equations, duration of load effects, effects due to moisture induced stresses, volume and length effects, reliable and uniform design equations for joints and the adoption of consequence classes for associated situations.

3.1 Different “material properties”

Timber is a rather complex building material. Its properties are highly variable, spatially and in time. In structural engineering, material properties of timber are in general understood as the stress and stiffness related properties of standard test specimen under given (standard) loading and climate conditions and the timber density. Test configurations are prescribed in e.g. ISO 8375 (1985) and any statement about stress and stiffness related properties of structural timber is conditional to the corresponding test configuration. In general it is distinguished between the different loading modes and “material properties” are given corresponding to the loading direction relative to the main fiber direction of a beam shaped element (Figure 2).

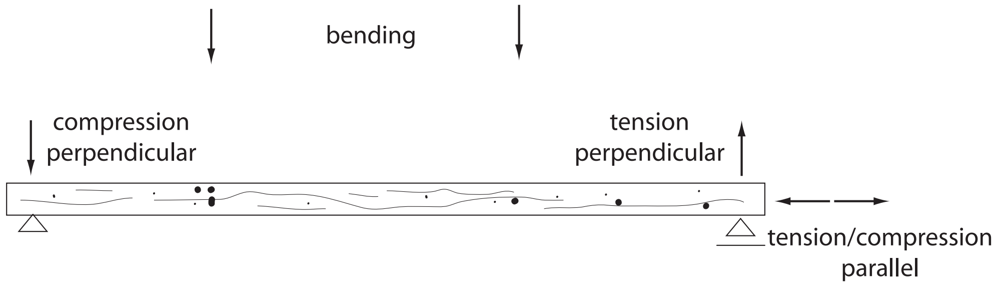

Figure 2: Different "material properties" dependent on the loading mode.

The "material properties" have different statistical properties and when using the design criterion introduced before and applying the same partial safety factor γ_m, as it is practiced in the Eurocode, the reliability of the corresponding design solutions differ.

The influence of different "material properties" was investigated in Kohler and Fink (2012). There, the distribution functions and the associated variability for different types of "material properties" were chosen, as recommended in the Probabilistic Model Code JCSS (2006), see also Köhler (2006) for background information. The results are summarized in Table 2. The obtained scatter in partial safety factors suggests a rather differentiated treatment of the different design situations in future developments of design codes.

The most extreme deviation from the values proposed in the Eurocode $\gamma_m = 1.30$ is obtained for the load case tension perpendicular to the grain $\gamma_m = 3.05$. This also indicated that if a structural element for this load case is designed with the current safety factor of $\gamma_m = 1.30$, very low reliability indices, in the order of magnitude of 3.1 are obtained. However, the results concerning this particular load case have to be considered with special care. In fact the material capacity under this loading mode is specified by EN 338 (2010) with a nominal value that does not correspond to the 5%-fractile value taken from the statistical distribution that is derived from test data for the same loading mode. It is rather a value well below the 5%-fractile value. Furthermore, in best practice timber engineering design this loading mode at its limit is avoided due to the high sensibility to aspects that are not directly controlled in design, as e.g. moisture induced stresses and macro and micro cracks in the timber.

On the other hand the current design for compression strength perpendicular to the grain seems to be rather conservative $\gamma_m = 1.20$. Here, it has to be considered that the consequences that are resulting from failure of the compression strength perpendicular to the grain are rather low (see also Chapter 3.7). Thus, the conservative approach has to questioned.

Table 2: Calibrated partial safety factors for the resistance, for constant $\gamma_G = 1.35$ and $\gamma_Q = 1.50$ (from Kohler and Fink, 2012).

Ultimate limit state	γ_m
Bending strength	1.33
Tension strength parallel to the grain	1.40
Tension strength perp. to the grain	3.05
Compression strength parallel to the grain	1.24
Compression strength perp. to the grain	1.20
Shear strength	1.33

3.2 Timber as a graded material

Due to the special way timber material properties are ensured by means of grading in the production line, special considerations must be made when modeling their probabilistic characteristics. Previous work on this subject is reported in (e.g. Rouger, 1996; Pöhlmann and Rackwitz, 1981). Further assessment of the probabilistic modelling on the properties of graded timber material was presented in Faber et al. (2004); Sandomeer et al. (2008). In the latter references it is reported that the scatter of strength related material properties is highly sensitive to the grading procedure applied and to the properties of the original ungraded material. This observation is confirmed by a large experimental campaign that took place recently in Europe in connection to the Gradewood project[3]. Here a large number of graded samples have been tested and a large between sample variability has been observed. Furthermore it has been shown that it is highly uncertain whether a sample that is graded to a specific grade actually meets the corresponding requirements in regard to minimum 5% fractile values of strength properties.

It is continued along the example introduced above, assuming that the grading accuracy directly affects the coefficient of variation of the timber bending capacity. The material partial safety factor are calibrated for different grading schemes that correspond to different coefficients of variation in the range from 0.2 – 0.4. The corresponding partial material safety factors rage between $\gamma_m = 1.2 - 1.65$ depending on the applied grading procedure. These results suggest a better differentiation of the grading procedure in future design codes. Alternatively, if no information about the accuracy of timber grading is utilized a larger coefficient of variation for representing the bending capacity should be used.

3.3 Non linear design equations

For common design equations a linear comparison of load effects and component resistance as in Equation (1) is not sufficient. One example is the design of slender columns where strength and stiffness properties and creep effects play an important role for assessing the stability. For the analysis of single members, standards generally give simplified calculation models that do not require a 2^{nd} order ultimate limit state analysis. However, for the analysis of more complex systems like unbraced frame structures, a 2^{nd} order structural analysis is more appropriate and accurate and an alternative design procedure is given e.g. in the Eurocode (2004). Compared to the simple design format as presented in Eq. (1), the design equations for slender columns are more complex containing uncertain properties as strength, stiffness and load eccentricity in non-linear combination. The problem was addressed in Köhler et al. (2008) and quite uneven reliabilities for different column slenderness have been reported. Figure 3 the reliability index of design solutions with different slenderness-ratio are presented. The different colors correspond to different design frameworks; I. EN 1995-1-1 (2004), 2^{nd} order method with the stiffness considered as the mean modulus of elasticity;. II. DIN 1052 (2004), 2nd order method with the stiffness considered as the 5% fractile of the modulus of elasticity, and; III. EN 1995-1-1 (2004) / DIN 1052 (2004) according to the so called simplified equivalent length approach. For more details compare Köhler et al. (2008).

In future code safety formats design strength and stiffness should be clibrated in order to obtain consistent reliability levels for different design situations.

---

[3] `http://www.woodwisdom.net/wp-content/uploads/2014/08/Gradewood_final_report.pdf`

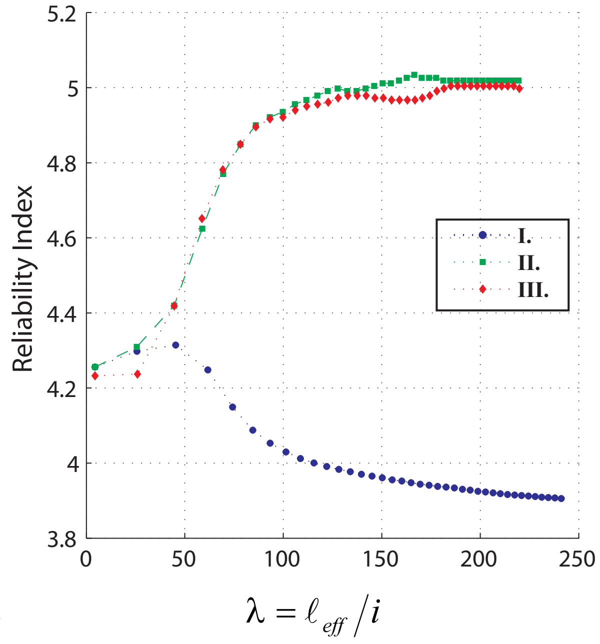

Figure 3: Reliability Index over slenderness for design solutions according to different design formats (Köhler et al., 2008).

3.4 Duration of load effect and moisture induced stress

The capacity of a timber structural element is highly dependent on the time duration of the load effect to which it is exposed to. As an example the capacity of a bending beam continuously loaded is only 60% of that of a similar beam exposed to an instant load (Wood, 1947).

Timber is a hygroscopic material, i.e. it adsorbs and desorbs moisture from the surrounding air. Variations in moisture content in the surrounding air will, with a corresponding time lack, lead to variations in moisture content in the timber, this affects the mechanical properties of the timber but more importantly it will induce stresses due to shrinkage and swelling alongside the moisture gradients in the timber. These moisture induced stresses have been a matter of intensive discussion in the timber engineering community in the last years.

Both, duration of load effect and moisture induced stresses are highly relevant phenomena to take into account in structural design. They are also challenging phenomena since the underlying physical mechanisms are not fully understood and empirical evidence is scarce. However, in practical design, as in the Eurocode 5 (2004), the effect of moisture on the duration of load effect is considered with the joint modification factor k_{mod} which is given for different climate exposures in design codes. Values for this factor are prescribed in a matrix for three different so-called service classes, i.e. different climate scenarios, and five different load classes, i.e. load scenarios.

This format appears to be oversimplified and further research and enhancement of the level of detail in structural design should be developed.

3.5 Volume and length effects

One major topic that is continuously discussed within the research community is the appropriate representation of size effects on strength in solid timber. For most loading modes as tension parallel or perpendicular to grain, shear or bending, timber predominately presents brittle failure behaviour. A (perfect) brittle material is defined as a material that fails if a single particle fails (see e.g. Bolotin, 1969). The strength of the material is thus governed by the strength of the 'weakest' particle; therefore the model for ideal brittle materials is also called the weakest link model (Weibull, 1939). This model was applied to the different failure modes in timber, the model parameters have been calibrated based on experimental evidence on the different failure modes. A literature review can be found e.g. in Kohler et al. (2013). There it is concluded that the size effects in timber are better represented with a model that takes into account the multi scale variability of structural timber and a corresponding model framework is suggested.

In present code formats size effects are often not completely taken into account or neglected. This is particularly critical when large scale engineered timber sections are used in modern timber construction. In a revision of the codes this aspect should earn appropriate attention and current research results should be implemented.

3.6 Joints

For timber structures, the structural performance depends to a considerable part on the connections or joints between different timber structural members; joints can govern the overall strength, serviceability and fire resistance. Despite their importance timber joint design frameworks are not based on a consistent basis compared to the design regulations of timber structural components.

Explanations for this difference in progress of design provisions for members and joints can be found in the relative simplicity of characterizing mechanical behaviour of members, as compared to connections. A diversity of joints types is used in practice and these types have infinite variety in arrangement. This usually precludes the option of testing large numbers of replicas for a reliable quantification and verification of statistical and mechanical models. The main and most important group of joints corresponds to the joints with dowel type fasteners, i.e. joints with dowels, nails, screws and staples belong to this group.

Different failure modes can be observed for dowel type fastener joints and the modes are partly captured by a simple mechanical model based on the works of Johansen (1949); Meyer (1957). These models build the basis for the current European design framework for dowel type connectors in the Eurocode. However, different failure modes correspond to different failure behavior and consequences (brittle or ductile). In Köhler (2006) is has also been observed that model uncertainty and model bias for the different failure modes is significantly different. This is not considered in the current version of the European design standard and should be subject for further investigation.

3.7 Consequence classes

In the previous chapter it was mentioned that different failure modes in dowel type fastener joint lead to different magnitudes of consequences. This is in principle true for all failure modes in timber structure. In Chapter 3.1 different failure modes of timber components have been compared to the same target reliability, implying that the consequences for all failure modes are classified uniformly. However, if a failure scenario for tension or bending failure is visualized and compared with a typical failure scenario for compression perpendicular to the grain, it might be agreed that the consequences are quite different and correspondingly the target reliability should be defined separately for the different cases.

4 CONCLUSIONS

Timber will play an important role in the future developments towards a more sustainable building sector. However, many stakeholders are still skeptical when it comes to the technological maturity of the material, especially compared to concrete and steel. The structural design regulations in general can be seen not only as the main interface connecting the state of knowledge in the engineering research community with the implementation of the real build environment; design standards are also the precondition for the implementation of building material on a high technological level.

In the present paper the major challenges for the future development of timber design standards have been highlighted from a European perspective; i.e. taking the Eurocodes as references. The challenges are hereby related to both, the further development of the knowledge basis for the behavior of timber in structures and the implementation of this knowledge into practicable rules in the future standards.

References

Bolotin, V. V. (1969). *Statistical Methods in Structural Mechanics*. Holden-Day Series in Mathematical Physics.

DIN 1052 (2004). Bemessungsregeln für Holzkonstruktionen. Normenausschuss Bauwesen (NABau) im DIN (Deutsches Institut für Normung e.V.), Berlin, Germany.

EN 1990 (2002). Eurocode 0: Basis of structural design. European Committee for Standardization, Brussels, Belgium.

EN 1995-1-1 (2004). Eurocode 5: Design of timber structures – Part 1-1: General – Common rules and rules for buildings; German version. European Committee for Standardization, Brussels, Belgium.

EN 338 (2010). Structural timber – Strength classes; German version. European Committee for Standardization, Brussels, Belgium.

Faber, M. H., Köhler, J., and Sørensen, J. D. (2004). Probabilistic modelling of graded timber material properties. *Structural safety*, 26(3):295–309.

Faber, M. H. and Sørensen, J. D. (2003). Reliability based code calibration – The JCSS approach. In *Applications of statistics and probability in civil engineering : proceedings of the 9th International Conference on Applications of Statistics and Probability in Civil Engineering, San Francisco, USA, July 6–9*, pages 927–935.

ISO 8375 (1985). Solid timber in structural sizes: Determination of some physical and mechanical properties. International Standards Organization, Geneva, Switzerland.

JCSS (2001). Probabilistic Model Code Part I - Basis of Design. http://www.jcss.byg.dtu.dk/Publications/Probabilistic_Model_Code.

JCSS (2006). Probabilistic Model Code Part III - Resistance Models (3.05 Timber). http://www.jcss.byg.dtu.dk/Publications/Probabilistic_Model_Code.

Johansen, K. (1949). Theory of timber connections. In *International Association of Bridge and Structural Engineering, Publication No. 9, pp. 249-262, Bern, Switzerland*.

Köhler, J. (2006). *Reliability of Timber Structures*. PhD thesis, ETH Zurich, Zurich, Switzerland.

Köhler, J., Andrea, F., and René, S. (2008). On the role of stiffness properties for ultimate limit state design of slender columns. In *Proceedings of the 41th Meeting, International Council for Research and Innovation in Building and Construction, Working Commission W18 - Timber Structures, St. Andrews, Canada, CIB-W18, Paper No. 41-1-1*.

Kohler, J., Brandner, R., Thiel, A., and Schickhofer, G. (2013). Probabilistic characterisation of the length effect for parallel to the grain tensile strength of central european spruce. *Engineering Structures*, 56:691–697.

Kohler, J. and Fink, G. (2012). Reliability Based Code Calibration of a Typical Eurocode 5 Design Equations. In Quenneville, P., editor, *World Conference on Timber Engineering 2012 (WCTE 2012) : The Future of Timber Engineering : Auckland, New Zealand : 15-19 July 2012. Volume 4*, pages 99–103, Red Hook, NY. Curran Associates, Inc.

Kohler, J. and Fink, G. (2015). Aspects of code based design of timber structures. In *Proceedings of the 12th International Conference on Applications of Statistics and Probability in Civil Engineering, Vancouver, Canada on July 12-15, 2015*.

Meyer, A. (1957). Die Tragfähigkeit von Nagelverbindungen bei Statischer Belastung. *Holz als Roh- und Werkstoff*, 15(2):96–109.

Pöhlmann, S. and Rackwitz, R. (1981). *Zur Verteilungsfunktion der Festigkeitseigenschaften bei kontinuierlich durchgeführter Sortierung*. Materialprüfung 23, Hanser, Munich, Germany.

Rouger, F. (1996). Application of a modified statistical segmentation method to timber machine strength grading. *Wood and Fibre Science*, 28(4).

Sandomeer, M. K., Köhler, J., and Faber, M. H. (2008). Probabilistic output control for structural timber - modelling approach. In *Proceedings of the 41th Meeting, International Council for Research and Innovation in Building and Construction, Working Commission W18 - Timber Structures, St. Andrews, Canada, CIB-W18, Paper No. 41-5-1*.

Weibull, W. (1939). *A statistical theory of strength of materials*. Nr. 151, Royal Swedish Institute for Engineering Research.

Wood, L. (1947). Behaviour of wood under continued loading. *Eng. News-Record*, 139(24):108–111.

Discussion

The paper was presented by G Fink

K Ranasinghe commented that simplicity would be needed by practicing engineers and asked the group whether we know who the target audience are for the standards. G Fink responded that the user of the standards is our aim; however, they needed to look deep into the problem to get the basic understanding to come up with provisions. H Blass commented that one would have to find the tools to translate these findings to the engineering world and practicing engineers would have deadlines and budget constraints and would use simple tools.

I Smith commented that sizing members would have easy ways but structural system considerations would be more challenging.

F Lam commented that the most needed area for reliability based design consideration would be connection design.

S Franke agreed that one needed a deeper understanding to transfer the information into simple equations; however, PhD students could be involved in the useful step of documentation of the steps from the deep understanding to the simple equation. G Fink responded that PhD students needed to be more focused and work on a topic in depth rather than looking into too many areas.

G Schickhofer agreed that COV should be considered but how to do this in a standard would be the question. G Fink agreed that it would not make sense to have different γ_m values to consider COV. F Lam added that in Canada, a reliability normalization procedure is available to consider different COVs in a reliability based approach.

U Kuhlmann suggested only one γ_m and provide calibration factor for γ_m and document clearly where these factors come from.

P Dietsch and G Fink discussed the aim of Eurocode 5 and the target audience. The fact that practicing engineers not familiar with wood might complain that the code would be too complicated.

The Reality of Seismic Engineering in a Modern Timber World

Tobias Smith, University of Canterbury, New Zealand
Daniel Moroder, University of Canterbury, New Zealand
Francesco Sarti, University of Canterbury, New Zealand
Stefano Pampanin, University of Canterbury, New Zealand
Andrew H. Buchanan, University of Canterbury, New Zealand

Keywords: Capacity design, ductile timber, seismic engineering, timber over-strength

Abstract

While timber structures are rapidly gaining in popularity, modern timber engineering codes are struggling to keep up with the rapid advancement of timber techniques, technologies and philosophies. One of the most evident areas of this struggle is in seismic design which combines timber engineering with the equally rapidly developing subject of earthquake resistant design.

This paper critically examines several key aspects of seismic design in the context of the modern timber world and discusses how to improve the inclusion of basic principles into international design codes. The items presented have been drawn from the authors' experience during their contribution to the writing of the new seismic section of the New Zealand timber design code.

1 Introduction

The use of timber in the construction of large scale structures has increased significantly in recent years. This trend has created structures which extend beyond the scope of traditional timber design and therefore beyond codified design approaches.

This is particularly true for seismic design as the potential for mass timber construction increases, thanks to the recent advances of timber technologies and calculation methods which have principally been developed for non-seismic applications in low seismic hazard countries.

Recent innovations in engineered wood products have reduced the variability between timber members and have allowed designers to assign higher loads. This reliance on smaller and higher performing members coupled with the increase in building bay length and building height has significantly increased the consequences of failure which could lead to structural collapse.

This paper summarises the general principles and aims of seismic design of structures. The implications of seismic design principles in relation to timber structures are then discussed. Finally the paper suggests codification of these principles and identifies gaps still needing to be addressed. Although these principles are not new (Blass et al. 1994), it is imperative that they are carefully considered in a modern timber world.

2 The Aim of Seismic Design

Earthquake engineering and seismic design have the principal goal of ensuring a certain response when a structure is subjected to a predetermined level of ground motion. Traditionally, both the level of ground shaking and the accepted level of response are set by seismic design codes.

Although the estimated likely level of ground shaking is material independent, the response of a structure to ground motion is dependent on structural form that is often dictated by the material used.

2.1 The role of non-linearity

A very stiff building designed for only elastic response will be subjected to very high accelerations and therefore high seismic forces. High seismic forces result in expensive buildings, and high accelerations lead to high levels of damage to the building's contents. Engineers have two weapons against these high accelerations: ductility and damping as shown in Figure 1. Both properties rely on the non-linear behaviour of materials or structural elements.

Displacement ductility is normally defined as the ratio of the ultimate displacement (defined by the fracture of the material or by a defined displacement limit) to the displacement at yielding, or in more general terms to the point where a distinctive change in stiffness can be observed. Ductility is therefore linked to non-linear behaviour, which can either be elastic (i.e. through rocking) or inelastic (i.e. material yielding). Damping is the ability of a material or structural element to dissipate energy; in seismic design this is normally in the form of plastic yielding (structural damping), friction (Coulomb damping) or viscous drag (viscous damping).

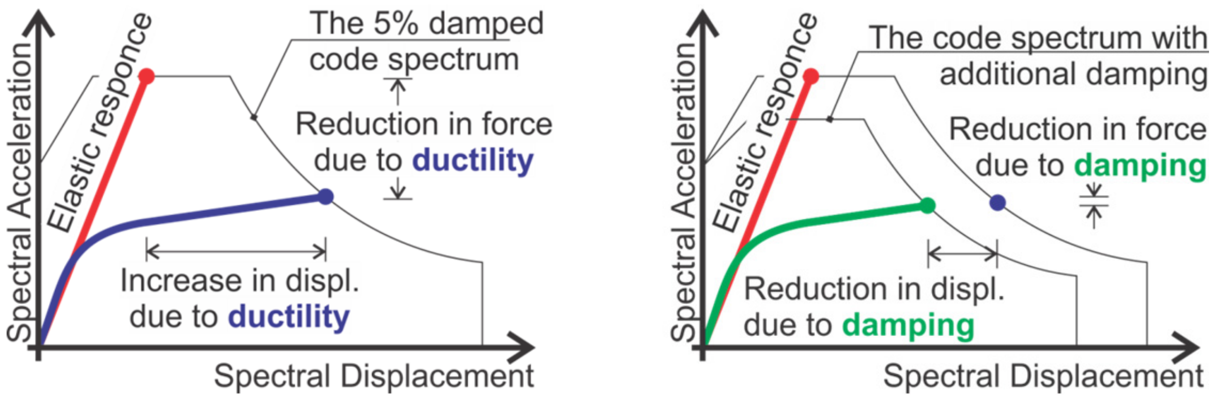

Figure 1: Effects of ductility and damping on the lateral load response of a structure.

Non-linearity also has a further function in seismic design, that of ensuring resilience by allowing a structure to deform beyond its design capacity. Seismic hazard, as defined by codified design methods, is based on probability and as such a likelihood of exceedance exists. This was demonstrated in the recent seismic sequence in Christchurch, New Zealand where seismic loading in some areas of the city was over twice the predicted design values (Bradley et al. 2011).

2.2 Representation of non-linearity in codified seismic design

All modern design codes for seismic areas use a force-based design approach. This approach requires an assumption to be made regarding the initial period of vibration of the structure and the amount of non-linear displacement (normally defined as ductility) that the structure will possess at its 'performance point'. The performance point is an idealization which represents the behaviour of the structure when subjected to the design spectrum acceleration.

Traditional seismic design assumes that the provision of some ductility will also provide the structure with hysteretic damping. It is worth noting however that ductility influences seismic response separately from the influence of damping, as shown in Figure 1.

2.2.1 Structural classification

The response of a structural system to lateral loading is classified as being either ductile or brittle. *Brittle Structures* (μ = 1) are designed for elastic behaviour and exhibit brittle failure under any loading greater than the Ultimate Limit State (ULS) loading. Example structures include, but are not limited to, moment-resisting frames or portals with glued knee joints, cantilevered timber poles, and all structures where capacity design principles are not complied with, such that brittle failure of a structural element or connection precedes the activation of the potential ductile elements.

Ductile structures are those in which non-linear behaviour is possible. These are often split into subcategories: Nominally Ductile, Limited Ductile and Fully Ductile. *Nominally Ductile Structures* (μ = 1.25) are capable of sustaining small inelastic material deformations in predefined ductile areas. Example structures include but are not limited to timber arch structures, walls with screw fixed sheathing, joints which rely on embedment-only failure modes, fully threaded screws in tension, and carpentry joints in compression.

Limited Ductile Structures (1.25 < $\mu \leq 3$) are designed to exhibit a ductile failure under any seismic loading greater than the ULS load levels. Significant inelastic material deformations are required in identified non-linear elements, to limit the earthquake design forces. Example structures include but are not limited to nailed plywood shear walls, well designed ductile moment frames, and braced frames with buckling restrained braces which are designed to yield in both tension and compression.

Similar to Limited Ductile Structures, *Fully Ductile Structures* ($\mu > 3$) are designed to exhibit an even more ductile failure mode under seismic loading greater than the ULS load levels. Inelastic material deformations beyond those of a Limited Ductile system are required.

2.2.2 Seismic reduction factors

Seismic hazard is represented in modern seismic design codes through the presentation of a single-degree-of-freedom elastic site hazard acceleration spectrum. Assumed approximations summarized in Figure 2 provide the relationship between the seismic response of elastic and non-linear systems which allow for the reduction of elastic accelerations by using a spectrum representing non-linear response. It now becomes possible to determine the required yield strength of the structural system based on the codified elastic hazard spectrum, the predicted system ductility, and the estimated period of vibration of the structure to be designed.

It is important to note that all of these modifications are based on the idealization that the force-deformation relationship is bi-linear elastic perfectly-plastic (Figure 2). When the force is between the positive and negative yield values ($-F_y$ and F_y) the stiffness is equal to the initial elastic stiffness, k, but when the force is equal to the yield force (either $-F_y$ or F_y) the stiffness is equal to zero (i.e. perfectly plastic). For this idealized system, both ductility and damping contribute in the reduction of seismic forces.

Moderate-to-long period structures: Equal displacement approximation

For extremely long period structures (e.g. 30 seconds, as an extreme example) the maximum system displacement will equal the maximum ground displacement (Figure 2a). The reason for this is that the system is so flexible that when the ground moves, the mass of the system essentially stays in its initial position. Hence, this maximum system displacement will be the same whether the system responds elastically or in-elastically. For moderate-to-long period structures the above explanation does not hold strongly, but practically speaking, the inelastic and elastic displacements are similar giving the equal displacement approximation.

For moderate-to-long period structures the equal displacement approximation means that the reduction in seismic force (R_y = F_u/F_y) is equal to the design displacement ductility ($\mu = \Delta_u/\Delta_y$).

Short period structures: Equal energy approximation

For structures with short-vibration periods the peak inelastic displacements tend to be larger than the peak displacement of the corresponding linear elastic system. Therefore the equal displacement approximation for moderate-to-long period structures is inappropriate for short-period structures.

An alternative approach is to compare the energy in both the elastic and inelastic structures at their peak displacement. Since at the peak displacement the velocity is zero, then at this point there is no kinetic energy and only potential strain energy, which can be computed as the area beneath the force-displacement relationship. Based on the assumption that the two areas are equal, it is possible to calculate the reduction in seismic force as a function of the system displacement ductility ($R_y = \sqrt{2\mu - 1}$). This assumption is independent of the building's period of vibration which is not completely accurate. For this reason some loading codes include building period in the application of the equal energy approximation.

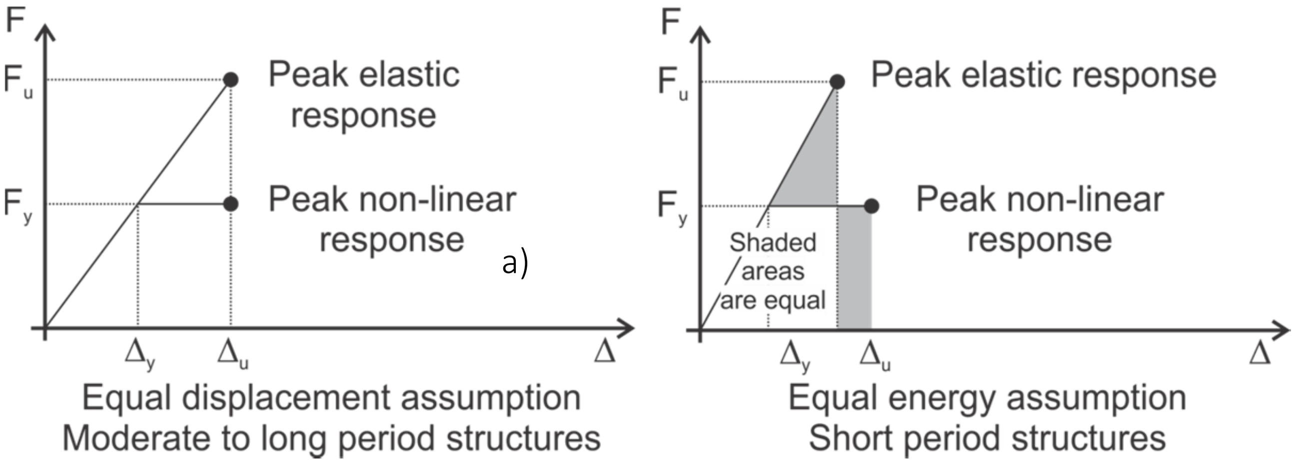

Figure 2: a) Equal displacement approximation and b) equal energy approximation allowing for non-linear system response

2.3 The role of capacity design and over-strength in ensuring ductility

Capacity design philosophy developed in New Zealand in the nineteen seventies for the seismic design of reinforced concrete structures is the most common way of ensuring structural ductility. Capacity design protects all brittle (or less ductile) parts of a structure by understanding the load exerted upon them from the selected ductile elements, even at large displacements.

This is similar to loading a chain where the maximum capacity is dictated by the weakest link, when the weakest link is ductile, the overall chain is ductile. In order to ensure the capacity of all the brittle elements within the lateral load resisting system is adequate, their strength demand is set equal to the "over-strength" of the ductile elements. Paulay et al. (1975) state that the over-strength should take into account all factors that may increase the strength of the weakest element or connection, however, there is little consensus on a common approach of how to determine over-strength values and what factors should be included for the design of ductile timber structures.

3 Non-linearity and Timber Design

Wood exhibits ductile behaviour in compression parallel to the grain because even though the fibres buckle, they still support a limited load. If member buckling can be excluded, timber in compression can be classified as ductile. Clear wood is strong but brittle in tension, with no non-linear behaviour.

Timber in bending will display limited non-linear capability when loaded monotonically, but has no ductility under reversed cyclic loading. .

3.1 Sources of non-linearity in timber structures

Steel is one of the few structural materials capable of sustaining repeated non-linear loading cycles without strength degradation or brittle fracture. As in concrete structures, the use of steel components is the most common method of providing non-linear behaviour in timber structures.

Dowel type fasteners have traditionally been used to obtain ductility in timber structures. Small diameter fasteners (nails, screws or rivets, Figure 3a) tend to be more ductile than large diameter fasteners (bolts, dowels and coach screws, Figure 3b), because steel yielding is the likely governing failure mode. More recently, specifically designed steel elements have been used to provide non-linearity at beam-column and foundation connections (Figure 3c).

The European Yield Model (Johansen 1949) for small and large dowel type fasteners defines seven potential non-linear failure modes for timber-to-timber or steel-to-timber connections under monotonic loading as shown in Figure 4. These failure modes are classified as ‘yielding’ due to their ability to provide non-linear response and therefore some ductility under monotonic loading. As shown in Figure 4 the non-linearity comes from the crushing of timber (a, b, c, g and h) or the combination of timber crushing and fastener yielding (d, e, f, j and k).

For a group of several fasteners making up a joint, failure of the fastener group may occur through block tear-out for small dowels or row shear and group tear out for large dowels. The fastener group must be designed so that none of these brittle failure mechanisms occur before the development of fastener yielding, if any ductility is to be achieved.

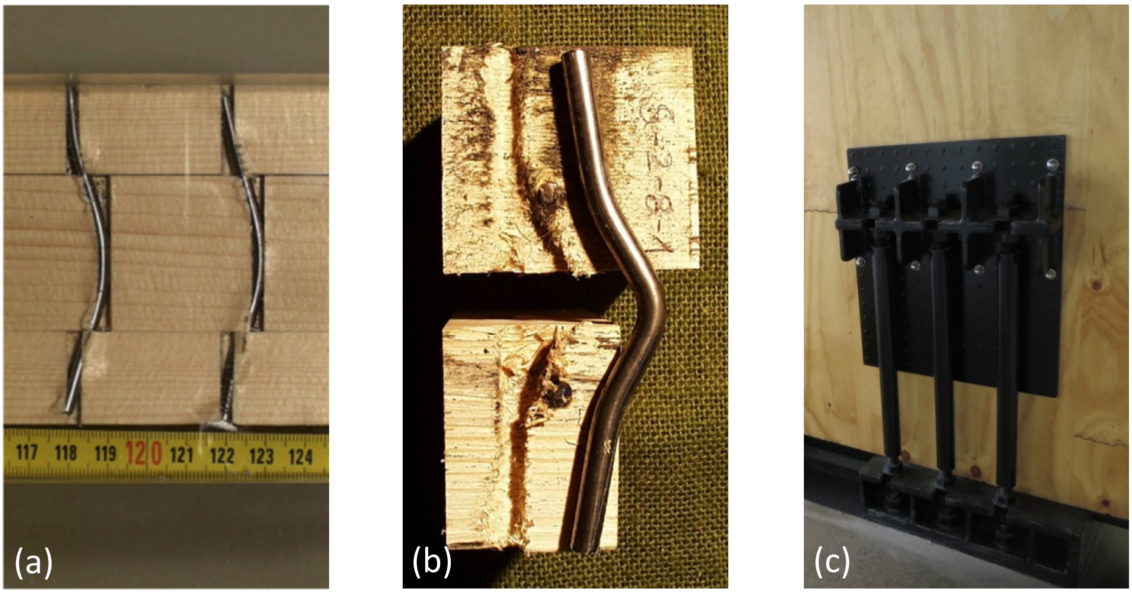

Figure 3: a) Small (Versuche zur DIN 1052 2010) and b) large dowel type fasteners (Bejtka 2005), c) specifically designed ductile steel hold downs as part of a wall system

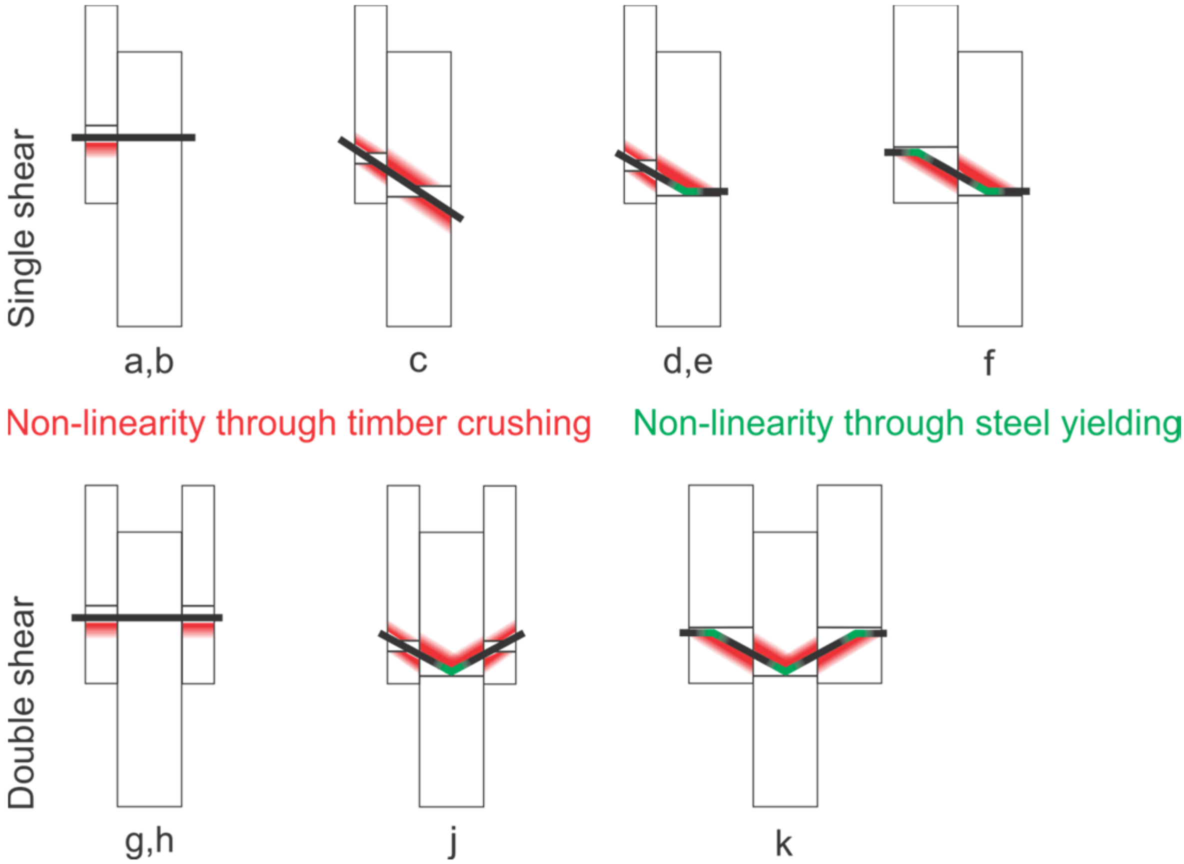

Figure 4: 'Yielding' failure modes combining timber crushing (shown in red) and steel yielding (shown in green)

3.2 Seismic non-linearity and damping

Seismic loading is cyclic and random in amplitude, therefore the ability of a connection to provide ductile seismic response must be evaluated within the context of the nature of this loading. Figure 4 showed the yielding failure modes of small and large dowel type connections and how the non-linear behaviour of these connections consists of timber crushing and in some cases flexural yielding of the fastener.Figure 5: Figure 5 shows schematically the cyclic behaviour of these failure modes. When non-linear behaviour is only through timber crushing, the timber can only yield in the first cycle, creating severely pinched force-displacement loops and a 'sloppy' connection similar to a braced structure with tension-only yielding. Figure 5 also shows how the amount of hysteretic energy dissipation in such a connection is significantly reduced. When timber crushing is combined with steel yielding the curves remain pinched, but the cyclic characteristics of the steel yielding mean that some ductile capacity always remains, which also creates more favourable hysteretic behaviour.

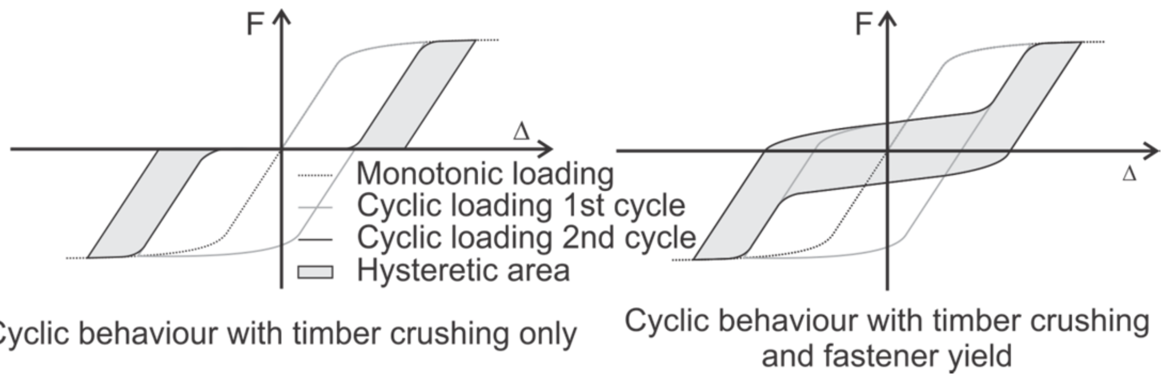

Figure 5: Comparison of hysteretic behaviour for cyclic behaviour of 'yielding' fastener failure modes

3.3 Global and local ductility and the displacement paradox

Design to control displacements is becoming increasingly important in the seismic design of buildings, to reduce the potential costs of both structural damage and non-structural damage. The damage potential of displacement is far beyond the damage potential of force; however, displacements are too often overlooked (Buchanan et al. 2015).

Section 2.1 discussed how non-linear behaviour of a structural system is typically quantified using the parameter of ductility, the ratio between the ultimate displacement of a structural system and the point in which yield has been deemed to occur. Section 3.1 and 3.2 described how this ductility is normally provided by steel fasteners at beam-column, wall-foundation or column-foundation connections. It is therefore evident that the ductility of a timber building is governed by the ductility of its connections. The seismic demand, however, is governed by the ductility of the entire seismic system. Therefore the elastic displacements of the structure must also be considered in design creating a displacement paradox.

The displacement paradox occurs because, on the one hand, designers need to control lateral displacements to reduce damage and the possibility of structural collapse, but on the other hand, they must provide enough displacement to ensure non-linear response if ductility has been used in the calculation of seismic forces (i.e. using the reduced design acceleration spectrum). These two objectives sometimes clash, creating a paradox. The displacement paradox can be a particular problem in timber structures because they tend to have larger elastic displacements than steel or concrete structures, giving a smaller displacement window in which to provide the required ductility. The displacement paradox often creates a severe mismatch between the intended ductility of a building and its actual response, especially if there are large linear elastic displacements before any non-linearity occurs. A large assumed ductility means that the structure is required to undergo very large displacements, creating large P-Delta and other undesired effects.

4 The Future of Seismic Timber Codes

New timber technologies and construction methods are creating new and exciting opportunities for timber in construction. Practical experience is being added to a wealth of new research significantly advancing our understanding of the seismic response of timber structures. Design codes are attempting to keep up with these developments. This section discusses the relationship between the response of timber structures as discussed in the previous sections and the intent of the seismic loading codes.

4.1 Ensuring resilience in timber structures

Non-linearity is used to reduce the seismic loading on a structure and to increase the resilience of a structure against collapse under loads which are higher than the design loading.

In modern seismic design using any structural materials, specific locations of non-linearity are identified and protected through capacity design. In well-designed concrete and steel structures, however, most regions outside the defined non-linear zones still possess some non-linear capacity. This is in contrast to timber buildings where the timber materials outside the identified non-linear zones are brittle. In the existing New Zealand Earthquake Loading Code (NZS 1170.5 2004) a structure of limited ductility has a 25% reduction in seismic loading but structural members in general need not adhere to capacity design principles. The resilience of such a lateral load resisting system made of timber is not adequate and as such it is recommended that although the connection may be designed for μ = 1.25 the surrounding timber members (those which would be capacity protected in a ductile structure) should be designed with some reserve strength, by using demands derived through an elastic assumption (μ = 1).

The current draft amendment to the New Zealand Earthquake Loading Code will further impose that earthquake actions on brittle structures be increased by 50%. This will apply to all materials including timber. This means that all brittle structures will have to be designed to resist Maximum Credible Event (MCE) loading, representative of an earthquake with a return period of 1 in 2500 years.

4.2 Ensuring desired response from timber connections

Timber is inherently a brittle material and non-linearity must come from its connections. These connections must therefore be designed to provide the required level of non-linear response without brittle failure.

It is clear that the pinched hysteretic loops shown in Figure 5 for a timber joint with combined fastener yielding and timber crushing shown in Figure 3 and Figure 4 does not match well to the elastic perfectly-plastic assumption of the equal displacement approximation or the equal energy approximation. The match is even worse for timber crushing with no yielding of steel, so it is recommended that connections with only timber crushing mechanisms should not be considered as ductile for seismic design.

Recent research (Franke et al. 2013; Schoenmakers et al. 2013; Zarnani et al. 2014a; Zarnani et al. 2014b; Jensen et al. 2015; Zarnani et al. 2015) has enabled the accurate calculation of the brittle failure modes of doweled connections. The formulas allowing this calculation are also currently being implemented in new design codes, in some cases replacing minimum edge distances.

Following the occurrence of yield, reached at the yield failure strength $N_{\alpha,y,y}$ the system will displace until the required level of non-linear behaviour, defined through displacement ductility, is reached, as shown in Figure 6. In order for a timber structure to continue to display good seismic behaviour, the yielding failure mode must continue to govern the connection behaviour until it has developed its ultimate yielding failure mode strength. To ensure this, all brittle failure modes in the connection must be excluded. Capacity design principles, as used to protect any other element outside the potential ductile zone, need to be applied for design of any components of the connection which could have brittle failure modes.

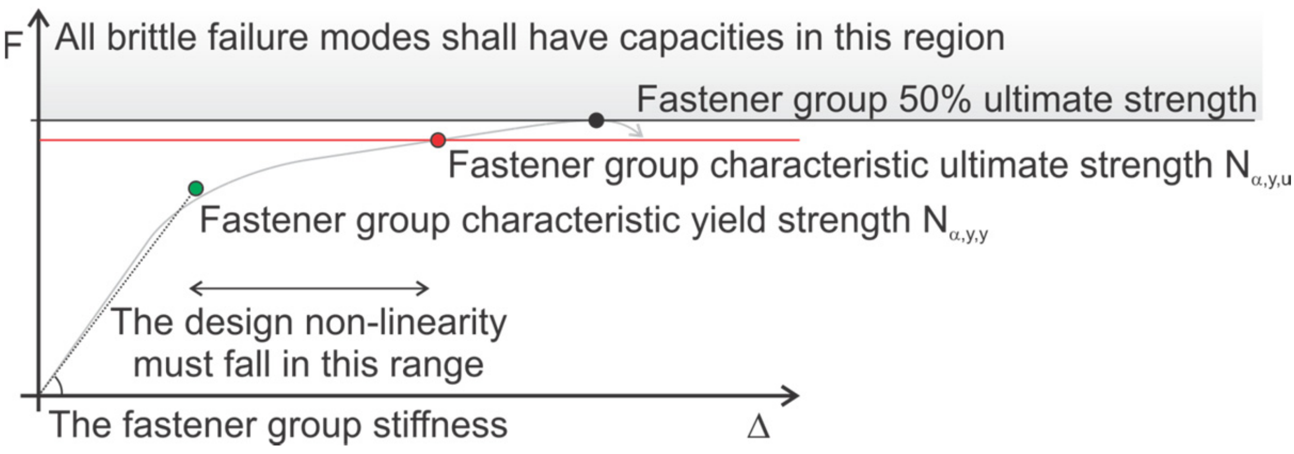

Figure 6: Strength hierarchy within the joint fastener group to ensure non-linearity

4.3 Ensuring desired response from timber structures

Section 3.3 recommended that a dowel type connection be designed to ensure the desired amount of non-linear capacity. These connections however are part of a wider lateral load resisting system and it is the non-linearity (ductility) of this entire system that was used in the determination of the seismic demand. It is therefore crucial that the structural beams, columns and walls or connections which are not intended to provide non-linear response: 1) have adequate capacity to avoid failure and 2) are adequately stiff to avoid excessive displacement before the required non-linearity is achieved.

4.3.1 Ensuring adequate strength of brittle elements which are designed to remain elastic

As stated in Section 2.3, over-strength is required to ensure that the intended non-linear element is the weakest link in the lateral load resisting system. Although several values for over-strength are available in literature (BRANZ 1999; Popovski et al. 2005; Jorissen et al. 2011; Sustersic et al. 2011; Schick et al. 2013; Brühl et al. 2014), the definition of what these values account for is unclear. Definitions of over-strength normally include one or more of the following items:

1. The difference between the demand on a joint and the capacity of the joint (over-capacity or over-design);
2. Material safety factors;
3. Strain hardening and the rope effect;
4. Statistical distribution of materials or joint capacities (characteristic strength values are given as the lower 5th percentile strength);
5. The difference between the real and calculated strength of a joint (i.e. experimental vs. European Yield Model values);
6. Mechanical effects or hidden reserves (such as friction).

Item 1 is based on the designer's choice and can easily be quantified. Items 2 and 3 are allowed for by designing the capacity-protected structural members for the fastener group's ultimate yield strength, $N_{\alpha,y,u}$. Item 4 is accounted for by calculating the upper characteristic value of the ultimate yield strength (i.e. calculating the ultimate yield strength using upper 95th percentile fastener yield and embedment strength).

Items 5 and 6 remain to be considered in the calculation of over-strength values for the capacity-protected members. Values for the partial over-strength factor regarding item 5 for dowel type connections were found to be between 0.94 (Brühl et al. 2012) and 1.18 (Jorissen et al. 2011), suggesting that a value of 1.0 could be used however further research into these partial factors is required.

4.3.2 Respecting displacement limits and the displacement paradox

As discussed in Section 3.3 a paradox can occur in seismic design where in order to obtain required levels of non-linear behaviour, excessive displacements may be required. Typical design codes place limits on maximum inter-storey drifts at ULS design levels, for example a limit of 2.5% is imposed by the New Zealand Earthquake Loadings Standard (NZS 1170.5 2004) while a limit of 2.0% generally exists in American codes with some allowance for building importance and period (ASCE 7-10 2010). Eurocode 8 defines maximum inter-storey deflection based on a stability coefficient which includes P-delta actions (Eurocode 8 2004). Often these deflection limits are reduced even further to limit the possibility of building pounding or to prevent damage to non-structural elements, which further reduces the ability of the designer to provide the required ductility.

The entire structural system, including all elastic deformation contributions, must be considered in the evaluation of non-linear behaviour and the definition of ductility. This means that horizontal deflection calculations must include not only the connections providing non-linearity but also the entire structural system containing the connections (accounting for the stiffness of all structural members and all other elastic connections).

For example, a 5 storey, limited ductile, moment resisting frame (moderate-to-long period, μ = 3) having a maximum allowable drift of 2.0%, must yield at 0.67% drift. This means that all horizontal displacements deriving from beam, column, and elastic connection deformations must be less than this value, which will require a very stiff structure to be provided.

4.4 The use of the mean material properties in capacity design

If it can be assumed that a correlation exists between material properties responsible for the yielding connection strength (timber density) and the brittle failure modes of the connection (i.e. fracture energy, tension perpendicular to grain strength) or the strength of the structural element (i.e. tension, compression or bending strength), then a similar statistical distribution can be assumed. This fact means that using the 95% material properties is overly conservative in some areas of the structure. However, to still guarantee a minimum level of safety, the mean ultimate yield strength $N_{\alpha,y,u}$ (i.e. calculated using the mean density) could be used instead (Priestley et al. 2007). As shown in Figure 7 this correlation can be applied to the brittle connection failure modes, as well as the brittle element where the ductile connection is located. All elements and connections outside the element where the ductile connection is located need to be verified against the upper characteristic ultimate yield strength.

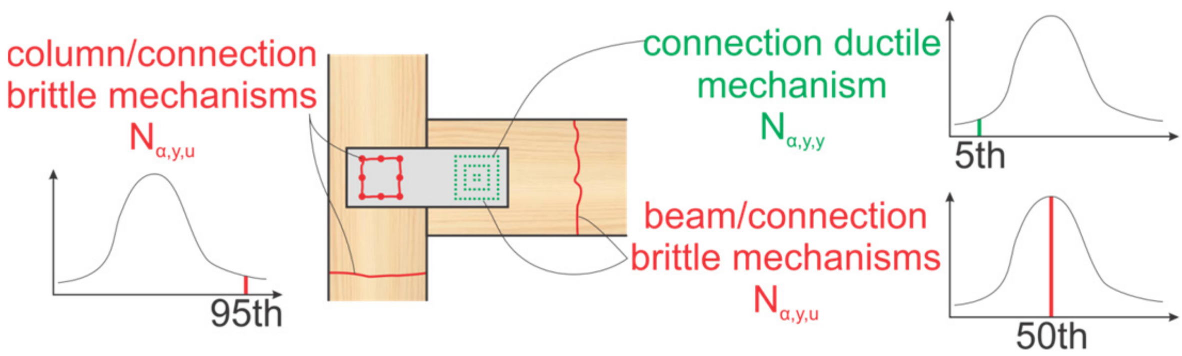

Figure 7: Material characteristics to be used in capacity design

4.5 Higher mode effects

Because of the more flexible nature of timber structures and the potentially delayed onset of yielding, higher modes can significantly affect the dynamic behaviour of taller timber structures. Especially wall structures can experience much higher storey shears and moments as well as peak floor accelerations when compared to values determined by methods based on a the first mode approximation (such as the equivalent static analysis). Until dynamic amplification factors for timber structures are available, more advanced methods like response spectrum analysis or time history analysis should be applied to taller timber buildings.

5 Conclusions

Assisted by the development of better materials and connections, timber buildings are pushing beyond traditional boundaries of height and size. Timber as a structural material is moving into structural types which have been traditionally dominated by reinforced concrete and steel. This paper has studied several of the foundation principles of modern seismic design, showing that some of the basic assumptions in calculating both seismic demand and structural resilience to seismic load are not as easily applicable to timber construction as they are to reinforced concrete or structural steel.

The following recommendations are therefore made for new codes specifying the seismic design of modern timber buildings:

Structural design

1. Brittle structures should be designed to resist MCE (1/2500 year) loading;
2. Brittle elements in limited ductility structures (μ = 1.25) should be designed for elastic seismic demand (μ = 1);
3. When assessing the ductility of a structural system, all components of displacement must be considered, including all local displacements and rotations resulting from deformations of the elastically responding elements and all the connections along the seismic load path;
4. For buildings taller than four stories, higher mode effects should be considered through special study, this remains a significant research gap in the implementation of tall timber buildings.

Connection design

1. The capacity of a joint in an intended ductile zone should be evaluated at the yielding state ($N_{\alpha,y,y}$);
2. Joints governed by crushing only failure modes should not be used in connections intended to provide damping;

Capacity design

1. No consensus on a unique definition of over-strength factors is currently available (Moroder et al. 2014) and therefore values for different connection types and different structural types are still missing. A partial over-strength factor of 1.2 is recommended, allowing for hidden reserves and the difference between analytical models and real behaviour, until further research is carried out;
2. The capacity of all brittle elements and elastically responding connections should exceed the capacity of the ultimate yielding failure mode ($N_{\alpha,y,u}$) of the non-linear connections, calculated using the upper limit (95%ile) material values multiplied by the partial over strength factor;
3. The capacity of all potential brittle failure modes within the connection should exceed the capacity of the ultimate yielding failure mode ($N_{\alpha,y,u}$) of the non-linear connections, calculated using the mean (50%ile) material values multiplied by the partial over strength factor.

6 References

ASCE 7-10 (2010). *Minimum design loads for buildings and other structures*. Reston, Va, American Society of Civil Engineers.

Bejtka, I. (2005). Verstärkung von Bauteilen aus Holz mit Vollgewindeschrauben, Versuchsanstalt für Stahl, Holz und Steine (VAKA)

Blass, H.J., Ceccotti, A., Dyrbye, C., Gnuschke, M., Hansen, K.F., Nielsen, J., Ohlsson, S., Parche, M., Reyer, E., Stieda, C.K.A., Vergne, A., Vignoli, A., Yasumura, M. and Dolan, J.D. (1994). Timber structures in seismic regions RILEM state-of-the-art report. *Materials and Structures* 27(3): 157-184.

Bradley, B.A. and Cubrinovski, M. (2011). Near-Source Strong Motions Observed in the 22 February 2011 Christchurch Earthquake. *Bulletin of the New Zealand National Society for Earthquake Engineering* 44(4).

BRANZ (1999). Evaluation and Test Method EM1: Structural Joints - Strength and Stiffness Evaluation. Porirua City, New Zealand.

Brühl, F. and Kuhlmann, U. (2012). Requirements on ductility in timber structures. *CIB Working Commission W18 - Timber Structures*, Växjö, Sweden.

Brühl, F., Schänzlin, J. and Kuhlmann, U. (2014). Ductility in Timber Structures: Investigations on Over-Strength Factors. *Materials and Joints in Timber Structures*. S. Aicher, H. W. Reinhardt and H. Garrecht, Springer Netherlands. 9: 181-190.

Buchanan, A.H. and Smith, T. (2015). The Displacement Paradox for Seismic Design of Tall Timber Buildings. *New Zealand Conference of Earthquake Engineering*. Rotorua, New Zealand.

Eurocode 8 (2004). EN 1998-1:2004/AC:2009 Design of structures for earthquake resistance. *Part 1: General rules, seismic actions and rules for buildings*, European Committee for Standardization.

Franke, B. and Quenneville, P. (2013). Design Approach for the Splitting Failure of Dowel-type Connections Loaded Perpendicular to Grain. *CIB Working Commission W18 - Timber Structures*, Vancouver, Canada.

Jensen, J.L., Quenneville, P., Girhammar, U.A. and Källsner, B. (2015). Brittle Failures in Timber Beams Loaded Perpendicular to Grain by Connections. *Journal of Materials in Civil Engineering*.

Johansen, K.W. (1949). Theory of timber connections. *International Association for Bridge and Structural Engineering*(9): 249-292.

Jorissen, A. and Fragiacomo, M. (2011). General notes on ductility in timber structures. *Engineering Structures* 33(11): 2987-2997.

Moroder, D., Smith, T., Pampanin, S., Palermo, A. and Buchanan, A.H. (2014). Design of Floor Diaphragms in Multi-Storey Timber Buildings. *International Network on Timber Engineering Research*. Bath, England.

NZS 1170.5 (2004). Structural Design Actions Part 5: Earthquake Actions - New Zealand. Wellington, New Zealand, Standards New Zealand.

Paulay, T. and Park, R. (1975). *Reinforced concrete structures*. New York, Wiley.

Popovski, M. and Karacabeyli, E. (2005). Framework for lateral load design provisions for engineered wood structures in Canada. *CIB Working Commission W18 - Timber Structures*. Karlsruhe, Germany.

Priestley, M.J.N., Calvi, G.M. and Kowalsky, M.J. (2007). *Displacement-Based Seismic Design of Structures*, IUSS Press.

Schick, M., Vogt, T. and Seim, W. (2013). Connections and anchoring for wall and slab elements in seismic design. *CIB Working Commission W18 - Timber Structures*. Vancouver, Canada.

Schoenmakers, J.C.M., Leijten, A.J.M. and Jorissen, A.J.M. (2013). Beams loaded perpendicular to grain by connections. *CIB Working Commission W18 - Timber Structures*. Vancouver, Canada.

Sustersic, I. and Dujic, B. (2011). Influence of connection properties on the ductility and seismic resistance of multi-storey cross-lam buildings. *CIB Working Commission W18 - Timber Structures*. Alghero, Italy.

Versuche zur DIN 1052 (2010). Teilprojekt II: „Einsatz visueller Medien in der Aus-, Fort- und Weiterbildung im Zimmerer- und Holzbaugewerbe". Bundesbildungszentrum des Zimmerer und Ausbaugewerbes GmbH.

Zarnani, P. and Quenneville, P. (2014a). Splitting Strength of Small Dowel-Type Timber Connections: Rivet Joint Loaded Perpendicular to Grain. *Journal of Structural Engineering* 140(10): 4014064.

Zarnani, P. and Quenneville, P. (2014b). Strength of timber connections under potential failure modes: An improved design procedure. *Construction and Building Materials* 60: 81-90.

Zarnani, P. and Quenneville, P. (2015). Group Tear-Out in Small-Dowel-Type Timber Connections: Brittle and Mixed Failure Modes of Multinail Joints. *Journal of Structural Engineering* 141(2).

Discussion

The paper was presented by G Fink

K Ranasinghe commented that simplicity would be needed by practicing engineers and asked the group whether we know who the target audience are for the standards. G Fink responded that the user of the standards is our aim; however, they needed to look deep into the problem to get the basic understanding to come up with provisions. H Blass commented that one would have to find the tools to translate these findings to the engineering world and practicing engineers would have deadlines and budget constraints and would use simple tools.

I Smith commented that sizing members would have easy ways but structural system considerations would be more challenging.

F Lam commented that the most needed area for reliability based design consideration would be connection design.

S Franke agreed that one needed a deeper understanding to transfer the information into simple equations; however, PhD students could be involved in the useful step of documentation of the steps from the deep understanding to the simple equation. G Fink responded that PhD students needed to be more focused and work on a topic in depth rather than looking into too many areas.

G Schickhofer agreed that COV should be considered but how to do this in a standard would be the question. G Fink agreed that it would not make sense to have different γ_m values to consider COV. F Lam added that in Canada, a reliability normalization procedure is available to consider different COVs in a reliability based approach.

U Kuhlmann suggested only one γ_m and provide calibration factor for γ_m and document clearly where these factors come from.

P Dietsch and G Fink discussed the aim of Eurocode 5 and the target audience. The fact that practicing engineers not familiar with wood might complain that the code would be too complicated.

An Execution Standard Initiative for Timber Construction

Tomi Toratti,

Wood working industries, Finland

Keywords: Execution, building works, quality control, weather protection, tolerances, construction process,

1 Introduction

At present, execution standards exist at the European level for concrete, steel and masonry construction. For timber construction such standards do not yet exist. However, in several European countries as well as at least in Canada and Australia, national standards or guidelines for the execution of timber structures have developed.

In Finland, the national execution standard for timber construction has recently been published [SFS 5978:2014 Execution of timber buildings – Rules for load-bearing structures of buildings]. In this national standard, quality requirements are set for the design and construction of timber buildings, so that sufficient overall quality of the building can be ensured and that the building is built as it has been designed.

Attention towards execution guidelines are also found in recent publications from Australia on fire during construction [England, 2014] and moisture controls [MacKenzie, 2012] and on tall timber buildings in general in Canada [Karacabeyli and Lum, 2014]. Such initiatives when followed will set a level on the quality of timber construction.

Currently Eurocode 5 has some pages related to detailing and execution of timber structures. These are given in chapter 10 and this consists of 3 pages. In the code committee CEN/TC250/SC5 there is a plan to produce a European full execution standard for timber structures, which may possibly be a separate new part of the Eurocode 5.

In a Nordic project named 'NEXT Timber', Nordic views on this document are discussed and this discussion will also be brought up at least in the Eurocode CEN group. This paper summarizes the fields of interest and anticipated results as a basis for future execution standards. This paper is also a continuation of an INTER note [Nore & al. 2014] on execution standardization. Here the backgrounds and ideas are brought a step forward.

2 Scope of an execution standard

Until now, the scope of an execution standard for timber construction has not been fully discussed or agreed at the European level. Additionally, the different structural materials have their execution standards structured in varying ways and there would also be a need on harmonizing the structure, contents as well as the scope of these different execution standards. This harmonization should take place at the CEN/TC250 level.

The scope of an execution standard is on the quality assurance of the end-product (which is the building) quality through execution rules, which are achieved by a functional cooperation among the project partners, sufficient coverage and quality of the design and on the documentation to be produced for the construction process. The standard should describe at least the following means for quality assurance in detail:

- The project description – A description of the project including all relevant information
- The moisture control plan – A plan of how moisture safety is achieved during the works
- The assembly plan – A plan how the members and elements are erected and the bracing required
- Tolerances of assembly – Description of tolerance classes and tolerance values for the construction works, manner of measuring and the checking scheme.

It is proposed here that the execution standard shall cover all the building site work and related quality control measures from the end of the design phase all the way to the stage of the finalized building. The recently published Finnish execution standard [SFS 5978:2014] does actually spread somewhat wider than this as quality aspects of design are also stated, as well as the ensuring of good communication between design and building site work. This initial point may vary as design work and on-site build work are often carried out simultaneously. The execution standard should cover the aspects related to the planning of the execution works. This should not be mixed with the design work of the structures.

The execution standard shall be based on producing the building with the intended level of quality given the design documentation as the starting point.

Two different targets for execution may be given:

1. To apply such a level of execution that the design rules given in Eurocodes apply. This could be related to assembly tolerances and moisture/weather protection for instance.
2. To apply execution rules which are known to produce sufficient quality level, work safety and which is economically sound based on earlier experience.

3 Contents of an execution standard

At present, chapter 10 of Eurocode 5 states some requirements for the execution. These are requirements on the following topics:

- Connectors and there holes, washers, predrilling etc.,
- Transportation, assembly and erection of elements,
- Detailing of diaphragm connections,
- Some rules for erecting nailplate trusses

The above list is in essence needed. However this is only a small part of the execution provisions that would be required in a standard to ensure the intended quality level. At least the following items need to be covered as well.

- The quality assurance on the building site. Definition of the parties involved, their tasks and responsibilities, quality control measures and inspection schemes. Execution classes: relevant execution classes (as in SFS5978 defined EXEC 1, 2 and 3) could be defined based on the consequence classification (EN 1990 annex B) and on the execution difficulty level assumed. This should be directly linked to the quality assurance scheme to be applied (the level of checking).
- The assembly plan. The assembly of prefabricated elements is a very central part of the execution of a building. Usually an assembly plan is required. This plan defines the responsibilities of the parties involved and solutions for Structural stability during each phase of the erection,
- Fire safety during the site work,
- The moisture control plan. Control of moisture during the building site work, weather protection methods applied, material storage conditions and the related inspection scheme.
- Definition of assembly tolerances, how these are measured and the inspection scheme

4 Requirements coming from the design (Eurocode 5) to the execution standard

The design documentation defines a set of requirements to the execution of the building. It is self-evident that the design as such has to be followed in the building phase. In addition, there are a set of requirements which are embedded in the design methods and therefore are conditions to be followed in the execution for the design to apply. Such characteristics are for instance:

4.1 Tolerances,

As the assembly of building parts and elements can never be done with exact precision, there has to be an assembly tolerance for which the design equations still apply. If wider tolerances should be applied, this should be allowed if it is considered in the design and alterations to the design equations or additional loads may apply. Considering the tendency towards an increased degree of prefabrication, defined tolerances are necessary to be agreed on and followed. Well-defined and agreed tolerances will simplify the communication between de different parties.

Tolerances are needed for:

1. Material sections, which are given in product standards,
2. Prefabricated elements, which should be given in a product standard (when finalised),
3. Connection and connector placings, which should be given either in the execution standard or in the design provisions,
4. Assembly of elements/parts on the building site, which should be given in the execution standard

Tolerance classes for the assembly shall be defined and these should be dependent on the execution class/consequence class of the building. The material tolerances are given in the relevant product standards (where available) and the assembly tolerances should be drafted together with the building contractors, code writers and designers in cooperation. No international discussion on this has yet followed.

4.1.1 Tolerance for compressed members

For compressed members the stability criterion in Eurocode 5 limits the straightness of members to L/300 for solid timber and L/500 for LVL and glulam. These are also given in the respective EN product standards. This is a basis also for the max assembly tolerance for wall straightness of ± 1,5 ‰ in table 1, which leaves some bow/crookedness for the member itself. If this is not fulfilled additional eccentricity loads should be considered.

Table 1. An example of assembly tolerances for timber wall structures (from SFS 5978)

	Maximum deviation allowed		
Dimension and location	Tolerance class 3	Tolerance class 2	Tolerance class 1
Wall structures			
Side location from base line	± 3 mm	± 5 mm	± 10 mm

Spacing of wall studs	± 3 mm	± 5 mm	± 10 mm
Size of windows and doors	± 3 mm	± 5 mm	± 10 mm
Location of windows and doors	± 3 mm	± 5 mm	± 10 mm
Distance between two adjacent walls	± 3 mm	± 5 mm	± 10 mm
Straightness of walls[1)]	± 1,5 ‰	± 1,5 ‰	± 1,5 ‰
Deviation of the wall frame from vertical line - height maximum 3 m - height over 3 m	 ± 5 mm ± 8 mm	 ± 5 mm ± 8 mm	 ± 5 mm ± 8 mm

4.1.2 Tolerances for connections

For connections there are many tolerance measures to be considered. A set of tolerances as given in SFS 5978 is presented here as an example in table 2. These tolerances may be on the placement of the connection itself, the measure and placement of the holes if predrilled, spacing's and edge distances etc. These tolerances should be considered in the design equations themselves. However, the present tolerance values are driven more by the practice: what is economically achievable with the applied production technologies. An interesting tolerance measure is also the support length where compression perpendicular to grain prevails from the reaction force of the horizontal member. In the example below for this measure a -10 mm tolerance is allowed and no plus tolerance is needed. This value is solely based on empirical judgement.

Table 2. Tolerances for connections in timber structures. The allowed deviation is given from the nominal location if not mentioned otherwise in the structural design. d is the diameter of the connector.

Connection type	tolerance	description / base value	Allowed deviation or gap
Nailed connections wood-wood	location of connector	spacing a_1,a_2 [1)]	± max(10%; d)
Screwed connection wood-wood		end distance a_3	-0 / +10 mm
		side distance a_4	-d / +10 mm
	penetration	head flat with surface	-0 / +3 mm
Nailing plate connection	location of hole	holes in the nailing plate	± 3 mm
(also screwed)	location of nailing plate	in both directions	± 5 mm

Metal framing plates and hangers	location of connector	general	± 5 mm
		from contact surface	± 2 mm 9)
	edge or end distance of connector		- d
	gap to wood surface	full contact	skewed gap max. 3 mm
Bolt connections	location of bolt	simultaneous drilling 2)	± 5 mm 5)
	location of hole	separate drilling	± 1,5 mm 3)
	tightening	full contact between members	skewed gap max. 3 mm
Dowel connections	location of connector 4)	simultaneous drilling	± 3 mm
	location of hole 4)	separate drilling	± 1 mm 6)
	length of dowel in wood member t		- max(2 mm; 0,05t) 7)
	gap of contact	grooved or battened members	≤ min(3 mm; 0,25t_t) 8)
Incline screw connections	angle of screw		± 5°
Glued-in rods	location of rod	position at wood surface	± 5 mm
Glued-screw connections	skewness of holes	drilling length L_a	± L_a/50
Contact connections	gap	contact required	skewed gap max. 3 mm
	contact length	contact length	- 10%
	length of notch	in grain direction	+ 10%
	depth of notch	perp. to grain direction	+ 5 mm

1) In the direction of grain, the nails have to be at least d out of line from each other if $a_1 < 14d$.

2) Drilling once through all members or using one drilled member as a template.

3) When wood members have 1 mm oversize holes and metal parts have 1,5..2 mm oversized holes.

4) In both surfaces of all wood members.

5) In the grain direction, the row may be out of line max. 5 mm from each other.

6) When in wood-metal connections have 1 mm oversized holes in metal parts.

7) t is the design smooth length of the connector in a wood member.

8) Gap between wood surface and metal plate, where t_t is the metal plate thickness.

9) For example the distance of a supporting L-plate from the wood-wood contact surface (i.e. preliminary assembly to truss).

4.2 Moisture control

The design is carried out for a defined service class. This boundary condition is to be followed during the execution. This may require special weather protection means for the execution. In some cases it may be allowed to carry out the execution in a higher moisture condition and then dry out before the execution is finalised or before the structures are insulated and closed. The designer should instruct the protection means for the works in such cases also.

Moisture control during the execution is of vital importance when building with wood. A moisture control plan, can ensure sound construction with minimal undesirable moisture influence. At first, a level of weather protection in the building process must be defined. Further, all stages must be followed from fabrication, transport, delivery, storage, assembly and use.

A moisture control plan should cover the whole chain of production and building process of the timber structure. It shall be ensured that the contractor follows the moisture control plan.

The content of the moisture control plan is proposed as the following:

1. Basic information of the building project (address and other coordinates of the building site, the person responsible for the construction on site, the main author of the moisture control plan),
2. List of wood materials and products to be used in the construction site,
3. The target moisture content of wood and wooden elements at different stages of the production,
4. The target moisture content of wood and wooden elements when delivered to the building site, during assembly and when the building is finalized,
5. Inspections on site and the person responsible for them,
6. Possible sources of moisture in the building site (for instance, rain, snow, ground water etc.),
7. The protection level (PL0-PL3, given in section 4.2.4) chosen for the building phase and an estimate on the necessary protection duration,
8. The protection of wood on the building site:
   - storage method and protection of storage

- protection during assembly (as determined by the protection level)
- drying methods applied for wood that has gained moisture (for some reason),

9. Controlled drying of structures to the service conditions of the building
   - analysis and prevention of risks caused by moisture, rain among others
   - sensitivity of the project to unfavourable weather and other exceptions
   - determination of moisture contents of wood, drying times and appropriate drying conditions
   - organizing of drying conditions
   - effects of onsite schedules (contingency plans),
10. Moisture measurement plan (measurement method, timetable, documentation and person responsible)

4.2.1 Design moisture content

In heated internal conditions, timber structures are design to service class 1, in which case the mean moisture content of wood shall be below 12 % (RH 65 %, 20^{o}C).

In sheltered unheated conditions, timber structures are designed to service class 2, in which case the target moisture content of wood shall not exceed 20 % (RH 85 %, 20^{o}C).

The internal air humidity of heated buildings may be very low during winter times. The moisture content of wood may decrease to even less than 5 % during the winter and during the fall it may increase to about 12 %. In sheltered unheated conditions the moisture content of wood may vary during the year between 12 – 18 %.

4.2.2 Moisture content of wood during delivery to building site

The moisture content of wood products at delivery varies greatly depending on the product. Unless otherwise agreed, the following delivery moisture contents may be assumed:

- sawn timber is delivered usually air-dried at 15 – 25 %. Due to risk of mould growth this should be lower than 20%.
- glue laminated timber is usually delivered at a moisture content of 10 - 12 %
- plywood and laminated veneer lumber are delivered at a moisture content of 8 – 10 %
- if delivered from storehouse the moisture content of glued laminated timber, plywood and laminated veneer lumber may be 20 % at most

Suitability of the moisture content measurement instrument for the actual product shall be checked.

4.2.3 Moisture during construction

Normally during the storage and assembly phases, the wood moisture content increases, except for sawn timber which is delivered usually at a high moisture content and usually this continues to dry on the building site. On the building site, during storage and assembly, the material moisture increase is controlled with weather protection.

The drying of wood should be carried out *sufficient slowly* so that drying cracks would not develop. Controlled drying is especially important with massive cross sections. Drying conditions shall be such that the difference between measured moisture content and equilibrium moisture content of the drying conditions is at most 6 %. If the need of the drying of wooden members is more than that, the drying shall be arranged in phases. The structure is not allowed to be sealed (covered, coated) before the desired moisture content is achieved.

4.2.4 Weather protection levels

In the *moisture control plan* and in the *assembly plan*, the *level of weather protection* is decided. During the selection of the weather protection level, exceptional weather conditions and additional moisture caused by the construction activities shall be considered.

The *weather protection levels* and the respective moisture contents expected are:

0. Protection level PL0, no protection:
   - moisture content depends on the climate and may not be assigned
   - recommended only in winter climates (freezing temperatures) and in short durations
   - ground contact is not allowed
1. Protection level PL1, plastic or tarpaulin covering:
   - moisture content below 20 %
   - sufficient ventilation shall be ensured
2. Protection level PL2, sheltered:
   - moisture content below 20 %
   - more reliable than PL1
3. Protection level PL3, internal conditions or a tent with heating:
   - moisture content below 15%

4.3 Assembly plan

The assembly of prefabricated elements is a very central part of the execution. Usually an assembly plan is required (often by the building law). This plan should define the responsibilities of the parties involved and the solutions for:

- Structural stability during each phase of the erection,
- Fire safety during the site work,
- Control of moisture during the site work, protection methods, element storage and related inspections

The assembly plan is a building project specific and requirements set in the moisture control plan have to be taken into account. Working methods for the safe assembly of timber structures are presented in the assembly plan. The proposed content of assembly plan is shown in table 3. This example is given for a high consequence class 3 (execution class 3) where the requirements are more rigorous. For other classes some rows may be omitted and there are fewer requirements.

The assembly plan has to be compatible with the project specification document described earlier. The assembly plan may differ from the project specification if there is a sound reason for it, for example changes in site conditions, and the safety of work is not decreased. Such changes shall be accepted in appropriate stakeholders and documented.

Table 3. Proposed content of the assembly plan for execution class 3

1. Site information	Building project, address Supplier of elements Building developer General contractor Designer General structural designer Element designer Site organization: - general foreman of the site - site manager of assembly performing contractor - general timber structures foreman
2. Building elements	Element types: - quantities, outer dimensions and weights, - required lifting equipment, lifting points and practises Crane information: crane type, lifting capacity, reach, maximum load of support on ground

3. Preliminary reports with the following requirements	- the building site fulfils the requirements of the security plans - the stability of the cranes used and their maintenance - the control of entry to the building site - ground and foundation conditions and safety on site - any requirements on dimensions and weights of building parts handled on site - environment and weather conditions to be considered (required protection) - information on neighbouring buildings effect on the assembly work and vice versa
4. Reception of building elements	- transportation and storage on site, storage method and location, strength of stock stands - working schedules on pre-assembly activities - initial inspection and unloading of the elements - transportation methods of the elements, machinery needed and pathways to be clear
5. Protection of elements	- Weather protection level applied - coatings applied during the execution
6. Lifting, assembling and assembly order	- assembly order per building or storey or building section - support of elements during assembly - protection of reaction and attachment points of elements - the stage when the additional supports are removed - actions caused by final stability and fastening of elements - detailed assembly order and moisture control relating to it - introduction of site personnel
7. Accuracies, tolerances, schemes	- tolerance class applied for the assembly - basic location point for tolerance measurements on site
8. Connection methods and details on assembly	Description of connection techniques and used connectors and work method
9. Work safety	- falling protection - temporary scaffolding, decking or fencing and other security measures, personal protective equipment
10. Assessment of fire risks	Fire risks on the building site and preparations for these

11. Inspection plan	Inspections, testing and repair activities are done on the performed work when compared to the project description structural plan requirements so that the timber structures have the strength and stability and are durable: - inspection of materials and products - inspection on storage - inspection of components, connections and structures - inspections and reviews during the process of assembly - inspection and measurement on moisture content and on building conditions - inspection on temporary protections
12. Approval of the assembly plan	Drafter of the assembly plan Contractor performing the assembly General timber structures foreman Main structural designer Element designer Main contractor on the site
13. Handling of fault incidents	Action procedure, security measures and communication

5 Conclusion

In this paper some thoughts, ideas and proposals have been presented for the contents of a future EN standard for the execution of timber structures. This work will be developed in the group CEN/TC250/SC5.

It will be important to identify all the requirements that the design procedures set on the execution phase of the building. In the present paper such identified cases are at least a) the assembly tolerances and b) the moisture content limits for wood. There could be also other overlapping conditions behind the design equations that set provisions for the execution. These should be identified.

The overall target of an execution standard is to set a defined level of quality on the building site works. This quality level may be different for different execution or consequence classes. Such a standard would underline good building practices and it should be simple for clients to use or demand and straightforward for the material producers, building companies and authorities to apply.

6 References

EN 1995 1-1 Eurocode 5. Design of timber structures - Part 1-1: General -Common rules and rules for buildings. Comité Européen de Normalisation (CEN), Brussels, Belgium. 2004.

England P. 2014 Fire Precautions during Construction of Large Buildings. Timber-framed Construction Technical Design Guide. Forest and Wood Products, Australia.

Karacabeyli E and Lum C. 2014. Technical Guide for the Design and Construction of Tall Wood Buildings in Canada. Special Publications SP-55E. FPInnovations, Canada.

MacKenzie C. 2012 Impact and Assessment of Moisture-affected Timber-framed Construction Technical Design Guide. Forest and Wood Products, Australia.

Nore, K. & al. 2014 Execution of Timber Structures. Note in INTER meeting 2014, Bath UK.

SFS 5978:2014 Execution of timber structures. Rules for load-bearing structures of buildings (In Finnish, an English translation is available).

Discussion

The paper was presented by T Toratti

U Kuhlmann commented and explained in steel there is an independent executive standard EN1090 which depends on executive class. The executive class and consequence classes are critical. U Kuhlmann recommended similar approach to be considered for timber.

S Winter commented that we need to learn from other material and people doing execution on site always fear too much regulation even though this is needed. He stated that national specification document not national standard would be interesting for industry. S Winter and T Toratti discussed responsibility of different parties in a building project as this is a grey area.

R Jockwer and T Toratti discussed issues related to tolerances in relationship to workability and practicality. Design equations have to consider these tolerances including length of members etc.

M Follesa stated in Italy foundation tolerances might not be compatible with timber tolerance. There are discussions that tolerance is an issue for all materials. In steel, basic tolerances are available with the consideration of additional tolerance. If basic tolerance is not followed, redesign might be needed to check if this is ok.

4 INTER Notes, Šibenik, Croatia 2015

Start time of charring of timber members protected with gypsum plasterboards

Alar Just, Tallinn University of Technology

Kairit Kraudok, Tallinn University of Technology

Keywords: Gypsum plasterboards –Start time of charring – Fire resistance

1 Introduction

Gypsum boards are widely used in timber frame assemblies because of their fire protective properties. The start time of charring and the failure time of the board are important properties for the fire safety design of timber frame constructions.

EN 1995-1-2 gives simplified design rules for calculation of pull-out failure. However, the failure time of gypsum plasterboard type F should be determined on the basis of tests.

As the thermo-mechanical properties of gypsum plasterboard type F are not part of the classification given in the European product standard for gypsum plasterboards EN 520, failure times of different makes may vary considerably

For the start time of charring there are rules in EN 1995-1-2 [1] and following the component additive method in „*Fire safety in timber buildings. Technical guideline for Europe*“ [2].

The aim of this study is to verify the calculation rules for start time of charring on EN 1995-1-2 and the component additive method in [2] by the extensive analyse of the database of full scale fire tests. The study is performed in co-operation with Tallinn University of Technology and SP.

2 Design methods

There are basically two different design methods regarding start time of charring.

EN 1995-1-2 provides following equation for start time of charring behind gypsum plasterboards Type A, F and H.

$$t_{ch} = 2{,}8 * h_p - 14 \quad (1)$$

The component additive method for design of separating function was developed in ETH by Schleifer [4] based on extensive experimental results and finite-element thermal analysis. According to this method the start time of charring can be calculated as sum of protection times of the cladding layers:

$$t_{ch} = \sum t_{prot,i} \tag{2}$$

Protection time is defined as the time when temperature rise behind the considered layer is reaching 250K. Protection times take into consideration the influence of the backing and preceding layers.

3 Analysis of the database

A database with data from full-scale fire test reports with assemblies including claddings made of gypsum plasterboards in accordance with EN 520 and gypsum fibre boards in accordance with EN 15283-2 was collected at SP Technical Research Institute of Sweden. The database consists of results of 388 full-scale tests from different institutes all over the world, although mainly from Europe.

The first analysis of the results of the full-scale fire tests was carried out by Just *et. al.* [3] and the results of the analysis were published in the „Fire Safety in Timber Buildings. Technical guideline for Europe“ [1]. The analysis is based on minimum values of the protection times

Present analysis is performed by finding 5% fractile values and is based on increased number of test data.

4 Discussions

Start time of charring is depending on thickness of gypsum plasterboards. One layer cladding consisting of Type A and Type F boards are analysed together. See Figure 1. Start times of charring behind two layers of the gypsum plasterboards, Type F are presented. See Figure 2.

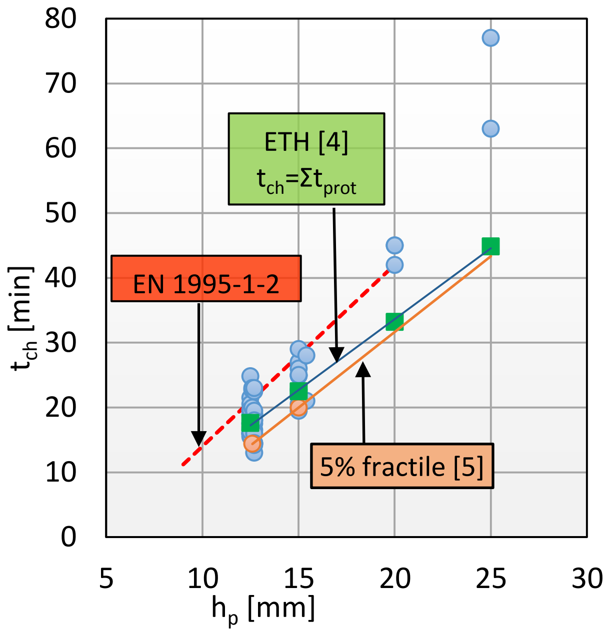

Figure 1. Full scale tests with recorded start time of charring behind one layer cladding of gypsum plasterboards. 5% fractile values compared to EN 1995-1-2 method and component additive method [4].

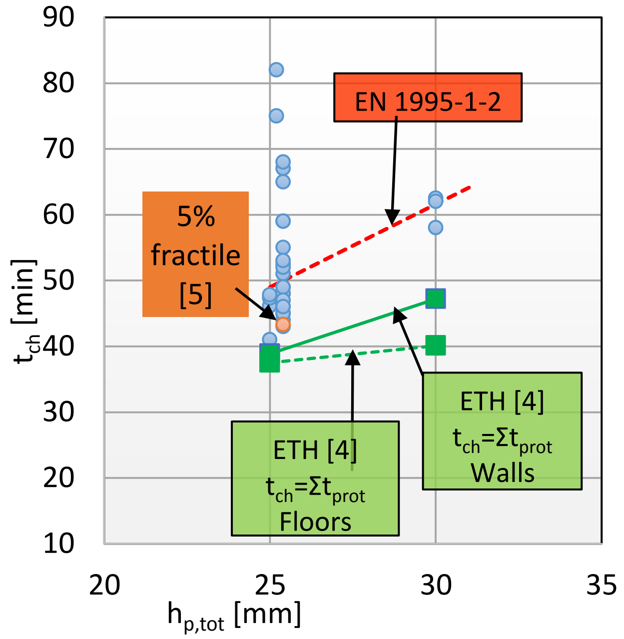

Figure 2. Full scale tests with recorded start time of charring behind two layers cladding of gypsum plasterboards, Type F. 5% fractile values compared to EN 1995-1-2 method and component additive method [4].

This study shows clearly that the generic values for start time of charring are overestimated in EN 1995-1-2 for the most cases. 5% fractile values of start times of charring from the database of full scale fire tests show good correlation with the component additive method.

Based on this analysis the component additive method [4] is recommended for the revision of EN 1995-1-2 for determining design start time of charring behind gypsum plasterboards.

5 References

[1]. Eurocode 5 (2004) Design of timber structures – Part 1-2: General – Structural fire design. CEN (EN 1995-1-2).

[2]. Fire safety in timber buildings (2010) Technical Guideline for Europe. SP Technical research Institute of Sweden, Wood Technology. SP Report 2010:19. Stockholm, Sweden.

[3]. Just, A, Schmid, J and König, J (2010). Gypsum Plasterboards Used as Fire Protection - Analysis of a database," SP Report: 2010:29, Stockholm, Sweden.

[4]. Schleifer, V (2009) Zum Verhalten von raumabschliessenden mehrschichtigen Holzbauteilen im Brandfall. Zürich, Switzerland.

[5]. Kraudok, K. (2015) Protective effect of gypsum plasterboards for the fire design of timber structures. Master thesis. TUT. Tallinn, Estonia.

Protective effect of insulation materials on charring of timber elements

Mattia Tiso, Tallinn University of Technology

Alar Just, Tallinn University of Technology

Keywords: Insulation materials –Timber assemblies – Fire resistance

1 Introduction

The insulation materials may give a contribution to the fire resistance of timber frame assemblies concerning the load-bearing (R criteria) and the separating function (EI criteria).

Current Eurocode 5 Part 1-2 [1] provides a model for fire design of the load bearing function of timber frame assemblies with cavities completely filled with stone wool. The extension of this model for the glass wool for post protection phase [2] is published in the European technical guideline Fire Safety in Timber Buildings [4]. For the verification of the insulation criteria a component additive model is available in Eurocode 5 Part 1-2 that is further improved and published in the European technical guideline *Fire Safety in Timber Buildings* [4].

Eurocode 5 Part 1-2 distinguishes clearly between stone wool and glass wool because of the different behaviour in fire of those mineral wools. There is similar behaviour of glass wool and stone wool as long as the wool is protected. According to the European product standard of mineral wools [2] those two materials are both mineral wool and there is no requirement to producer to declare the type (stone or glass). Beside mineral wool there are other insulation materials that are not included in the design models according to Eurocode 5 Part 1-2.

The aim of this study is to provide the classification methodology of different insulation materials in terms of fire design of timber structures and improvement of the fire design model for timber frame assemblies.

The study is performed by Tallinn University of Technology and SP with co-operation with the international reference group. Since now the investigation of different insulation materials was performed to study the contribution of insulations to the fire resistance of timber frame assemblies.

2 Test method

Ten specimens of timber frame assemblies have been tested in horizontal position in a cubic meter furnace following the standard fire curve according to ISO 834. The specimens consisted of timber beam with cross-section 45 x 145 mm and the insulation materials applied. The fire side of the tested assembly was protected by 15 mm thick gypsum plasterboard; Type F. On the unexposed side the particle board with thickness of 19 mm was used. Thermocouples have been embedded on the timber beam and insulation material in different depths to follow the charring scenario. In order to obtain comparable results for the post-protection phase among the insulation materials, the fall off of the gypsum plasterboard was imposed after 45 minutes from the test start. This was done by releasing the special fastening system. The expected duration of the tests was 60 minutes; in some tests the specimen was removed earlier due to start of charring in particle board.

At the end of the tests the instrumented beam has been cleaned from the char layer and the minimum residual cross section has been obtained.

3 Discussions and future works

Ratios between minimum residual moments of inertia and initial moment of inertia for the tests have been compared with the models in Eurocode 5 Part 1-2 and Fire Safety in Timber Buildings (Figure 1).

The first comparison indicates that the insulation materials could be divided according to their ability to stay only in the protected charring phase and also post-protection charring phase.

The protection provided by most of the materials is on the safe side respect to the two existing models analysed. Anyhow the validity of the models for other materials than stone wool or glass wool is not declared in [1] and [4].

Hence the improved model for timber frame assemblies should be open for wide range of the insulation materials.

Charring of the timber member has to be considered as two dimensional as general. Different charring rates have to be regarded for different sides of timber members and different phases of protection.

There is necessity to develop a qualification methodology that considers the contribution of any insulation materials to the fire protection of timber member. The qualification should not be simply related on the typology of material but on its performance.

For comparison reasons in this first step the experiments have been performed with the same fire protection boards on the exposed side of the specimens and the same cross sections of timber members. These factors could influence the charring behaviour in the protection phase and the load-bearing resistance.

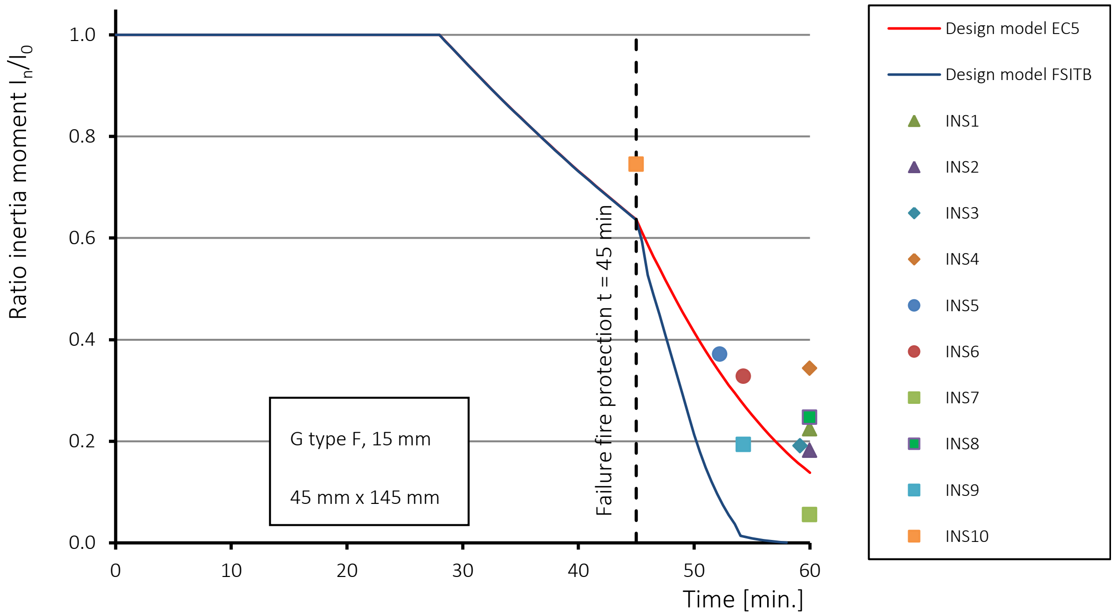

Figure 1. Minimum residual moments of inertia divided initial moment of inertia for the ten tests compared with the models for stone wool and glass wool

The study will continue with the investigations in order to consider the other cross-sections and protections. Comprehensive study with more fire tests and thermal simulations is planned following by analysis and proposals for the classification methodology of the insulation materials as well as for the improved design model for timber frame assemblies.

4 References

[1]. Eurocode 5 (2004) Design of timber structures – Part 1-2: General – Structural fire design. CEN (EN 1995-1-2).

[2]. EN 13162:2012, “Thermal insulation products for building – Factory made mineral wool (MW) products – Specification” European Standard. European Committee for Standardization, Brussels.

[3]. Just, A, Schmid, J and König, J (2010) Post protection behaviour of wooden wall and floor structures completely filled with glass wool, Structures in Fire (SIF).

[4]. Fire safety in timber buildings (2010) Technical Guideline for Europe. SP Technical research Institute of Sweden, Wood Technology. SP Report 2010:19. Stockholm, Sweden.

Investigation of thread configuration for self-tapping screws as reinforcement for embedment strength

Cong Zhang, University of Bath

Wen-Shao Chang, University of Bath

Richard Harris, University of Bath

Keywords: self-tapping screw, thread pattern, embedment strength

1 Introduction

Dowel-type connections are the most common type of connections in timber structural design, especially in large-scale structures. Recent studies, Blass and Schmid (2001), Bejtka and Blass (2005) & Blass and Schadle (2011), have shown improvement on load-carrying capacity of dowel type connections using self-tapping screws (STS).

Similar to other reinforcement such as fibre-reinforced polymers and glued-on plywood panels, the effectiveness of screw reinforcement is implemented and influenced by the bond between wood and screw. Promoting this bond will enhance the performance of reinforcement. The aim of this study is to investigate the influence of thread configuration on self-tapping screws to reinforce the embedment strength. Following this work, the project will progress to optimisation of self-tapping screws and their use in reinforcement of dowel-type connection.

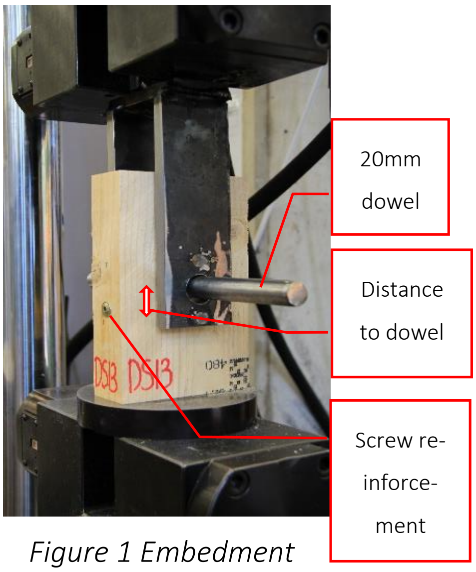

Figure 1 Embedment test set-up

2 Methodology

Following the guidance by BS EN 383-2007, a total of 150 embedment tests were conducted as shown in Figure 1. The embedment strength of timber specimens with varying thread location and length (see Figure 2) was determined. The purpose was to find the most crucial part of the thread over the whole length of the screw.

Description	Distance to dowel (d=20mm)
N, 0% thread	1d
S, 100% thread	1d
BS, 33% thread on the pin end	1d
DS, 33% thread on the head end	1d
ES, 100% thread	0.5d
FS, l_{thread}/l_{eff}=0.15 on the pin end	1d
GS, l_{thread}/l_{eff}=0.35 on the pin end	1d
TTS, 66% thread, two thread segments	1d

Figure 2 Different thread arrangements used in the embedment tests.

3 Results & discussion

Statistical analysis shows that the embedment strength between specimens reinforced by a screw with complete thread (S) and screw with 33% thread on the pin end (BS) does not differ significantly. This implies the thread on the pin side is crucial in providing the required bonding to prevent splitting failure due to tensile stress perpendicular to the grain.

It is hypothesised that a relationship exists between the embedment strength and the length of thread on the most effective pin end, shown in Figure 3. Embedment tests with group FS (l_{thread}/l_{eff}=0.15) and GS (l_{thread}/l_{eff}=0.35) were carried out and the results of embedment strength vs l_{thread}/l_{eff} were plotted in Figure 4. The hypothesis is based on the assumption that a crack will appear in the middle axis of the specimen.

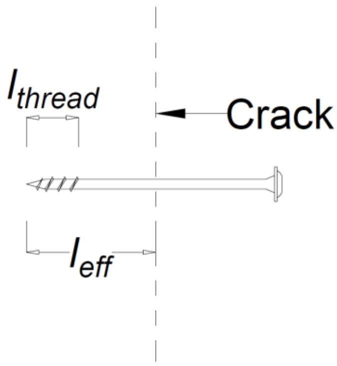

Figure 3 Indication of length of thread (l_{thread}) on the effective length (l_{eff})

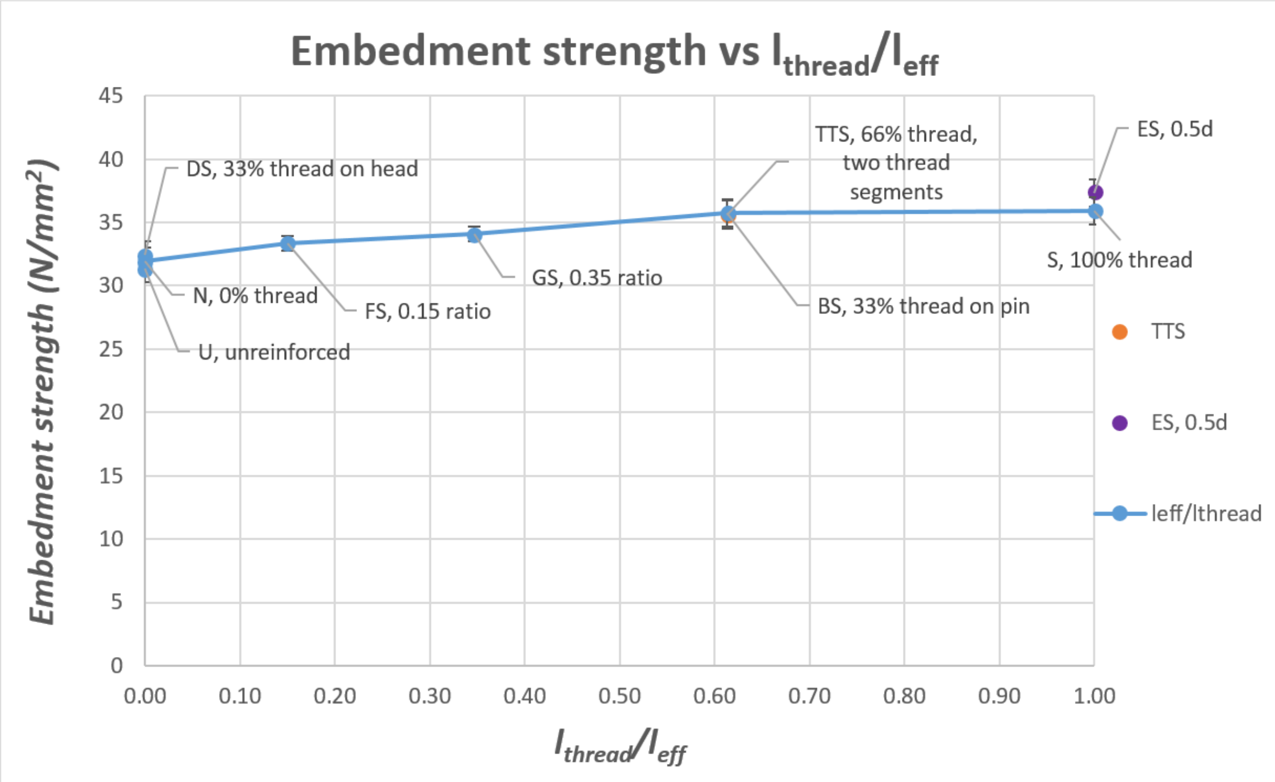

Figure 4 l_{thread}/l_{eff} vs strength enhancement (150 specimens)

4 Conclusion

This study found that the thread location and length can influence the effectiveness of reinforcement. A relationship between embedment strength and thread length over the most effective pin end on a screw is also discovered.

The work continues in tests on screw reinforced connections.

5 References

Bejtka, I. & Blass, H.J., 2005. Self-tapping screws as reinforcements in connections with dowel-type fasteners. In: CIB-W18 2005.

Blass, H.J. & Schadle, P., 2011. Ductility aspects of reinforced and non-reinforced timber joints. *Eng Struct,* 33(11), pp. 3018-3026.

Blass, H.J. & Schmid, M., 2001. Self-tapping screws as reinforcement perpendicular to the grain in timber connections. *Joints in Timber Structures.* Stuttgart, Germany.

BSI, 2007. BS EN 383:2007. *Timber structures. Test methods. Determination of embedment strength and foundation values for dowel type fasteners.*

5 Peer review of papers for the INTER Proceedings

Experts involved:

Members of the INTER group are a community of experts in the field of timber engineering.

Procedure of peer review

- Submission of manuscripts: all members of the INTER group attending the meeting receive the manuscripts of the papers at least four weeks before the meeting. Everyone is invited to read and review the manuscripts especially in their respective fields of competence and interest.

- Presentation of the paper during the meeting by the author

- Comments and recommendations of the experts, discussion of the paper

- Comments, discussion and recommendations of the experts are documented in the minutes of the meeting and are printed on the front page of each paper.

- Final acceptance of the paper for the proceedings with

    - no changes
    - minor changes
    - major changes
    - or reject

- Revised papers are to be sent to the editor of the proceedings and the chairman of the INTER group

- Editor and chairman check, whether the requested changes have been carried out.

6 Meetings and list of all CIB W18 and INTER Papers

CIB Meetings:

1 Princes Risborough, England; March 1973
2 Copenhagen, Denmark; October 1973
3 Delft, Netherlands; June 1974
4 Paris, France; February 1975
5 Karlsruhe, Federal Republic of Germany; October 1975
6 Aalborg, Denmark; June 1976
7 Stockholm, Sweden; February/March 1977
8 Brussels, Belgium; October 1977
9 Perth, Scotland; June 1978
10 Vancouver, Canada; August 1978
11 Vienna, Austria; March 1979
12 Bordeaux, France; October 1979
13 Otaniemi, Finland; June 1980
14 Warsaw, Poland; May 1981
15 Karlsruhe, Federal Republic of Germany; June 1982
16 Lillehammer, Norway; May/June 1983
17 Rapperswil, Switzerland; May 1984
18 Beit Oren, Israel; June 1985
19 Florence, Italy; September 1986
20 Dublin, Ireland; September 1987
21 Parksville, Canada; September 1988
22 Berlin, German Democratic Republic; September 1989
23 Lisbon, Portugal; September 1990
24 Oxford, United Kingdom; September 1991
25 Åhus, Sweden; August 1992
26 Athens, USA; August 1993
27 Sydney, Australia; July 1994
28 Copenhagen, Denmark; April 1995
29 Bordeaux, France; August 1996
30 Vancouver, Canada; August 1997
31 Savonlinna, Finland; August 1998
32 Graz, Austria; August 1999

33 Delft, The Netherlands; August 2000
34 Venice, Italy; August 2001
35 Kyoto, Japan; September 2002
36 Colorado, USA; August 2003
37 Edinburgh, Scotland; August 2004
38 Karlsruhe, Germany; August 2005
39 Florence, Italy; August 2006
40 Bled, Slovenia; August 2007
41 St. Andrews, Canada; August 2008
42 Dübendorf, Switzerland; August 2009
43 Nelson, New Zealand; August 2010
44 Alghero, Italy; August 2011
45 Växjö, Sweden; August 2012
46 Vancouver, Canada; August 2013

INTER Meetings:

47 Bath, United Kingdom; August 2014
48 Šibenik, Croatia; August 2015

The titles of the CIB W 18 and INTER papers (starting from 2014) are included in the complete list of CIB/INTER papers: http://holz.vaka.kit.edu/392.php